SEISMIC PERFORMANCE OF SUSPENDED CEILINGS

A thesis submitted in partial fulfilment of the requirements
for the degree of Doctor of Philosophy in
Structural Engineering
by

ATEFEH POURALI BEJARBANEH

Supervised by:
Professor Rajesh P. Dhakal
Associate Professor Gregory A. MacRae
Dr. Ali S. Tasligedik

Department of Civil and Natural Resources Engineering
University of Canterbury
Christchurch, New Zealand

September 2017

To

Mom, Dad and Merrick

ABSTRACT

Non-structural elements (NSEs) have frequently proven to contribute to significant losses sustained from earthquakes in the form of damage, downtime, injury and death. In New Zealand (NZ), the 2010 and 2011 Canterbury Earthquake Sequence (CES), the 2013 Seddon and Cook Strait earthquake sequence and the 2016 Kaikoura earthquake were major milestones in this regard as significant damage to building NSEs both highlighted and further reinforced the importance of NSE seismic performance to the resilience of urban centres. Extensive damage in suspended ceilings, partition walls, façades and building services following the CES was reported to be partly due to erroneous seismic design or installation or caused by intervening elements. Moreover, the low-damage solutions developed for structural systems sometimes allow for relatively large inter-story drifts -compared to conventional designs- which may not have been considered in the seismic design of NSEs. Having observed these shortcomings, this study on suspended ceilings was carried out with five main goals: i) Understanding the seismic performance of the system commonly used in NZ; ii) Understanding the transfer of seismic design actions through different suspended ceiling components, iii) Investigating potential low-damage solutions; iii) Evaluating the compatibility of the current ceiling system with other low-damage NSEs; and iv) Investigating the application of numerical analysis to simulate the response of ceiling systems.

The first phase of the study followed a joint research work between the University of Canterbury (UC) in NZ, and the Politecnico Di Milano, in Italy. The experimental ceiling component fragility curves obtained in this existing study were employed to produce analytical fragility curves for a perimeter-fixed ceiling of a given size and weight, with grid acceleration as the intensity measure. The validity of the method was proven through comparisons between this proposed analytical approach with the recommended procedures in proprietary products design guidelines, as well as experimental fragility curves from other studies. For application to engineering design practice, and using fragility curves for a range of ceiling lengths and weights, design curves were produced for estimating the allowable grid lengths for a given demand level.

In the second phase of this study, three specimens of perimeter-fixed ceilings were tested on a shake table under both sinusoidal and random floor motion input. The experiments considered the relationship between the floor acceleration, acceleration of the ceiling grid, the

axial force induced in the grid members, and the effect of boundary conditions on the transfer of these axial forces. A direct correlation was observed between the axial force (recorded via load cells) and the horizontal acceleration measured on the ceiling grid. Moreover, the amplification of floor acceleration, as transferred through ceiling components, was examined and found (in several tests) to be greater than the recommended factor for the design of ceilings provided in the NZ earthquake loadings standard NZS1170.5. However, this amplification was found to be influenced by the pounding interactions between the ceiling grid members and the tiles, and this amplification diminished considerably when the high frequency content was filtered out from the output time histories. The experiments ended with damage in the ceiling grid connection at an axial force similar to the capacity of these joints previously measured through static tests in phase one.

The observation of common forms of damage in ceilings in earthquakes triggered the monotonic experiments carried out in the third phase of this research with the objective of investigating a simple and easily applicable mitigation strategy for existing or new suspended ceilings. The tests focused on the possibility of using proprietary cross-shaped clip elements ordinarily used to provide seismic gap as a strengthening solution for the weak components of a ceiling. The results showed that the solution was effective under both tension and compression loads through increasing load bearing capacity and ductility in grid connections.

The feasibility of a novel type of suspended ceiling called fully-floating ceiling system was investigated through shaking table tests in the next phase of this study with the main goal of isolating the ceiling from the surrounding structure; thereby arresting the transfer of associated seismic forces from the structure to the ceiling. The fully-floating ceiling specimen was freely hung from the floor above lacking any lateral bracing and connections with the perimeter. Throughout different tests, a satisfactory agreement between the fully-floating ceiling response and simple pendulum theory was demonstrated. The addition of isolation material in perimeter gaps was found effective in inducing extra damping and protecting the ceiling from pounding impact; resulting in much reduced ceiling displacements and accelerations. The only form of damage observed throughout the random floor motion tests and the sinusoidal tests was a panel dislodgement observed in a test due to successive poundings between the ceiling specimen and the surrounding beams at resonant frequencies

Partition walls as the first effective NSE in direct interaction with ceilings were the topic of the final experimental phase. Low-damage drywall partitions proposed in a previous study in the UC were tested with two common forms of suspended ceiling: braced and perimeter-

fixed. The experiments investigated the in-plane and out-of-plane performance of the low-damage drywall partitions, as well as displacement compatibility between these walls and the suspended ceilings. In the braced ceiling experiment, where no connection was made between ceiling grids and surrounding walls no damage in the grid system or partitions was observed. However, at high drift values panel dislodgement was observed on corners of the ceiling where the free ends of grids were not restrained against spreading. This could be prevented by framing the grid ends using a perimeter angle that is riveted only to the grid members while keeping sufficient clearance from the perimeter walls. In the next set of tests with the perimeter-fixed ceiling, no damage was observed in the ceiling system or the drywalls. Based on the results of the experiments it was concluded that the tested ceiling had enough flexibility to accommodate the relative displacement between two perpendicular walls up to the inter-storey drifts achieved.

The experiments on perimeter-fixed ceilings were followed by numerical simulations of the performance of these ceilings in a finite element model developed in the structural analysis software, SAP2000. This model was relatively simple and easy to develop and was able to replicate the experimental results to a reasonable degree. Filtering was applied to the experimental output to exclude the effect of high frequency noise and tile-grid impact. The developed model generally simulated the acceleration responses well but underestimated the peak ceiling grid accelerations. This was possibly because the peak values in time histories were affected by impact occurring at very short periods. The model overestimated the axial forces in ceiling grids which was assumed to be caused by the initial assumptions made about the tributary area or constant acceleration associated with each grid line in the direction of excitation. Otherwise, the overall success of the numerical modelling in replicating the experimental results implies that numerical modelling using conventional structural analysis software could be used in engineering practice to analyse alternative ceiling geometries proposed for application to varying structural systems. This however, needs to be confirmed through similar analyses on other ceiling examples from existing instrumented buildings during real earthquakes.

As the concluding part of this research the final phase addressed the issues raised following the review of existing ceiling standards and guidelines. The applicability of the research findings to current practice and their implications were discussed. Finally, an example was provided for the design of a suspended ceiling utilising the new knowledge acquired in this research.

ACKNOWLEDGEMENTS

A PhD is not simply a degree you obtain. It's a once-in-a-lifetime experience and like many other life experiences, you don't survive it alone.

It's been an honour working under the supervision of Rajesh Dhakal who I've come to admire and respect greatly. He's been an incredibly meticulous mentor, supportive, bright and patient. I was also lucky enough to have two other great minds on board. Gregory MacRae and Sahin Tasligedik have been always there to introduce new angles into the research and provide me with great advice. I am also grateful to the Natural Hazards Research Platform for providing the financial support through a research scholarship which made this study possible.

I would like to express my endless gratitude to Merrick, Sudi and Azi; the three people who probably listened to me fuss and grumble about my PhD the most.

Merrick, I am ever so grateful for your unearthly patience, your enthusiasm and encouragement. You've been through this and know best how tough it can be at times to stay motivated and not lose focus. I couldn't have done this without your support.

Sudi, I applaud your passion, your sympathy, and above all, your everyday presence that kept me motivated. Thank you for sharing the pain and joy and for pushing me. I specially owe you and Milad, for having me at your place on my -many- visits to Christchurch and for being such lovely people to be around.

Thank you Azi, for being more motivating than you possibly imagine. Your positivity and encouragement were as effective -and appreciated- as your serious motivational rebukes.

I am very grateful to the technical staff in the University of Canterbury laboratories, John Maley and Alan Poynter who helped me during my long and challenging experiments. I specially appreciate your knowledge, reliability and experience in the lab, your meticulousness with the devices and your support and patience throughout different phases of this study. It was great working with you.

During the course of this project I have been fortunate enough to collaborate with some of the best people from the industry; I am so grateful to Steve Clements, who made himself available several times and carried out the installation of all the ceiling specimens in the experimental phases of this study. I would also like to thank John Keen and John Dobier from USG Boral for providing advice and generously sharing their experience and knowledge at

different stages of this study. We were lucky to have GIB on board for the experimental work we carried out on the integrated system of suspended ceilings and low-damage drywalls. I appreciate the support from Hans Gerlich, Richard Hunt and Clara Sumner who supplied the technical backup and test material for the installation of drywall specimens. Doug Connors and Peter were amazingly thorough, skilful and responsible during the installation process and their professional help is much appreciated.

My sincere thanks go to Trevor Yeow, Karim Tarbali, Arsalan Niroomandi, Maria Pianigiani, Ali Abdolahirad and Nikoo Hazaveh who each in some way helped me during the course of this thesis. I appreciate your patience with my questions. I would also like to thank Michael Robson and Darren Kho who devoted their 3rd Professional Year project to the initial experiments that formed the starting steps towards one of our interesting experiments and findings in this research. Special thanks to Weng Yuen Kam who found time in his busy schedule to meet me and answer my questions.

To my amazing former colleagues at GHD Structures team Auckland; Neil, Paula, Marlon, Sam, Willy, Brad, Piyush, Cameron and Andrew, thank you so much for providing me with much-needed company during my most isolated year of the PhD. Thank you for asking about my thesis and encouraging me many times. Working with you was one of the best things that happened during 2016.

And last but not least, I would like to express my endless appreciation to my amazing family, mum, dad, Arameh, Elham, Mohammad and Arian, who I have deeply missed during the past years. Thank you for supporting me each in your own way and for making my journey to NZ possible.

LIST OF PUBLICATIONS

1) A. Pourali, R. P. Dhakal, G. A. MacRae and A. S. Tasligedik. (2017-in press). Fully-Floating Suspended Ceiling System: Ex-perimental Evaluation of Structural Feasibility and Challenges. *Earthquake Spectra*.

2) Pourali, A., R. P. Dhakal, G. A. MacRae, and A. S. Tasligedik. (2016). Fully-floating suspended ceiling system: experimental evaluation of the effect of mass and elastic isolation. *Proceedings of the 16th World Conference on Earthquake Engineering, 9-13 January 2017, Santiago, Chile*

3) Dhakal, R. P., MacRae, G. A., Pourali, A., & Paganotti, G. (2016). Seismic fragility of suspended ceiling systems used in NZ based on component tests. *Bulletin of the New Zealand Society for Earthquake Engineering, Vol. 49, No. 1, March 2016*

4) Dhakal, R. P., Pourali, A., & Saha, S. (2016). Simplified Seismic Loss Functions for Suspended Ceilings and Drywall Partitions. *Bulletin of the New Zealand Society for Earthquake Engineering, Vol. 49, No. 1, March 2016*

5) Dhakal, R. P., Pourali, A., Tasligedik, A. S., Yeow, T., Baird, A., MacRae, G., ... & Palermo, A. (2016). Seismic performance of non-structural components and contents in buildings: an overview of NZ research. *Earthquake Engineering and Engineering Vibration*, *15*(1), 1-17.

6) Pourali, A., Dhakal, R. P., MacRae, G. A., & Tasligedik, A. S. (2015). Fully-Floating Suspended Ceiling System: Experimental Evaluation of Structural Feasibility & Challenges. *Proceedings of the Ninth Pacific Conference on Earthquake Engineering Building an Earthquake-Resilient Pacific 6-8 November 2015, Sydney, Australia*

7) Pourali, A., Dhakal, R. P., MacRae, G. A., & Tasligedik, A. S. (2015). Shake table tests of perimeter-fixed type suspended ceilings. In *Proceedings of NZSEE Conference*,

Auckland, New Zealand. (pp. 648-659).

8) Pourali, A., Dhakal, R. P., & MacRae, G. A. (2014). Seismic performance of suspended ceilings: Critical review of current design practice. In *Proceedings of NZSEE Conference, Auckland, New Zealand*.

9) Robson, M. J., Kho, D., Pourali, B. A., & Dhakal, R. P. (2014). Feasibility of a Fully Floating Ceiling System. In *Proceedings of NZSEE Conference, Auckland, New Zealand*.

TABLE OF CONTENTS

1 Introduction 22

1.1 Suspended ceilings: Current practice 22

1.2 Common damage types 26

1.3 Previous studies 32

1.4 Existing Standards and Guidelines 33

1.4.1 Limit States 35

1.4.2 Actions and load combination 35

1.4.3 Seismic design & installation requirements 36

1.5 Proprietary systems: USG Generic Seismic Design 53

1.5.1 Assumption & Limitations 53

1.5.2 Panel Range Provided 54

1.5.3 Seismic design method 54

1.6 Proprietary systems: Armstrong Seismic Design 57

1.6.1 Assumptions and limitations 57

1.6.2 Panel Range Provided 58

1.6.3 Armstrong Seismic RX Suspension System 58

1.6.4 Seismic design method 60

1.7 Design examples 61

1.7.1 Design based on NZ Standard 61

1.7.2 Design based on USG Guideline 64

1.7.3 Design based on Armstrong Guideline 67

1.8 Research motivations 68

1.9 Research aim and objectives 69

1.10 Thesis outline 70
1.11 References 72
2 Seismic Fragility of Suspended Ceiling Systems Used in NZ Based on Component Tests 79
2.1 Introduction 79
2.2 Suspended ceiling systems in New Zealand 81
2.2.1 Typical Layout 81
2.2.2 Current Design/Installation Approach 83
2.2.3 Seismic performance 86
2.3 Methodology 90
2.3.1 Tests on Components and Connections 90
2.4 Results and discussion 96
2.4.1 Ceiling Component Test Results 96
2.4.2 Fragility Curves for Ceiling Components 99
2.4.3 Fragility Curves for Ceiling System 101
2.4.4 Effect of Ceiling Area and Tile Weight 104
2.4.5 Comparing the Proposed Analytical Method with Existing Experimental Data 109
2.5 Conclusions 112
2.6 References 113
3 Experimental Assessment of Seismic Response of Suspended Perimeter-Fixed Ceilings 120
3.1 Introduction 120
3.2 Literature review 120
3.3 Objectives 122
3.4 Experimental program 123
3.4.1 Test setup 123

3.4.2 Instrumentation 124
3.4.3 Test specimens 125
3.4.4 Test input motion 127
3.5 Results and discussions 128
3.5.1 Amplification of input motion 128
3.5.2 Effect of boundary restraint 133
3.5.3 Force-acceleration relationship 137
3.5.4 Effect of filtering on the experimental output 142
3.5.5 Damage observations 145
3.6 Conclusions 146
3.7 References 147
4 Experimental Evaluation of the Influence of Seismic Clips on Grid Joints in a Suspended Ceiling System 151
4.1 Introduction 151
4.2 Description of experimental program 152
4.2.1 Test setup 152
4.2.2 Test specimens 152
4.2.3 Methodology 153
4.3 Experimental results & observations 154
4.3.1 Load carrying and failure mechanism 154
4.3.2 Discussion of Results 159
4.4 Fragility studies 163
4.4.1 Damage state and definition of failure 163
4.4.2 Fragility curves 163
4.5 Implications and recommendations for further studies 166
4.6 Conclusions 167

4.7 References 168
5 Fully-Floating Suspended Ceiling System 173
5.1 Introduction 173
5.2 Mechanics of fully-floating ceiling system 175
5.3 Design of the experiment 176
5.3.1 Test specimens 176
5.3.2 Test setup and instrumentation 180
5.4 Input motions to the Shaking Table 181
5.5 Results and discussions 182
5.5.1 Dynamic properties of the specimen 182
5.5.2 Ceiling displacement range 185
5.5.3 Ceiling weight 187
5.5.4 Arrangement of hanger wires 190
5.5.5 Effect of perimeter isolation 191
5.5.6 Amplification of input acceleration 196
5.5.7 Damage observations 196
5.5.8 Applications and implications 198
5.6 Conclusions 200
5.7 References 202
6 Experimental Evaluation of Seismic Compatibility between Low-Damage Drywall Partitions and Suspended Ceilings 206
6.1 Introduction 206
6.1.1 Existing systems and common damage forms 206
6.1.2 Review of previous studies 210
6.1.3 Motivation and objectives 210
6.1.4 Limitations 211

6.2 Methodology 212
6.2.1 Test Setup 212
6.2.2 Specimens and installation details 213
6.2.3 Instrumentation 218
6.2.4 Input motion 220
6.3 Results 221
6.3.1 Inter-storey drift levels 221
6.3.2 Phase I: Low-damage drywalls with back-braced ceiling 222
6.3.3 Phase II: Low-damage drywalls with perimeter-fixed ceiling 224
6.4 Discussions 227
6.4.1 Phase I 227
6.4.2 Phase II 229
6.5 Conclusions 229
6.6 References 230
7 Perimeter-Fixed Ceiling: Comparison of Numerical Modelling and Shaking Table Experiments 235
7.1 Introduction 235
7.2 Section 1: Review of experiments 236
7.2.1 Test setup 236
7.2.2 Test specimen 237
7.2.3 Instrumentation 238
7.2.4 Input motions 239
7.2.5 Filtering the time histories 239
7.3 Section 2: Numerical modelling 240
7.3.1 Model of test frame and perimeter-fixed ceiling 240
7.3.2 Data collection 243

7.3.3 Summary of simplifying assumptions 244
7.4 Section 3: Results and discussion 246
7.4.1 Effect of overhanging beams on frames vertical excitation 246
7.4.2 Natural periods 246
7.4.3 Comparisons of results in a ground motion test without filtering 247
7.4.4 Comparisons of results in a sinusoidal test without filtering 251
7.4.5 Comparisons of results in a ground motion test with filtering 253
7.4.6 Comparisons of results in a sinusoidal motion test with filtering 259
7.4.7 Comparisons of results for all tests 260
7.4.8 Effect of filtering level 266
7.4.9 Numerical model of ceiling specimen incorporating the tile-grid impact 268
7.5 Summary and Conclusions 275
7.6 References 275
8 Implications of Research Findings 278
8.1 Introduction 278
8.2 Findings and implications 278
8.2.1 The design working life of the suspended ceiling system 278
8.2.2 Suspended ceiling system's ductility factor for the ULS design 279
8.2.3 Understanding the mechanics of the force transfer within the components of suspended ceilings and development of a hierarchy of strength 281
8.2.4 Ceiling grid acceleration – axial force relationship 282
8.2.5 Part spectral shape coefficient for suspended ceilings 283
8.2.6 Alternative ceiling systems or solutions 284
8.3 Research limitations and shortcomings 285
8.4 Seismic design example of a suspended ceiling based on NZ Standard 286
8.4.1 Calculation of seismic demand: 286

8.4.2 Envelope fragility curves 286
8.4.3 Design plots 287
8.4.4 Estimation of allowable lengths 288
8.4.5 Comparison of Standard mandated seismic force with manufacturer's guidelines 289
8.5 Conclusions 291
8.6 References 291
9 Conclusions and Recommendations 294
9.1 Main Findings 294
9.1.1 Component-based seismic fragility of suspended ceilings 294
9.1.2 Experimental investigations on the seismic performance of perimeter-fixed ceilings 295
9.1.3 Effect of seismic clips on the performance of ceiling grid joints 297
9.1.4 Experimental evaluation of fully-floating ceilings as a low-damage solution 297
9.1.5 Compatibility between low-damage drywall partitions and common suspended ceilings 299
9.1.6 Numerical modelling of perimeter-fixed ceilings 300
9.2 Recommendations for Future Research 301
9.2.1 Effect of seismic clips 301
9.2.2 The fully-floating ceiling 301
9.2.3 Numerical modelling of perimeter-fixed ceiling 302
9.3 References 302
10 Original and Filtered Ground Motions Used in Experiments on Perimeter Fixed Ceiling Specimens 306
11 List and Location of Instruments on Specimens and Test Frame 320
11.1 Test frame 320
11.2 Perimeter-fixed ceiling Pr-F-A 322

11.3 Perimeter-fixed ceiling Pr-F-B 324
11.4 Fully-floating ceiling 326
11.5 Low-damage drywall 328
11.6 Braced ceiling 329
11.7 Unbraced ceiling 330
12 Photos 333
12.1 Test frame 333
12.2 Experiments on perimeter-fixed ceilings 336
12.3 Experiments of fully-floating ceiling system 342
12.4 Experiments on low-damage drywall & ceiling 349
12.5 Experiments on CT-MT joints with seismic clip 360

CHAPTER 1

INTRODUCTION

1 INTRODUCTION

1.1 Suspended ceilings: Current practice

Suspended ceilings are non-structural components used widely in modern buildings as an alternative for direct gypsum plasterboards, concrete or wood ceiling finishes. They provide a more appealing interior and serve a wide range of other purposes. Dropped ceilings and ceiling tiles were used in Japan for aesthetic reasons since the 14th century. US Patent No. 1,470,728 (1923) for modern dropped ceilings was granted to Hall in 1923. Initially modern dropped ceilings were built using interlocking tiles which made the repair or inspection very time-consuming and expensive. In 1961 Donald A. Brown was granted a patent for Accessible Suspended Ceiling Construction (US Patent No. 2,984,946 A). This invention provided suspended ceiling construction which allowed easy access at any desired location. Ever since, suspended ceilings have gained increasing popularity in commercial, educational and residential areas due to their advantageous qualities such as sound absorption, sound correction and insulation, providing an enclosed hidden space for mechanical and electrical services underneath the floor while providing easy access for repair, light reflection, prevention of fire spread, aesthetic and architectural variability, energy and heat retention and simplicity of installation process. This widespread application combined with damage observations in several earthquakes, has given the design and installation of suspended ceilings a reasonable level of significance.

The main commercial ceiling systems used in New Zealand are two-way exposed ceilings which consist of drop in tiles/panels supported by the flanges of inverted ‘T’ shaped grid members known as main tees and cross tees (Figure 1-1). This system can be fixed directly to the surrounding walls or to the floor above.

Figure 1-2 shows the typical main tee and cross tee cross sections used in NZ and their interlocking connections and splices which use a click-fit mechanism.

In the case of surrounding confinement, the system is called “Perimeter-fixed ceiling” (Figure 1-4a & b). The perimeter fixtures can be proprietary clips or aluminium rivets as shown in Figure 1-3.The lateral load in the form of acceleration is transmitted from the structure to the system through columns and walls at the height of the ceiling. In this configuration, the hanging wires fixing the ceiling to the above floor are flexible enough to transfer no lateral action. Loads are applied to the ceiling via perimeter contacts. Additional loads may be induced in the ceiling from attached services.

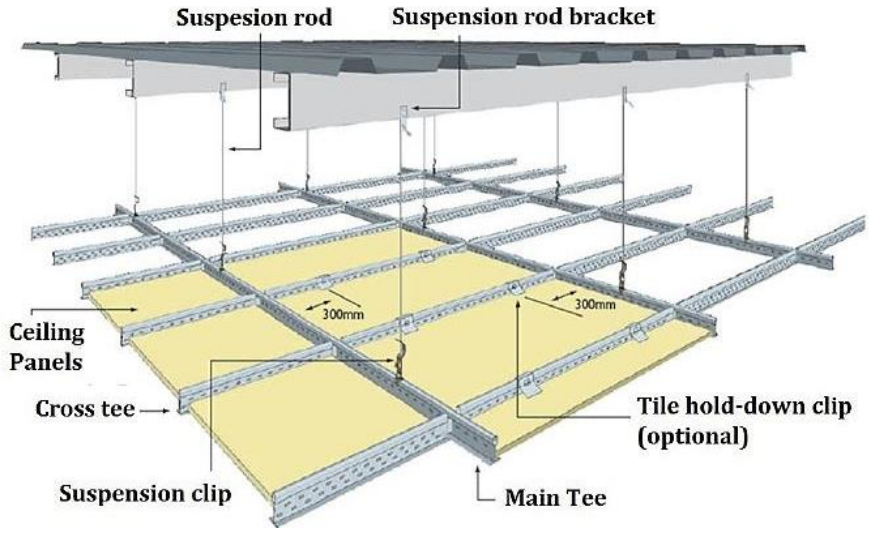

Figure 1-1- A typical suspended ceiling system (Rondo, 2008)

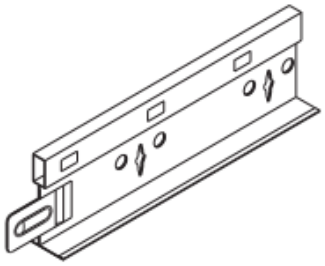

Main tee (USG, 2012)

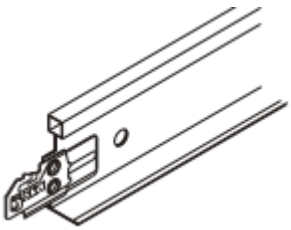

Cross tee (USG, 2012)

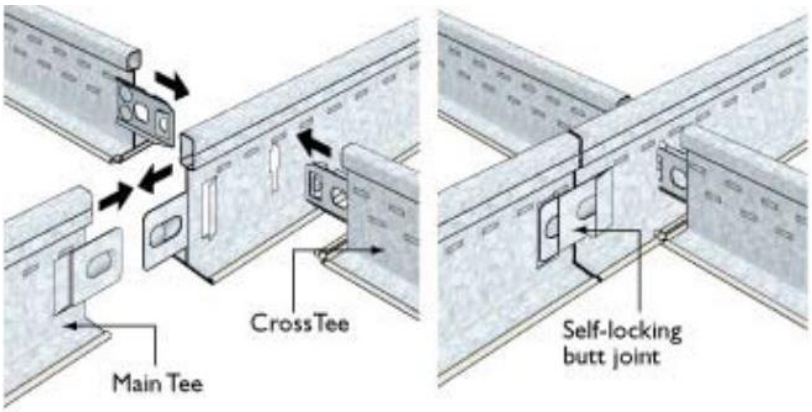

Connection between cross tees and main tees, and main tee splice (Rondo, 2008)

Figure 1-2 – Typical tee sections and their connections

The second ceiling system is the floating ceiling which is not connected to the perimeter but is supported by the floor above by means of diagonal bracing elements (Figure 1-4c). The gaps at the ends of the ceiling have to be large enough to accommodate the inter-story drift demands plus some extra clearance for the additional ceiling displacement due to the flexibility/slackness of braces. Insufficient gaps on the grid ends may result in pounding which could impose large impact forces on the ceiling (Singh, 2011).

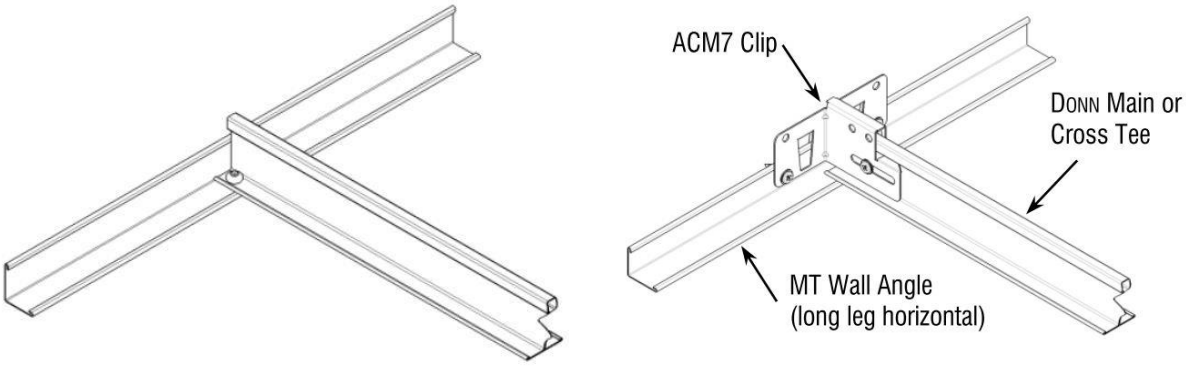

(a) (b)

Figure 1-3 – Typical end fixtures to perimeter wall angle: (a) rivet, and (b) clip (USG, 2011)

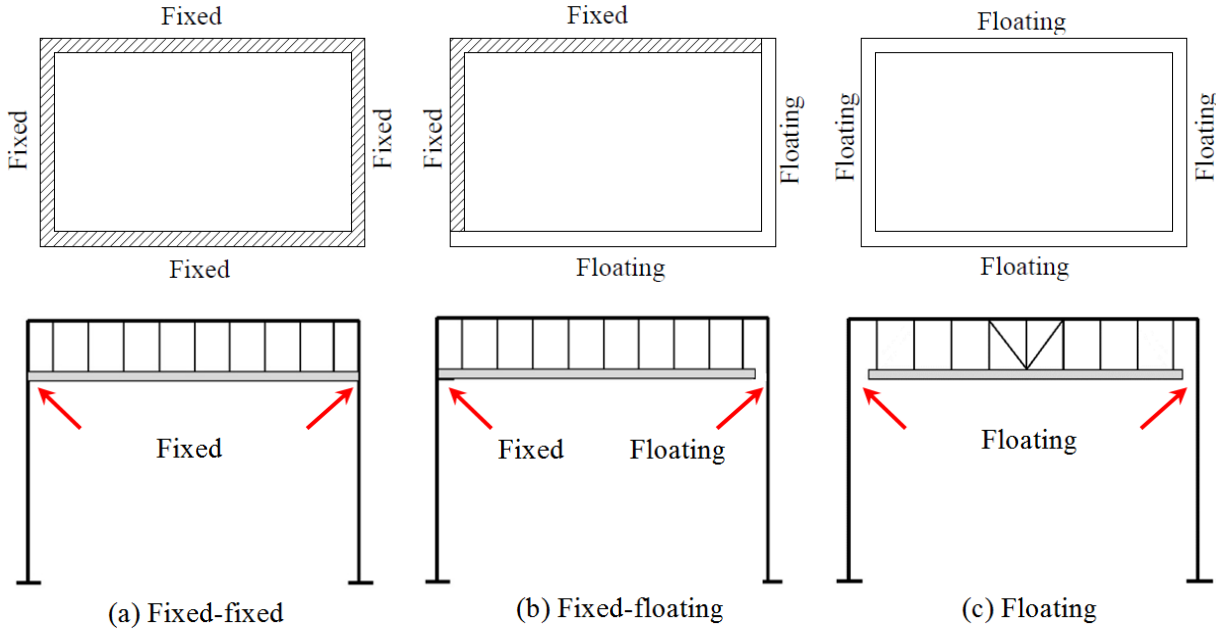

Figure 1-4 – Suspended ceiling types and perimeter connections

Grid members have a limited capacity defined in standards and determined through testing. Once this limit is passed, other members should be added to the system to contribute to load carrying. In ceilings with large areas and considerable load carried, back-bracing is applied in which, grid members are supported by the structure above through diagonal members. The bracing is made more robust using various additional elements such as compression conduits and struts and diagonal angle or channel profiles instead of wires. In this system, rigid braces carry all lateral forces applied to the ceiling and the ceiling is free to displace on all perimeters. Figure 1-5 to Figure 1-7 show examples of back-bracing options provided by two manufacturers in New Zealand (Armstrong, 2013; USG, 2012).

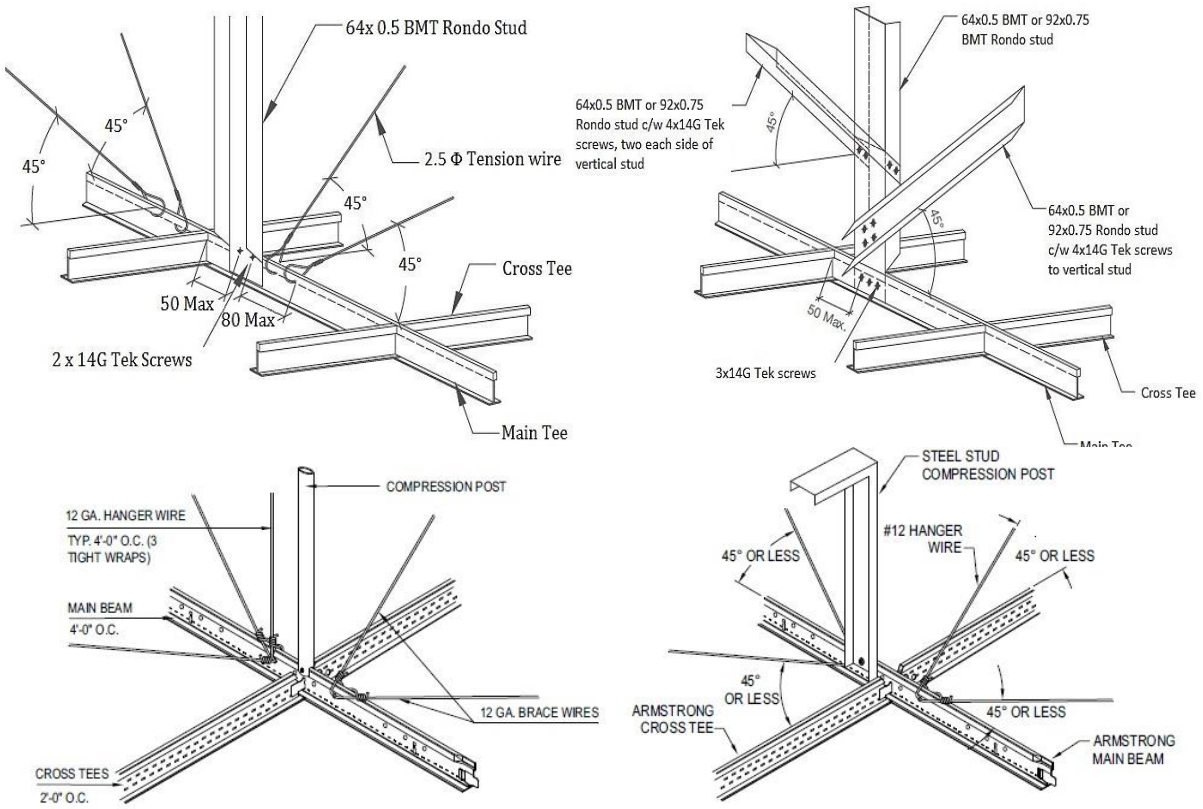

Figure 1-5 - Details of back-bracing options (Armstrong, 2013)

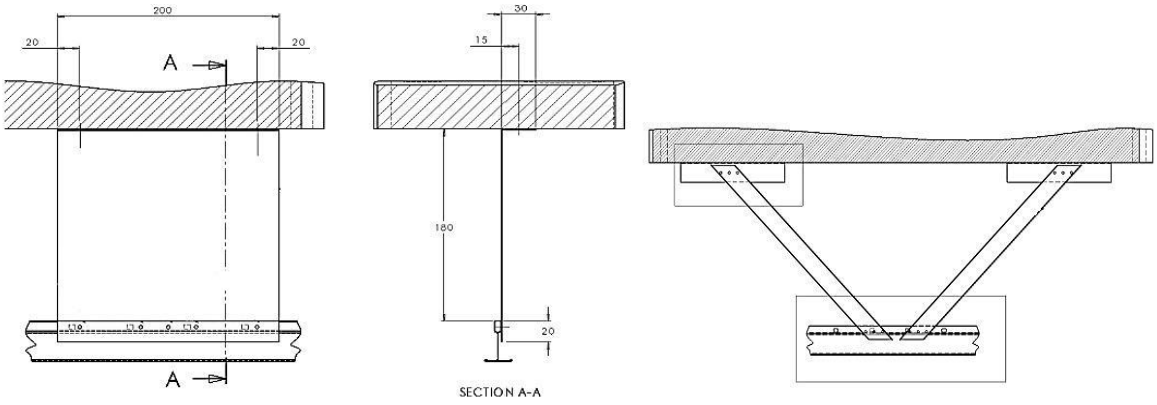

Figure 1-6 - Direct fix bracing for plenum depth ≤ 0.18 m (left), K Bracing for 0.18 m ≤ plenum depth ≤ 1.25 m (right) (USG, 2012)

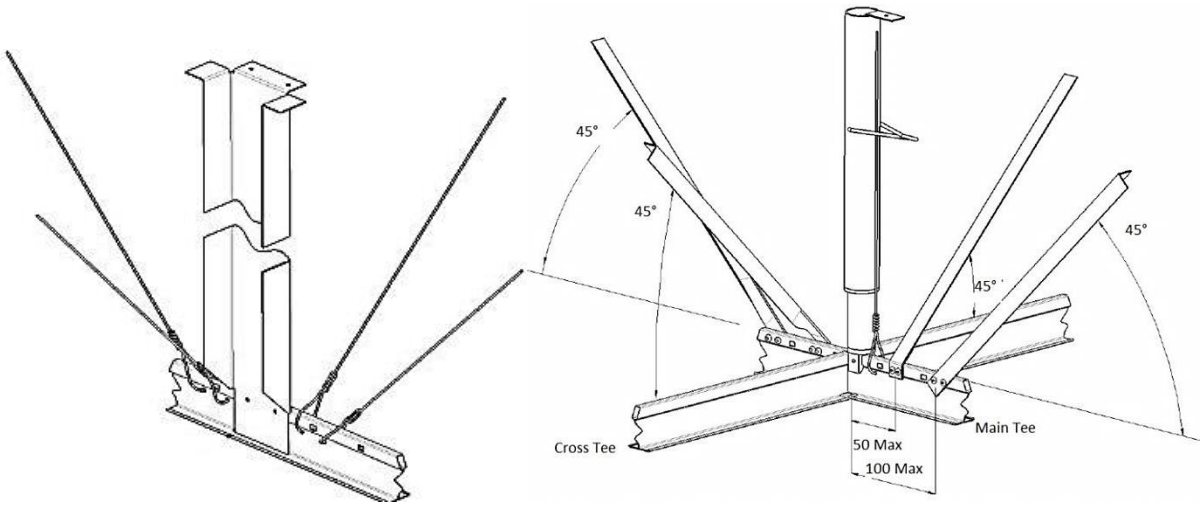

Figure 1-7 – Seismic wire and strut bracing options (USG, 2012)

1.2 Common damage types

According to FEMA E-74 (2011), the structural components of a commercial building account for approximately 15-25% of the original construction cost, while the non-structural (mechanical, electrical, plumbing, and architectural) components and contents account for the remaining 75-85% of the cost. The comparison of the costs related to these 3 components in three common types of commercial construction in Figure 1-8 by Miranda & Taghavi (2003) highlights the financial implications associated with the damage to non-structural elements.

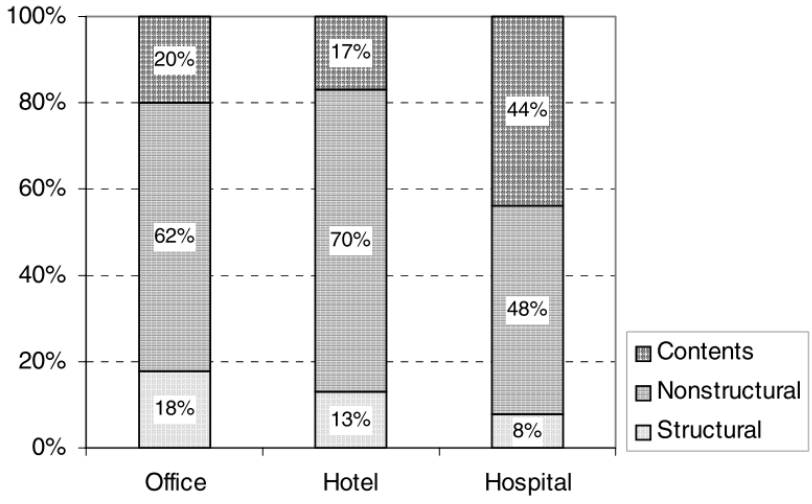

Figure 1-8 - Typical cost of building construction (Miranda & Taghavi, 2003)

The seismic resilience of Non-structural elements (NSEs) plays an important role in the overall seismic performance of buildings as they can pose various risks to the occupants including property loss, loss of functionality of spaces, fire hazard and potential for injury or

even loss of life. Moreover, due to their relatively lower capacity, NSEs experience damage at demand levels lower than what the structure is designed for. This results in considerable financial losses due to damage, downtime (resulting in business interruption and relocation) and injuries even when the structure remains intact or undergoes insignificant damage following a seismic event. Studies show that non-structural damage accounts for 79% of the total earthquake damage in office buildings (Miranda & Taghavi, 2003). Suspended ceilings are one of the key contributors to NS damage as shown by Bradley et al. (2010). In New Zealand, inspections following the 2010 and 2011 Canterbury earthquakes showed that many of the damaged ceilings were not designed to withstand seismic forces. In other cases, the installation method was found to be inefficient (Dhakal, 2010; Dhakal et al., 2011; MacRae et al., 2011)

The types of damage commonly observed in suspended ceilings as reported in FEMA E-74 (2011) include:

- Damage caused by the differential movement of the ceiling relative to structural elements such as columns or walls or nonstructural elements such as partitions, sprinklers heads, or fixed lighting (Figure 1-9).
- Dislodgment and failure of acoustical tiles out of the ceiling grid; separation and dislodgement of grid members, especially at the perimeter or at penetration points for other elements (Figure 1-10).
- Damage caused by lights, diffusers, and sprinkler heads' swing and displacement (Figure 1-11)
- Hazard caused by lights, diffusers and other services within the ceiling which are not independently supported by safety wires
- Post-earthquake damage to content caused by water leaks from broken sprinklers (Figure 1-11)

Magnitude 7.1 Mw Darfield Earthquake which occurred on 4 September 2010 near the town of Darfield, east of Christchurch, New Zealand caused significant damage to non-structural elements in almost all buildings in the area affected. According to Dhakal (2010), ceiling damage was observed both in low-rise residential houses and commercial buildings. Damage was less significant in residential ceilings which typically consist of plasterboard nailed and/or glued to a light timber frame, where the common form of ceiling damage was cracks on the plasterboard, crushed plasterboard particles falling on the floor and plasterboards being detached from the frame (due to punching though the nail or tearing off at the glue).

Ceilings in commercial buildings consist of grid and tile suspended ceilings anchored to the floor above. The damage observed in these types of structures included i) dislodging and breaking of the tiles, ii) failure of the ceiling grid members and connections, iii) failure of perimeter angles, and iv) damage of ceiling tiles due to interaction with the services. In a crude approximation, 10%-15% of commercial/industrial buildings incurred ceiling damage to different extents (Dhakal, 2010).

Figure 1-9 - Damage to suspended metal panel ceiling system around column obstructions in the 2010 Chile Earthquake (FEMA E-74, 2011)

Figure 1-10 - Generalized failure of ceiling grid, tiles, lights, and diffusers at the Los Angeles Hospital in the 2010 magnitude-8.8 Chile Earthquake (FEMA E-74, 2011)

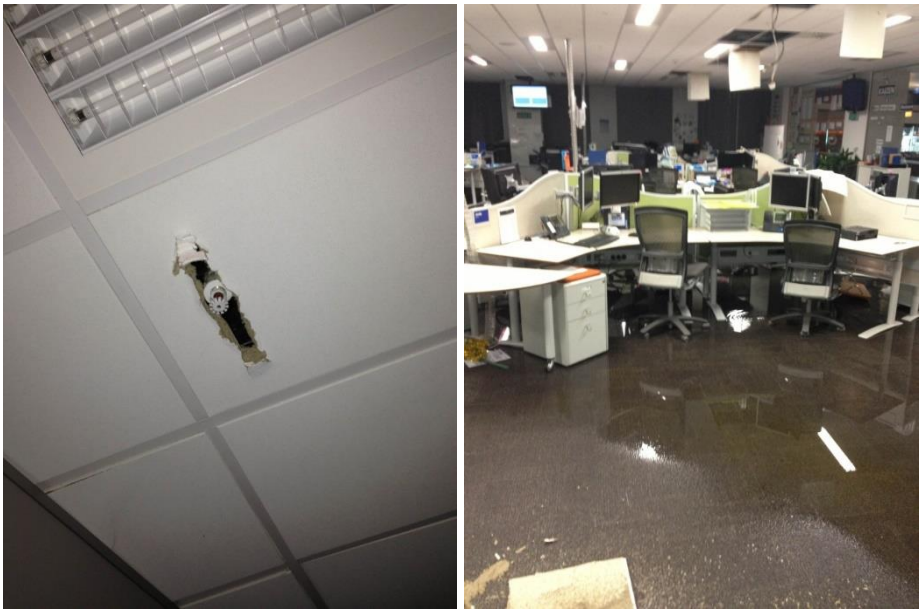

Figure 1-11 – Ceiling and content damage caused by sprinklers in the 2013 Cook Strait earthquake in NZ (Photograph courtesy of T. Johnson)

(a) (b)

Figure 1-12 – Failure of (a) main tee splices, and (b) perimeter fixing (Dhakal, 2010; MacRae et al., 2011)

Several examples of main tee splice failure and disconnection of the cross tees from the main tees were observed which resulted in localized collapse of the grid and loss of tiles (Figure 1-12a). The other type of grid damage occurred in one-way suspended ceilings where panels were supported by main tees spanning one way and hung from the structure above. There were typically no transverse tees. In such a system, as soon as the first panel fails the system loses integrity and grid members are free to spread resulting in failure of adjacent panels.

Perimeter damage was also found which resulted from the main tee or cross tee losing seating on the perimeter angle around the ceiling. Loss of seating can result due to insufficient

seating edge, absence of rivets to connect the grid member to the angle or failure of the rivet itself. This resulted in the grid members and tiles dropping from the ceiling. Perimeter hanger wires on grid ends were effective in preventing the grid and tiles from falling, however, this could result in the tile and members being forced back into the angle causing damage to the tiles and members (Figure 1-12b).

Suspended ceilings were also subject to damage caused by services above the ceiling being forced down, displacing haphazardly or impairing the proper hanger support. In a standard installation of a suspended ceiling the hanger wires are placed at 1200mm/c. However, the presence of services (such as HVAC units) above the ceiling can occasionally make this setting impossible. As a result, suspended ceilings were sometimes partially hung from services within the ceiling (most commonly HVAC ducting and plant). As these plants were rarely secured properly, their movement imparted force into the ceiling causing damage. Suspended ceilings were not designed to take the additional force from the plant. Figure 1-13 shows examples of this type of damage. Ceilings also underwent damage due to the elements supported by the system which are supposed to be independently braced, such as partitions.

Both in residential and commercial buildings the ceiling systems were generally not engineered for seismic performance. Unlike in earthquake prone countries like USA and Japan, properly designed seismic braces were not used in the ceilings in the inspected buildings. Observations following this event revealed the need for the improvement of existing ceiling systems and their seismic bracing in particular.

Figure 1-13 – Damage caused by services (Dhakal, 2010; MacRae et al., 2011)

On 22nd February 2011, a M6.3 earthquake hit Christchurch resulting in significant damage in both high-rise and medium height buildings. Due to the nature of the ground motions, tall

buildings suffered both structural and non-structural damage but in low-rise structures the damage was mostly non-structural while the structure remained mainly intact.

According to Dhakal et al. (2011), among the different non-structural building components, ceilings stood out as the most severely damaged component in the Christchurch earthquake. In general, two thirds of office buildings in Christchurch visited by the authors after the earthquake had suffered non-trivial damage to suspended ceilings.

Most of the medium-high rise office/commercial buildings observed had suspended ceilings. In these systems damage included detachment of the cross-tee from the main tees resulting in tile dislodgement, failure of the main tee splice joint, breaking or buckling of main tees due to compression and torsion-induced rotation of the joints, grid spreading, perimeter damage due to inadequate fixing of grid members to the wall angles, damage caused by services above the ceiling, dislodged tiles in case of large –above 1g– vertical acceleration and damage due to interaction with other non-structural components which should be supported independently from the ceiling.

In general, a combination of smaller ceilings and lighter tiles resulted in lower demand on the grid members and connections, which led to safer ceilings. The observations showed that smaller ceilings performed much better due to smaller demands on the system and in the case of ceilings of similar size, using heavy tiles resulted in considerable damage.

According to Dhakal et al. (2011), the observed damage in ceilings was very severe in many cases and it was only a coincidence that nobody was killed due to ceiling failure in these earthquakes. As the 2011 Japan earthquake had proved, heavy ceiling tiles falling from several meters can easily be fatal. Even in rooms without heavy tiles, cross members bent down like skewers can cause a major hazard for anyone exiting the building. Hence, ceilings should be designed for life safety (i.e. Ultimate limit state) rather than for serviceability. In many cases also, the damages were the result of poor installation rather than weak design. Therefore, the need for mandatory installation practices and quality control seems obvious.

Goltz (1994) reported the ceiling damages observed after 1994 Northridge earthquake which include widespread dropping of acoustical panels, dropped light fixtures when not directly attached with a safety wire and perimeter damage with occasional grid drops for ceilings with unbraced vertical breaks.

In a report prepared by Kawaguchi (2012), damage to non-structural components and particularly suspended ceilings in large rooms after 2011 Japan earthquake has been

documented. Extensive damage was reported in a large number of buildings including schools, sports and entertainment centers which are of special significance both because of the large number of occupants and post-earthquake application.

The damages reported include: failure of plasterboard connection to furring strips in inclined and curved gymnasium ceilings, collapse of large ceilings in swimming pools due to the weak performance of clips connecting panels to grid system, damage to acoustic curved ceilings of auditoriums due to large spans and plenum spaces and use of heavy acoustic panels and extensive collapse of ceiling in an airport entrance hall despite no damage in the structure.

The 6.6M earthquake in Japan in 2007 caused extensive ceiling and equipment damage. The unbraced suspended ceiling on the 3rd floor of a building underwent significant damage although there was no damage to the structure; panels fell, the grid system buckled, and connections came loose. Damage was concentrated either at the perimeter or at the column lines where the flexible ceiling impacted rigid structural components. Another structure investigated was the Supercenter store which was a large, one-story structure and had a floor area of more than 500,000 ft^2 [46,000 m^2]. The structural systems performed well, however, the building area experienced close to 12 inches [300 mm] of settlement. There was non-structural damage at the site which included the collapse of the suspended ceiling system. The damage affected 20 percent of the building, and the facility was shut down for a week after the earthquake. The collapsed ceiling system was a main contributor to the resulting business interruption.

Actual earthquake experience (most notably Northridge and Loma Prieta earthquakes) suggested three critical elements which are effective in ensuring good performance of ceiling systems during earthquakes:

- Independent safety wires on light fixtures to prevent dropout
- Minimum strength requirements for splices and cross tee/main tee intersections
- Spreader bars and independent support of grid ends at wall closures through hanger wires, which prevent panel dropout if the perimeter grid end loses support on edges due to differential movement.

1.3 Previous studies

Several different research publications and reports were reviewed and studied prior to the commencement of this research. These studies included

- Monotonic and cyclic tests on the components of the ceiling with the aim of capturing their force-displacement response and load bearing capacities. Fragility curves were proposed based on these experiments. (Paganotti et al., 2011; Soroushian et al., 2015a & b)
- Shake table tests on different configurations of perimeter-fixed and back-braced (floating) ceilings with the aim of determining their overall performance and fragility functions at different acceleration levels. These studies also investigated the common forms and causes of damage in ceilings and defined their damage states. (Badillo-Almaraz et al., 2007; Gilani et al., 2010 & 2012; Glasgow et al., 2010; Huang et al., 2013; Ryu et al., 2012; Soroushian et al., 2016)
- Shake table tests on proposed pendulum ceilings (Robson et al., 2014; Yao et al., 2000)
- Shake table tests on combined non-structural elements studies, e.g. suspended ceilings and partition walls or services and the performance of the system as a whole as well as interactions between different elements (Huang et al., 2013; Soroushian et al., 2014)
- Experiments on specimens of as-built and proposed low-damage drywall partitions developed and tested at the University of Canterbury (Tasligedik et al., 2014; Tasligedik, 2015)
- Numerical analysis models developed to simulate the seismic performance of suspended ceilings (Zaghi et al., 2016; Ryu et al., 2012 & 2013)

Each of these categories have been reviewed in more details in the corresponding chapter of this thesis.

1.4 Existing Standards and Guidelines

Currently design and installation criteria exist for suspended ceilings through a number of compliant documents. Manufacturers also provide guidelines specific to their products that assist designers and tenderers with the details of installation and a simple design method.

The following list includes some of the documents available in NZ providing guidance on different aspects of the suspended ceiling system and other inter-related elements:

- (NZS 1170.5:2004) – Structural design actions, earthquake actions, New Zealand
- (AS/NZS 2785:2000) – Suspended ceilings: Design and installation
- (NZS 4219:2009) – Seismic performance of engineering systems in a building.

- Generic seismic design for USG DONN exposed grid suspended ceilings, 2012
- Armstrong seismic design guide, suspended ceiling systems, New Zealand version, 2013

The following Standards were also used in conjunction with the NZ Standards and guidelines to create a summary in this chapter:

- (ASTM C636) – Standard practice for installation of metal ceiling suspension systems for acoustical tile and lay-in panels
- (ASTM E580) – Standard practice for installation of ceiling suspension systems for acoustical tile and lay-in panels in areas subject to earthquake ground motions
- (ASCE/SEI 7–10) – Minimum design loads for buildings and other structures
- (CISCA Seismic Zones 3-4) – Guidelines for seismic restraint for direct hung suspended ceiling assemblies

In NZ, the AS/NZS 2785:2000 Suspended Ceilings Standard sets out the minimum requirements for the design, construction, installation, maintenance and testing of internal and external non-trafficable suspended ceiling systems and it is intended for use in commercial, industrial and residential applications (AS/NZS 2785:2000). NZS 1170.5 (2004) is the Standard for the design of structural and non-structural elements (i.e. parts) for earthquake actions in NZ. Chapter 8 of this Standard is used for determining the seismic actions on suspended ceilings. Suspended ceilings are outside the scope of NZS 4219:2009. However, this Standard (NZS 4219:2009) is applicable to the services installed in the vicinity of or in interaction with suspended ceilings.

Suspended ceilings commonly used in NZ are proprietary products. These products are provided with installation and design recommendations that users need to adhere to. Two of these proprietary guidelines are also included in this chapter as a reference for the common installation and design practice in NZ.

As one of the common non-structural elements used in residential, commercial and educational spaces, suspended ceilings need to conform to the relevant fire resistance and acoustic performance requirements. For this purpose, manufacturers provide special ceiling tiles compliant with the requirements of Standards (NZS/BS 476.20:1987, AS/NZS 1530.3:1999, AS/NZS 2499:2000). However, design of suspended ceilings with considerations for fire protection and acoustics is outside the scope of this research project and therefore, will not be discussed in this chapter.

1.4.1 *Limit States*

Based on the importance level of the ceiling and the risk associated with its failure (risk factor), a ceiling may be designed for serviceability or ultimate limit state (SLS or ULS) (NZS 1170.5:2004). The ceiling is serviceable as long as it maintains its intended performance level throughout its working life. According to AS/NZS 2785:2000, the total deflection of ceiling grid system under service conditions for exposed two ways ceilings and finish level 2 (i.e. minimum finish, applicable in non-critical areas, department stores etc.) and level 3 (i.e. normal finish, used in shops, offices etc.) are *L/250* and *L/300*, respectively, where *L* is the distance between the supports.

The Ultimate limit state (ULS) is reached when the ceiling system or any of its parts ruptures, becomes unstable or loses equilibrium (AS/NZS 2785:2000). The Standard does not define the type of damage at ULS. However, it is assumed the damage should result in a life safety threat, such as tile dislodgment from heights greater than 3 m (NSZ 1170.5:2004).

For both limit states, load combinations are defined for the design action effect (i.e. S_s^* or S_u^*) according to Table 1-1 in Section 1.4.2 of this chapter.

1.4.2 *Actions and load combination*

According to AS/NZS 2785:2000, while designing a ceiling for ultimate and/or serviceability limit states, the following actions must be taken into account: Dead load, live load, wind load, earthquake load and air pressure fluctuations. Moreover, a minimum distributed service load (U) of 3 kgf/m^2 [30 N/m^2] must be included in seismic weight in all ceilings.

The design action effect S_u^* in the AS/NZS 2785:2000 Standard is determined from the combinations in Table 1-1. For suspended ceilings that are installed indoors, wind is not a key factor in design. Therefore, the load combinations including the effect of wind load have been excluded.

Table 1-1 – Load combinations for design action effects (AS/NZS 2785:2000)

Load combinations for SLS design	Load combinations for ULS design
$S_s^* \geq G + U$	$S_u^* \geq 1.4G + 1.7U$
$S_s^* \geq G + U + E_s$	$S_u^* \geq 1.2G + 1.2U + E_u$
	$S_u^* \geq 0.9G + E_u$

Where *G* is the nominal seismic mass of the ceiling, *U* is the design distributed or point service load, and E_u is the design earthquake load for ULS including both horizontal and

vertical components.

For design to ULS, the member or component shall be proportioned so that the design action effect (S_u*) is not greater than the design ultimate strength (ΦR_u):

$$S_u^* \leq \Phi R_u \qquad \text{Equation 1-1}$$

The design ultimate strength (ΦR_u) must be determined by either the nominal capacity (R_u) and the capacity (strength) reduction factor (Φ) determined in accordance with the relevant Australian or New Zealand Standard. The values of reduction factors for some components have been shown in Table 1-2.

Table 1-2 - Capacity reduction factor for cold-formed steel members – (Table 1.6 – AS/NZS 4600:2005)

Design Capacity	Capacity reduction factor (Φ)
Members subject to axial tension (φ_t)	0.9
Concentrically loaded compression members (φ_c)	0.85
Blind riveted connections in shear	0.6 - 0.7

1.4.3 *Seismic design & installation requirements*

According to FEMA E-74 (2011) guideline, in order to perform engineering calculations for a non-structural element, an engineer may have to consider the following factors:

- the proximity of the building site to an active fault
- soil conditions at the site (other than stiff soil)
- the flexibility of the building structure
- the location of the item in the building
- the flexibility of the floor framing or walls in the immediate vicinity of the item
- the flexibility and strength of the item and its attachments
- the weight and configuration of the item
- the characteristics of any connection details between the item and the structure
- the expected relative displacement between two connection points in adjacent stories or across a seismic gap
- the function of the item
- the function of the facility

In the same light, the required steps and components in the design and installation of a

suspended ceiling have been collected and presented as a chart in Figure 1-14, followed by subsections that provide detailed recommendations and references for each of the steps in the charts.

1.4.3.1 A) Project specifications

Includes the primary information required for starting the design and installation process.

1.4.3.1.1 *A-a) Seismic zone*

Determines the seismic hazard factor associated with the region the building is located in. This factor which is defined as Z factor in NZS 1170.5:2004 can be determined using Table 3.3 and associated graphs in Clause 3.1.4 of this Standard for all regions of NZ. This factor cannot be taken less than 0.1.

1.4.3.1.2 *A-b) Design working life*

According to NZ Standard NZS 2785:2000, ceiling systems must be designed and installed so that the suspension system and frame will remain structurally sound and without maintenance for a period of 15 years. However, the Standard also requires the ceiling systems that provide structural stability to the building (e.g. acting as diaphragm) to have a design life not less than that of the building.

1.4.3.1.3 *A-c) Site subsoil class*

This information is required in order to determine the spectral shape factor (Section 1.4.3.4.1.3.1). The description of subsoil classes A-E and their methods of evaluation are provided in Clause 3.1.3 of NZS 1170.5:2004.

1.4.3.1.4 *A-d) Building/room application*

The seismic design actions vary depending on the occupancy, the use of the building and the locality of the ceiling. Table 3.1 and Table 3.2 in Section 3.3 of AS/NZS 1170.0:2002 provide the importance levels for different structures. This classification should then be used in combination with Table 8.1 in Clause 8.1.2 of NZS 1170.5:2004 to determine the value of risk factor specific to the ceiling.

1.4.3.1.5 *A-e) Height*

Both total height of the structure and the height of the ceiling supporting floor are required for the design of ceilings. These values are used in Section 1.4.3.4.1.1 (D-a-a) of the chart.

Figure 1-14 - Design and installation chart

1.4.3.1.6 *A-f) Story drift*

The drift value at each story is required for determining the safe gap on the perimeters of ceilings as will be discussed in Section 1.4.3.5.

1.4.3.2 B) Room size

The dimensions of the room where the ceiling is installed are key factors in the choice of the possible ceiling system. According to ASTM E580 (2011), "lateral force bracing is required for all ceiling areas greater than 1000 ft^2 [92.9 m^2]". For all continuous ceiling areas greater than 2500 ft^2 [232 m^2], this Standard requires a seismic separation joint, bulkhead braced to the structure or full height partition. This separation joints should break the ceiling into areas of no more than 2500 ft^2 [232 m^2] and having a ratio of the long to short dimensions less than or equal to 4. Each area must accommodate ±3⁄4 in. [18 mm] axial movement (ASTM E580, 2011).

Based on ceiling manufacturers' guidelines (Armstrong, 2013; USG, 2012) and supported by our experiments on perimeter-fixed ceilings (Dhakal et al., 2016), the applicability of the perimeter-fixed system is limited by either area or length of the ceiling grids. This allowable length is determined by the seismic demand and capacity of the ceiling elements used.

1.4.3.3 C) Seismic mass

According to AS/NZS 2785:2000, seismic mass of the ceiling must include: ceiling tiles and grid system, partitions connected to the underside of the ceiling, supported luminaries, services such as air-conditioning registers and insulation. This Standard also requires a minimum distributed service load of 3 kgf/m^2 [30 N/m^2] to be included in seismic weight in all ceilings.

ASCE 7-10, Chapter 13 applies similar definitions for the weight of ceilings in the expression of seismic force. According to ASCE 7-10, the ceiling weight including all supported components and used in the calculation of seismic force should not be taken as less than 4 psf [19.5 kg/m^2].

1.4.3.4 D) Seismic action

According to NZ Standard for the seismic design of parts (NZS 1170.5:2004), parts are required to withstand i) the horizontal and vertical forces imposed by the part through its inertial response to the earthquake excitation of the buildings, and ii) the secondary stresses induced by deformations imposed on the part by the response of the structural system. NZS

1170.5:2004 defines the horizontal and vertical seismic design action on a ceiling through the following equations:

$$F_{ph} = C_p(T_p) \cdot C_{ph} \cdot R_p \cdot W_p \qquad \text{Equation 1-2}$$

$$F_{pv} = C_{vd} \cdot C_{pv} \cdot R_p \cdot W_p \qquad \text{Equation 1-3}$$

The equation consists of various coefficients and parameters defined in Table 1-3:

Table 1-3 – Seismic action, definitions and references.

Parameter	Definition	Reference
F_{ph}, F_{pv}	Horizontal & vertical seismic design actions	Clause 8.5.1, NZS 1170.5:2004
$C_p(T_p)$	Horizontal design coefficient	Clause 8.2, NZS 1170.5:2004
T_p	Period of the part (i.e. ceiling)	N/A
R_p	Part risk factor	Table 8.1, NZS 1170.5:2004
W_p	Part seismic weight	Clause 3.3.4.2, AS/NZS 2785:2000
C_{ph}, C_{pv}	Part response factor	Clause 8.6, NZS 1170.5:2004
C_{vd}	Vertical design action coefficient	Clause 5.4, NZS 1170.5:200

The components in Table 1-3 are defined in more details below:

1.4.3.4.1 *D-a) Horizontal and vertical design coefficient ($C_p(T_p)$, Cvd)*

These coefficients are determined for the level of structural support of the ceiling from Equations below:

$$C_p(T_p) = C(0) \cdot C_{Hi} \cdot C_i(T_p) \qquad \text{Equation 1-4}$$

$$C_{vd} = C_v(0) = 0.7C(0) \qquad \text{Equation 1-5}$$

The horizontal acceleration coefficient depends on the site hazard coefficient, the height in structure where the ceiling is supported and the spectral shape coefficient for the ceiling designed. Table 1-4 includes these components and the referenced standards where they can be determined.

Table 1-4 – Horizontal acceleration coefficient, definitions and references.

Parameter	Definition	Reference
$C(0)$	Elastic site hazard coefficient for horizontal loading at T=0	Clause 3.1.1, NZS 1170.5:2004
C_{Hi}	Floor height coefficient for level i	Clause 8.3, NZS 1170.5:2004
$C_i(T_p)$	Part spectral shape coefficient	Clause 8.4, NZS 1170.5:2004
$C_v(0)$	Elastic site hazard spectrum for vertical loading at T=0	Clause 3.2 and C3.2, NZS 1170.5:2004

1.4.3.4.1.1 D-a-a) Floor height coefficient (C_{Hi})

This coefficient varies between 1 and 3 (Figure 1-15a). It shows how the floor acceleration is affected by the magnification and frequency filtering of the ground motion along the structure height taking into account the effect of higher modes on floor acceleration. As stated in Table 1-4, this coefficient can be determined using equations provided in Section 8.3 of NZS 1170.5:2004.

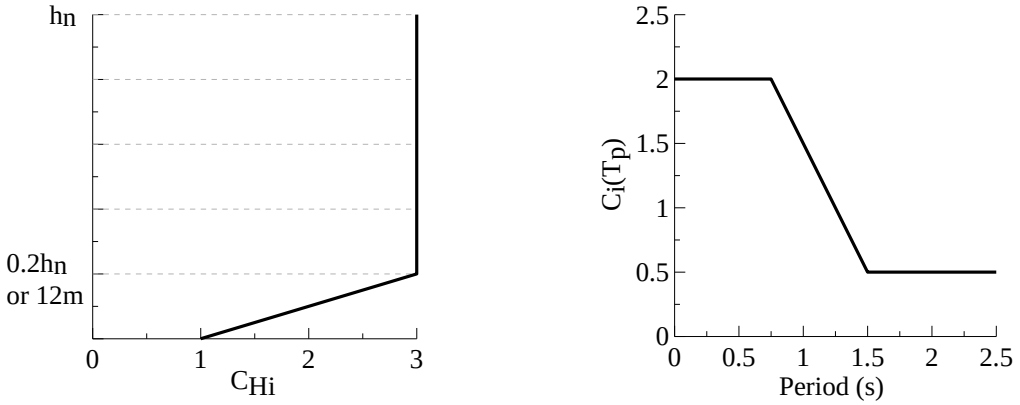

(a) (b)

Figure 1-15 - (a) Height coefficient; and (b) spectral shape coefficient for parts (NZS 1170.5:2004)

1.4.3.4.1.2 D-a-b) Part spectral shape coefficient ($C_i(T_p)$)

This coefficient, as illustrated in Figure 1-15b, is a tri-linear function for the spectral shape coefficient of the part with a given period. Ceilings are assumed to have a period of less than 0.75s. Therefore, the value of this coefficient for ceilings is taken as 2. However, for special ceilings with longer periods, the coefficient of spectral shape can be determined through Equations in NZS 1170.5:2004 or graph shown in Figure 1-15b.

1.4.3.4.1.3 D-a-c) Elastic site hazard coefficient at zero second period (C(0))

This coefficient is a combination of different parameters factoring in the effects of location and hazard probability. It is provided in the form of spectra covering different periods. However, for the design of all parts the coefficient for zero second period is used. The parameters are introduced and referenced in Table 1-5 and described in more details below:

1.4.3.4.1.3.1 D-a-c-a) Spectral shape factor for parts ($C_h(0)$)

This factor is determined for each site subsoil class and can be found in Table 3.1 of

NZS 1170.5:2004. For design of parts including ceilings the value of the spectral shape factor at zero second period is used.

1.4.3.4.1.3.2 D-a-c-b) Seismic zone factor (Z)

Also called hazard factor, is the quantity produced by probabilistic hazard models for all areas in NZ and presented in tables and graphs in NZS 1170.5:2004. The hazard factor multiplied by spectral shape factor ($C_h(T)$) results in the code defined 500-year spectrum for the associated location and site condition excluding near fault effects. Seismic zone factor cannot be taken as less than 0.1.

1.4.3.4.1.3.3 D-a-c-c) Return period factor (R_s, R_u)

This factor is required for scaling the spectra to earthquake return periods other than 500 years. Return period factors for serviceability (R_s) or ultimate (R_u) limit states can be obtained from Table 3.5 of NZS 1170.5:2004. The required annual probability of exceedance provided in this Table can be determined according to Table 3.3 of AS/NZS 1170.0:2002 for the associated design working life, importance level and limit state.

1.4.3.4.1.3.4 D-a-c-d) Near-fault factor (N(T,D))

This factor accounts for the near-fault effects from earthquake ground motions on structures located less than 20 km from a major fault. The factor can be determined using equations provided in Clause 3.1.6 of NZS 1170.5:2004. A list of major faults in NZ can also be found in Table 3.6 of this Section of the Standard.

Table 1-5 – Elastic site hazard coefficient, definitions and references.

Parameter	Definition	Reference
$C_h(0)$	Spectral shape factor for parts at T=0	Clause 3.1.2, NZS 1170.5:2004
Z	Seismic zone factor	Clause 3.1.4, NZS 1170.5:2004
R_s, R_u	Return period factor for SLS (R_s) or ULS (R_u).	Clause 3.1.5, NZS 1170.5:2004
N(T,D)	Near-fault factor	Clause 3.1.6, NZS 1170.5:2004

1.4.3.4.2 *D-b) Part response factor (C_{ph})*

This factor accounts for the effect of the period and ductility of ceilings (or parts in general) and can be obtained from Table 8.2 of NZS 1170.5:2004. This Standard suggests the ductility of parts to be assumed μ_p=1 unless advised otherwise through testing or established engineering methods. Table C8.2 in the commentary of NZS 1170.5:2004 suggests ductility

and deformation limits for common parts in buildings. According to this table, suspended (lay-in tile proprietary) ceilings have a ductility of μ=2. However, some ceiling manufacturers assume a ductility factor of 1 for ceiling grids in their seismic design guideline. Moreover, NZS 1170.5:2004 requires the ductility factor of 1 to be used for the design of parts for serviceability limit state.

1.4.3.4.3 *D-c) Part risk factor (R_p)*

This factor is associated with the classification of parts (i.e. ceilings) based on their importance and the consequences of their failure as well as the limit state used for their design. Table 8.1 of NZS 1170.5:2004 sets out the criteria for determining this factor which varies between 1 and 2.

1.4.3.5 E) Suspended ceiling types

Ceilings with an area smaller than 93 m^2 are exempt from the lateral bracing requirements (ASTM E580, 2011). However, special consideration must be taken of the maximum allowable length of grids (cross tee or main tee) in each direction. American Standard ASTM E580 (2011) and Ceilings and Interior Systems Construction Association (CISCA, 2004) provide different forms of boundary conditions for suspended ceilings depending on the seismic risk and ceiling weight. In areas of light to moderate seismic risk (i.e. Category C), ceilings are only supported by vertical hanger wires and free-sliding seating on perimeter wall angles. No permanent end fixture (e.g. pop rivet) is allowed in this category. In areas with high seismic risk (i.e. Categories D-F), ceilings are either perimeter-fixed on two sides or back-braced with free sliding perimeters (ASTM E580, 2011).

1.4.3.5.1 *E-a) Free-floating*

This category covers areas with light to moderate earthquake potential and is limited to ceiling systems with an average weight of 2.5 lb/ft^2 [120 N/m^2] or less. This average weight includes grid members, tiles, light fixtures, supported flexible sprinkler drops and air terminals (ASTM E580, 2011). The design is intended to provide an unrestrained (free-floating) ceiling system that will accommodate the movement of the structure during a seismic event.

As shown in the Figure 1-16, a minimum of 7/8 in. [22 mm] support ledge must be provided by perimeter angles on all sides of the ceiling. Is case this perimeter support ledge cannot be provided, hanger wires must support the free ends of all cross tees and main tees within 200 mm from any wall or ceiling discontinuity (ASTM E580, 2011). The terminal ends of tees

must have a minimum of 3⁄8 in. [10 mm] clearance from the wall with no permanent fixing to the perimeters. Similar clearance must be provided between ceiling and other rigid penetrating objects such as columns, sprinklers etc. Wire hangers and their connections must carry a minimum of 90 lb [0.4 kN] allowable load.

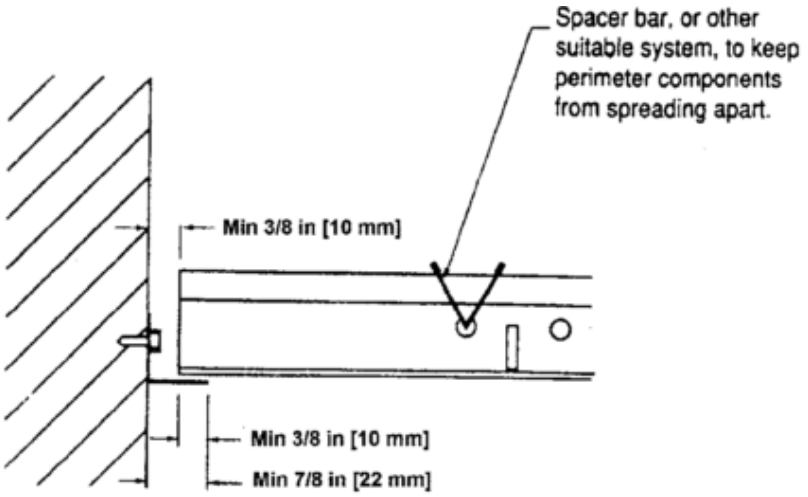

Figure 1-16 - Category C treatment of cross tees, main tees, and wall closures at terminal ends (ASTM E580, 2011)

1.4.3.5.2 *E-b) Perimeter-fixed*

This category covers areas with high earthquake potential and is limited to ceiling systems with a maximum area of 1000 ft^2 [93 m^2]. For the satisfactory seismic performance of this type of ceiling it is important to ensure the width of the wall angles around the perimeters can accommodate ceiling motion and enough clearance is provided around rigid penetrating objects, such as columns and piping. The perimeter wall angle must supply a minimum support ledge of 2 in. [50 mm]. Main tees and cross tees are attached to the perimeter on two adjacent walls. On the two opposite walls, a clearance of 3⁄4 in. [18 mm] must be provided between the main tee and cross tee ends and the walls. At the terminal end of each cross tee and main tee, a vertical hanger wire must be provided at a maximum of 8 in. [200 mm] from each wall or ceiling discontinuity (ASTM E580, 2011). On the fixed end of tees, pop rivets are commonly used as a permanent method of attachment. Seismic clips are also introduced for this purpose by proprietary manufacturers. These clips can be used on both fixed and floating ends. Application of seismic clips on the floating end has the advantage of preventing spreading in the direction perpendicular to the grid.

1.4.3.5.3 *E-c) Back braced*

Suspended ceilings are either perimeter-fixed or back-braced. As mentioned earlier, back-bracing is required for all ceilings with an area greater than 1000 ft^2 [93 m^2] or when the perimeter-fixed option is not acceptable due to large seismic demands. The most basic form of lateral bracing consists of four No. 12-gauge [2.70 mm] wires fixed to the main tee within 2 in. [50 mm] of the cross tee intersection and splayed 90° from each other at an angle not exceeding 45° from the plane of the ceiling. A vertical strut is connected to the main tee and the structure above to resist the vertical component induced by the bracing wires. These lateral force bracing points must be placed 12 ft [3600 mm] on center in both directions with the first point within 6ft [1800 mm] from each wall. They must also be spaced at least 6 in. [150 mm] from all horizontal piping or duct work that is not provided with bracing restraints for horizontal forces. Rigid bracing options that have been designed to limit relative lateral deflections at the point of attachment of the ceiling grid to less than 0.25 in. [6 mm] are a possible alternative for splay wire braces. These usually consist of four struts, channels or angle sections splayed 90° from each other at an angle not exceeding 45° from the plane of the ceiling. For more details on the requirements for vertical struts, splay and vertical hanger wires refer to Sections (G-c), (G-b) and (G-a), respectively.

1.4.3.6 F) Suspension system's capacity

The load bearing capacity of a suspended ceiling depends on the capacity of its components, i.e. fixtures and grid/suspension system. It is quite difficult to obtain the strength of the proprietary suspension systems (i.e. cross tees, main tees and their connections) due to the confidentiality of manufacturer information. Therefore, the only available sources are tests conducted on similar elements. The components of a common suspended ceiling consist of:

i. Grid members: cross tees and main tees
ii. Grid connections: cross tee-main tee intersection joints
iii. Rivets or end clips

The load bearing capacities of each of these components will be discussed in the following sections:

1.4.3.6.1 *F-a) Grid/suspension system: cross tees, main tees and their intersections*

ASTM standard E580 (2011) classifies suspended ceilings into two categories based on the seismicity of the site where the ceiling is located. Design and installation of the ceilings are either done for Category C (light to moderate seismic risk) or Categories D-F (high seismic

risk). For a ceiling in Category C, all main tees, cross tees and their splices, intersection connectors, and expansion devices are required to carry a mean ultimate test load of not less than 60 lb [0.27 kN] in tension and in compression.

According to this standard, for design and installation of Category D-F ceilings, only heavy-duty main tees can be used. The terms intermediate and heavy-duty refer to the capacities of gird members and are defined based on the maximum load on the grid associated with an allowable midspan deflection (ASTM C636, 2013). According to this standard, main tees and cross tees of the Category D-F ceiling systems and their splices, intersection connectors, and expansion devices must be designed and constructed to carry a mean ultimate test load of not less than 180 lb [0.8 kN] in compression and in tension. The connectors at splices and intersections must be the mechanical interlocking type (ASTM E580, 2011).

However, studies by Gilani et al. (2010) and Glasgow et al. (2010) showed that the substitution of intermediate for heavy-duty main tees did not adversely affect the seismic response of the system.

1.4.3.6.2 *F-b) Rivets*

Pop rivets due to their easy and quick application are the more common method of fixture in perimeter-fixed ceilings. These connectors vary in size and capacity and their application in suspended ceilings is only acceptable in shear (AS/NZS 2785:2000). Table 1-6 shows the shear and tensile strengths of rivets commonly used in suspended ceilings in NZ. As per the specifications of AS/NZS 2785:2000, rivets are only acceptable to be used to resist shear forces in ceilings.

Table 1-6 – Shear and tensile strength of aluminium rivets with steel mandrel (IFI-114)

Rivet type	Diameter	Shear strength (kN)	Tensile strength (kN)
aluminium rivet/ aluminium mandrel	2.4 mm or 3/32"	0.30	0.37
	3.2 mm or 1/8"	0.53	0.67
	4 mm or 5/32"	0.85	1.00
aluminium rivet/ steel mandrel	2.4 mm or 3/32"	0.42	0.55
	3.2 mm or 1/8"	0.76	0.98
	4 mm or 5/32"	1.16	1.56

According to NZ manufacturers' specifications, perimeter-fixing rivets must be made of aluminium, and sizes should be either ϕ3.2 or ϕ4 and may be used in single or double layouts depending on the design seismic force (Armstrong, 2013; USG, 2012). Some other

type of end fixture for suspended ceilings is introduced by proprietary manufacturers in the form of end clips (Figure 1-17) which, depending on the installation detail, can be used as sliding or fixed end connection.

These manufacturer guidelines determine the allowable fixing connection load of 0.7 kN for Φ3.2 aluminium rivet, 1 kN for Φ4.0 aluminium rivet and 0.6 kN for BERC2 Clip.

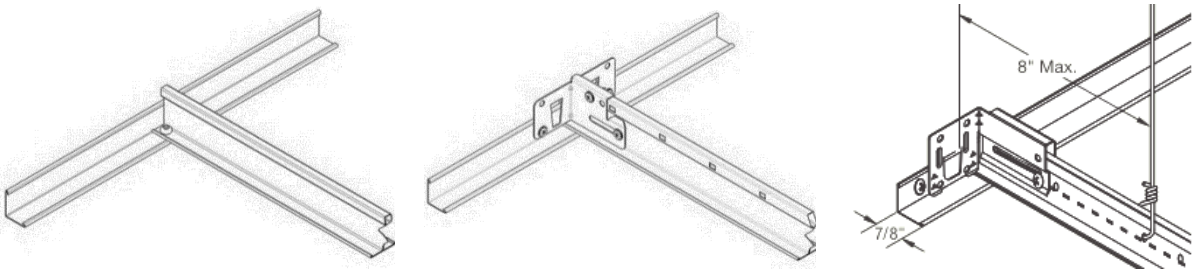

(a) Riveted connection (USG) (b) ACM7 clip (USG) (c) BERC2 clip (Armstrong)

Figure 1-17 – Common end fixtures used in NZ (Armstrong, 2013; USG, 2012)

1.4.3.7 G) Vertical and lateral support details

Suspended ceilings are supported by the structure on perimeter walls and overhead floor slab/joists. In a perimeter-fixed suspended ceiling, the vertical support consists of perimeter wall angle fixtures and vertical hanger wires. In this ceiling type, the perimeter fixtures also provide lateral resistance. A floating or back-braced suspended ceiling on the other hand, is designed to float/slide on perimeter wall angles and the diagonal wires or struts connecting the main tees to the floor above provide rigid or semi-rigid lateral bracing. The following sections summarise the standard requirements for each of these connectors.

1.4.3.7.1 *G-a) Hanger wires*

These vertical wires carry part of the gravity load from the ceiling and anything supported by it (e.g. services, luminaries etc.). According to ASTM C636 (2013) hanger wires are required to be a minimum of No. 12-gage [2.70 mm] galvanized, soft-annealed, mild steel wire. These wires are usually wrapped through or around main tees. As shown in Figure 1-18, the wire loops must be tightly wrapped and sharply bent to prevent any vertical movement or rotation of the member within the loops. The wire must be wrapped around itself a minimum of three full turns (360° each) within a 3-in [75 mm] length (Figure 1-18). These hanger wires are fixed to main tees at 4 ft [1200 mm] intervals. In addition, it is required to provide hanger wires on the terminal end of all cross tees and main tees at a maximum of 8 in. [200 mm] from each wall or ceiling discontinuity for all seismic Categories (ASTM E580, 2011). Extra

hangers may be required where additional loads, such as luminaries are superimposed on the ceiling. This will be discussed in Section 1.4.3.9.

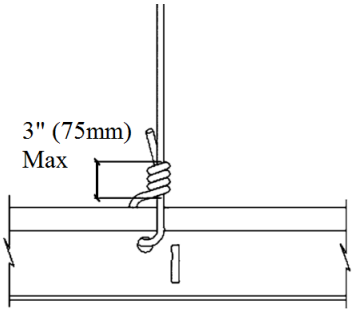

Figure 1-18 – Hanger wire loop detail

According to ASTM E580 (2011), connection devices to the supporting structure must be capable of carrying a minimum of 90 lb [0.4 kN] allowable load. This minimum design load is specified in AS/NZS 2785 to be 0.5 kN for non-trafficable ceiling system (i.e. ceilings where access by personnel on to the ceiling system for any purpose is prohibited).

According to AS/NZS 2785:2000, where the ceiling is likely to be subjected to upward movement, the hangers should be rigid or be of a proprietary or engineered system adequate to resist the upward force. This Standard does not allow bends or kinks in the hangers or struts, as a means of levelling the ceiling or to avoid plenum services. Where hangers or struts cannot be fitted at the specified spacing, secondary members should be installed in accordance with the requirements specified in Design section of the Standard. If hangers have to be fixed diagonally, the horizontal force should be offset by equal and opposite hangers or suitable bracing.

1.4.3.7.2 *G-b) Splay wires:*

According to ASTM E580 (2011), lateral force bracing can be in the form of four splay wires fastened to the main tee as described in Section 1.4.3.5.3. Attachment of the restraint wires both to the structure above and to the main tees must be adequate for the load imposed (ASTM E580, 2011). The connections of bracing wires to the grid and to the structure must support a minimum load of 250 lb [1.11 kN]. Connections of vertical hanger wires and bracing wires to suspension members must be tested in tension and is required to demonstrate a minimum capacity of 100 lb [0.45 kN] for vertical hanger wire; and 200 lb [0.9 kN] or the actual design load, with a safety factor of 2, whichever is greater, for bracing wires (ICC-ES-AC368, 2012).

1.4.3.7.3 *G-c) Vertical struts*

According to AS/NZS 2785:2000, where the ceiling is likely to be subjected to upward movement, it is required to provide rigid hangers or a proprietary or engineered system adequate to resist the upward force. The common practice is to fix a vertical strut to main tees at 3600 mm spacing to resist the vertical component induced by the bracing wires (AS/NZS 2785:2000; ASTM E580, 2011). These vertical struts are fastened to the main tees at the location of the lateral bracing elements.

Struts or hangers must be installed without bends or kinks as a means of levelling the ceiling or to avoid plenum services. If for any reason hangers or struts cannot be fitted at the specified spacing, secondary members need to be installed. All the fasteners between struts and ceilings or supporting structure need to be capable of carrying the minimum design loads for the ceiling. The fixings are required to be of a corrosion-resistant material.

1.4.3.8 H) Splices

Main tees are produced in the standard length of 3600 mm. In practice however, the length of the direction main tees support may be greater than this value in which case main tee splices are used. These splices are formed of proprietary manufactured self-locking clips fastened to both ends of each tee (Figure 1-19a) or can be added to the two cut ends of main tees (Figure 1-19b). The self-locking clips are designed with an interlocking mechanism and no external/additional mechanical fasteners are used at the location of splices. According to the manufacturer's guideline, main Tee integral splices must be offset from each other across the ceiling (USG, 2011). AS/NZS 2785:2000 also recommends placing splice joints in a staggered layout. Where this cannot be achieved, aligned splices must be mechanically fastened (e.g. with a pop-rivet) (USG, 2011). According to a manufacturer's guideline, vertical hangers are required 150 mm from the main tee splices or 200 mm from the main tee-cross tee joints (USG, 2011).

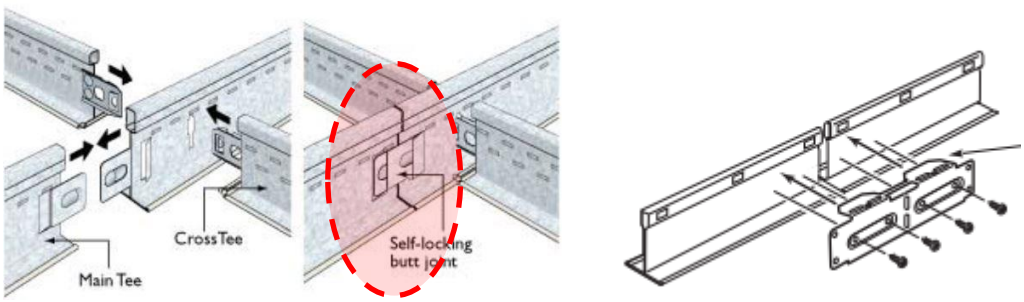

(a) Self-locking splice clips (Rondo, 2008) (b) Splice clip (USG, 2011)

Figure 1-19 – Examples of proprietary main tee splice connections

The splices of main tees must be designed to carry a mean ultimate load equal to that of main tees in tension and compression (i.e. 60 lb [0.27 kN] in areas of low to moderate seismic risk and 180 lb [0.8 kN] in areas of high seismicity, according to ASTM E580 (2011).

1.4.3.9 I) Services

According to AS/NZS 2785:2000 all ceiling hangers and their fixing should be designed for a minimum design action effect of 0.5 kN (50 kgf) for non-trafficable ceiling systems.

According to ASTM E580 (2011), all lighting fixtures must be positively attached to the suspended ceiling system by mechanical means unless independently supported. The fixture must not exceed the design carrying capacity of the supporting members. Details of attachment requirements for areas of low to moderate seismicity (Category C) and high seismicity (Category D, E & F) are summarised in Table 1-8 and Table 1-9, respectively.

According to NZ Standard for the Seismic Performance of Engineering Systems in Buildings (NZS 4219:2009), the clearances listed in Table 1-7 must be maintained between structural and non-structural elements. According to this Standard, ceiling hangers and braces are considered restrained components. Use of flexible connections within the service may allow for smaller penetration clearances.

Except where rigid bracing is used or substantiating design calculations have shown that lateral deflections are limited to less than 0.25 in. [6 mm], sprinkler heads and other penetrations must have a 2-in. [50 mm] oversize ring, sleeve or adapter through the ceiling tile to allow for free movement of at least 1 in. [25 mm] in all horizontal directions. Alternatively, a flexible sprinkler hose fitting that can accommodate 1 in. [25 mm] of ceiling movement shall be permitted to be used without the oversized ring, sleeve or adapter (ASTM E580, 2011).

Table 1-7 – Clearances (NZS 4219:2009)

Restraint condition of components	Min clearance (mm)	
	Horizontal	Vertical
Unrestrained to unrestrained	250	50
Unrestrained to restrained	150	50
Restrained to restrained	50	50
Penetration through structure	50	50

Table 1-8 - Requirements for services and attachments in areas of low to moderate seismicity as per ASTM E580 (2011)

Type of services or fixtures	Requirement
Lighting fixtures	• Positive attachment to ceiling system • Attachment must carry 100 % of the fixture weight in any direction • Min 2 attachment devices
Surface-mounted lighting fixtures	• Positive attachment to the ceiling system • Clamping device surrounding the supporting member • Safety wires between the clamping device and the adjacent ceiling hanger or to the structure above
Lighting fixtures weighing ≤ 10 lb [5 kg]	• One no. 12-gauge [2.70 mm] safety wire from the fixture housing to the structure above • Safety wires not necessary to be taut
10 lbs [5kg] > lighting fixtures weighing ≤ 56 lb [25 kg]	Two no. 12-gauge [2.70 mm] safety wires from the fixture housing to the structure above
Lighting fixtures weighing > 56 lb [25 kg]	Supported directly from the structure above by approved hangers
Pendant-hung lighting fixtures	Supported directly from the structure above using a minimum no. 9-gauge [3.80 mm] wire or an approved alternate support
Flexible sprinkler hose fittings, ceiling mounted air terminals or other services weighing ≤ 20 lb [9 kg]	Positive attachment to main tees or cross tees that of same carrying capacity
20 lb [9 kg] > flexible sprinkler hose fittings, air terminals or other services weighing ≤ 56 lb [25 kg]	(in addition to the requirements above) two no. 12-gauge [2.70 mm] hanger wires connected from the terminal or service to the ceiling system hangers or to the structure above
Flexible sprinkler hose fittings, air terminals or other services weighing > 56 lb [25 kg]	Supported directly from the structure above by approved hangers
Walls or partitions	The ceiling system must not provide lateral support. They can only be attached to the ceiling suspension provided they allow the ceiling mem- brane to move laterally to accommodate the required clearance

Table 1-9 - Requirements for services and attachments in areas of high seismicity as per ASTM E580 (2011)

Type of services or fixtures	Requirement
Lighting fixtures	• Positive attachment to ceiling system • Attachment must carry 100 % of the fixture weight in any direction • Min 2 attachment devices • When the load carrying capability of cross tees supporting light fixtures is less than 16 lbs/ft (241.7 N/m), supplemental hanger wires are required
Surface-mounted lighting fixtures	• Positive attachment to the ceiling system • Clamping device surrounding the supporting member • Safety wires between the clamping device and the adjacent ceiling hanger or to the structure above
Lighting fixtures weighing ≤ 10 lb [5 kg]	• One no. 12-gauge [2.70 mm] safety wire from the fixture housing to the structure above • Safety wires not necessary to be taut
10 lbs [5kg] > lighting fixtures weighing ≤ 56 lb [25 kg]	Two no. 12-gauge [2.70 mm] safety wires from the fixture housing to the structure above
Lighting fixtures weighing > 56 lb [25 kg]	Supported directly from the structure above by approved hangers
Pendant-hung lighting fixtures	Supported directly from the structure above using a minimum no. 9-gauge [3.80 mm] wire or an approved alternate support
Flexible sprinkler hose fittings, ceiling mounted air terminals or other services weighing ≤ 20 lb [9 kg]	Positive attachment to main tees or cross tees that of same carrying capacity
20 lb [9 kg] > flexible sprinkler hose fittings, air terminals or other services weighing ≤ 56 lb [25 kg]	(in addition to the requirements above) Two no. 12-gauge [2.70 mm] hanger wires connected from the terminal or service to the ceiling system hangers or to the structure above
Flexible sprinkler hose fittings, air terminals or other services weighing > 56 lb [25 kg]	Supported directly from the structure above by approved hangers
Walls or partitions	Partitions that are tied to the ceiling and all partitions greater than 6 ft [1.8 m] in height must be laterally braced to the building structure. Bracing must be independent of any ceiling splay bracing and be spaced to limit horizontal deflection at the partition head to be compatible with ceiling deflection requirements as determined for suspended ceilings.

1.5 Proprietary systems: USG Generic Seismic Design

Suspended ceilings installed in New Zealand are mainly produced by two manufacturers; USG Boral (2012) and Armstrong (2013). These manufacturers provide their design guidelines, in which their main assumptions, design criteria and installation requirements are determined along with the details of the systems they offer.

1.5.1 *Assumption & Limitations*

According to this guideline, earthquake forces need to be considered for all suspended ceilings in New Zealand and Australia, to comply with AS/NZS 2785:2000. Lateral bracing (restraint) options include perimeter fixing and back bracing which comply with NZS1170.5:2004 and AS/NZS2785:2000. It is the installer's job to make sure the installed ceilings do not exceed the limits defined by the guideline. For all ceilings falling outside the scope of the guideline's limitations and assumptions, the design must be undertaken by a qualified engineer with experience in ceiling design.

According to USG seismic design guide (USG, 2012), ceilings in areas with low seismic risk are designed to withstand serviceability level earthquake only (25-year return period), without incurring significant damage to ceiling components or allowing tiles to fall out. If a ceiling grid is rigidly perimeter fixed to the supporting structure at both ends, there is the possibility that the ceiling will be damaged by differential movement of the building. To avoid this, this guideline recommends a 10-15mm gap to be provided between one end of each ceiling grid and the adjacent building structure (USG, 2012). A similar isolation gap is also required around rigid objects that penetrate through the ceiling (e.g. central columns). USG has introduced the ACM7 Seismic Clip as an alternative option for creating this seismic isolation gap, while increasing the strength of the ceiling.

Ceilings must be installed in accordance with the documents and brochures required by the USG guideline (USG, 2012). Building must be no more than 40 meters tall and must not be of Importance Level 4 having special requirements for "post disaster" functionality (e.g. hospitals, police stations etc.). Maximum grid spacing must be 1200 mm in any direction. Ceiling must be non-structural and non-trafficable (does not provide structural stability to the building). The ceiling ductility is assumed to be $\mu=1.0$ (for serviceability level earthquake).

For the seismic design, ceiling weight must include ceiling tiles, suspension grid, lighting, any other services, and insulation if laid on the grid. Individual ceiling tiles must not weigh more than 10 kg. All items weighing more than 10 kg must be supported independently from

the ceiling. All lay-in ceiling panels must be installed and fixed with correct hold-down clips in full conformance with USG specifications. Perimeter fixing rivets must be aluminium and no substitution is permitted.

All interior partition walls must be supported independently from the ceiling (including independent horizontal restraint to top of wall), or their weight must be included in the ceiling seismic mass calculations, including specific consideration of the seismic load on each individual ceiling grid. Also, all evacuation and life safety systems must be supported independently from the ceiling and must be likely to remain functional even if the ceiling collapses.

AS/NZS2785:2000 has been interpreted in light of the more detailed guidance in NZS1170.5:2004, Section 8 "Requirements for Parts and Components". It is assumed that non-structural, non-trafficable suspended ceilings that satisfy the definition of a Category P.7 part in NZS1170.5:2004, are only required to satisfy Serviceability Limit State criteria. For design of ceilings for Ultimate Limit State loads, further detailed technical and engineering assumptions and guidance on specific engineering design has been provided by the generic design guide (USG, 2012).

1.5.2 *Panel Range Provided*

USG offers a wide variety of lay-in panels. Panels vary in material, durability and performance, acoustical qualities, fire-resistance, color, size and weight. For the purpose of this study a thorough study was conducted on the size and weight variation of the panels. Choices were narrowed down to the 600 mm by 1200 mm tiles which are most commonly used in residential and commercial buildings. According to the product catalogue presented in 2013, the maximum and average weights for USG panels were identified as 9.76 kg/m^2 and 5.5 kg/m^2, respectively.

1.5.3 *Seismic design method*

According to the table provided in the USG guideline, New Zealand is divided into 6 seismic zones one of which requires specific engineering design. To all other zones a Z value is assigned. The seismic zone factor for Christchurch area following the amendments provided by Department of Building and Housing (2011) is 0.3.

Height factor is not provided independently. Instead Table 1-10 gives a factor which is derived by defining the relevant zone & height. According to Table 1-10, for Christchurch and buildings above 9 m the factor is 4.6.

Table 1-10– Combined zone and height factor according to (USG, 2012)

Height[5] (metres)	ZONE FACTOR				
	1a	1	2	2a	3
0-3	0.8	1.2	1.8	2.3	2.7
3.1-6	1.0	1.6	2.4	3.1	3.6
6.1-9	1.3	2.0	2.9	3.9	5.0
9.1-12	1.5	2.4	3.5	4.6	6.0
12.1-20	1.5	2.4	3.5	4.6	7.3
20.1-40	1.5	2.4	3.5	4.6	8.5[6]

Seismic Force is calculated through the multiplication of:

F_p = Ceiling Weight (kg/m^2) × Combined Height & Zone factor × Teg Tab factor × Tee spacing (m)

Teg tab factor is only applied for perimeter fixing and when the teg tab is used. Teg tabs are proprietry plastic pieces used for levelling the grids in areas where there is elevation difference. These tabs are riveted to the grid.

There are 2 perimeter fixing options: Fixed on two adjacent sides only and fixed on all 4 sides. This installation configuration does not allow for any seismic gaps and must be used only with approval of the building structural engineer. Alternatively, the four-sided fixture can be used with seismic separation joins in rooms with large areas exceeding the allowable tee length.

To establish the correct grid and perimeter fixing to use, USG (2012) provides 3 sets of graphs shown in Figure 1-20 to Figure 1-22. For each component to be designed, graphs provide a number of possible options of grid or fixing types. The intersection point of the seismic force value and the actual length of the grid in the building, defines the option possible for a certain ceiling.

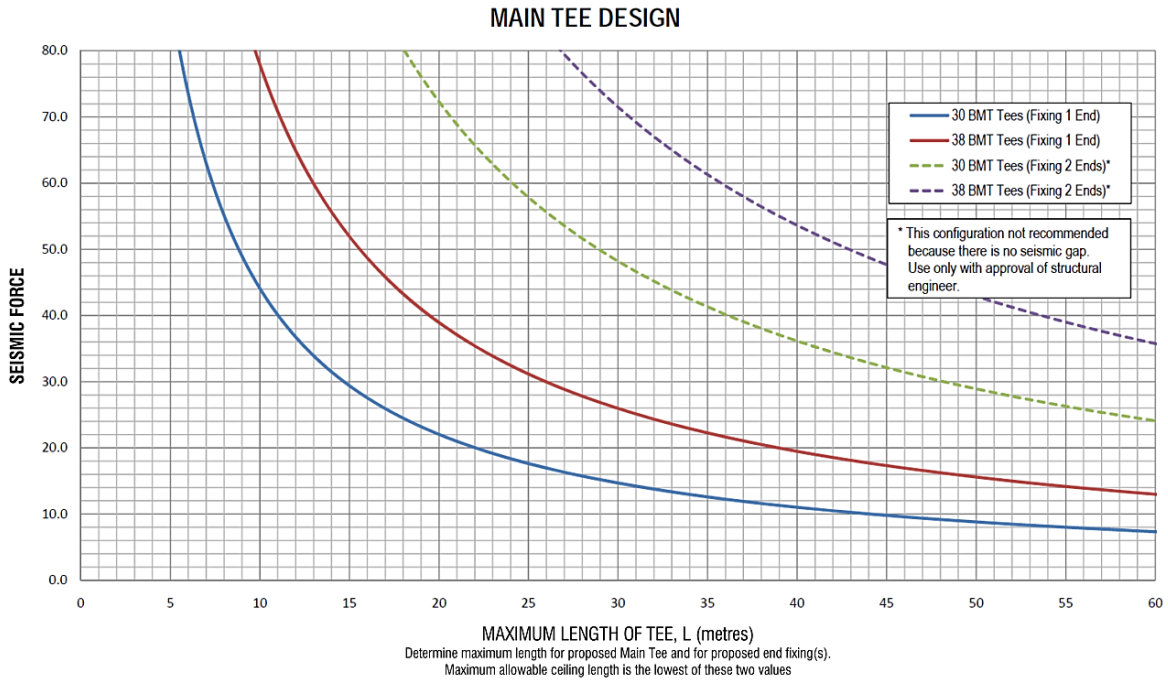

Figure 1-20 – Main Tee Design graphs (USG, 2012)

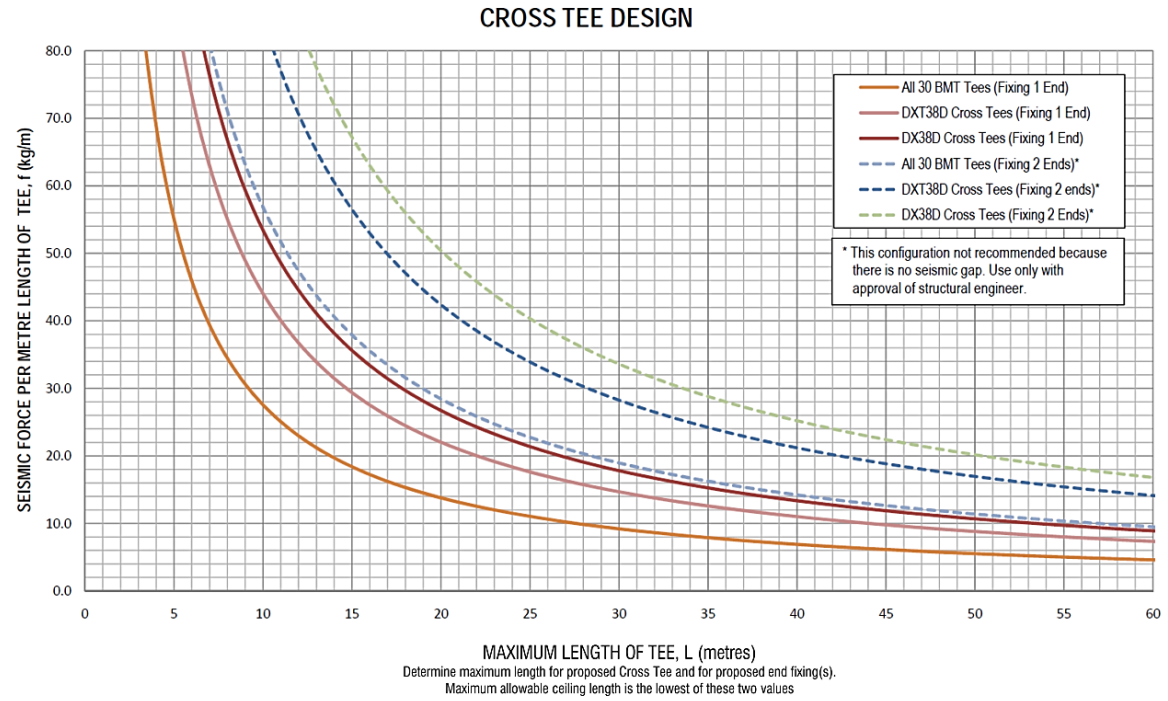

Figure 1-21 - Cross Tee Design graphs (USG, 2012)

As it can be observed in Figure 1-22, USG offers 6 options for end fixing. Four of these options are rivets of 2 sizes in single and double configurations. The next two fixing types are the ACM7 Seismic Clips introduced by USG to be used as fixed or free end connections.

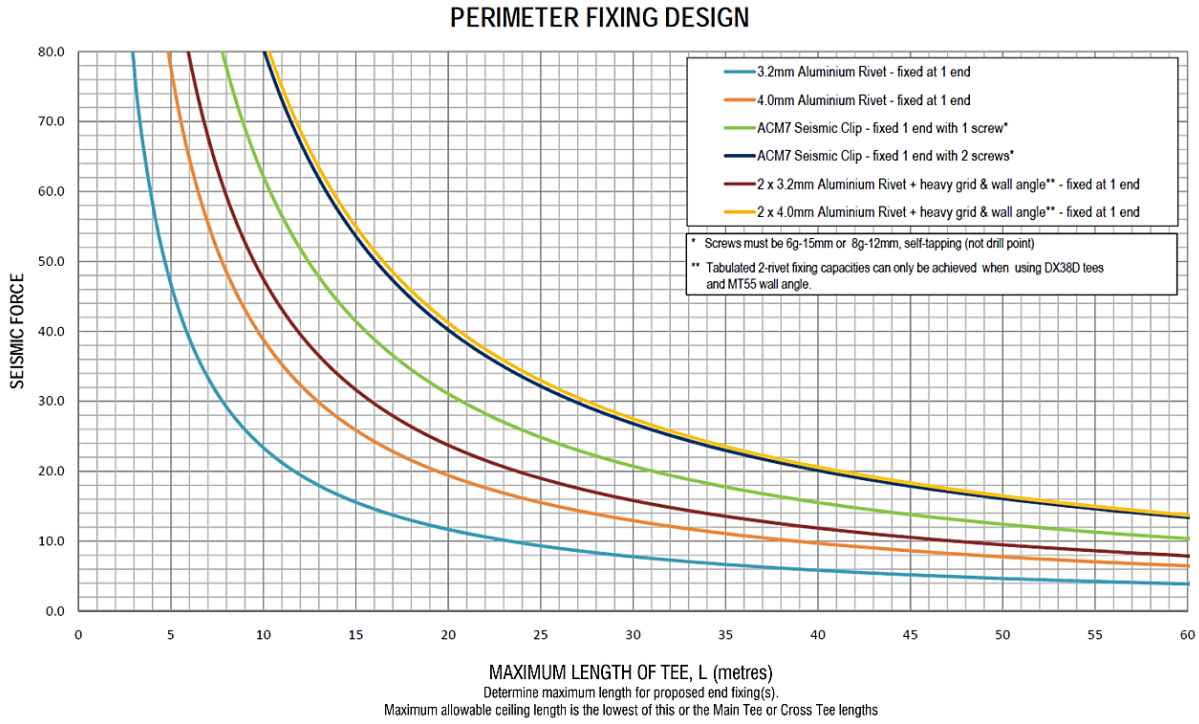

Figure 1-22 – End Fixing Design graphs (USG, 2012)

The USG ACM7 Seismic Clip, shown in Figure 1-17b, is designed and engineered to provide a more robust perimeter restraint. According to the manufacturer's guideline, use of ACM7 clips at both ends (fixed at one, floating at the other) can increase the strength and allowable length of a ceiling tee by more than 3 times, compared to single end fixing using a ϕ3.2 aluminium rivet. However, this conclusion seems to conflict with the hierarchy of strength. The use of end fixture clips may result in a more robust perimeter connection on grid ends and affect the force transfer by increasing their rigidity. However, it does not alter the strength of the whole system. The capacity of the ceiling system is governed by its weakest component. After strengthening the end fixtures, the weakest component of the ceiling may be the cross tee - main tee joints which according to the findings in Chapter 2 of this thesis, have a load bearing capacity close to that of a riveted end fixture. Moreover, the application of these end fixtures needs to be recommended with special considerations for the required gaps on the sliding ends of the ceiling grids, as most of these proprietary clips have a displacement limit (e.g. ± 10 mm).

1.6 Proprietary systems: Armstrong Seismic Design

1.6.1 *Assumptions and limitations*

Armstrong design guideline meets the requirements of NZS 1170.5:2004. According to this

manufacturer's guideline, all individual objects weighing over 10 kg need independent bracing unless specifically designed by a structural engineer. Similarly, ceiling tiles must weigh less than 10 kg each unless a structural engineer is consulted (Armstrong, 2013).

There are three different options for bracing the ceiling against lateral loading. Options 1 (Perimeter fixing on adjacent edges) and 2 (Perimeter fixing on more than two edges and separated by seismic joints) involve bracing the ceiling to the perimeter. In these configurations, lateral loads are transferred from the ceiling to the structure through perimeter fixings.

Option 3 involves bracing back to the structure above with compression struts and tension wire braces or diagonal tension/compression struts. A seismic sliding/floating joint around the entire perimeter is required as the ceiling cannot be braced to both the structure above and the perimeter.

Figure 1-5 in Section 1.1 shows typical seismic bracing details for a wall-to-wall ceiling.

Plenum depths greater than 1.4 m may need a perimeter gap of greater than 19 mm provided by the BERC2 clip discussed in Section 1.6.3. Consultation with buildings structural engineer is needed to determine the gap required and the required edge distances must be followed when fixing rivets, screws etc.

For ceilings with a plenum of less than 300 mm back bracing cannot be used without consulting a qualified structural engineer. Ceilings should not be attached to two opposite walls unless there is a seismic gap between them. Design and installation of ceilings braced/fixed both on perimeters and the roof/structure above is also prohibited by this guideline, due to differential movement (Armstrong, 2013).

The period of the ceiling is assumed to be $T \leq 0.75$ s and the assumed ceiling grid ductility is $\mu=1$.

1.6.2 *Panel Range Provided*

Similar to the manufacturer mentioned in Section 1.5, Armstrong provides a wide range of options for lay-in panels. According to the product catalogue presented in 2013 the maximum and average weights for Armstrong panels were identified as 7.42 kg/m^2 and 5.5 kg/m^2, respectively.

1.6.3 *Armstrong Seismic RX Suspension System*

BERC and BERC2 clips introduced in Seismic RX Suspension System can be used both in the free end and fixed ends as an alternative for rivets. According to the manufacturer's

guideline (Armstrong, 2013), using these clips allows for a minimum 7/8" [22 mm] wall support instead of the 2" [50 mm] IBC Installation requirement providing a more sleek architecturally desired finish. The need for end ties (stabilizer bars) in main and cross tees at free ends is also eliminated. Figure 1-23 shows the possible details on fixed and unattached ends.

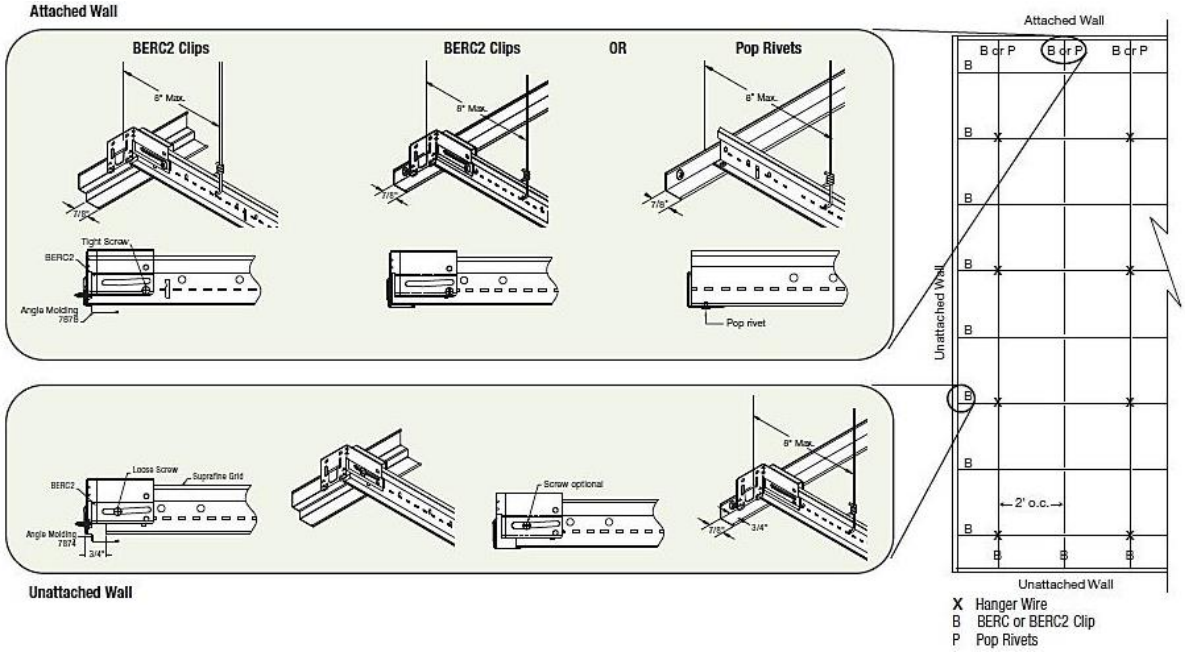

Figure 1-23 – Details of end fixing types in Armstrong Seismic RX (Armstrong, 2013)

ASCE7-10 (1994) Section 13.5.6.2.2, mandates application of seismic separation joints, closure angles and horizontal restraints for ceiling with areas greater than 2,500 ft^2 [232 m^2]. Armstrong provides Seismic Joint Clip for main tees (SJMR) and Seismic Joint Clip for cross tees (SJCG & SCJSI) supported by full-scale testing results (Figure 1-24).

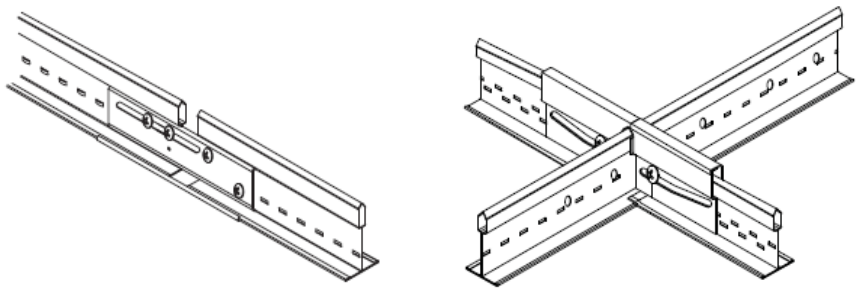

(a) (b)

Figure 1-24 – Seismic Joint Clip for (a) main tees (SJMR), and (b) cross tees (SJCG & SCJSI) (Armstrong, 2013)

1.6.4 *Seismic design method*

All elements that are supported by the ceiling grid -including the grid- must be included in the seismic weight. Note that no individual element may weigh more than 10 kg. The total service load must be taken as at least 3 kg/m² [30 N/m²].

The Armstrong design guideline provides tables for the seismic zone factor in New Zealand. For instance, Christchurch is located in zone 4 with a Z value of 0.396.

Ceiling height factor has been considered by this guideline with values between 1 and 2 depending on the supporting structure's height (Table 1-11). For ceilings supported at levels higher than 9 m, the height factor is taken as 2.

Table 1-11 – Height factors recommended by the guideline (Armstrong 2013)

Ceiling Support Height	Ceiling Height Factor, H
0 - 3m	1.0
3 - 6m	1.33
6 - 9m	1.66
> 9m	2.0

The guideline also provides values for considerations of slopes in ceilings, varying in the range of 1 to 1.305. For a ceiling with zero degree slope this factor is equal to 1.

Seismic force (F_p) is then calculated trough the multiplication of above factors:

$$F_p\ (kg/m^2) = \text{Seismic Zone (Z)} \times \text{Height Factor (H)} \times \text{Ceiling Slope Factor} \times \text{Ceiling Weight } (W_t)\ (kg/m^2)$$

The applicability of bracing options 1 & 2 is checked through the calculation of the maximum force in the main and cross tees. These grid forces then must be less than the grid capacity F_g (i.e. $F_t \leq F_g$), which the guideline defines as 100 kg for main tees and 60 kg for cross tees (Armstrong, 2013). This force also must not exceed the allowable fixing connection load F_c which is 70 kg for Φ3.2 Alum Rivet, 100 kg for Φ4.0 Alum Rivet and 60 kg for BERC2 Clip.

$$\text{Total Force } (F_t)\ (kg) = \text{Seismic Force } (F_p)\ (kg/m^2) \times \text{Tee Spacing (m)} \times \text{Tee Length (m)}$$

The minimum allowable force from chosen grid connection type and grid type is used to control the allowable grid length. The length used in the design of the ceiling must not exceed

this length.

Maximum Allowable Length (m) = Allowable Force (Grids and Connections) (kg) ÷ Grid Spacing (m) ÷ Seismic Force (F_p) (kg/m^2)

In bracing layout option 3 (Back Bracing), any Armstrong grid may be used as in this layout the back-bracing strengths govern the design. After choosing a brace type & knowing the plenum height, the maximum ceiling area per brace is calculated. At least every second main tee should be braced to avoid the ceiling having to perform as a diaphragm.

1.7 Design examples

In the following sections, suspended ceilings are designed based on the proprietary guidelines summarised in Sections 1.5 and 1.6 as well as NZ Standards.

The ceilings are designed to be installed on the 4th floor of a 6-storey office building in Christchurch. The tiles chosen have an average mass of 5.5 kg/m^2.

1.7.1 *Design based on NZ Standard*

Based on the requirements of NZS 1170.5:2004, ceilings in this example are classified in two categories: i) P.7 which are ceilings in areas of ordinary activity, such as offices, and ii) P.4: ceiling in corridors and exit routs, which are required to be operational for evacuation after an earthquake. The first category is designed for SLS1 and the second category is designed for ULS.

Table 1-12 lists the parameters required for determining the seismic design actions for both limit states. This design example follows the procedure shown in Figure 1-25.

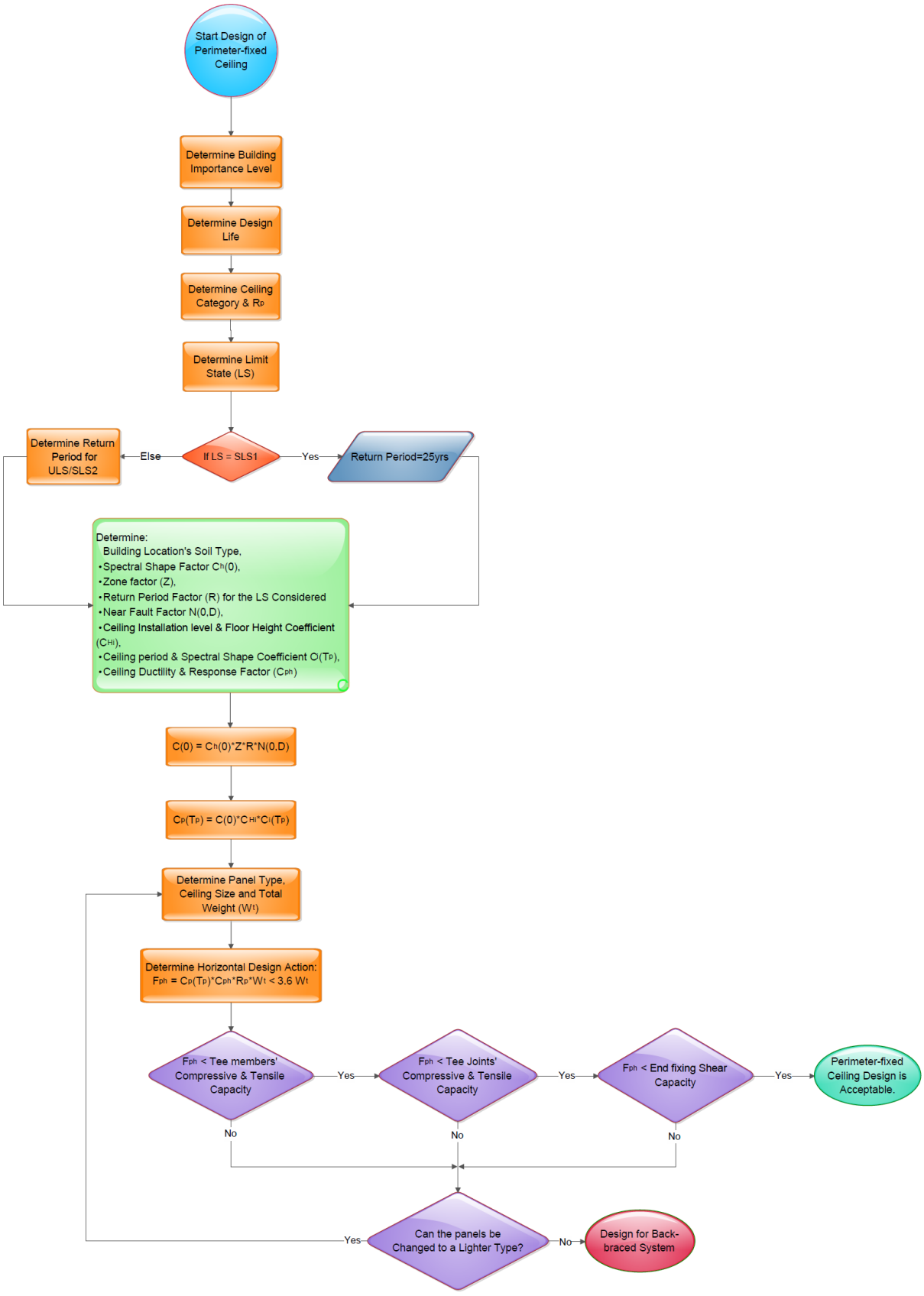

Figure 1-25 – Design procedure for a perimeter-fixed ceiling

Table 1-12 – Design parameters based on NZS 1170.5:2004

Seismic weight for SLS design (including tile, grid system and 3 kg/m^2 service load)	$W_p = (5.5+1+3)\times 9.81 = 93.2$ *N/m^2 = 9.5 kg/m^2*
Ceiling category in office rooms	*P.7*
Design limit state for office rooms	*SLS1*
Ceiling category in egress areas	*P.4*
Design limit state for egress areas	*ULS*
Return period factor for SLS design	$R_s = 0.25$
Return period factor for ULS design, 1/500 year event	$R_u = 1$
Ceiling risk factor	$R_p = 1$
Design working life of building	*50 years*
Soil class	*C*
Spectral shape factor (T=0s)	$C_h(0) = 1.33$
Seismic zone factor	$Z = 0.3$
Near fault factor	$N(T,D) = 1$
Elastic site hazard coefficient for horizontal loading at T=0, SLS	$C_{SLS}(0) = \cdot C_h(0) \cdot Z \cdot R_s \cdot N(T,D) = 0.1$
Elastic site hazard coefficient for horizontal loading at T=0, ULS	$C_{ULS}(0) = \cdot C_h(0) \cdot Z \cdot R_u \cdot N(T,D) = 0.4$
Floor height coefficient for level 4	$h_i = 12$, $h_n = 18$ $C_{Hi} = 1 + \frac{h_i}{6} = 1 + \frac{12}{6} = 3$
Part spectral shape coefficient	$T_p < 0.75$ *s* $C_i(T_p) = 2$
Horizontal design coefficient (SLS)	$C_p(T_p) = C_{SLS}(0) \cdot C_{Hi} \cdot C_i(T_p) = 0.6$
Horizontal design coefficient (ULS)	$C_p(T_p) = C_{ULS}(0) \cdot C_{Hi} \cdot C_i(T_p) = 2.4$
Ceiling ductility factor	$\mu = 1$
Ceiling response factor	$C_{ph} = 1$
Horizontal SLS design earthquake actions	$F_{ph} = C_p(T_p) \cdot C_{ph} \cdot R_p \cdot W_p$ $F_{ph} = 0.6 \times 93.2 = 56 N/m^2 = 5.7 kg/m^2$
Horizontal ULS design earthquake actions	$F_{ph} = C_p(T_p) \cdot C_{ph} \cdot R_p \cdot W_p$ $F_{ph} = 2.4 \times 93.2 = 223.7 N/m^2 = 22.8 kg/m^2$

The seismic design actions on each grid line (main tee or cross tee) is determined in Table 1-13. These values along with the load bearing capacities of the cross tee (CT), main tee (MT), their joints and rivets determine the allowable lengths or dimensions of the ceiling. As mentioned in Section 1.4.2, Table 1-2, appropriate capacity reduction factors need to be

considered when comparing the demand and capacity on the elements.

Table 1-13 – Horizontal seismic force on CTs and MTs

	CT (600 mm spacing)	MT (1200 mm spacing)
Horizontal SLS design earthquake actions	*56 × 0.6 = 33.6 N/m = 3.4 kg/m*	*56 × 1.2 = 67.2 N/m = 6.8 kg/m*
Horizontal ULS design earthquake actions	*223.7 × 0.6 = 134 N/m = 13.7 kg/m*	*223.7 × 1.2 = 268.4 N/m = 27.4 kg/m*

1.7.2 ***Design based on USG Guideline***

Based on the requirements of NZS 1170.5:2004, ceilings in this example are classified in two categories: i) P.7 which are ceilings in areas of ordinary activity, such as offices, and ii) P.4: ceiling in corridors and exit routs, which are required to be operational for evacuation after an earthquake. The first category is designed for SLS1 and the second category is designed for ULS.

1.7.2.1 Design of ceilings for serviceability:

The seismic forces on cross tees and main tees are calculated using the USG design guideline in Table 1-14 (USG, 2012). The values obtained are then plotted over the graphs shown in Figure 1-26 to Figure 1-28 to determine the maximum allowed length of cross tees and main tees based on the end fixture used. Note that in the option with two ends fixed, the ceiling requires separation joints. According to the guideline (USG, 2012), the values of seismic force obtained from this table are in non-standard units and need to be multiplied by a factor of 1.33×0.13 = 0.1729 to be compared with seismic forces in kg/m.

Table 1-14 – Seismic design parameters based on USG (2012)

Seismic weight for SLS design (including tile, grid system and 3 kg/m^2 service load)	$W_p = 5.5 + 1 + 3 = 9.5$ *kg/m^2*
Seismic zone 2a	*Z = 0.3*
Height and zone factor	*4.6*
Teg tab factor	*1*
CT spacing (m)	*0.6*
MT spacing (m)	*1.2*
Seismic force	*F = 9.5 × 4.6 = 43.7 (or 7.5 kg/m^2)*
Seismic force on CT	*F = 9.5 × 4.6 × 1 × 0.6 = 26.2*
Seismic force on MT	*F = 9.5 × 4.6 × 1 × 1.2 = 52.4*

The allowable lengths for the CTs and MTs are the lesser of the two from the grid plots and

fixture plots. For example, if single 3.2 mm rivets are chosen as the fixture type, the lengths of MTs and CTs are limited to 4.5 m and 9 m, respectively. This is while the grid plots allowed for a maximum of 8.5 m for MTs and 10.5 m for CTs in the worst case (weakest grid type).

In case the areas of the ceilings exceed these dimensions, the areas are divided by seismic separation joints. Alternatively, back bracing is installed on every other MTs at maximum 3.6 m intervals.

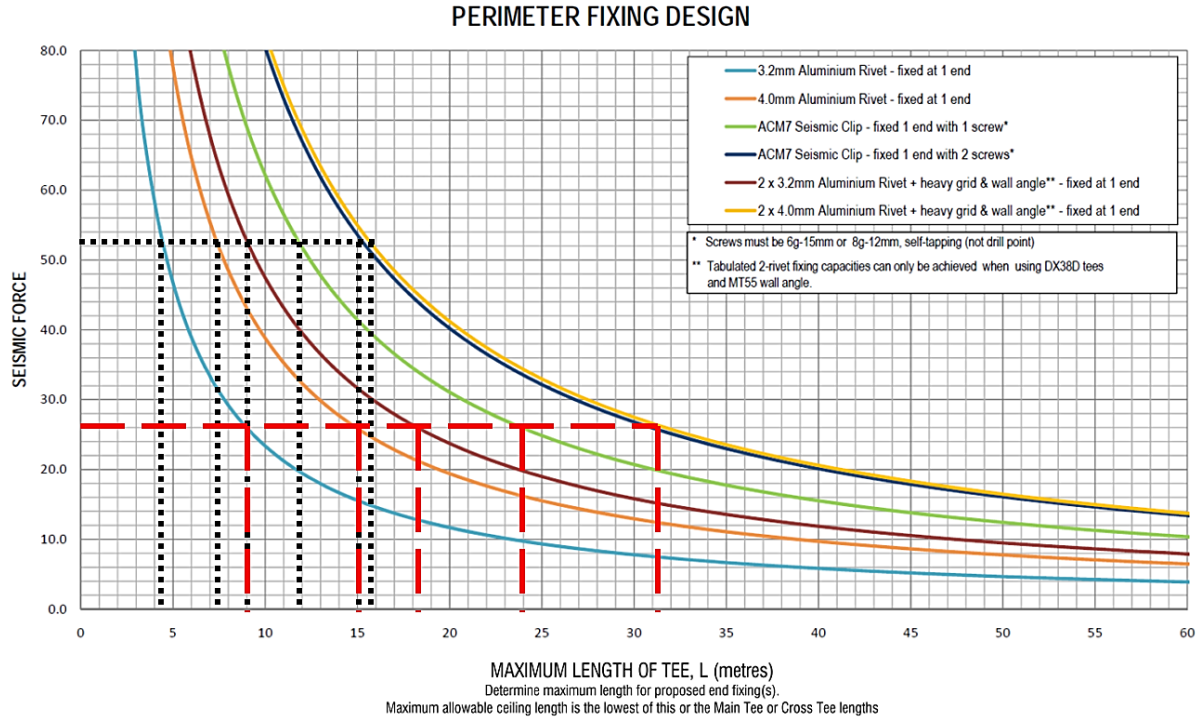

Figure 1-26 – The allowable length of CTs and MTs based on end fixture (USG, 2012)

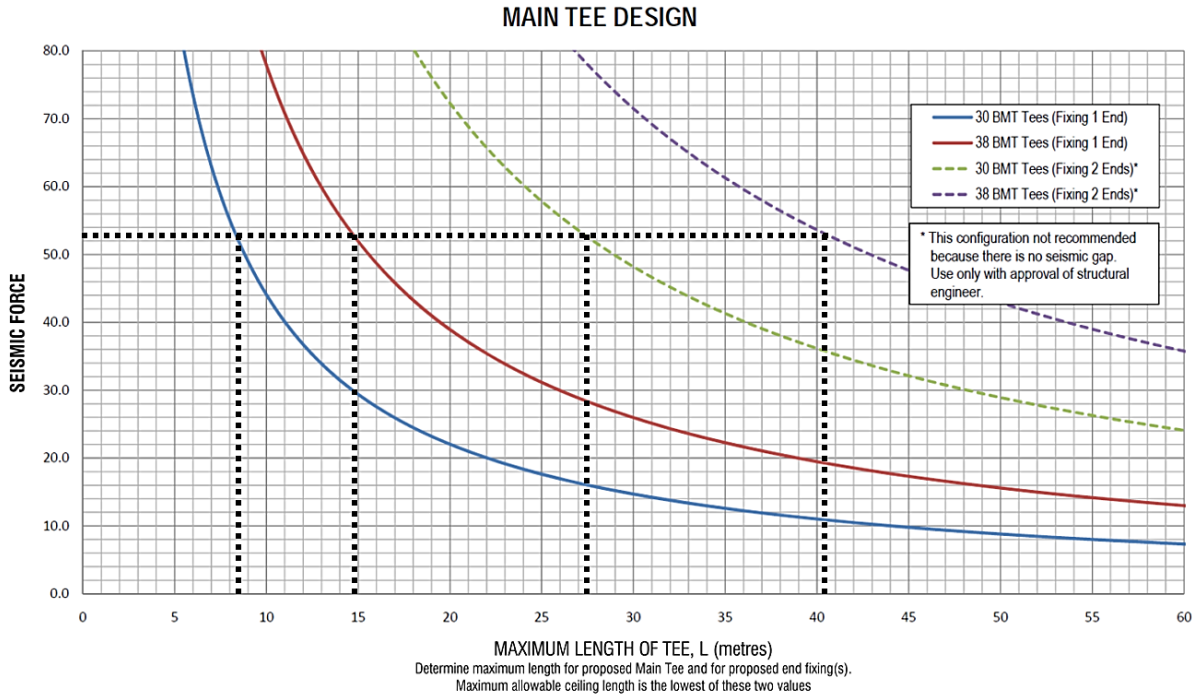

Figure 1-27 – Maximum allowable MT length for different grid types (USG, 2012)

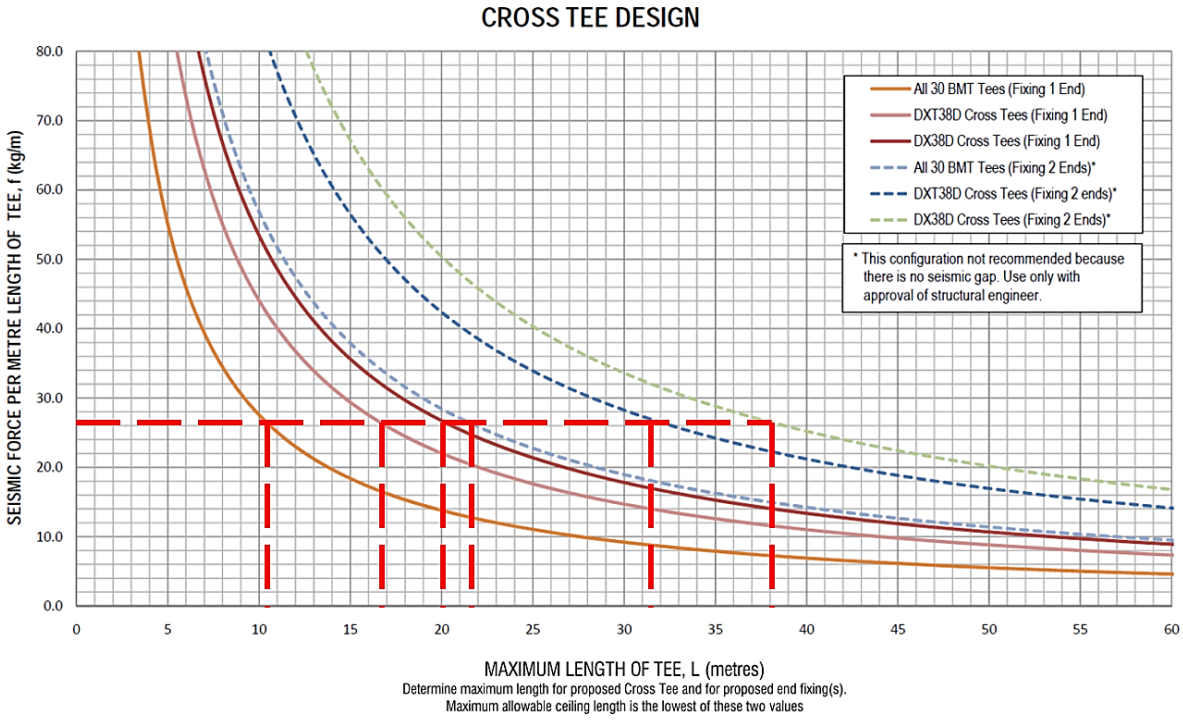

Figure 1-28 – Maximum allowable CT length for different grid types (USG, 2012)

1.7.2.2 Design of ceiling for ultimate limit state

When the determined ceiling category requires ULS design, USG guideline provides

additional factors to include the effect of return period and ductility factors (USG, 2012). The table provided by this guideline recommends a factor of 4 for category P.4 to be applied to the seismic force calculated, which is the ratio between the return period of 1 for ULS and 0.25 for SLS design.

1.7.3 *Design based on Armstrong Guideline*

The design parameters listed in Table 1-15 were determined based on the Armstrong guideline (2013). These values only correspond to design for SLS. This guideline does not have any recommendations for ULS design.

Table 1-15 – Seismic design parameters based on Armstrong (2013)

Seismic weight for SLS design (including tile, grid system and 3 kg/m^2 service load)	$W_p = 5.5 + 1 + 3 = 9.5$ *kg/m^2*
Seismic zone 4	*Z = 0.396*
Height factor for support heights > 9 m	*2*
Slope factor (slope = 0)	*1*
CT spacing (m)	*0.6*
MT spacing (m)	*1.2*
Seismic force	*F = 9.5 × 0.396 ×2 = 7.5 kg/m^2*
Seismic force on CT	*F_{CT} = 9.5 × 0.396 × 2 × 1 × 0.6 = 4.5 kg/m*
Seismic force on MT	*F_{MT} = 9.5 × 0.396 × 2 × 1 × 1.2 = 9 kg/m*
Allowable CT length with single 3.2 mm rivet fixture	*L_{CT} = 60/4.5 = 13 m*
Allowable MT length with single 3.2 mm rivet fixture	*L_{MT} = 70/9 = 7.8 m*

Note that the SLS seismic forces calculated based on the two proprietary guidelines are equal (7.5 kg/m^2) and both larger than the seismic force obtained from NZS 1170.5:2004 (5.7 kg/m^2). This discrepancy was assumed to be related to the SLS return period factor of 0.33 instead of 0.25 for Canterbury region, adopted by the guidelines (Armstrong, 2013; USG, 2012). As shown in the calculation of seismic force below, the force based on NZ standard becomes equal to those obtained from guidelines above, upon the use of R_s = 0.33. Further discussions comparing these design methods and their outcomes will be presented in Chapter 8 of this thesis.

$$C_{SLS}(0) = C_h(0) \cdot Z \cdot R_S \cdot N(T,D) = 1.33 \times 0.3 \times 0.33 = 0.13$$

$$C_p(T_p) = C_{SLS}(0) \cdot C_{Hi} \cdot C_i(T_p) = 0.79$$

$$F_{ph} = C_p(T_p) \cdot C_{ph} \cdot R_p \cdot W_p$$
$$F_{ph} = 0.79 \times 93.2 = 73.6 N/m^2 = 7.5 kg/m^2$$

1.8 Research motivations

Following the review of existing documents (standards, guidelines and previous research mentioned in the earlier sections of this chapter, the following were identified as the potential areas for further study and discussion:

i. The current NZ Standard (NZS2785:2000) requires ceilings to be designed for a working life of 15 years without maintenance. The standard also requires ceilings that provide structural stability to the building to be designed for the design life not less than the building. This requirement has a significant effect on the seismic design coefficient in ultimate limit state design. Moreover, the restriction of "providing structural stability" leads to the exclusion of almost all suspended ceilings as they are not expected to contribute to the structure's load resistance. This is while ceiling damage has repeatedly proven to be a major cause of operational disruption in previous earthquakes (Dhakal, 2010; Ferner et al., 2014).

ii. The application of different areas and rooms of a single building needs to be taken into consideration when determining the design category. Ceilings installed in one building may fall into several different categories and require different design and installation methods.

iii. The ductility factor for the ultimate limit state design of ceilings is not clearly defined by the standard. The guidelines also refer to the structural engineer consulted for the special design. However, the engineer may not have the means required to advise this factor.

iv. The load bearing capacities of the ceiling components are a crucial part of the seismic design process. This information is usually difficult to obtain from the manufacturers. Other methods available are through laboratory testing of the components. Interpretation of the results and relating them to the design parameters was considered an area of potential improvement.

v. The other essential part of every successful design lies within the correct estimation of demand. The part spectral shape coefficient currently set by the NZ Standard requires a factor of 2 for most ceilings (parts with a natural period less than 0.75 s). The appropriateness/validity of this factor needs to be evaluated through tests.

vi. The possibility of employing analysis software commonly used for modelling the structure for predicting the demand on the suspended ceilings.

vii. Currently, the two options recommended for suspended ceilings consist of perimeter-fixed and back braced systems. Extensive studies have been conducted regarding the fragility of these two systems and the damage states. These studies have clarified the weaknesses of the current practices. However, no strengthening or improvement methods are currently suggested for existing or new ceilings.

viii. The interactions of suspended ceilings with traditional vertical non-structural elements (partitions) has been investigated in previous studies. Considering the progress made towards the development of low-damage structural and non-structural systems, the compatibility among these interacting systems needs to be evaluated.

1.9 Research aim and objectives

This study aims to investigate the seismic performance of the currently used suspended ceiling system and identify the deficiencies to propose the concept of a low damage suspended ceiling option. In light of the review of the existing systems, the research carried out and the potential areas for research, this study intends to achieve the following:

i. Evaluating the mechanics of the force transfer within the components of suspended ceilings commonly used in NZ and establishing a strength hierarchy for the critical components,

ii. Development of a simple method for deducing the global capacity of the suspended ceiling system from components capacities. Providing fragility functions in terms of ceiling acceleration for the suspended ceiling using the component capacity data,

iii. Verification of the simple method of estimating seismic actions in connections and members based on PFA via shake table tests,

iv. Development of a simple numerical model for the perimeter-fixed ceiling in SAP2000 software and performing nonlinear time history analysis. Verification of the numerical model using the obtained experimental results,

v. Experimental investigations on the feasibility of a low-damage fully-floating (pendulum) ceiling for seismic applications and use of perimeter isolation material through full scale shake table tests,

vi. Experimental evaluation of the out-of-plane performance of an existing low-damage drywall partition system and its compatibility with existing suspended ceilings in a series of shake table tests,

vii. Recommendations for improving the existing design practice Incorporating the findings from this research.

1.10 Thesis outline

The thesis format has been organised as a mixture of chapters and submitted or accepted/published peer reviewed papers. Different distinctive aspects of the research conducted are presented in the following chapters:

- **Chapter 1** - Introduction into the system researched, its significance and importance followed by the review of relevant Standards, reports and studies. This chapter also outlines the motivations and objectives and layout of this study.
- **Chapter 2** - Derivation of ceiling system fragility functions based on the fragility of ceiling components: This chapter follows after experiments previously conducted in the University of Canterbury on the capacity of the suspended ceiling components common in NZ. In this chapter, the capacities of the ceiling members and connections (in terms of failure forces) are used to build the hierarchy of strength in the ceiling. This method is then expanded from component level to system level by incorporating the other parameters of ceiling, i.e. dimensions and weight, to reinterpret the capacity in terms of ceiling acceleration. Derivation of analytical ceiling fragility curves with the ceiling acceleration as the intensity measure and design curves were the other outcomes of this chapter.
- **Chapter 3** - Experimental assessment of the seismic performance of perimeter-fixed ceilings: This chapter focuses on the shake table tests and sensitivity studies carried out on two specimens of perimeter-fixed ceilings. The validity of a simple design approach based on the linear relationship between inertial forces and accelerations in the ceilings is checked using the experimental results. The chapter also investigates the amplification of accelerations in the ceiling grids and compares the observations with NZ Standard mandated factors.
- **Chapter 4** - Experiments on the influence of seismic clips on capacity and strength of the cross tee-main tee connection of a suspended ceiling system: This chapter reports the monotonic tension and compression tests that were carried out on suspended ceiling cross tee-main tee (CT-MT) connection specimens with and without proprietary seismic clips. Different failure modes are identified in the connection area and fragility curves are derived for the as-built and the improved connections. Results of these

experiments show that using seismic clips improved CT-MT connection performance in two ways: i) increasing the maximum and residual capacity, and ii) adding ductility.

- **Chapter 5** - Fully-floating suspended ceiling system: experimental evaluation of structural feasibility and challenges: Through extensive shake table experiments and sensitivity studies carried out in this chapter, the seismic response of a pendulum type ceiling is evaluated and quantified. The Combination of perimeter isolators with this system proves to be effective in damping the ceiling displacements and impact accelerations.
- **Chapter 6** - Experimental evaluation of seismic compatibility between low-damage drywall partitions and suspended ceilings: This chapter is focused on shake table tests on a combined system of low-damage drywalls and two existing suspended ceilings, identifying any possible incompatibilities and proposing solutions. The main aspect of compatibility investigated in these experiments is the relative displacement between the adjacent drywalls and the suspended ceilings. Throughout these experiments, no damage is observed in the low-damage drywalls. Large relative displacements in the back-braced ceiling result in pounding to the perimeter walls. However, the only form of ceiling damage is observed as tile dislodgement in the back-braced ceiling, due to grid spreading. A trimming element is introduced to overcome this shortcoming.
- **Chapter 7** - Development and verification of numerical models of the perimeter-fixed ceiling based on shake table experimental results: Two types of models were developed in this chapter. The model of the test frame including the perimeter-fixed ceiling specimen was developed with ceiling tiles modelled only as distributed loads. The model was capable of simulating the experimental acceleration and axial force time histories well, except for the high frequency peaks. Comparison was repeated with filtered experimental results which showed better agreement after the removal of higher frequency content from the response. The results showed an acceptable level of accuracy for an initial estimation of ceiling response. The second model incorporated the impact between ceiling tiles and grids in a smaller specimen. The pounding effect was apparent in the form of high frequency spikes in the response at the closure of gaps between grids and tile corner nodes.
- **Chapter 8** - Implications of the achieved experimental results: The practical applications and implications of the experimental and analytical findings of this study are

discussed in this chapter, followed by an example for seismic design procedure for a typical suspended ceiling.

- **Chapter 9** - Summary and conclusions

1.11 References

Accessible suspended ceiling construction. U.S. Patent No. 2,984,946, issued May 23, 1961.

American Society of Civil Engineers. (1994). *Minimum Design Loads for Buildings and Other Structures (ASCE/SEI 7-10.), Vol. 7, Chapter 13: Seismic Design Requirements for Non-Structural Components.* USA: American Society of Civil Engineers.

American Society for Testing and Materials. (2013). *Standard Specification for the Manufacture, Performance, and Testing of Metal Suspension Systems for Acoustical Tile and Lay-in Panel Ceilings (C635/C635M)*. PA, USA.

American Society for Testing and Materials. (2013). *Standard Practice for Installation of Metal Ceiling Suspension Systems for Acoustical Tile and Lay-in Panels (C636/C636M)*. PA, USA.

American Society for Testing and Materials International. (2011). *Standard Practice for Installation of Ceiling Suspension Systems for Acoustical Tile and Lay-in Panels in Areas Subject to Earthquake Ground Motions (E580/E580M-11b 2011)*. PA, USA.

American Standard. Blind Rivet. Break Mandrel Rivets, Industrial Fasteners Institute (IFI 114). USA

Armstrong (2013). *"Seismic Design Guide New Zealand Version, Suspended Ceiling Systems"*. Armstrong, Auckland, New Zealand.

Australian/New Zealand Standard. (1999). *Methods for Fire Test on Building Materials, Components and Structures - Simultaneous Determination of Ignitability, Flame Propagation, Heat Release and Smoke Release (AS/NZS 1530.3:1999)*. Wellington, NZ: Standards New Zealand.

Australian/New Zealand Standard. (2000). *Acoustics - Measurements of sound insulation in buildings and of buildings elements - Laboratory measurement of room-to-room airborne sound insulation of a suspended ceiling with a plenum above it (AS/NZS 2499:2000).* Wellington, NZ: Standards New Zealand.

Australian/New Zealand Standard. (2000). *Suspended ceilings - Design and Installation (AS/NZS 2785:2000).* Wellington, NZ: Standards New Zealand.

Australian/New Zealand Standard. (2002). *Structural design actions - Part 0: General principles (AS/NZS 1170.0:2002).* Wellington, NZ: Standards New Zealand.

Australian/New Zealand Standard. (2002). *Structural design actions – Part 1: Permanent, Imposed and Other Actions (AS/NZS 1170.1:2002).* Wellington, NZ: Standards New Zealand.

Australian/New Zealand Standard. (2005). *Cold-formed steel structures (AS/NZS 4600:2005).* Wellington, NZ: Standards New Zealand.

Australian Standard. (1991). *Suspended Ceilings, Recessed Luminaires and Air Diffusers – Interface Requirements for Physical Compatibility (AS 2946:1991).* Sydney, Australia: Standards Australia.

Badillo-Almaraz, H., Whittaker, A. S., & Reinhorn, A. M. (2007). Seismic fragility of suspended ceiling systems. *Earthquake Spectra*, *23*(1), 21-40.

Bradley, B. A., Dhakal, R. P., MacRae, G. A., & Cubrinovski, M. (2010). Prediction of spatially distributed seismic demands in specific structures: Structural response to loss estimation. *Earthquake Engineering & Structural Dynamics*, *39*(6), 591-613.

British Standards Institution. (1987). *Fire Tests on Building Materials and Structures - Method for determination of the fire resistance of elements of construction (general principles) (NZS/BS 476.20:1987).*

Ceilings and Interior Systems Construction Association CISCA. (2004). "Guidelines for Seismic Restraint for Direct Hung Suspended Ceiling Assemblies, Seismic Zones 3-4". Illinois, USA: Ceiling and Interior Systems Construction Association.

Department of Building and Housing. (2011). Compliance Document for New Zealand Building Code Clause B1 Structure. Wellington, NZ: NZ Government.

Dhakal, R. P. (2010). Damage to Non-structural Components and Contents in the 2010 Darfield earthquake. *Bulletin of the New Zealand Society for Earthquake Engineering*, *43*(4), 404.

Dhakal, R. P., MacRae, G. A. & Hogg, K. (2011). Performance of Ceilings in the February 2011 Christchurch Earthquake. *Bulletin of the New Zealand Society for Earthquake*

Engineering, *44*(4), 379-389.

Dhakal, R. P., MacRae, G. A., Pourali, A., & Paganotti, G. (2016). Seismic fragility of suspended ceiling systems used in NZ based on component tests. *Bulletin of the New Zealand Society for Earthquake Engineering*, *49*(1), March 2016

Dhakal, R. P., Pourali, A., Tasligedik, A. S., Yeow, T., Baird, A., MacRae, G., ... & Palermo, A. (2016). Seismic performance of non-structural components and contents in buildings: an overview of NZ research. *Earthquake Engineering and Engineering Vibration*, *15*(1), 1-17.

FEMA. (2011). *Reducing the Risks of Non-Structural Earthquake Damage – A Practical Guide (FEMA E74)*. Washington D.C., USA.

Ferner, H., Wemyss, M., Baird, A., Beer, A., & Hunter, D. (2014, March). Seismic performance of non-structural elements within buildings. In *Proceeding of the NZSEE Conference* (pp. 21-23).

Gilani, A. S., Reinhorn, A. M., Glasgow, B., Lavan, O., & Miyamoto, H. K. (2010). Earthquake simulator testing and seismic evaluation of suspended ceilings. *Journal of architectural engineering*, *16*(2), 63-73.

Glasgow, B., Gilani, A. S., & Miyamoto, H. K. (2010). Resilient suspended ceilings for sustainable design of buildings. In *Structures Congress 2010* (pp. 2575-2587).

Goltz, J. D. (1994). The Northridge, California earthquake of January 17, 1994: General reconnaissance report. Rep. No. NCEER-94-0005.

Huang, W., Mcclure, G., & Hussainzada, N. (2013). Experimental Study on the Seismic Performance of Suspended Ceiling Systems in Interaction with Partition Walls, *In The 2013 World Congress*, Jeju, Korea, Sep 8-12, 2013 (pp. 2304–2323).

International Code Council. (2012). *Acceptance Criteria for Suspended Ceiling Framing Systems (ICC-ES-AC368)*. USA

Kawaguchi, K. I. (2012). Damage to Non-structural Components in Large Rooms by the Japan Earthquake. In *Structures Congress 2012* (pp. 1035-1044).

MacRae, G. A., Hair, J., & Dhakal, R. P. (2011, March). Ceiling damage in the 2010 Canterbury earthquake. In *Joint 8th Center for Urban Earthquake Engineering (CUEE) and 8th International Conference on Earthquake Engineering (ICEE) Conference Proceedings*, March 7-8, 2011, Tokyo Institute of Technology, Tokyo, Japan.

Miranda, E., & Taghavi, S. (2003). Response assessment of nonstructural building elements. *Pacific Earthquake Engineering Research Center, University of California Berkeley, California, USA*.

New Zealand Standard. (2004). *Structural Design Actions Part 5: Earthquake Actions-New Zealand (NZS 1170.5:2004)*. Wellington, NZ: Standards New Zealand.

New Zealand Standard. (2009). *Seismic Performance of Engineering Systems in Buildings (NZS 4219:2009)*. Wellington, NZ: Standards New Zealand.

New Zealand Standard. (2013). *Automatic fire sprinkler systems (NZS 4541:2013)*. Wellington, NZ: Standards New Zealand.

Paganotti, G. (2010). *Behaviour of Suspended Ceiling System during Seismic Events: Development of Fragility Curves*. (Masters Thesis, Politecnico Di Milano, Italy).

Paganotti, G., MacRae, G. A., & Dhakal, R. P. (2011, April). Development of typical NZ ceiling system seismic fragilities. In *Ninth Pacific Conference on Earthquake Engineering (PCEE)* (pp. 14-16).

Robson M. J., Kho D. N., Pourali A. and Dhakal R. P., 2014. Feasibility of a fully floating ceiling system, *in proceedings of the New Zealand Society for Earthquake Engineering Conference*, 21-23 March, 2014, Auckland, NZ.

Rondo. (2008). *DUO Two-way Exposed Suspended Ceiling Grid System*. Rondo, Auckland, NZ.

Ryu, K. P., Reinhorn, A. M., & Filiatrault, A. (2012). Full scale dynamic testing of large area suspended ceiling system. In *Proceedings 15th World Conference on Earthquake Engineering, September 23-28, 2012, Lisbon Portugal-Paper* (Vol. 5474).

Ryu, K. P., Reinhorn, A. M., & Filiatrault, A. (2013). Capacity evaluation of suspended ceiling systems. *Technical Report MCEER-13-XXXX*.

Sato, Y., Motoyui, S., MacRae, G. A., & Dhakal, R. P. (2011, April). Ceiling Fragility of Japanese Ceiling Systems. In *Proceedings of the Ninth Pacific Conference on Earthquake Engineering*.

Singh, J., MacRae, G. A., Dhakal, R. P., & Pampanin, S. (2011). Building seismic ceiling fragility using spectral acceleration. In *Ninth Pacific Conference on Earthquake Engineering*. Auckland, NZ, 14-16 April 2011.

Soroushian, S., Zaghi, A. E., Maragakis, E. M., & Echevarria, A. (2014). Seismic fragility study of displacement demand on fire sprinkler piping systems. *Journal of earthquake engineering*, *18(7)*, 1129-1150.

Soroushian, S., Maragakis, E. M., & Jenkins, C. (2015a). Capacity evaluation of suspended ceiling components, part 1: experimental studies. *Journal of Earthquake Engineering*, *19*(5), 784-804.

Soroushian, S., Maragakis, E. M., & Jenkins, C. (2015b). Capacity evaluation of suspended ceiling components, part 2: analytical studies. *Journal of Earthquake Engineering*, *19*(5), 805-821.

Soroushian, S., Rahmanishamsi, E., Ryu, K. P., Maragakis, M., & Reinhorn, A. M. (2016). Experimental fragility analysis of suspension ceiling systems. *Earthquake Spectra*, *32(2)*, 881-908.

Suspended ceiling. U.S. Patent 1,470,728, issued October 16, 1923.

Tasligedik, A. S., Pampanin, S., & Palermo, A. (2015). Low damage seismic solutions for non-structural drywall partitions. *Bulletin of Earthquake Engineering*, *13*(4), 1029-1050.

Tasligedik, A. S. (2014). *Damage mitigation strategies for non-structural infill walls* (Doctral thesis, Civil and Natural Resources Engineering Department. University of Canterbury, Christchurch/New Zealand), pp. 304.

USG Australia. (2011). *DONN Brand Grid Suspension System*. USG Australia, Auckland, NZ.

USG Australia. (2012). *Generic Seismic Design for USG DONN Exposed Grid Suspended Ceilings*, Auckland, New Zealand.

Yao, G. C. (2000). Seismic performance of direct hung suspended ceiling systems. *Journal of architectural engineering*, *6*(1), 6-11.

Zaghi, A. E., Soroushian, S., Echevarria Heiser, A., Maragakis, M., & Bagtzoglou, A. (2016). Development and Validation of a Numerical Model for Suspended-Ceiling Systems with Acoustic Tiles. *Journal of Architectural Engineering*, *22*(3), 04016008.

CHAPTER 2

SEISMIC FRAGILITY OF SUSPENDED CEILING SYSTEMS USED IN NZ BASED ON COMPONENT TESTS

2 SEISMIC FRAGILITY OF SUSPENDED CEILING SYSTEMS USED IN NZ BASED ON COMPONENT TESTS

(Accepted and published in the *Bulletin of the New Zealand Society for Earthquake Engineering, Vol. 49, No. 1, March 2016)*

2.1 Introduction

Non-structural elements (NSEs) in a building (also sometimes referred to as secondary elements) are components, which despite adding to building design dead loads, do not always contribute to the resistance against design actions. NSEs are indispensable because without them buildings are incomplete and cannot function as intended. While the load resisting structural components provide strength and stiffness to a building, NSEs are required to provide heat/sound insulation, compartmentalization, and protection from sun/rain which are vital in making the building inhabitable. Some of the most common NSEs in residential, as well as commercial buildings are ceilings, roofs, partitions, claddings, façades, windows, parapets, canopies, chimneys etc. Other movable components in buildings which contribute to the live load (e.g. furniture, appliances, equipment etc.) are generally categorised separately as contents.

NSEs and building contents make up a considerable 70-80% of the total construction cost in commercial buildings. (Miranda & Taghavi, 2003). In recent earthquakes, damage to NSEs has been reported to be significant (more so than the structural damage) (Dhakal, 2010; MacRae & Lehman, 2001; MacRae et al., 2012). Predictions using risk assessment methods have also suggested that the economic implication from non-structural damage is generally more significant than those of structural damage. For example, Bradley et al. (2010) conducted a detailed component based seismic loss estimation on a typical office building in New Zealand and found that the direct repair cost of NSEs amounted to 44% of the total direct loss, which is higher than the structural loss (25%) and contents (31%). Among the NSEs, two major contributors were partitions (20%) and ceilings (14%).

When business downtime is included in the comparison, the criticality of NSEs is further elevated. In the 2010-2011 Canterbury earthquake sequence, many buildings remained unoccupied weeks after the event due to non-structural damage despite the buildings retaining their structural integrity. Observations from recent earthquakes have shown that if buildings do not collapse, it is mainly the NSEs and contents which dictate the extent of downtime. Even in the 2013 Seddon earthquake, which induced only minor-moderate level of shaking in

Wellington, NZ, there was significant damage to NSEs (Ferner et al., 2014). The relatively new BNZ building suffered severe damage to its suspended ceilings requiring building closure for several weeks despite no significant structural damage.

In addition to significantly contributing to direct financial loss and downtime, damage to NSEs and contents can also be a life threat. For example, the collapse of ceiling boards led to loss of four lives in the 2011 Tohoku (Japan) earthquake (Motosakaa & Mitsujib, 2012; Nation Media, 2011). Similarly, collapse of parapets was the cause of some of the fatalities in the 2011 Christchurch earthquake and the extensive collapse of parapets, chimneys, canopies, façades, ceilings reported in the 2010 Darfield earthquake (Dhakal, 2010) could easily have caused loss of life or serious injury had the quake occurred at a different time of day.

In order to minimise such losses in earthquakes, it is necessary to realise the importance of designing NSEs to withstand design level earthquakes. This requires a clear understanding of the capacity of the NSEs and defining the limits of their use to meet design seismic demand in different locations. The main purpose of this paper is to provide a simple and practical method for the evaluation of the impact of floor acceleration on typical perimeter-fixed suspended ceilings currently designed and used in New Zealand. According to the principles of capacity design, a system is only as strong as its weakest member. Once the weakest element reaches its capacity, the system is considered a failure. Hence, the method of observation of ceilings in this study is the evaluation of its components to identify the weakest link. For this purpose, a series of tension-compression tests were conducted on components of a typical suspended ceiling in New Zealand. Results from these experiments were used to derive fragility curves for each ceiling component leading to identification of the weakest members. In the next phase of the study, perimeter-fixed suspended ceilings of various size and weight were designed based on current available guidelines. The component fragility curves were then used to evaluate the probability of failure in the designed ceilings when subject to acceleration as the intensity measure. These evaluations provide an insight into the level of reliability of current perimeter-fixed ceilings at serviceability and ultimate limit states.

The objectives of this paper can be summarised in the following questions:

1. What standards or guidelines exist for suspended ceiling systems?
2. What damage has been observed in the past?
3. What is the capacity of typical ceiling components?

4. How do ceiling components contribute to the overall ceiling system performance?
5. Comparing examples of different ceiling systems, what parameters result in a more susceptible response?

2.2 Suspended ceiling systems in New Zealand

2.2.1 *Typical Layout*

Suspended ceilings are architectural components sensitive to both acceleration and displacement (FEMA, 2011). Depending on the structure and load bearing system, they are categorised as perimeter-fixed, with one or more sides connected to the adjacent wall as shown in Figure 2-1a or Figure 2-1b, or floating systems which have no connection to any walls but are braced to the floor above, as shown in Figure 2-1c.

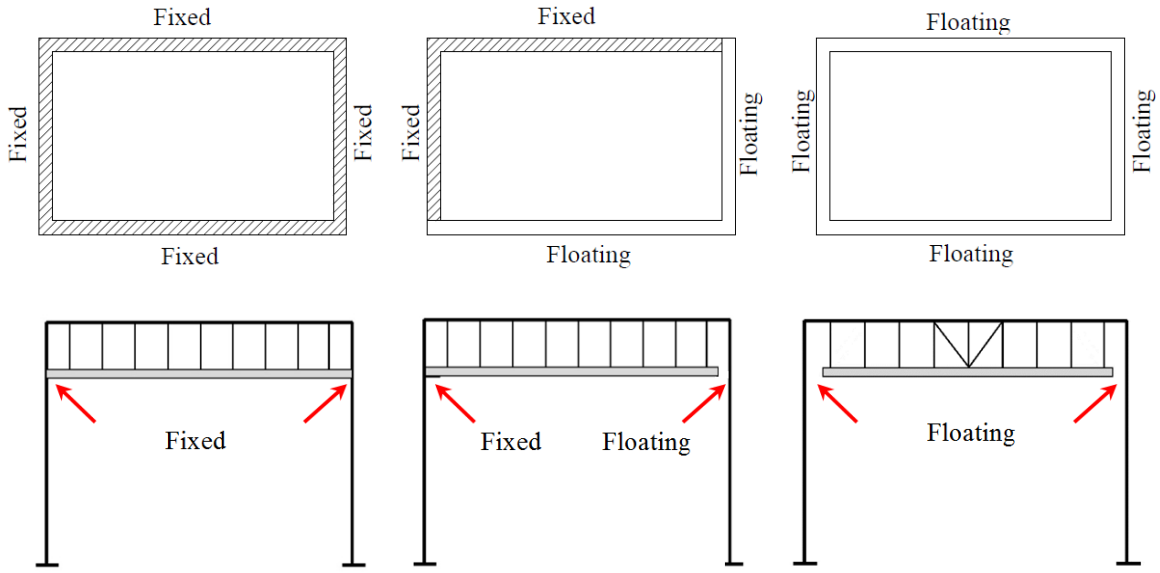

(a) Fixed-fixed (b) Fixed floating (c) Floating

Figure 2-1 - Schematic of different ceiling systems

The fixed-fixed system of Figure 2-1a was recommended by many ceiling supplier systems for small ceilings until recent earthquakes, with force designed to be carried on one or both sides. However, in such systems any relative movement of the adjacent walls applies force to the ceiling system. Such movement may occur during the dynamic motion of the structure and walls, or due to beam elongation effects.

More recently, to avoid these issues, the fixed-floating approach in Figure 2-1b has been recommended (e.g. by USG (2011)). This system also works well for small ceilings because it avoids any forces due to relative wall movement, as long as the gaps on the floating sides

remain open. A thin covering is placed over the separation to provide an acceptable appearance. Here, all inertial forces are transferred to the perimeter fixings on the fixed sides, making these connections the most vulnerable components of the system.

For larger ceilings, the ceiling grid may not to be strong enough to carry the expected lateral forces, so additional ceiling bracing to the floor above may be used while fully separating the ceiling perimeters from the structure. For instance, ASTM E580 (2011) mandates the application of lateral restraints for all suspended ceilings in seismic category D-F, should the size of the ceiling exceed 1000 ft^2 [93 m^2]. The braced ceiling, also referred to as a floating ceiling, or fully separated ceiling, shown in Figure 2-1c, carries horizontal force due to the horizontal accelerations of the floor above through the braces and it is disconnected from the surrounding walls.

A typical suspended ceiling consists of a grid system of inverted T-shaped beams assembled perpendicular to each other forming square or rectangular grids for the lay-in tiles to sit on (Figure 2-2a). The grid system consists of 3600 mm long main tees and 600 mm or 1200 mm long cross tees. Main tees are generally placed perpendicular to the upper floor joists or in shorter direction. For cases where the length of the main tee direction exceeds 3600 mm, they may be extended via splices. Cross tees pass through special slots in the main tee webs and are connected to the next cross tee via click-fit clips (Figure 2-2c). No additional mechanical fasteners are used in the assembly of the grid system itself.

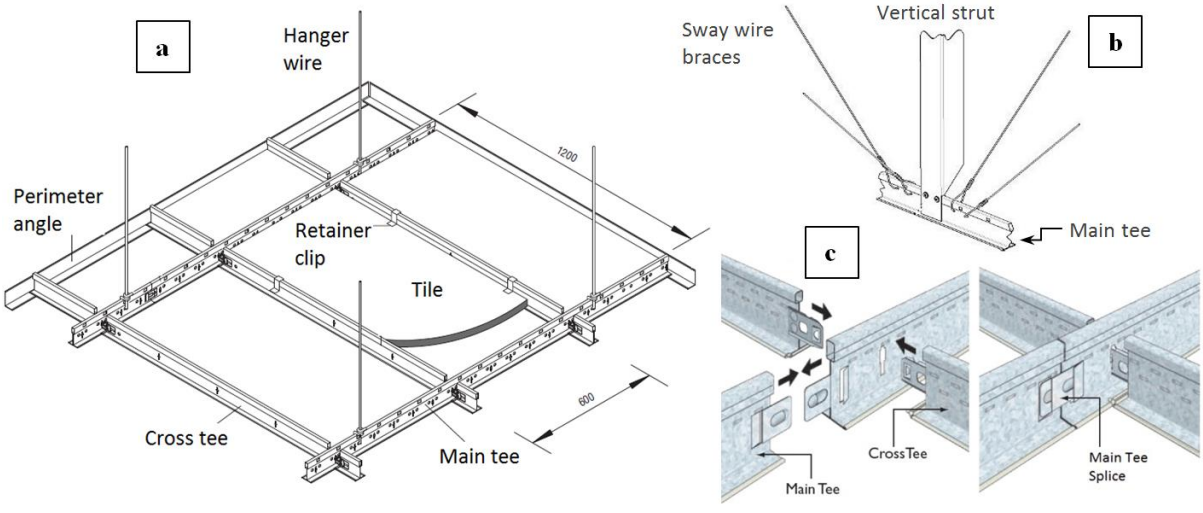

Figure 2-2 - (a) Typical suspended ceiling components (USG, 2011); (b) Typical back bracing options (USG, 2012) & (c) tee joint details (Rondo, 2008)

On the fixed ends, the grid system is connected to the perimeter angle fastened to the

surrounding walls using mechanical fixtures such as rivets, screws or proprietary clips. The lay-in tiles are not fastened to the grids but rather sit freely on the inverted tee flanges. AS/NZS 2785 (2000) recommends the use of retainer clips to control the upward movement of the tiles. However, these clips are not commonly used due to installation difficulties. The grid system is hung from the structure above via hanger wires connected to main tees at 1200 mm intervals. The hanger wires are a minimum of 12-gauge galvanized, soft annealed mild steel wire (ASTM C636, 2013). The wire must be wrapped around itself a minimum of 3 full turns within 75 mm. These vertical wires don't have any lateral resistance but their application, particularly on perimeters, has proven advantageous in limiting the spreading of grid ends and consequent damage during earthquakes. For this purpose, all terminal ends of grid members should be supported via vertical hanger wires at a maximum 200 mm from each wall or ceiling discontinuity. Ceilings designed for seismic design categories D, E and F should have a minimum perimeter support ledge of 50 mm and grid ends are required to have a clearance of 18 mm from the perimeter member (ASTM E580, 2011). The bracing can consist of four diagonal wires and a vertical strut performing as a compression post (Figure 2-2b). Diagonal channel or strut members can also be used instead of the wires.

2.2.2 *Current Design/Installation Approach*

There are a number of standards and documents specific or relevant to the design or installation of suspended ceilings (Dhakal & MacRae, 2013). The following documents are available in New Zealand:

- (NZS 1170.5:2004) Structural Design Actions, Earthquake Actions, New Zealand.
- (AS/NZS 2785:2000) – Suspended Ceilings: Design and Installation.
- (NZS 4219:2009) – Seismic performance of engineering systems in a building.
- (NZS 4541:2013) – Automatic Fire Sprinkler Systems in a building.
- (Ministry of Works PW/81/10/1:1985) - Guidelines for the Seismic Design of Public Buildings: Appendix D Suspended Ceilings and Associated Fittings and Fixtures.
- (AS/NZS 1170.1:2002) - Structural design actions - Permanent, imposed and other actions.
- (AS/NZS 1530.3:1999) - Methods for fire test on building materials, components and structures - Simultaneous determination of ignitability, flame propagation, heat release and smoke release.

- (AS 2946:1991) - Suspended ceilings, recessed luminaries and air diffusers – Interface requirements for physical compatibility.

Some other documents and standards providing guidelines for suspended ceilings in the United States include:

- FEMA E74 (2011) – Reducing the Risks of Non-structural Earthquake Damage – A Practical Guide.
- ASCE/SEI 7-10 (1994) – Minimum Design Loads for Buildings and Other Structures – Chapter 13 Seismic Design for Non-structural Components.
- ASTM C635 (2013) – Standard Specification for the Manufacture Performance and Testing of Metal Suspension Systems for Acoustical Tile and Lay-in Panels.
- ASTM C636 (2013) – Standard Practice for Installation of Metal Ceiling Suspension Systems for Acoustical Tile and Lay-in Panels.
- ASTM E580 (2011) – Standard Practice for Installation of Ceiling Suspension Systems for Acoustical Tile and Lay-in Panels in Areas Subject to Earthquake.
- ASTM E1414-11 (2011) – Standard Test Method for Airborne Sound Attenuation between Rooms Sharing a Common Ceiling Plenum (Two room method).
- CISCA (2004) – Guidelines for Seismic Restraint for Direct Hung Suspended Ceiling Assemblies – Seismic Zones 3-4.

Some of the key contributions of these documents are listed below:

NZS 1170.5 (2004) New Zealand standard for design of structures subject to earthquake actions provides a section for determining the seismic demand on parts (NSEs) including suspended ceilings. The horizontal acceleration coefficient for parts according to NZS 1170.5 (2004), is an expression consisting of the following factors:

i) site hazard coefficient which is a factor of site hazard, spectral shape factor and the probability of occurrence of the seismic event relevant to the limit state,

ii) height coefficient which depending on the location of the part along building height can vary between 2 to 3 (Figure 2-3b) and

iii) part spectral shape factor which varies between 0.5 and 2 based on the period of the part (Figure 2-3a).

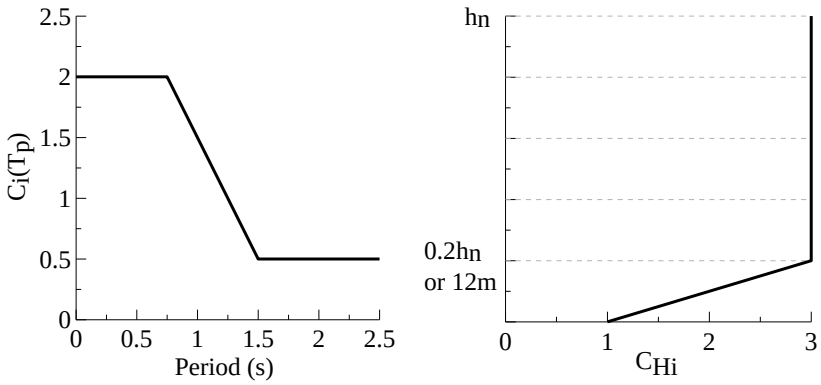

(a) (b)

Figure 2-3 – (a) Part spectral shape coefficient; (b) height coefficient (NZS 1170.5:2004)

The detailed design of ceilings is carried out based on the recommendations of ceiling manufacturers which comply with these standards. The general trend in current manufacturers' guidelines (Armstrong, 2013; USG, 2012) is to design ceilings to satisfy serviceability limit state.

AS/NZS 2785 (2000) Australia and New Zealand standard for suspended ceilings sets out the minimum requirements for the design, construction, installation, maintenance and testing of internal and external non-trafficable suspended ceilings for use in commercial, industrial and residential buildings. The standard includes the design loads, definition of limit states and installation recommendations. However, the recommendations are mainly qualitative rather than specifying quantitative limits. In many cases the users are referred to the proprietary manufacturers' specifications.

Suspended ceilings are outside the scope of NZS 4219 (2009). However, this document provides minimum clearance limits to be applied between components of suspended ceiling system and other services and equipment within ceiling plenum.

ASCE7–10 (1994) in Chapter 13 provides an expression for the seismic design force taking into account component's importance and amplification factors, spectral acceleration for short period, component's response modification factor, height in structure and component's operating weight.

ASTM E580 (2011) sets out minimum requirements for the installation of suspended ceilings. This document which is mainly adopted by most proprietary guidelines, provides quantitative requirements and limits for grid members and connections load capacity, grid spacing, bracing, maximum allowable weight and layout and details for installation. The

requirements are provided for areas of light to moderate as well as high seismicity.

Proprietary manufacturers also provide guidelines specific to their products (Armstrong, 2013; USG, 2012). These documents provide brief design methods and installation techniques which need to be strictly followed in case the final work requires inspection to be signed off.

Based on NZS 1170.5 (2004), suspended ceilings are mainly designed for serviceability limit state (SLS) unless they are located in buildings of high post-disaster significance such as hospitals and police stations or in case they cover egress areas. However, performance of suspended ceilings in recent seismic events has proven that damage to suspended ceilings can pose a life threat and cause considerable financial loss (Dhakal, 2010; Dhakal et al., 2011).

Suspended ceilings do not exhibit a great level of ductility. Hence the point where the system loses its originally intended operation -SLS- and the point where it loses integrity and undergoes collapse, thereby endangering occupants -ultimate limit state ULS- are close. Therefore, the reconsideration and thorough evaluation of design and installation practices in New Zealand seem inevitable and highly beneficial in reducing future losses.

2.2.3 *Seismic performance*

Based on Dhakal (2010), following the magnitude 7.1 Darfield earthquake in September 2010 in New Zealand, ceiling damage was observed both in low-rise residential houses and commercial buildings. Damage was less significant in residential ceilings which were typically plasterboard type. Ceilings in commercial buildings were the suspended type which is discussed in this paper. The damage observed in these types of ceilings included dislodging and breaking of the tiles, failure of the ceiling grid members and connections, failure of perimeter angles and damage to ceiling tiles due to interaction with the services (Figure 2-4). In a crude approximation, 10%-15% of commercial/industrial buildings incurred ceiling damage to different extents.

The other type of grid damage occurred in one-way suspended ceilings where tiles are supported by main tees spanning one way and hung from the structure above. There are typically no transverse tees. As soon as the first tile fails the system loses integrity and grid members are free to spread resulting in failure of adjacent tiles (Figure 2-4e).

A large portion of grid damage observed was concentrated around perimeters which results from the main tee or cross tee either being compressed into the rigid surrounding structure or losing support on the perimeter angle around the ceiling. Loss of support can be due to the

absence of proper perimeter hanger wires, absence of rivets to connect the grid member to the angle or failure of the rivet itself (Figure 2-4b & f). Perimeter fixings are especially prone to damage as they transfer the largest inertial force from the suspension system to the rigid supporting structure. As acceleration is applied to the ceiling, the inertial force induced by the seismic mass increases throughout the length of the grid carrying ceiling tiles.

Magnitude 6.3 Christchurch earthquake in February 2011 resulted in significant damage in both high-rise and medium height buildings. Tall buildings due to the nature of the event suffered both structural and non-structural damage but in low-rise structures the damage was in most cases non-structural while the structure remained intact. Among these non-structural elements, ceilings were conspicuous as the most severely damaged NSEs according to Dhakal et al. (2011). Similar forms of damage in suspended ceilings were observed in this earthquake compared to 2010 Darfield earthquake. A combination of smaller ceilings and lighter tiles was reported to result in lower demand on the grid members and connections, which led to safer ceilings (Dhakal, 2010; Dhakal et al., 2011).

Services and fire sprinklers are frequently reported as one of the causes of ceiling damage. In July 2013, following the magnitude 6.5 earthquake centred in Cook Strait, widespread non-structural damage was reported in the BNZ Harbour Quays building in Wellington. The suspended ceilings and sprinkler pipes were extensively damaged and showed signs of large deformations (Figure 2-5). Based on reports, it took nearly 6 months before the tenants (BNZ) could reoccupy the building, resulting in large financial loss due to downtime as well as repair (Stuff, 2014).

In many damage cases observed, ceilings and services either lacked suitable seismic design, or were not correctly installed. The extent and nature of the loss due to suspended ceiling failure observed in recent earthquakes is an indication of the significance of the issue. These observations highlight the need for a thorough investigation, and enforcement of consistent methods for design and installation of NSEs and suspended ceilings in particular.

Figure 2-4 – Failure due to (a) main tee splices; (b) perimeter fixings; (c & d) services support; (e) grid spreading; and (f) perimeter fixing damage (Dhakal, 2010)

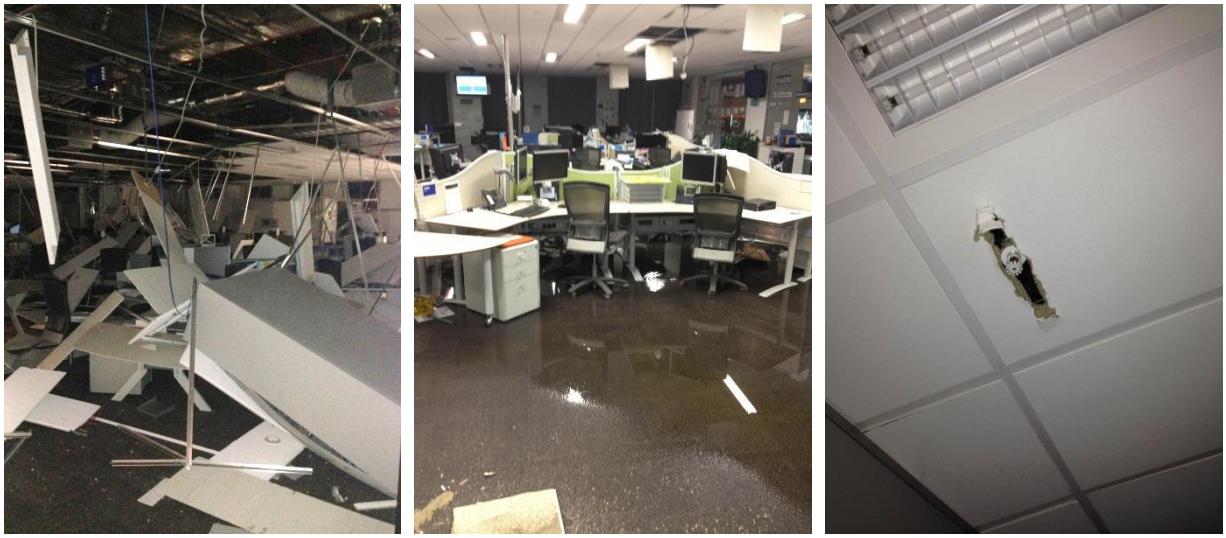

Figure 2-5 – Damage in BNZ building (Photo: Terry Johnson)

There have been a number of research projects investigating the seismic fragility of suspended ceilings and performance of different configurations of ceiling system. One of the early experiments done by ANCO Engineers Inc. (1983) on a prototypical suspended ceiling concluded that the most common locations for damage in suspended ceiling systems were around the perimeter of a room at the intersection of the walls and ceilings, where the grids buckle or detach from the perimeter angle. Their research also showed that pop rivet installation was more influential than sway wires and that sway wire braces, if installed with perimeter fixing, will not be active in the system's lateral restraint.

Rihal & Granneman (1984) investigated the effectiveness of current building code provisions and installation practices for braced and unbraced suspended ceilings with and without partitions in a series of dynamic tests. According to their results, specimens with vertical strut showed less uplift which occurs due to the vertical excitation in ceilings. Extensive damage to the ceiling system was observed at unattached (floating) perimeters. The addition of vertical hanger wires located at cross tees, 8-inch max from unattached perimeter, prevented tiles from crashing down, but damage was instead caused by pounding of cross tees to perimeter angles.

Badillo-Almaraz et al. (2007) conducted fragility studies on suspended ceiling systems. In their full-scale earthquake-simulator testing they evaluated the effect of size and weight of tiles, use of retainer clips, installation of compression posts, and physical condition of grid components on the performance of ceilings. Four limit states were proposed to evaluate the damage observed in the systems and the threshold peak floor accelerations associated with each limit state were found.

In a series of studies by Gilani et al. (2010; 2012) and Glasgow (2010), an experimental procedure and a performance matrix based on limit states were developed to evaluate and qualify innovations and quantitatively assess the efficacy of various code prescribed design and installation requirements. A fragility curve was derived for ceiling tile failure as one of the damage states. The use of intermediate duty main runners in high seismic regions was also tested through a case study which showed that the substitution of intermediate for heavy-duty main runners does not adversely affect the seismic response of the system. The terms intermediate and heavy-duty refer to gird members of various capacities. These categories are defined based on the maximum load on the grid associated with an allowable midspan deflection (ASTM C636, 2013).

Ryu et al. (2013) published a report on full scale shake table tests on large area suspended ceilings using 3D motions. In their tests they compared the seismic response of suspended ceilings with different areas (6.1 m × 15.2 m, 6.1 m × 6.1 m, 4.8 m × 4.8 m and 3.6 m × 3.6 m). They also investigated the effect of tile weight, multidirectional excitation and end fixing type. Three different failure mechanisms were observed during tests and fragility curves were derived for four damage states. Based on their results, the observed failure was concentrated on connections rather than grid body. Simplified uniaxial numerical models were also developed to track the behaviour of the system.

2.3 Methodology

2.3.1 *Tests on Components and Connections*

2.3.1.1 Test setup

A series of destructive static tests were carried out on components of a typical suspended ceiling system manufactured by two of the major ceiling providers in New Zealand (T1 for Type 1 and T2 for Type 2) (Paganotti, 2010; Paganotti et al., 2011). The experiments focused on grid members -main tees and cross tees- as well as connections including cross tee connections, main tee splices and end fixing rivets. Tension, compression and shear tests were carried out on the 100 kN Avery Universal Testing machine and the 250 kN Instron Universal Testing machine at the University of Canterbury (Figure 2-6a). The first machine provides loading at a range of 50 kN by 0.1 kN divisions and the second machine applies load at a range of 5 kN by 0.01 kN divisions. For tension and compression tests on members Avery Universal testing machine was used. Instron Universal testing machine was used to conduct all other tests on connections. The choice of machine depended on maximum load searched as well as the length of the specimens tested. The loading rate for connection tests was lower than the member tests as connections were expected to fail at an earlier stage.

In order to provide a good grip between the specimens and the test machine, the two flanges of the inverted T-shape section on either end of the specimens were removed and the web was compressed (Figure 2-6b). In connection tests, specimens consisted of a main tee and two cross tees connected through the main tee slot (Figure 2-7).

The tensile tests on grid members were standardized by AS/NZS 2785 (2000). However, there is no standard suggesting methods for testing connections, which are suspected to be the weakest part of the ceiling system. Also, there is no specific test standard for compression. In this case the design of the experiment is very important as the test configuration can easily

affect the results. Therefore, a rig was constructed (Figure 2-7a) for compression tests which not only maintained the joint position during the test, but also allowed for the compressive action to take place without restraining the system too greatly, as this would potentially give higher values.

During the tensile loading, the main tee in the specimen needs to remain horizontal. This replicates the real condition in an as-built ceiling system, where ceiling tiles provide in-plane stiffness to the grids modules. If the main tee is not supported horizontally, the rotation in the joint could result in early failure.

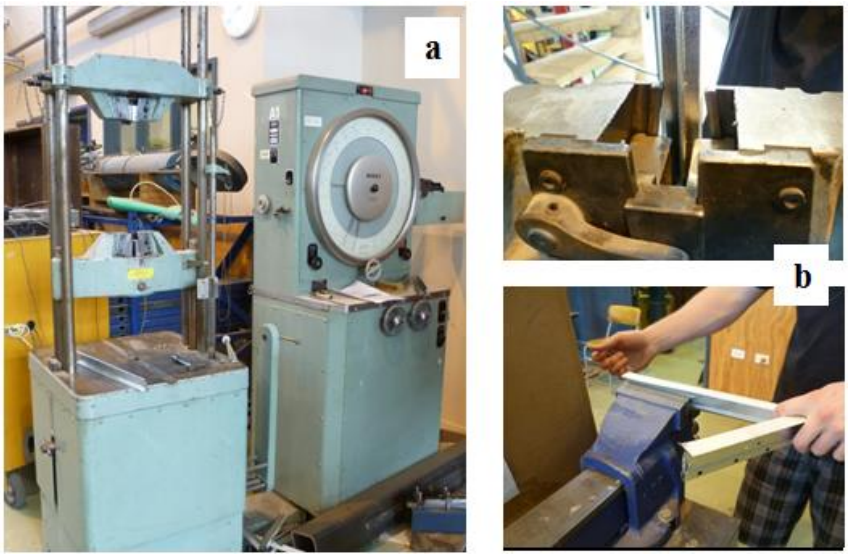

Figure 2-6 – (a) Test apparatus and (b) preparation of specimens

The rig consisted of a piece of laminated veneer lumber, with a thickness of 15 mm. Eight 50 mm × 50 mm × 2.5 mm steel angles of 50 mm length were screwed to the surface of the lumber as shown in Figure 2-7a. The angles kept the main tee in the horizontal position while the vertically positioned cross tees were being loaded by the machine. The angles simulated the effect of ceiling tiles, as they help with the orthogonality of fully installed ceiling systems.

Cross tee connections were also tested in shear. This loading condition was created using an in-plane force which simulated the effect of tile pressure and impact on the connection. For this purpose, a different rig was created which consisted of two steel members fixed to the testing machine and accommodating two cross tees in horizontal position. The main tee is placed perpendicular to the cross tees and pushed down (Figure 2-7c).

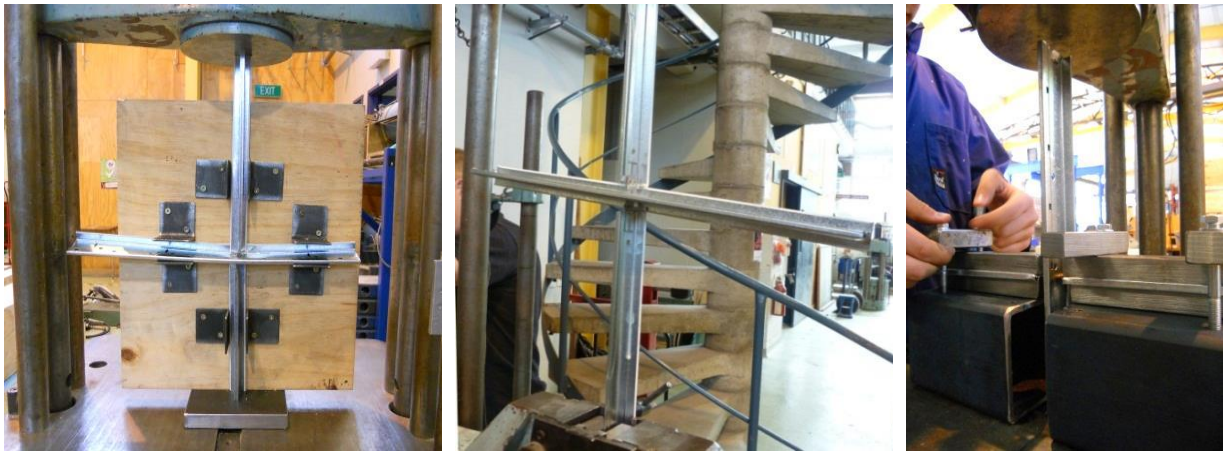

(a) (b) (c)

Figure 2-7 – Setup for (a) Compression, (b) Tension and (c) Shear test

No flexural tests were carried out on these specimens. According to Soroushian et al. (2015), bending tests on the as-built cross tee - main tee joints showed that these connections have almost no rotational strength and under bending their failure is abrupt and brittle. In a real setup, the combination of large vertical accelerations with heavy services/luminaries supported by the grids could result in large bending moments with the potential to cause flexural damage. However, this flexural response needs to be quantified in conjunction with axial loading, compressive forces in particular. In the absence of such experimental data, the effect of bending on the overall capacity of the system was ignored in this study.

2.3.1.2 Test specimens

The length of each specimen was approximately 600 mm, which is equal to the actual length of a short cross tee. This length was chosen to be as close as possible to the actual components dimension while satisfying the limits imposed by the test facility. Specimens were subjected to gradually increasing static load. Failure point was identified as the point when the applied force started decreasing.

A minimum of ten specimens of every component type from each manufacturer were tested to make sure that the obtained test results were enough to statistically interpret the strength of all components tested. For tests on tee to perimeter angle connections 3.2 mm aluminium rivets were used. The cross sections and locations of the components tested are shown in Figure 2-8 and Figure 2-9. Table 2-1 lists the components and number of specimens tested. The results from the component tests were used for derivation of fragility curves which showed each component's probability of failure for a given force value.

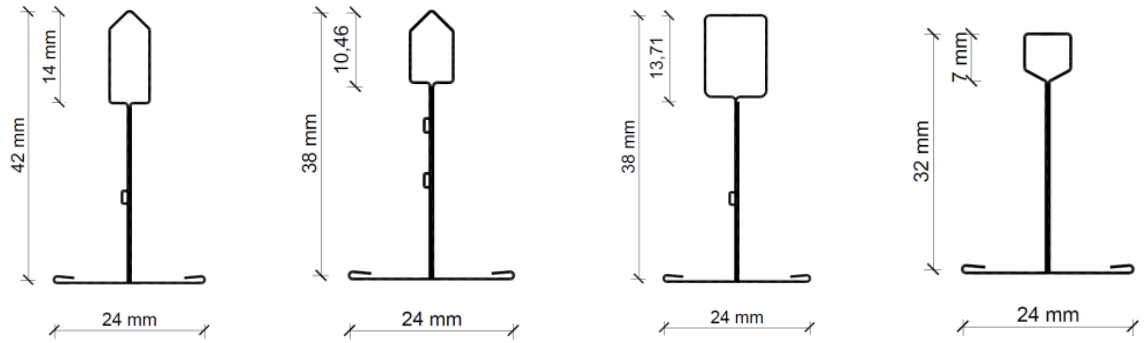

Type 1 Main tee Type 1 Cross tee Type 2 Main tee Type 2 Cross tee

Figure 2-8 – Cross section view of test specimens from two manufacturers

Table 2-1: Number of tests

No.	Component	Tension	Compression	Shear
1	Main tee member	10	10	-
2	Cross tee member	10	10	-
3	Main tee splice	10	10	-
4	Cross tee connection	10	10	10
5	Tee to perimeter angle rivet connection	40	-	-

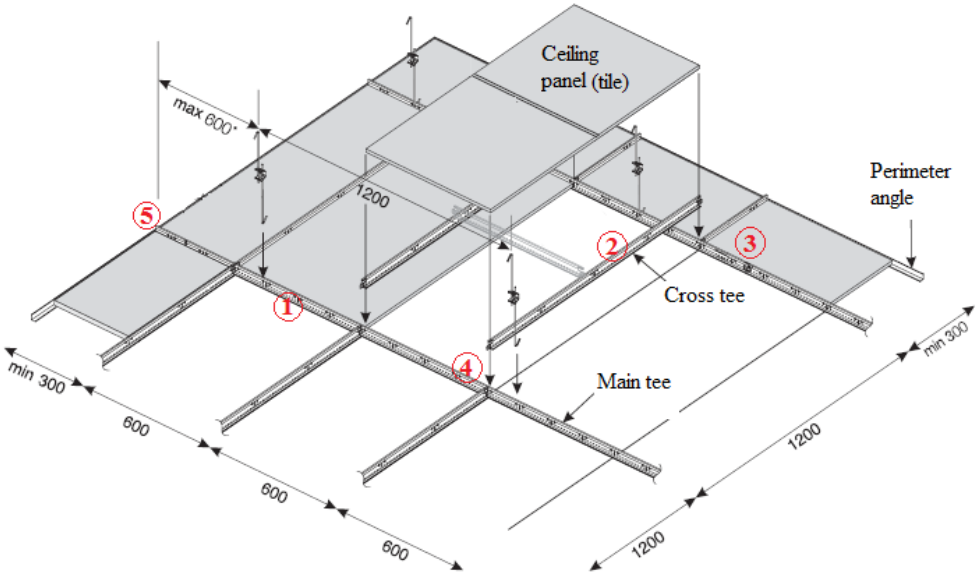

Figure 2-9 – Components tested

2.3.1.3 Simplified Analysis of a Suspended Ceiling System

Ceiling systems are acceleration sensitive NSEs, and consequently are designed for the peak acceleration they are subjected to. This acceleration differs from the one reaching the supporting structure both in intensity and characteristics and can be considered the response of the supporting structure to the ground motion. When the arriving strong ground motion

interacts with a structure, and propagates to the respective floors of the building, its frequency content and intensity are modified by the building response. These changes vary from structure to structure based on the building's dynamic properties (i.e. stiffness, mass and damping characteristics). Consequently, a ceiling system may be subjected to unique demands when installed in different structures, or even at different elevations or parts of the same building. Therefore, ceilings should be assessed and designed for peak floor acceleration (PFA) rather than peak ground acceleration (PGA).

New Zealand Standard NZS 1170.5 (2004) in section 8 introduces C_{Hi}, a floor height factor of up to 3, to be applied to the horizontal acceleration coefficient for NSEs supported at various elevations of a structure.

Analytical investigations by Singh et al. (2011) showed that the negligible addition of mass from suspended ceilings compared to the total structure mass does not alter the dynamic properties of the floor and the building noticeably. It was also concluded that the typical connection between ceilings and perimeter structure is rigid enough to assume the input acceleration to the ceiling was equal to the floor acceleration (Figure 2-10).

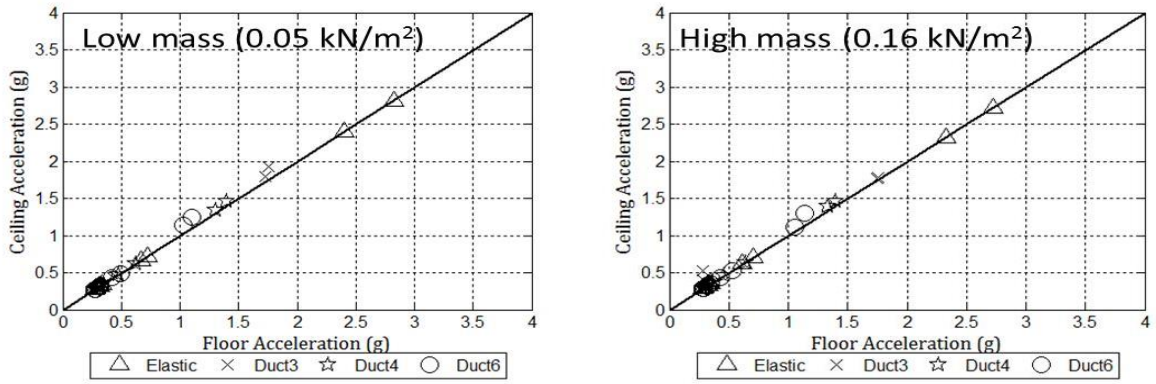

Figure 2-10 – Perimeter-fixed ceiling acceleration vs. floor acceleration for light and heavy ceiling (Singh et al., 2011)

The acceleration transferred to the level of ceiling is distributed among the ceiling components. As the ceiling, itself has an inherent flexibility, the peak acceleration induced in the various components of the system might vary from the PFA. New Zealand Standard NZS 1170.5 (2004) in section 8 recommends a spectral shape coefficient of 2 to be applied in the calculation of the horizontal acceleration coefficient for parts with a natural period of less than 0.75 s. Pourali et al. (2015) also showed that the acceleration recorded on various locations of the perimeter-fixed ceiling grid tested were up to 3.5 times larger than the PFA.

Since the method used in this study is based on the capacity of ceiling grid joints, the acceleration used as the intensity measure in all fragility curves derived are the peak ceiling grid acceleration (PCGA) which is expected to be larger than the PFA.

Figure 2-11 shows the perimeter connections between the suspended ceiling grids and walls. The ceiling grids are riveted to wall supports on two adjacent ends and floating on the opposite ends. According to common practice, proprietary clips are recommended on free ends which only allow the grids to slide along their longitudinal axis and are fixed to the wall in the other directions. This forms some fixity on the floating ends which is schematically shown in Figure 2-11b. In this paper, the effect of this partial fixity on the load path is overlooked and the load transfer is assumed direct and uninterrupted.

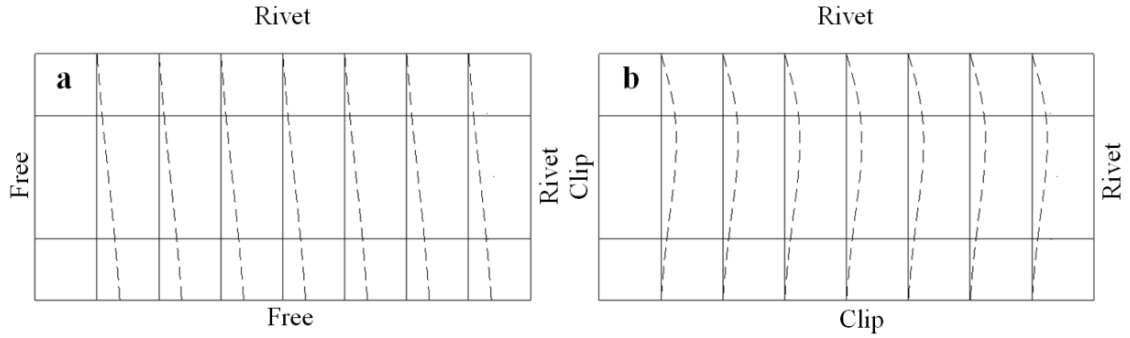

Figure 2-11 – Schematic view of grid end fixings

The seismic mass of the ceiling system is mainly associated with the ceiling tiles supported by the grids. It is assumed that these tiles perform like a rigid diaphragm and transfer the inertial force to the transverse tees as shown in Figure 2-12. In this figure, longitudinal tees are assumed in the direction of loading and transverse tees are perpendicular to them. The force induced in transverse tees is transferred to longitudinal tees through a shear force equal to ($m.S.l.a/2$), where m is the ceiling mass per unit area (kg/m^2), l is tile length in the direction of loading (m), S is tee spacing (m) and a is the PCGA (g). The longitudinal tee at each node is subjected to an axial force of ($m.S.l.a$). It is possible to consider connections between grid members pinned and therefore gradually sum up the inertial force from all tiles at the grid joints. The inertial force accumulated in end connection shown in Figure 2-12 can be expressed through Equation 2-1, where ($L=\Sigma l$) is the total tee length in the direction of loading (m).

$$F = m \cdot L \cdot S \cdot a \qquad \text{Equation 2-1}$$

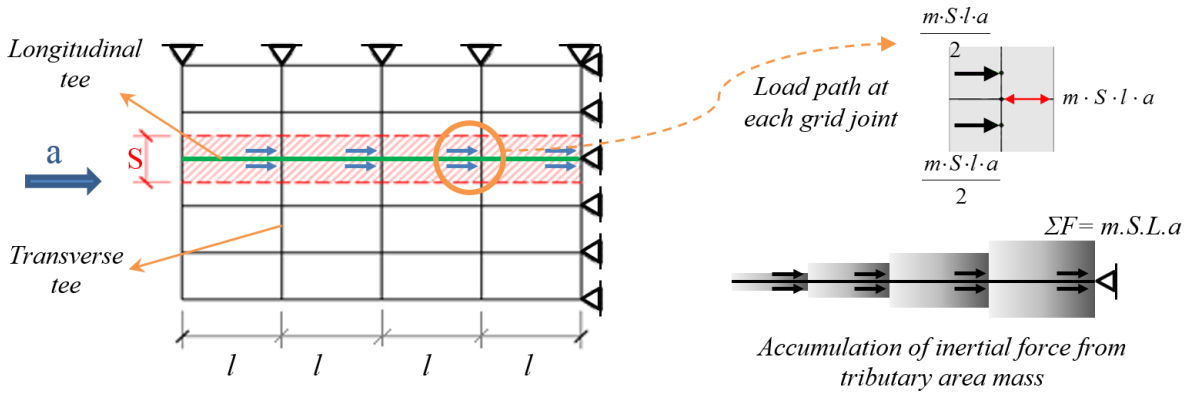

Figure 2-12 – Schematic of load path on perimeter-fixed ceiling

These axial forces (both in compression and tension) form the demand on the grids and their spliced connections. Consequently, any member of this force-transfer system with the lowest capacity undergoes yielding first and triggers failure. Therefore, the overall capacity of the ceiling system can be approximated by the capacity of the weakest element of the system. The results of component tests show that connections between the grid members undergo failure long before grid buckling occurs. Consequently, in this system, the buckling of the grids under compression has not been considered as a failure mode. Using these assumptions and the failure probability of components obtained through tests, fragility curves can be drawn for a perimeter-fixed ceiling of any given size and weight.

2.4 Results and discussion

2.4.1 *Ceiling Component Test Results*

In tension tests on grid members, the failure loads characteristically caused tearing of the thin walls of the sections at the position of reduced area where the slots for the insertion of cross tees or hanging wires are situated (Figure 2-13a). In case of main tee splices and cross tee connections, the failure happened in the connection clip and not the connected member itself (Figure 2-13b).

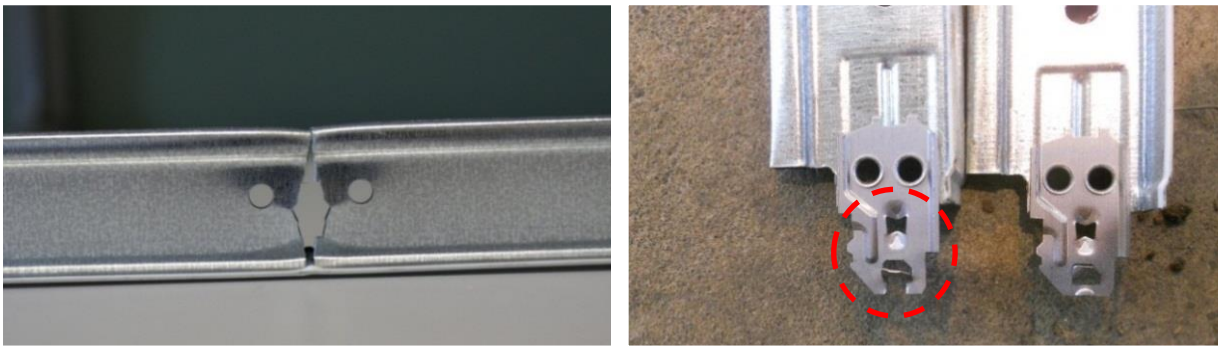

(a) (b)

Figure 2-13 – Failure modes in tension tests in (a) member; and (b) cross tee connection

In compression tests on members, failure mode was the local buckling of the member at the location of reduced cross section (Figure 2-14a). In compression tests on splices, the failure load was much lower than ones of the member tests and specimens all failed due to buckling, compression and deformation of splice connection. However, the failure loads of splices in compression were larger than the failure loads of splices in tensile tests. This was due to the different nature of the failure process under the two loading types. When under compression, before the two pieces of the splice connection came apart, there was a phase where the clips got crushed into each other. During this phase, the connection still carried load and failure only happened after excessive buckling which finally broke the splice (Figure 2-14b).

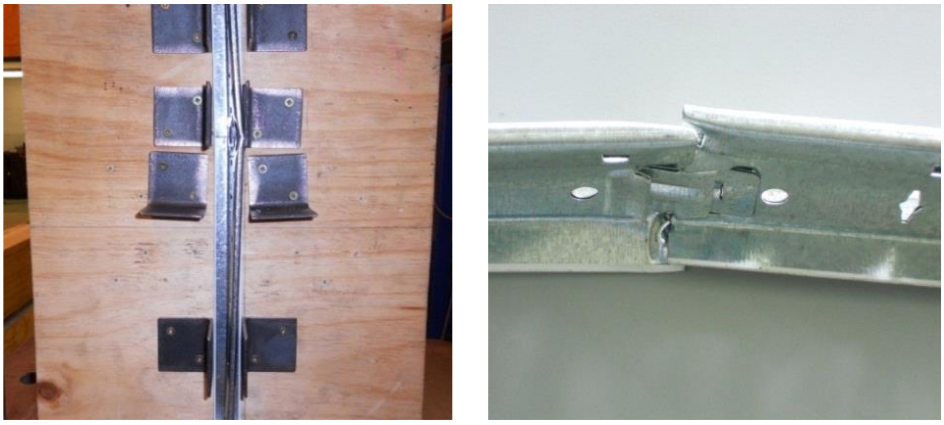

(a) (b)

Figure 2-14 – Failure in (a) main tee; and (b) splice in compression

Compression tests on cross tee connections showed that the failure mode was buckling and distortion of the clips (Figure 2-15a). The values of failure loads in compression tests on cross tees were less than those of tensile tests. This made cross tee connections in compression so far, the weakest member of the grid system. Results of shear tests on cross tee connections showed that failure occurred when the connection clips were pulled out by the main tee (Figure 2-15b).

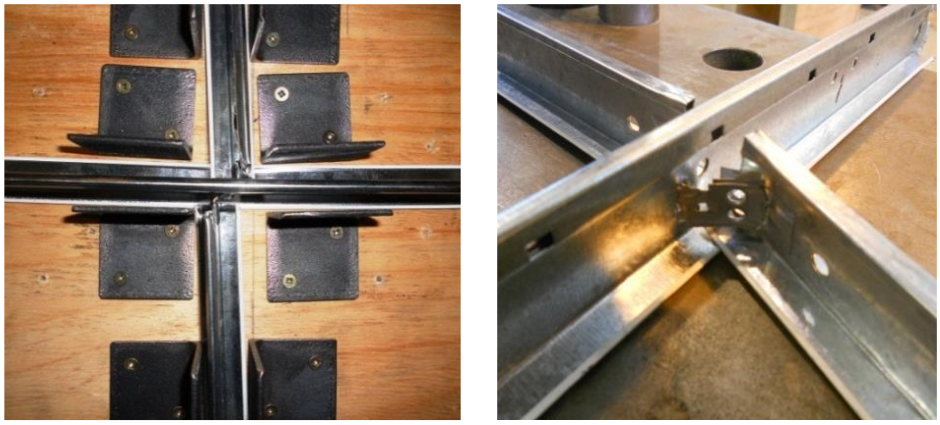

(a) (b)

Figure 2-15 – Failure in cross tee connection due to (a) compression; and (b) shear

Rivet tests were carried out using a variety of positions for the rivet. These configurations varied in the distance of the rivet from the free edge of the connected elements i.e. perimeter angle and tee. The failure force was lower in cases where rivets were inserted close to the free edge of the tees, leading to tearing of the tee flange. When the rivet insertion point was shifted to further in the centre, failure force increased and mode of failure changed to hole enlargement and rivet pull-out. The highest value of failure load was found in the configuration where rivets were inserted near the edge of the perimeter angle and far inside the tee flange. This configuration provided good resistance both to hole enlargement and flange tearing (Figure 2-16). The last configuration tested was for connections with double rivets. The capacity of these connections was larger than all previous rivet connections tested, as expected. Table 2-2 shows the values of median and standard deviation for components tested and described above. A quick comparison shows that cross tee connections and single rivets were the weakest components of the system.

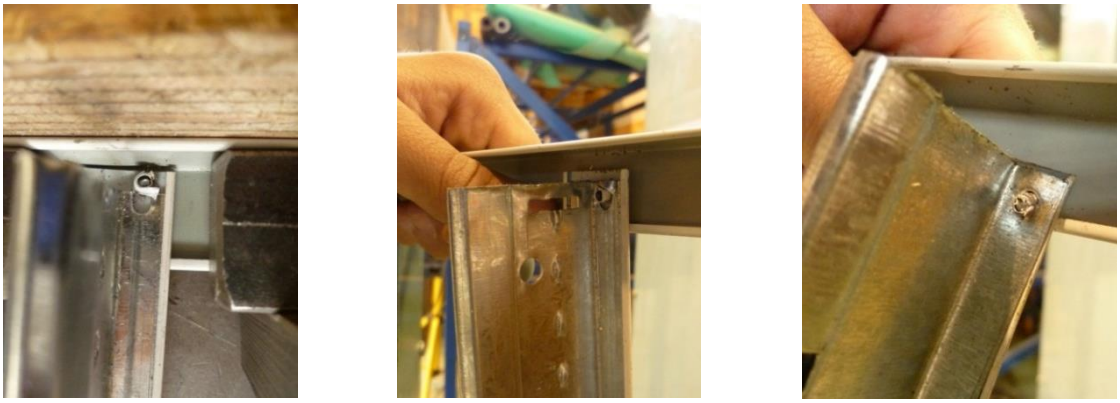

(a) (b) (c)

Figure 2-16 – Failure modes in (a) far; (b) centre; and (c) near edge positions

Table 2-2 – Component test results

Component Tested	Median Failure Force (kN)		Standard Deviation (kN)	
	Type 1	Type 2	Type 1	Type 2
Main T in Compression	3.86	3.47	0.15	0.13
Main T in Tension	9.4	8.35	0.11	0.10
Cross T in Compression	2.61	2.92	0.14	0.23
Cross T in Tension	8.55	8.15	0.18	0.08
Cross T Connection in Compression	0.73	0.86	0.10	0.11
Cross T Connection in Tension	1.04	1.29	0.27	0.37
Main T Splice in Compression	2.11	2.42	0.12	0.09
Main T Splice in Tension	1.09	1.02	0.07	0.05
Cross T Connection in Shear	1.00	0.80	0.11	0.15
Single 3.2mm Rivet – Far	0.69	0.77	0.06	0.04
Single 3.2mm Rivet – Centre	0.75	0.88	0.05	0.07
Single 3.2mm Rivet – Near Edge	0.97	0.97	0.09	0.06
Double 3.2mm Rivets	1.51	1.52	0.11	0.19

2.4.2 *Fragility Curves for Ceiling Components*

The conditional probability of reaching or exceeding a damage state is given by

$$P_{Lik} = P\,[D \geq d_{Li} \mid Y = y_k] \qquad \text{Equation 2-2}$$

where P_{Lik} is the probability of damage reaching or exceeding damage limit state d_{Li} given that the excitation is y_k; D is a damage random variable defined on damage state vector $D=\{d_0, d_1, \ldots, d_n\}$; and Y is an excitation random variable (Badillo-Almaraz et al. (2007)).

Following the completion of tests, values of median and standard deviation for each component (Table 2-2) were used to derive a cumulative distribution of failure loads. Both normal and lognormal distributions were derived for each component. To compare the appropriateness of the theoretical distribution functions, Kolmogorov-Smirnov (K-S) goodness-of-fit (GOF) tests were carried out. The K-S statistic ($D_{n,max}$) for the normal and lognormal distribution functions are reported in Figure 2-17 for comparison. In most cases, both distributions fit the data with similar error. In few cases which showed some difference, lognormal distribution was found to be a better fit. Therefore, for consistency lognormal distribution was used for all component fragility curves.

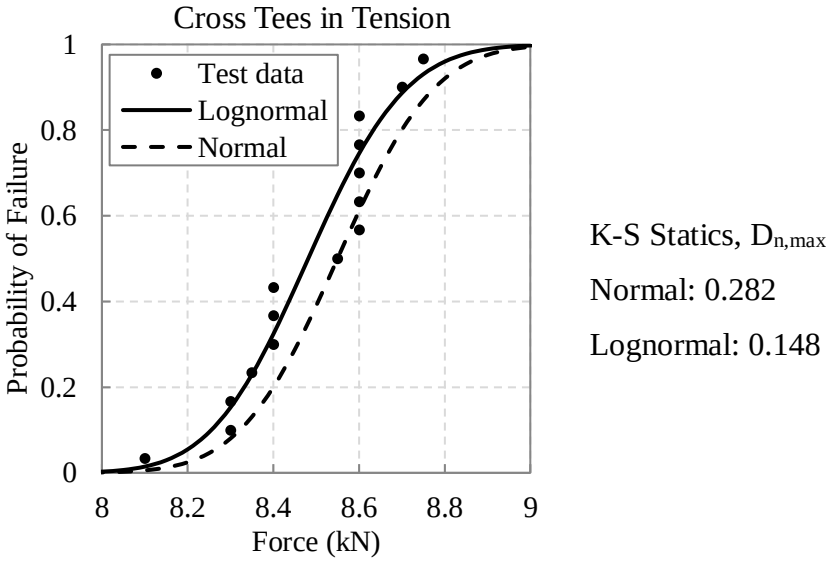

Figure 2-17 – Fitted data vs. normal and lognormal distributions

Figure 2-18 shows the fragility curves for all components tested under tension. Based on this figure, cross tee connections (shown as CT-con) were the weakest elements when under tension.

Comparing fragility curves of components tested under compression showed that i) cross tee

connections were the weakest components under compression; and ii) capacity of components in general was lower under compression than tension except for main tee splices which were discussed in the previous section. Fragility curves for components tested under compression can be found in Figure 2-19.

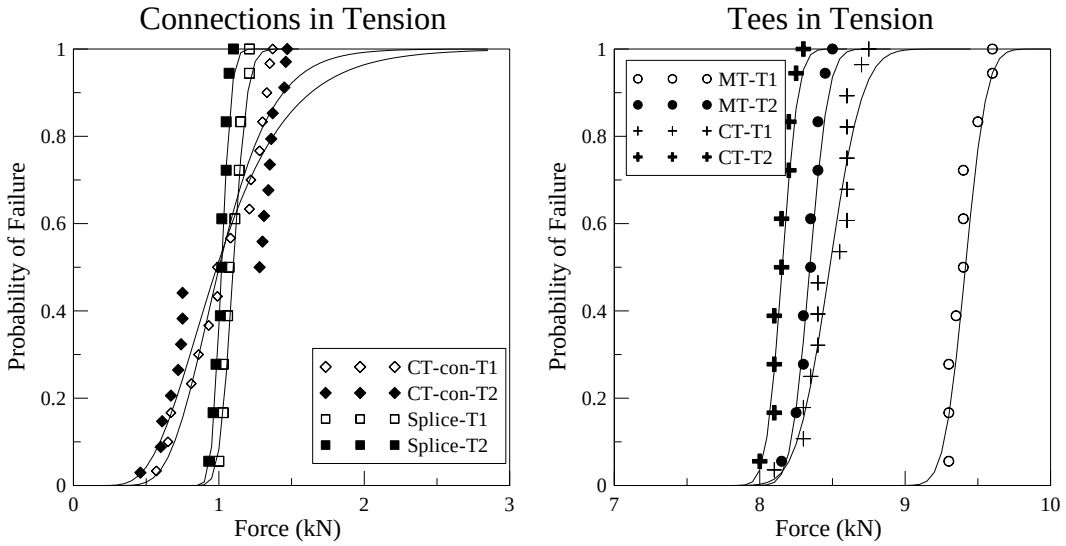

Figure 2-18 – Fragility curves for tension tests in (a) connections; and (b) tees

Perimeter fixed suspended ceilings are connected to the surrounding walls on two adjacent sides via pop rivets. This type of rivets due to its financial and application advantages is most commonly used for fixing the ceiling grid to the perimeter angles. The capacity of various configurations of single and double 3.2 mm aluminium rivet connections under tensile loads (which causes shear in the rivet) were evaluated. As expected, using double rivets instead of one improved the capacity of the fixing. Figure 2-19 shows the fragility curves for 3.2 mm single and double rivets. The single rivets in this figure were in the centre position. Note that the following abbreviations have been used in Figure 2-18 to Figure 2-20: CT: cross tee, MT: main tee, con: connection, 3.2R: 3.2mm Rivet, T1: Type 1 and T2: Type 2.

The general trend in all tests as per Figure 2-18 and Figure 2-19 showed that both under compression and tension, connections failed before the members, making connections the weakest link in the overall capacity chain. In the case of cross tee connections and main tee splices, failure occurred due to the breakage of small fasteners in the joint and in few cases the rivets connecting the joint clip to the member. This means although the tee section performance was satisfactory according to code requirements, the overall system was

exposed to failure at demands much lower than the members' capacity due to the weak performance of the connections.

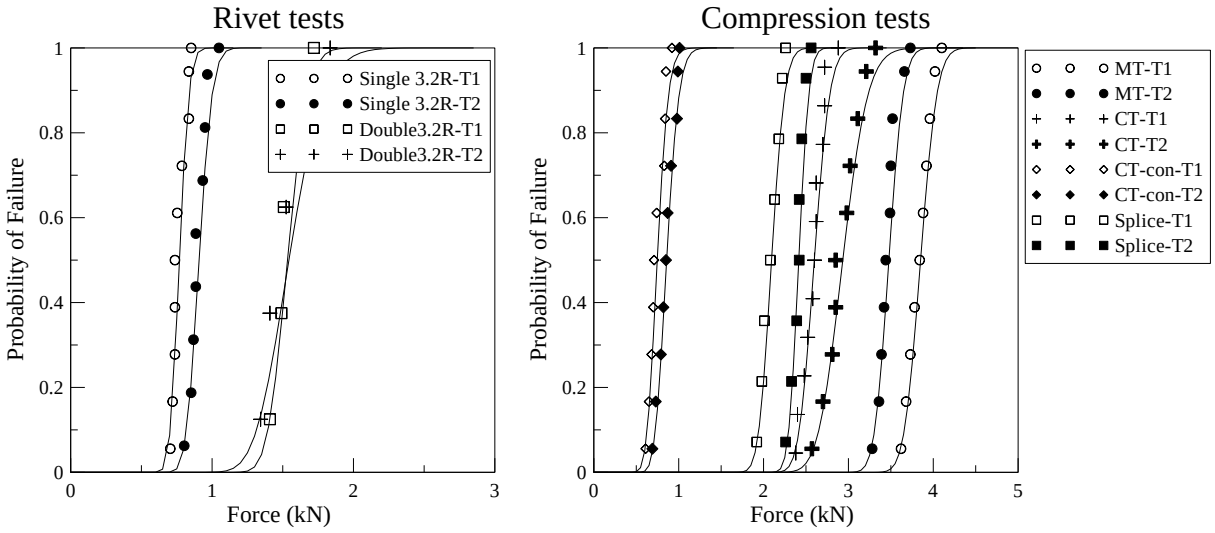

Figure 2-19 – Fragility curves for (a) rivet; and (b) compression tests.

Based on the values of median and standard deviation presented in Table 2-2 and fragility curves derived in this section, the capacities of components tested can be compared. It can then be concluded that single rivet connections, cross tee connections under compression, main tee splices under tension, cross tee connections under tension and double rivet connections were the more critical components of the system and may dictate the overall capacity of the ceiling system.

2.4.3 *Fragility Curves for Ceiling System*

Currently, most residential and commercial suspended ceilings in New Zealand are categorised under serviceability limit state and are therefore designed for a low level of demand. However, the extensive damage suffered by suspended ceilings in recent New Zealand earthquakes (Dhakal, 2010; Dhakal et al., 2011) proves the need for reconsiderations in the assignment of limit state and risk factor applied in the design of these NSEs.

For designing a ceiling, knowing the weight of the ceiling chosen, the horizontal design action can be calculated. This horizontal action is a factor of

i. ceiling total weight (W_p),
ii. horizontal acceleration coefficient ($C_p(T_p)$) described in previous sections of this paper,

iii. the part horizontal response factor (C_{ph}) which is equal to 1 for ceilings with a ductility of 1, and
iv. part risk factor (R_p) which based on the importance of the building or room the ceiling is installed in, can vary between 0.9 and 2.

The dimensions of the appropriate ceiling for each case are determined based on the allowable capacity of the grid system. According to ASTM E580 (2011), "only heavy-duty main tees can be used in areas of seismic category D-F i.e. high seismic risk. The main tees and cross tees of the ceiling system and their splices, intersection connectors, and expansion devices shall be designed and constructed to carry a mean ultimate test load of not less than 180 lb [0.8 kN] in compression and in tension. The connectors at splices and intersections shall be the mechanical interlocking type." This is almost in agreement with the test results presented in Table 2-2 as the weakest components of the ceiling system -cross tee to main tee connections- have a median capacity of 0.73 kN and 0.86 kN for the two manufacturers.

In this section, fragility of a perimeter-fixed ceiling with ceiling grid acceleration as the intensity measure is developed using the components fragility curves from the previous section and considering that the ceiling system is as strong as its weakest component. The analysis presented herein uses perimeter fixed ceilings without any vertical struts and/or diagonal bracing, which are very common in NZ as bracing is not required for ceilings of small to moderate size. Also, the fragility analysis presented in the paper does not account for vertical acceleration effect and falling of tiles due to distortion (before mechanical failure) of ceiling grid members and connections.

The ceiling example was assumed to be located in an area of relatively high seismicity risk (seismic zone factor Z = 0.3) and on various levels of a 5-story commercial building having an importance level of 2. According to proprietary guideline requirements (USG, 2012; Armstrong, 2013), individual ceiling tiles must not weigh more than 10 kg. Seismic weight used in the design of the ceiling must also include the grid mass (1 kg/m^2) and a minimum service load of 3 kg/m^2. Assuming the size of tiles as 1200 mm × 600 mm and each weighing 10 kg, in the worst case the seismic mass of the ceiling will be:

$$(10 \text{ kg} / 0.72 \text{ m}^2) + 3 \text{ kg/m}^2 + 1 \text{ kg/m}^2 = 17.9 \text{ kg/m}^2 \qquad \text{Equation 2-3}$$

The total seismic mass of the ceiling for the design was therefore assumed 17.9 kg/m^2. This mass was used to design ceilings based on the recommendations of ceiling manufacturers (USG, 2012; Armstrong, 2013). One example of the designed ceilings on the forth level was

4.1 m × 7.1 m with main tees in the shorter direction and single 3.2 mm Aluminium rivets connecting the tees to wall angles on two adjacent sides. Fragility curves were derived based on three most vulnerable components: single rivets, cross tee connections in compression and main tee splices in tension. For any given grid acceleration, the seismic force on the longer dimension of the ceiling is calculated using the assumed seismic mass and Equation 2-1. The probability of failure of the weakest component in that direction - e.g. cross tee in compression - is derived for the associated seismic force from the fragility curve in Figure 2-19. This probability of failure will be assigned to the grid acceleration considered. After considering all weak components, an envelope curve is drawn on the furthest left end of the group of fragility curves. This envelope represents the system capacity of the perimeter-fixed ceiling being considered (Figure 2-20).

The horizontal design coefficient on level four was determined for both SLS with a 25-year return period and an ULS event with a 500-year return period (structural design level). The probability of failure of the designed ceiling was evaluated for both limit states (Figure 2-20). AS it can be observed in the fragility curves, the designed system on level 4 performs satisfactorily when subject to a serviceability level acceleration (probability of failure ~5%). However, when compared with the ultimate level excitation demand, the probability of failure is 100%, i.e. failure is inevitable.

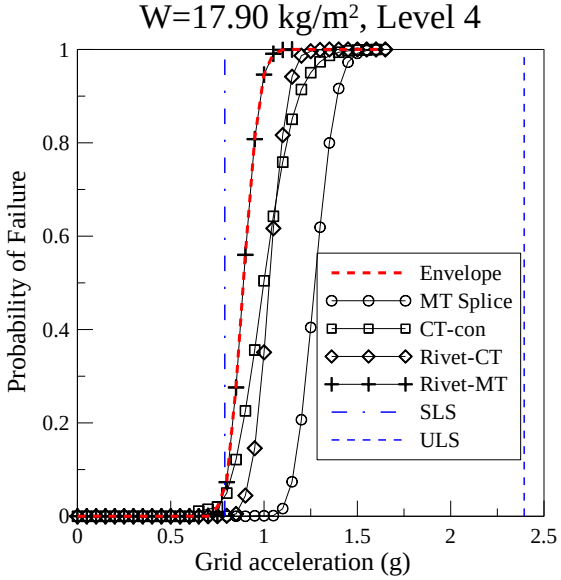

Figure 2-20 – Fragility curves for the designed ceiling on Level four

Notations: CT-con: Cross tee connection, MT: Main tee, Rivet-CT: Rivet on cross tee, Rivet-MT: Rivet on main tee SLS: Serviceability limit state, ULS: Ultimate limit state.

2.4.4 *Effect of Ceiling Area and Tile Weight*

Based on Equation 2-1, the force induced in a grid member increases as the grid expands in length. Also, heavier tiles lead to greater demand on the ceiling grid. The effect of these factors is shown in fragility curves in this section.

To investigate the effect of area, three ceilings were designed with the same seismic mass of 17.9 kg/m^2 but having three different seismic demands basically due to the difference in height of the floor supporting the designed ceiling. Ceilings consequently vary in size but all are within the 93 m^2 area limit of perimeter-fixed ceiling without seismic bracing (Figure 2-21). The design of the ceilings is carried out according to the guidelines provided by the ceiling manufacturer. Details of the seismic demand also calculated based on NZS 1170.5 (2004) are provided below. These seismic demands showed a close proximity to the demand calculated based on the recommendations of the manufacturer's guideline.

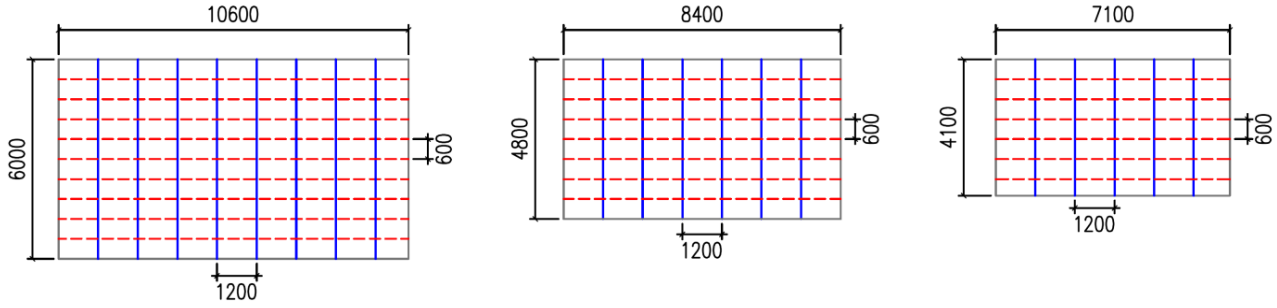

Figure 2-21 – Ceiling schematic, main tees in bold and cross tees in dashed line

Seismic demand on ceiling type A, located in Christchurch (Seismic zone factor, Z = 0.3 & Near-fault factor, $N(T,D)$ =1) on soil type C (Spectral shape factor at zero second period, $C_h(0)$ = 1.33)), for SLS (Return period factor, R = 0.33, on the second floor (Floor height coefficient, C_{Hi} = 2):

$$C(0) = C_h(0) \cdot Z \cdot R \cdot N(T,D) = 1.33 \times 0.3 \times 0.33 \times 1 = 0.132 \quad \text{Equation 2-4}$$

$$C_p(T_p) = C(0) \cdot C_{Hi} \cdot C_i(T_p) = 0.132 \times 2 \times 2 = 0.527 \quad \text{Equation 2-5}$$

$$F_{ph} = C_p(T_p) \cdot C_{ph} \cdot R_p \cdot W_p = 0.527 \times 1 \times 1 \times 17.9 = F_{ph} = 9.43 kg/m^2 \quad \text{Equation 2-6}$$

Where $C_p(T_p)$ is horizontal acceleration coefficient, $C(0)$ is the elastic site spectra at zero second period, $C_i(T_p)$ is the part spectral shape coefficient, W_p is the part seismic weight, C_{ph} is part response factor, R_p is part risk factor and F_{ph} is the horizontal seismic design action.

Using the demand above and the capacity of ceiling components: Main tee length = 6,000 mm, cross tee length = 10,600 mm.

Seismic demand on ceiling type A with same location and return period properties but on the third floor (C_{Hi} = 2.5):

$$F_{ph} = C_p(T_p) \cdot C_{ph} \cdot R_p \cdot W_p = 0.658 \times 1 \times 1 \times 17.9 = \\ F_{ph} = 11.78 kg/m^2$$

Equation 2-7

Using the demand above and the capacity of ceiling components: Main tee length = 4,800 mm, cross tee length = 8,400 mm.

Seismic demand on ceiling type A with same location and return period properties but on the forth and higher floors (C_{Hi} = 3):

$$F_{ph} = C_p(T_p) \cdot C_{ph} \cdot R_p \cdot W_p = 0.79 \times 1 \times 1 \times 17.9 = \\ F_{ph} = 14.14 kg/m^2$$

Equation 2-8

Using the demand above and the capacity of ceiling components: Main tee length = 4,100 mm, cross tee length = 7,100 mm.

Based on the length of the tees and the seismic demand on ceiling components, fragility curves were derived for each of the ceilings shown in Figure 2-21. The fragility curves shown in Figure 2-22a are the envelope curve of the most critical components identified through testing, i.e. single 3.2 mm rivets, cross tee connections in compression and main tee splices in tension.

In order to investigate the effect of ceiling weight, ceilings were then designed assuming three different seismic mass values; Light: 5.5 kg/m^2; Average: 9.5 kg/m^2 compared with the previously mentioned; Heavy: 17.9 kg/m^2 example. These ceilings are all assumed to have the same area of 7.1 m × 4.1 m and are located in similar conditions. Figure 2-22b shows the fragility curves associated with these ceilings.

As it can be observed in Figure 2-22, the demand on a ceiling is proportional to its size and weight. Using lighter tiles can increase the failure acceleration demand as much as 3 times. Ceilings of a relatively small size (29.1 m^2) but supporting heavy tiles (17.9 kg/m^2) show 50% chance of failure at a horizontal grid acceleration of about 0.9 g. The same ceiling with light tiles (5.5 kg/m^2) instead has median failure probability at 2.9 g.

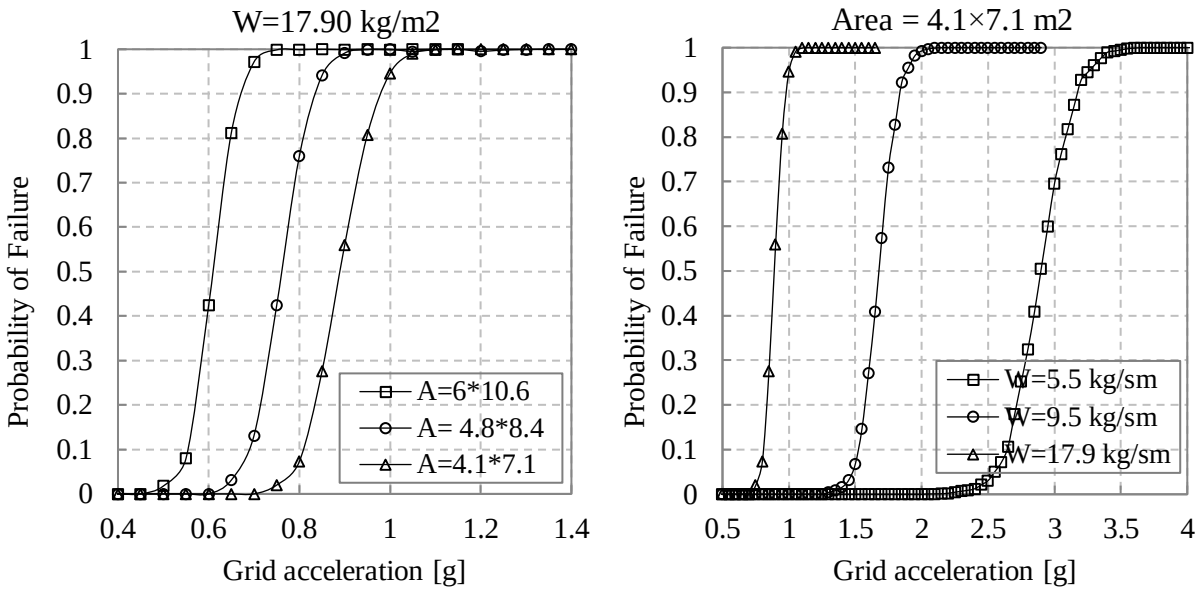

(a) (b)

Figure 2-22 – Fragility curves for ceilings with different (a) areas; and (b) weights

Table 2-3 provides the values of horizontal acceleration coefficient $C_p(T_p)$ for serviceability and ultimate limit states at different levels in an example building in Christchurch based on the amendments to New Zealand code (NZS 1170.5:2004) described in detail earlier in this section. Note that the SLS return period factor has been raised to 0.33 based on the new draft of the aforementioned code.

Table 2-3 – Horizontal acceleration coefficient

Floor Level	SLS (25yrp*) $Z=0.3$ $R_s=0.33$ $C_i(T_p)=2$ $N(D,T)=1$ $C_h(0)=1.33$	ULS (500yrp) $Z=0.3$ $R_u=1$ $C_i(T_p)=2$ $N(D,T)=1$ $C_h(0)=1.33$
2 ($C_{hi}=2$)	0.527	1.596
3 ($C_{hi}=2.5$)	0.628	1.995
4 & higher ($C_{hi}=3$)	0.790	2.394

** yrp: year return period*

The 4.1 × 7.1 m^2 perimeter-fixed ceiling with heavy tiles, if for instance is installed on the second floor of a building in Christchurch on a location with soil type C, will probably sustain some damage in an ultimate limit state seismic event (structural design earthquake). That is because the horizontal acceleration coefficient C_pT_p at the second level of the supporting structure is 1.596 which according to Figure 2-22b will have a 100% probability of failure. Using average weight tiles (9.5 kg/m^2) on the same ceiling area should decrease

the probability of failure to about 25% and the ceiling with very light tiles is expected to not sustain any damage.

When subject to serviceability level demand, all three ceilings with very light, average and heavy tiles are expected to perform satisfactorily. Only in ceilings with heavy tiles on the fourth or higher floor levels a 5% probability of failure is observed in fragility curves.

A larger area has similar effect on the overall demand on the perimeter-fixed ceiling. Figure 2-22a shows the probability of failure in ceilings with heavy tiles and different areas. All three ceilings undergo 100% failure when subject to ultimate limit state level event. With 6 × 10.6 m^2 area on the first or second floors, the ceiling has less than 10% probability of failure at serviceability level event. The probability of failure is almost similar for ceilings with areas 4.8 × 8.4 m^2 and 4.1 × 7.1 m^2 designed to be located on the 3rd and 4th floors, respectively.

Considering a variety of ceiling weights and dimensions and using envelope fragility curves, graphs presented in Figure 2-23 and Figure 2-24 show the correlation between ceiling size and weight and the peak ceiling grid acceleration. These graphs have been derived based on the component tests presented in this study and apply to perimeter-fixed ceilings of the same properties (refer to Methodology section for size of rivets, cross tees and main tees). The graphs presented in Figure 2-23 have been created using the median capacity of the weakest element of the load path in a ceiling, while graphs in Figure 2-24 use the 5th and 16th percentile failure values. In each figure two sets of graphs have been presented; for main tees and cross tees. This is due to the difference in grid spacing. Main tees are installed at 1200 mm spacing and cross tees at 600 mm intervals. Therefore, their tributary areas and the inertial force carried are different. According to Figure 2-23, for instance, if the ceiling grid acceleration at the desired level of structure is 1 g, main tees can be between 3.6 m to 12 m based on the weight of the ceiling. Cross tees similarly can expand across a length of 7.1 m to about 12 m or more.

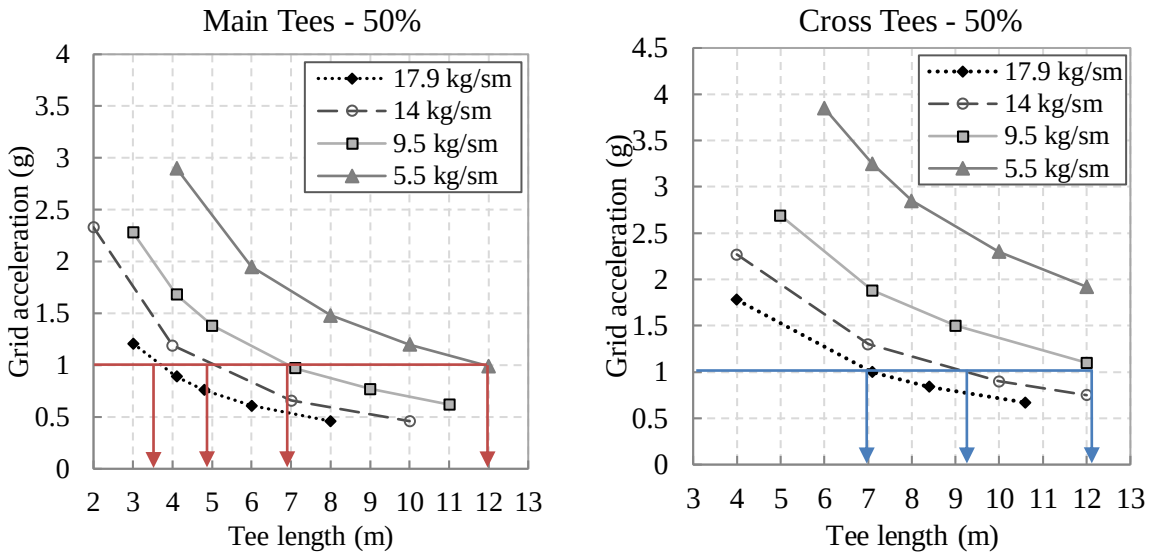

Figure 2-23 – Correlations among grid length, ceiling weight and allowable acceleration using median probability of failure

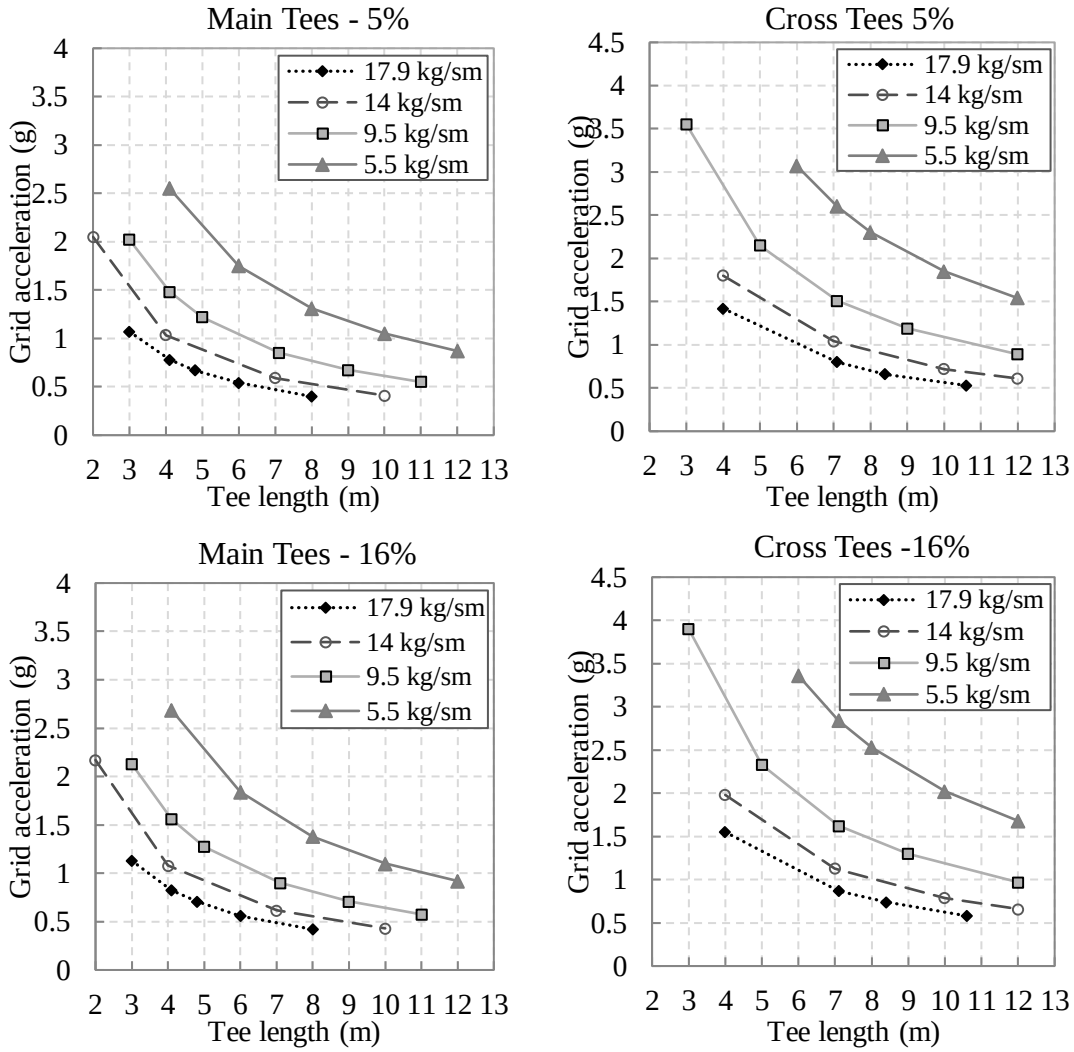

Figure 2-24 – Correlations among grid length, ceiling weight and allowable acceleration using 5% and 16% probability of failure

Graphs and fragility curves shown in this study emphasise the importance of grid length and weight of the ceiling tiles or any other devices supported by the suspension system in finalising the capacity of the perimeter-fixed ceiling system. Therefore, the limit of 93 m^2 area for the requirement of back bracing seems insufficient. A ceiling may be perfectly within this area limit but the length of the grid members may exceed the allowable limit. Similarly, a combination of small length but heavy tiles may lead to large demands which are beyond the system capacity. It seems more advisable to set the requirements of seismic bracing based on the capacity of components and therefore, the allowable combination of grid length and weight rather than area alone.

It is worthwhile to mention that the above observations are merely for the purpose of study. Ceilings currently designed based on the manufacturers' guidelines and New Zealand codes are proportioned in size and weight such that a serviceability level event does not induce damage. According to current practice in New Zealand as reported by manufacturers (USG, 2011; Armstrong, 2013), when ceilings are exposed to high seismic demand or covering large areas of high financial or vital importance, bracing to the above structure is mostly applied as the seismic solution.

2.4.5 *Comparing the Proposed Analytical Method with Existing Experimental Data*

In order to evaluate the validity of the proposed simple method of estimating ceiling fragility described in previous sections, comparisons have been made with experimental results from Badillo-Almaraz et al. (2007) and Ryu et al. (2013). Both of these experiments were carried out on a similar grid system to what has been tested in this paper. Due to limits of the available experimental data, the following conditions need to be considered in this comparison:

(i) Ceilings in Badillo-Almaraz et al. (2007) were fixed on two sides via aluminium rivets. On the other hand, the ceilings tested by Ryu et al. (2013) used seismic clips which have slightly less capacity compared to rivets (Armstrong 2013).

(ii) The ceiling tested by Badillo-Almaraz et al. (2007) was also back braced to the frame roof which makes it stiffer compared to the perimeter-fixed ceiling used for this proposed analytical method.

(iii) Although Ryu et al. (2013) reported the recorded peak ceiling grid accelerations (PCGA) associated with the commencement of two damage states considered, Badillo-Almaraz et al. (2007) provide fragility curves with PFA as the intensity measure. The proposed analytical method in this paper is based on PCGA. To overcome this

discrepancy, a simplifying assumption has been made; the values of PFA are amplified by a factor of 3 to obtain the PCGA. This amplification factor is based on the observations made by Ryu et al. (2013) and Pourali et al. (2015).

(iv) The fragility curves available in Badillo-Almaraz et al. (2007) are for ceilings with undersized tiles. Use of undersized tiles decreases the resilience of the ceiling. However, the threshold PFA for grid failure damage state was the same for undersized and normal-sized ceiling specimen.

(v) In the proposed method, the capacity of the ceiling is estimated only under horizontal excitation as opposed to 3D in Ryu et al. (2013) and 2D in Badillo-Almaraz et al. (2007). The effect of bidirectional and vertical motions has not been considered.

Using the tile weight and dimensions of the ceilings tested by Ryu et al. (2013) and Badillo-Almaraz et al. (2007) (Figure 2-25) and components fragility curves in earlier sections, ceiling fragility curves are derived based on the simplified method presented in this paper. Values of acceleration at the onset of repairable damage and collapse based on Ryu et al. (2013) are shown in Table 2-4.

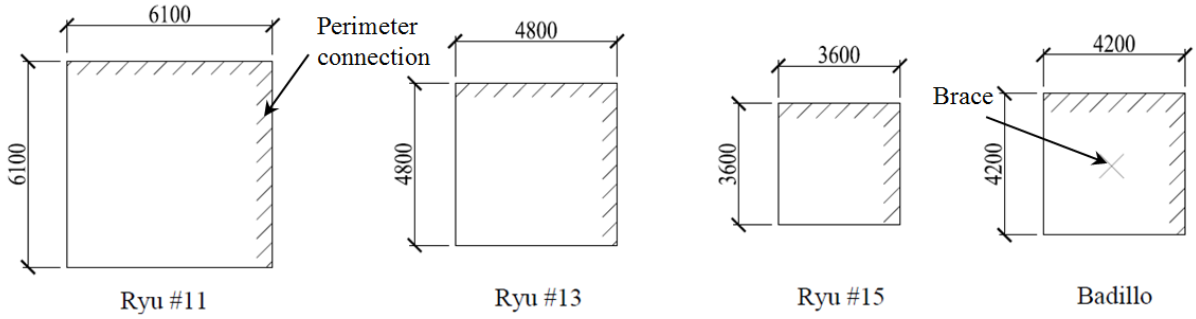

Figure 2-25 – Specimens used in comparison (Badillo-Almaraz et al., 2007; Ryu et al., 2013)

Table 2-4 – Acceleration levels at the onset of repairable damage and collapse in tests (Ryu et al., 2013)

Ceiling Dimension	Damage State	Onset of Repairable Damage*		Onset of Collapse**	
	Assembly	PFA (g)	PCGA*** (g)	PFA (g)	PCGA*** (g)
6 m × 6 m	#11	-	-	1.54	3.48
6 m × 6 m	#12	1.76	3.57	2.02	3.75
4.8 m × 4.8 m	#13	-	-	1.99	3.72
4.8 m × 4.8 m	#14	1.65	3.22	1.95	3.57
3.6 m × 3.6 m	#15	2.66	5.32	2.65	5.59

** Repairable damage: "minor dislocations of tiles or grids in isolated places of ceiling without losing stability and the support of the rest of the ceiling." This damage may require*

*** Collapse: loss of grid and tiles requiring complete replacement of the ceiling. This state is defined as the failure of 10% of the total number of girds or tiles (Ryu et al., 2013).*

**** PCGA: Peak ceiling grid acceleration*

In Table 2-4 assemblies #12 and #14 have only been included for comparison with #11 and #13. These assemblies were similar to #11 and #13 respectively with the exception of back bracing added. The perimeter connections were also rivets instead of seismic clips.

Figure 2-26a shows the experimental fragility curves obtained from Badillo-Almaraz et al. (2007) tests plotted after converting the peak floor acceleration (PFA) to ceiling grid acceleration (PCGA). The experimental fragility curves corresponding to two different damage stated monitored in the tests are compared with an analytical fragility curve derived for a perimeter-fixed ceiling of the same size and weight. As can be noticed in the figure, the analytical fragility curve is in better agreement with the experimental grid failure fragility. This is expected as the analytical procedure considers the failure of any grid member (and connections) as the damage state.

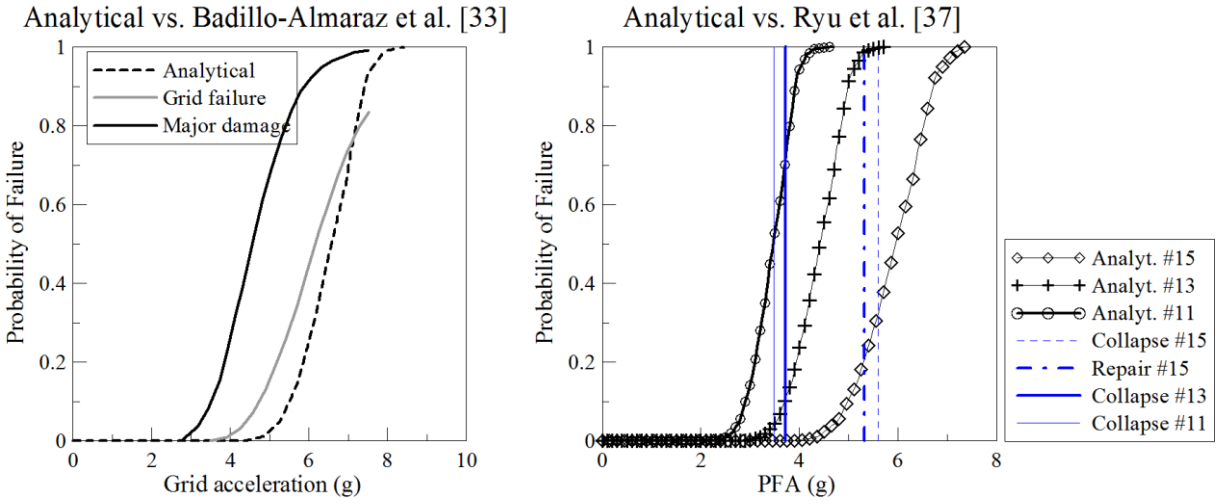

(a) (b)

Figure 2-26 – Comparison between experimental (Badillo-Almaraz et al., 2007; Ryu et al., 2013) and proposed analytical fragility curves

Figure 2-26b shows the proposed analytical fragility curves associated with three test specimens in Ryu et al. (2013) along with grid accelerations at the onset of repair or collapse. In all three specimens, the experimentally obtained ceiling grid acceleration capacity lies within the range covered by the analytical fragility curves. In assembly #11, which is the largest of the three, the peak grid acceleration at the onset of collapse is associated with 50% probability of failure in the proposed fragility curve. In assembly #13 the onset of collapse happens at the PCGA corresponding to 10% failure probability in the analytical fragility curve. In assembly #15 the PCGA at the onset of repair and collapse are associated with 20% and 32% probability of failure, respectively. Considering all the simplifications and

assumptions mentioned above, the analytical fragility curve provides a relatively good estimation of the experimental results. Given that failure or damage in suspended ceilings depends on the type of suspension system used, size and weight of the particular ceiling, it is unlikely that relevant experimental reference can be found for the design of each particular ceiling. Therefore, this initial estimate can be useful in the preliminary prediction of probable loss in perimeter-fixed ceilings.

2.5 Conclusions

A study was conducted on typical suspended ceilings in NZ. The following conclusions have been drawn from this study:

1. Standards exist for loading, design and installation of suspended ceilings or related non-structural elements. However, since most ceilings are proprietary systems, reliance is made on the ceiling manufacturers to ensure that these conditions are satisfied.

2. Significant damage has been observed in suspended ceilings in past earthquakes in NZ and oversees. Damage types include: i) dislodging and breaking of the tiles, ii) failure of the ceiling grid members and connections, iii) grid spreading, iv) failure of perimeter tiles v) perimeter damage due to failure of grids or end fixings in compression to rigid walls or columns, vi) failure caused by insufficient bracing on supporting partition walls and vii) damage to ceiling tiles and grids due to interaction with services.

3. Experimental and analytical results concerning the capacity of typical suspended ceilings in New Zealand were presented. Results from static tests on these ceiling components in the form of component fragility curves show that most critical components of the perimeter-fixed ceiling can be identified as: single rivet connections (3.2mm), cross tee connections under compression, main tee splices under tension, cross tee connections under tension and double rivet connections (3.2mm) (in order of weakness).

4. A simple method has been proposed for the analysis of perimeter-fixed suspended ceilings with peak grid acceleration as the demand and the length of the grid members and the overall seismic mass as parameters limiting the capacity. Using the component fragility curves, the overall fragility of the ceiling system has been estimated based on the principles of capacity chain and assumption of linear accumulation of seismic force in ceiling components.

5. Effect of ceiling weight and grid length on the overall capacity of the ceiling has been investigated through comparison of designed example ceilings. Results show that a

combination of ceiling weight and grid length needs to be considered for estimating the allowable acceleration applied to the ceiling. The performance of designed ceilings of various sizes and weights has also been compared with serviceability and ultimate limit state demands. The simple method provided in this study can be used for a quick estimation of the allowable length and weight for a typical perimeter-fixed ceiling subject to a given grid acceleration.

6. The analytical fragility curves proposed for the perimeter-fixed ceilings in this paper have been compared with relatively similar experimental fragility curves by other researchers. The comparison shows that the proposed method is relatively conservative in estimating the fragility of the system but can be used as an initial estimation of the probability of failure.

This study has proposed fragility functions for perimeter fixed ceiling systems assuming that the forces in different grid member and their connections are directly proportional to the ceiling acceleration and the total force in each direction is uniformly distributed among different grid members acting in that direction. As an extension to this study, the authors are currently assessing the validity of (and deviations from) these assumptions by conducting shaking table tests on different types of ceiling systems including the unbraced perimeter-fixed ceilings considered herein. Although detail results will be reported in future publications, the study has so far indicated that the axial force in a grid member can be reliably taken as being proportional to its acceleration but the forces in different grid members in a direction can differ substantially depending on the nature of the perimeter connections.

2.6 References

American Society of Civil Engineers. (1994). *Minimum Design Loads for Buildings and Other Structures (ASCE/SEI 7-10.), Vol. 7, Chapter 13: Seismic Design Requirements for Non-Structural Components.* USA: American Society of Civil Engineers.

American Society for Testing and Materials International. (2011). *Standard Test Method for Airborne Sound Attenuation Between Rooms Sharing a Common Ceiling Plenum (Two room method) (E1414-11).* PA, USA.

American Society for Testing and Materials International. (2011). *Standard Practice for Installation of Ceiling Suspension Systems for Acoustical Tile and Lay-in Panels in Areas Subject to Earthquake Ground Motions (E580/E580M-11b 2011).* PA, USA.

American Society for Testing and Materials. (2013). *Standard Specification for the Manufacture, Performance, and Testing of Metal Suspension Systems for Acoustical Tile and Lay-in Panel Ceilings (C635/C635M)*. PA, USA.

American Society for Testing and Materials. (2013). *Standard Practice for Installation of Metal Ceiling Suspension Systems for Acoustical Tile and Lay-in Panels (C636/C636M)*. PA, USA.

ANCO Engineers Inc. (1983). *Seismic Hazard Assessment of Non-Structural Ceiling Components: Phase I* (Report No. 1249.12). Grant 8114155, National Science Foundation, Culver City, California, USA.

Armstrong (2013). *"Seismic Design Guide New Zealand Version, Suspended Ceiling Systems"*. Armstrong, Auckland, New Zealand.

Australian Standard. (1991). *Suspended Ceilings, Recessed Luminaires and Air Diffusers – Interface Requirements for Physical Compatibility (AS 2946:1991)*. Sydney, Australia: Standards Australia.

Australian/New Zealand Standard. (1999). *Methods for Fire Test on Building Materials, Components and Structures - Simultaneous Determination of Ignitability, Flame Propagation, Heat Release and Smoke Release (AS/NZS 1530.3:1999)*. Wellington, NZ: Standards New Zealand.

Australian/New Zealand Standard. (2000). *Suspended ceilings - Design and Installation (AS/NZS 2785:2000).* Wellington, NZ: Standards New Zealand.

Australian/New Zealand Standard. (2002). *Structural design actions – Part 1: Permanent, Imposed and Other Actions (AS/NZS 1170.1:2002)*. Wellington, NZ: Standards New Zealand.

Badillo-Almaraz, H., Whittaker, A. S., & Reinhorn, A. M. (2007). Seismic fragility of suspended ceiling systems. *Earthquake Spectra, 23*(1), 21-40.

Bradley, B. A., Dhakal, R. P., MacRae, G. A., & Cubrinovski, M. (2010). Prediction of spatially distributed seismic demands in specific structures: Structural response to loss estimation. *Earthquake Engineering & Structural Dynamics*, *39*(6), 591-613.

Ceilings and Interior Systems Construction Association CISCA. (2004). "Guidelines for Seismic Restraint for Direct Hung Suspended Ceiling Assemblies, Seismic Zones 3-4". Illinois, USA: Ceiling and Interior Systems Construction Association.

Dhakal, R. P. (2010). Damage to Non-structural Components and Contents in the 2010 Darfield earthquake. *Bulletin of the New Zealand Society for Earthquake Engineering*, *43*(4), 404.

Dhakal, R. P., MacRae, G. A. & Hogg, K. (2011). Performance of Ceilings in the February 2011 Christchurch Earthquake. *Bulletin of the New Zealand Society for Earthquake Engineering*, *44*(4), 379-389.

Dhakal, R. P., MacRae, G. A. (2013). Ceiling Systems Design and Installation Lessons from the Canterbury Earthquakes. *Proceedings of 10th International Conference on Urban Earthquake Engineering (10CUEE)*, Tokyo Institute of Technology, Tokyo, Japan, 1-2 March 2013.

FEMA. (2011). *Reducing the Risks of Non-Structural Earthquake Damage – A Practical Guide (FEMA E74)*. Washington D.C., USA.

Ferner, H., Wemyss, M., Baird, A., Beer, A., & Hunter, D. (2014, March). Seismic performance of non-structural elements within buildings. In *Proceeding of the NZSEE Conference* (pp. 21-23).

Gilani, A. S., Reinhorn, A. M., Glasgow, B., Lavan, O., & Miyamoto, H. K. (2010). Earthquake simulator testing and seismic evaluation of suspended ceilings. *Journal of architectural engineering*, *16*(2), 63-73.

Gilani, A. S., Takhirov, S. M., & Tedesco, L. (2012). Seismic evaluation procedure for suspended ceilings and components new experimental approach. In *Proceedings of the 15th World Conference on Earthquake Engineering*. Lisbon, Portugal, 20-24 September 2012.

Glasgow, B., Gilani, A. S., & Miyamoto, H. K. (2010). Resilient suspended ceilings for sustainable design of buildings. In *Structures Congress 2010* (pp. 2575-2587).

MacRae, G. A. & Lehman, D. (2001). *Chapter 4, Buildings: The Nisqually Washington Earthquake, February 28, 2001 Preliminary Reconnaissance Report*. Co-authored by the Nisqually Earthquake Clearinghouse Group, University of Washington, Seattle. Earthquake Engineering Research Institute, EERI Learning from Earthquakes Project, March 2001, USA.

MacRae, G. A., Pampanin, S., Dhakal, R., Palermo, A., Baird A & Tasligedik, S. (2012). *Review of Design and Installation Practices for Non-Structural Components*, Report

prepared for the Engineering Advisory Group of the Department of Building and Housing by New Zealand Consultants, Industry and Related Experts, NZ, June 2012.

Ministry of Works. (1985). *Guidelines for the Seismic Design of Public Buildings: Appendix D Suspended Ceilings and Associated Fittings and Fixtures (PW/81/10/1:1985)*. Wellington, NZ: MoW.

Miranda, E., & Taghavi, S. (2003). Response assessment of nonstructural building elements. *Pacific Earthquake Engineering Research Center, University of California Berkeley, California, USA*.

Motosaka, M., & Mitsuji, K. (2012). Building damage during the 2011 off the Pacific coast of Tohoku Earthquake. *Soils and Foundations*, *52*(5), 929-944.

Nation Media. (2011). Retrieved from http://www.nationmultimedia.com/headlines/At-least-20-dead-after-8-8-magnitude-tremor-30150675.html

New Zealand Standard. (2004). *Structural Design Actions Part 5: Earthquake Actions-New Zealand (NZS 1170.5:2004)*. Wellington, NZ: Standards New Zealand.

New Zealand Standard. (2009). *Seismic Performance of Engineering Systems in Buildings (NZS 4219:2009)*. Wellington, NZ: Standards New Zealand.

New Zealand Standard. (2013). *Automatic fire sprinkler systems (NZS 4541:2013)*. Wellington, NZ: Standards New Zealand.

Paganotti, G. (2010). *Behaviour of Suspended Ceiling System during Seismic Events: Development of Fragility Curves*. (Masters Thesis, Politecnico Di Milano, Italy).

Paganotti, G., MacRae, G. A., & Dhakal, R. P. (2011, April). Development of typical NZ ceiling system seismic fragilities. In *Ninth Pacific Conference on Earthquake Engineering (PCEE)* (pp. 14-16).

Pourali, A., Dhakal, R. P., MacRae, G. A., & Tasligedik, A. S. (2015). Shake table tests of perimeter-fixed type suspended ceilings. In *New Zealand Society for Earthquake Engineering Annual Technical Conference* (pp. 648-659).

Rihal, S. S. & Granneman, G. (1984). *Experimental Investigation of the Dynamic Behavior of Building Partitions and Suspended Ceilings during Earthquakes*. Report No. ARCE R-84-1, California Polytechnic State University, San Luis Obispo, California, USA.

Rondo. (2008). *DUO Two-way Exposed Suspended Ceiling Grid System*. Rondo, Auckland,

NZ.

Ryu, K. P., Reinhorn, A. M., & Filiatrault, A. (2013). Capacity evaluation of suspended ceiling systems. *Technical Report MCEER-13-XXXX*.

Singh, J., MacRae, G. A., Dhakal, R. P., & Pampanin, S. (2011). Building seismic ceiling fragility using spectral acceleration. In *Ninth Pacific Conference on Earthquake Engineering*. Auckland, NZ, 14-16 April 2011.

Soroushian, S., Maragakis, E. M., & Jenkins, C. (2015). Capacity evaluation of suspended ceiling components, part 1: experimental studies. *Journal of Earthquake Engineering*, *19*(5), 784-804.

Stuff (2014). *Long wait for BNZ workers* Retrieved from http://www.stuff.co.nz/dominion-post/business/commercial-property/9209910/Long-wait-for-BNZ-workers

USG Australia. (2011). *DONN Brand Grid Suspension System*. USG Australia, Auckland, NZ.

USG Australia. (2012). *Generic Seismic Design for USG DONN Exposed Grid Suspended Ceilings*, Auckland, New Zealand.

CHAPTER 3

EXPERIMENTAL ASSESSMENT OF SEISMIC RESPONSE OF SUSPENDED PERIMETER-FIXED CEILINGS

3 EXPERIMENTAL ASSESSMENT OF SEISMIC RESPONSE OF SUSPENDED PERIMETER-FIXED CEILINGS

3.1 Introduction

Non-structural elements (NSEs) in buildings are the components which, despite adding to the design dead loads, are not generally considered to contribute to the structure's design resistance. These elements make up approximately 70% of the total construction cost in commercial buildings (Miranda & Taghavi, 2003) and are often reported as contributing to a significant portion of post-earthquake financial loss in the forms of damage and downtime.

In recent earthquakes, suspended ceilings were observed to have suffered significant damage despite the supporting structure sustaining minimal or no damage. This observation indicates an incompatibility between the performance requirements for structural and non-structural elements. Based on post-earthquake observations (Dhakal, 2010; Dhakal et al., 2011), the most common damage types in typical suspended ceilings include:

i. failure of end rivets in perimeter-fixed ceilings;
ii. failure of suspension system at grid intersections;
iii. dislodgment and downfall of acoustical tiles due to grid spreading;
iv. damage caused by the differential movement of the ceiling relative to vertical structural elements or non-structural elements such as partitions and sprinkler heads; and
v. failure due to the absence of sufficient bridging, clearance and support for other services within or in the vicinity of ceilings, e.g. pipes, ductwork and light fixtures located in ceiling plenum space.

3.2 Literature review

Perimeter-fixed ceilings consist of inverted T-shaped galvanized steel beams that form 1200 mm × 600 mm or 600 mm × 600 mm modules to support ceiling tiles (Figure 3-1). The suspension system is hung from the structure above (usually floor slab or joists) via steel hanger wires. These hangers are a minimum of 12-gauge galvanized, soft annealed mild steel wire (ASTM E580, 2013). On the perimeters, the ceiling is fixed to the walls via rivets or special clips on two adjacent sides while the opposite sides are free to slide on wall angles (Figure 3-2). ACM7 clips are one of the proprietary products that can be installed on both fixed and free ends. Based on the installation method (i.e. use of tight or loosely fit screws), they can allow or prevent displacement along the grid axis but they always prevent grid

spreading (i. e. displacements normal to the grid axis).

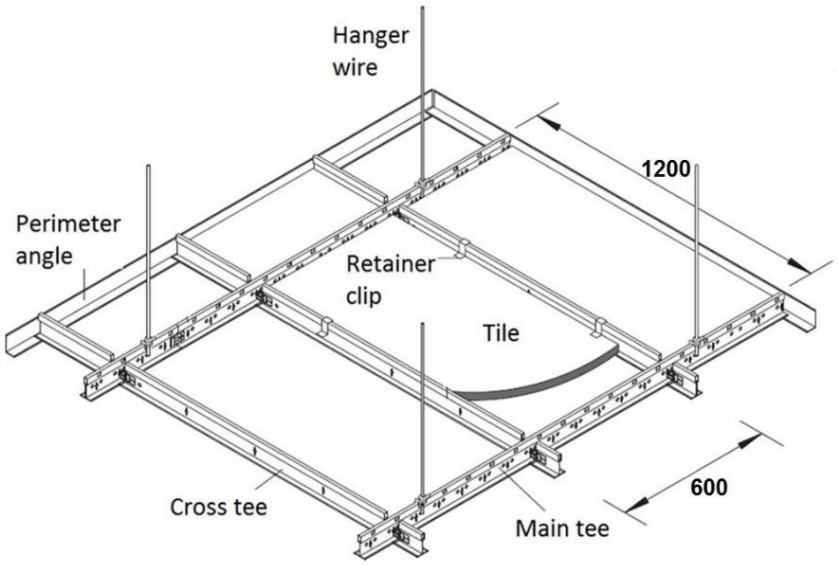

Figure 3-1 - Typical suspended ceiling components (USG, 2012)

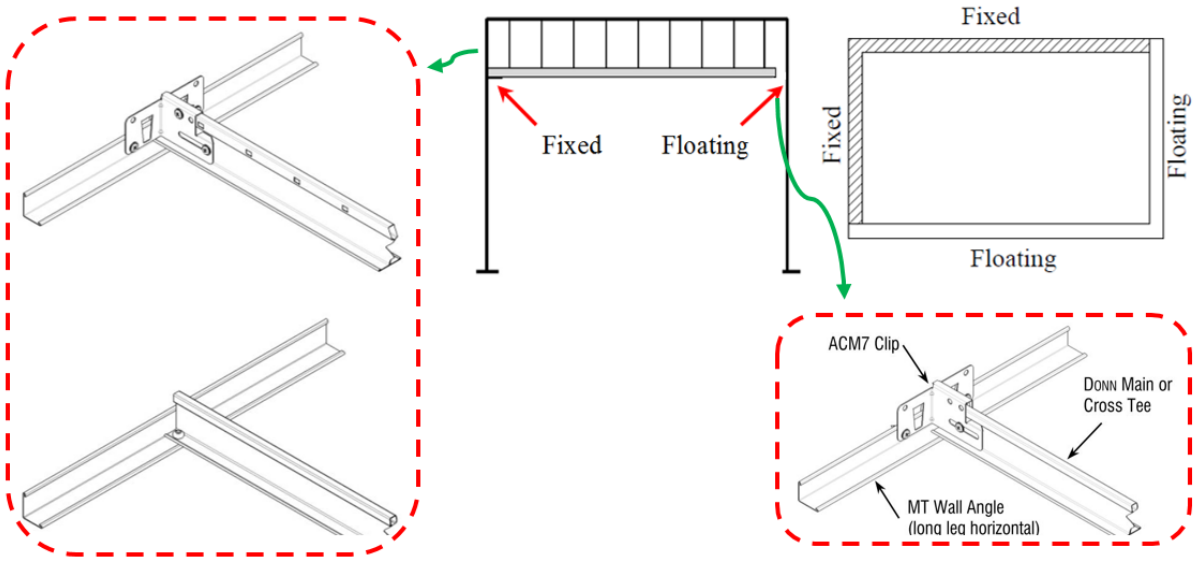

Figure 3-2 – Schematic of perimeter-fixed suspended ceiling and end fixings (USG, 2012)

NZS 1170.5:2004 specifies the seismic actions for the design of suspended ceilings in terms of peak floor acceleration (PFA). The acceleration coefficient used as ceiling demand incorporates the effect of seismic risk, importance factor, soil type, location over the height of the building and a maximum coefficient of 2 to account for the amplification of floor acceleration.

Seismic research on the performance of non-structural elements and suspended ceilings in particular has gained popularity in recent decades, following the extensive non-structural

damage reported in recent earthquakes. A brief review of some of these studies follows.

The industry-sponsored tests by ANCO Engineers Inc. (1983) on a prototypical suspended ceiling concluded that the most common locations for damage in suspended ceiling systems were around the perimeter of a room at the intersection of the walls and ceilings, where the runners buckle or detach from the wall angle. Their research also showed that pop rivet installation is more influential than sway wires and that sway wire braces, if installed with perimeter fixing, will not be active in the system's lateral restraint. Badillo-Almaraz et al. (2007) conducted fragility studies on suspended ceiling systems. In their full-scale earthquake-simulator testing they evaluated the effect of size and weight of tiles, use of retainer clips, installation of compression posts, and physical condition of grid components on the performance of ceilings. Four limit states were proposed to evaluate the damage observed in the systems and the threshold peak floor accelerations associated with each limit state were found. In a series of studies by Gilani et al. (2010) and Glasgow (2010), an experimental procedure and a performance matrix based on limit states were developed to evaluate and qualify innovations and quantitatively assess the efficacy of various code prescribed design and installation requirements. Fragility curve for panel failure as one of the damage states was derived. The use of intermediate duty main runners in high seismic regions was also tested through a case study which showed that the substitution of intermediate for heavy-duty main runners does not adversely affect the seismic response of the system.

3.3 Objectives

This paper reports an extensive series of shaking table tests conducted on the typical perimeter-fixed suspended ceilings commonly used in New Zealand with the main goal of understanding the mechanics of the system, the contributing elements in its performance and finally finding a simple method for its seismic design. The objectives of this study can be listed as follows:

1. To obtain experimental shaking table data from which simple design procedures can be developed and compared,
2. To develop a simple procedure for design, and
3. To perform a sensitivity study with the model to quantify the effects of variations in parameters.

3.4 Experimental program

3.4.1 *Test setup*

The test setup was constructed on a 2 m by 4 m unidirectional shake table. The test frame built was 5.20 m long, 2.6 m wide and 2.6 m high and could accommodate a 2.4 m by 4.8 m ceiling (Figure 3-3). The frame was cross-braced in the direction of excitation. Connections at column bases were pinned and rigid fixed end plate connections were used at the beam to column joints.

Figure 3-3 – Test frame on shake table

At the ceiling hanging level; i.e. 500 mm below the roof of the frame, timber beams were fixed to the columns on four sides and 19 mm × 40 mm wall angles were screwed to the timber beams to provide support for the ceiling tee ends. In real installation practice of such suspended ceilings, the perimeter angles are often supported by plasterboard partitions or drywalls. In such conditions, perimeter angles are screwed to the drywalls at 600 mm centres and are expected to be fixed onto the vertical timber studs rather than only the gypsum boards. This reasonably replicates the testing condition in this experiment, concerning the perimeter stiffness provided by timber beams.

Suspended ceilings react to floor accelerations and as they are located on different elevations inside a building, the demand imposed on them will depend on the floor response and can be significantly different from the ground acceleration. To have a degree of control on the input motion to ceilings in shake table tests, it is desirable to have an infinitely rigid test frame so that the floor motion at the ceiling level is the same as the one applied to the shake table

(ground motion). However, such a frame would be inefficiently heavy and expensive. Therefore, a more reasonable alternative is to use a less rigid frame and consider the ceiling level motion on the frame as the input. To account for any unintended difference between the shaking table and ceiling support excitations, the acceleration at the top of the test frame was recorded and used as the input to the ceiling system in analysing and interpreting the test results. The frame used in this study had a horizontal natural frequency of 12.5 Hz.

3.4.2 *Instrumentation*

A total of 21 accelerometers, potentiometers and load cells were used for recording the test outputs in the first two series of tests. The number of instruments and their locations were slightly changed in the remaining series as accelerometers with higher capacities were used. A schematic view of the location of these instruments is shown in Figure 3-4 with more details on the instruments in Table 3-1. Further details on the instruments can be found in Appendix B.

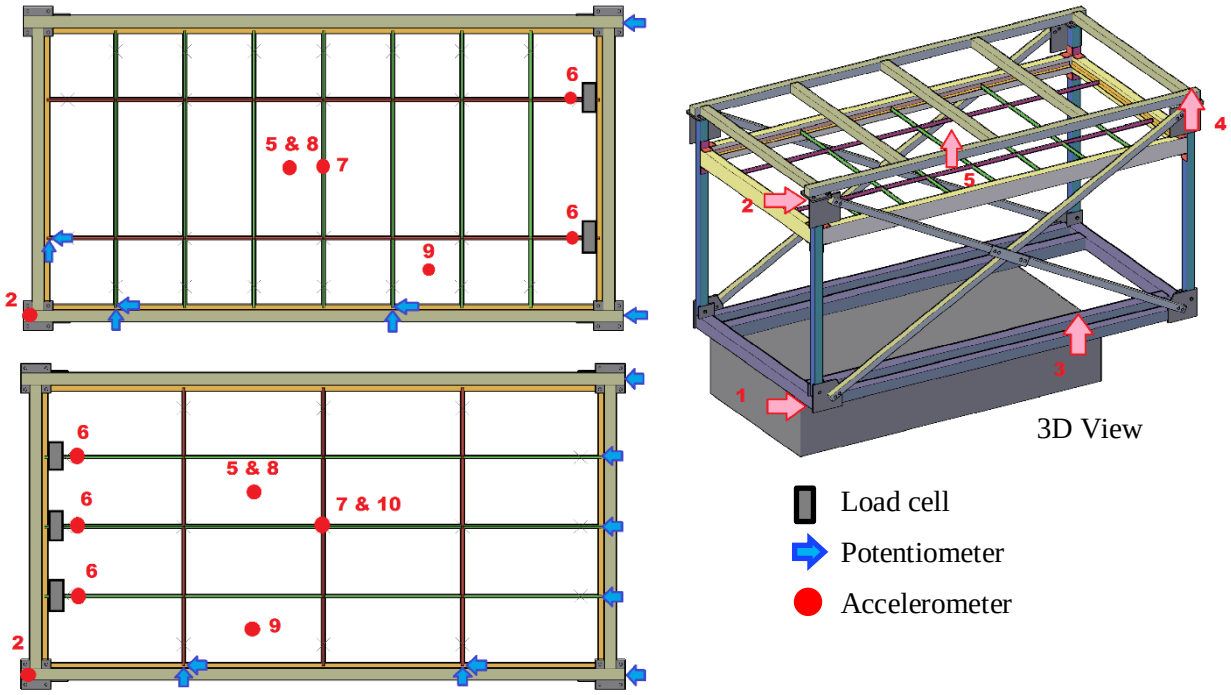

Figure 3-4 - Instruments in test series Pr-F-A & Pr-F-B

Table 3-1 – List of accelerometers

No.	Location	No.	Location
1	Shake table input (Hrz.)	6	Grid end (Hrz.)
2	Frame top (Hrz.)	7	Central grid (Hrz.)
3	Shake table input (Vrt.)	8	Central tile (Hrz.)
4	Frame top (Vrt.)	9	Perimeter tile (Hrz.)
5	Central tile (Vrt.)	10	Central grid (Vrt.)

3.4.3 *Test specimens*

Four configurations of ceilings were tested in this experimental study. The specimens were 2.4 m × 4.8 m in size and varied in suspension system layouts (Figure 3-5) and end fixing details (Figure 3-6) (details provided in Table 3-2).

Table 3-2 – Details of test specimens

No.	Test Series	Grid loaded	Fixed end	Free end	Tile mass ea. (kg)
1	Pr-F-A-RC[4]	Main tee	3.2 mm Rivet[1]	Clipped[2]	2.75
2	Pr-F-A-RF[5]	Main tee	3.2 mm Rivet	Free[3]	2.75
3	Pr-F-B-RC	Cross tee	3.2 mm Rivet	Clipped	2.75
4	Pr-F-B-HRC	Cross tee	3.2 mm Rivet	Clipped	4.65
5	Pr-F-B-HCC[6]	Cross tee	ACM7 clips	Clipped	4.65
6	Pr-F-B-HRF	Cross tee	3.2 mm Rivet	Free	4.65

Note: Three types of end fixings were used in these experiments:

1. *Riveted: Single 3.2 mm rivets.*
2. *Clipped: ACM7 clips with loosely fit screws that allow the grids to slide along their axis but prevent movement perpendicular to their axis. When applied with tightly fit screws, displacement is prevented in both directions (Figure* 3-6*).*
3. *Free: The grids simply rest on the wall angles provided on perimeters.*

Based on these end fixings, three boundary configurations of perimeter-fixed ceilings were tested:

4. *Riveted – Clipped*
5. *Riveted – Free*
6. *Heavy tiles – Clipped – Clipped*

In the first ceiling type referred to as Pr-F-A (Figure 3-5a), main tees were in the longitudinal direction and cross tees in transverse direction. The tiles used on this ceiling were light weight. Two configurations of this ceiling type were tested to evaluate the effect of boundary conditions: i) Pr-F-A-RC with rivets on fixed sides and ACM7 clips on the floating sides, and ii) Pr-F-A-RF with rivets on fixed sides and no fixings on the floating sides. To resemble a floating grid end in the Pr-F-A-RC specimen, ACM7 clips were installed with loosely fit screws (Figure 3-5). In the second specimen, Pr-F-A-RF, the ACM7 clips are removed and grids are free to slide on the seating wall angle along and normal to the grid axis.

The second type of ceiling, Pr-F-B, was installed with cross tees placed in the longitudinal direction and main tees in transverse direction (Figure 3-5b). Four configurations of this ceiling were tested with changes in tile weight and boundary conditions as detailed in Table 3-2.

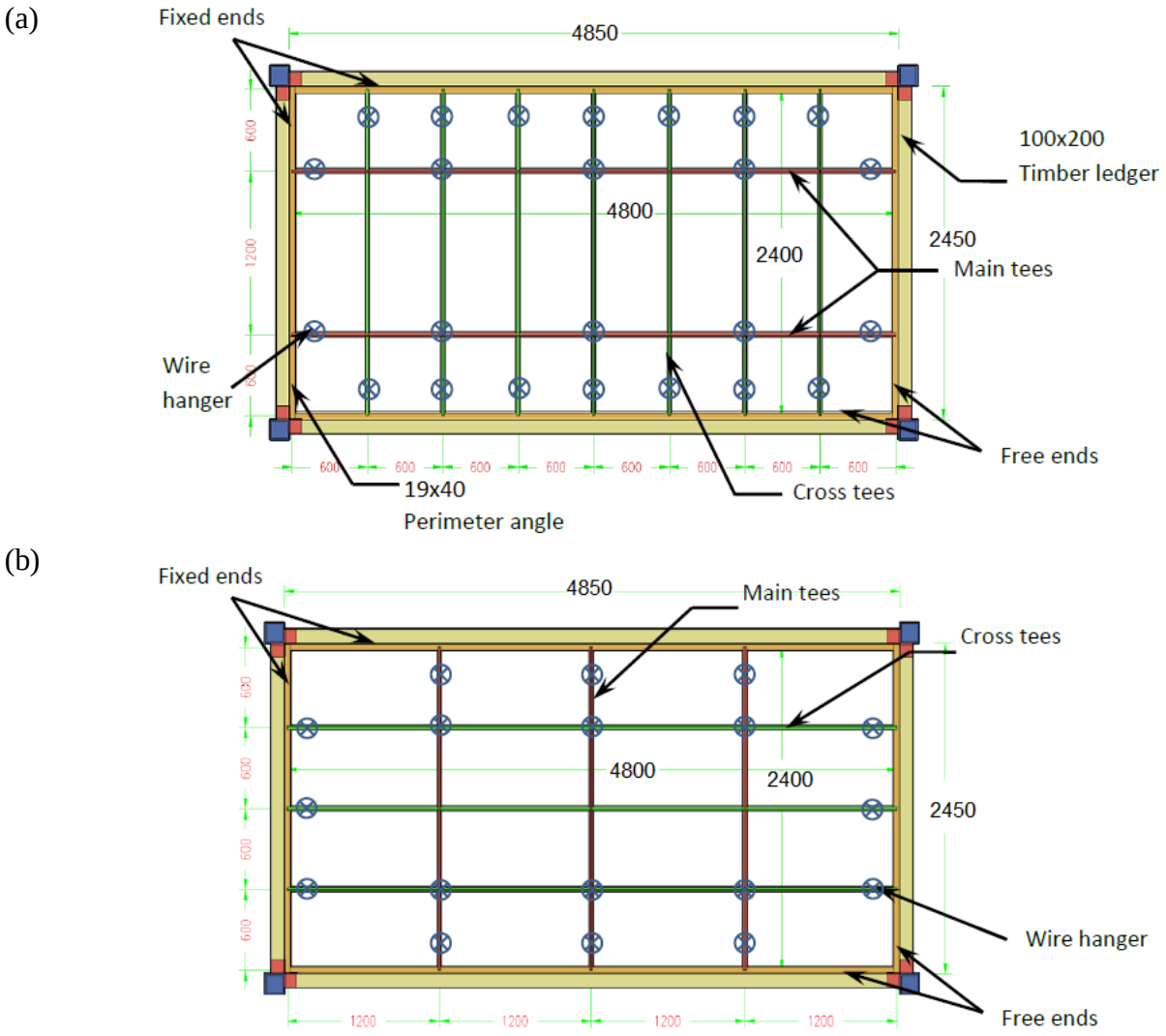

Figure 3-5 – Plan view of ceiling specimens (a) Pr-F-A, and (b) Pr-F-B (Dimensions in mm)

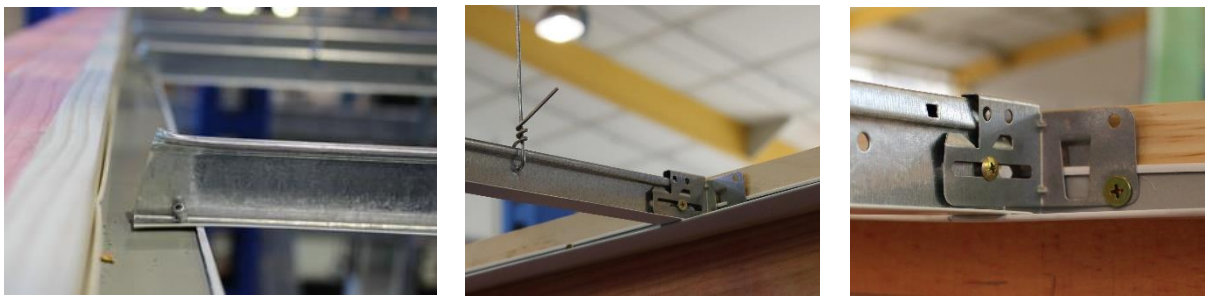

Rivet on fixed end ACM7 clip with loosely fit screw on free end

Figure 3-6 – Fixtures on grid ends

Due to the observation of considerable vertical (out-of-plain) vibrations in some tests, finding the natural vertical frequency of the ceiling was important in this study. This resulted in the vibration or displacement of ceiling tiles and the consequent pounding between them and

ceiling grids. This will be further discussed in the discussion of results.

For estimating the natural frequency of the ceiling specimens, a simplified theoretical method was employed (Young et al. 2012). This method uses the formula shown in Equation 3-1 for estimating the natural frequencies of a simply supported beam.

$$f_n = \frac{K_n}{2\pi}\sqrt{\frac{EIg}{wl^4}} \qquad \text{Equation 3-1}$$

Where E is modulus of elasticity, I is moment of inertia, g is gravitation acceleration, w is uniform load per unit length of the beam and l is the beam length. In this equation, K_n is a constant which varies depending on the mode of vibration. Values of K_n for the first 4 modes are: $K_1=9.87$, $K_2=39.5$, $K_3=88.8$ and $K_4=158$.

To apply this formula to the ceiling specimen, the longitudinal grids are assumed to be beams supported on perimeters through rivets and seating which act as hinge and roller supports, respectively. This assumption excludes the effect of transverse grids which are expected to increase the stiffness of the longitudinal grids/beams and result in higher natural frequencies. Using this simplified method, the first four vertical natural frequencies of the Pr-F-B ceiling with heavy tiles were calculated as: $f_1=0.64$ Hz, $f_2=2.56$ Hz, $f_3=5.76$ Hz *and* $f_4=10.25$ Hz. The vertical natural frequency of Pr-F-A ceiling was assumed fairly similar to Pr-F-B. Moreover, most of the tested configurations and results were obtained from Pr-F-B specimen.

3.4.4 *Test input motion*

One of the main objectives of these series of tests is to better understand the mechanism with which the suspended ceiling system resists the floor acceleration and how the inertial force is transferred through different components. Therefore, it is more desirable to have a controlled loading regime through which the effect of various parameters of loading can be controlled and separately investigated. A series of sinusoidal motions varying in displacement amplitude and frequency were therefore chosen as input motion for these tests. This provides a variety of input PFAs applied to the ceiling. Table 3-3 shows the parameters of motions used for each test series. In addition to the sinusoidal motions, a suite of random motions obtained from actual ground motions were also used in these experiments. These motions are provided in more detail in Appendix A.

Table 3-3 – Details of input motions in test series Pr-F-A-RC, Pr-F-A-RF, Pr-F-B-RC & Pr-F-B-HRC

	Frequency of Vibration (Hz)	Displacement Amplitude (mm)	Input acceleration (g)
Pr-F-A-RC & Pr-F-B-RC	1	20 & 28	0.08 & 0.11
	1.5	20 & 28	0.18 & 0.25
	2	12-28 (at 4 mm intervals)	0.19 – 0.45
	2.5	12-24 (at 4 mm intervals)	0.3 – 0.6
	3	2-20 (at 2 mm intervals)	0.07 – 0.72
	3.5	2-16 (at 2 mm intervals)	0.1 – 0.8
	4	2-12 (at 2 mm intervals)	0.13 – 0.77
	4.5	2-10 (at 2 mm intervals)	0.16 – 0.81
	5	2-8 (at 2 mm intervals)	0.2 – 0.8
Pr-F-A-RF	2	12, 16, 20	0.19 – 0.32
	3	2-12 (at 2 mm intervals)	0.07 – 0.50
	4	4, 6, 8	0.26 – 0.52
Pr-F-B-HRC	2	12-24 (at 4 mm intervals)	0.19 – 0.45
	2.5	12-24 (at 4 mm intervals)	0.30 – 0.60
	3	4-20 (at 2 mm intervals)	0.14 – 0.72
	3.5	4-16 (at 2 mm intervals)	0.20 – 0.79
	4	4-10 (at 2 mm intervals)	0.26 – 0.64
	4.5	2-10 (at 2 mm intervals)	0.16 – 0.81

3.5 Results and discussions

3.5.1 *Amplification of input motion*

Since suspended ceilings are located on different elevations of a building, the peak floor acceleration (PFA) and the frequency content of the motion applied to them are different from the peak ground acceleration (PGA). Moreover, the acceleration applied to the supporting floor is amplified while being transferred to different components of the ceiling. NZ Standard for the seismic design of parts (NZS 1170.5:2004) specifies a maximum spectral shape factor ($C_i(T_p)$) of up to 2 to be applied to ceilings acceleration to account for these amplifications. To evaluate this provision and to quantify the amplification of acceleration in the ceiling, acceleration outputs at different locations of the frame and the ceiling were compared in Figure 3-7 to Figure 3-10.

Figure 3-7 shows the amplification in peak horizontal acceleration when transferred from shake table to the frame top (Point 2 in Figure 3-4). The values of amplification in the two tests are in a reasonably similar range since the grid layout of ceilings does not change the properties of the supporting frame. Since the frequencies of input motions are far less than the

natural frequency of the frame, no significant variation in amplification is observed in different motions. The amplification factors vary between approximately 0.8 and 1.4.

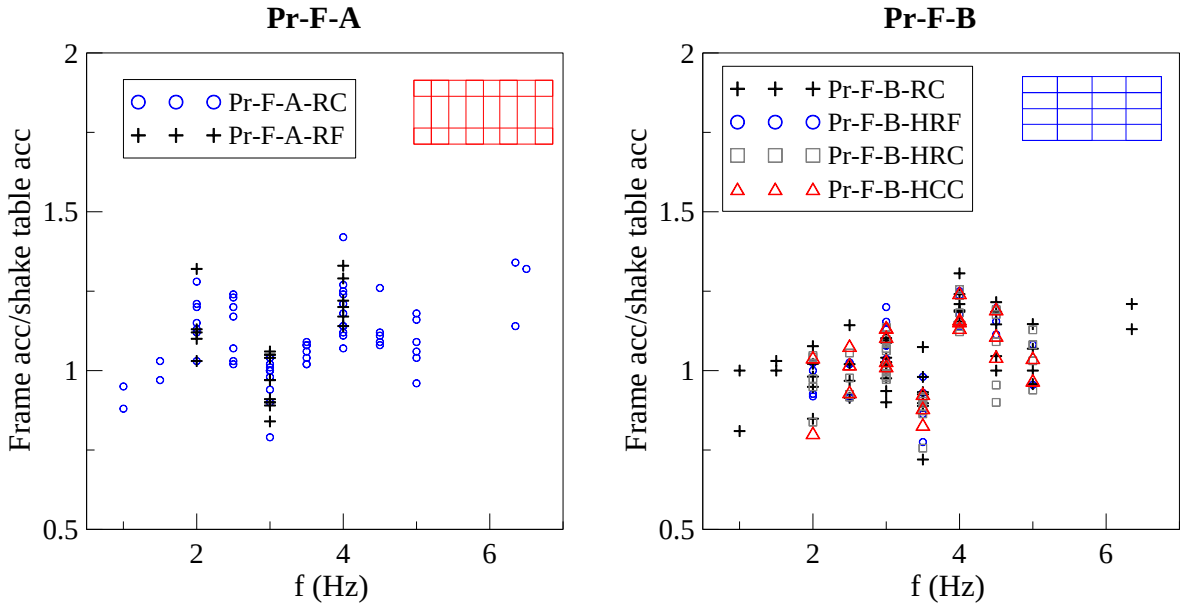

Figure 3-7 – Amplification of input acceleration on frame top

The acceleration applied at the floor level is transferred to the ceiling grid members and tiles, and in a perimeter-fixed ceiling it is resisted by the end fixing connections (i.e. rivets). In Figure 3-8, the values of peak horizontal acceleration recorded on grid members in specimen Pr-F-B are compared with the peak acceleration at roof support level (herein floor acceleration). Three accelerometers were located on grid ends (identified as No. 6 in Figure 3-4 and referred to as #1 to #3 here) and one at the central grid or joint (identified as No. 7 in Figure 3-4), which are used in the plots shown in Figure 3-8. The values of peak acceleration recorded on the centre and grid ends were up to 3 and 4.5 times larger than the peak acceleration at the roof level, respectively. This amplification increased as higher floor accelerations and higher input frequencies were applied. Note that in Figure 3-8, floor accelerations were limited to 1g in the central grid as in higher accelerations the accelerometers in this location reached their capacity and their recordings were eliminated from the data set.

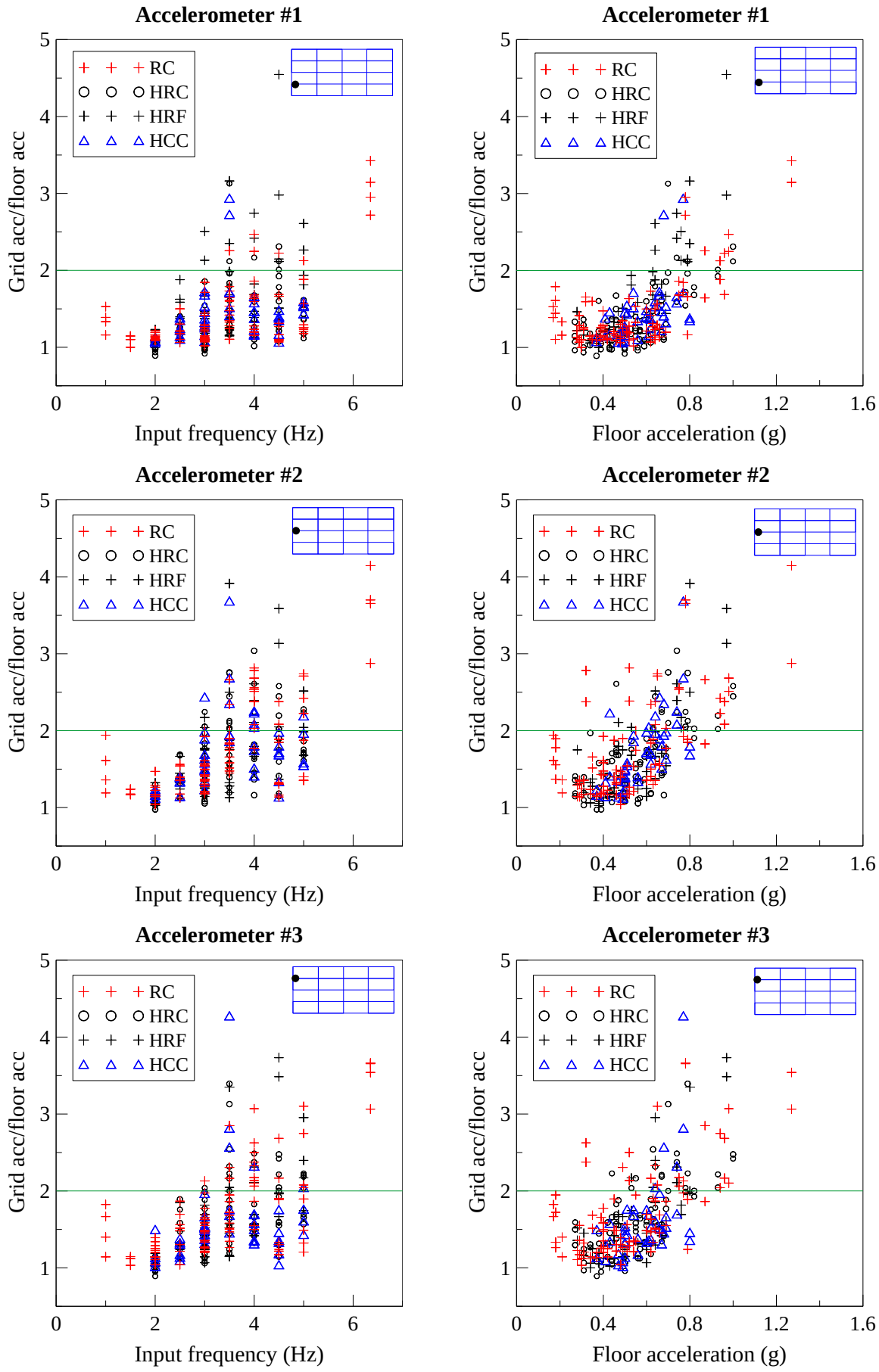

Figure 3-8 – Acceleration amplification factor on grid members

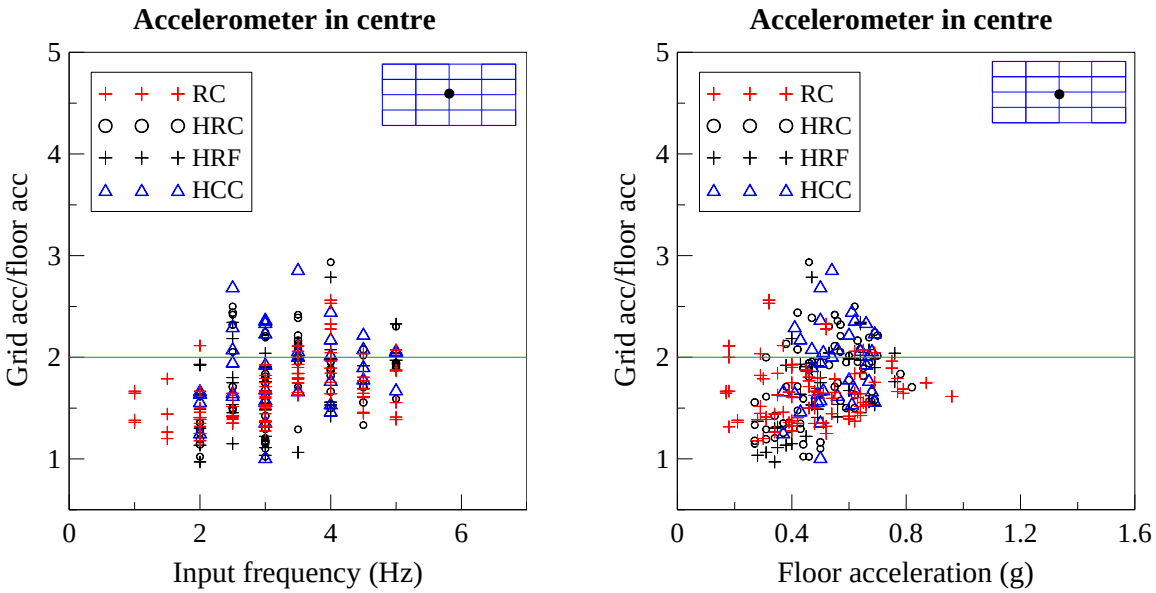

Figure 3-8 (Cont'd) – Acceleration amplification factor on grid members

Based on the current NZ Standard (NZS 1170.5, 2004), the acceleration considered for design of ceilings is amplified using several coefficients such as floor height and part spectral shape coefficients. This acceleration applied at the ceiling level can be up to 3.6 times the acceleration due to gravity in a high seismic region. In case of suspended ceilings which have a natural period of less than 0.75s, the part spectral shape coefficient has a value of 2. This amplification value was exceeded by a significant number of data points in the graphs provided in Figure 3-8 which implied that grid members could be subject to much larger accelerations, in the worst cases up to 4.5 times the peak floor acceleration.

Due to the presence of gaps between tiles and the surrounding grids, tiles tend to slide in their grid modules and in some cases hit the grid members. This excitation is greater in the ceiling centre where large vertical movements were also observed in tiles. As it can be observed in Figure 3-9, large values of amplification -up to 3.5 times the floor motion- were recorded in central tiles. In general, lighter tiles -used in specimen RC- were observed to result in higher acceleration amplifications compared to specimens with heavy tile -i.e. HRC, HRF and HCC.

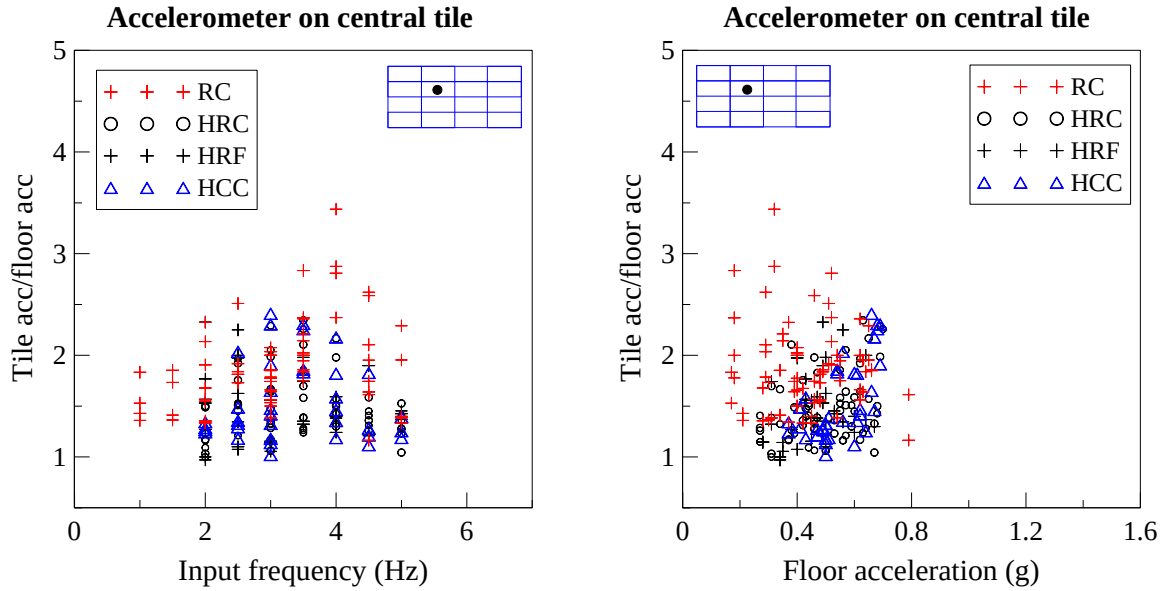

Figure 3-9 – Acceleration amplification factor on tiles

Although the shake table was only capable of unidirectional horizontal motion, vertical vibrations were observed and recorded in the ceiling grids and tiles. To expand the size, the test frame was built on slightly longer beams which overhung from one end of the shake table. This overhang may have partly contributed to the vertical accelerations recorded at the frame top -i.e. ceiling support. The peak vertical accelerations recorded on the frame top on the overhanging side are shown in Figure 3-10a. Figure 3-10b shows the peak vertical acceleration on the ceiling grid centre. Figure 3-10c and Figure 3-10d show the amplification of vertical acceleration recorded on ceiling grid centre compared to the vertical acceleration on frame top -herein supporting floor.

The amplifications are especially larger in the input frequency range of 3.5-4.5 Hz which is close to the natural frequency of the specimen calculated in Section 3.4.3. These large vertical accelerations which show the flexibility of the suspended ceiling system, could cause uplift which along with the simultaneous horizontal acceleration of the undersized tiles could lead to dislodgment of the tiles, potentially triggering a cascading system failure. Considering that all ground shaking events have an inherent vertical component and the large amplifications observed in these experiments even at low vertical acceleration levels, this could become a commonly occurring issue at any shaking level. One possible mitigation or preventing measure for the tile dislodgment damage is advised by the ceiling manufacturers in the form of tile hold-down clips. Although this solution is not very popular among practitioners due to installation difficulties, it may be the required step to limit the movement of ceiling tiles.

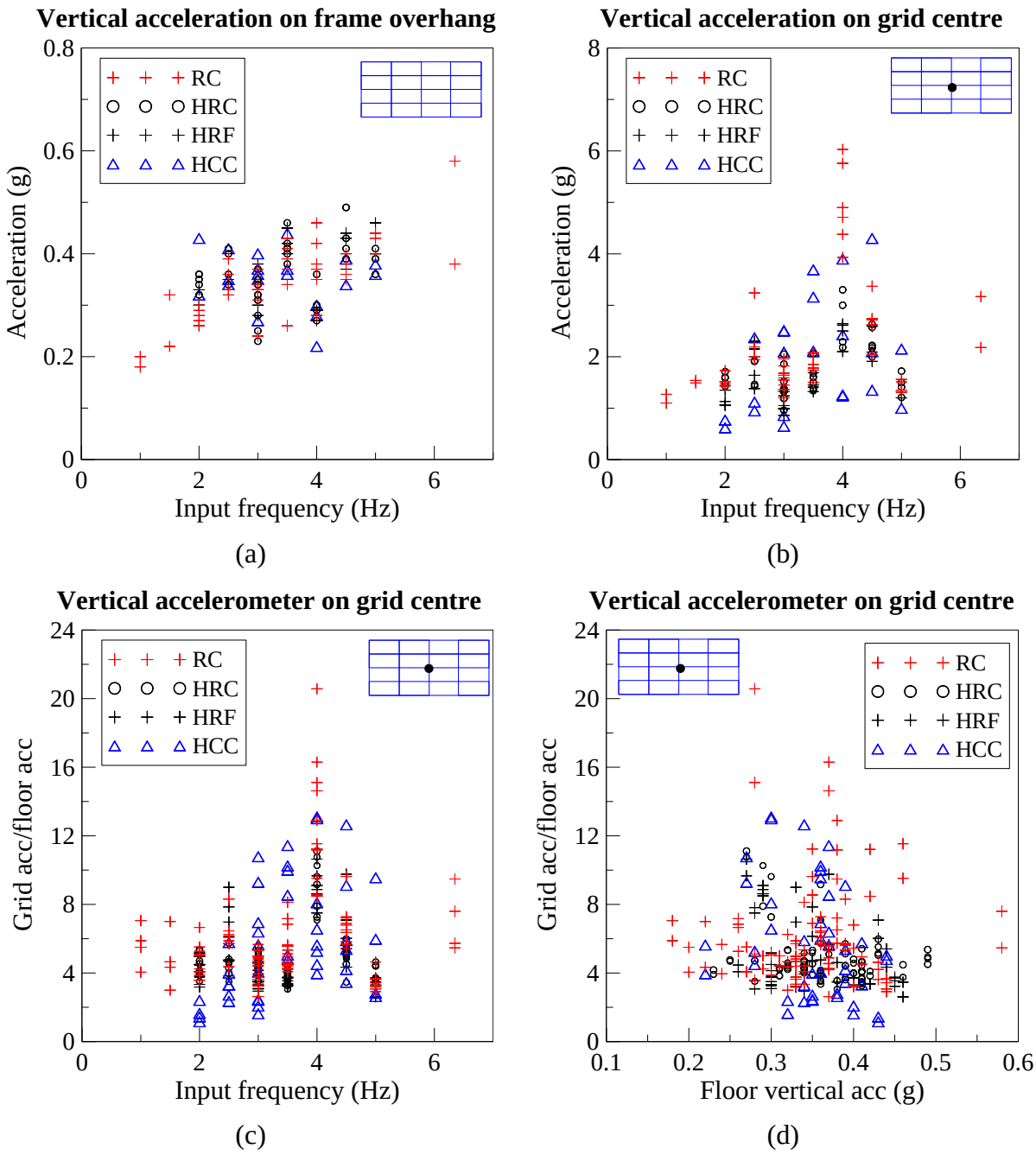

Figure 3-10 – Amplification of vertical acceleration in ceiling specimens

3.5.2 *Effect of boundary restraint*

Figure 3-11 shows a schematic view of the assumed rotations and deformations in transverse tees (i.e. vertical grids in the figure) for the three boundary conditions mentioned earlier in a Pr-F-B specimen. The aim is to explain their effect on the transfer of loads through longitudinal tees. In these schemes, the rivets (marked as R) resembled pinned connections while clips (marked as C) provided some constraint to the end rotation.

At the grid joints, the forces in transverse grids were transferred to the longitudinal grids (i.e. horizontal grids in Figure 3-11) and finally to their end fixings which were equipped with load cells and potentiometers (Figure 3-12). Measurement of displacements at the free ends of longitudinal tees in Pr-F-B ceilings showed that removing ACM7 clips increased the overall motion of the ceiling (Figure 3-13). Reducing or removing the rotational and transverse resistance in the end fixing (by removing clips) also led to a larger tributary area and larger forces in the longitudinal grid members closest to the free end (LC1) (Figure 3-14). It was expected that in this manner, changing the boundary conditions from C-C to R-F would result in a decrease in the contribution of perimeter fixtures and an increase in the forces transferred by longitudinal grids.

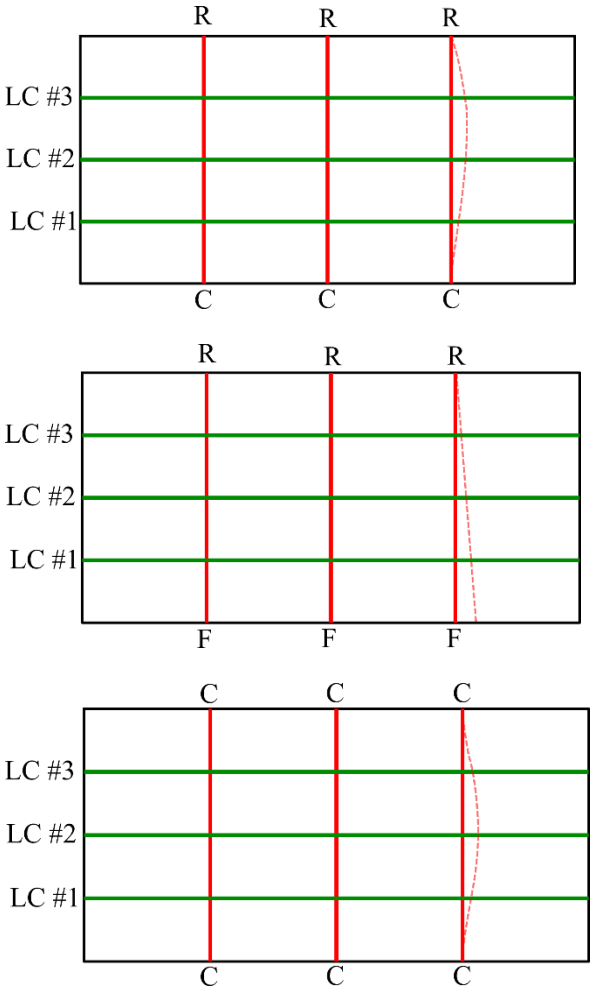

(a) R – C:

Rivet on the top end of transverse tees and clips on the bottom ends.

(b) R – F:

Rivet on the top end of transverse tees and free on the bottom ends.

(c) C – C:

Clips on the top and bottom ends of transverse tees

Figure 3-11 - Schematic view of displacement mechanism on grid ends with different fixings (Boundary conditions: R-C, R-F, C-C)

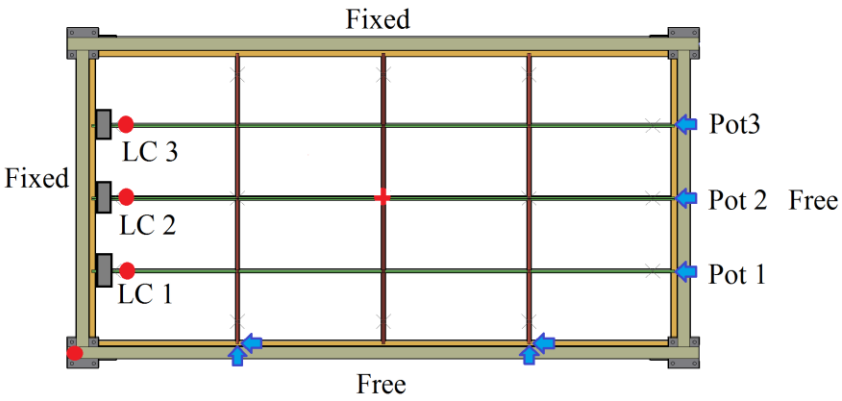

Figure 3-12 – Location of potentiometers (Pot) and load cells (LC) on specimen Pr-F-B

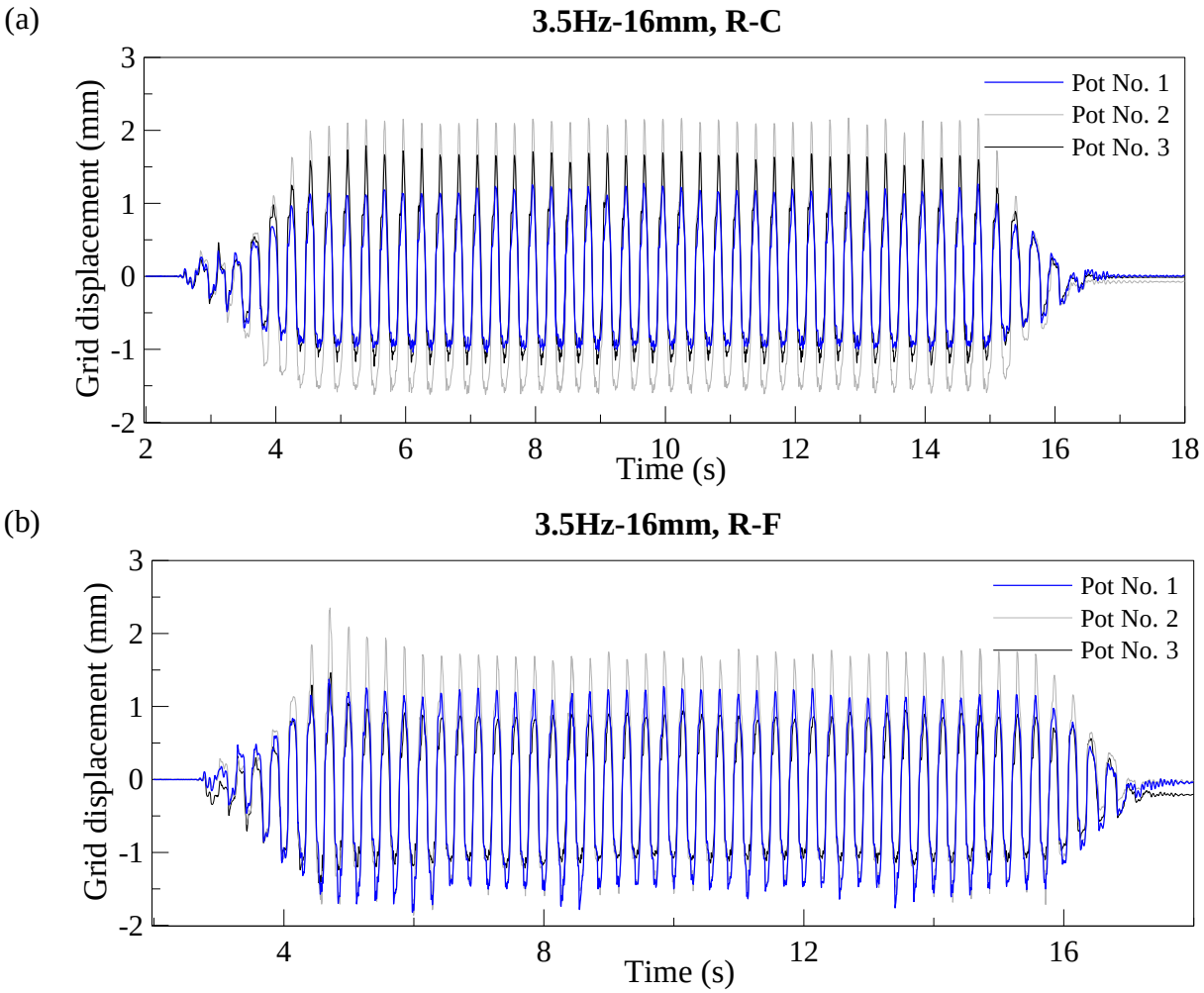

Figure 3-13 – Displacement time history in longitudinal grids in sinusoidal tests on Pr-F-B specimens with two boundary conditions (a) R-C and (b) R-F.

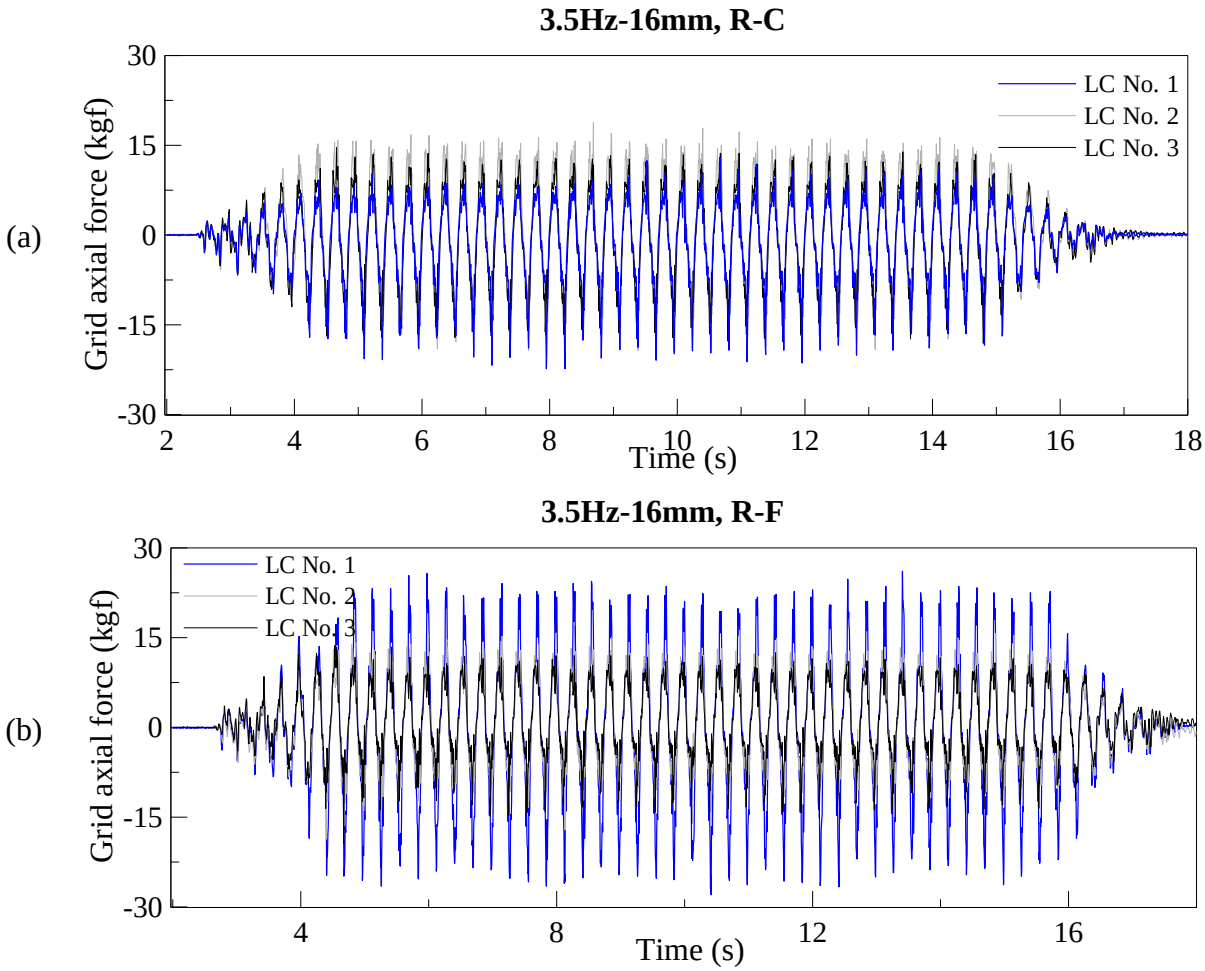

Figure 3-14 – Axial force time history in longitudinal grids in sinusoidal tests on Pr-F-B specimens with two boundary conditions (a) R-C and (b) R-F.

Figure 3-15 compares results of sinusoidal tests on Pr-F-B specimens with three different boundary conditions: R-C, R-F and C-C. Each bar shows the sum of axial forces recorded via load cells on the three longitudinal grid ends on the ceiling. Each of the test numbers represent one sinusoidal wave with frequency of vibration varying from 2 Hz to 5 Hz. Of the three specimens tested under the same sine wave, R-F had the largest values of total longitudinal grid force. This indicated that the rigidity added to the end fixings increased the contribution of perimeter fixings on transverse grids to the total seismic forces and reduced the forces in longitudinal grids. This could be beneficial in decreasing the demand on end fixing rivets and connections in long grids.

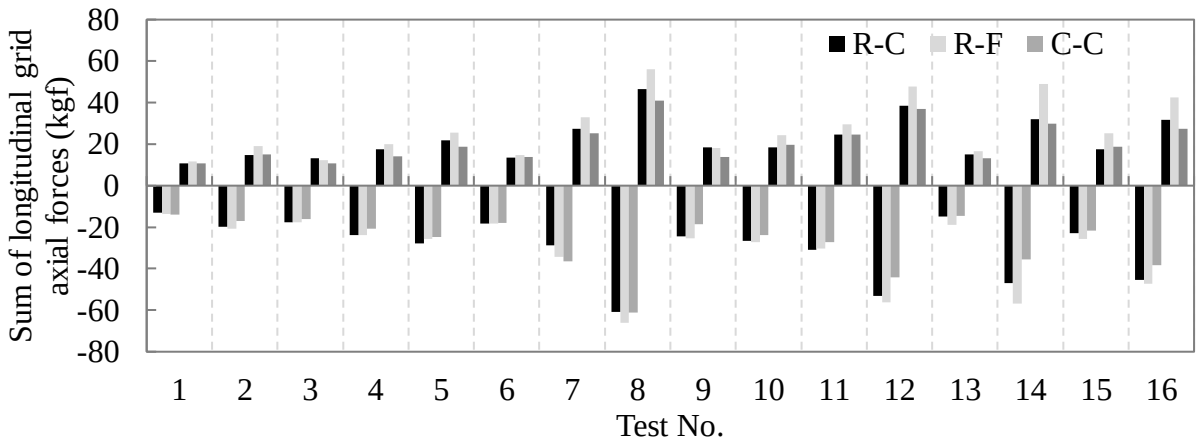

Figure 3-15 – Comparison of the sum of axial forces in three longitudinal grids in three Pr-F-B specimens with different boundary conditions

3.5.3 *Force-acceleration relationship*

If we assume the suspension system as an elastic grid of beams carrying the seismic force from suspended tiles and supported services, then we can consider the transfer of force through these beams to be linear and cumulative. In other words, this assumption allows us to estimate the inertial force in the end connections as the product of horizontal acceleration and mass associated with the tributary area of the considered beam (Figure 3-17). To verify this assumption in experiment, load cells and accelerometers were installed at the fixed end of the tees (Figure 3-16). The axial forces measured by the load cells in tees were compared with the product of measured accelerations and mass carried by each beam. The masses associated with tributary areas in different specimens are listed in Table 3-4.

Table 3-4 – Mass and tributary areas in specimens

Test Series	Area on tee (m^2)	Tile mass (kg/m^2)	Tributary area mass (kg)
Pr-F-A-RC	4.8×0.9 = 4.32	3.8	4.32×3.82 = 16.5
Pr-F-A-RF	4.32	3.8	16.5
Pr-F-B-RC	4.8×0.6 = 2.88	3.8	2.88×3.8=11
Pr-F-B-HRC	2.88	6.4	2.88×6.4=18.5
Pr-F-B-HRF	2.88	6.4	18.5
Pr-F-B-HCC	2.88	6.4	18.5

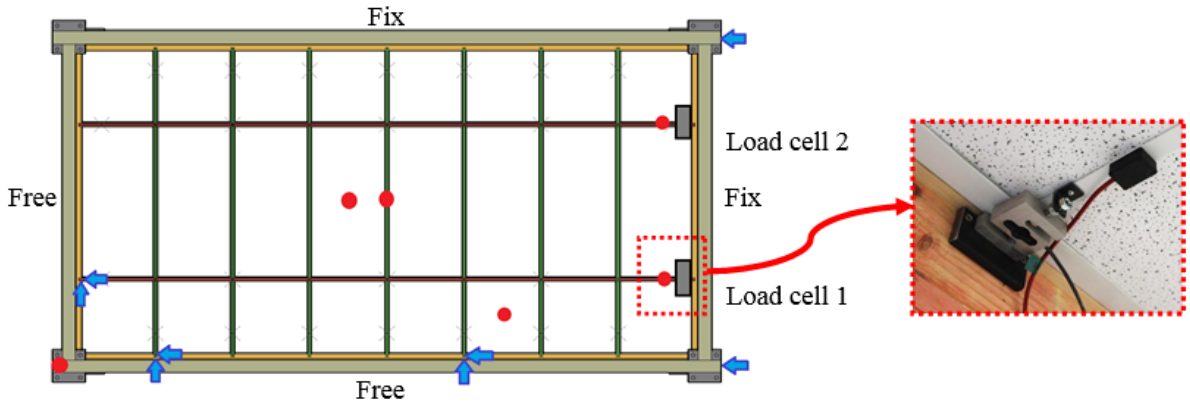

Figure 3-16 – Layout of instruments and location of load cells on Pr-F-A specimen

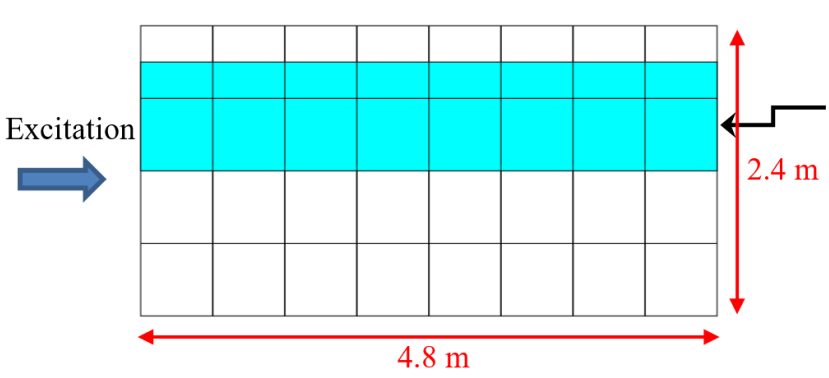

Tile average mass = 3.82 kg/m^2

Tributary area = 0.9×4.8=4.32 m^2

Mass of tributary area =

= 3.82×4.32 = 16.5 kg

F = m × a Equation 3-2

Figure 3-17 – Schematic view of tributary area per main tee

Figure 3-18 compares the peak forces measured by the load cells -filled black circles- with the forces calculated as the product of mass and the recorded peak grid accelerations -hollow blue circles- in the two load cells used in sinusoidal tests in Pr-F-A-RC. In both graphs, the values of force from the load cells are slightly lower than what was calculated or expected based on Equation 3-2 shown in Figure 3-17. In other words, the assumption of linear relationship among axial force, tributary area mass and grid acceleration resulted in a conservative overestimation for grid axial forces. This discrepancy in axial force values may be caused by the initial assumptions about the two contributors of the equation: mass and acceleration. In reality, the mass distributed and associated to the grid members may be different from what assumed in the tributary area. This was shown partly in the previous section considering the effect of boundary conditions and their level of contribution to axial force transfer. Moreover, the acceleration considered in this equation (and the predicted axial force) is the peak grid acceleration. This acceleration may not be constant throughout the

length of the longitudinal grids. As the variation in our experimental tests recordings from the accelerometers on the grid ends and grid centre showed, different sections of the grid may be excited by accelerations different from the peak value considered. This implies that assuming a single peak acceleration value for the mass associated with the entire length of the grid is a simplification and possibly different from the actual conditions.

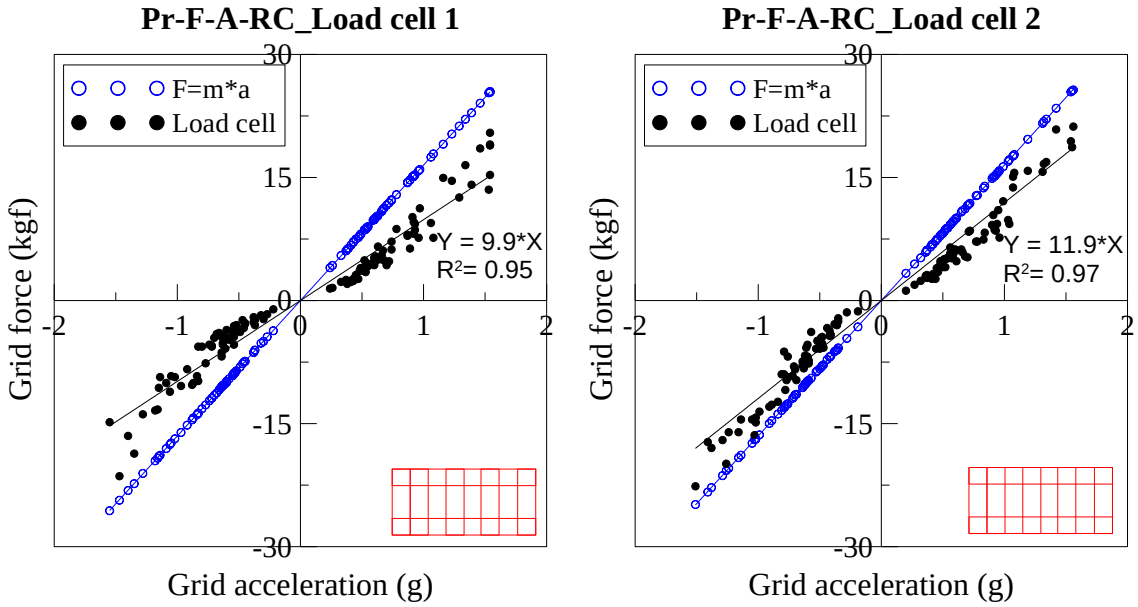

Figure 3-18 – Peak force-acceleration relationship Pr-F-A-RC

The effect of boundary fixtures on the axial force on grids was tested in a different layout used in Pr-F-A-RF. It this specimen, the clips used on the free ends of the grids in Pr-F-A-RC were removed, so that the free ends of the grids could slide and move while the fixed ends were riveted. As shown in Figure 3-19, with the removal of end clips, the boundary stiffness was reduced and the axial forces recorded in load cells increased. This resulted in maximum axial forces in load cells being closer to the estimated/predicted values from mass and grid acceleration. This is more apparent in the results of load cell 1 which was installed on longitudinal grid closer to the free end.

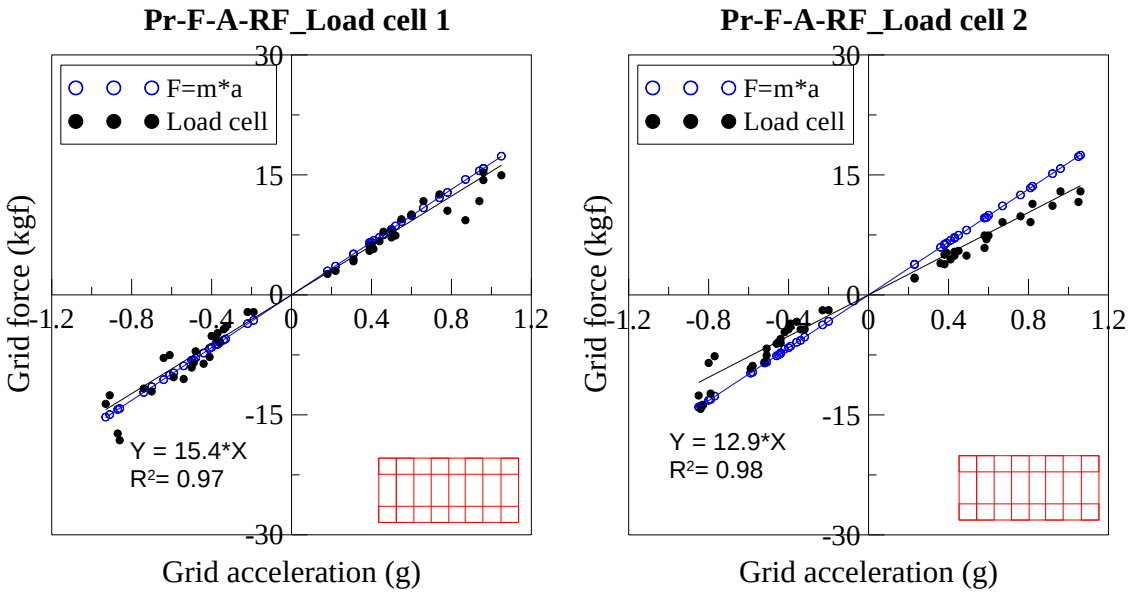

Figure 3-19 – Peak force-acceleration relationship Pr-F-A-RF

In the linear equations shown on the graphs in Figure 3-18 and Figure 3-19, the slope of each fitted line indicates the mass associated with the grid connected to the load cell. The highest value of the slope (or mass) was 15.4kg on load cell 1 in Pr-F-A-RF. Since no damage was observed at this stage it can be concluded that the system was still at its elastic stage and the linear assumption was relevant.

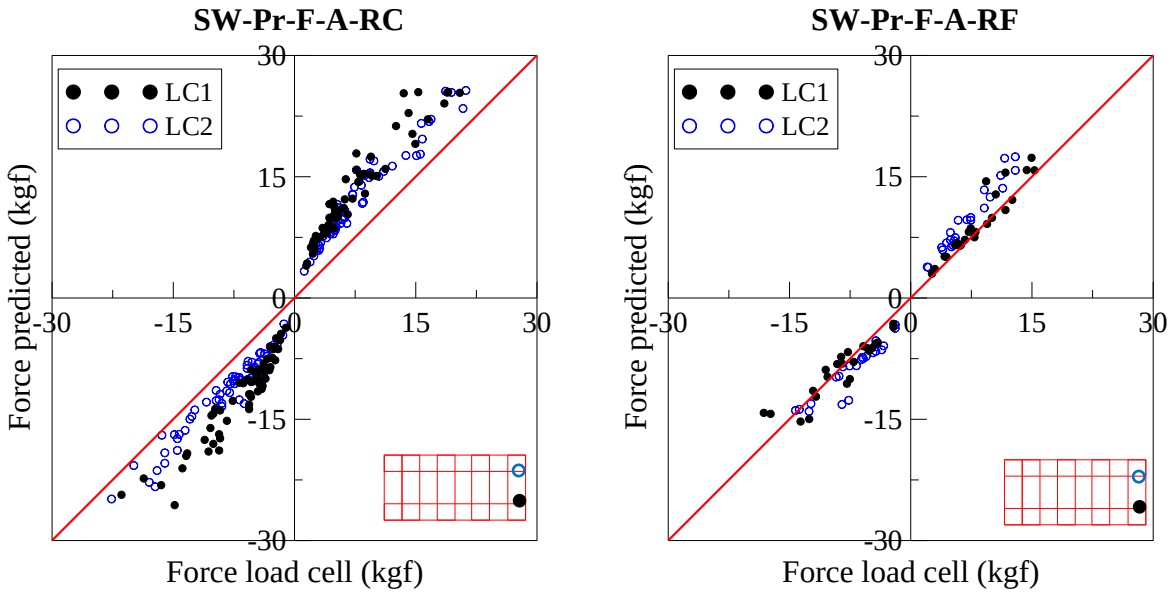

(a) (b)

Figure 3-20 – Comparison between recorded and predicted peak force in sinusoidal tests on ceiling specimens Pr-F-A

In Figure 3-20 to Figure 3-22 values of force measured by the load cells are plotted against the values of predicted force based on Equation 3-2 for all the specimens in sinusoidal and ground motion tests. The first graph in Figure 3-20 is related to series Pr-F-A-RC where ACM7 clips were used on the free ends of grids (Figure 3-20a). This graph shows lower values of load cell force than the second graph where ACM7 clips were removed in series Pr-F-A-RF (especially noticeable in LC1) (Figure 3-20b). A similar trend was observed in the sinusoidal tests on Pr-F-B specimens (Figure 3-21) and also tests under earthquake ground motions (Figure 3-22).

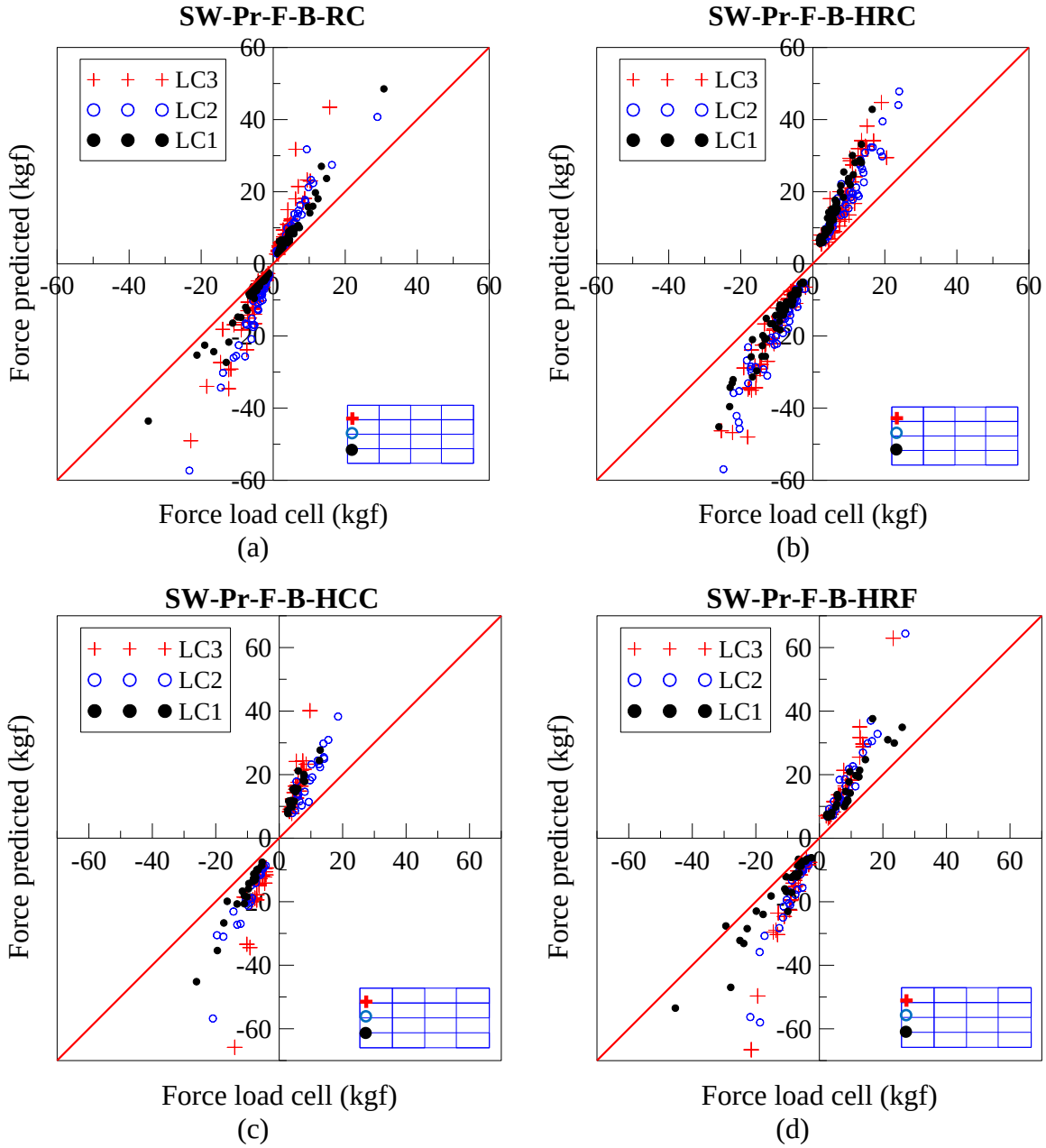

Figure 3-21 – Comparison between recorded and predicted peak force in sinusoidal tests on ceiling specimens Pr-F-B

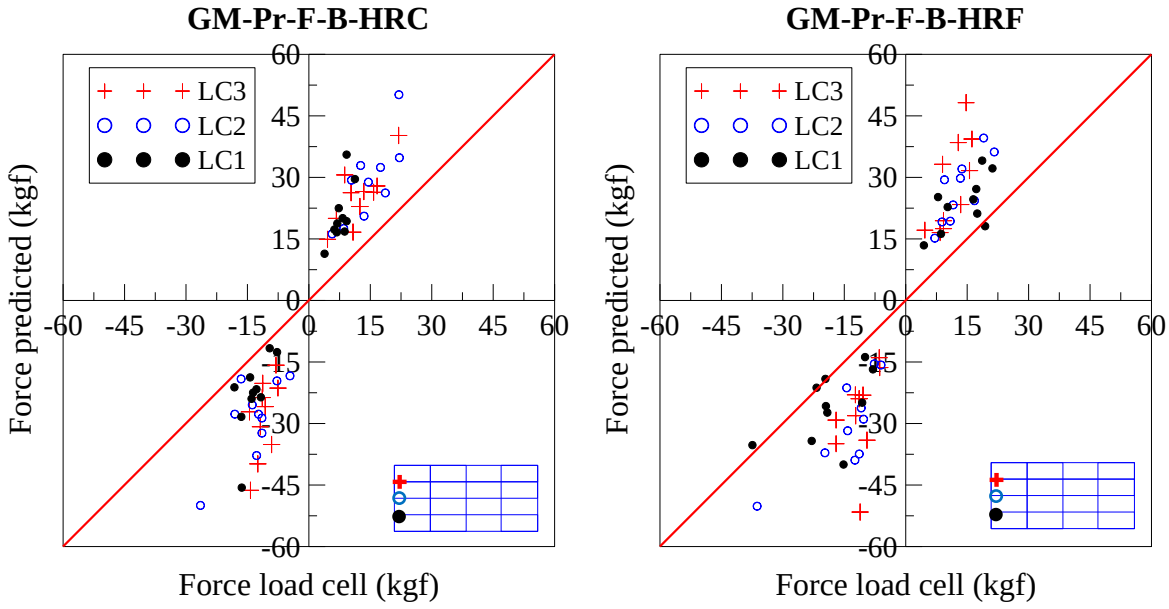

Figure 3-22 – Comparison between recorded and predicted peak force in ceiling specimens in tests with ground motion input

Based on these comparisons, it can be deducted that applying the end clips increased the rigidity of the end connections on transverse tees, which also affected the load transfer in the longitudinal tees. This additional rigidity on transverse grid ends appeared to have forced the clips to carry some initial force; thereby resulting in a reduction of the inertial force in the longitudinal grid ends.

3.5.4 *Effect of filtering on the experimental output*

As mentioned earlier, some of the large accelerations recorded on the ceiling specimen during shake table tests were most likely caused by the haphazard movement of tiles and their impact against ceiling grids. Moreover, in shake table experiments, high frequency noise induced by the test apparatus is also possible. To eliminate these two factors, low-pass filtering was applied to ceiling time history outputs using Seismosignal software (2013). The low-pass filtering excluded all frequencies higher than 25 Hz from the acceleration and axial force time histories recorded by accelerometers and load cells. This frequency limit was chosen far enough from the natural frequencies of the test frame and the ceiling specimens. Figure 3-23 shows the effect of this filtering on the amplifications in the ceiling grid acceleration. Compared to graphs of similar test specimens shown in Figure 3-8 and Figure 3-9, the amplification of peak ceiling grid acceleration with respect to the peak floor acceleration is now below 2 in majority of cases. This indicates that the large amplifications

observed in the test results prior to filtering mainly corresponded to pounding between tiles and grids (which can occur in suspended ceilings) or the noise inherent within the time histories. The part spectral shape coefficient of 2 recommended by NZ Standard (NZS 1170.5:2004) appears to exclude these local grid-tile ponding effects on the ceiling acceleration. Since these large accelerations also occurred at very short periods of time and were mostly observed as random spikes, this recommended coefficient appears to be reasonable for the design. However, given the uncertainties, for a more conservative approach larger values may seem more appropriate.

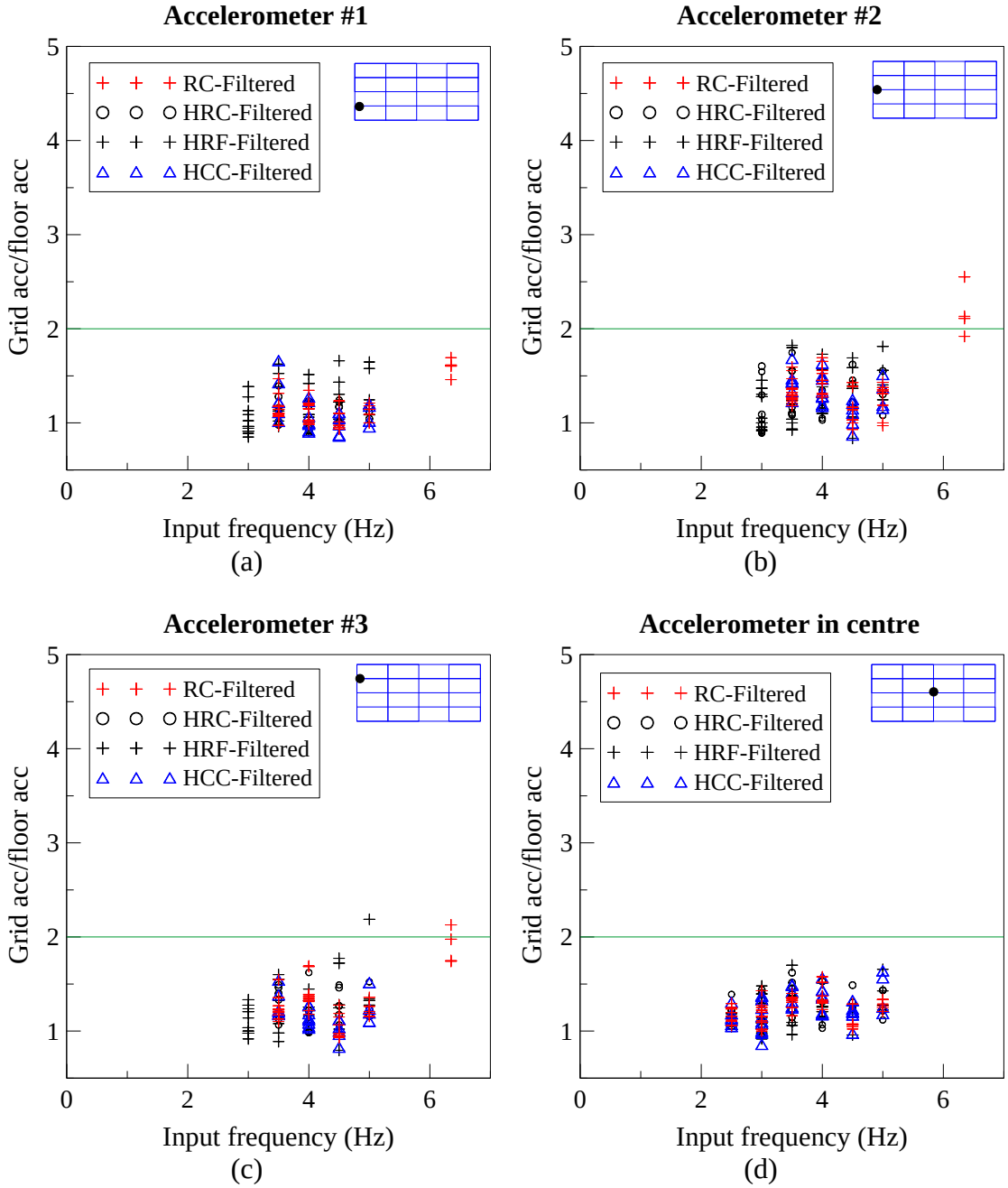

Figure 3-23 – Amplification of peak ceiling grid acceleration compared to peak floor acceleration after applying low-pass filtering

The filtered results were also used to evaluate the relevance of the linear force-acceleration assumption, using the load cells and accelerometers outputs as shown in Figure 3-24. Comparing these plots with those presented in Figure 3-21 shows that in all tests, filtering reduced the scatter in data points. Moreover, the predicted forces (product of mass and acceleration) appeared to be more comparable with the actual recorded forces.

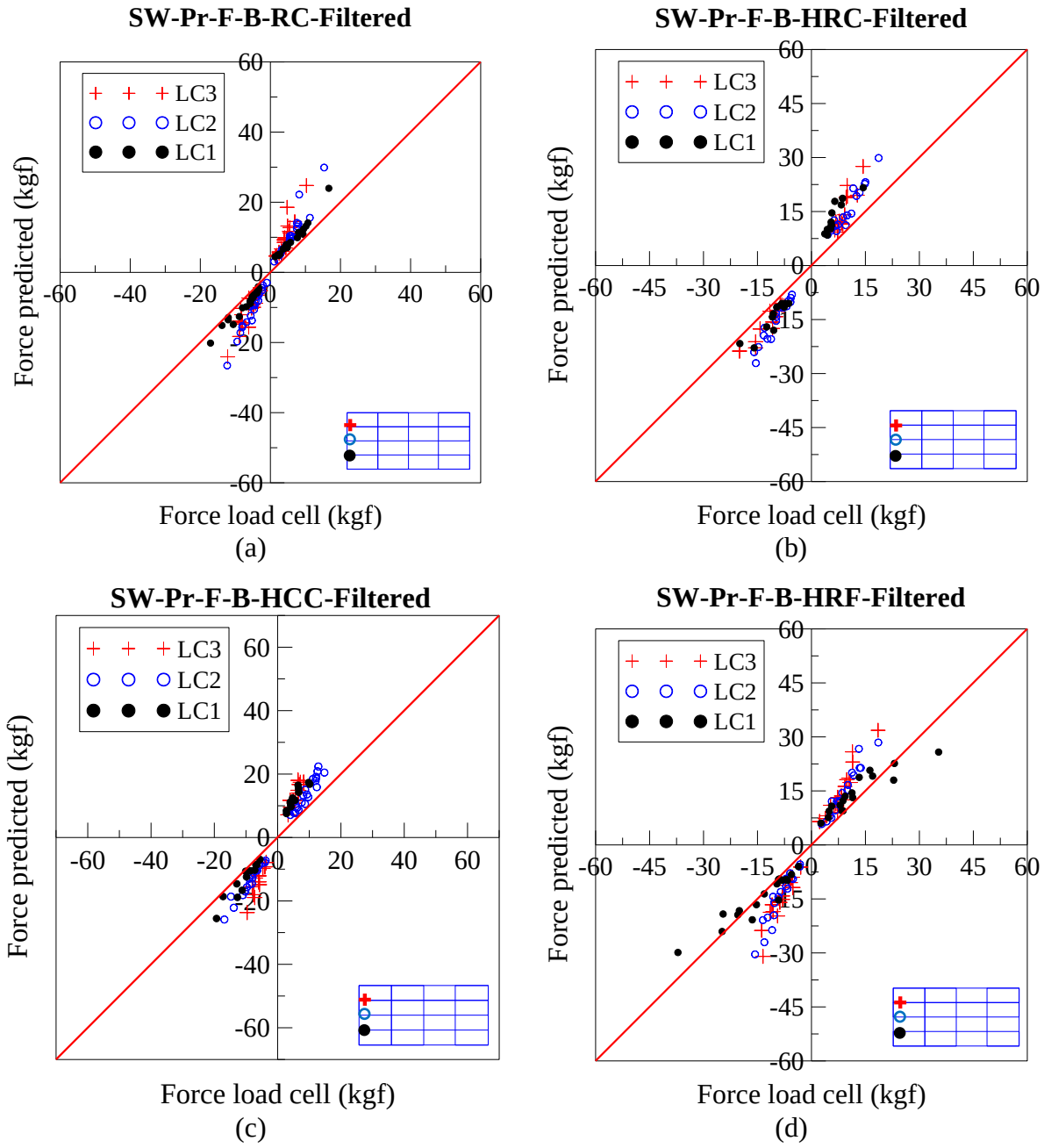

Figure 3-24 – Comparison between peak axial force obtained from load cells vs. peak axial force obtained from peak grid acceleration times tributary area mass of each grid after applying filtering

The low-pass filtering decreased and eliminated the high spikes in the sinusoidal time

histories, resulting in more consistent time histories and peak values. As it can be seen in Figure 3-24, the trend of the peak axial forces was closer to the 45-degree lines which meant that the predicted peak forces were closer to the actual recorded values after the 25 Hz filtering was applied.

3.5.5 *Damage observations*

Damage in the suspended ceiling specimens was observed in a sinusoidal motion test at the input frequency of 6.5 Hz and displacement amplitude of 6 mm. At this input motion the following peak recordings were obtained:

Table 3-5 – recording of instruments at destructive tests

Shake table horizontal acceleration (g)	Frame top horizontal acceleration (g)	Ceiling grid end horizontal acceleration (g)	Ceiling grid centre vertical acceleration (g)	Load cell (kgf)
1.2	1.5	9-10	5.4	65

The damage was observed only in the connection between main tees and cross tees and on the last row of connections before the fixed end. At the failure point where the cross tee clips came apart, enlargement of transverse grid (main tee) slots was observed along with the bending of cross tee (longitudinal grids) end clips that connected through the transverse grid slot (Figure 3-25). This form of damage was observed in previous earthquakes to be followed by dislodgement of tiles and expansion of the failure to surrounding grids. As the system loses its integrity and the additional rigidity provided by tiles is eliminated, the suspension system becomes more susceptible to shaking (Dhakal et al., 2011). The value of axial force recorded in the longitudinal grid at the occurrence of this damage was close to the capacity of cross tee-main tee connections found by Paganotti (2010) in experimental tests of similar grids. The acceleration recordings in grids however were larger than expected which could be explained by the impact of tiles vibrating at high frequency.

When interpreting the PFA and peak grid acceleration at failure point in the experiment, the size and mass of the ceiling tested must be considered. The capacity of the suspended ceiling is governed by the shear capacity of the rivets and axial force capacity of the cross tee-main tee joints (Refer to Chapter 2 of this thesis). Damage can occur when the combination of ceiling mass, grid length and grid acceleration results in a force large enough to exceed these capacities. Therefore, for the design of a safe ceiling, all of the above-mentioned elements (length, mass and acceleration) must be considered simultaneously.

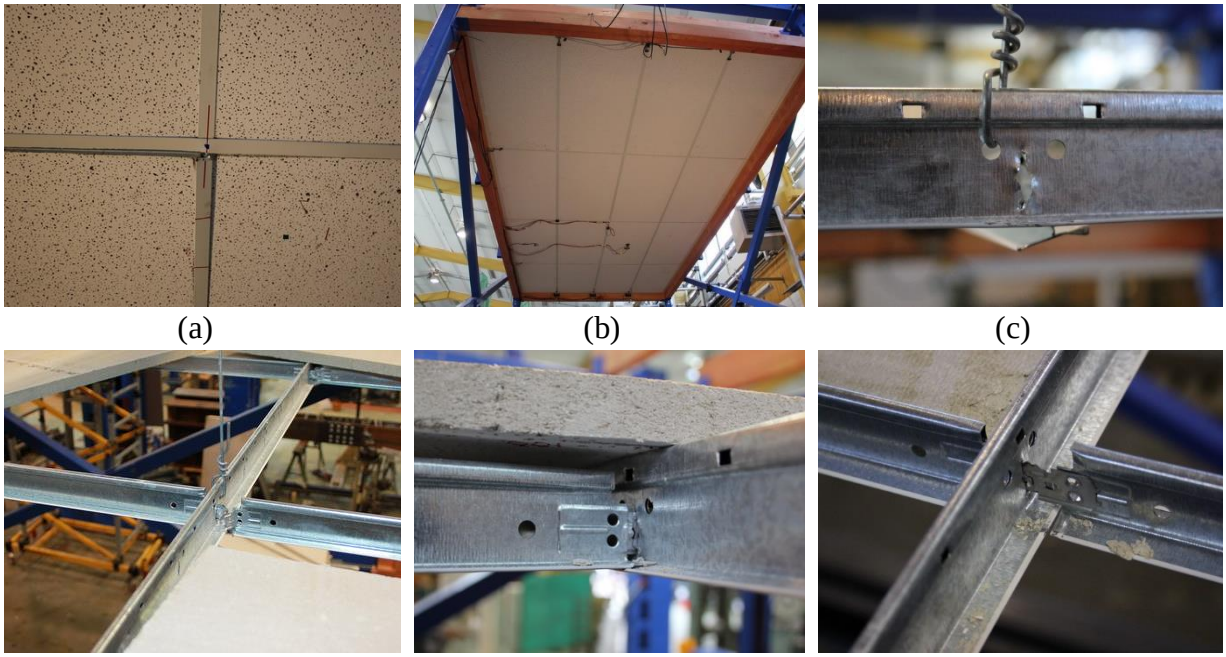

(a) (b) (c)

(d) (e) (f)

Figure 3-25 – Damage in suspended ceiling: (a) connection damaged and partial dislodgement of tiles; (b) location of the last row of connections before the fixed end; (c) tearing in main tee slot; (d) bending in cross tee clips (tiles were manually removed for these observations); (e) & (f) the cross tee clips pushed into the torn main tee slot

3.6 Conclusions

Shake table tests were carried out on two configurations of perimeter-fixed suspended ceilings. Specimens varied in grid layout, weight and end fixing type and were subject to sinusoidal and ground motion excitations. Through these experiments, the relevance of the assumption for linear accumulation of inertial forces in grid members in the direction of loading was checked. Based on the preliminary results and observations, the tributary mass concept to relate grid axial forces with ceiling acceleration appeared to be reasonable and conservative (hence acceptable for design purposes). The reason could lie within the initial assumptions made about the tributary areas and the constant acceleration along the entire length of the grids. In these experiments, the boundary conditions and connections on the transverse grids were observed to affect the distribution of tributary area mass and consequent axial forces in grids.

The amplification of the input acceleration was also investigated in various components of the system including the test frame, grid members and tiles. These amplification factors varied in different locations of the system but appeared to also depend on the frequency and amplitude of excitation. The level of amplification in floor acceleration as it is transferred to

the ceiling grids was observed to be greater than the factor recommended by the NZ design Standard (NZS 1170.5:2004) and in some cases this amplification was more significant than previously thought. Upon the application of low-pass filtering to the recorded acceleration outputs, it was observed that these amplification factors were consistently reduced and remained below the code recommended factor. The filtering eliminated the high frequency contents in the acceleration and axial force time histories which were assumed to result from the impact between ceiling tiles and grids and vertical excitations due to the flexibility of the specimens. This indicated that these high frequency large amplifications which occurred at short periods of time may not be a great concern for the overall design, especially when considered with the overestimation of axial forces predicted.

One of the limitations of these experiments was the unidirectional shake table input. However, due to the special condition of the test frame (overhanging beams), some small vertical accelerations were induced in the frame and at the ceiling level. These vertical accelerations were not controlled and considerable. It is our understanding that in the presence of 3D excitation, larger demands would be expected on the test specimens including potential bending in grid joints and panel dislodgment risk. However, the review of similar experiments on suspended ceilings with 3D excitations showed that the modes of failure and capacity of the system are generally comparable.

In the final destructive test, the system was damaged in the cross tee-main tee connections that could potentially lead to tile dislodgement. Failure occurred at an axial force in the connection similar to the capacity obtained through previous experiments for that type of connection, and it required a shaking with a PFA equal to 1.5 g to damage the ceiling. However, for evaluating the safe design of the ceiling, length of the grids, mass and acceleration on the ceiling grids must be considered simultaneously.

3.7 References

American Society for Testing and Materials International. (2011). *Standard Practice for Installation of Ceiling Suspension Systems for Acoustical Tile and Lay-in Panels in Areas Subject to Earthquake Ground Motions (E580/E580M-11b 2011)*. PA, USA.

ANCO Engineers Inc. (1983). *Seismic Hazard Assessment of Non-Structural Ceiling Components: Phase I* (Report No. 1249.12). Grant 8114155, National Science Foundation, Culver City, California, USA.

Badillo-Almaraz, H., Whittaker, A. S., & Reinhorn, A. M. (2007). Seismic fragility of

suspended ceiling systems. *Earthquake Spectra*, *23*(1), 21-40.

Dhakal, R. P. (2010). Damage to Non-structural Components and Contents in the 2010 Darfield earthquake. *Bulletin of the New Zealand Society for Earthquake Engineering*, *43*(4), 404.

Dhakal, R. P., MacRae, G. A. & Hogg, K. (2011). Performance of Ceilings in the February 2011 Christchurch Earthquake. *Bulletin of the New Zealand Society for Earthquake Engineering*, *44*(4), 379-389.

Gilani, A. S., Reinhorn, A. M., Glasgow, B., Lavan, O., & Miyamoto, H. K. (2010). Earthquake simulator testing and seismic evaluation of suspended ceilings. *Journal of architectural engineering*, *16*(2), 63-73.

Glasgow, B., Gilani, A. S., & Miyamoto, H. K. (2010). Resilient suspended ceilings for sustainable design of buildings. In *Structures Congress 2010* (pp. 2575-2587).

Miranda, E., & Taghavi, S. (2003). Response assessment of nonstructural building elements. *Pacific Earthquake Engineering Research Center, University of California Berkeley, California, USA*.

New Zealand Standard. (2004). *Structural Design Actions Part 5: Earthquake Actions-New Zealand (NZS 1170.5:2004)*. Wellington, NZ: Standards New Zealand.

Seismosoft (2013). "SeismoSignal v5.1 – A computer program for signal processing of strong-motion data," available from http://www.seismosoft.com.

USG Australia. (2012). *Generic Seismic Design for USG DONN Exposed Grid Suspended Ceilings*, Auckland, New Zealand.

CHAPTER 4

EXPERIMENTAL EVALUATION OF THE INFLUENCE OF SEISMIC CLIPS ON GRID JOINTS IN A SUSPENDED CEILING SYSTEM

4 EXPERIMENTAL EVALUATION OF THE INFLUENCE OF SEISMIC CLIPS ON GRID JOINTS IN A SUSPENDED CEILING SYSTEM

4.1 Introduction

Perimeter-fixed suspended ceilings commonly used in commercial buildings in New Zealand (NZ) consist of a grid system and lay-in acoustic tiles. The grid/suspension system consists of main tees (MTs) and cross tees (CTs) forming frame modules that support the tiles. The CT and MT ends are either fixed to perimeters via rivets or the suspension system is back braced to the floor above. Unsatisfactory performance of such ceilings during earthquakes has raised concerns in the past (Dhakal et al., 2011; Dhakal, 2010). Failure of ceilings results in costly and time-consuming repairs and replacements. Damage to services and engineering systems within the ceiling plenum space can be critical and may negatively affect the operation of buildings. Identifying the performance issues and damage states in suspended ceilings has been the subject of many recent studies. Some of these studies were focused on shake table tests of full sized suspended ceilings (Anco Engineers Inc., 1983; Rihal & Granneman, 1984; Badillo-Almaraz et al., 2007; Gilani et al., 2010 & 2012; Glasgow et al., 2010; Pourali et al.; 2015; Ryu et al., 2013), while others investigated the capacity of individual ceiling components under monotonic and cyclic loads (Dhakal et al., 2016; Paganotti, 2010; Paganotti et al., 2011; Soroushian et al., 2015a; 2015b; 2016). Although there are guidelines and recommendations for seismic design and installation of suspended ceilings (Armstrong, 2013; ASCE/SEI7-10, 1994; ASTM C635, 2013; ASTM C636, 2013; ASTM E580, 2011; AS/NZS 2785, 2000; CISCA, 2004; FEMA, 2011; NZS 1170.5, 2004; USG, 2012) as well as fragility curves for ceiling systems and components (Badillo-Almaraz et al., 2007; Ryu et al., 2013) developed for the use of industry, there is still a gap in the areas of retrofitting existing ceilings or development of more resilient ceiling systems.

According to the basic capacity design principles (i.e. weakest link of a chain), a ceiling system's strength is governed by its weakest load-bearing component, which are the CT-MT connections and rivet fixtures around the perimeters of the ceiling grid (Dhakal et al., 2016; Paganotti et al., 2011). Although, the rivets can be strengthened by increasing their size, the CT-MT connection still remains the weakest element contributing to ceiling system failure. Therefore, if ceiling performance is to be improved, this would need to be accomplished by improving the connections.

This study aims to investigate the effects of a proprietary seismic clip on the load carrying capacity and the ductility of ceiling grids. Monotonic tension and compression tests are conducted on two configurations of CT-MT joints;

i) the connection used in as-built practice, and

ii) the connection with a cross-shaped seismic clip.

Based on the experiments, the applicability of these seismic clips for strengthening the CT-MT joints in real life applications is discussed.

4.2 Description of experimental program

4.2.1 *Test setup*

An Instron uniaxial loading apparatus was used for applying tension and compression with strain control. The forces and displacements were measured using a load cell and a potentiometer (Figure 4-1a). The test setup in the tensile tests consisted of the cross-shaped specimens and measurement instruments. The seismic clip maintained the orthogonality between CTs and MT. In specimens without seismic clips, elastic strings were used to straighten up the MT without interfering with the load path. In compression tests, boundary conditions were introduced via additional constraining angle sections in the test setup in order to simulate the effect of ceiling tiles (Figure 4-1b). The rig consisted of a timber panel and eight 50 mm × 50 mm × 5 mm angles. The angles were screwed to the timber panel 4 mm from the edge of the grids to allow for limited in-plane buckling. The MT piece was held horizontal to represent the effect of tiles, however small lateral displacements were allowed (i.e. in practice, tiles are about 5 mm smaller than the module formed by the grids and this difference in size facilitates the installation of tiles).

4.2.2 *Test specimens*

Commonly available standard CT and MT sections in NZ were selected for testing (USG, 2011; USG, 2012), which are also compatible with previous experimental research conducted at the University of Canterbury (Dhakal et al., 2016; Paganotti et al., 2011). The seismic clips (DH4) used are proprietary products provided as a 4-way seismic separation joint (Figure 4-2a). Details of the sections and the used components are given in Table 4-1.

The first configuration, cross-shaped specimens without clips (as-built connections), consisted of one horizontal MT and two vertical CTs that passed and connected through the MT slot. The length of the MT was such that the specimens could easily fit into the test apparatus (uniaxial loading system). Each of the CTs was 300 mm long, summing up to 600

mm in total. The cut ends of the CTs were flattened by pressure and screwed to the loading arms of the test apparatus. In the second configuration, a seismic clip was pushed in place on top of the CT-MT joints and was fastened to CTs via two 3.2 mm Aluminium rivets (Figure 4-2b). The rivet on each wing was placed 10 mm from the edges of the clip.

(a) (b)

Figure 4-1 – Test setup in (a) tension, and (b) compression tests

Table 4-1 – Details of components used in tests (USG, 2011)

CT section	MT section	Seismic clip	Rivet
DX30M-1200 (24 mm × 32 mm)	DX38D-3600 (24 mm × 38 mm)	DH4	1/8” or 3.2 mm AA 4-4
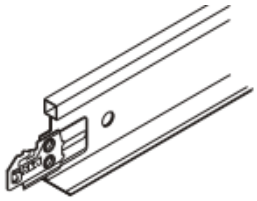	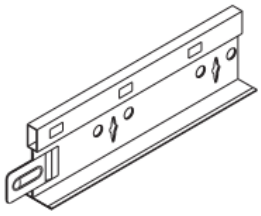	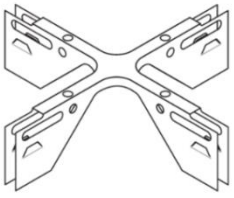	

4.2.3 *Methodology*

Four series of tests were carried out on the two types of test specimens with 40 monotonic tests recorded in total (Table 4-2). The loading rate in both tensile and compressive tests was 0.5 mm/min and the tests were monotonically continued until either brittle failure or very large deformations occurred at the CT-MT joint.

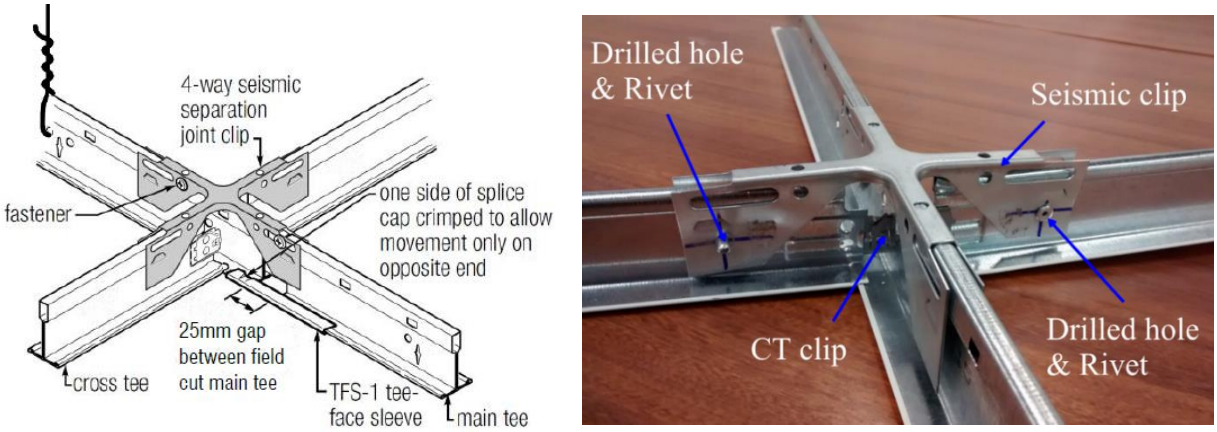

(a) (b)

Figure 4-2 – (a) A 4-way DH4 clip used as seismic separation joint (USG, 2011); (b) CT-MT connection specimen with the 4-way seismic clip for strengthening and 2 rivets on CTs

Table 4-2 – List and number of specimens

Test Series Name	Test Description	Specimen count
CT-MT-T	CT-MT connection in tension	10
CT-MT-C	CT-MT connection in compression	10
CT-MT-CL-T	CT-MT connection with seismic clips in tension	10
CT-MT-CL-C	CT-MT connection with seismic clips in compression.	10

4.3 Experimental results & observations

4.3.1 *Load carrying and failure mechanism*

4.3.1.1 Tests under tension

A typical CT-MT connection consists of two CT members attached through a MT web. This is achieved by the CT clips on the two ends of the CTs passing through the special slot in the MT web and clicking as the CT latches connect (Figure 4-3). This proprietary connection takes advantage of a special interlocking mechanism and no other form of fastening (e.g. rivet or screw) is used on the joint area.

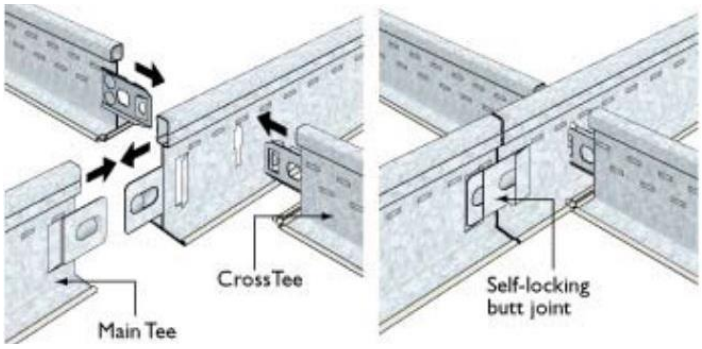

Figure 4-3 – Typical CT-MT connection (Rondo, 2008)

The CT-MT joint tested here was observed to carry the axial load through a special interlocking mechanism shown in Figure 4-4. For this interlocking mechanism to work to its desired capacity, the small latches (Figure 4-4a) must be fully engaged and the load path needs to be aligned with the joint. Any rotations or small deformations may lead to disengagement of the CT clip latches and since there is no other mechanical fastening in the joint, they may carry a lower force than expected and easily disconnect under tension.

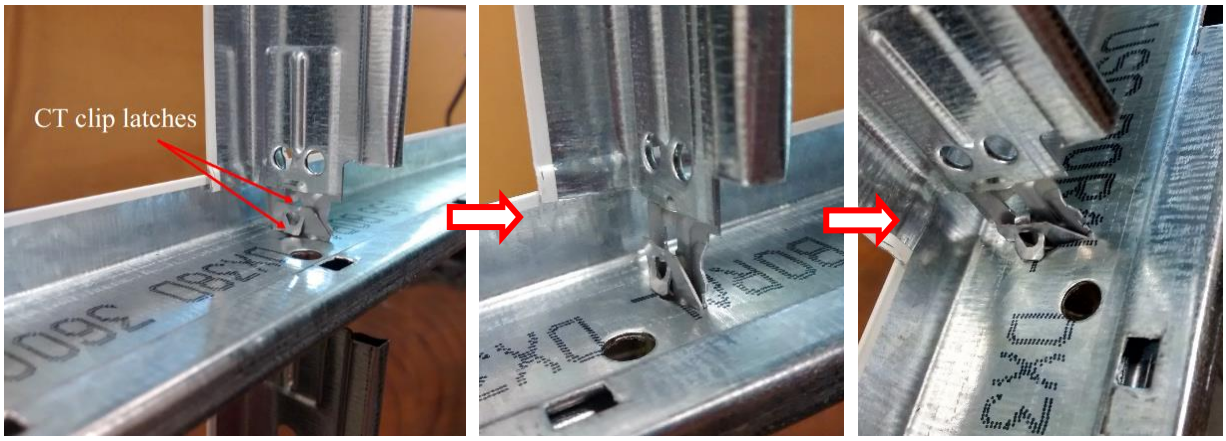

Figure 4-4 – Mechanism of failure due to yielding in CT clip with the clip well engaged (yielding of CT clip latches visible in the second and third images)

a) Tensile tests without seismic clip

In tension tests of the joints without seismic clips, the failure mode understandably depended on the level of engagement of the CT clips. With complete engagement of the CT clips, i.e. the latches on two connected CTs engaged in the load carrying process, as shown in Figure 4-4a-c the connection failed by gradual yielding of the CT clip (referred to as "TF1"). In other tests without engagement of the CT clips, the latches prematurely released and caused the CT clips to slide past each other. When this occurred only the top and bottom dents on the CT clips were observed to pull against the MT slot briefly before the joint disconnected (referred to as "TF2"). This type of premature failure can expose a ceiling to local failure of grids and panel dislodgement. An example of force-displacement response for two similar CT-MT joints tested in tension is shown in Figure 4-5a. In this example, the premature failure in the CT clip resulted in failure at almost 30% of the actual capacity of the joint with good engagement.

b) Tensile tests with seismic clip

CT-MT joints with seismic clips showed increased force carrying capacity compared to the joints without seismic clips. While the induced displacements got larger, the force carried by

the seismic clip system did not drop severely and there was a residual force carrying capacity within the yielding plateau (where the CT clip latches had disengaged already). Therefore, the seismic clip application added ductility to the otherwise fragile CT-MT joints. In tests with seismic clip, the failure of the specimen was governed mostly by the buckling of the joint (Figure 4-6). In the specimen with disengaged CT clips, as shown in Figure 4-5b, the failure occurred at approximately 0.8 kN due to disengagement of CT clips, which was still higher than the as-built CT-MT joint. After this premature failure, unlike connections without seismic clip, the joint continued carrying forces up to 1.4 kN. Complete failure of the joint occurred after a relative displacement of about 11 mm between the two ends of the disconnected CT clips, which corresponds to total loss of load bearing capacity. The use of seismic clips in this example increased the ductility of the CT-MT joint significantly.

The final modes of failure in tension tests with seismic clip were; i) failure of the lower rivet connections between the seismic clips and CTs (Figure 4-6c), ii) tearing of the CT web at the location of rivet hole (Figure 4-6b) (referred to as “TF3”).

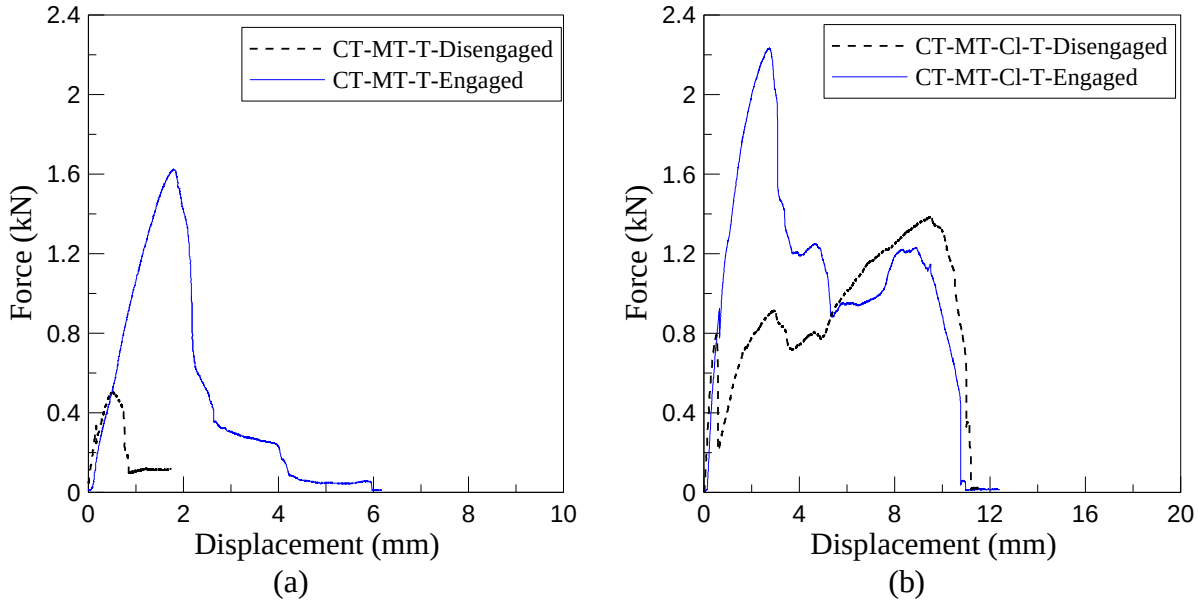

Figure 4-5 – Examples of tension tests showing effect of CT clip engagement (a) without seismic clip, and (b) with seismic clip

(a) (b) (c)

Figure 4-6 – Failure of CT-MT joint with seismic clip in tension: (a) yielding in CT clip, (b) tearing of CT web, and (c) yielding and shear failure in rivet

4.3.1.2 Tests under compression

The mechanism of load bearing and failure of CT-MT joints under compression are different from those in tension. These failures include in-plane and out-of-plane yielding of CT clips and penetration of CT section into MT web.

a) Compression tests without seismic clip

Under compression, majority of specimens without seismic clips first showed yielding in the small CT clip latches, followed by the lateral buckling of the CT clip (Figure 4-7a) (referred to as "CF1"). However, in some cases, the CT clips were not engaged in the load bearing process and the two CT clips slid parallel to each other and into the MT slot (Figure 4-7b). Eventually the CT clip tore into the web of the MT (Figure 4-7c) (Referred to as "CF2").

Figure 4-8a shows two examples of force-displacement curves for the CT-MT connection under compression. The sudden drop in the dashed curve corresponds to the premature disengagement of the CT clip latches. After this point the lateral buckling of the CT clips commenced. Unlike tensile tests, the ultimate forces in these two specimens were not significantly different as the load bearing mechanism was relatively similar after the disengagement of the CT clip latches.

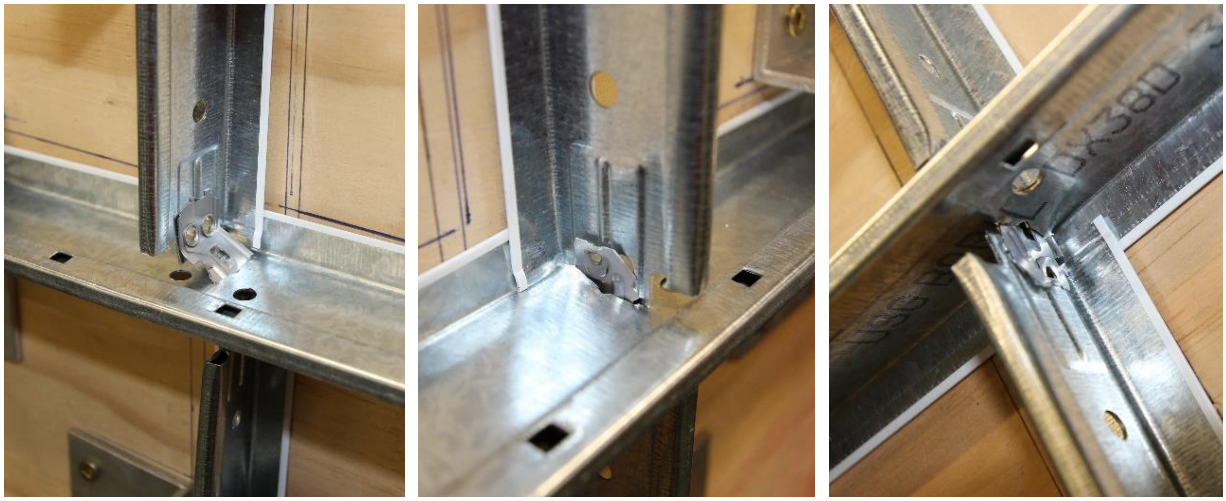

(a) (b) (c)

Figure 4-7 – Failure of CT-MT joint in compression: (a) in-plane buckling of CT clips, (b) CT section pressed to MT web, and (c) CT clips sliding through and tearing MT web

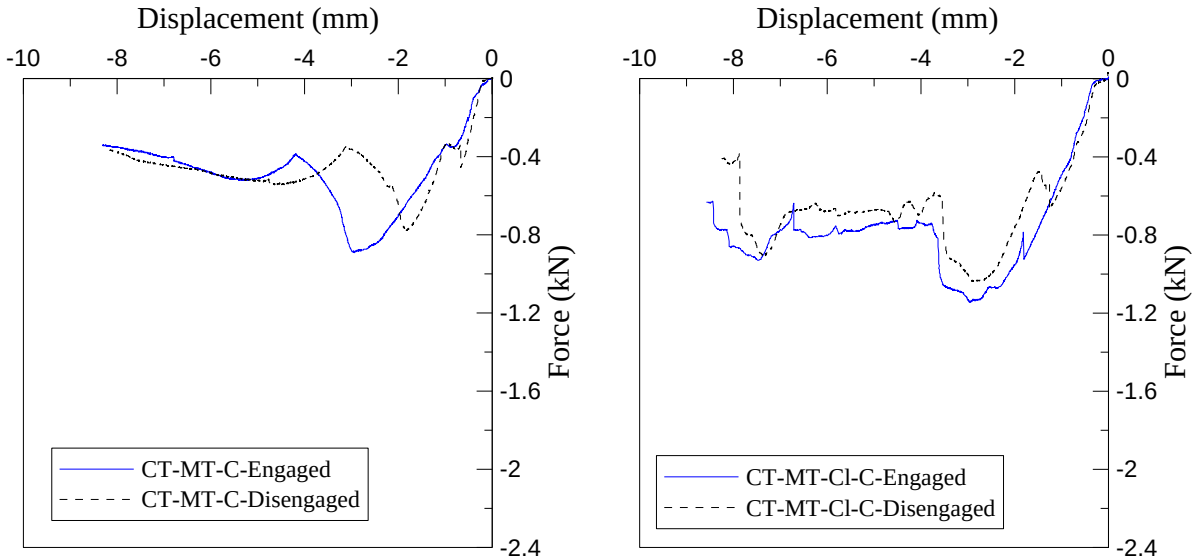

(a) (b)

Figure 4-8 – Examples of tests showing effect of CT clip engagement on connections' load bearing capacity in compression tests (a) without seismic clip, and (b) with seismic clip

b) Compression tests with seismic clip

With the addition of seismic clips, the deformation in the joint area changed to out-of-plane buckling as the seismic clip reduced the sideway deformation of the CT clip (Figure 4-9) (referred to as "CF3"). However, still bending in the CT clip was observed under compression. The ultimate force carried by the connection was higher in specimens with seismic clips (Figure 4-8b). The failure of rivets or tee sections were not observed in any of

these tests. The tests were stopped when the deformations in the joint area reached high enough values to cause buckling, posing damage risk to the instruments.

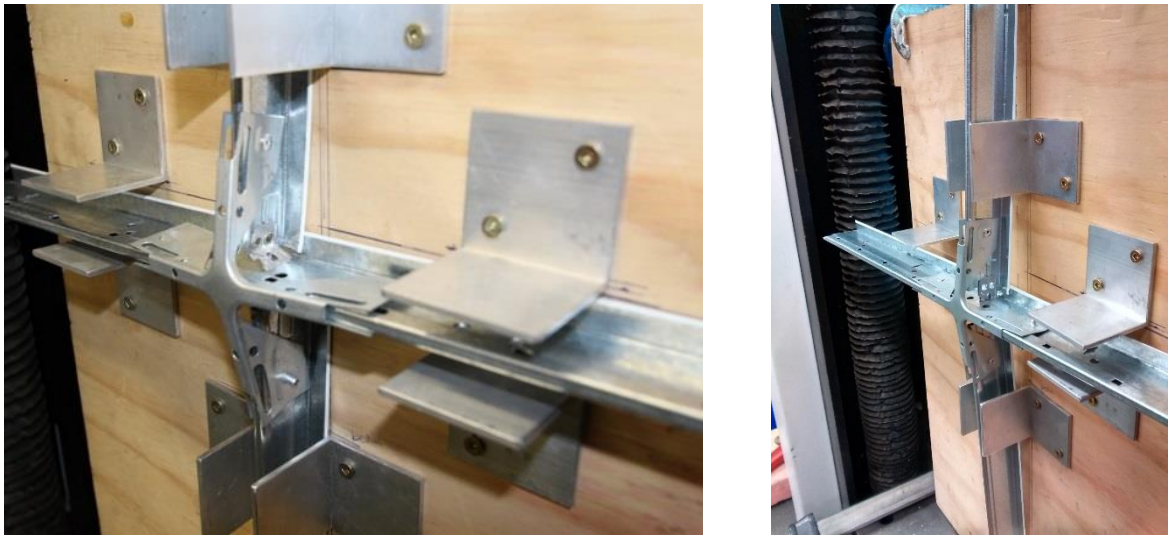

(c) (d)

Figure 4-9 – Failure in CT-MT joints with seismic clip: (a) bending in CT clip, and (b) out of plane buckling

4.3.2 *Discussion of Results*

4.3.2.1 Response of joints in tension

Figure 4-10 summarises all test types carried out along with the modes of failure observed.

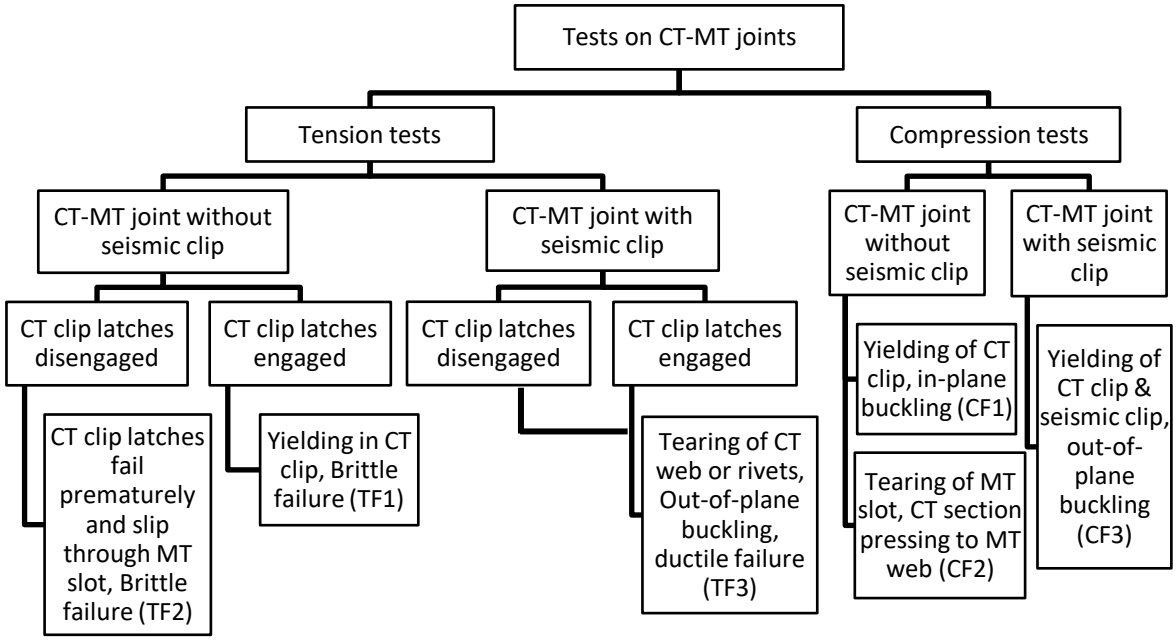

Figure 4-10 – summary of tests and failure modes

Considering the tensile failure mechanisms TF1 and TF2, Figure 4-11 shows the performance comparison of the CT-MT joints for these two mechanisms. As expected, the load bearing capacity of the engaged CT clips was clearly higher (Figure 4-11a). In both conditions, after the connections capacity was exceeded, brittle response was observed in the form of sudden drop of the recorded force values.

Results of these experiments showed that proper engagement of CT clip latches had a significant effect on the overall capacity of the joint. During the preparation of the specimens, special care was taken to make sure the CT clips were not damaged or improperly connected. Also, the MTs were kept horizontal throughout all the tests. It is evident that in practice any workmanship error during installation may pose a risk to the proper engagement of the CT clips when loaded and may lead to premature failures in the joints. Moreover, in as built CT-MT joints (without any seismic clips), the clips and latches are the only forms of fixture at the connection area so their failure is essentially brittle without any remaining load carrying capacity.

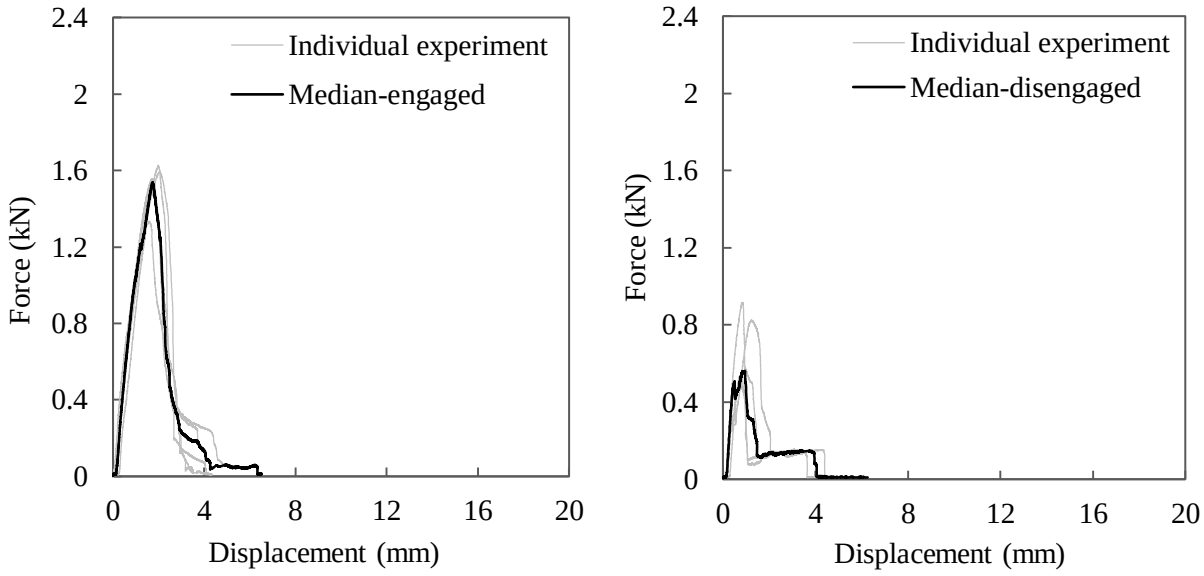

Figure 4-11 – Results of tensile tests on CT-MT joints without seismic clips with (a) complete CT clip engagement (TF1) and (b) CT clip disengaged (TF2)

The addition of seismic clips in the second phase of tension tests proved to be a satisfactory solution for this shortcoming in the CT-MT joint. In both conditions (whether or not the CT clip latches were engaged) the connection with seismic clip had higher capacities than those without (Figure 4-12). More importantly even after the CT clip failed, the joint continued to carry forces with increasing deformations (i.e. signs of ductility). This means that the addition

of seismic clips was beneficial in increasing both the maximum and residual load carrying capacities of the connection in addition to its ductility.

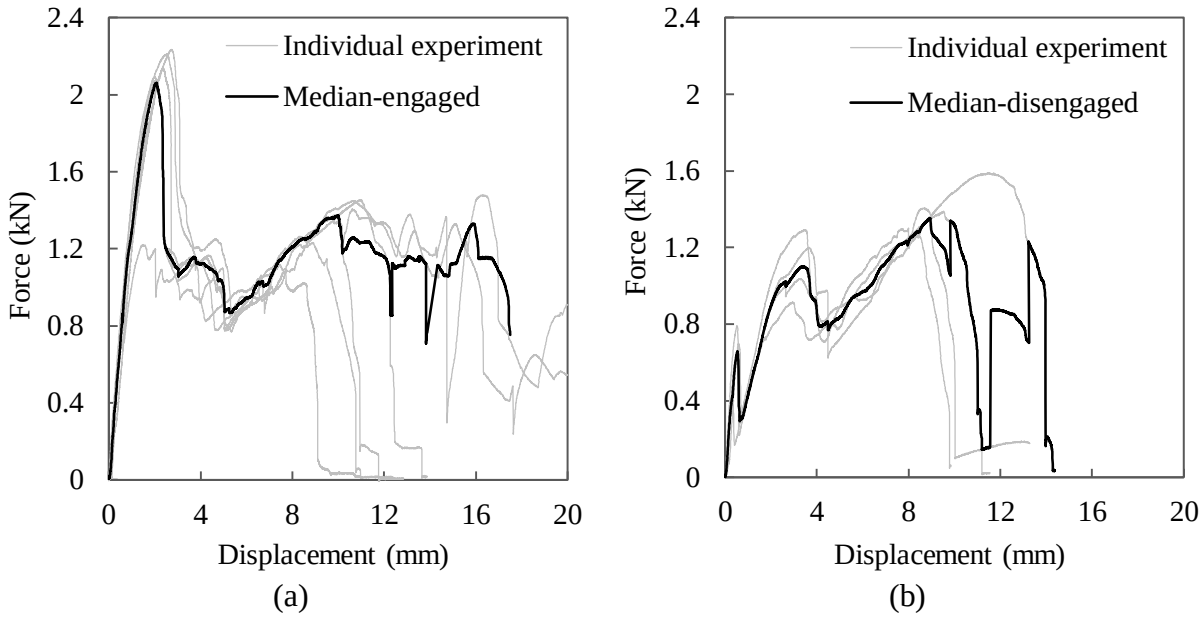

Figure 4-12 – Results of tensile tests on CT-MT joints with seismic clips with (a) complete CT clip engagement (TF1) and (b) CT clip disengaged (TF2)

Comparing the median curves for specimens tested under tension in the two aforementioned categories based on CT clip engagement (Figure 4-13) shows that in both categories, adding seismic clips increased the load bearing capacity and deformability of the joint. The stiffness of the joint was not significantly affected by this change.

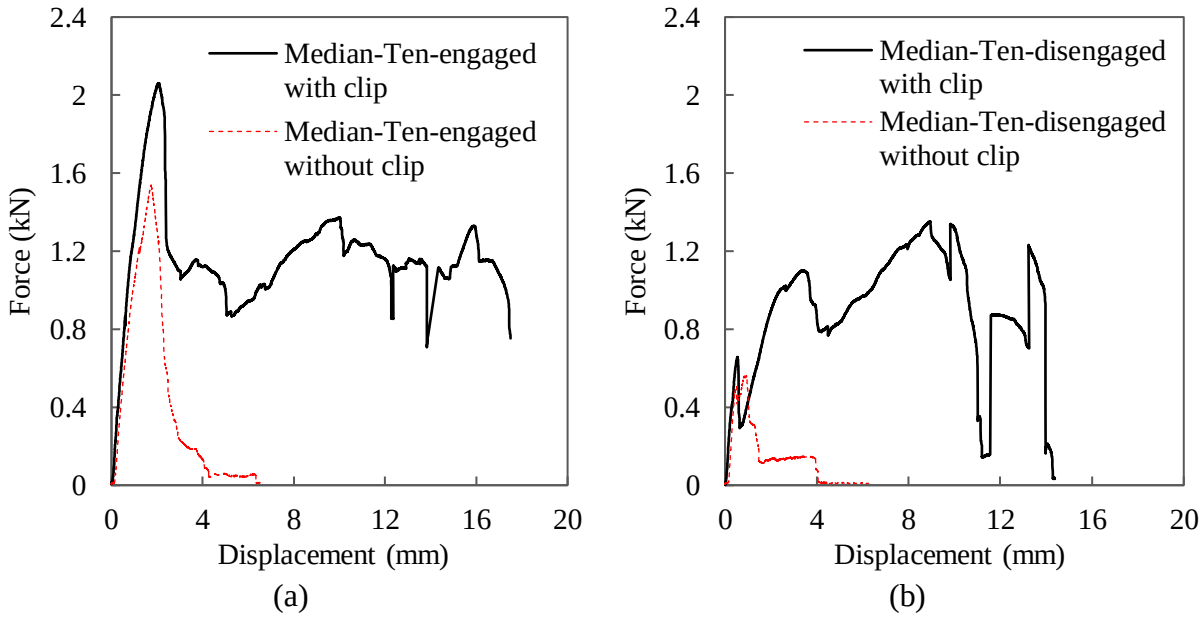

Figure 4-13 – Comparison of CT-MT joints response under tension with and without seismic clips, (a) with CT clip engaged, and (b) with CT clip disengagement

4.3.2.2 Response of joints in compression

Since the mechanism of failure under compression is different from tension, the engagement of the CT clip latches did not play an important role in these tests. Under compression, the CT clips bent about their major axis and after that the CT section was pressed to the MT web. Therefore, the force-displacement curves did not show a brittle failure as observed in tension tests (Figure 4-14). Moreover, similar to the tension tests, the addition of seismic clips increased the maximum force carried by the joint (Figure 4-15) while having no effect on the stiffness of the CT-MT joint.

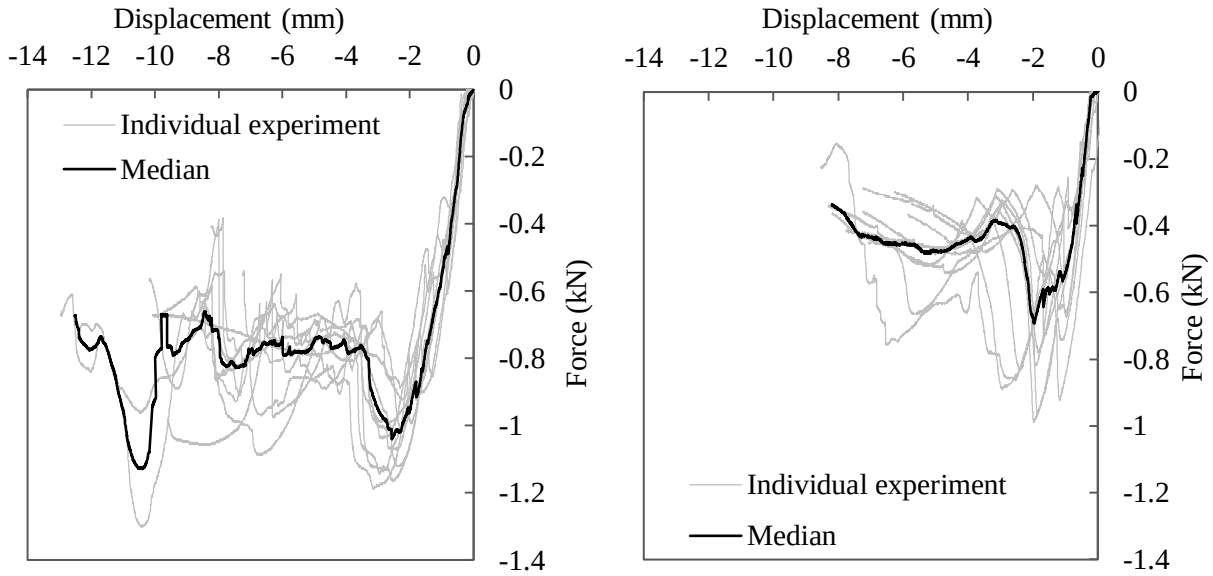

Figure 4-14 – Results of compression tests on CT-MT joints (a) with, and (b) without seismic clips

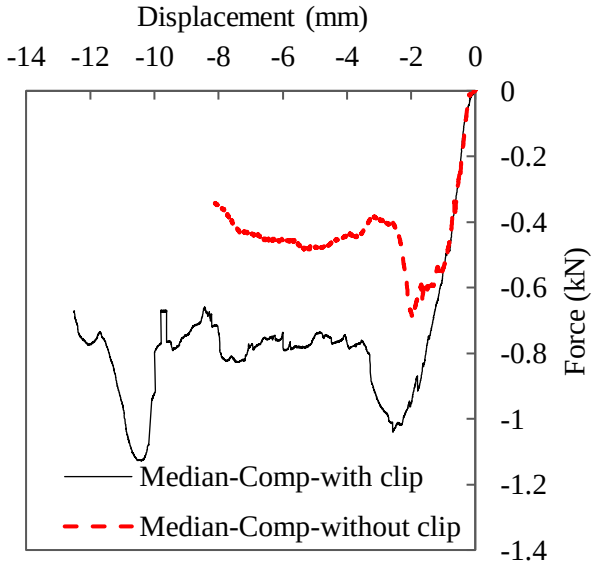

Figure 4-15 – Comparison of CT-MT joints response under compression with and without seismic clip

4.4 Fragility studies

4.4.1 *Damage state and definition of failure*

Fragility curves reported in this section were based on a single damage limit state. The failure force is the maximum force carried by the joint before the occurrence of brittle failure. In some of the compression tests, the maximum force was recorded at the end of the tests and that was associated with CT section being pressed against the MT web. This maximum force was ignored and the failure force reported was the initial maximum observed in the tests (Figure 4-16).

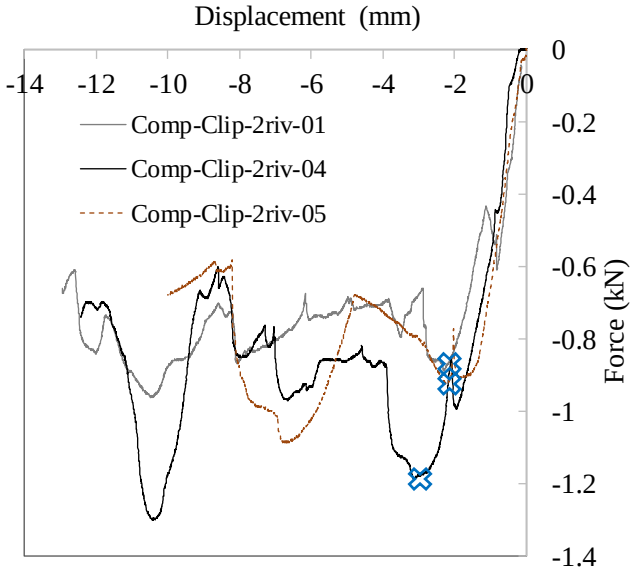

Figure 4-16 – Example of determining failure force (crossed) in compression tests

4.4.2 *Fragility curves*

Fragility curves for the tested specimens are created using lognormal distributions based on the results of the goodness-of-fit tests performed by the authors on distribution of suspended ceiling component test results (Dhakal et al., 2016). Under tension, the results showed a larger dispersion than in compression tests (Figure 4-17a). This was due to the different performance of the joint with regard to the engagement of CT clip in carrying load. Therefore, these results were classified into two groups (i.e. engaged vs. disengaged) and fragility curves were derived for them separately. Figure 4-17a shows the cumulative lognormal distribution of failure forces in all CT-MT joints under tension and compression as well as the experimental results. In Figure 4-17b lognormal cumulative distributions are shown for tension tests with the results classified with respect to the engagement or

disengagement of CT clip latches.

Separating the fragility curves in two categories based on the addition of seismic clips (Figure 4-18) showed the improvement resulting from the seismic clip application. This improvement was more noticeable in tension tests due to the failure mode and the level of involvement of the seismic clip in load bearing.

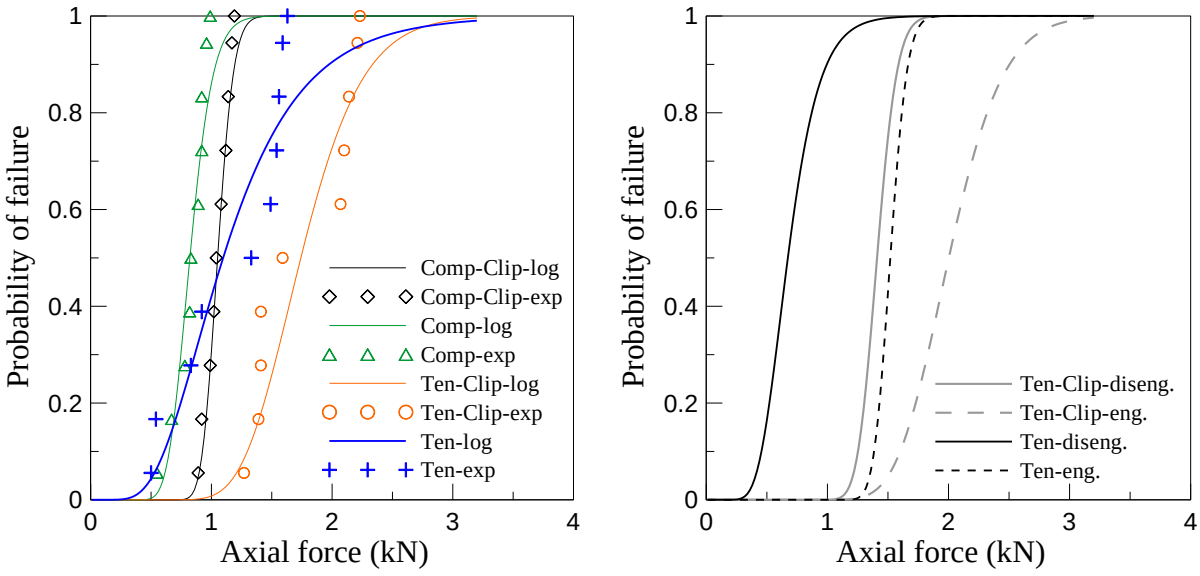

(a) (b)

Figure 4-17 – (a) Lognormal fragility curves for the axial failure force vs. experimental data; (b) Fragility curves for tension tests with & without clips

(*Note: Comp: Compression, log: lognormal distribution, exp: experimental result, Ten: tension, eng.: engaged and diseng.: disengaged.)*

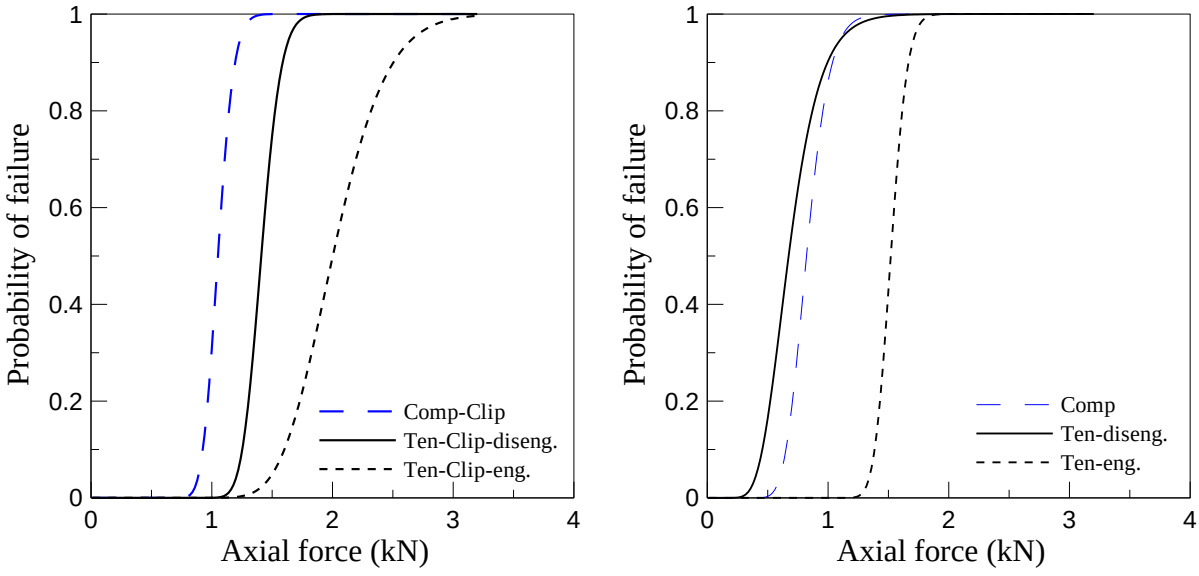

(a) (b)

Figure 4-18 – Fragility curves for all CT-MT joint tests (a) with, and (b) without seismic clip

To determine the capacity of the entire ceiling system, fragility curves from Figure 4-18 need to be compared with the fragility curves previously derived for other components of a suspended ceiling e.g. end fixing rivets or MT splices (Figure 4-19) (Dhakal et al., 2016; Paganotti, 2010). When making such comparisons, it is important to consider that these results were obtained for standard grids which have lower capacities than heavy-duty grids (Refer to details of cross sections in Section 4.2). Based on the comparison between fragility curves of different components shown in Figure 4-19, it is clear that the addition of seismic clips significantly improved the performance of the CT-MT clip in tension, and some improvement can be observed in compression, too. However, Figure 4-19b emphasises that the seismic clip application needs to be accompanied with improvements in other components such as end fixing rivets, to result in the overall improvement of the ceiling system.

(a)

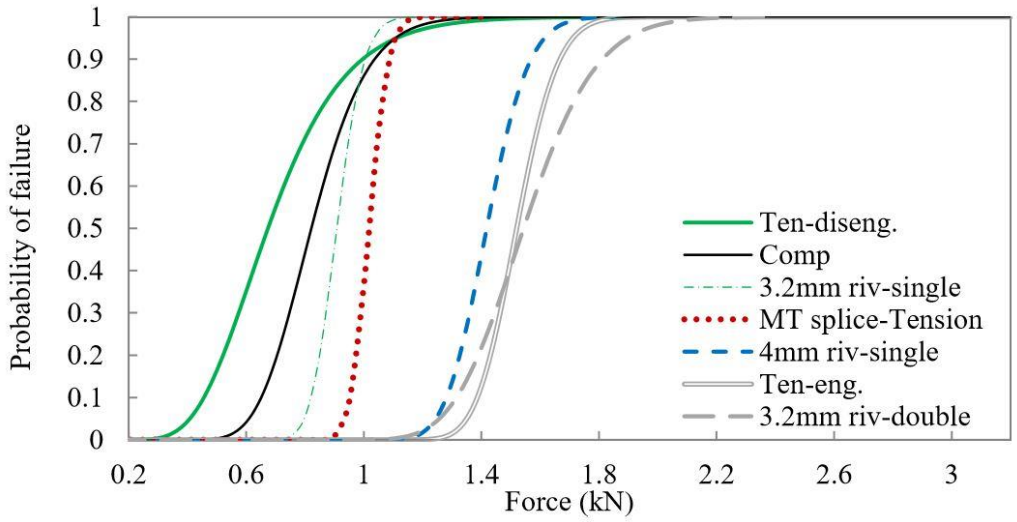

(b)

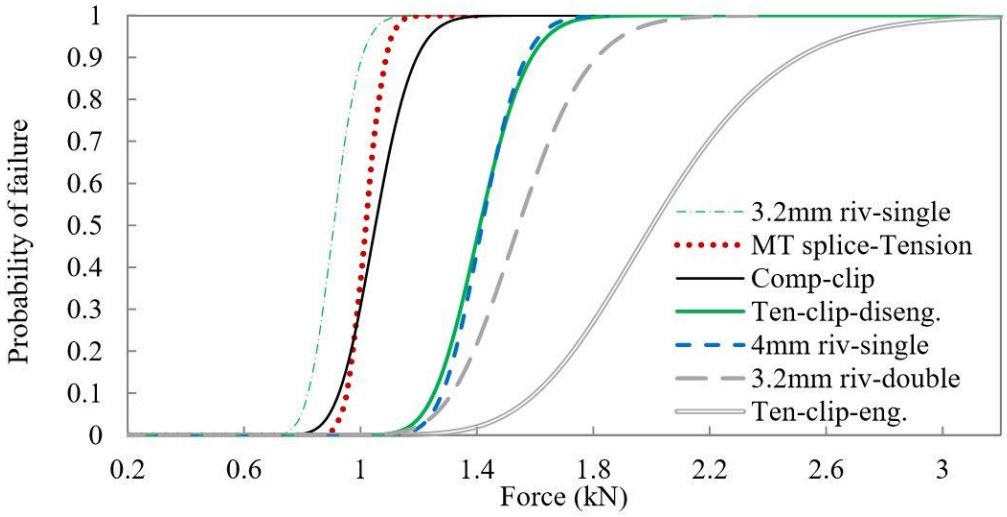

Figure 4-19 – Fragility curves comparing other ceiling components (Dhakal et al., 2016; Paganotti, 2010) with CT-MT connections (a) without, and (b) with seismic clips

The majority of the expense of the installation of suspended ceilings is associated with labour cost. After acquiring a quote from a quantity surveyor, the cost of installation of a simple suspended ceiling is estimated to be approximately $60 per square meter, including material and labour. The labour cost alone is estimated to be $55-70 per hour (assuming $60/hr). Assuming an average cost of $6 per clip ($3 for material and $3 for labour), the overall extra cost associated with adding these clips to a suspended ceiling is estimated to be approximately 10% of the total ceiling cost (material and labour).

4.5 Implications and recommendations for further studies

The information reported in this paper can help with the evaluation of a designed ceiling or retrofitting an existing ceiling using these seismic clips. According to previous studies (Paganotti, 2010), CT-MT joints and perimeter rivets are the weakest elements of a suspended ceiling. Several experimental studies have also reported the failure in these two components as the initial forms of damage observed in shake table tests (Anco Engineers Inc., 1983; Badillo-Almaraz et al., 2007; Gilani et al., 2010 & 2012; Glasgow et al., 2010; Rihal & Granneman, 1984; Ryu et al., 2013). Based on the experiments reported in this paper, one simple improvement method can be through the application of seismic clips at CT-MT joints. Results of the experiments showed that the CT-MT joint with seismic clips had a higher capacity in carrying axial forces. However, this improvement must be accompanied by strengthening the splices on MTs and increasing the size or the number of end fixing rivets. The possibility of strengthening MT splices using 2-way seismic separation clips needs to be further investigated through experiments.

The connection capacities reported here were associated with standard grids which are made out of thinner base metal than heavy-duty grids recommended for high seismic areas. As one of the failure modes recorded in tension tests was tearing in the CT web, it is recommended that similar investigations should be conducted on the effects of seismic clips on heavy-duty grids. Since the type of CT clips used on both standard and heavy-duty grids are the same, it is expected that the overall connection capacity in the as-built connection (i.e. CT-MT joint without clip) would not be significantly different in tests on heavy-duty grids.

The other significant improvement in the strengthened CT-MT joint lies within the increased ductility/residual load carrying capacity of the joints strengthened with seismic clips. In the tests carried out, after the failure of the CT clip latches, seismic clips came into action and prevented the two CTs from separating and creating a local failure. This mechanism in a

ceiling can delay the spread of damage and allow for the safe evacuation of occupants while still showing damage signs. With large deformations of CT-MT joint, there is a risk of panel dislodgement. However, this is considered less dangerous in lighter ceilings than the loss of the suspension system which usually results in domino effect and loss of the system's unity and complete collapse. However, the deformability of a ceiling grid is limited by the panels and other services installed within the grid. The interaction of seismic clips with these services can be investigated in a full scale ceiling experiment strengthened by seismic clips.

The experiments reported here were carried out using axial loads and results showed no significant change in the initial slope of the force-displacement graphs with the addition of seismic clips. With the limited loading conditions, it is difficult to comment on the generic effect of seismic clips on the overall stiffness of the suspension system under diagonal loads. However, based on the observations made in these tests, the seismic clips limited the free rotation of CTs and MTs at the connection point and increased the rigidity of the joint area. This can result in an overall more rigid suspension system which could withstand bidirectional loads better. It is recommended that this effect be tested in a full-size ceiling system under bidirectional loads.

4.6 Conclusions

Monotonic tension and compression tests were carried out on suspended ceiling cross tee-main tee (CT-MT) connection specimens with and without seismic clips. During these tests, different failure modes were observed in the connection area and fragility curves were derived for the as-built and the strengthened connections. Results showed that using seismic clips improved CT-MT connection performance in two ways: i) increasing the maximum and residual capacity, and ii) adding ductility. When seismic clips were added, initial failure always occurred in the CT clip, followed by larger deformations and buckling in the seismic clips. Comparisons showed that using seismic clips in all cases increased the failure force in the connection. However, to transfer this component level gain to the performance of the whole suspended ceiling system, use of these 4-way seismic clips must be accompanied by strengthening other critical components of the ceiling such as the splices on MTs and increasing the size or number of end fixing rivets. With the addition of seismic clips, the connection's failure mode was no longer brittle. The connection with seismic clips experienced a number of failure and yielding phases while still carrying forces as large as that of the as-built CT-MT connection. This ductility together with substantial residual load carrying capacity in the grid of suspended ceilings can delay the spread of damage and allow

for the safe evacuation of occupants while still showing signs of damage.

4.7 References

American Society of Civil Engineers. (1994). *Minimum Design Loads for Buildings and Other Structures (ASCE/SEI 7-10.), Vol. 7, Chapter 13: Seismic Design Requirements for Non-Structural Components*. USA: American Society of Civil Engineers.

American Society for Testing and Materials. (2013). *Standard Specification for the Manufacture, Performance, and Testing of Metal Suspension Systems for Acoustical Tile and Lay-in Panel Ceilings (C635/C635M)*. PA, USA.

American Society for Testing and Materials. (2013). *Standard Practice for Installation of Metal Ceiling Suspension Systems for Acoustical Tile and Lay-in Panels (C636/C636M)*. PA, USA.

American Society for Testing and Materials International. (2011). *Standard Practice for Installation of Ceiling Suspension Systems for Acoustical Tile and Lay-in Panels in Areas Subject to Earthquake Ground Motions (E580/E580M-11b 2011)*. PA, USA.

ANCO Engineers Inc. (1983). *Seismic Hazard Assessment of Non-Structural Ceiling Components: Phase I* (Report No. 1249.12). Grant 8114155, National Science Foundation, Culver City, California, USA.

Armstrong (2013). *"Seismic Design Guide New Zealand Version, Suspended Ceiling Systems"*. Armstrong, Auckland, New Zealand.

Australian/New Zealand Standard. (2000). *Suspended ceilings - Design and Installation (AS/NZS 2785:2000).* Wellington, NZ: Standards New Zealand.

Badillo-Almaraz, H., Whittaker, A. S., & Reinhorn, A. M. (2007). Seismic fragility of suspended ceiling systems. *Earthquake Spectra*, *23*(1), 21-40.

Ceilings and Interior Systems Construction Association CISCA. (2004). "Guidelines for Seismic Restraint for Direct Hung Suspended Ceiling Assemblies, Seismic Zones 3-4". Illinois, USA: Ceiling and Interior Systems Construction Association.

Dhakal, R. P. (2010). Damage to Non-structural Components and Contents in the 2010 Darfield earthquake. *Bulletin of the New Zealand Society for Earthquake Engineering*, *43*(4), 404.

Dhakal, R. P., MacRae, G. A. & Hogg, K. (2011). Performance of Ceilings in the February

2011 Christchurch Earthquake. *Bulletin of the New Zealand Society for Earthquake Engineering, 44*(4), 379-389.

Dhakal, R. P., MacRae, G. A., Pourali, A., & Paganotti, G. (2016). Seismic fragility of suspended ceiling systems used in NZ based on component tests. *Bulletin of the New Zealand Society for Earthquake Engineering, 49*(1), March 2016

FEMA. (2011). *Reducing the Risks of Non-Structural Earthquake Damage – A Practical Guide (FEMA E74)*. Washington D.C., USA.

Gilani, A. S., Reinhorn, A. M., Glasgow, B., Lavan, O., & Miyamoto, H. K. (2010). Earthquake simulator testing and seismic evaluation of suspended ceilings. *Journal of architectural engineering, 16*(2), 63-73.

Gilani, A. S., Takhirov, S. M., & Tedesco, L. (2012). Seismic evaluation procedure for suspended ceilings and components new experimental approach. In *Proceedings of the 15th World Conference on Earthquake Engineering*. Lisbon, Portugal, 20-24 September 2012.

Glasgow, B., Gilani, A. S., & Miyamoto, H. K. (2010). Resilient suspended ceilings for sustainable design of buildings. In *Structures Congress 2010* (pp. 2575-2587).

New Zealand Standard. (2004). *Structural Design Actions Part 5: Earthquake actions-New Zealand (NZS 1170.5:2004)*. Wellington, NZ: Standards New Zealand.

Paganotti, G. (2010). *Behaviour of Suspended Ceiling System during Seismic Events: Development of Fragility Curves*. (Masters Thesis, Politecnico Di Milano, Italy).

Paganotti, G., MacRae, G. A., & Dhakal, R. P. (2011, April). Development of typical NZ ceiling system seismic fragilities. In *Ninth Pacific Conference on Earthquake Engineering (PCEE)* (pp. 14-16).

Pourali, A., Dhakal, R. P., MacRae, G. A., & Tasligedik, A. S. (2015). Shake table tests of perimeter-fixed type suspended ceilings. In *New Zealand Society for Earthquake Engineering Annual Technical Conference* (pp. 648-659).

Rihal, S. S. & Granneman, G. (1984). *Experimental Investigation of the Dynamic Behavior of Building Partitions and Suspended Ceilings during Earthquakes*. Report No. ARCE R-84-1, California Polytechnic State University, San Luis Obispo, California, USA.

Rondo. (2008). *DUO Two-way Exposed Suspended Ceiling Grid System*. Rondo, Auckland,

NZ.

Ryu, K. P., Reinhorn, A. M., & Filiatrault, A. (2013). Capacity evaluation of suspended ceiling systems. *Technical Report MCEER-13-XXXX*.

Soroushian, S., Maragakis, E. M., & Jenkins, C. (2015a). Capacity evaluation of suspended ceiling components, part 1: experimental studies. *Journal of Earthquake Engineering*, *19*(5), 784-804.

Soroushian, S., Maragakis, E. M., & Jenkins, C. (2015b). Capacity evaluation of suspended ceiling components, part 2: analytical studies. *Journal of Earthquake Engineering*, *19*(5), 805-821.

Soroushian, S., Maragakis, M., & Jenkins, C. (2016). Axial Capacity Evaluation for Typical Suspended Ceiling Joints. *Earthquake Spectra*, *32*(1), 547-565.

USG Australia. (2011). *DONN Brand Grid Suspension System*. USG Australia, Auckland, NZ.

USG Australia. (2012). *Generic Seismic Design for USG DONN Exposed Grid Suspended Ceilings*, Auckland, New Zealand.

CHAPTER 5

FULLY-FLOATING

SUSPENDED CEILING SYSTEM

5 FULLY-FLOATING SUSPENDED CEILING SYSTEM

(Accepted for publication in the Journal of *Earthquake Spectra* in August 2017 under the title of "Fully-Floating Suspended Ceiling System: Experimental Evaluation of Structural Feasibility and Challenges", in press.)

5.1 Introduction

Suspended ceilings serve a wide range of purposes in a building. They provide sound absorption, fire protection and an aesthetically pleasing, safe and clean finish over engineering systems and services in the plenum space. Consequently, satisfactory performance of these components is necessary for continued occupancy of buildings following an earthquake. Damage to suspended ceilings causes significant financial loss in the form of direct damage (Dhakal, 2010; MacRae et al., 2012), downtime (Ferner et al., 2014) and casualties (Motosakaa & Mitsujib, 2012; Nation Media, 2011). To mitigate the risks associated with the failure of ceiling systems, two approaches can be followed: i) identifying the ceiling weaknesses and carrying out a detailed design; and ii) minimizing the imposed demand. In the case of suspended ceilings, which are sensitive to horizontal acceleration, one solution is to isolate ceilings from the walls and floors. This can be achieved by eliminating the stiff connections to the suspended ceilings. A fully-floating ceiling is a system with no stiff lateral restraints to the supporting structure, unlike a perimeter fixed or braced ceiling. The ceiling is suspended from the floor via vertical steel hanger wires and is provided with gaps around the perimeter. Given sufficient gap is provided to accommodate the deflections resulting from earthquakes, minimal contact between the edges of the ceiling and the perimeter walls is expected. In an ideal gravity pendulum, if the pendulum cords only provide axial resistance and their lateral stiffness is zero, according to classic pendulum mechanics, none of the lateral forces induced in the support should be transferred to the pendulum mass. As a result, there should be very low interaction with the walls and the ceiling damage is expected to be very little, if any. Nevertheless, the free and uncontrollable swing of the ceiling in a pendulum-like fashion may result in undesirable interactions with other services within the plenum space.

Considering post-earthquake observations which highlight the significance of non-structural elements in buildings overall performance, several research projects have targeted the seismic behavior of suspended ceilings. These experimental and analytical studies mainly focused on the performance and damage states of common perimeter-fixed and back-braced -also known

as floating- ceilings (Badillo-Almaraz et al., 2007; Magliulo et al., 2012; Ryu et al., 2013; Soroushian et al., 2016). Despite the extensive research on these common types of ceilings, not many studies have explored the prospect of developing new ceiling systems with an aim to reduce ceiling damage in earthquakes. This study explores the possibility of a novel low-damage ceiling system by experimentally investigating the seismic performance of fully-floating ceilings without any rigid/semi-rigid bracings (i.e. pendulum type ceilings). There are not many works on fully-floating ceiling systems; a report dating back to the 1980s (ANCO Engineering Inc., 1983) concludes that in comparison to the back-braced ceilings supported by 45-degree splay wires, the pendulum ceilings have lower peak acceleration whilst having higher peak displacement. In another study (Yao, 2000), shaking table tests of fully-floating ceiling systems used in Taiwan showed that the period of these ceilings could be accurately calculated by pendulum theory. Moreover, the results suggested that the ceiling performance was sensitive to the use of transverse cross tees on edges. In a preliminary study carried out by the authors' research group at University of Canterbury (Robson et al., 2014), the feasibility of a ceiling that performs as a simple pendulum was investigated through simple pendulum tests. The numerical and experimental study showed that: i) The length of the hanger wire -herein the pendulum rod- controls the natural frequency of the pendulum as well as its sensitivity to a particular motion, ii) The mass has a negligible effect on pendulum peak displacement and does not change the natural frequency, iii) Displacement amplifications were observed at resonance frequencies of the input motion, and iv) Displacement amplifications were observed also at higher input acceleration amplitudes. The limited extent of the experimental work mentioned reveals the need for a more extensive study into the characteristics of a pendulum ceiling and its practicality. Through shake table experiments using a wide range of sinusoidal and ground motions, this paper aims at addressing the following:

1) Comparison of fully-floating ceiling response with the response of a pendulum,
2) Maximum displacement levels in a fully-floating ceiling under a particular motion,
3) Effect of ceiling mass on the fully-floating ceiling response,
4) Effect of the layout of hanger wires on the pattern and magnitude of the displacement in the ceiling,
5) Amplification of ceiling acceleration with respect to the floor acceleration,
6) Effect of elastic isolation material as confinement around the perimeter of the fully-floating ceiling,
7) Any instances of damage to the tested ceiling and their probable cause,

8) The efficiency and effectiveness of the tested ceiling typologies for practical applications.

5.2 Mechanics of fully-floating ceiling system

A simple pendulum is a weight hanging from a frictionless pivot point through a massless cord (Gitterman, 2010). This system, in an idealised frictionless condition, swings at a constant amplitude with a period (T) that depends on the length of the pendulum (l) and the acceleration due to gravity (g). Equation 5-1 shows this interrelation.

$$T = 2\pi\sqrt{\frac{l}{g}} \qquad \text{or} \qquad \omega = \sqrt{\frac{g}{l}} \qquad \text{Equation 5-1}$$

The equation of motion for a simple frictionless pendulum with a swinging mass of m and length of l can be derived through energy method.

$$E = \tfrac{1}{2}mv_\theta^2 + mgl(1-\mathrm{Cos}\theta) \qquad \text{Equation 5-2}$$

$$\frac{dE}{dt} = 0 \Rightarrow ml^2\ddot{\theta} + mgl \cdot Sin\theta = 0 \qquad \text{Equation 5-3}$$

(for small rotations $sin\ \theta \approx \theta$)

$$\ddot{\theta} + \tfrac{g}{l}\theta = 0 \quad \Rightarrow \quad \ddot{\theta} + \omega^2\theta = 0 \qquad \text{Equation 5-4}$$

According to Equation 5-4, the displacement, velocity and acceleration of a pendulum are independent of its mass. These parameters are only affected by the pendulum's change of natural frequency, ω, which, as shown in Equation 5-1, depends on the pendulum length, l and acceleration due to gravity, g.

In case of the support moving with small oscillations of $X = X_0\cos(\Omega t)$, after initial transients the pendulum mass will oscillate with the same frequency Ω and its motion can be described as $\theta = \theta_0\cos(\Omega t)$ where θ_0 is:

$$\theta_0 = \frac{X_0}{l}\frac{\Omega^2}{\omega^2 - \Omega^2} \qquad \text{Equation 5-5}$$

As can be deduced from Equation 5-5, if the frequency of the input motion is much lower than the natural frequency of the system ($\Omega^2 << \omega^2$), the pendulum will follow the support and the pendulum displacement will be close to the amplitude of the input motion. At very high driving frequencies ($\Omega >> \omega$) the pendulum mass stays near the equilibrium point, independent of the support motion (Gonzalez, 2006). At input frequencies near the natural

frequency of the pendulum, $\Omega \approx \omega$, the motion will grow very large due to resonance. Hence, in fully-floating ceilings, the perimeter gaps may not be enough when the floor excites in a motion that releases significant energy at and around the resonant frequency of the ceiling. In such cases, pounding will occur between the ceiling and the perimeters and the instantaneous acceleration (and hence the force) in the ceiling grid becomes large enough to cause substantial damage to the system. To avoid such situations, perimeter isolations are proposed in this study as a possible method to limit the ceiling displacements, accelerations and damage.

5.3 Design of the experiment

5.3.1 *Test specimens*

The ceiling specimen tested was 2.15 m × 4.55 m in size (Figure 5-1) and was hung from the test frame roof joists through a number of vertical steel hanger wires. These hanger wires are minimum 12-gauge galvanized, soft annealed mild steel (ASTM C636, 2013). The ceiling consisted of DONN brand DX30D-3600 main tees and DX30M-1200 cross tees, both of which are standard grids. The ceiling tiles were 1200 mm × 600 mm USG Boral Radar ClimaPlus^{TM} which are commonly used in NZ (USG, 2011; USG Boral, 2012).

The fully-floating (pendulum) ceiling is different from other common suspended ceilings (e.g. perimeter-fixed or floating/back-braced) in its boundary connections. In a typical perimeter-fixed ceiling, the perimeters are connected to the surrounding structure on two adjacent sides while the opposite sides are free to slide. A fully-floating ceiling on the other hand is not fixed to the surrounding structure on the perimeters on any side. It is supported from the structure above through vertical hanger wires, similar to a perimeter-fixed ceiling. In a back-braced or floating ceiling the perimeters of the ceiling are not fixed to the surrounding structure, but the suspension system is connected to the structure above through rigid or semi-rigid braces.

Since the fully-floating ceiling was not attached to the perimeter walls/beam on any side, to maintain the integrity of the system and prevent grid spreading, DONN brand US45 channels were used on all four sides of the ceiling (Figure 5-2). These channels were connected to the tee ends via single 3.2 mm aluminium rivets. For ease of installation, standard MT45 or MT55 angles are recommended instead of channels (Figure 5-2).

The perimeter isolation material was a type of industrial foam (Dunlop Foams^{TM}) with hardness and density values of 70 N and 16 kg/m^3, respectively. Here, density refers to the

weight of the foam in kilograms per cubic metre. Hardness (load bearing) is a measure of the 'feel' of a foam. To establish the hardness, a standard size piece of foam is compressed to 40% using a cylindrical apparatus. ASTM D3574 – 11 (2016) standard lays out the details and test method for acquiring the measure of hardness of foams in Test B1, Indentation Force Deflection (IFD) Test. In consultation with the ceiling manufacturer, the foam material was chosen because it has relatively similar density and stiffness to those of an elastic fibrous material commonly used to fill ceiling perimeter gaps in NZ, which was not available at the time of fabrication of the specimen.

Four configurations of this specimen were tested with variations in the following properties: hanger layout (Figure 5-5), ceiling weight and perimeter isolators (Table 5-1). As given in Table 1, in the first configuration, the ceiling was tested with tiles weighing approximately 2.75 kg each (3.82 kg/m^2) resulting in a total tile weight of 37.4 kg. In this configuration, hanger wires were placed in the layout of Figure 5-5a (Layout A). In the second configuration, 22 kg of extra mass was distributed on the ceiling to study the effect of mass on the ceiling response. To avoid delay due to re-installation, instead of using heavy tiles, small sand bags were evenly distributed over the ceiling grid (Figure 5-4) to increase the mass of the ceiling. In the third configuration, the extra mass was removed, and hanger wires layout was changed to layout B (shown in Figure 5-5b). In the first three setups a 150 mm wide gap was provided between the ceiling and perimeter beams. In the final configuration in Table 5-1, due to installation limits, the gap was reduced to 100 mm which was fully-filled with isolation material to experiment a possibly more practical and safer form of the fully-floating ceiling. This specimen was tested with hanger layout B only.

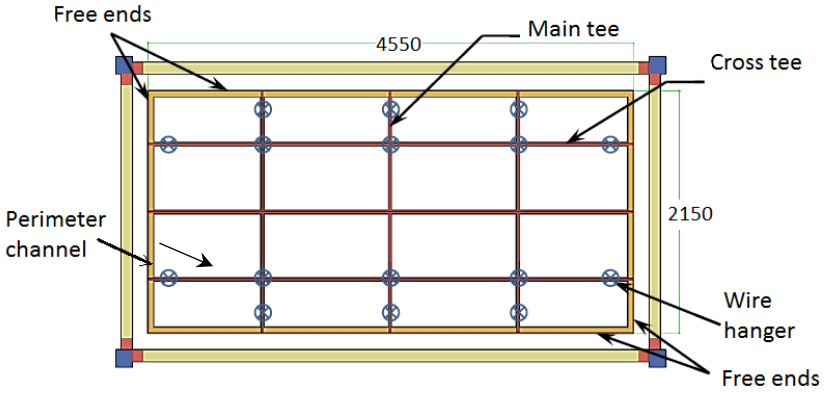

Figure 5-1 – Plan view of fully-floating ceiling specimen (dimensions in mm)

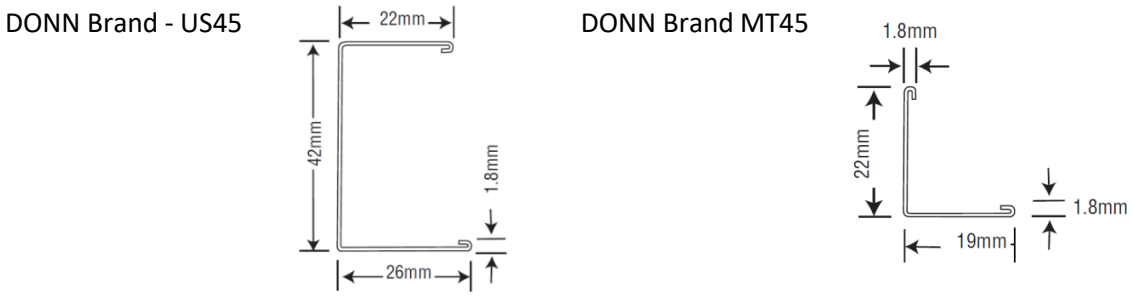

Figure 5-2 – Cross section view of perimeter channel and angle (USG, 2011)

Figure 5-3 – Top and bottom views of test specimen and test frame showing the gap between fully-floating ceiling and the timber perimeter beams of the test frame

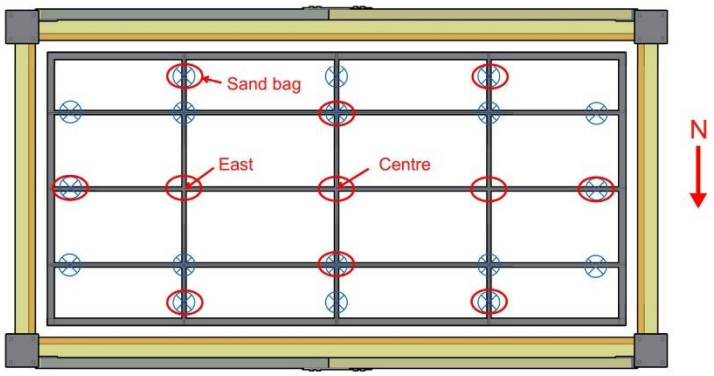

Figure 5-4 – Plan view of specimen with hanger layout A, position of sand bags and centre and east grid joints

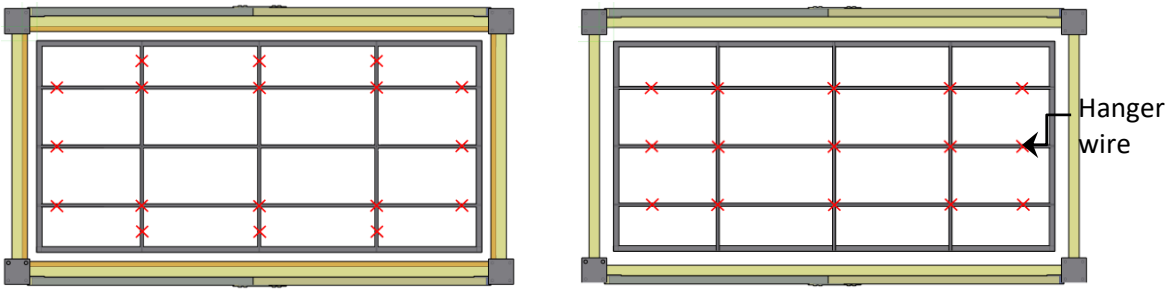

(a) (b)

Figure 5-5 – Ceiling specimen with (a) hanger layout A, and (b) hanger layout B

Table 5-1 – Details of specimens

No.	Symbol	Layout of vertical hanger wires	Total tile mass (kg)	Perimeter Isolation
1	WPA	A	37.4	No
2	Add. mass	A	59.4	No
3	WPB	B	37.4	No
4	Foam	B	37.4	Yes

Notation: WPA: Hanger layout A, WPB: Hanger layout B., Foam: Foam isolated, and Add. Mass: Hanger layout A with additional mass.

In these tests, the length of ceiling vertical hangers was 450 mm. For this hanger length, the period of the ceiling was expected to be approximately 1.34 s (0.75 Hz), assuming simple pendulum motion (Equation 5-1). The minimum plenum depth or hanger wire length depends on ceiling tile dimensions and clearances for services within the plenum space. For instance, in case of 1200 mm × 600 mm tiles, a minimum 200 mm depth is required for installation purposes (USG, 2011). In common practice, the plenum depth in suspended ceilings is usually between 200 mm and 500 mm, which could be as high as 3000 mm in some industrial applications. Considering this range of plenum depth, the natural period of a pendulum ceiling can vary between 0.9 s and 1.4 s (up to 3.5 s for some rare cases).

Note that the period of the ceilings governs the extent of the effect different excitations have on these ceilings. Typical near source seismic ground motions, when scrutinized in frequency domain, will have little energy in the range of period beyond 1 s. In contrast, ground motions from long distance earthquakes are likely to have substantial energy in the moderate to long period range. It is hence plausible that long distance earthquakes will induce greater displacement responses from these floating ceilings; thereby increasing the possibility of insufficient perimeter gap and pounding. It is important here to note that the ceilings do not respond to the ground motions; rather they respond to the floor motions, which are a part of the building's response to the ground motion. Obviously, the frequency characteristics of the floor motion will be greatly influenced by the building properties; mainly its period. A relatively stiff low-rise building will have the floor response dominated by high frequency modes regardless of the input ground motion, and similarly floor response in a tall flexible building will be dominated by low frequency modes. In this pretext, it can be argued that the floating ceilings will induce less displacement in low-rise buildings but in high rise buildings the ceiling response could exceed the perimeter gap and suffer pounding if the gap is not filled with a compressive isolation material to damp the response.

5.3.2 *Test setup and instrumentation*

The setup was constructed on a 2 m by 4 m unidirectional shake table. The assembled frame was 5.20 m long, 2.65 m wide and 2.6 m high, which could accommodate a 2.15 m by 4.55 m ceiling. The frame was cross-braced in the direction of excitation. Connections of the frame at the column base level were pinned while rigid end plate connections were used at beam-column joints. At the ceiling level, 450 mm from the top of the frame, timber beams were fixed to the columns on four sides to provide perimeter support for the ceiling assembly when needed.

For the purpose of this experiment, a relatively rigid braced frame (horizontal natural frequency of 12.5 Hz) was used to ensure that the motion applied to the shaking table would be transferred to the ceiling level without any substantial alteration. To account for any unintended difference between the shaking table and ceiling support excitations, the acceleration at the top of the test frame was recorded and used as the input to the ceiling system in analysing and interpreting the test results. A total of 12 accelerometers and 3 potentiometers were used for recording the outputs in these tests. The location and details of these instruments is shown in Figure 5-6 and Table 5-2. In addition to these devices, a high-speed video camera was also put underneath the ceiling on the west end of the test setup (marked as W in Figure 5-6). The recordings from this camera were digitised and analysed in MATLAB using the Hedrick tracking software (Hedrick Lab) to derive the displacement of the ceiling. Further details on the instruments can be found in Appendix B.

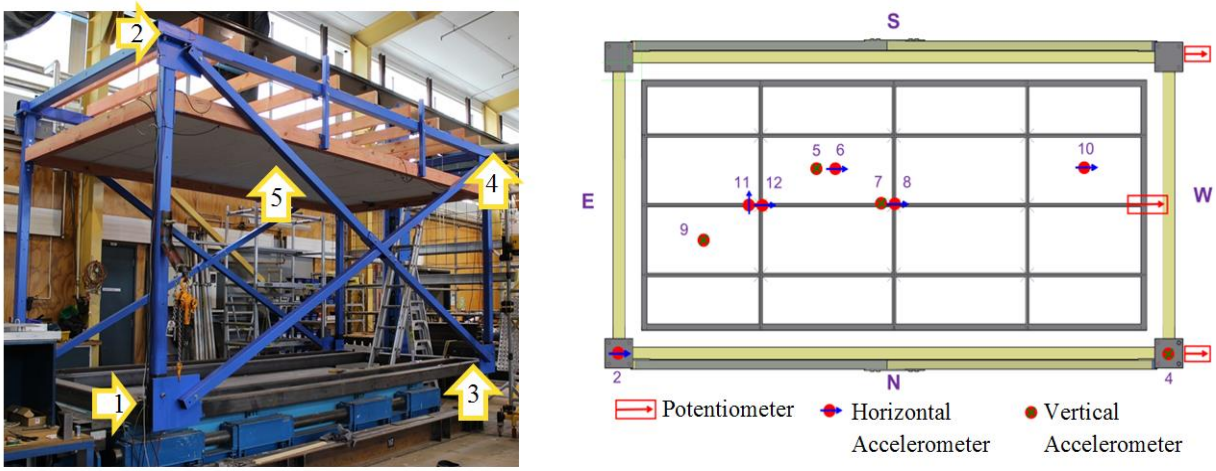

Figure 5-6 – Instruments in test frame and test specimen

Table 5-2 – List of accelerometers

No.	Location	No.	Location	No.	Location
1	Shake table input (Hrz.)	5	Central tile (Vrt.)	9	Perimeter tile (Vrt.)
2	Frame top (Hrz.)	6	Central tile (Hrz.)	10	Perimeter tile (Hrz.)
3	Shake table input (Vrt.)	7	Central grid (Vrt.)	11	East grid (NS)
4	Frame top (Vrt.)	8	Central grid (Hrz.)	12	East grid (EW)

5.4 Input motions to the Shaking Table

A series of 54 sinusoidal motions with different displacement amplitudes (2 mm – 75 mm) and frequencies (0.75 Hz – 4.5 Hz) was chosen for the initial tests. Each sinusoidal wave (SW) consisted of a 2 s long starting and ending ramp phase. The motion between these two ramps continued with constant displacement amplitude and frequency for approximately 15 s. Figure 5-7 shows the range of peak floor accelerations (PFAs) intended at the floor level (i.e. at the top of the frame) considering different frequencies.

Following these sinusoidal tests, a suite of ground motions (GM), chosen to cover a variety of frequency content, was used as the input. The plot of acceleration response spectra shown in Figure 5-8 is based on the acceleration time histories recorded on the shake table and may vary from the original data due to the slight changes induced by the table. Table 5-3 also provides additional information about these ground motions with their lowest scaling factor in the tests. The record amplitudes were scaled according to the limitations of the shake table and the objective of the tests. Values of the scaling factor are presented in Figure 5-8 legend within brackets. These scaling factors were gradually increased throughout the tests up to the limits allowed by the test setup. For the specimen with isolation foam, the same set of records (as applied to the specimen without foam) was used except that some records with higher accelerations were also added. Further details on the input motions can be found in Appendix A.

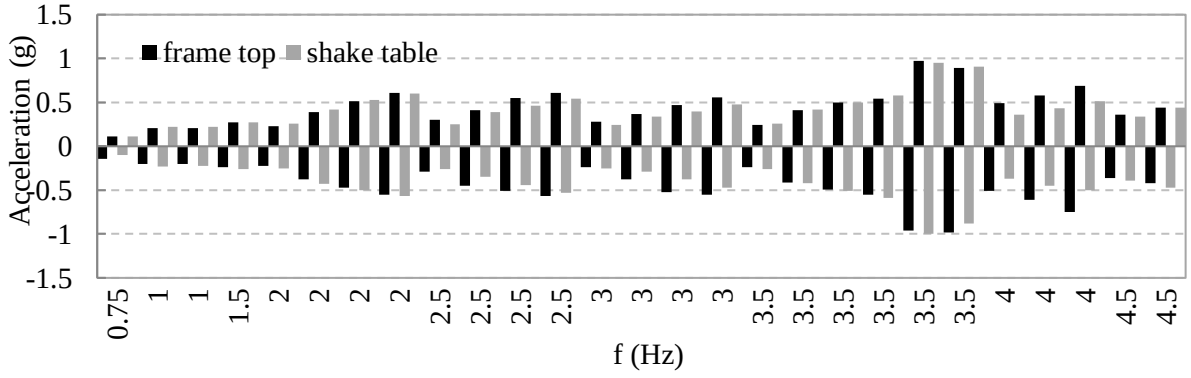

Figure 5-7 – Acceleration recorded on shake table and acceleration response on frame top

Table 5-3 – Details of ground motions used in tests

Ground motion ID	Scaling factor	Time history duration [s]	Peak shake table displacement [mm]	Peak test frame displacement [mm]	Peak shake table acceleration (PGA) [g]	Peak test frame acceleration (PFA) [g]
Sep-CCCC	0.6	50	122	122	0.30	0.26
Sep-CBGS	0.9	65	128	127	0.22	0.23
Sep-GDLC	0.1	25	126	125	0.14	0.19
Feb-CCCC	0.6	25	122	122	0.38	0.39
Feb-CBGS	0.55	25	123	123	0.37	0.42
Feb-HVSC-1	0.2	15	44	43	0.37	0.48
Feb-HVSC-2	0.2	20	17	17	0.32	0.36
North-1048	0.5	30	42	0.42	0.25	0.26
North-1063	0.35	20	103	102	0.37	0.43
IMPV	1	45	85	85	0.42	0.44
Mana	1	25	63	62	0.48	0.55
NWCal	5	30	25	25	0.86	0.90
SFern	1	45	22	23	0.36	0.45

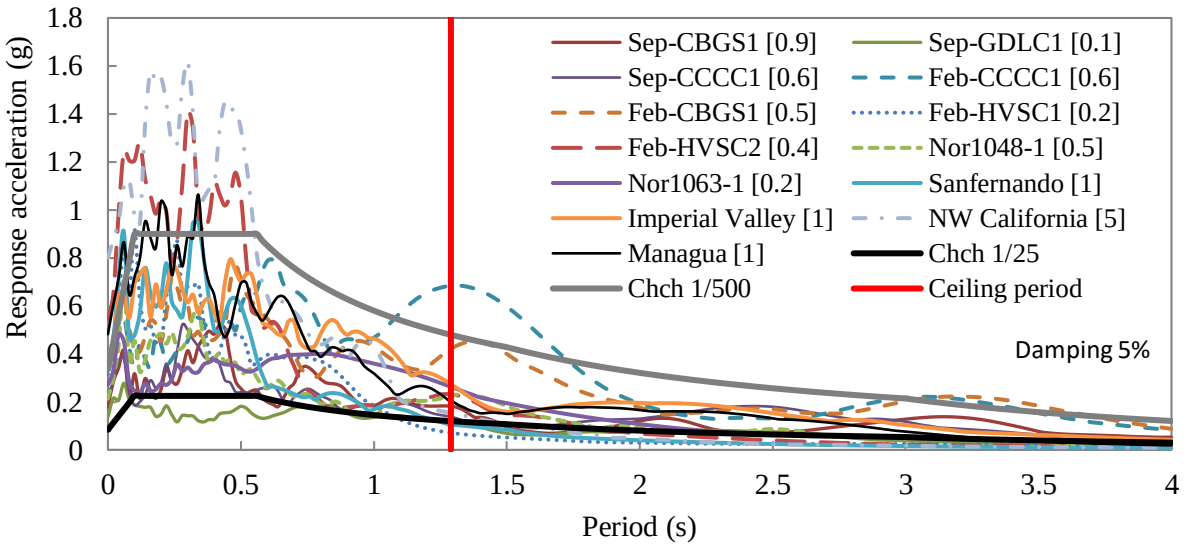

Figure 5-8 – Response spectra of the input ground motions as recorded on shake table (Damping 5%)

5.5 Results and discussions

5.5.1 *Dynamic properties of the specimen*

5.5.1.1 Ceiling specimen without isolation foam

Given the plenum height used in the specimen, the period of the ceiling was approximately

1.34 s (i.e. f = 0.75 Hz) (using Equation 5-1). The natural frequency and damping ratio of the ceiling specimen were measured using the free vibration phase of the experiments (Table 5-4). Figure 5-9 shows an example of free vibration in the first specimen and the associated frequency (f = 0.775 Hz) and damping ratio (Equation 5-6). The average values of natural frequency and damping ratio for all tests carried out in each series are presented in Table 5-4.

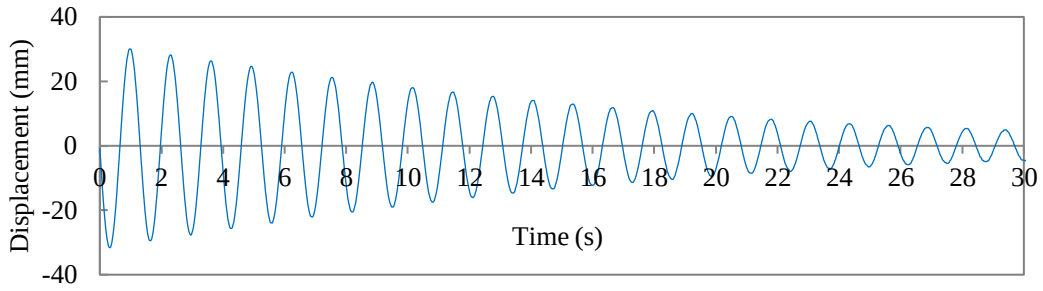

Figure 5-9 – Free vibration of fully-floating ceiling with hanger layout A

$$\xi = \frac{1}{2\pi j}\ln\left(\frac{u_i}{u_{i+j}}\right) = 0.0133 \qquad \text{Equation 5-6}$$

Table 5-4 – Natural frequencies and damping ratios obtained from ceiling

Test description	No. of tests	Average natural frequency [Hz]	Average damping ratio
Fully-floating ceiling – Hanger layout A	21	0.774	0.012
Fully-floating ceiling with additional mass	25	0.751	0.0074
Fully-floating ceiling – Hanger layout B	26	0.772	0.0111

It may be seen in Table 5-4 that the fundamental frequency of the ceiling specimen was insensitive to the mass and hanger layout. It was close to the calculated frequency of 0.75 Hz for a pendulum length of 450 mm. However, a 38% decrease was recorded in the damping ratio as the total mass of the ceiling increased by 59% (22 kg). Using basic interrelationship between damping and mass (see Equation 5-7), such a reduction is expected and justified if the damping value, *c*, does not significantly change.

$$\xi = \frac{c}{2m\omega_n} \qquad \text{Equation 5-7}$$

5.5.1.2 Ceiling specimen with isolation foam

To estimate the mechanical properties of the specimen with the isolation foam, the specimen and foam can be assumed as a mass and spring system. Since the foam was not connected to the ceiling, at each stroke only one layer of foam was resisting the motion. The surface

friction in the longitudinal direction (along the direction of loading) was not considered in this model. Figure 5-10 shows the stress-strain relationship for the perimeter foam used in these experiments. This plot was obtained through force-displacement monotonic tests on a specimen of the foam and normalised by its thickness and area. The permanent deformation in the foam was observed to return to zero as the specimen rested after being unloaded. From this graph, it was concluded that the foam had a multilinear stiffness which increased at different rates as the material was compressed.

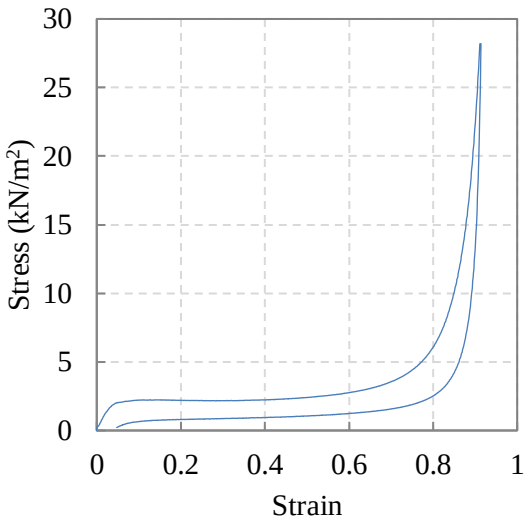

Figure 5-10 – Stress-strain relationship obtained for the foam used in the experiments

Any numerical modelling attempt to simulate the behaviour of the isolated fully-floating ceilings should implement compression only springs around the perimeter, and the spring's force displacement properties should match with the behaviour of the isolation foam used. A simple example of such a model is developed and presented in Figure 5-11 followed by the comparison with the experimental results in Figure 5-12. In this numerical model, the cross tees and main tees are defined using the cross sections of the members used in experiment. The tile is modelled with a cross braced assembly and four compression-only multilinear spring link elements are defined using the force-displacement properties of the foam material used in the experiments.

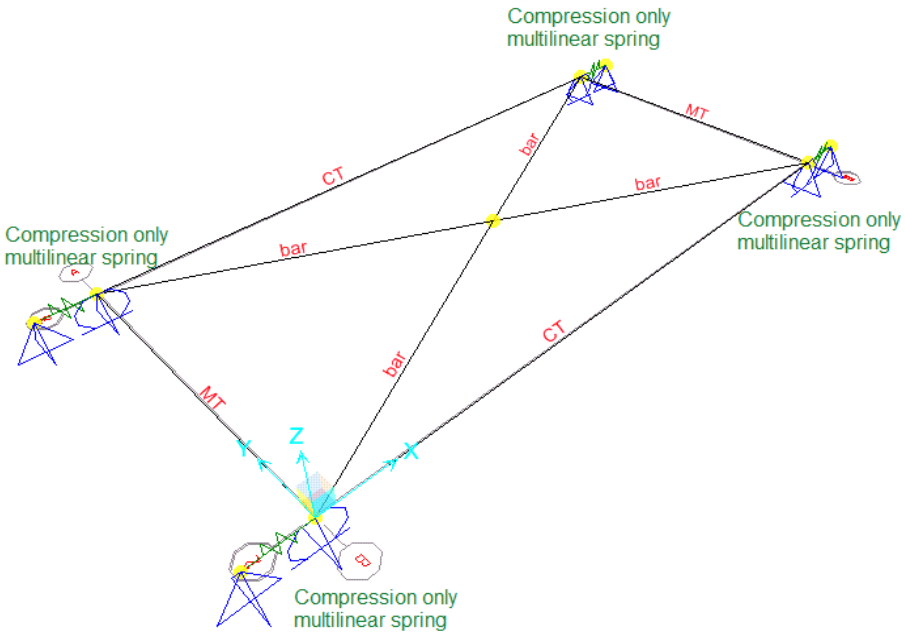

Figure 5-11 – Simple model of the fully-floating ceiling with perimeter isolation foam in SAP2000

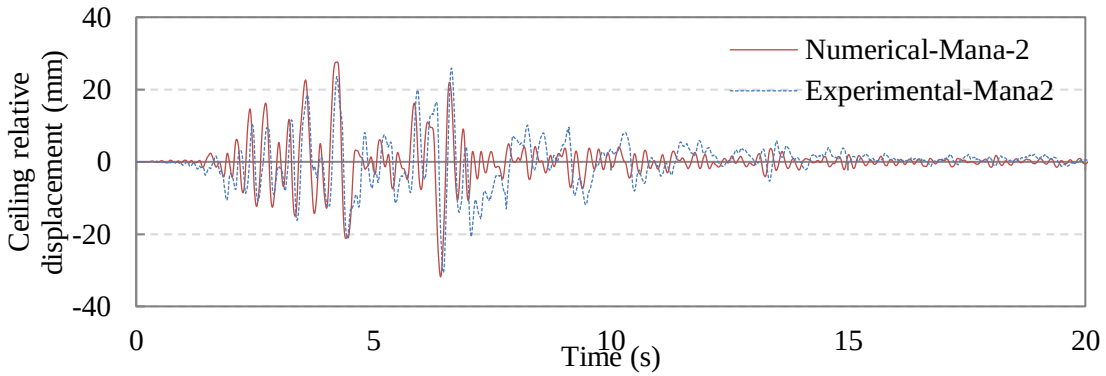

Figure 5-12 – Preliminary results comparing experimental results with modelling output

5.5.2 *Ceiling displacement range*

In a fully-floating ceiling it is desirable to limit the peak ceiling displacement so that any interference with the surrounding objects can be avoided. Plots of relative and absolute displacements during sinusoidal tests in Figure 5-13 and Figure 5-14 indicate that:

i. At frequencies higher than the natural frequency of the pendulum ceiling, the fully-floating ceiling was almost stationary or moved very little. Values of ceiling absolute displacement remained below 5 mm in all tests with input motion frequencies over 1 Hz (Figure 5-13a).

ii. As the frequency of the input sine wave approached the natural frequency of the specimen (i.e. 0.77 Hz), an increase in displacement was generally observed as shown in Figure 5-13 and Figure 5-14. At excitation frequency of 0.75 Hz pounding occurred.

iii. For a given input motion frequency, a slight increase in peak ceiling displacement was noticed as the floor acceleration increased (Figure 5-14). Nevertheless, the response of the specimens was more influenced by the frequency of the motion rather than the amplitude of acceleration.

Tests under actual earthquake ground motions generally resulted in larger displacements than the sinusoidal motions for all configurations and regardless of the peak acceleration. Displacements varied greatly with the change in frequency content of the acceleration time histories applied (Figure 5-15). The addition of isolation foam in these tests resulted in consistently smaller peak displacements. This will be further discussed later.

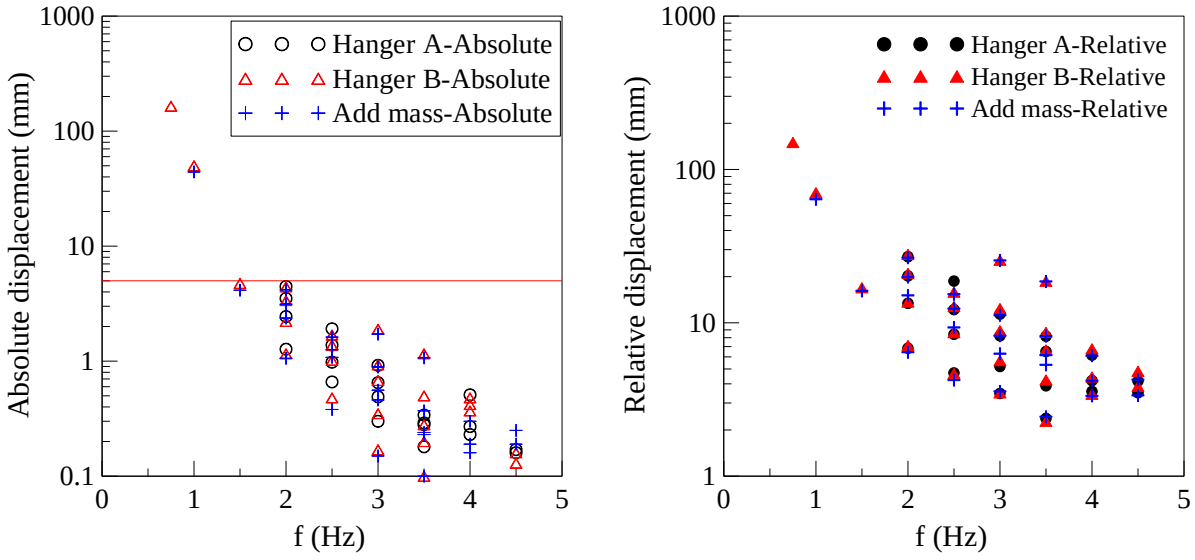

(a) (b)

Figure 5-13 – (a) Peak absolute displacements, and (b) peak relative displacements in ceilings in sinusoidal tests without foam

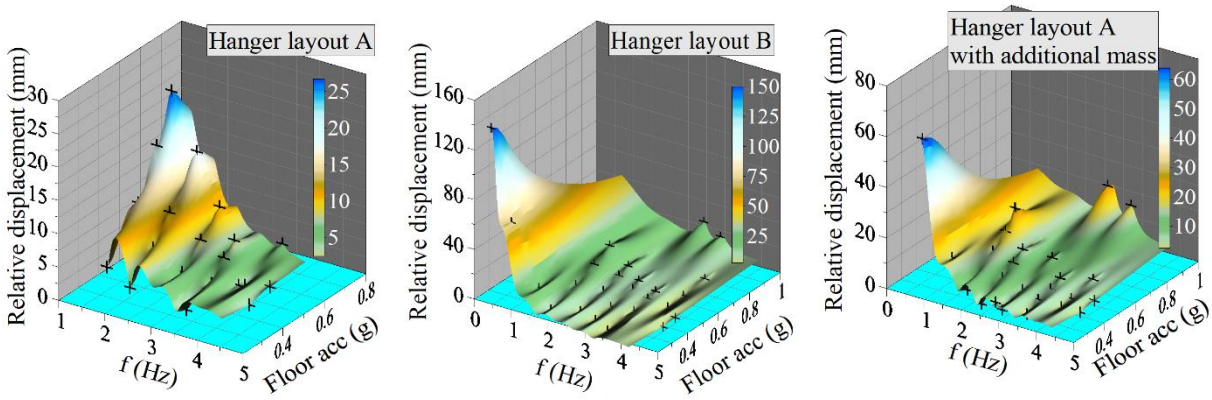

Figure 5-14 – Ceiling peak relative displacement in sinusoidal tests

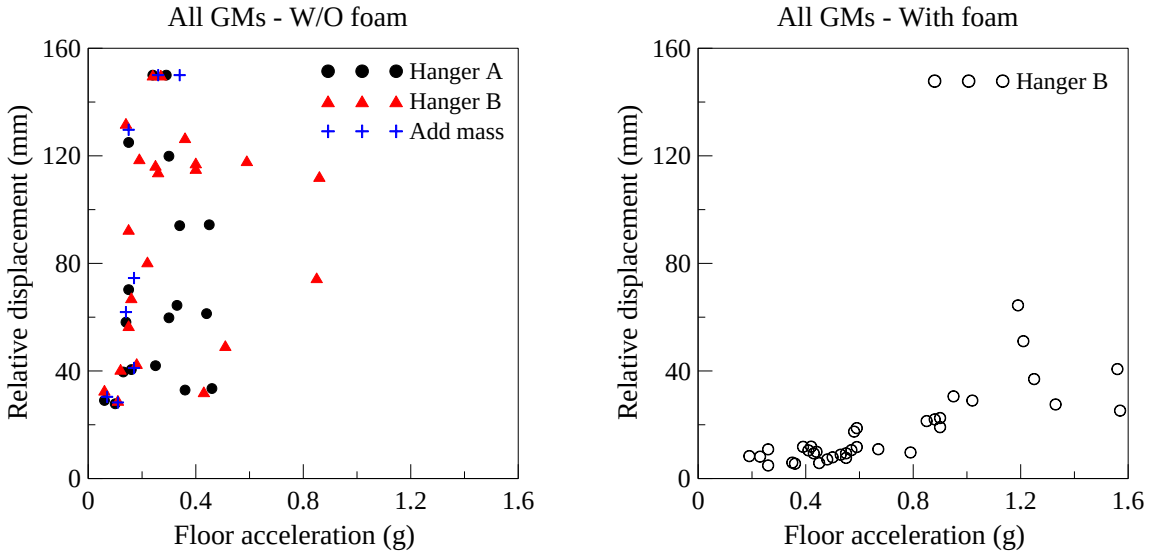

Figure 5-15 – Ceiling peak displacement in ground motion tests

5.5.3 *Ceiling weight*

Ceiling tiles are in general loosely fitted in grid modules with a minimum gap of 5mm in each direction and were observed to vibrate chaotically in vertical and horizontal directions during tests. The placement of additional masses (i.e. sand bags) over the tiles limited their vibrations and sliding.

As discussed earlier, increasing the mass of the ceiling by 22 kg (59%) did not have a significant effect on the natural frequency of the system. The displacement of a pendulum is a factor of its natural frequency which is not influenced by mass. Comparing the peak relative displacements recorded in tests under actual earthquake ground motions in Figure 5-16 shows either similar or slightly larger displacements in the heavier specimen. These differences vary between 1-6 mm (0.5-6.5 percent of the total displacement). Since all displacement data in these tests are derived from digitised videos, the results are accurate enough, but not exact.

Similar comparisons were made between displacements recorded in sinusoidal tests in Figure 5-17. As it can be observed, the differences in displacement are relatively small and rather negligible.

In addition to displacements, the peak horizontal accelerations recorded at the centre of the ceiling grid are also compared in Figure 5-16b and Figure 5-18. In both sinusoidal and ground motion tests, majority of the grid accelerations recorded on the heavier ceiling were smaller than those on the lighter ceiling.

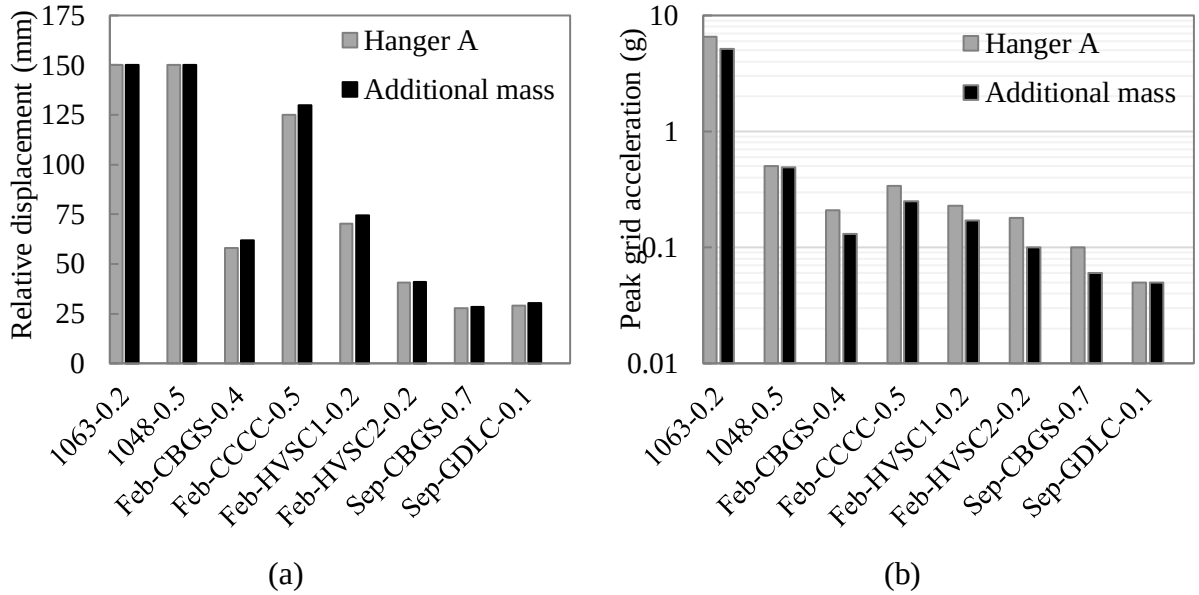

(a) (b)

Figure 5-16 – (a) Peak ceiling relative displacement, and (b) grid acceleration in ground motion tests

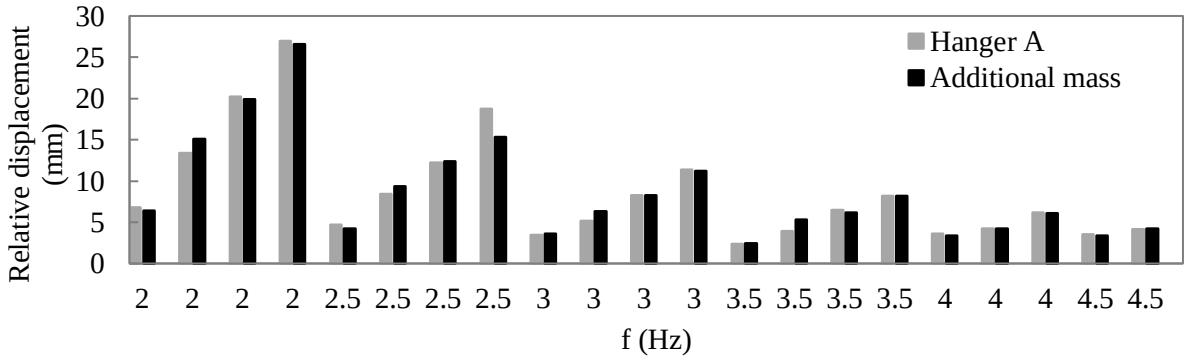

Figure 5-17 – Peak relative displacement in sinusoidal tests, hanger layout "A" with & without added mass

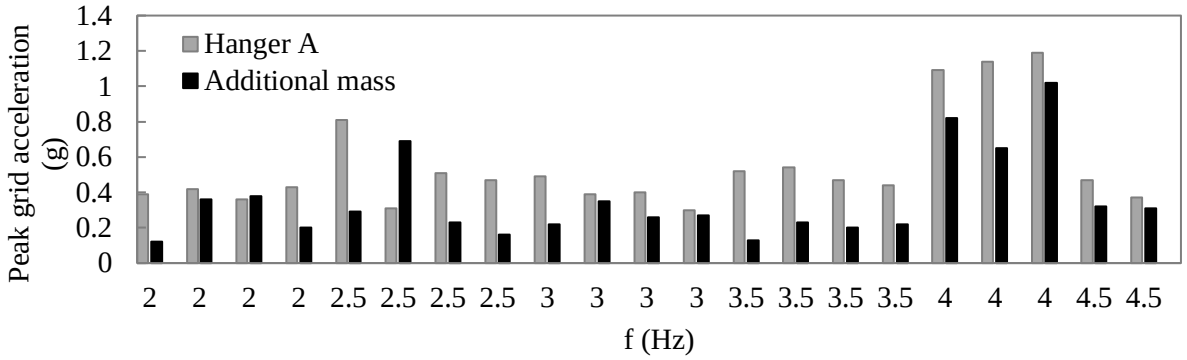

Figure 5-18 – Peak grid acceleration at ceiling center, hanger layout A, with & without added mass

Figure 5-19 shows two sets of horizontal acceleration time histories corresponding to two similar sinusoidal tests with the frequency and displacement amplitudes of 2.5 Hz and 4 mm, respectively; first without and then with the additional mass. The accelerometers were placed on a grid intersection at the centre of the ceiling which was more restrained by sand bags. This resulted in smaller acceleration values at this location. Also, the recorded response acceleration time history had a more even distribution with rare spikes in the response. Similar behaviour was observed in other sinusoidal and ground motion tests. The observed large accelerations on the ceiling grids may have been partly caused by the impact between tiles and grid members as the tiles slid within the grids. Since these impacts occur at very short periods of time, their effect was expected to be less destructive than the acceleration induced by the structure. This ill-effect due to tiles' movement can be restrained by using ceiling retainer clips available in market. A study by Badillo-Almaraz et al. (2007) showed that using retainer clips substantially improved the performance of the suspended ceiling systems by preventing tiles dislodgement failure.

The results of these experiments indicated that the displacement response of the fully-floating ceiling was not significantly affected by the increased mass. Acceleration responses were slightly less in the heavier ceiling. This meant that higher mass resulting from the addition of services and lights attached to the fully-floating ceiling might not be a risk to the ceiling's satisfactory performance by itself. However, issues might arise from insufficient clearances and attachments between services and the hangers of the ceiling, as pounding is probable in this system.

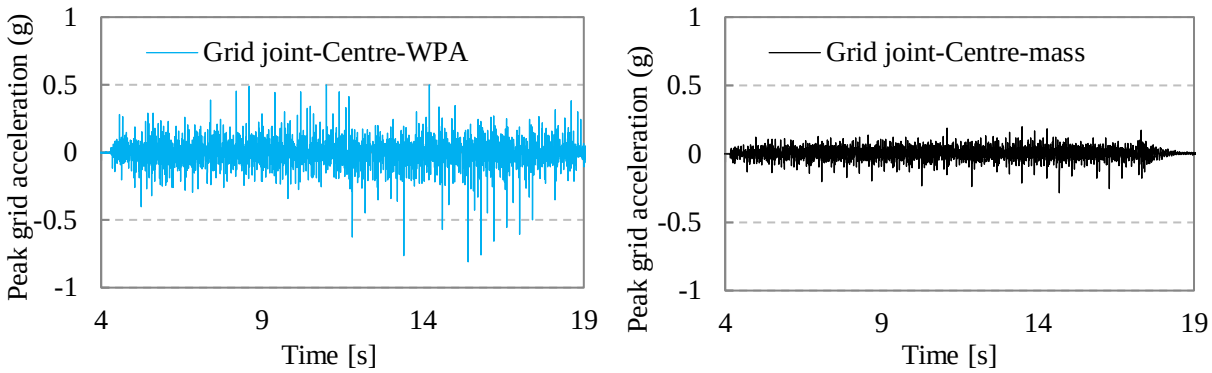

(a) (b)

Figure 5-19 – Acceleration time histories on ceiling grid in sinusoidal tests, hanger layout "A" (a) without & (b) with added mass

5.5.4 *Arrangement of hanger wires*

For the two layouts of the vertical hanger wires discussed earlier (and shown in Figure 5-5), it was shown that changing the layout did not affect the natural period or damping ratio as per simple pendulum theory. Nevertheless, as can be seen in Figure 5-20, the ceiling displacement pattern recorded in the test was affected by the layout.

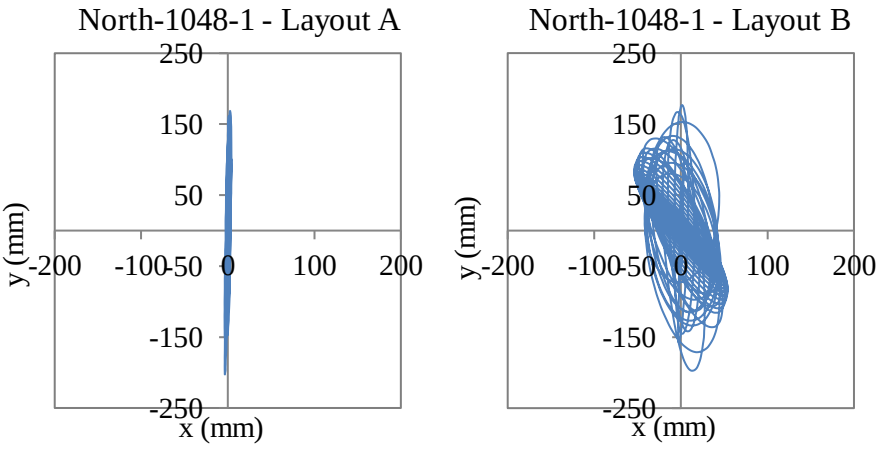

Figure 5-20 – Position of a tracked point on the ceiling with hanger layouts A and B

As the hangers in layout B were concentrated in the center of the ceiling, the displacement perpendicular to the direction of excitation (i. e. x axis in Figure 5-20) increased significantly and the ceiling followed a more circular displacement pattern. Based on the results and observations made during these series of tests, it was concluded that a symmetrical hanger wire layout evenly distributed around the four sides of the perimeter was more advantageous in the fully-floating ceiling system. In order to eliminate the haphazard movement of the

ceiling, hangers were required at most 200 mm from the terminal ends of all grid members.

Even though the displacement patterns were different in the two hanger layouts, the observed peak ceiling displacements in the direction of excitation were not notably different (Figure 5-21).

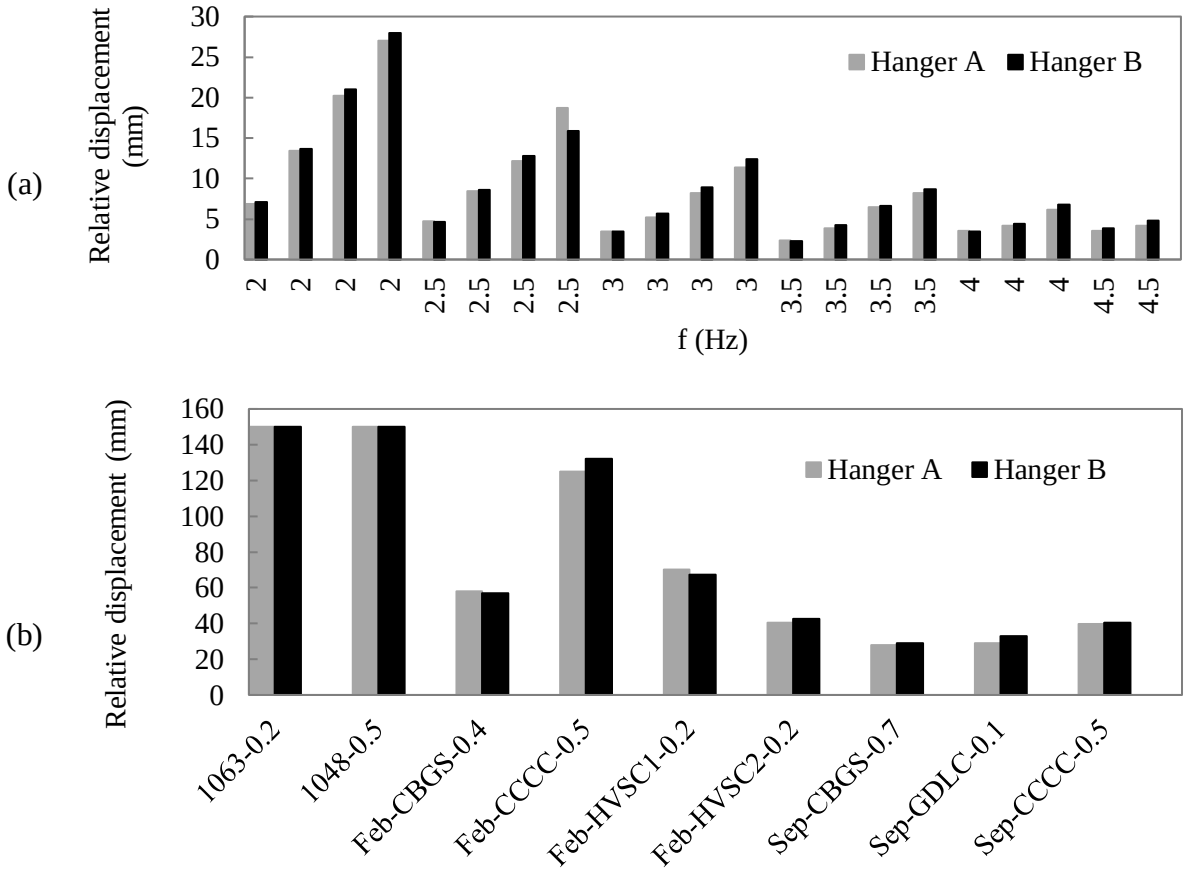

Figure 5-21 – Displacement with hanger layouts A and B in: (a) sinusoidal, and (b) ground motion tests

5.5.5 *Effect of perimeter isolation*

In the final set of tests, the gap on ceiling perimeters was filled with acoustic isolation foam (Figure 5-22). This material is flexible and allows the ceiling to move, serving two purposes: i) to work as a shock absorber at resonance induced pounding, and ii) to reduce the ceiling displacement. The effectiveness of this material was tested through sinusoidal tests (SW) and tests under actual earthquake ground motions (GM).

An overall look at the displacements measured in all tests with isolation foam shows that about 80% and 70% of cases in the sinusoidal and earthquake ground motion tests, respectively, had displacements less than 20 mm (Figure 5-23c-d). In contrast, in ground

motion (GM) tests without isolation foam all recorded displacements were above 20 mm (Figure 5-23a). In foam isolated tests, larger displacements mainly coincided with larger floor acceleration (Figure 5-23c).

Figure 5-22 – Isolation foam placed in and filling the perimeter gap

When comparing similar specimens with and without isolation foam, it was observed that in all tests with earthquake ground motions (GM), use of isolation foam effectively decreased the displacements of the ceiling (Figure 5-25a). In sinusoidal tests without isolation foam, generally small displacements were recorded at input motion frequencies far enough from the natural frequency of the ceiling. When isolation foam filled the perimeter gap, the movement of the test frame initiated the movement of the ceiling as the two elements were in contact. Consequently, slightly larger displacements were measured in some of the foam isolated specimens compared to similar tests without foam (i.e. hanger layout B). However, when subjected to sine waves close to the natural frequency of the pendulum ceiling, similar to tests under actual earthquake ground motion, the isolation foam proved effective in limiting the displacement (Figure 5-24). In other words, when displacements were generally greater than the initial movement induced by the foam, the damping effect of foam in limiting these large motions was noticeable.

The effect of isolation foam on the acceleration recorded at the central ceiling grid joint is shown in Figure 5-25b. Considering Figure 5-25a and Figure 5-25b together, in all tests where the peak displacement was about 100 mm (gap width in these series of tests was modified to 100 mm) and consequently included pounding, using foam isolators reduced the peak ceiling grid acceleration significantly.

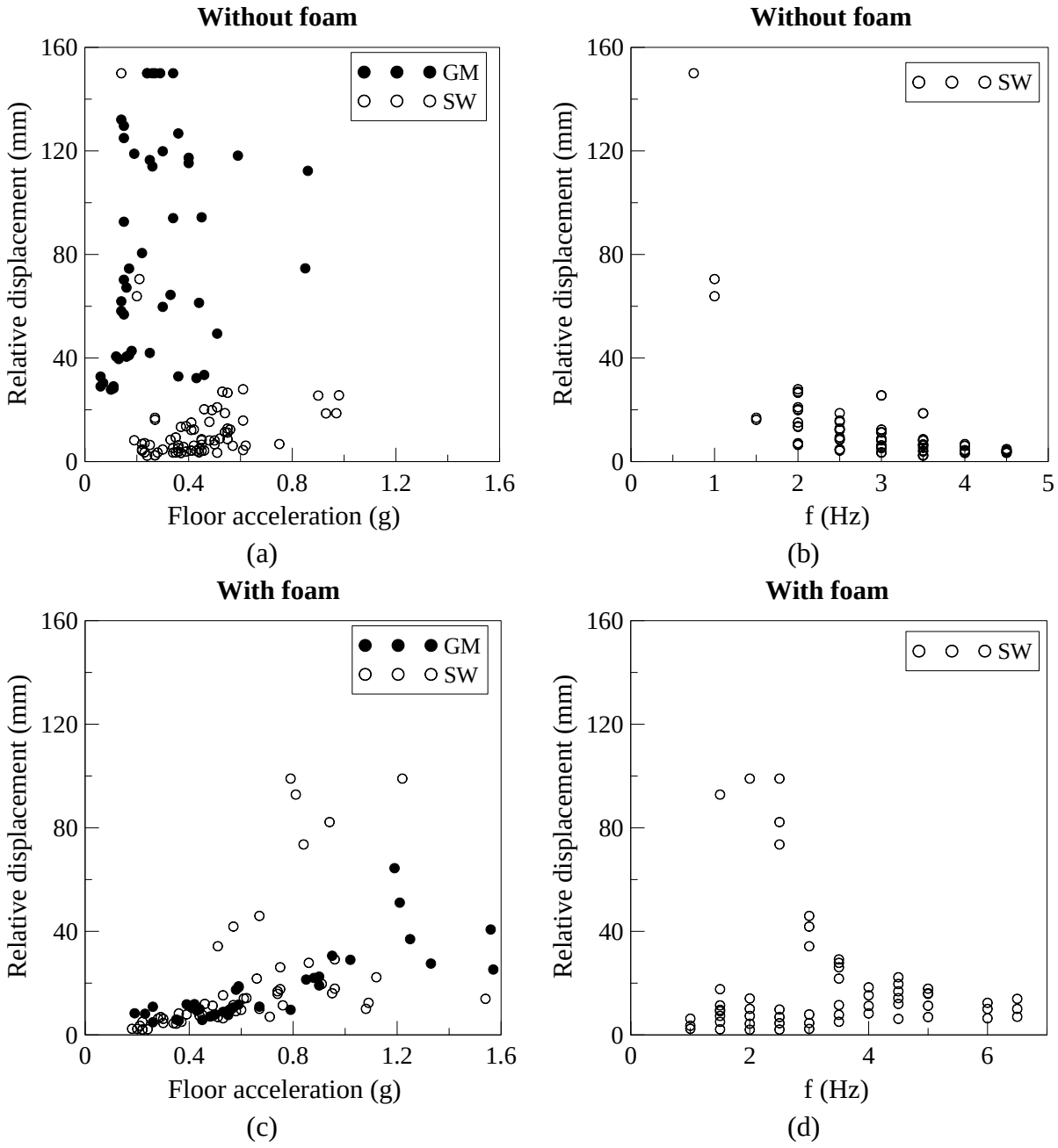

Figure 5-23 – Peak ceiling relative displacement in sinusoidal (SW) and ground motion (GM) tests with and without foam isolation

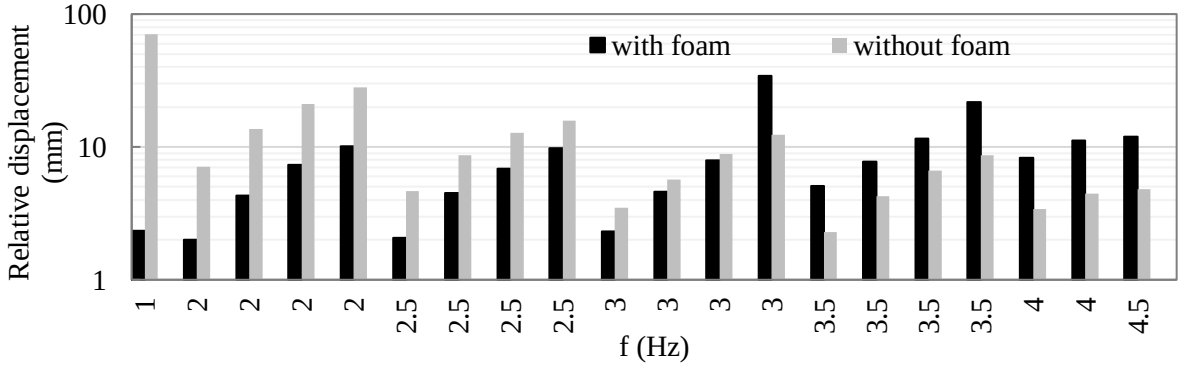

Figure 5-24 – Peak ceiling displacement with and without foam isolation in sinusoidal tests

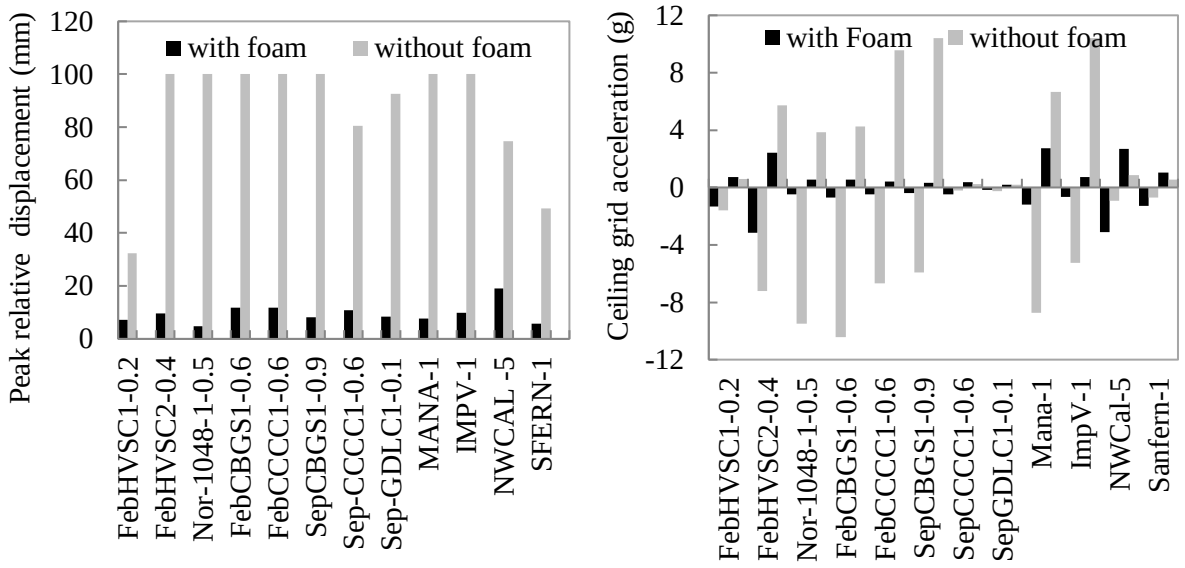

(a) (b)

Figure 5-25 – (a) Peak ceiling displacement; and (b) acceleration on central grid joint with & without isolation foam

Figure 5-26 shows the cumulative distributions of the peak relative displacements in all tests carried out on ceilings with and without isolation foam. The effect of isolation foam was especially noticeable in tests with GM records as these tests generated large displacements in the ceiling without foam (due to the wide range of frequencies in a ground motion).

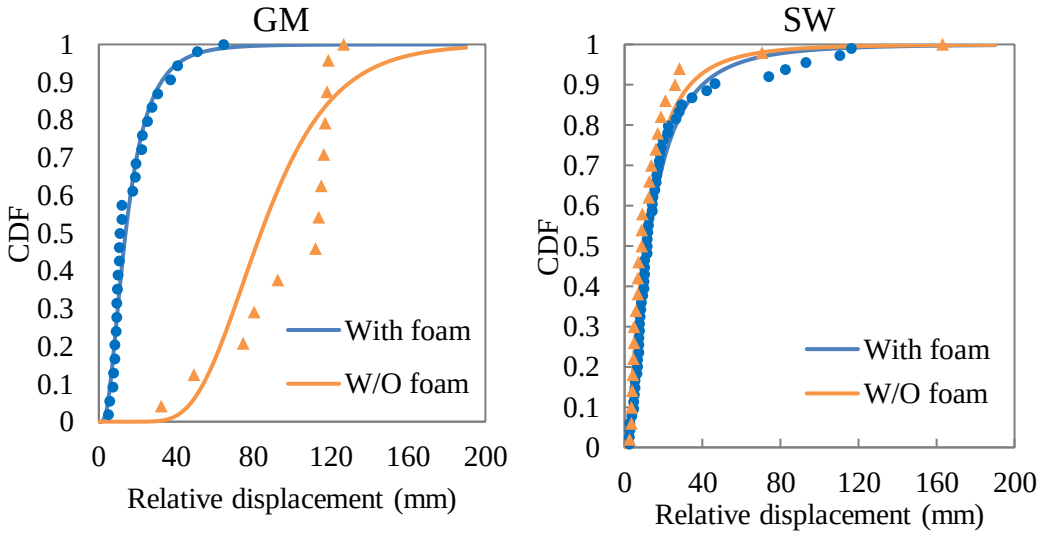

Figure 5-26 – Distribution of ceiling peak relative displacement in ground motion (GM) and sinusoidal (SW) tests, with & without isolation foam

In the isolated specimens, the foam was glued to the perimeter beams but the side in contact with the ceiling was disconnected. Figure 5-27 shows a simple model of the fully-floating

ceiling consisting of mass and springs to represent isolation material. In Figure 5-27a, the mass is shown before the motion is applied. Figure 5-27b shows the position of the mass (i.e. ceiling) as it travels towards one side. This was the configuration tested in the experiments reported herein. Due to the displacement of the mass, the spring (i.e. foam) at one end was compressed. Since the spring was not connected to the mass, at the opposite end a gap was formed between mass and spring. This meant that during each stroke of the shake table only one of the two springs was active in damping the motion. When the motion changed direction, the mass travelled the gap and came into contact with the spring at the opposite end causing an impact. The impact was followed by the compression of the spring and damping of the displacement, as the mass continued to travel towards the perimeter. The observed impact at the closure of the gap explains some of the relatively large accelerations recorded on the ceiling grids during foam-isolated tests.

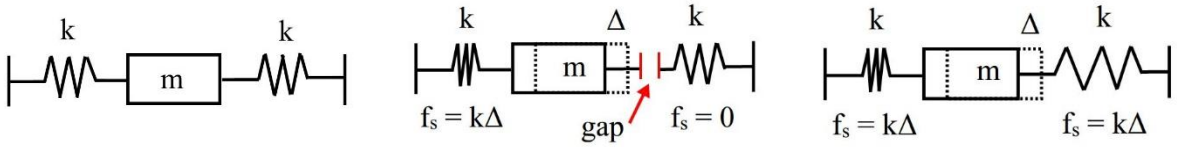

(a) (b) (c)

Figure 5-27 – Simplified spring and mass model of fully-floating ceiling with isolation foam

A possible variation to the experiment carried out is shown in Figure 5-27c. In this configuration, the foam is connected or glued to the ceiling as well as the perimeter beams. This means that during each stroke, the foam on both ends is effective in resisting the motion. This would prevent the formation of gaps between the foam and ceiling, thus eliminating the impact between the two. In the simplified model shown in Figure 5-27, the stiffness of the foam is assumed to be equal in tension and compression and any effect of side shear was ignored. In a more accurate model it would be necessary to include the resisting effect of foam on the sides (in shear) as well as on ends (tension and compression) (as shown in Figure 5-28).

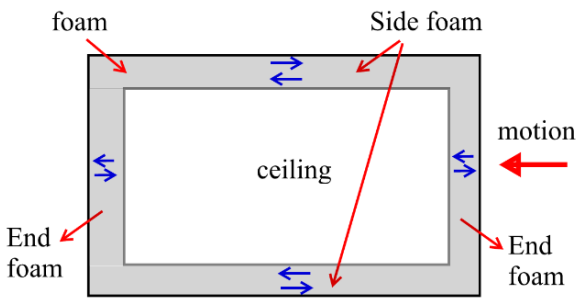

Figure 5-28 – Schematic view of ceiling with surrounding foam

5.5.6 *Amplification of input acceleration*

Figure 5-29 shows the amplifications of horizontal acceleration in the fully-floating ceiling specimens subjected to sinusoidal and ground motion excitations. The accelerations measurements were taken at two locations on the ceiling: east and centre grid intersection (for information on the location of these grid joints refer to Figure 5-4).

In fully-floating ceiling without foam (Figure 5-29a-b), the amplification factors were mainly below 2 with a large number of results less than 1, i.e. in many cases, the acceleration recorded on the ceiling grids was less than the floor acceleration. These values are also lower than the results obtained from a perimeter-fixed specimen (Pourali et al., 2015), where for all tests the amplification factor was higher than 1 and in some cases it was as high as 4.5. The considerably large amplifications noticed in some data points in Fig 28a-b were associated with resonance induced large displacements which resulted in pounding.

Figure 5-29c-d show similar graphs for foam isolated specimen. In sinusoidal tests, as shown in Figure 5-29c, the large amplification factors could be mainly associated with two factors: i) input frequencies of 4-5 Hz, and ii) large displacements that include the effect of pounding and impact. In tests with earthquake ground motion smaller displacements obviously resulted in smaller amplifications (Figure 5-29d). The acceleration amplification factors in majority of tests with foam exceed the spectral shape coefficient for ceilings recommended by the New Zealand Earthquake Loadings Standard (NZS1170.5, 2004) which has a maximum limit of 2. Nevertheless, these rather significant amplifications in the response accelerations did not result in damage in the ceiling grids.

5.5.7 *Damage observations*

Throughout more than 230 tests run on the specimen in various configurations, no damage was observed in the ceiling grid system. The only mode of failure was recorded in the final sinusoidal test on the fully-floating ceiling with isolation foam in the form of panel dislodgment (Figure 5-30). This happened due to pounding against perimeter beams coinciding with large vertical acceleration in the ceiling centre. The values of acceleration recorded at various locations of the setup are shown in Table 5-5. The test was stopped as soon as the panel dislodgment occurred. It is likely that if the shaking was continued in this test, damage in grid members would have possibly developed.

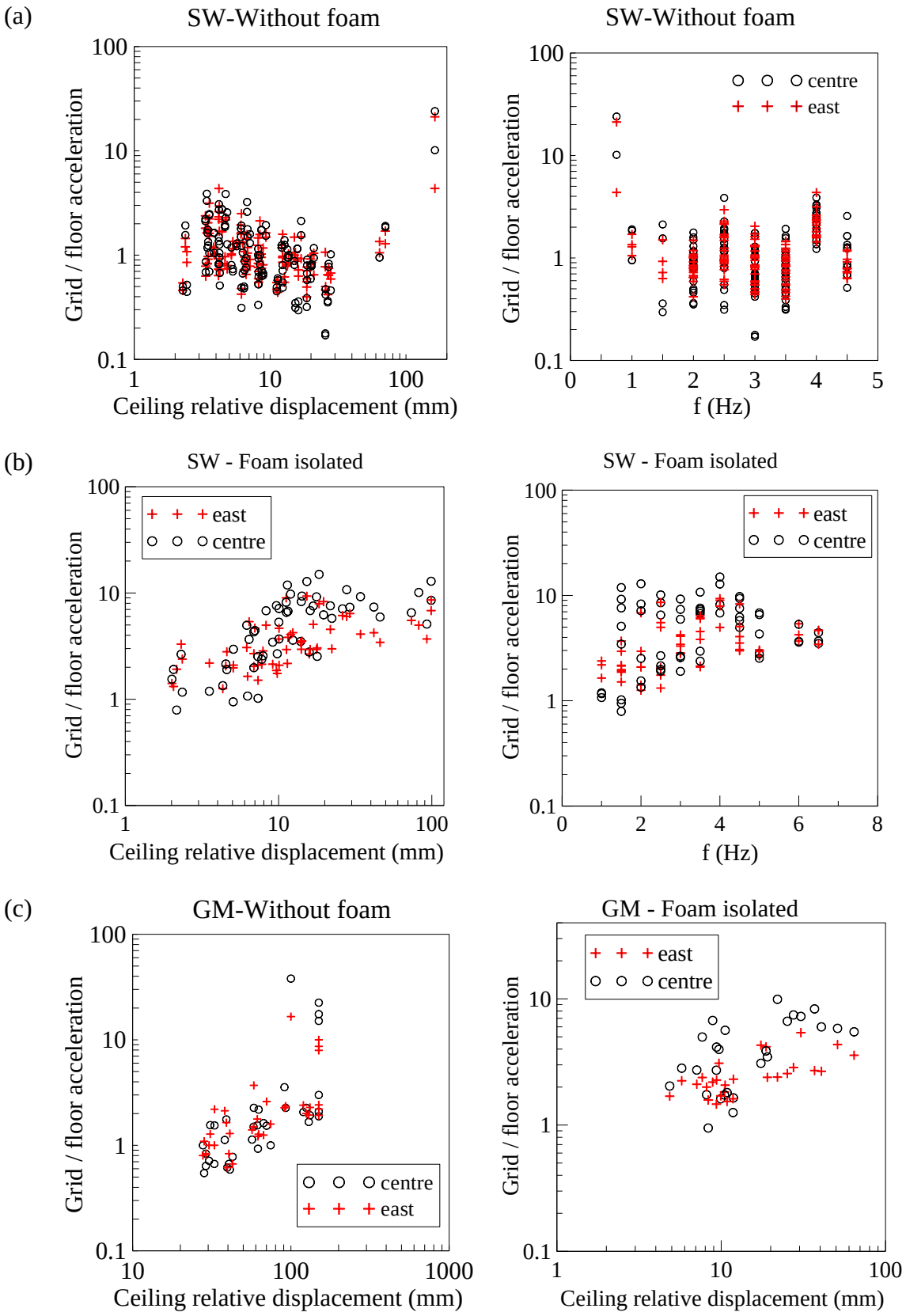

Figure 5-29 – Amplification of ceiling acceleration in (a & b) sinusoidal, and (c) ground motion tests

Table 5-5 – Acceleration recorded in failure test

Location	Acceleration (g)	Location	Acceleration (g)
Frame top (Vrt.)	0.73	Shake table input (Hrz.)	1.14
Central tile (Vrt.)	>22.7	Frame top (Hrz.)	1.22
Central grid (Vrt.)	>10.47	Shake table overhang (Vrt.)	0.77
Central grid (Hrz.)	>10.39*		

**Accelerometers reached their capacity. Real value was probably higher.*

Figure 5-30 – Panel dislodgment in the final sinusoidal test

5.5.8 *Applications and implications*

A suspended ceiling in general application is not an independent and isolated element. There are other parts interacting with and occasionally supported by them, such as luminaries, partitions and building services. Consequently, and as per NZS4219 (2009), the seismic performance of the ceiling must be compatible with these elements. Since a fully-floating ceiling is disconnected from walls on all sides, the room partitions need to be separately braced to the upper floor and the design also needs to account for the pounding from ceilings. The fully-floating ceiling itself has a framing component connected to all terminal grid ends. Therefore, the integrity of the ceiling system is not dependent on the surrounding elements.

It needs to be considered that these experiments were conducted to observe the performance of the fully-floating ceiling and to compare it with theory. An actual fully-floating ceiling needs to be compatible with any objects that can be affected by the ceiling displacement, such as fire sprinklers and braced services within plenum. The clearances provided between this type of ceiling and rigid penetrating or adjacent objects need to accommodate the maximum displacement of the ceiling.

A fully-floating ceiling is a displacement-sensitive component rather than acceleration-sensitive, which makes the provision of sufficient clearances a crucial element in design. Table 5-6 shows the minimum clearances required according to Clause 5.2 of the NZ Standard for the Seismic Performance of Engineering Systems in Buildings (NZS4219, 2009). Unlike current suspended ceilings, a fully-floating ceiling is considered an unrestrained component. Consequently, the clearances mentioned in Table 5-6 must be maintained between all ceiling components and other restrained or unrestrained elements. For example, the clearance between the fully-floating ceiling and a restrained partition wall needs to be a minimum of 150 mm. Any objects penetrating through the ceiling (e.g. fire sprinklers) need to have 25 mm clearance all around. Such penetrating objects need to be provided with flexible joints if used with a fully-floating ceiling. As advised in Clause C5.2.2 of this Standard (NZS 4219, 2009), use of flexible connections, such as foam isolation tested in this paper can reduce this clearance. Further investigation is recommended on the effect of the mechanical properties of the isolation material on the required clearance.

Table 5-6 – Clearances required between building and non-building components as per NZS4219 (2009)

Condition being considered	Minimum clearance (mm)	
	Horizontal	Vertical
Unrestrained component to unrestrained component	250	50
Unrestrained component to restrained component	150	50

The horizontal acceleration coefficient for ceilings can be calculated according to NZS1170.5 (2004) for serviceability and ultimate limit states (SLS & ULS). For example, this coefficient for a ceiling located in Christchurch, NZ equals 0.6 as shown in Equation 5-8 and Equation 5-9. In these equations: seismic zone factor Z=0.3, near-fault factor N(T, D)=1, spectral shape factor for soil type C at zero second period $C_h(0)$=1.33, return period factor for SLS design R = 0.25, floor height coefficient C_{Hi}=3 and part spectral shape factor $C_i(T_p)$=2.

$$C(0) = C_h(0) \cdot Z \cdot R \cdot N(T, D) = 1.33 \times 0.3 \times 0.25 \times 1 = 0.1 \quad \text{Equation 5-8}$$

$$C_p(T_p) = C(0) \cdot C_{Hi} \cdot C_i(T_p) = 0.1 \times 3 \times 2 = 0.6 \quad \text{Equation 5-9}$$

According to Figure 5-23c, for a fully-floating ceiling isolated with foam, up to the floor acceleration of 0.3g in SLS (excluding the factor of $C_i(T_p)$ = 2 in Equation 5-9), in none of the 13 tests the peak relative displacement exceeded 25 mm. If considering ULS horizontal

acceleration coefficient which is 4 times the SLS (i.e. 1.2g), in total of 86 tests, 13 exceeded 25 mm displacement. In other words, in sinusoidal and ground motion tests altogether, 100% of the tests subjected to SLS and 85% of tests subjected to ULS level acceleration, the displacements remained below 25 mm. In one of the tests up to 1.2g floor acceleration pounding occurred as the relative displacement closed the 100-mm gap provided. This indicates that in terms of clearances and damage to grid system, the fully-floating ceiling tested with the flexible isolation material provided had a satisfactory performance in n SLS event. When subjected to an ULS event, the overall performance of the floating ceiling (in terms of damage) was satisfactory but the displacement in some cases could be more than the current 25 mm clearance suggested by the standards. If the displacement is to be reduced within the limits of required clearances, minor modifications may be required in terms of the stiffness of the isolation material used.

5.6 Conclusions

In this paper, a novel pendulum-type fully-floating ceiling system with and without isolation layer around the perimeter has been tested on a shake table using sinusoidal and earthquake induced ground motions, and the results are scrutinised to investigate the feasibility of the floating ceiling system and potential challenges in its implementation. The following conclusions can be made based on the results of this experimental investigation.

1) The recorded response of the tested fully-floating ceiling was consistent with the simple pendulum theory. The natural frequency of the fully-floating ceiling tested was independent of the ceiling total mass. Larger displacements were recorded at input frequencies close to the natural frequency of the ceiling due to resonance effects.
2) In all sinusoidal motion tests without isolation foam and with excitation frequency above 2 Hz, peak absolute displacement remained below 5 mm. In about 80% of the sinusoidal tests and 70% of the tests under earthquake ground motions with foam isolation, ceiling peak relative displacement was less than 20 mm and larger displacements mainly coincided with larger floor accelerations.
3) Increasing the mass of the ceiling did not significantly affect the peak ceiling displacement. Adding mass on the ceiling grid and tiles limited the vibrations and sliding in ceiling tiles, resulting in smaller peak acceleration on ceiling grids. This indicates that extra load on fully-floating ceilings from the electrical and mechanical ducting above the ceiling will not make the ceiling more vulnerable.

4) Changing the number and arrangement of the vertical hanger wires did not affect the natural frequency of the fully-floating ceiling or the peak displacement in specimens. However, a more spread-out layout of hangers covering perimeters rather than center of the ceiling reduced the displacement perpendicular to the direction of excitation resulting in a linear motion pattern.
5) The ceiling grids' horizontal accelerations varied depending on the frequency and amplitude of the input motion and ceiling peak displacement. In the fully-floating ceiling without isolation, the ceiling grid to floor acceleration ratios were mostly below 2 (the value inferred in NZ seismic standard) with a large number of results less than 1. In ceilings without isolation, high amplifications were observed only in a few cases where the provided perimeter gap was exhausted, thereby resulting in pounding. With the addition of isolation foam, accelerations were amplified even when the displacements were small as the ceilings started pushing the foam very early, and the amplification was as high as 15 times at large displacement around the resonance frequencies. Nevertheless, the fully floating ceilings with the isolation foam were able to sustain the induced large acceleration without any damage.
6) The isolation foam appeared effective in damping the ceiling displacement and avoiding the large acceleration peaks due to pounding and impact. These gains were most noticeable in tests under ground motions where very large displacements were induced (mostly exceeding the gap provided and causing pounding) when the perimeter gap was not filled with foam. Overall, a 100-mm thick isolation foam was found enough to safeguard the floating ceiling from any untoward effects causing any noticeable damage.
7) Throughout the tests, damage was only observed in a sinusoidal test with the isolation foam in the form of panel dislodgement. The panel failure was assumed to be caused by large ceiling accelerations due to impact combined with the vertical movement of the untied/loose tiles due to significant vertical acceleration induced. No grid failure occurred in these experiments.
8) Based on these experiments, it can be said that the fully-floating ceiling isolated with perimeter foam showed a satisfactory performance in excitations with floor accelerations matching (in some cases, exceeding) an ULS level event. Although the outcomes from this investigation are promising and point towards viability of the fully floating ceilings as a low damage solution, more investigation is needed to confirm its ability to interact positively with surrounding structural and non-structural elements.

5.7 References

ANCO Engineers Inc. (1983). *Seismic Hazard Assessment of Non-Structural Ceiling Components: Phase I* (Report No. 1249.12). Grant 8114155, National Science Foundation, Culver City, California, USA.

American Society for Testing and Materials. (2013). *Standard Practice for Installation of Metal Ceiling Suspension Systems for Acoustical Tile and Lay-in Panels (C636/C636M)*. PA, USA.

American Society for Testing and Materials. 2016. *Standard Test Methods for Flexible Cellular Materials—Slab, Bonded, and Molded Urethane Foams (ASTM D3574 – 11)*, USA.

Badillo-Almaraz, H., Whittaker, A. S., & Reinhorn, A. M. (2007). Seismic fragility of suspended ceiling systems. *Earthquake Spectra*, *23*(1), 21-40.

Dhakal, R. P. (2010). Damage to Non-structural Components and Contents in the 2010 Darfield earthquake. *Bulletin of the New Zealand Society for Earthquake Engineering*, *43*(4), 404.

Ferner, H., Wemyss, M., Baird, A., Beer, A., & Hunter, D. (2014, March). Seismic performance of non-structural elements within buildings. In *Proceeding of the NZSEE Conference* (pp. 21-23).

Gonzalez, G. (2006). *A pendulum with a moving support point*. Retrieved from http://www.phys.lsu.edu/faculty/gonzalez/Teaching/Phys7221/PendulumWithMovingSupport.pdf . Louisiana State University, USA.

Gitterman, M., (2010). The c*haotic pendulum*. Singapore: World Scientific.

Hedrick Lab Digitizing tool, Department of Biology University of North Carolina available at http://www.unc.edu/~thedrick/software1.html

MacRae, G. A., Pampanin, S., Dhakal, R., Palermo, A., Baird A & Tasligedik, S. (2012). *Review of Design and Installation Practices for Non-Structural Components*, Report prepared for the Engineering Advisory Group of the Department of Building and Housing by New Zealand Consultants, Industry and Related Experts, NZ, June 2012.

Motosaka, M., & Mitsuji, K. (2012). Building damage during the 2011 off the Pacific coast

of Tohoku Earthquake. *Soils and Foundations*, *52*(5), 929-944.

Nation Media. (2011). Retrieved from http://www.nationmultimedia.com/headlines/At-least-20-dead-after-8-8-magnitude-tremor-30150675.html

New Zealand Standard. (2004). *Structural Design Actions Part 5: Earthquake actions-New Zealand (NZS 1170.5:2004)*. Wellington, NZ: Standards New Zealand.

New Zealand Standard. (2009). *Seismic Performance of Engineering Systems in Buildings (NZS 4219:2009)*. Wellington, NZ: Standards New Zealand.

Pourali, A., Dhakal, R. P., MacRae, G. A., & Tasligedik, A. S. (2015). Shake table tests of perimeter-fixed type suspended ceilings. In *New Zealand Society for Earthquake Engineering Annual Technical Conference* (pp. 648-659).

Robson M. J., Kho D. N., Pourali A. and Dhakal R. P., 2014. Feasibility of a fully floating ceiling system, *in proceedings of the New Zealand Society for Earthquake Engineering Conference*, 21-23 March, 2014, Auckland, NZ.

Ryu, K. P., Reinhorn, A. M., & Filiatrault, A. (2013). Capacity evaluation of suspended ceiling systems. *Technical Report MCEER-13-XXXX*.

Soroushian, S., Rahmanishamsi, E., Ryu, K. P., Maragakis, M., & Reinhorn, A. M. (2016). Experimental fragility analysis of suspension ceiling systems. *Earthquake Spectra, 32(2)*, 881-908.

USG Australia. (2011). *DONN Brand Grid Suspension System*. USG Australia, Auckland, NZ.

USG Australia. (2012). *Generic Seismic Design for USG DONN Exposed Grid Suspended Ceilings*, Auckland, New Zealand.

CHAPTER 6

EXPERIMENTAL EVALUATION OF SEISMIC COMPATIBILITY BETWEEN LOW-DAMAGE DRYWALL PARTITIONS AND SUSPENDED CEILINGS

6 EXPERIMENTAL EVALUATION OF SEISMIC COMPATIBILITY BETWEEN LOW-DAMAGE DRYWALL PARTITIONS AND SUSPENDED CEILINGS

6.1 Introduction

Non-structural elements have been identified as the dominant contributor to the overall cost of the buildings. They are also crucial to the continued occupancy and uninterrupted use following natural hazards such as earthquakes. In some instances, damage to non-structural elements has also been reported as a life hazard (Motosakaa & Mitsujib, 2012; Nation Media, 2011). Non-structural elements are now included in the buildings seismic assessment process and can contribute to a building being rated as potentially earthquake prone (NZSEE Guidelines, 2017a, 2017b). Following recent earthquakes in New Zealand, many instances of non-structural damage were reported, many of which resulted in downtime and in many cases repeated repairs (Dhakal, 2010; Dhakal et al., 2011; Dhakal et al., 2016). Suspended ceilings and partition walls were among the frequently reported non-structural elements damaged in Canterbury earthquake sequence (Mw 7.1 on 4th September 2010, and Mw 6.3 at 5km depth on 22nd February 2011) (Dhakal, 2010; Dhakal et al., 2011; Baird et al., 2014). In many occasions during these earthquakes, the structural damage in modern buildings was small. For a more uniform earthquake resilience, both structural and non-structural performances need to go hand in hand as currently the non-structural elements suffer damage at much smaller demand levels than the structure itself. Performance compatibility among structural and non-structural elements needs to be checked to provide assurance that extensive deformations in one element will not impose unforeseen demands on adjacent elements.

6.1.1 *Existing systems and common damage forms*

The suspended ceiling types currently constructed in New Zealand can be classified as follows:

- Plasterboard ceilings: the ceiling boards are fixed (usually glued) to the ceiling framing and the surrounding structure (Figure 6-1). These are often used in residential buildings.
- Perimeter-fixed ceilings: the ceiling consists of grids and tiles (Figure 6-2). The grids are fixed to the perimeter structure (walls) on two adjacent sides and free to move on the two opposite sides (Figure 6-4b) where gaps are provided. This is a modification

to an older system which was fixed to walls on all four sides (Figure 6-4a). The ceiling is suspended from the floor above via hanger wires.

- Back-braced or floating ceiling: the ceiling is not connected to perimeter walls but is separated by a gap. The loads are carried through rigid or semi-rigid braces between the ceiling grids and the floor above (Figure 6-3). Hanger wires also provide gravity support, as shown in Figure 6-4c.

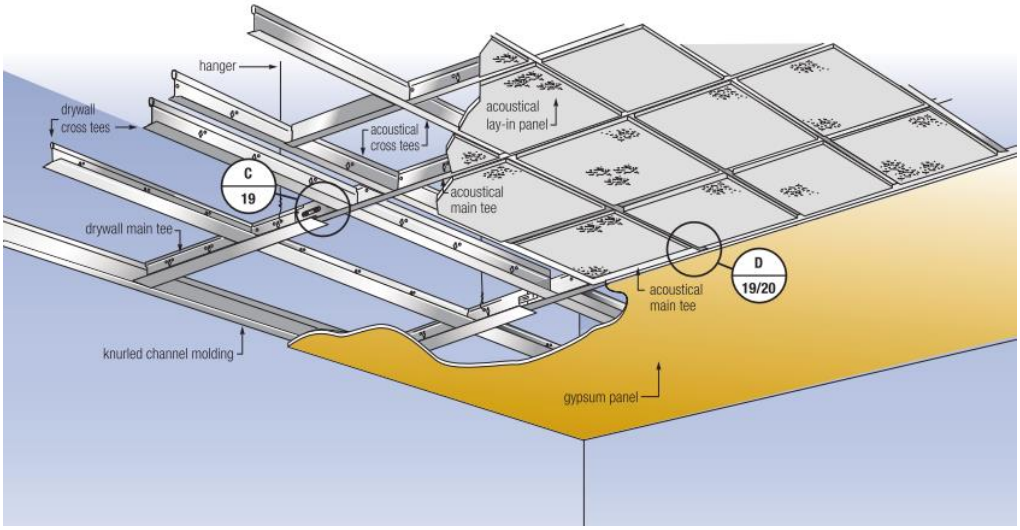

Figure 6-1 - Typical plasterboard ceiling components (USG, 2011)

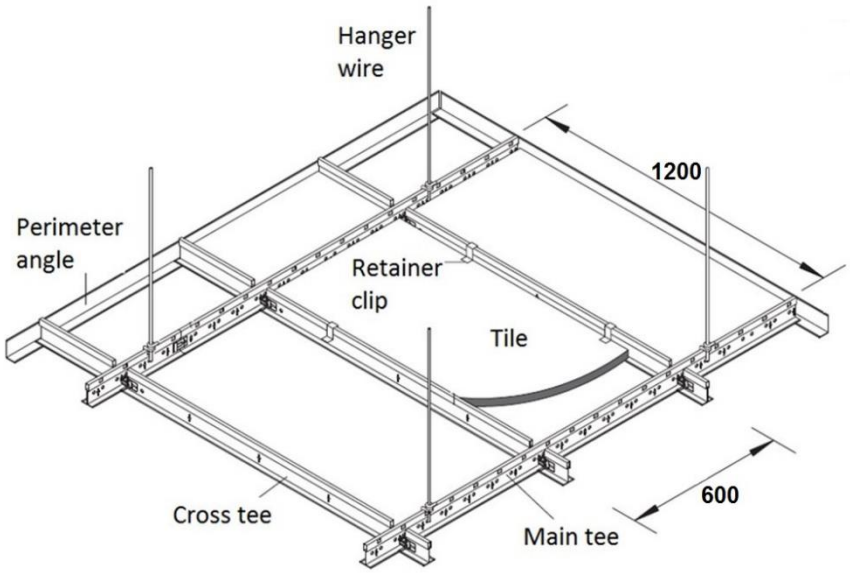

Figure 6-2 – Typical grid and tile ceiling components (USG, 2011)

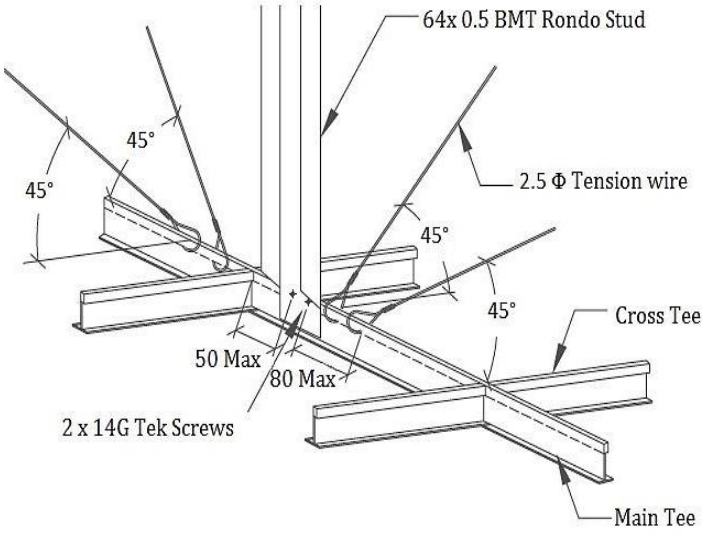

Figure 6-3 – Typical grid and tile ceiling components (Armstrong, 2013)

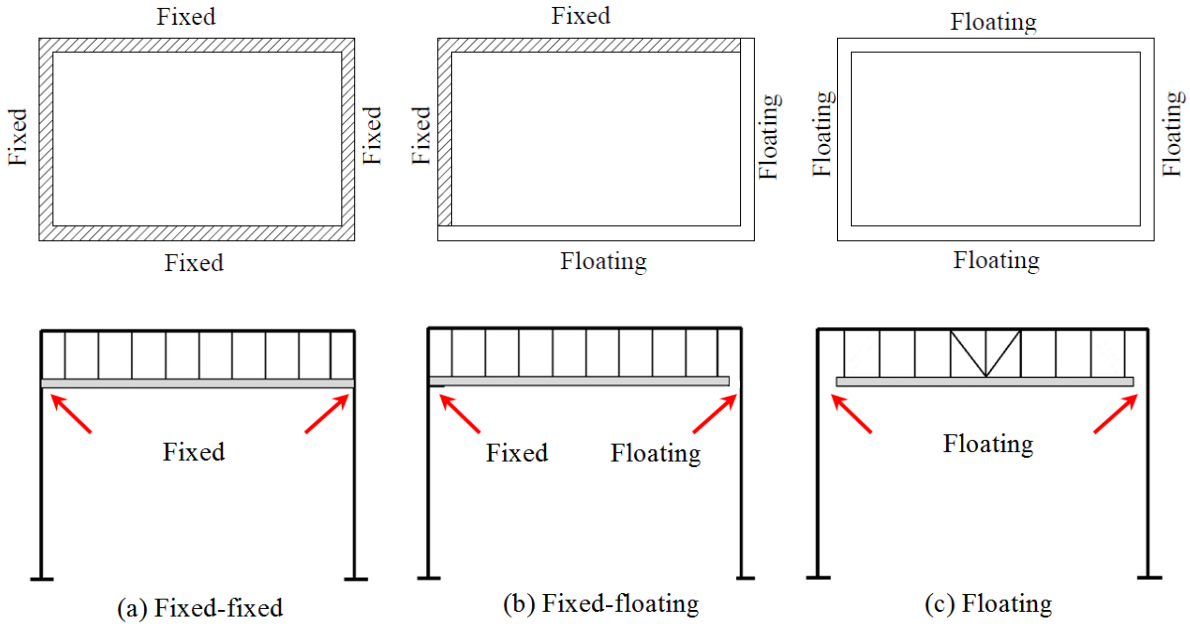

Figure 6-4 – Schematic view of common suspended ceiling types

The potential damage types in the grid and tile suspended ceilings include (Dhakal, 2010):

- dislodgment and breakage of the ceiling tiles,
- failure of the ceiling grid members and connections,
- failure of perimeter support angles, and
- damage due to interaction with the services.

Damage in residential ceilings, which typically consist of plasterboards nailed and/or glued to a light timber frame, was mainly caused by force transferred to the ceiling from the roof

framing and adjacent walls. In these ceiling types, the common forms of damage included cracking, crushing and detachment of plasterboards from their frame. This was mainly caused by punching though the nail or tearing off at the glue or the differential movement between the ceiling and structural frame or walls (Dhakal, 2010).

The commonly used drywall partitions in New Zealand can be classified into two categories, which are based on the type of the underlying framing system:

- Light gauge steel framed drywalls (Figure 6-5)
- Timber framed drywalls

The construction specifications for these drywalls are usually mandated by the manufacturer (GIB, 2006, 2010). In these two scenarios, underlying frame systems are usually either attached to the surrounding structural elements or to the upper and lower floor slabs, depending on their location in the floor plan. This results in the transfer of inter-storey drifts from the structural frame to the walls and potential damage. In many cases a gap is provided above the drywall boards to accommodate the floor deformations under live loads and relative displacement between the floors through sliding. However, often the absence of proper detailing results in extensive cracking and tearing at joints and points of attachment (FEMA, 2011). For such a system to not damage the panels, a gap is also needed at both ends of the panel to prevent loading under in-plane deformations (Canterbury Earthquake Royal Commission, 2012). In a study by Tasligedik et al. (2015), a low-damage drywall partition system was proposed and tested. The fundamental methodology and construction details of this low-damage drywall can be found in Tasligedik (2014).

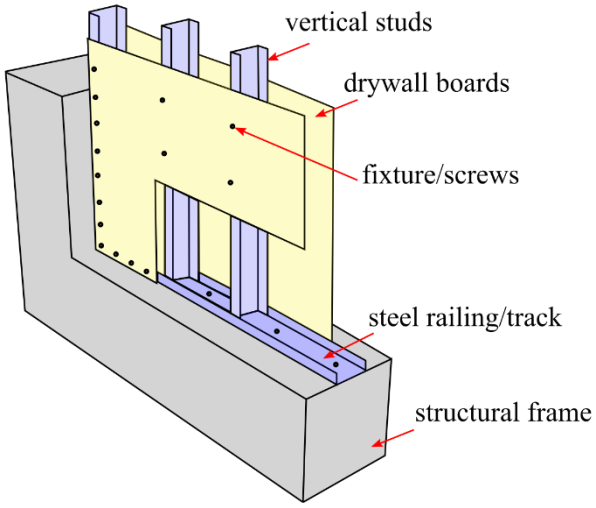

Figure 6-5 – Schematic view of the components of an as-built steel framed drywall (Tasligedik et al., 2015)

In earthquakes, drywall partitions typically incur damage in the form of boundary and interface cracks around individual drywall linings (Tasligedilk et al., 2015). After the Canterbury earthquakes, these walls suffered moderate to extensive levels of damage, which required repair or complete replacement repeatedly.

6.1.2 *Review of previous studies*

Extensive studies have been carried out to date on the seismic performance and damage states of typical suspended ceilings and drywall partitions. Some studies have also investigated the behaviour of these two non-structural elements combined. Shake table tests by Badillo-Almaraz et al. (2007), Gilani et al. (2010, 2012), Glasgow et al. (2010), Ryu et al. (2012), and Soroushian et al. (2016) were carried out to determine the overall performance and fragility functions of different suspended ceilings at increasing levels of shaking. These studies also investigated the common forms and causes of damage in ceilings and defined their damage states. Shake table tests by Huang et al. (2013) and Soroushian et al. (2014) investigated the seismic performance of combinations of non-structural elements, e.g. suspended ceilings in conjunction with partition walls or services. In the shake table experiments by Huang et al. (2013), damage was observed in seismic and non-seismic (i.e. without bracing or perimeter fixtures) ceilings as well as in partitions' connections. In the tests on the combined system of suspended ceilings and partition walls, damage was observed in the form of tile dislodgement and failure of the partition's top railing. The damage was reported to be more extensive in the non-seismic ceiling due to the absence of a rational load path and sufficient lateral restraints.

To avoid the common earthquake damage to partition walls mentioned in Section 6.1.1, Tasligedik (2014) proposed a low-damage drywall solution following their reverse cyclic quasi-static experiments on different drywall specimens. The low-damage drywalls used were distinguished from the common as-built drywalls in their isolation from the structural frame. These walls are detailed such that the drywall boards are only fixed to the drywall frames that are able to slide within the steel channel tracks, which allow rigid body motion following the structure's displacements -i.e. inter-storey drifts- through friction and sliding. The construction details of these low-damage drywalls can be found in Tasligedik (2014) and Tasligedik et al. (2015).

6.1.3 *Motivation and objectives*

Shake table tests on a combined system of two non-structural elements (i.e. existing suspended ceilings and low-damage drywalls) were carried. These tests are considered

innovative on three fronts:

i. The low-damage drywalls proposed by Tasligedik et al. (2015) were only tested under quasi-static motion and their dynamic performance will be tested for the first time in this project.
ii. Tasligedik et al. (2015) tested their low-damage drywalls under in plane loading on a single wall specimen. The response of these drywalls when combined with similar drywalls in a roomlike setting and under out-of-plane displacements has not been investigated earlier.
iii. The seismic performance of these low-damage drywalls will be evaluated in conjunction with other non-structural elements, herein and most importantly, suspended ceilings.

The tests carried out aimed at investigating the performance and compatibility of the low-damage drywalls with two existing suspended ceilings, identifying any possible incompatibilities and proposing solutions (if needed). The main aspect of compatibility investigated in these experiments was the relative displacement between the adjacent drywalls and the suspended ceilings. The low-damage drywalls were installed and tested on three faces of the test frame on a shaking table in a C-shaped setting and were tested in two configurations:

- Low-damage drywall with back-braced (floating) ceiling
- Low-damage drywall with perimeter-fixed ceiling

The experiments were designed and conducted to seek answers to the following questions:

1. How does the proposed low-damage drywall perform under seismic loading, both in-plane and out-of-plane?
2. Are there any incompatibility issues when this low-damage drywall system is used in multiple directions (similar to a room)?
3. How does the back-braced ceiling perform in combination with the low-damage drywall system?
4. How does the perimeter-fixed ceiling perform in combination with the low-damage drywall system?
5. What modifications could be applied to improve the overall performance?

6.1.4 *Limitations*

The shake table used in these experiments applied uni-directional horizontal excitations along

the longitudinal direction of the specimens (E-W). Therefore, the results and conclusions reached here do not include the effect of bidirectional and vertical excitations. Another restriction arose from the size of the test frame and ceiling specimen. It is expected that the results and consequent recommendations may vary in a larger ceiling size, where bracing conditions could be more realistic. Using heavier ceiling tiles could also affect the type and extent of the damage observed. Due to time restrictions, tests were only conducted on ceilings with average weight tiles.

6.2 Methodology

6.2.1 *Test Setup*

The experiments were carried out on a unidirectional shaking table at the University of Canterbury and provided motion along the longitudinal direction of the frame (East-West). The test setup consisted of a steel frame, three low-damage timber stud drywall partitions on three sides of this frame (C-shaped wall setting) and two types of suspended ceilings supported by the frame (Figure 6-6). The test frame built was 5.20 m long, 2.65 m wide and 2.6 m high and could accommodate a 2.4 m by 4.8 m ceiling. The test frame had pinned column base connections and moment resisting beam to column joints. The roof structure provided support for the suspended ceiling and consisted of 45 mm by 140 mm timber joists extending in the transverse direction of the frame. The horizontal natural frequency of the frame was calculated through transfer function of the test frame and shake table responses. The calculated natural frequency was approximately 4 Hz (i.e. natural period of 0.25 s).

Figure 6-6 – The exterior and interior views of the test frame with partitions and ceiling specimen installed

6.2.2 *Specimens and installation details*

The low-damage drywalls were provided and installed on three faces of the frame: North, South and East by GIB (2010) and according to the recommendations of Tasligedik (2014). The two drywalls in the longitudinal direction (N & S faces) were 2.3 m by 5 m and the third in the transverse direction (E face) was 2.3 m by 2.5 m. The key installation details are shown both in drawings and in the real specimen in Figure 6-7. These key points are crucial to the low-damage performance of the partition walls. Details B and C show the sliding mechanism at the top and bottom ends of vertical studs in the low-damage drywall. The vertical wall studs (45 mm by 140 mm) were designed to slide along steel channels that were fixed to the top and bottom structural beams. This connection can be done through nail guns or special glue depending on the material of the structure. Unlike a traditional partition wall, in these details the vertical wall frame studs were not connected to the top and bottom steel channel elements (i.e. members of the supporting structure), but they were friction fitted. On the top end of the partition's vertical stud, a 10-15 mm vertical gap was provided to ease this sliding mechanism and allow for vertical deflections from the floor beams. As the structure (herein the test frame) undergoes lateral deformation, the beams and the connected channels displace and slide around the vertical studs. This way, the vertical studs and the gypsum wallboards connected to them remain stationary while the frame deforms around them. For these motions to take place without causing damage to wallboards, appropriate gaps need to be provided between the drywall boards and any obstructions (e.g. at the intersections with the perpendicular wall boards, roof and floor structure). These gaps need to be large enough to accommodate the design drifts.

To allow wall re-centering, Tasligedik et al. (2015) recommended the use of gaps and pivot points on two ends of each wall as shown in Detail A in Figure 6-7. In these experiments, horizontal gaps were provided between the frame columns and the two ends of the walls vertical studs to accommodate inter-storey drifts up to 3.8% at the frame roof level without causing structural damage to the drywalls and the linings. To accommodate this drift level, a 50-mm horizontal gap was required (3.8% = 50/1300). A vertical timber stud was fixed to each structural column in the frame and a 50-mm long piece of timber was fixed to this vertical stud on the column and acted as the pivot point. The next vertical studs of the drywall were placed after this pivot point at about 600 mm intervals. Horizontal studs (45 mm by 140 mm) were fixed between the inner vertical studs to maintain the orthogonality of the timber frame of the walls. The other important installation point was the fixture of drywall boards to

the wall studs. These boards could only be screwed to those horizontal and vertical timber studs that were not fixed to the structural/test frame. Any connections between the drywall boards and the top and bottom channels or beams and columns of the main structure (herein test frame) would impair the low-damage performance of this type of drywall partition (Tasligedik et al. 2015).

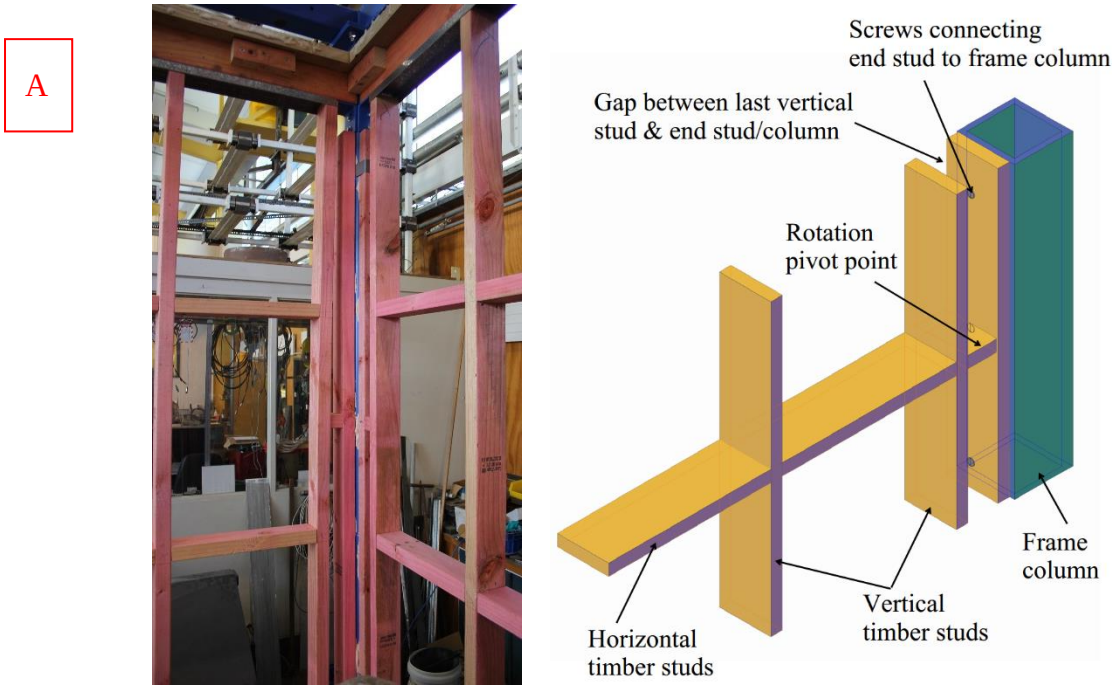

Detail A: the pivot point (The pivot point location shown in the schetch may vary in different specimens with different heights. The pivot point is located in mid-height of the wall frame)

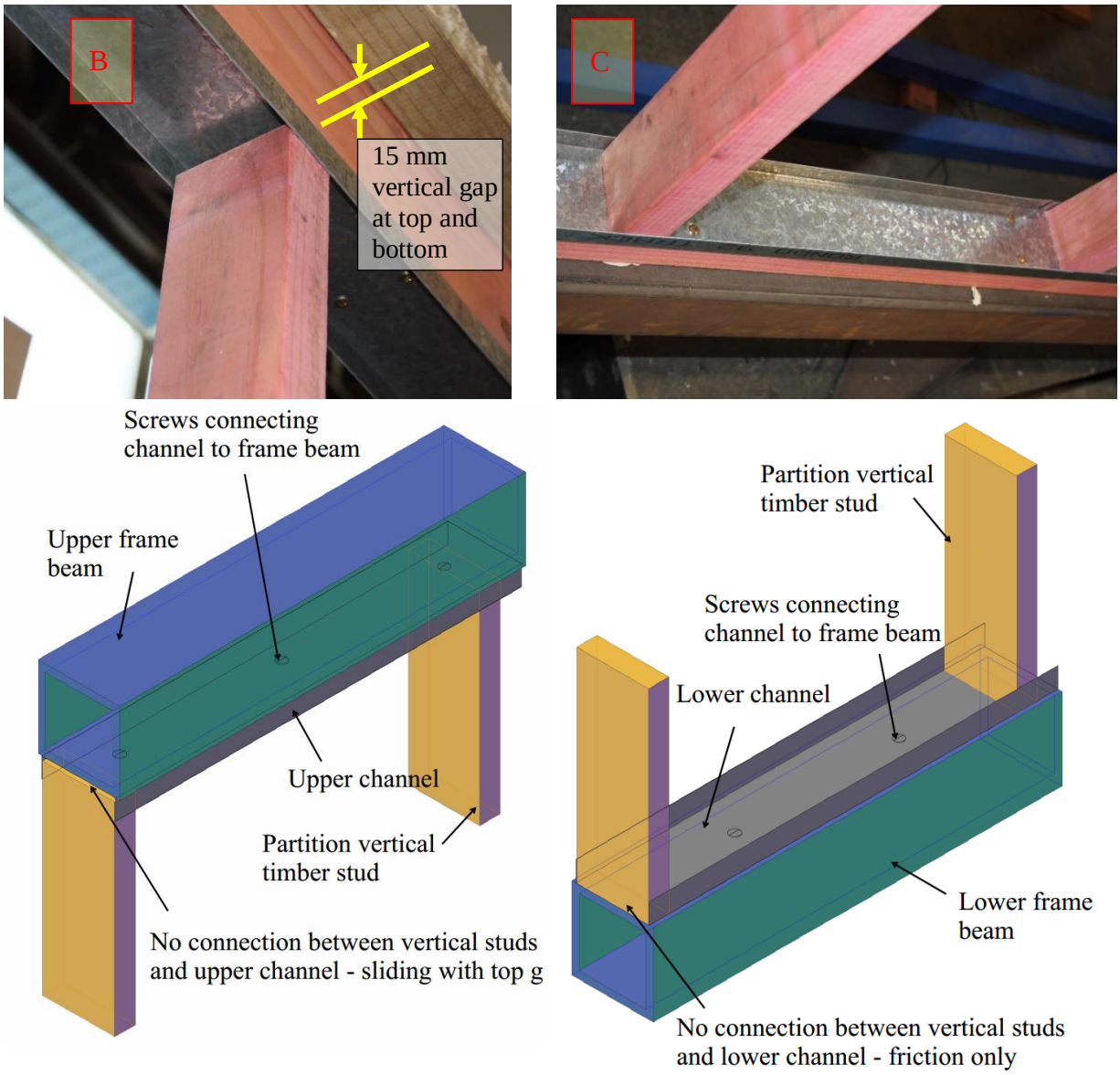

Detail B: top beam, track and studs Detail C: bottom beam, track and studs

Figure 6-7 – Details of specimen construction

Two types of ceilings were tested with the low-damage drywall partitions: i) back-braced, and ii) perimeter-fixed ceilings. The bracing locations on the ceiling grid for the braced ceiling are shown in Figure 6-8a and the perimeter types in the perimeter-fixed ceiling are shown in Figure 6-8b.

(a)

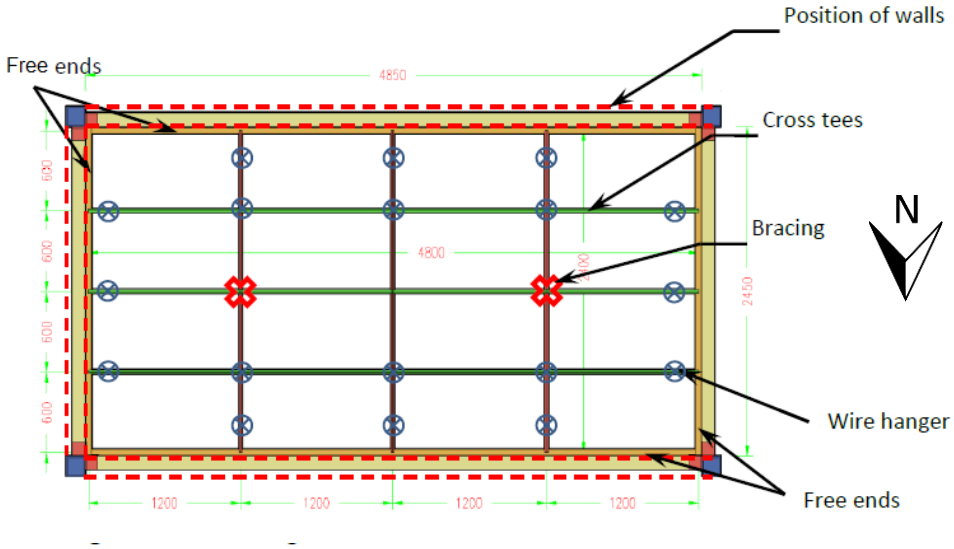

(b)

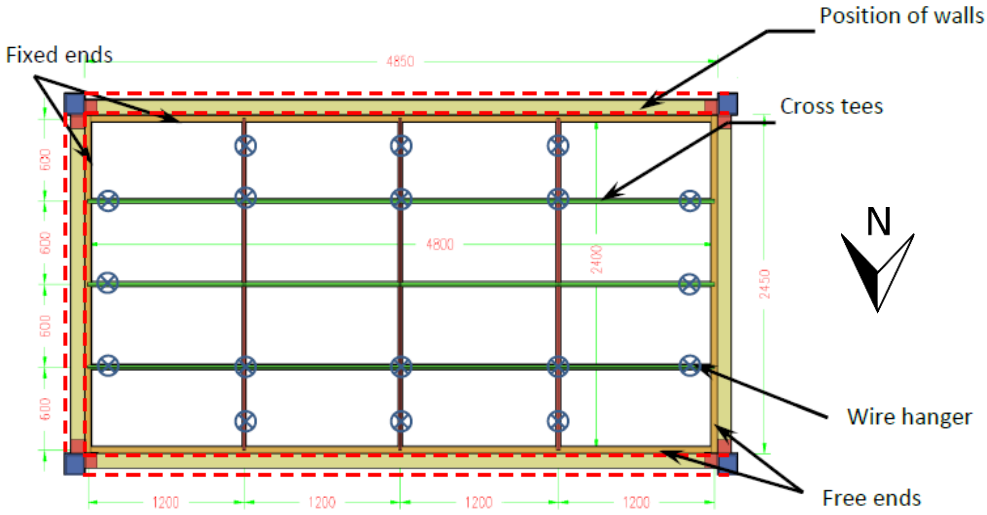

Figure 6-8 – Suspended ceiling specimens (a) back-braced, and (b) perimeter-fixed (dimensions in mm)

The ceilings consisted of DONN brand DX30D-3600 main tees and DX30M-1200 cross tees, both of which are standard grids. The ceiling tiles were 1200 mm × 600 mm USG Boral Radar ClimaPlus™ which are approximately 2.75 kg each and are commonly used in NZ (USG, 2012, USG, 2011). The perimeter-fixed ceiling was fixed to the drywall boards on two adjacent sides (i.e. south and east faces) and free to slide on the opposite ends (i.e. north and west faces). In common and good practice, ceiling manufacturers provide special clips for the fixed and free ends of the ceiling grids which restrain the displacement perpendicular to the grid axis and therefore, prevents grid spreading at free ends (USG, 2012; Armstrong, 2013). However, the use of these proprietary clips is not mandatory by the standards and they only allow for a limited gap (e.g. ±10 mm). To consider the worst case, the fixed ends were installed via 3.2 mm rivets and free ends were simply resting on the perimeter angle. To

support the ceiling, 50 mm by 50 mm angles were screwed to the drywall boards. In the case of the opening on the West end of the frame, a timber perimeter beam was fixed to the frame at the same height and supported the perimeter angle. A 20-mm gap was provided on all grid ends in both ceilings to accommodate the relative displacements (Figure 6-9d).

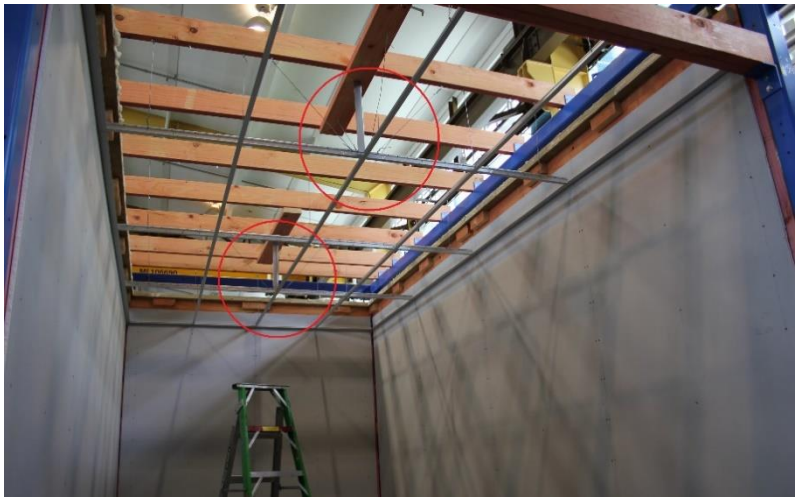

(a)

(b)

(c)

(d)

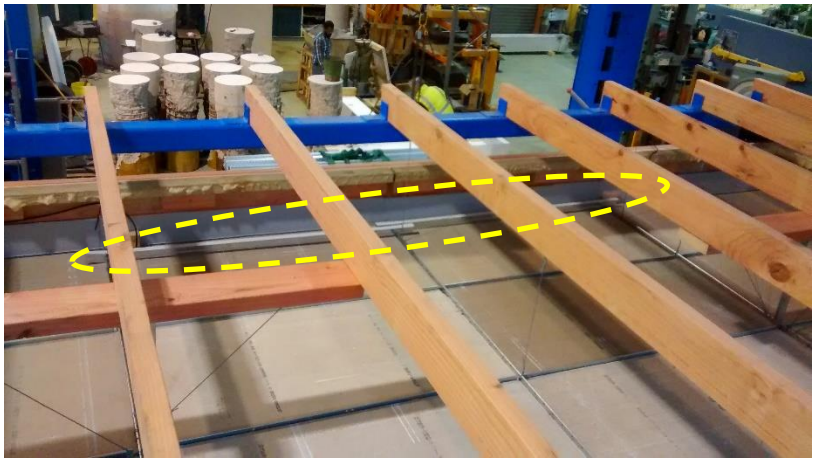

(e)

Figure 6-9 – (a) Position of braces and (b) bracing detail, (c) ceiling grids and vertical hangers in back-braced ceiling specimen, (d) gap on grid ends (in both ceiling specimens), and (e) spacer bars

The back-braced ceiling was not fixed to any walls or perimeter beams. The ceiling grid ends sat on the perimeter angles and were free to slide. Two ceiling braces were provided 2.4 m apart and 1.2 m from ceiling grid ends (Figure 6-8a). In common practice and manufacturer guidelines, ceiling braces are required at 3600 mm intervals in both directions and 1800 mm from each wall (CISCA zone 3-4). The braces consisted of four wires installed 90 degrees apart and with a 45-degree slope from the ceiling plane, in accordance with the manufacturer's guideline (Figure 6-9a & b) (USG, 2012). These wires were 12-gauge galvanized, soft annealed mild steel similar to those used as hanger wires and were connected to the ceiling at the intersection of cross tees and main tees. A 40×40×0.05 mm galvanized steel angle was used as the vertical support element at the bracing point (Figure 6-9b). The installation of the braces (and both ceiling specimens in general) was carried out by an experienced contractor recommended by the ceiling manufacturer. Therefore, the installation of the ceiling was assumed as per the common practice.

Both ceilings had vertical hanger wires at 1200 mm intervals and 200 mm from all grid ends (Figure 6-9c). During the experiments, considerable displacements were observed at the free end of the ceiling grids. To limit this grid spreading, some spacer bars were added to the ceilings as shown in Figure 6-9e.

6.2.3 *Instrumentation*

A total of 18 potentiometers and 21 accelerometers in the horizontal (i.e. x, y) and vertical (i.e. z) directions were installed on the frame, walls and ceilings to record the displacements and accelerations during tests. The potentiometers shown in Figure 6-11a were installed to measure the relative displacements between the frame and the shake table, and between the frame and drywalls. The displacements of the ceiling relative to the walls were recorded in two horizontal directions as shown in Figure 6-10 and Figure 6-11b. These instruments were partly effective in the measurement of the displacements but were later removed from the setup as they were observed to be unable to return to their zero position and cope well with the dynamic motion or reached their capacity (±10 mm). This was confirmed by comparing the displacements recorded by the potentiometers on the outer grids and the digitised video data from the middle grid without any instruments attached (Figure 6-10). Therefore, in the last set of tests on back-braced ceilings all potentiometers on the ceilings were removed.

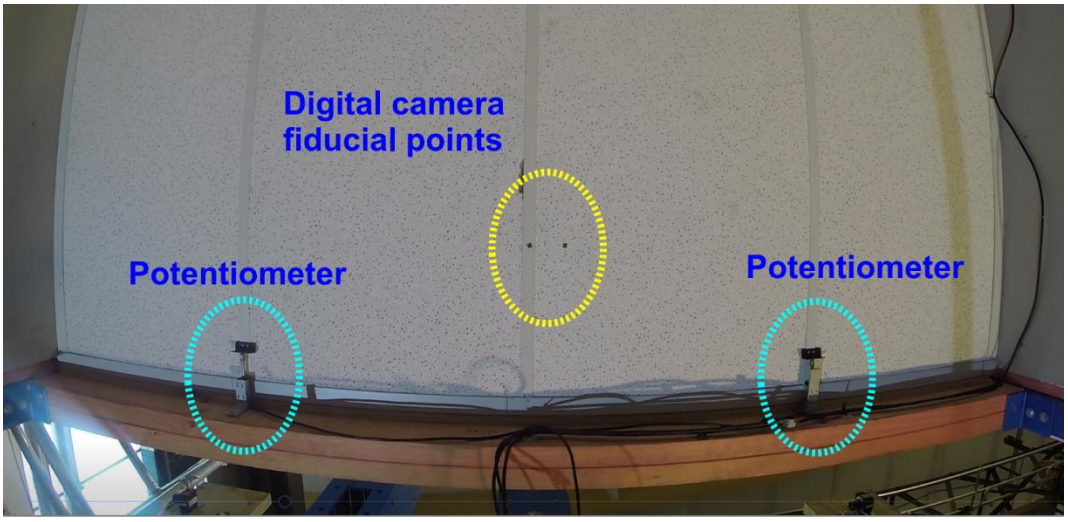

Figure 6-10 – Position of potentiometers and fiducial point

(a)

(b)

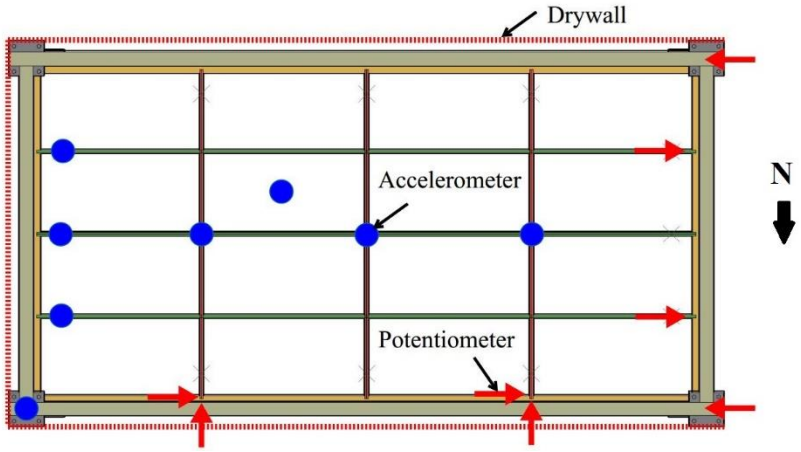

Figure 6-11 – Accelerometers and potentiometers installed (a) on the drywall and test frame (elevation view), and (b) on the ceiling specimen (plan view)

6.2.4 *Input motion*

A suite of ground motions was chosen from a mix of significant local and global seismic events. The ground motion time histories were applied with scaling factors gradually increasing to reach the target inter-storey drift level. Figure 6-12 shows the spectral accelerations and spectral displacements obtained from the scaled acceleration time histories recorded on the shaking table. In the spectral acceleration plot, it must be noted that these accelerations correspond to the peak acceleration applied to the non-structural element which varies from the PGA or PFA (e.g. based on the location of the element along the height of the building). Further details on the input motions can be found in Appendix A.

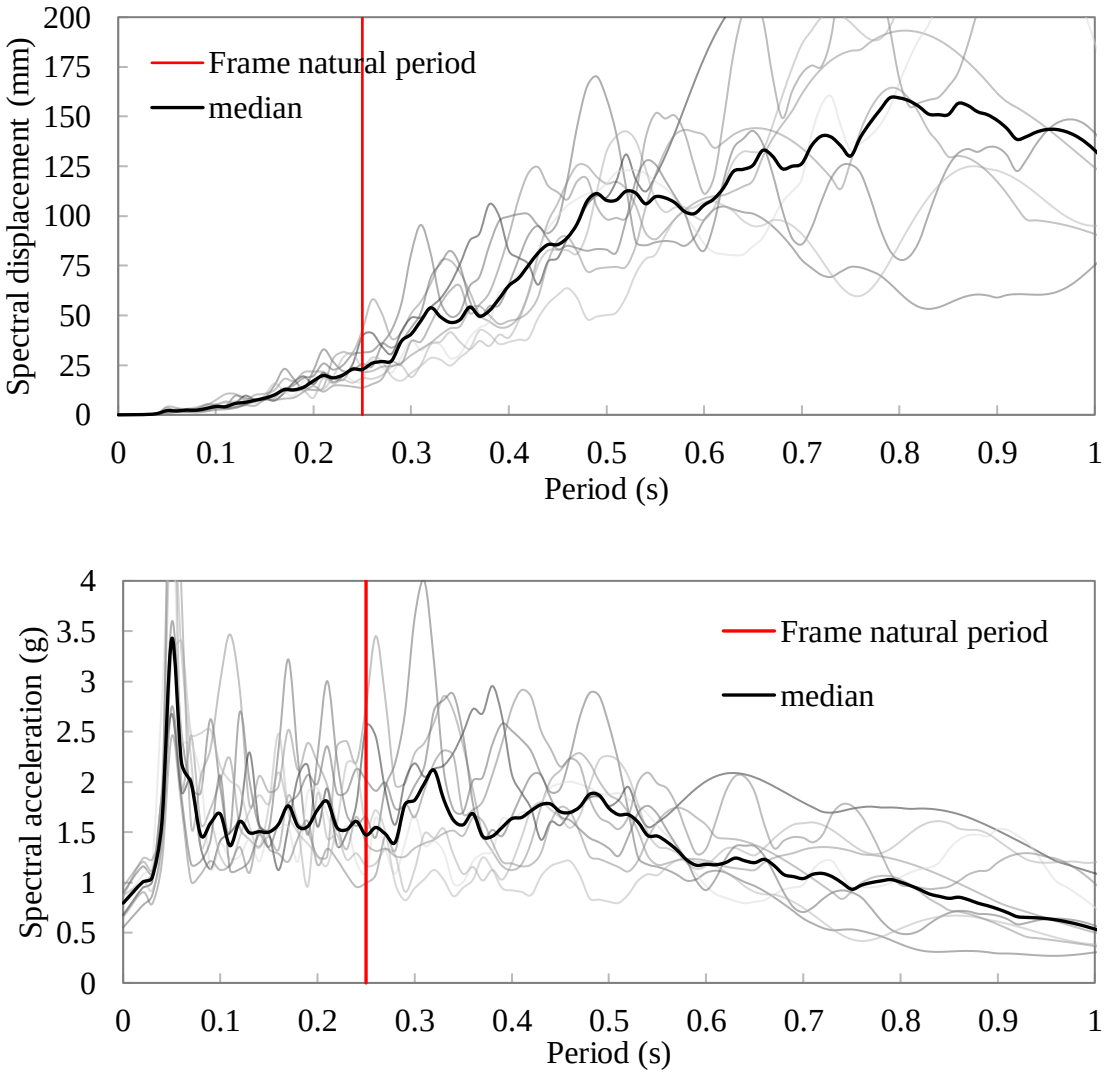

Figure 6-12 – Spectral displacements and accelerations from ground motions recorded on the shaking table (damping ratio 1.5%)

6.3 Results

6.3.1 *Inter-storey drift levels*

In both phases of experiments, the seismic compatibility of the two non-structural systems (drywall partitions and ceilings) were evaluated when subjected to increasing levels of inter-storey drift. The ground motion records chosen were applied with an increasing scaling factor. The displacements were recorded both at the frame roof level and the corners of the drywall frame relative to the test frame (Figure 6-11a). During these experiments, an inter-storey drift of approximately 1.3% was achieved at the test frame roof level (height of 2.5 m). Figure 6-13 shows the peak inter-storey drifts from steel frame displacements in all tests vs. the peak horizontal accelerations measured at the top of the frame in the direction of applied shaking. These accelerations are referred to as peak floor acceleration (PFA), which is dependent on the structural system type, inter-storey height and the induced floor accelerations during an earthquake.

Table 6-1 shows the spectral accelerations and spectral displacements for the ground motions recoded on the shake table at periods close to the estimated natural period of 0.25s. The experimental results for the peak accelerations on the frame top (PFA) and peak displacements on the frame roof level have been provided in the last column on the table for comparison.

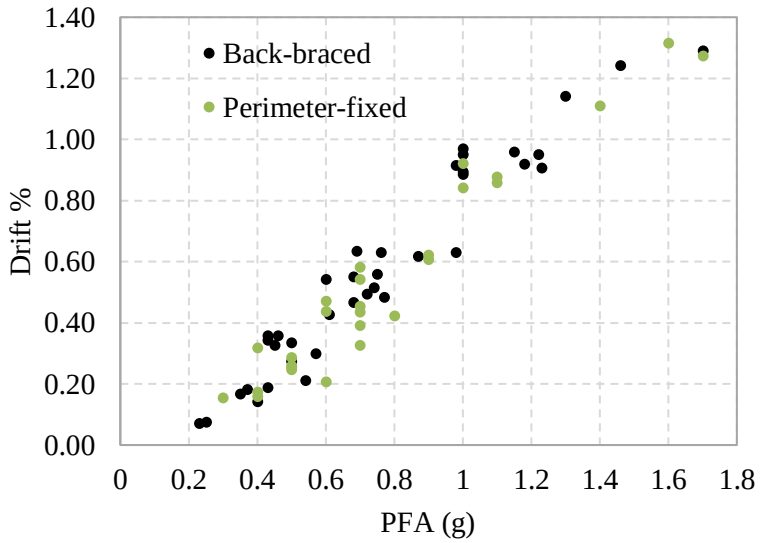

Figure 6-13 – Inter-storey drifts and peak floor accelerations (PFA) achieved in tests

Table 6-1 – Spectral accelerations and displacements of the different ground motions used in the tests vs. the experimental peak displacements and PFAs

	Period (s)	0.23	0.24	0.25	0.26	0.27	Experimental
HVSC-2-0.6	S_d (mm)	22.0	22.3	25.6	24.3	35.3	**31.9**
	S_a (g)	1.7	1.6	1.7	1.4	1.9	**1.7**
HVSC-2-0.4	S_d (mm)	15.2	15.8	17.6	16.0	23.5	**11.5**
	S_a (g)	1.2	1.1	1.1	1.0	1.3	**0.7**
HVSC-1-0.5	S_d (mm)	31.6	31.3	42.7	58.0	50.9	**32.9**
	S_a (g)	2.4	2.2	2.8	3.5	2.8	**1.6**
North1063-1-1	S_d (mm)	19.5	25.4	39.6	41.1	34.5	**27.8**
	S_a (g)	1.5	1.8	2.6	2.4	1.9	**1.4**
GDLC-2-1	S_d (mm)	20.5	17.2	17.1	27.6	24.0	**23.0**
	S_a (g)	1.6	1.2	1.1	1.6	1.3	**1.0**
GDLC-1-1	S_d (mm)	16.1	18.5	18.1	19.9	24.1	**22.2**
	S_a (g)	1.2	1.3	1.2	1.2	1.3	**1.2**
North1048-2-1	S_d (mm)	14.2	13.7	15.4	18.1	26.5	**22.5**
	S_a (g)	1.1	1.0	1.0	1.1	1.5	**1.1**
North1048-1-1.5	S_d (mm)	25.0	30.4	31.3	32.1	36.0	**23.2**
	S_a (g)	1.9	2.1	2.0	1.9	2.0	**1.2**
183-2-1.2	S_d (mm)	28.7	30.9	24.1	28.8	27.1	**15.0**
	S_a (g)	2.2	2.2	1.6	1.7	1.5	**0.9**
183-1-1.5	S_d (mm)	17.5	23.6	21.6	22.0	24.2	**22.0**
	S_a (g)	1.3	1.7	1.4	1.3	1.3	**1.2**

6.3.2 *Phase I: Low-damage drywalls with back-braced ceiling*

Phase I of the experiments consisted of dynamic tests on low-damage drywall partitions combined with the back-braced ceiling. In these experiments, peak floor accelerations (PFAs) up to 1.7 g and inter-storey drifts up to 1.3% were measured at the top of the test frame. The highest peak ceiling accelerations (PCAs) recorded was 9 g (this includes the random spikes at 0.005 s time steps, which were caused by the impact between tiles and pounding of longitudinal grid ends to perimeter beams). Up to these levels of input, no damage was observed in the drywall partitions. It means the gaps provided between the gypsum lining and the steel test frame was large enough to cater for the relative displacements. Moreover, due to the lack of connection between the back-braced ceiling and the low-damage drywall, no damage occurred due to interaction between the two systems. The only interaction occurred as a result of the lateral displacements of the ceiling components, which is explained in more details below.

As discussed in Section 6.2.3, in the last set of tests on back-braced ceilings all

potentiometers on the ceilings were removed. This coincided with more significant grid spreading as the grids were no longer restrained by the instruments.

During several tests at higher levels of shaking, ceiling damage was observed in the forms of grid spreading and tile dislodgement (Table 6-2). The ends of main tees and cross tees were free to slide on all sides beside the perimeter gaps. As the ends of the grids in the direction of shaking moved apart up to 5mm, the corner tiles dislodged from the grid as shown in Figure 6-14. The values of inter-storey drift and PFA and peak ceiling acceleration (PCA) recorded in tests with tile dislodgment are listed in Table 6-2.

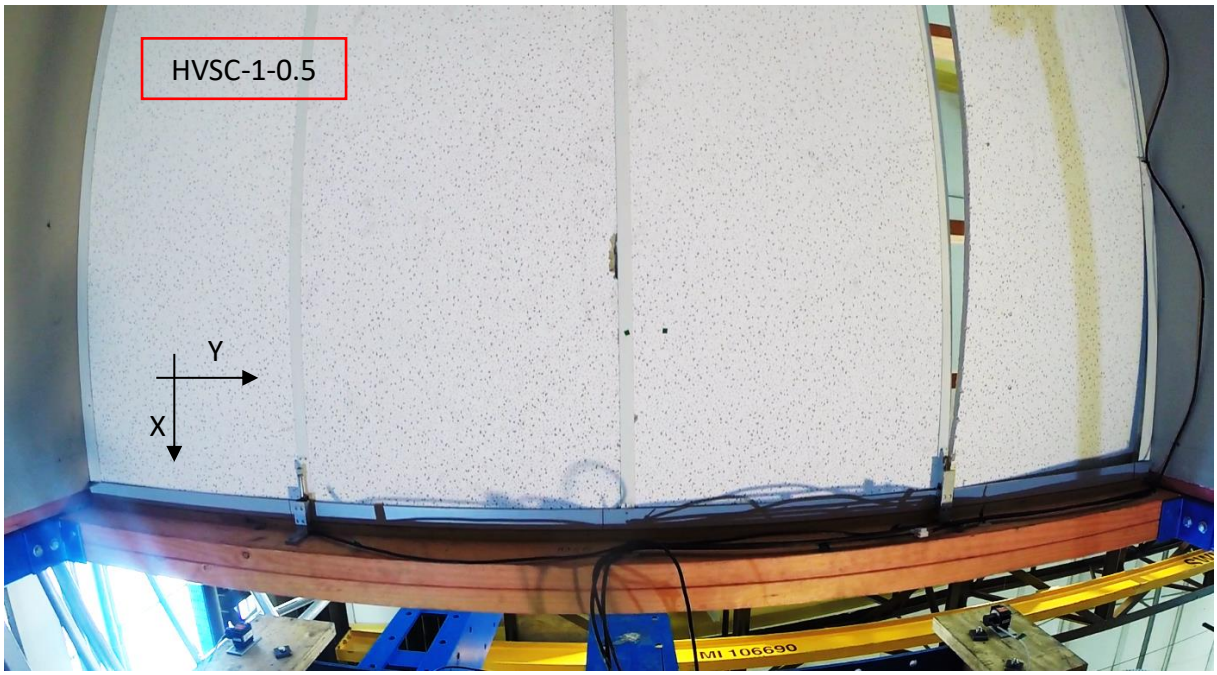

Figure 6-14 – Dislodgement of ceiling tiles

Table 6-2 – Tests with Tile Dislodgement

Ground motion	PFA (g)	Peak frame drift %	Peak ceiling grid displacement-x (mm)	Peak ceiling grid displacement-y (mm)
North-1048-1-1.5	1	0.97	20	4
North-1048-2-1	0.98	0.92	20	5
HVSC-1-0.5	1.6	1.28	20	4
HVSC-2-0.6	1.7	1.29	20	5

As mentioned earlier, on all four sides of the ceiling, perimeter gaps of 20 mm were provided between grid ends and the support angles (Figure 6-9d) which covered the suspended ceiling installation requirements in seismic areas (ASTM E580, 2011). The tested ceiling had two braces installed 2400 mm apart from each other and this bracing interval can be considered

conservative for the size of the specimen. The 45° wire braces only act in tension. They are fastened to the structure and ceiling grids through looped wires which are not taut or tight and consequently, have an inherent level of slackness which results in their lateral flexibility. Under shake table excitations, the relative displacements in ceilings reached the 20-mm limit during several of the tests carried out, including those which caused tile dislodgement as listed in Table 6-2. These displacements resulted in pounding between the grid ends and the perimeter structure. In one of the tests (HVSC-1-0.5), this impact resulted in partial damage to the cross tee-main tee intersection at the point of the connection of the ceiling brace as shown in Figure 6-15. In this test, the main tee-cross tee clip was observed to have disconnected but no damage was noticed and the clip ends were popped back inside. No other form of damage was observed in the ceiling grids in these series of tests.

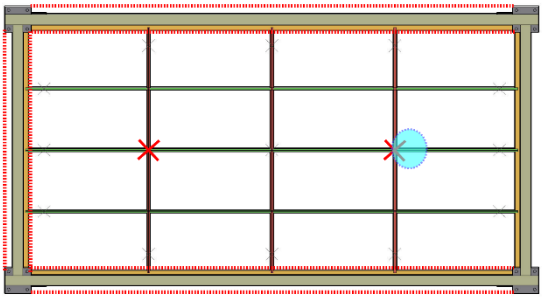

Figure 6-15 – The back-braced ceiling specimen with the location of the disconnected MT-CT connection marked in circle

6.3.3 *Phase II: Low-damage drywalls with perimeter-fixed ceiling*

In phase II, the low-damage drywall partitions were tested with a perimeter-fixed ceiling. In this configuration, the suspended ceiling was fixed to the drywall boards on two adjacent and perpendicular sides (i.e. East and South) and free to slide on the opposite sides (i.e. North and West). The schematic deformations of the system are shown in Figure 6-16 in solid lines compared to the original position before shaking in dashed lines. As shown in the figure, at each stroke of the (shake table) motion the displacement of the steel frame at the top was *2a* with the centre of rotation at column bases. The East wall and the grids connected to it (herein cross tees) displaced at the top by *2a* as well, rotating at the column bases. In the North and South walls, there were two systems moving: i) the structural frame with the centre of rotation at columns bases and displacing *2a* at the top and *a* at mid-height, and ii) the drywall frame and boards displacing by a length *a* at the mid-height with the structure while allowing for further sliding movement of the structural frame at the top and bottom. The overall displacement of the drywall boards (which did shift as a rigid body but did not

deform) was equal to *a* at the column mid-height as well as at the top. This resulted in relative displacement of *a* between the N and S walls and structural frame at the top and bottom. The ceiling cross tees were fixed and pushed by the East wall for a distance of *2a*. The main (transverse) tees were consequently pushed by the cross (longitudinal) tees for the same length of *2a*. On the North wall, where the main tees were not fixed to the wall, this displacement was not resisted. However, on the South wall the main tees were riveted and could only move as far as the wall moved (i.e. *a*). This resulted in the deformation of the last span of the main tees fixed to the South wall as shown in Figure 6-16 to accommodate the remaining relative displacement of *a*. In summary, when the frame underwent a deformation of Δ, the grids needed to be able to withstand a deformation of Δ/2 without damage. This ratio has been shown for the results obtained in this experiment in Figure 6-17.

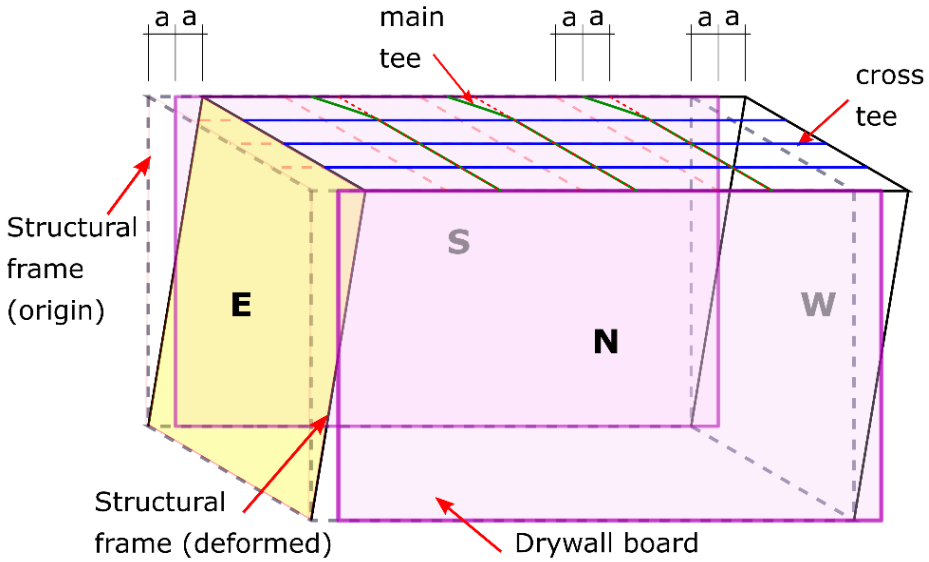

Figure 6-16 – Schematic view of the deformations in the frame, drywalls and ceiling

Potentiometers were installed on the ceiling grid, drywall boards and test frame to measure the relative displacements (Figure 6-11). Figure 6-18 shows the E-W relative displacements between the drywall frame and steel frame columns recorded by potentiometers on the four corners of the North wall. The recordings from the potentiometer installed on the ceiling main tee are also included for comparison. This potentiometer recorded the E-W relative displacements between the main tee and the drywall board on the North wall.

The variation in the ratios shown in Figure 6-17 and displacements presented in Figure 6-18 must be considered with the limits of the measurements with the potentiometers in a dynamic test. In some cases, the readings in the positive and negative directions in the top and bottom

potentiometers varied as the instruments were not always fully engaged or the components underwent permanent displacement (i.e. grid spreading) and the instruments did not return to their zero position. Therefore, some of the small recordings could be excluded from the data range (e.g. the positive readings of the wall potentiometer at the bottom left)

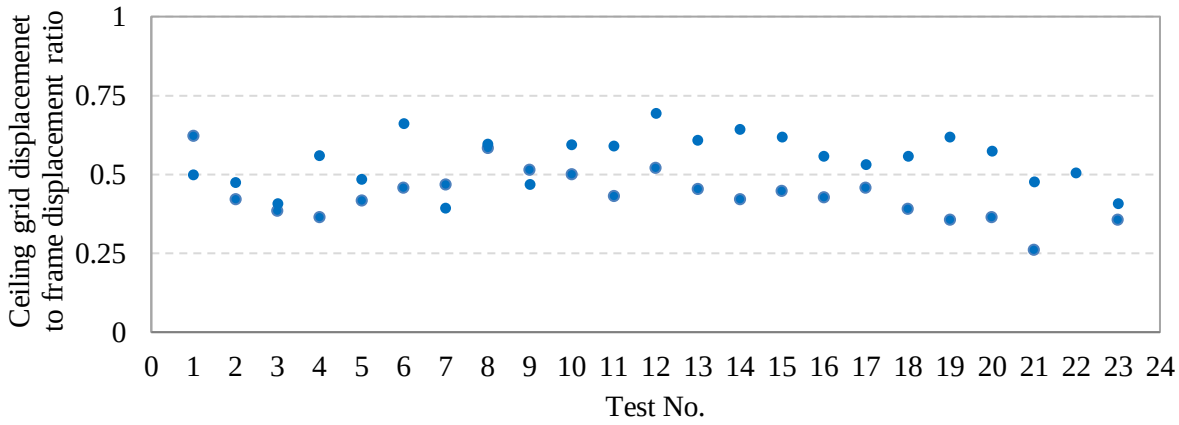

Figure 6-17 – Ratio of the relative displacement between ceiling main tees and drywall board on North wall to the relative displacements at the top of the frame

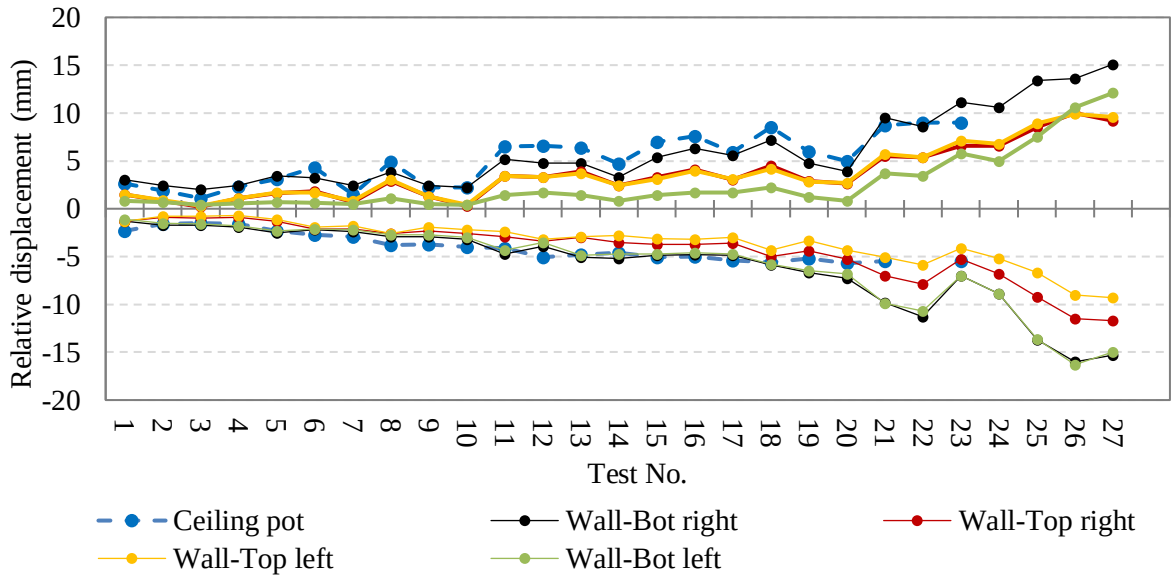

Figure 6-18 – Displacements between the ceiling main tees and drywall board on North wall vs. the displacements between the frame and the drywall board on the North wall during E-W shaking

Throughout the tests no damage was observed in the perimeter-fixed ceiling or the low-damage drywalls. In these experiments, peak floor accelerations (PFAs) up 1.7 g and inter-storey drifts up to 1.3% were measured at the top of the tests frame. The highest peak ceiling accelerations (PCAs) recorded was 4.8 g (This includes the random spikes due to impact between tiles and grids).

Based on the outcomes of this experiment, the perimeter-fixed ceiling had enough flexibility to accommodate the relative displacements between the two perpendicular walls.

6.4 Discussions

As shown in Figure 6-16, under E-W excitation, the wall on the East face rotates and displaces along the steel frame and perpendicular walls on the North and South faces. It is estimated that in presence of plaster finish and paint, these relative displacements would result in some cosmetic damage in the corners of the drywall boards. In these experiments, the gaps and lines between the drywall boards were not filled and no damage of that kind was observed. As shown in Figure 6-19, in the absence of sufficient gaps, the clash between two adjacent walls is possible and could impair the performance of the wall. In an optimum layout, gaps need to be provided around structural columns in both directions, minimising the damage to cracks in cosmetic layers and paint on edges.

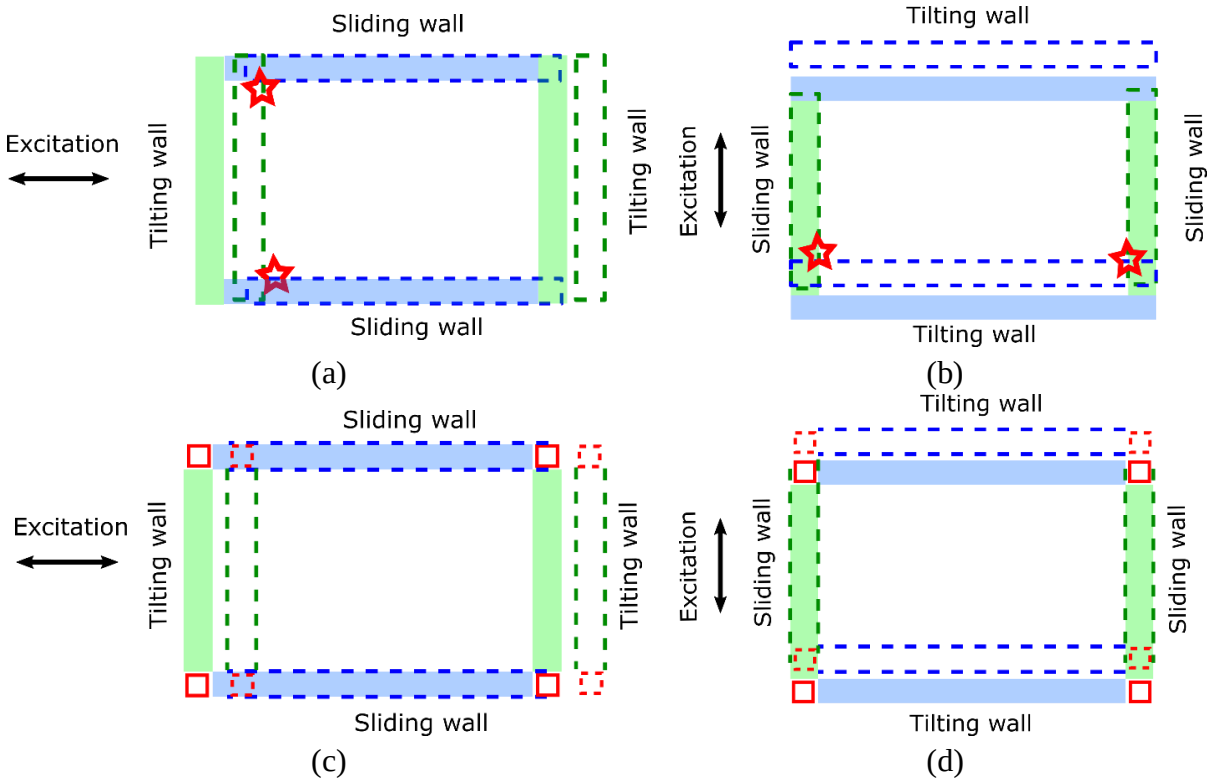

Figure 6-19 – Relative displacements of low-damage drywalls in (a) E-W excitation and (b) N-S excitation with clash; and (c) E-W excitation and (d) N-S excitation with gaps

6.4.1 *Phase I*

From the tests carried out it was concluded that low-damage drywall partitions showed good compatibility with the back-braced ceiling up to the level of inter-storey drift achieved. However, the spreading at grid ends resulting in the dislodgement of ceiling tiles needed to be

controlled. This could be achieved by using spacer bars. However, a more effective and simple solution could be the use of perimeter angles fixed to all ceiling grids as a perimeter trim element as shown in Figure 6-20b & Figure 6-20d. In Figure 6-20a, the ceiling grids have free ends and can rotate and spread on the perimeter support which can result in tile dislodgement. In Figure 6-20b, the red dashed line on perimeters shows the perimeter trim element which provides integrity/confinement for the entire ceiling. This can be achieved simply by riveting all grid ends to an angle element which is not connected to any supporting structure. Gaps of various lengths can be provided between the trimmed/framed ceiling and the structure or walls. This gap can be covered using wider perimeter angles fixed to the walls similar to the current practice with no mechanical fastening to the ceiling (detail shown in Figure 6-20d). Using this trimming solution isolates the ceiling as a rigid confined horizontal element from the surrounding vertical elements (i.e. walls) and minimises their interaction.

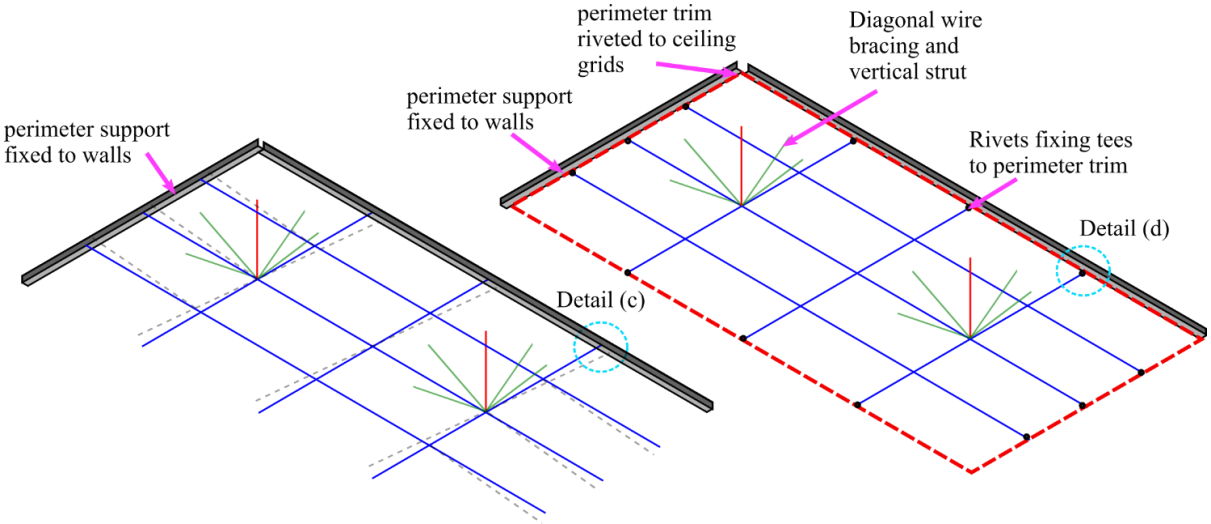

(a) Back-braced ceiling with free grid ends

(b) Back-braced ceiling with trimming angle element connected to grid ends

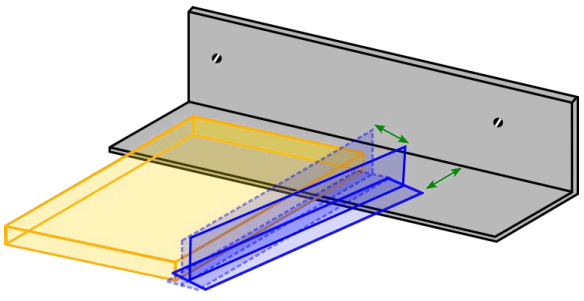

(c) Detail of free floating grid end without trimming element in ceiling (a)

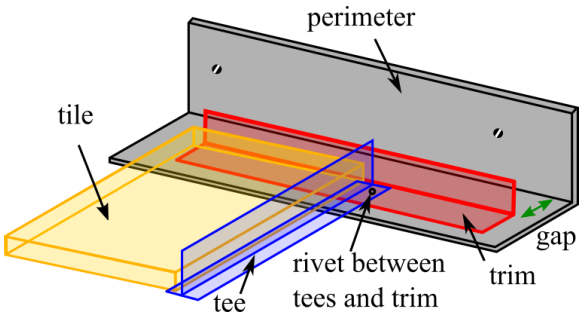

(c) Detail of trimming angle element riveted to grid end in ceiling (b)

Figure 6-20 – Recommended framing/trimming angle solution for the prevention of grid spreading

The observations also suggested that a more accurate estimation of the probable/expected relative displacements between ceiling grid ends and perimeter walls is required to provide adequate perimeter gaps and prevent pounding between these two non-structural elements. Alternatively, a more rigid bracing solution using struts rather than sway wires can reduce the lateral flexibility of the ceiling and the relative displacements. However, this study cannot be used to comment on the possibility of other forms of grid damage due to the increased lateral stiffness in the ceiling system.

6.4.2 *Phase II*

As in these experiments, the excitation was uniaxial and the grids undergoing deformations were the main tee which were single consistent elements without any splices and connection clips, the ceiling performed well and the bending in main tees did not result in permanent deformation and disconnection. In the presence of bidirectional loading or bending in cross tee elements (which are shorter and connected through clips without mechanical fasteners, the grid joint may not be able to resist the rotation and hence disconnect. Therefore, these outcomes may not be applicable to a different suspension system with less flexible main tee-cross tee connections. One possible mitigation is using cross tee-main tee seismic clips (Refer to Chapter 4) on the joints close to the walls on the fixed sides of the ceiling to increase the load bearing capacity and the rigidity of these joints.

6.5 Conclusions

Shake table tests were carried out on two combinations of suspended ceilings and low-damage drywall partitions with the aim of investigating their deformation compatibility. In the first combination, low-damage drywalls were tested with a back-braced ceiling. In the second combination, the same drywalls were tested with a perimeter-fixed ceiling. Inter-storey drifts of up to 1.3% were applied to the subassemblies in these two series of tests. Based on the results obtained the following conclusions and recommendations are made:

1. In both combinations, the drywalls showed no damage and with the gaps provided, the low-damage solution proved effective under dynamic loading.
2. It was estimated that in the presence of plaster and paint finish, some cosmetic damage could occur in the drywall boards due to the out-of-plane relative displacements between adjacent walls. Gaps are required between the low-damage drywall boards and the structural columns in both directions.

3. In the tests with the back-braced ceiling, the damage was observed in the form of grid spreading and tile dislodgement. The back-braced ceiling also showed considerable lateral displacements resulting in closure of the perimeter gaps and impact with the perimeter support beams/walls. No permanent damage was observed in these tests, but it is recommended to use more rigid braces or increase the perimeter gaps.
4. No damage was observed in the perimeter-fixed ceilings and the drywall interfaces in these experiments. It was concluded that the main tees had enough capacity to accommodate the relative deformations resulting from the different fixtures on the two ends of the grids.
5. The grid spreading in the tested back-braced ceiling was restrained using spacer bars. Alternatively, a framing/trimming element could be added surrounding the ceiling, binding all grid ends together while still maintaining free sliding ends. In the perimeter-fixed ceiling, use of seismic clips was recommended to increase the rigidity and limit the rotation of the joints near the walls on the fixed sides of the ceiling.

6.6 References

American Society for Testing and Materials International. (2011). *Standard Practice for Installation of Ceiling Suspension Systems for Acoustical Tile and Lay-in Panels in Areas Subject to Earthquake Ground Motions (E580/E580M-11b 2011)*. PA, USA.

Badillo-Almaraz, H., Whittaker, A. S., & Reinhorn, A. M. (2007). Seismic fragility of suspended ceiling systems. *Earthquake Spectra, 23*(1), 21-40.

Baird, A., Tasligedik, A. S., Palermo, A., & Pampanin, S. (2014). Seismic performance of vertical nonstructural components in the 22 February 2011 Christchurch earthquake. *Earthquake Spectra, 30*(1), 401-425.

Canterbury Earthquake Royal Commission. (2012). *Final Report: Volume 2 – The Performance of Christchurch CBD Buildings*. NZ.

Dhakal, R. P. (2010). Damage to Non-structural Components and Contents in the 2010 Darfield earthquake. *Bulletin of the New Zealand Society for Earthquake Engineering, 43*(4), 404.

Dhakal, R. P., MacRae, G. A. & Hogg, K. (2011). Performance of Ceilings in the February 2011 Christchurch Earthquake. *Bulletin of the New Zealand Society for Earthquake Engineering, 44*(4), 379-389.

Dhakal, R. P., Pourali, A., Tasligedik, A. S., Yeow, T., Baird, A., MacRae, G., ... & Palermo, A. (2016). Seismic performance of non-structural components and contents in buildings: an overview of NZ research. *Earthquake Engineering and Engineering Vibration*, *15*(1), 1-17.

FEMA. (2011). *Reducing the Risks of Non-Structural Earthquake Damage – A Practical Guide (FEMA E74)*. Washington D.C., USA.

GIB. (2006). *GIB Noise Control Systems-Specifications for Drywalls*. NZ.

GIB. (2010). *GIB Site Guide for Residential and Commercial Installations: CBI 5113. The Manufacturer's Installation Guidelines*. NZ.

Gilani, A. S., Reinhorn, A. M., Glasgow, B., Lavan, O., & Miyamoto, H. K. (2010). Earthquake simulator testing and seismic evaluation of suspended ceilings. *Journal of architectural engineering*, *16*(2), 63-73.

Glasgow, B., Gilani, A. S., & Miyamoto, H. K. (2010). Resilient suspended ceilings for sustainable design of buildings. In *Structures Congress 2010* (pp. 2575-2587).

Huang, W., Mcclure, G., & Hussainzada, N. (2013). Experimental Study on the Seismic Performance of Suspended Ceiling Systems in Interaction with Partition Walls, *In The 2013 World Congress*, Jeju, Korea, Sep 8-12, 2013 (pp. 2304–2323).

Motosaka, M., & Mitsuji, K. (2012). Building damage during the 2011 off the Pacific coast of Tohoku Earthquake. *Soils and Foundations*, *52*(5), 929-944.

Nation Media. (2011). Retrieved from http://www.nationmultimedia.com/headlines/At-least-20-dead-after-8-8-magnitude-tremor-30150675.html

New Zealand Society for Earthquake Engineering Guidelines. (2017a). *The Seismic Assessment of Existing Buildings Guidelines - Part A – Assessment Objectives and Principles*. NZ: NZSEE. July 2017.

New Zealand Society for Earthquake Engineering Guidelines. (2017b). *The Seismic Assessment of Existing Buildings Guidelines - Part B – Initial Seismic Assessment*. NZ: NZSEE. July 2017.

Ryu, K. P., Reinhorn, A. M., & Filiatrault, A. (2012). Full scale dynamic testing of large area suspended ceiling system. In *Proceedings 15th World Conference on Earthquake Engineering, September 23-28, 2012, Lisbon Portugal-Paper* (Vol. 5474).

Soroushian, S., Zaghi, A. E., Maragakis, E. M., & Echevarria, A. (2014). Seismic fragility

study of displacement demand on fire sprinkler piping systems. *Journal of earthquake engineering*, *18(7)*, 1129-1150.

Soroushian, S., Rahmanishamsi, E., Ryu, K. P., Maragakis, M., & Reinhorn, A. M. (2016). Experimental fragility analysis of suspension ceiling systems. *Earthquake Spectra, 32(2)*, 881-908.

Tasligedik, A. S., Pampanin, S., & Palermo, A. (2015). Low damage seismic solutions for non-structural drywall partitions. *Bulletin of Earthquake Engineering*, *13*(4), 1029-1050.

Tasligedik, A. S. (2014). *Damage mitigation strategies for non-structural infill walls* (Doctral thesis, Civil and Natural Resources Engineering Department. University of Canterbury, Christchurch/New Zealand), pp. 304.

USG Australia. (2011). *DONN Brand Grid Suspension System*. USG Australia, Auckland, NZ.

USG Australia. (2012). *Generic Seismic Design for USG DONN Exposed Grid Suspended Ceilings*, Auckland, NZ.

CHAPTER 7

PERIMETER-FIXED CEILING: COMPARISON OF NUMERICAL MODELLING AND SHAKING TABLE EXPERIMENTS

7 PERIMETER-FIXED CEILING: COMPARISON OF NUMERICAL MODELLING AND SHAKING TABLE EXPERIMENTS

7.1 Introduction

Following the experimental shake table tests on the perimeter-fixed ceiling, numerical models were developed in the finite element analysis program SAP2000 (CSI Software 2010). This chapter is therefore presented in three main sections:

i. Review of experiments carried out and used as verification reference
ii. Numerical model development
iii. Comparison of experimental and numerical results and conclusions

The primary objective of this chapter was to develop a simple model to replicate the experimental results with an acceptable level of accuracy. Such a model could be used for system level investigation of seismic performance of suspended ceilings of different configurations in different buildings/floors. To avoid complications in analysis, different simplifying approaches were examined which are discussed in detail in this chapter.

Two types of models were developed in the numerical modelling Section.

i. Model of the steel test frame and ceiling specimen
ii. Model of a grid and tile assembly

The first model consisted of the entire test setup used in the experimental Section, including the full-sized steel test frame and the ceiling specimen. This model excluded the interaction between ceiling tiles and grids and the pounding between these elements. Low-pass filtering of experimental results was introduced to compensate for this simplification.

In the second model, the simulation focused on the ceiling specimen only, with the objective to replicate the effect of pounding between ceiling components. Link elements are incorporated in this model to simulate the gaps between ceiling tiles and grids and the effect of pounding.

The chapter aims at addressing the following questions:

1. How closely does the simple numerical model replicate the experimental results?
2. Is filtering out the high frequency response an effective and valid simplification?
3. Are the high frequency spikes in the ceiling response similar to the effect of pounding between grids and tiles modelled with link elements?

4. Can the outcome of numerical analysis be used to predict the accelerations and forces induced in the ceiling system?

7.2 Section 1: Review of experiments

7.2.1 *Test setup*

The dimensions of the steel test frame shown in Figure 7-1 were 2.6 m (h), 2.6 m (w) and 5.2 m (l). Due to the limits of the shake table dimensions (2 m by 4 m) and its position in the laboratory, the length and width of the specimen had to be extended beyond the table surface to allow for the 2.4 m by 4.8 m ceiling specimen. This extension was made on the west end of the table to accommodate the required length as shown in Figure 7-2 through overhanging beams.

Steel square hollow sections (SHS) were used for building the test frame with a grade conservatively estimated as Gr250. The frame was designed to remain elastic throughout the tests and was checked that it did not yield. Figure 7-1 shows the experimental test frame with cross sections marked. The details of these cross sections can be found in Table 7-1.

Figure 7-1 – Experimental test frame and shake table

Figure 7-2 – Extension beams in the experimental test frame

Table 7-1 – Cross sections (dimensions in mm)

Section ID	Size	Section type	Section ID	Size	Section type
C100	100 × 100 × 9	SHS	Br75	75 × 75 × 3	SHS*
B125	125 × 125 × 5	SHS	CT*	32 × 24 × 0.3	Inverted T
B150	150 × 150 × 6	SHS	MT**	38 × 24 × 0.3	Inverted T
B100	100 × 100 × 5	SHS	Timber	140 × 45 (x2)	Rectangular

** Cross tee*
*** Main tee*

The lower beams were bolted to the shake table at 600 mm intervals. The connection between the shake table and lower beams was rigid and the column bases were connected to lower beams through single bolts with a gap underneath the column to allow for rotation. The connections between the upper beams and tops of the columns in the test setup were bolted end plates. At the ceiling height, timber beams were fixed to frame columns as perimeter support for the ceiling specimen. For these beams two timber studs were used to provide larger cross section. The end connection between these beams and the columns was in the form of top and seat connections using steel angle sections, with double bolts to the column and double screws to the timber beam. Single timber joists were added to the test frame roof for ceiling vertical hanger support. The connections between these beams and frame beams were single bolted angle connections.

7.2.2 *Test specimen*

The ceiling specimen was 2.4 m by 4.8 m and consisted of 4 rows of tiles in each direction, making up a total of sixteen 0.6 m by 1.2 m tiles (Figure 7-3). The ceiling tested was a perimeter-fixed type which means the grid ends were riveted on two perpendicular sides of the ceiling through single 3.2 mm aluminium rivets and the opposite sides were free to slide.

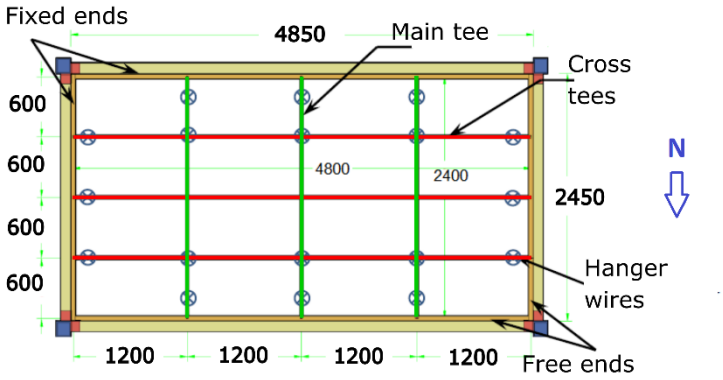

Figure 7-3 – The schematic plan view of the ceiling specimen (dimensions in mm)

On the free sliding ends, the grids were unrestrained in the translational direction along and perpendicular to the axis of the grid (x & y). In the experiment, clips were used on the free ends of the grids which prevented movement in the direction perpendicular to the grid axis (Figure 7-4a &b).

(a) Clips on free end

(b) Loosely fit screw on clip allows displacement along grid

(c) Riveted connection on fixed end

Figure 7-4 – Restraint conditions on grid ends

7.2.3 *Instrumentation*

Three types of instrument were used for recording test data in the experiments: accelerometers, potentiometers and load cells. The load cells were installed between the ceiling grids and perimeter supports on the fixed end of the ceiling in the direction of excitation (longitudinal direction or x). Potentiometers recorded the displacements on the free ends of the grids in x and y directions. Accelerometers were installed on the shake table, test frame, ceiling grids and tiles in x, y and z directions. Figure 7-5 shows the location of some of these instruments on the test setup and specimen. Further details on the instruments can be found in Appendix B.

Figure 7-5 – Location of instruments marked on test frame

7.2.4 *Input motions*

The input motions applied to the shake table were in the form of displacement time histories. An accelerometer installed on the shake table recorded the acceleration time histories resulting from these motions. These recordings were used as the input for the model created in SAP2000. Both sinusoidal waves and actual earthquake ground motions were used in these experiments.

The shake table used in the experiment applied unidirectional excitation in the East-West (longitudinal or X) direction and a similar loading regime was used in the numerical model input.

7.2.5 *Filtering the time histories*

The main sources of high frequency content in experimental response were assumed to be the noise created by the shake table and the interaction between grids and tiles. To eliminate this high frequency content and noise from the results, low-pass filtering was applied to the experimental time histories using SeismoSignal software (Seismosoft 2013). Two sets of data were created with two filtering levels which were chosen far from the natural frequency of the test frame: filtering out all frequencies above i) 18 Hz, and ii) 25 Hz. The filtering value of 25 Hz was chosen as the common noise removal limit for ground motions. The lower 18 Hz filtering was chosen randomly for sensitivity study which is still far from the natural frequency of the system. These two sets were created to investigate both the effect of filtering

and the sensitivity of the outcome to the filtering frequency.

The numerical study was generally summarised in two main categories:

i. Unfiltered numerical input and output, compared with unfiltered experimental results,
ii. Unfiltered output of numerical analysis with filtered shake table acceleration time histories used as input, compared with filtered experimental results.

For the section of numerical analyses concerned with the effect of filtering, two sets of filtered time histories (low-pass filtering of 18 Hz and 25 Hz) recorded on the shake table were used as input to the model. No further filter was applied to numerical results. All experimental time histories were filtered for the section of the study on the effect of filtering.

7.3 Section 2: Numerical modelling

7.3.1 *Model of test frame and perimeter-fixed ceiling*

The model was developed in the finite element structural analysis software SAP2000 (CSI 2008). It was created with size and material properties of the actual test setup and the specimen mentioned in Sections 7.2.1 and 7.2.2, respectively.

The material used for modelling the steel frame elements was steel with elastic modulus of 200 GPa, minimum yield strength of 250 MPa and a minimum tensile strength of 320 MPa (AS/NZS 1163:2016). Figure 7-6 shows the stress-strain relationship defined for this material. For modelling the steel test frame, square hollow section (SHS) elements were defined with the same section sizes as used in the experiment. The timber beams were modelled with material properties as follows: elastic modulus of 10 GPa. Figure 7-7 shows the model developed in SAP2000 with cross sections marked and materials shown in different colours. The details of these cross sections can be found in Table 7-1. All materials used in the model were defined with zero density and their self-weight was calculated and applied as uniformly distributed line loads. In the test frame, the dead load associated with the frame elements was calculated based on the elements cross section and steel density of 7849 kg/m^3. This uniform load was applied to the top beams of the frame.

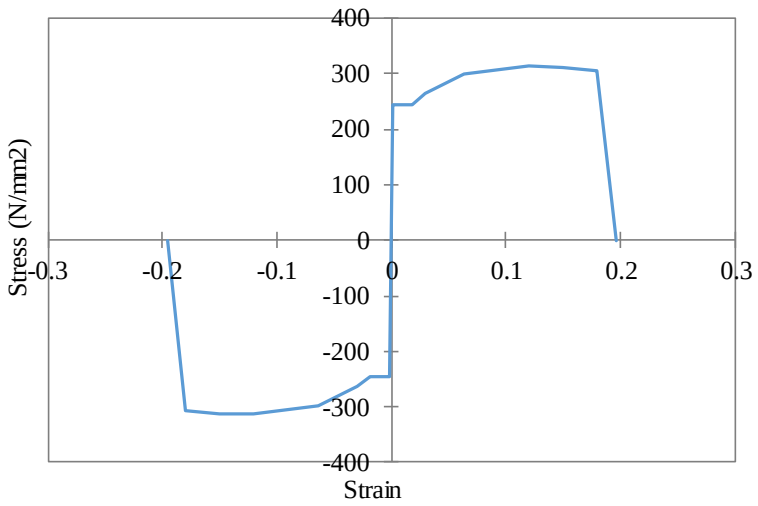

Figure 7-6 – Stress-strain relationship definition for steel C250 material

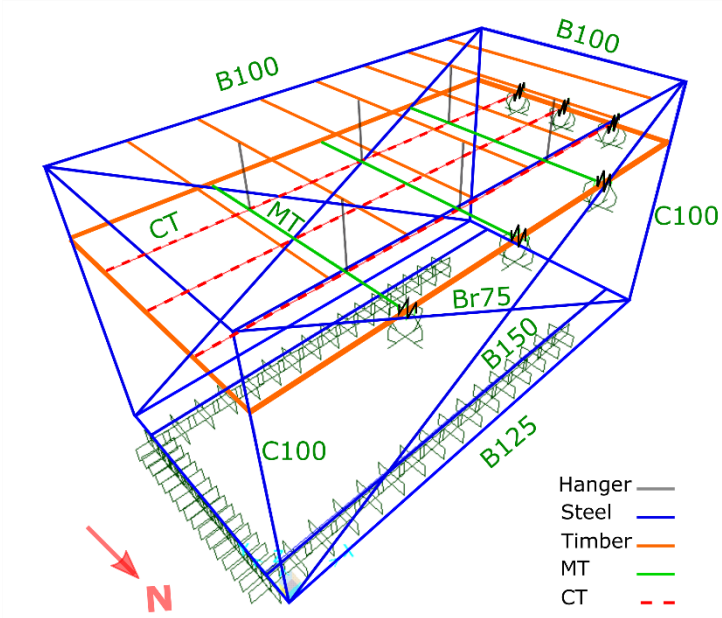

Figure 7-7– Test frame and test specimen with materials and cross sections marked

The connection between the shake table and lower beams was modelled as rigid and the overhanging length of the beams was also included in the model. The column base connections were modelled as pinned joints. The connections between the upper beams and tops of the columns were modelled rigid. At the ceiling height, timber beams for providing perimeter support were introduced into the model. The end connections of these timber beams to columns were modelled as rigid joints in the numerical model. Similar to the experimental setup, timber beams were added to the model at roof level to provide vertical hanging support for the ceiling. The connection between these secondary beams and the frame top beams was also modelled as pinned.

The hot-dipped galvanised steel ceiling grid elements were modelled using inverted T sections defined into the program with their actual cross section properties (Table 7-1) and the same material properties as the steel frame elements (Langill, 2009). The single riveted connectors between grid ends on the fixed (i.e. axially restrained) ends were modelled using pinned joints.

The ceiling tiles were excluded from this model and instead, an equivalent uniformly distributed line dead load associated with the mass of the tiles was applied to the grids. In the calculation of these dead loads, a simplifying assumption was made based on equal tributary areas for all beams in the direction of excitation (i.e. cross tees) (Figure 7-8). Considering the contribution of perimeter timber beams, the tributary mass of all ceiling elements in each row of cross tees was assumed to be ¼ of the total ceiling mass.

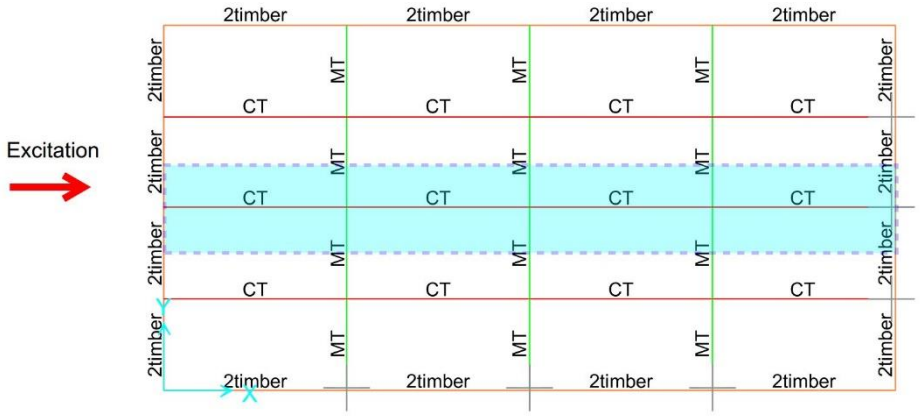

Figure 7-8 – The schematic plan view of the ceiling specimen modelled with the cross tees tributary area highlighted

On the free ends of the grids, gaps were introduced into the model using multilinear elastic link elements (Figure 7-9). These elements allowed for 20 mm displacement - which was the gap provided in the test specimen - with negligible stiffness representing the gap at grid ends. The second stiffness was significantly higher than the initial stiffness representing the closure of the perimeter gap and contact between grid ends and timber beams. In none of the experiments and the corresponding analyses of the model this gap was closed by differential movement.

Disp (m)	F (N)
-1	-9810
-0.0201	-9810
-0.02	-0.00098
0	0
1	0.000098

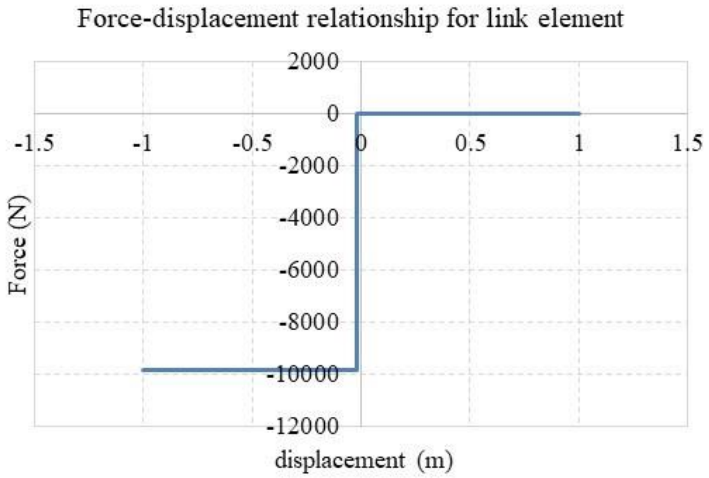

Figure 7-9 – Multilinear elastic link element used at free ends of the ceiling grids

The vertical hanger wires were modelled as steel rods to only resist tension. The position of the hanger wires/rods on CT-MT intersections was similar to the experiment. However, the perimeter hanger wires positioned at 200 mm from grid ends were excluded from the model for simplification. Instead, all grid ends were restrained in the translational degree of freedom in vertical direction. This condition partly resembled the seating support provided by the perimeter angles fixed to the perimeter timber beam. Since all other 5 restraints were released (2 translational in horizontal direction and 3 rotational), this simplification does not affect the overall result.

Since in the simplified model the dead loads from the tiles were only applied to longitudinal grids (i.e. cross tees), the lack of restraint in the model did not result in considerable displacements in main tees. It must be noted that in reality, the tiles are about 5 mm smaller than the grid modules.

7.3.2 *Data collection*

For the verification of the model, recordings from the instruments mentioned in Section 7.2.3 were compared with the results from the numerical model at corresponding joints and beam elements listed in Table 7-2. Figure 7-10 shows the locations of these joints and elements on the model.

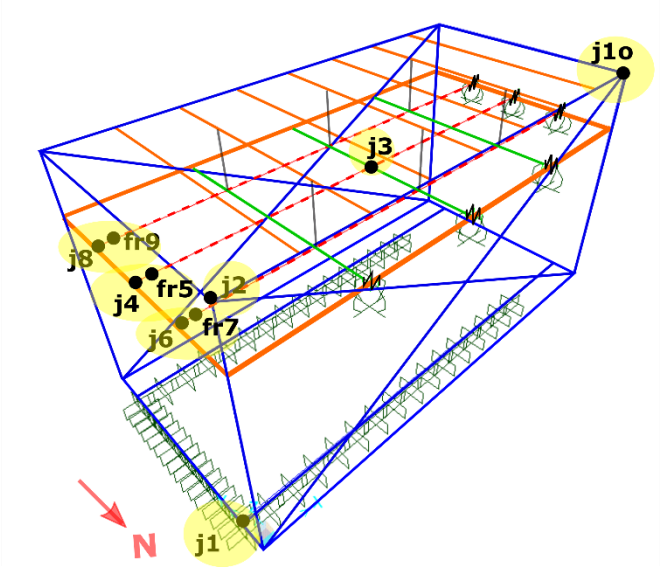

Figure 7-10 – Location of data points marked on numerical model

Table 7-2 – List of channels and joints referenced in experiments and model

Location	Instrumentation	Direction	ID in experiment	ID in model
Shake table	accelerometer	H	Ch1	j1
Frame top	accelerometer	H	Ch2	j2
Grid centre	accelerometer	H	Ch3	j3
Grid end	accelerometer	H	Ch4	j4
Grid end	Load cell	H	Ch5	fr5
Grid end	accelerometer	H	Ch6	j6
Grid end	Load cell	H	Ch7	fr7
Grid end	accelerometer	H	Ch8	j8
Grid end	Load cell	H	Ch9	fr9
Frame top	accelerometer	V	Ch10	j10

7.3.3 *Summary of simplifying assumptions*

In previous studies by Zaghi et al. (2016) and Ryu and Reinhorn (2014), numerical models were developed to capture the response of a suspended ceiling. These models showed a good level of accuracy and in some cases, included very detailed and rather complex elements. One of the objectives of the numerical analyses conducted in the study presented here was to develop a simple model that would be easy to replicate with programs commonly available to designers. Hence, the following simplifications were applied to the models developed in Phase 1 and Phase 2 of this study:

- Exclusion of ceiling tiles from the model and replacement with equivalent dead load (Phase 1)
- Exclusion of gaps between tiles and grids and the consequential horizontal and vertical vibration of the tiles and contact with grids (Phase 1)
- Exclusion of the vertical vibration/displacement of grid ends on the free sliding sides of the ceiling by applying vertical restraint (Phase 1 & 2)
- Assuming zero density for materials and using equivalent uniformly distributed dead load on top beams (Phase 1 & 2)
- Assumption of equal tributary area for all ceiling grids (Phase 1)
- Assumption of pinned connections for riveted grid ends (Phase 1 & 2)

The validity of the assumption of equal tributary areas for all longitudinal ceiling grids depends on the definition of the boundary conditions of the transverse grids. In this case, one end of the transverse grids are restrained in all translational degrees of freedom and the other ends are free in x and y (in plane) directions. Therefore, it is more accurate to assign half of the tributary width on the restrained (i.e. riveted) end and all of the tributary width on the free end to the longitudinal grid as shown in Figure 7-11. However, as the detailed comparison of forces transferred by individual grids was not the main focus of this study, the equal tributary area assumption was considered acceptable.

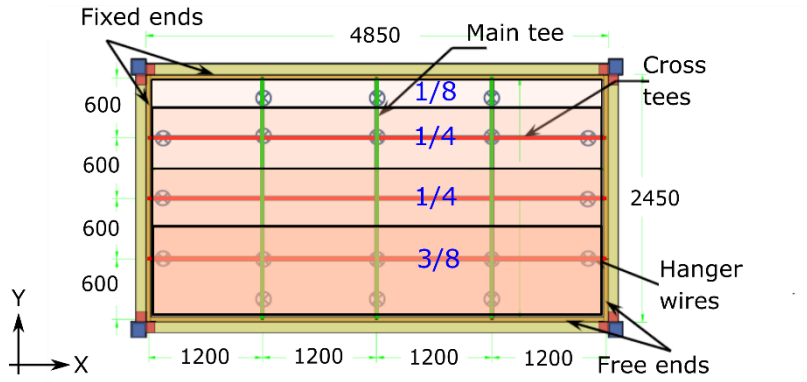

Figure 7-11 – Tributary areas for each longitudinal grid considering the boundary conditions

In this study pinned joints were employed for modelling the rivetted end connections instead of defining bilinear elastic link elements. This simplification was considered acceptable due to the brittle failure of rivets. As tested in a capacity evaluation study by Paganotti (2011), rivets undergo a brittle shear failure at a known level of loading. Since the perimeter-fixed ceiling is considered an elastic system, beyond this loading point the system has very little residual capacity and is considered as failed. Therefore, by knowing the shear capacity of the

rivet type used and controlling the forces achieved in the pinned joint, the failure point of the rivet and consequently the overall ceiling can be determined without including a more detailed link element.

7.4 Section 3: Results and discussion

7.4.1 *Effect of overhanging beams on frames vertical excitation*

As discussed in Section 7.2.1, the test frame was larger than the shake table used and therefore, the lower beams of the frame were extended on 3 sides (Figure 7-2). During the experiments, relatively large vertical accelerations were recorded on the ceiling grids. Based on the observation of tile movement during the tests, it was deduced that many of the large spikes in vertical and horizontal acceleration outputs were affected by the impact between vibrating tiles and grids. However, it was also expected that the overhanging beams could affect the vertical excitation in the frame response. Therefore, the vertical accelerations at the extended end of the overhanging frame were recorded and compared with the numerical results.

Based on the experimental results, the vertical accelerations on the frame top corner on the West end (i.e. Ch10 in test setup and j10 in the model) were measured to vary between 0.23 g to 0.49 g in sinusoidal tests and 0.38 g to 0.87 g in tests with ground motion input. The same joint in the numerical model had vertical accelerations ranging between 0.19 g to 0.53 g in sinusoidal analyses and 0.33 g to 0.99 g in ground motion analyses. It was concluded that the effect of overhanging beams was similarly captured in both experimental and numerical analyses.

7.4.2 *Natural periods*

To determine the natural frequency of the test frame, transfer functions were used between the acceleration time history on the shake table as the input (Ch1 or J1) and the acceleration time history at the top of the frame (Ch2 or J2). These transfer functions are shown in Figure 7-12 and Figure 7-13 for the experimental and numerical results, respectively. According to these figures, the horizontal natural frequency of the test frame was estimated to be 12-13 Hz. This was compatible with the natural frequency in the dominant mode, obtained from the model's output.

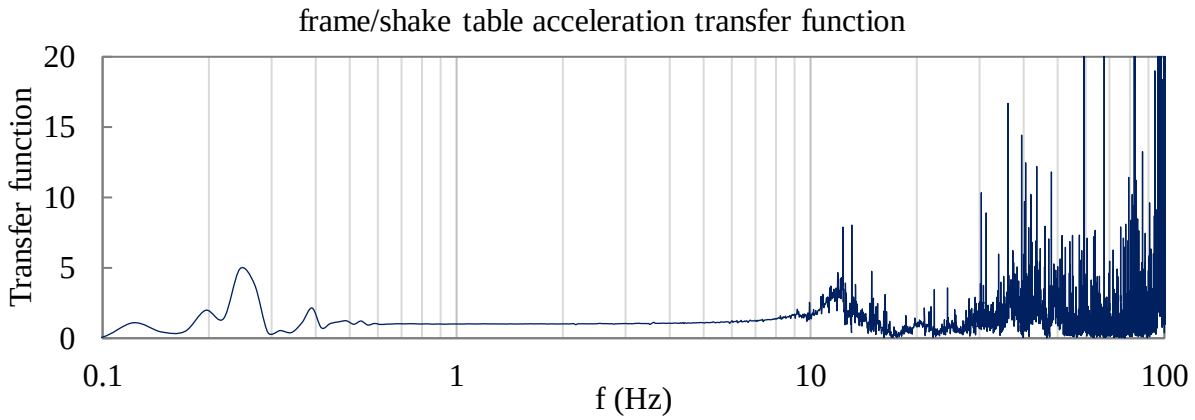

Figure 7-12 – Transfer function of frame to shake table response in experiment

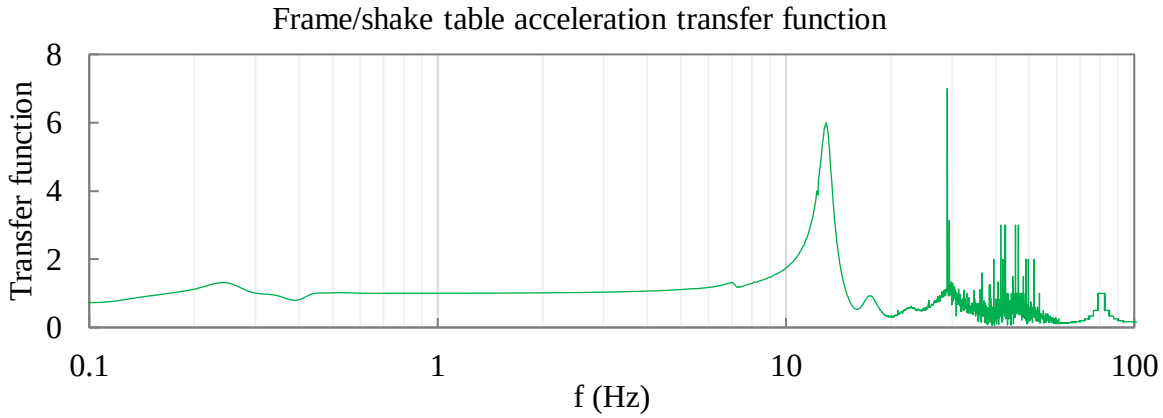

Figure 7-13 – Transfer function of frame to shake table response in model

7.4.3 *Comparisons of results in a ground motion test without filtering*

Graphs shown in Figure 7-14 through to Figure 7-17 compare the experimental and numerical results without any filtering applied to the records. The record used in this ground motion test was Northridge1063-1 as shown in Figure 7-14.

The experimental accelerations recorded on the ceiling grids were generally observed to have peaks that occurred in the form of high frequency spikes as shown in Figure 7-15 and Figure 7-16. The grid accelerations from numerical analysis were generally lower than the experimental records, and this difference was especially considerable in the peaks. As the zoomed-in image of the first 5 seconds of the plots in Figure 7-15 and Figure 7-16 show, these high accelerations occurred for very short periods of time. These spikes in the experimental acceleration time histories could be due to the impact between ceiling elements or noise produced by the shaking table. As the numerical model excluded the tiles and their pounding against grids, this discrepancy was expected. Unlike grid accelerations, the axial

forces in ceiling grids (in Figure 7-17) did not show a large high frequency content and fewer spikes were observed in the experimental record. This could be related to the sensitivity of the measuring device.

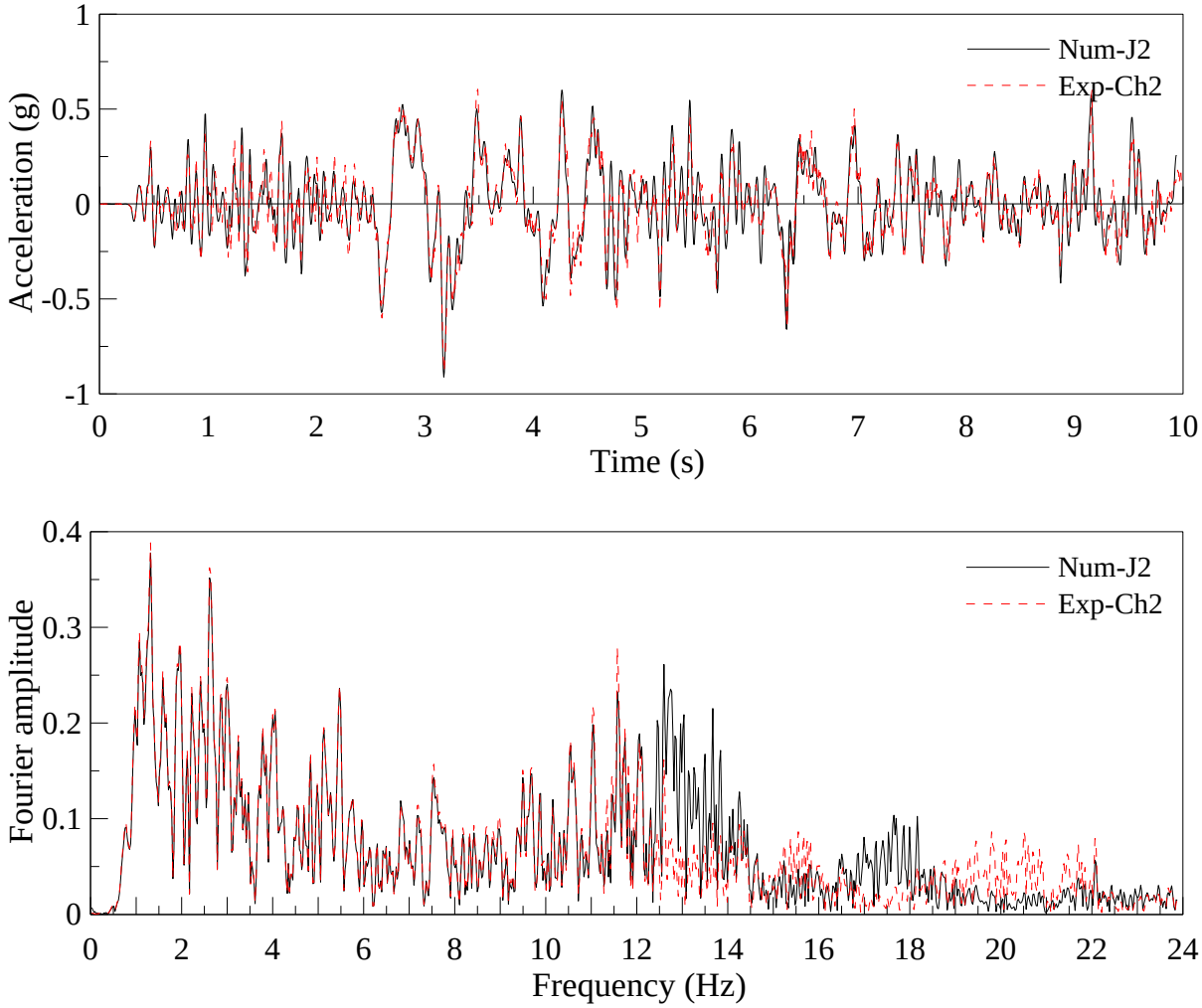

Figure 7-14 – Comparisons between frame acceleration response in the experiments (Ch2) and numerical model (J2) in a ground motion test without filtering

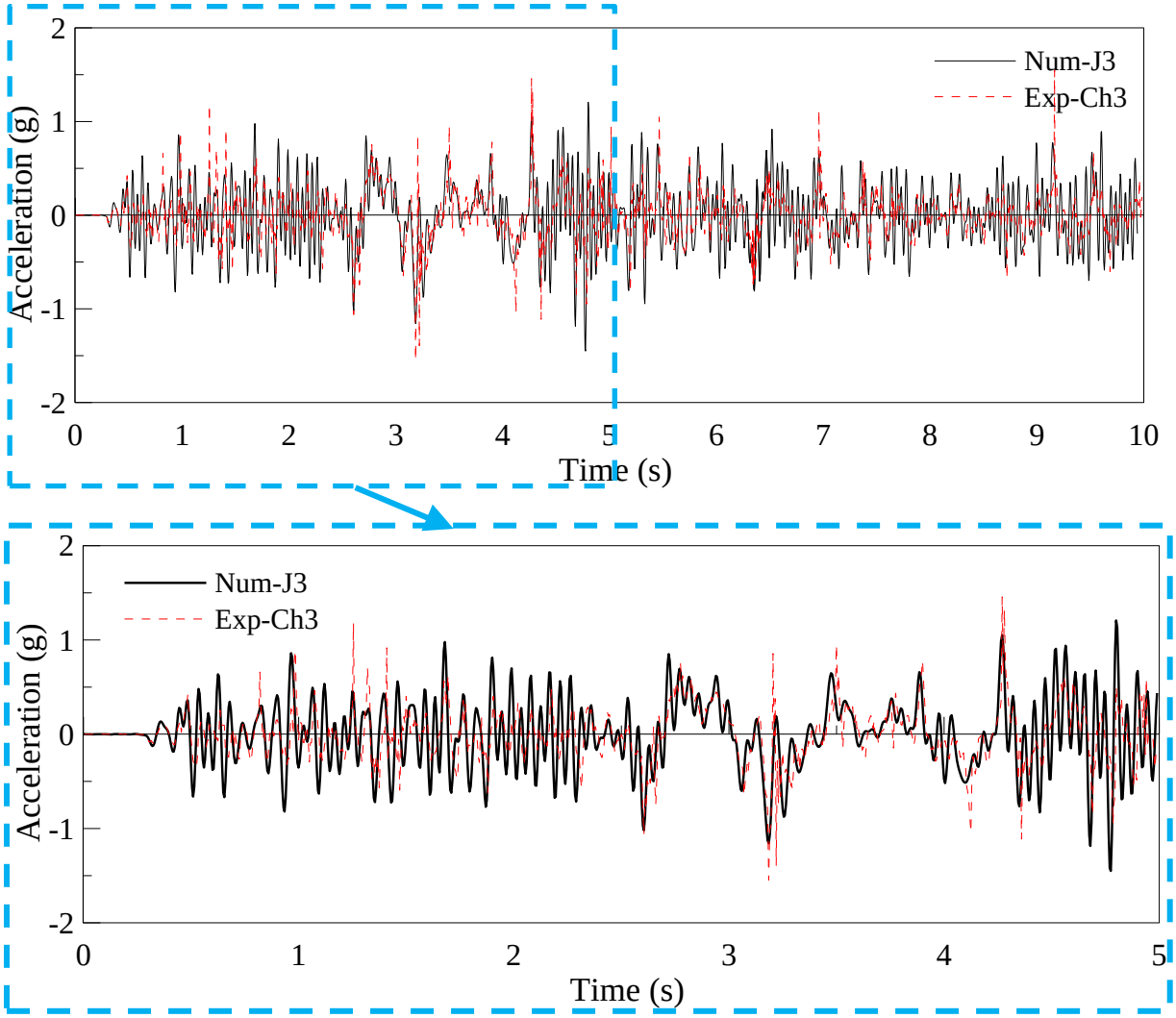

Figure 7-15 – Horizontal acceleration in ceiling grid centre in experiment and model in a ground motion test without filtering

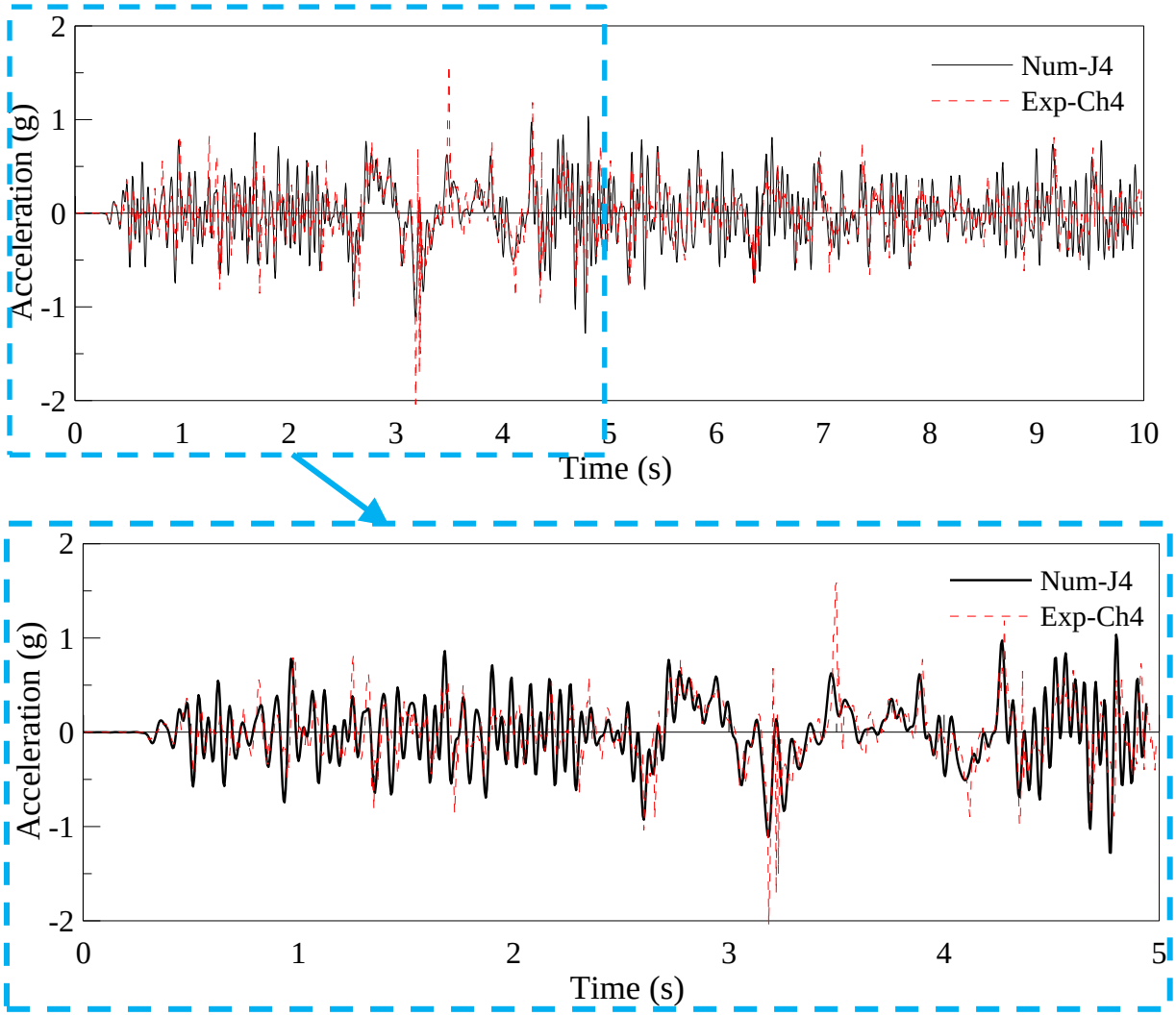

Figure 7-16 – Horizontal acceleration in ceiling grid end in experiment (Ch4) and model (J4) in a ground motion test without filtering

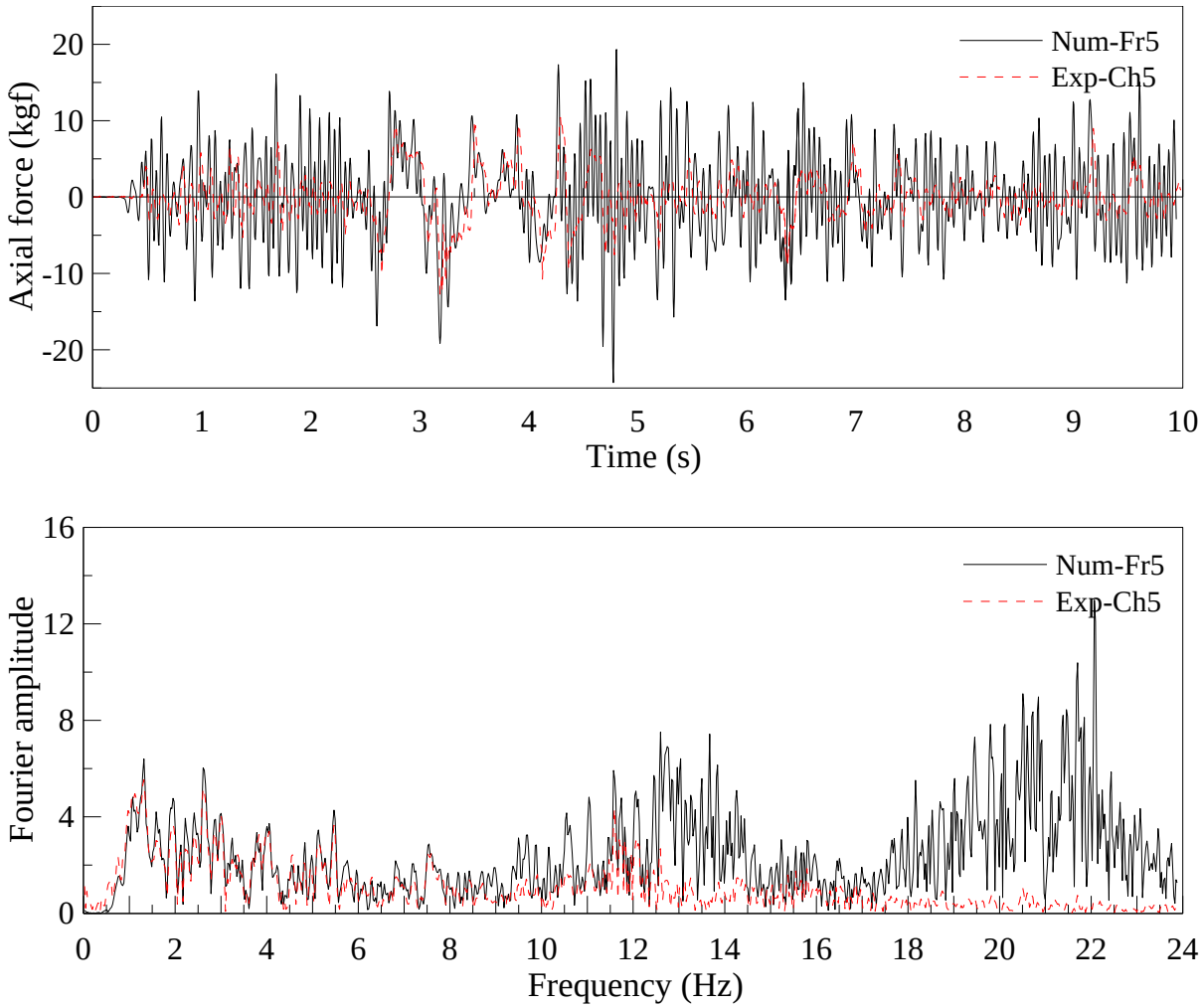

Figure 7-17 – Axial force in ceiling grid in experiment and numerical model in a ground motion test without filtering

7.4.4 *Comparisons of results in a sinusoidal test without filtering*

Similar results to those in the previous Section are shown in Figure 7-18 to Figure 7-21 for a sinusoidal test with frequency of vibration of 3 Hz and displacement amplitude of 20 mm.

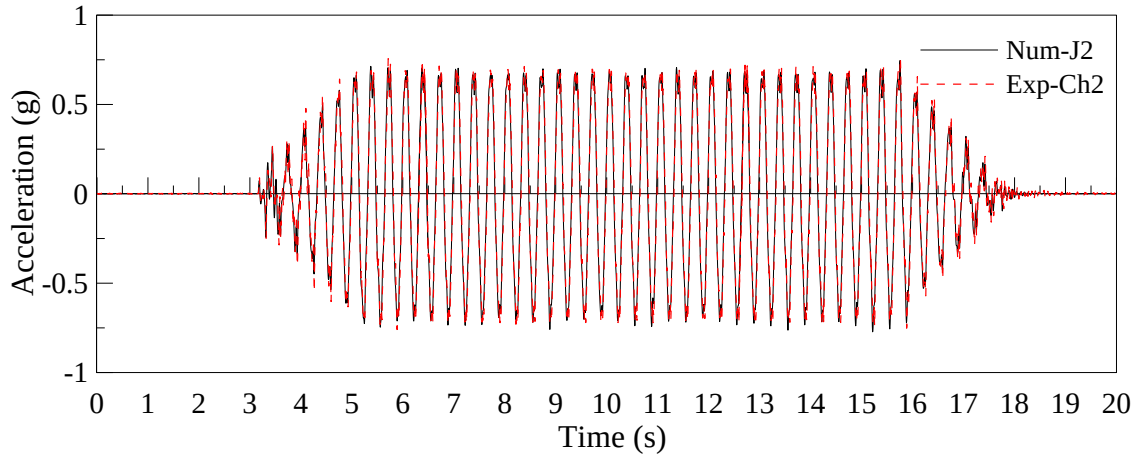

Figure 7-18 – Comparisons between frame acceleration response in the experiments and numerical model in a sinusoidal test without filtering

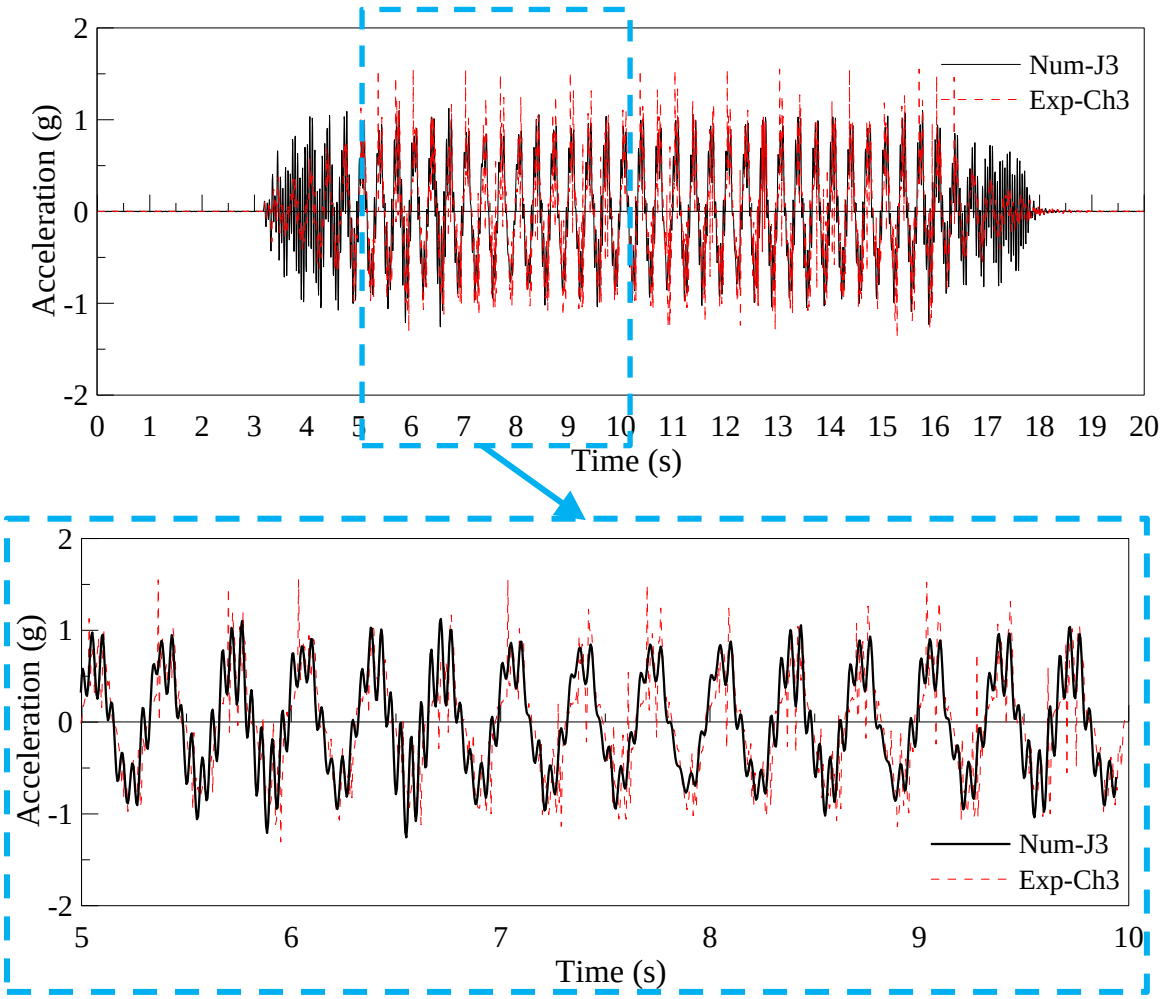

Figure 7-19 – Horizontal acceleration in ceiling grid centre in experiment (Ch3) and model (J3) in a sinusoidal test without filtering

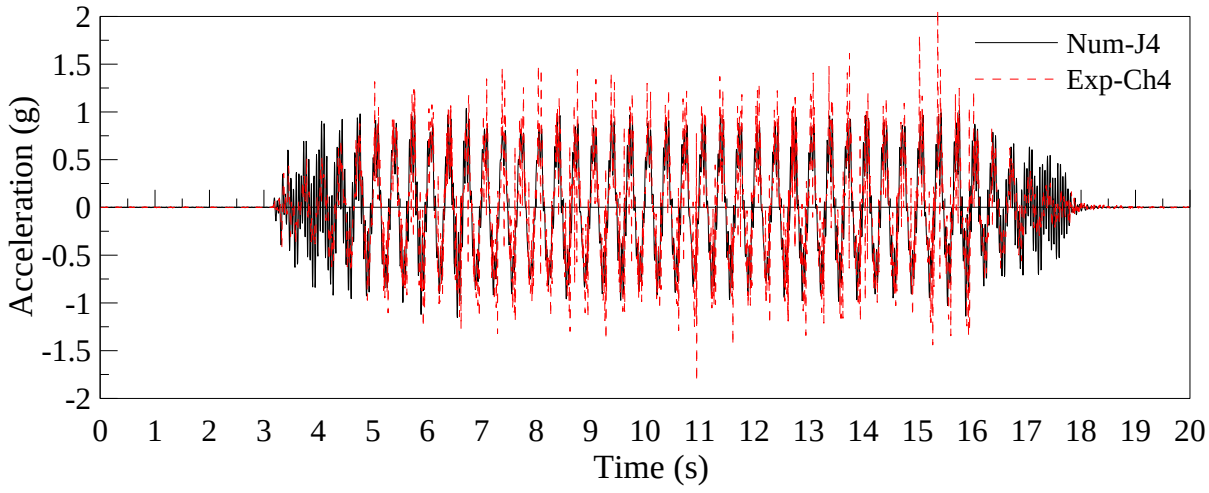

Figure 7-20 – Horizontal acceleration in ceiling grid end in experiment (Ch4) and model (J4) in a sinusoidal test without filtering

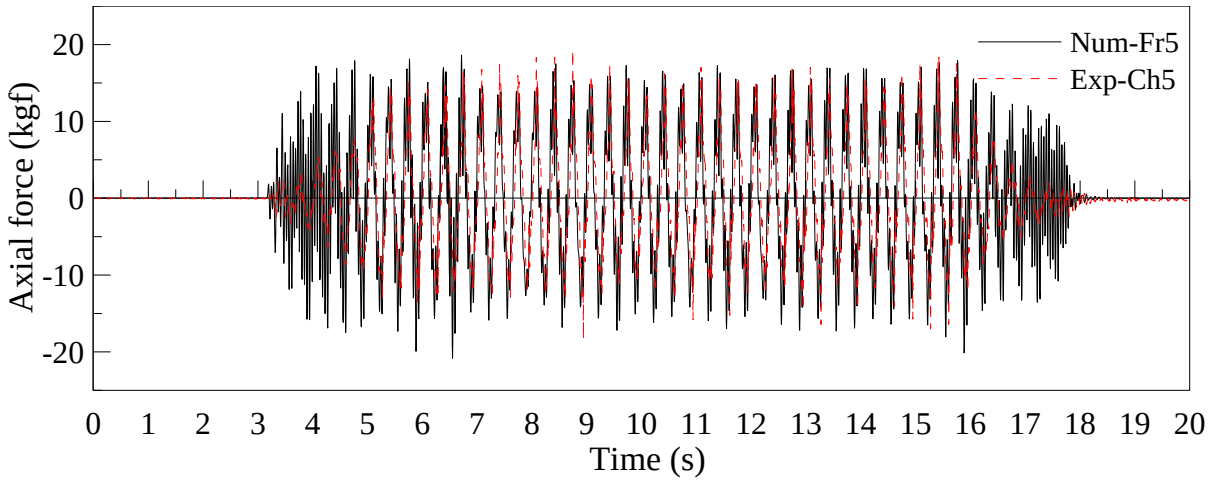

Figure 7-21 – Axial force in ceiling grid in experiment (Ch5) and numerical model (Fr5) in a sinusoidal test without filtering

7.4.5 *Comparisons of results in a ground motion test with filtering*

In this Section, the results of numerical modelling are compared with experimental results for a ground motion record (Northridge 1063-1). In all comparisons, the 18 Hz low-pass filtering is applied to the experimental results and a filtered shake table acceleration time history is used as input in the numerical analyses. The 25 Hz low-pass filtered results are compared with the 18 Hz filtered results in Section 7.4.7 in the form of peak responses of all tested motions.

7.4.5.1 Horizontal acceleration on shake table

Low-pass filtering was applied to the acceleration time history recorded on the shake table (i.e. Ch1) with 18 Hz as the upper limit (i.e. frequencies above 18 Hz were filtered out). The filtered time history was used as the input for the model (Joint 1). Figure 7-22a and b show the effect of low-pass filtering on the shake table acceleration history in frequency and time domains, respectively.

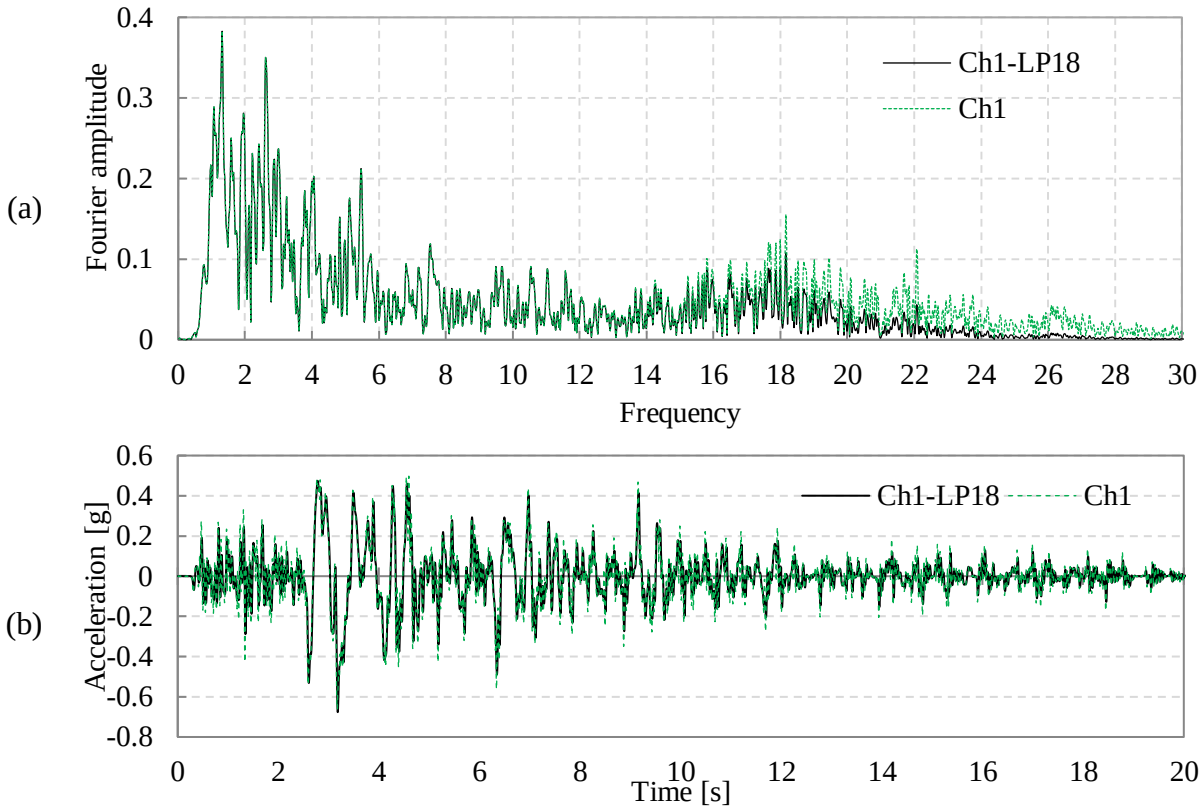

Figure 7-22 – Comparison between filtered (Ch1-LP18) and unfiltered (Ch1) input: (a) shake table acceleration history in frequency domain; and (b) shake table acceleration history in time domain in ground motion record Northridge1063-1.

7.4.5.2 Horizontal acceleration at frame top

To verify the modelled test assembly, the response of the modelled test frame was compared with the response of the steel frame in the experiment. This is to make sure the input to the ceiling or the peak floor acceleration (PFA) was similar in the experiments and analyses. All the time histories of experimental results were filtered as described above with low-pass 18 Hz filtering. Numerical results were reported without filtering as the input time history was already filtered. Figure 7-23 shows the experimental acceleration time history at the top of the test frame (i.e. Ch2) in comparison with the numerical results at the similar location in the model (i.e. Joint 2). This comparison shows a good agreement between the experimental and numerical results for the record used. This confirms that the model simulated the response of the experimental test frame reasonably well. In the frequency domain plot, the model shows higher amplitudes around 12-13 Hz which can be associated with the natural frequency of the frame. For better visibility in the time domain plots, only the first 10 s of the motion are shown.

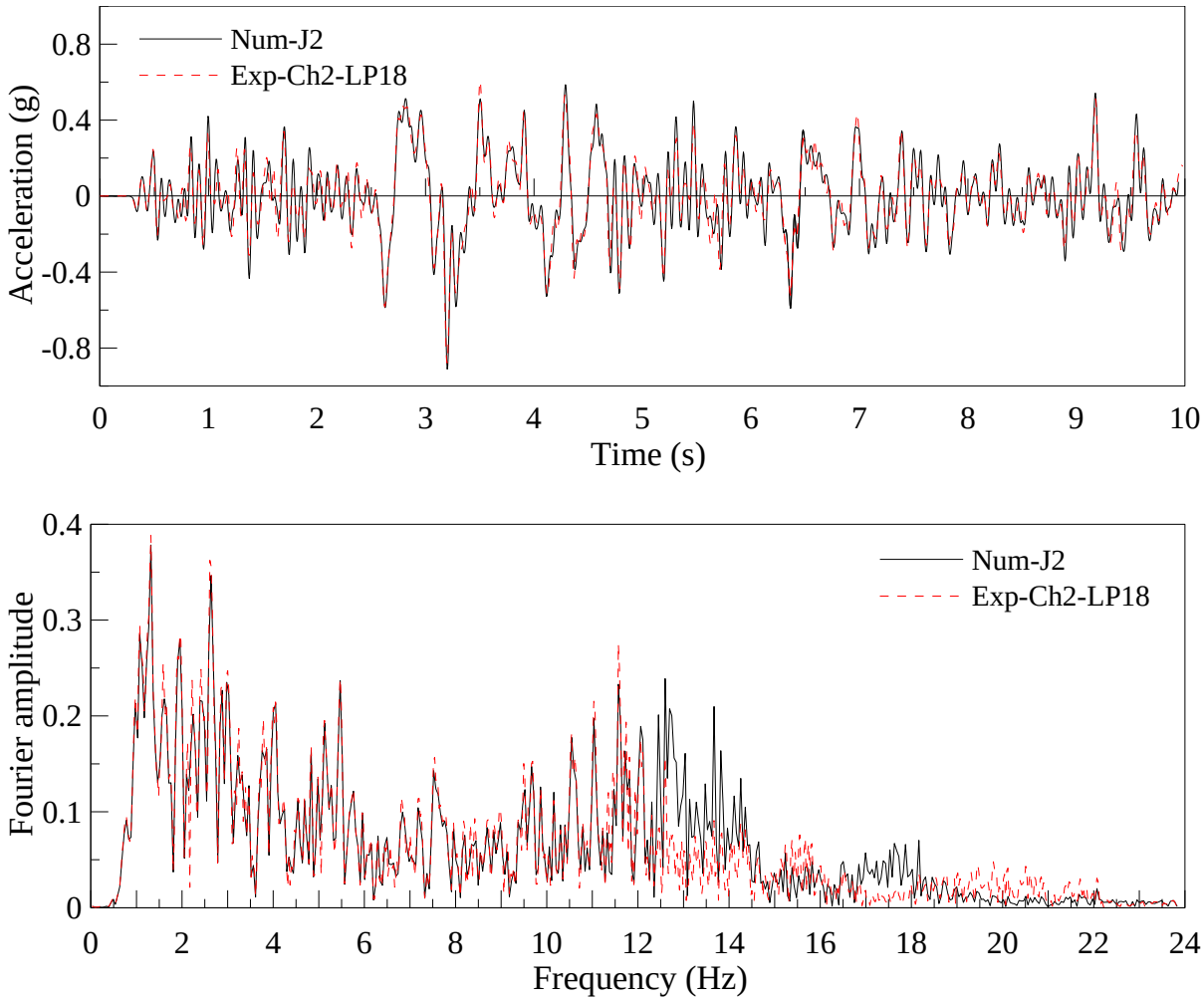

Figure 7-23 – Comparisons between frame acceleration response in the experiments (CH2) and numerical model (J2) with low-pass 18 Hz filtering, in time and frequency domains

7.4.5.3 Horizontal acceleration on ceiling grids

The horizontal accelerations recorded on the ceiling grids have been shown to vary from the floor acceleration by a factor of 2 or more (Refer to Chapter 3). This peak acceleration can determine the axial forces carried by the ceiling grids and the overall capacity of the ceiling. Therefore, the modelled behaviour approximately predicts the experimental results (in terms of ceiling grid acceleration). Ceiling grid accelerations were recorded in 2 different locations; i) intersection of CT and MTs in the centre of the ceiling, and ii) fixed (i.e. riveted) end of the CTs. The comparison between the horizontal acceleration recorded on the ceiling grid and the acceleration obtained from the numerical model in the central grid joint is shown in Figure 7-24. Figure 7-25 shows a similar comparison for an accelerometer located on the grid (CT) end. For better visibility in the time domain plots, only the first 10 s of the motion are shown. Based on the results, the model appeared to simulate the ceiling response relatively well at

frequencies lower than 10 Hz. Discrepancies were observed around the natural frequency of the frame (12-13 Hz). Except for this frequency range, the model seemed to slightly underestimate the experimental response.

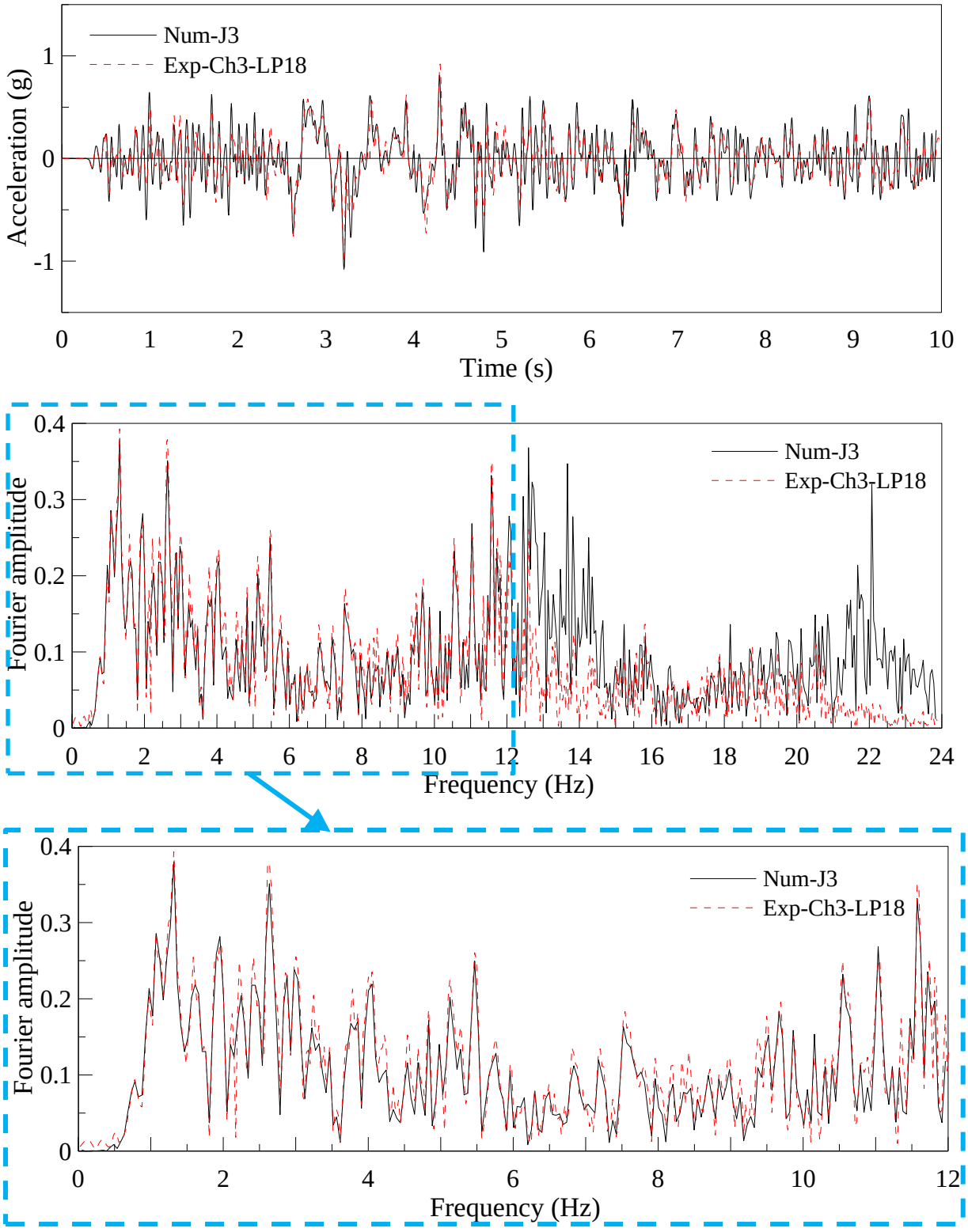

Figure 7-24 – Horizontal acceleration in ceiling grid centre in experiment (Ch3) and model (J3) with low-pass 18 Hz filtering in time and frequency domains

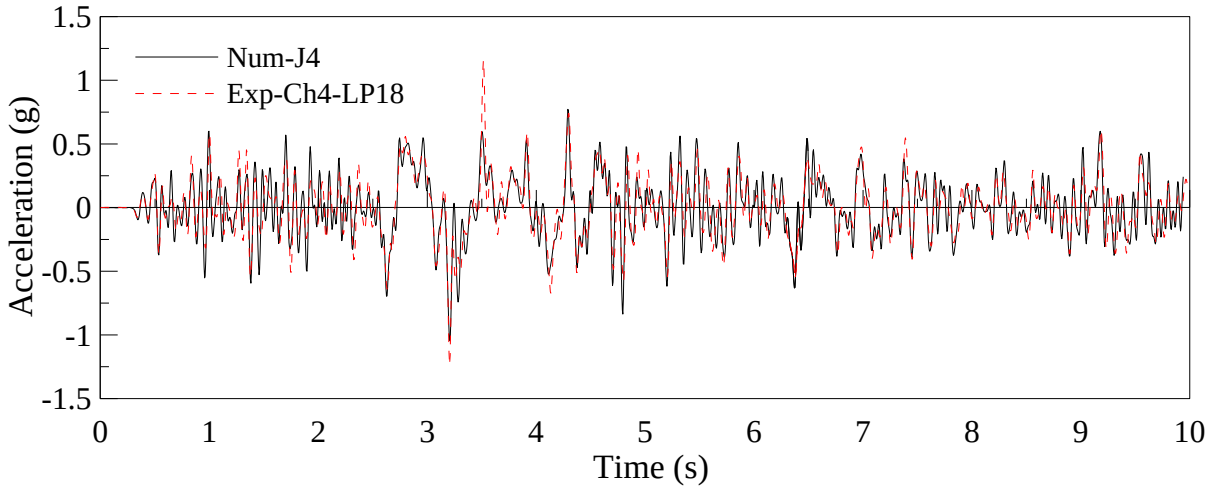

Figure 7-25 – Horizontal acceleration in ceiling grid end in experiment (Ch4) and model (J4) with low-pass 18 Hz filtering

7.4.5.4 Axial force on ceiling grids

The axial forces induced in the ceiling grids in the experiments were measured through load cells installed on grid ends. After low-pass filtering, these measurements were compared with the axial force in the corresponding beam elements in the model in Figure 7-26. As it can be seen both in time and frequency domains, the model captures the overall trend (i.e. fluctuations in the amplitude) but slightly overestimates the axial force; especially at the peaks.

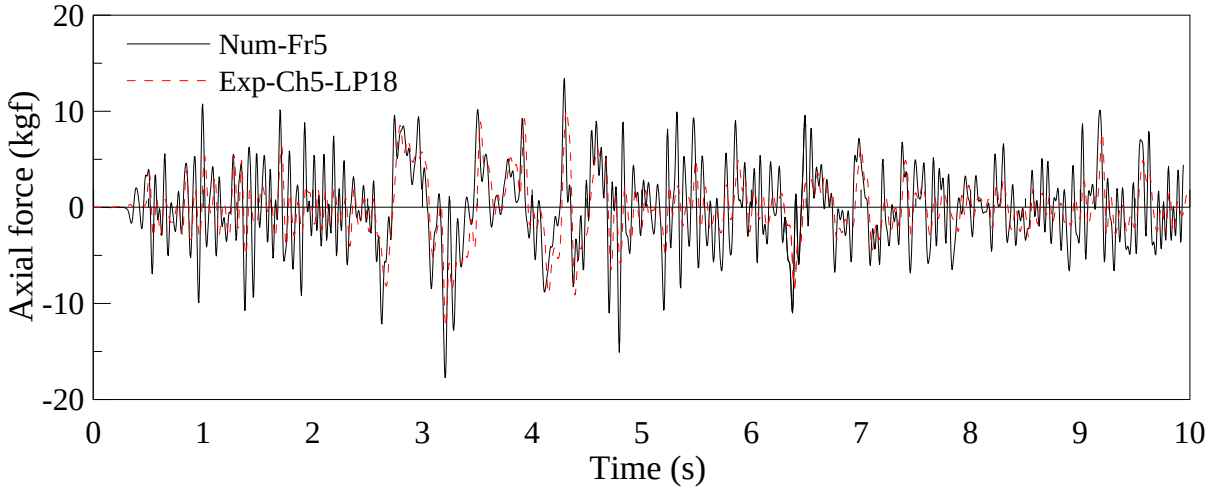

Figure 7-26 – Axial force in ceiling grid in experiment (Ch5) and numerical model (Fr5) with low-pass 18 Hz filtering

In comparing the experimental and numerical results for axial forces in grids, note must be taken of the relationship between the axial force, the tributary area assumed and accelerations in the grids. In the numerical analysis, the axial force is directly proportioned to the

acceleration in the grid by the factor of its tributary area mass. Figure 7-27a shows the axial force in the beam element in the model (Frame 5) compared with the acceleration time history on the frame end joint (joint 4), multiplied by the tributary area mass associated with that beam element (i.e. uniform dead load times the grid length of 4.8 m). This comparison shows a good similarity between the two values. A similar comparison was made for the results from the experiments in Figure 7-27b. In this figure, the values of axial force recorded by loadcells are noticeably lower than the expected values based on the mass and acceleration relationship. This trend was generally visible in majority of the results (Refer to Chapter 3 of this thesis). This could partly be due to the overestimation of the tributary area for the grid in consideration or the exaggeration inherent in grid acceleration recordings due to impact or vibration of ceiling tiles (Refer to Chapter 3 of this thesis). Therefore, the overestimation in the grid axial forces in the model could be also interpreted by the lower than expected axial forces recorded in the experiments.

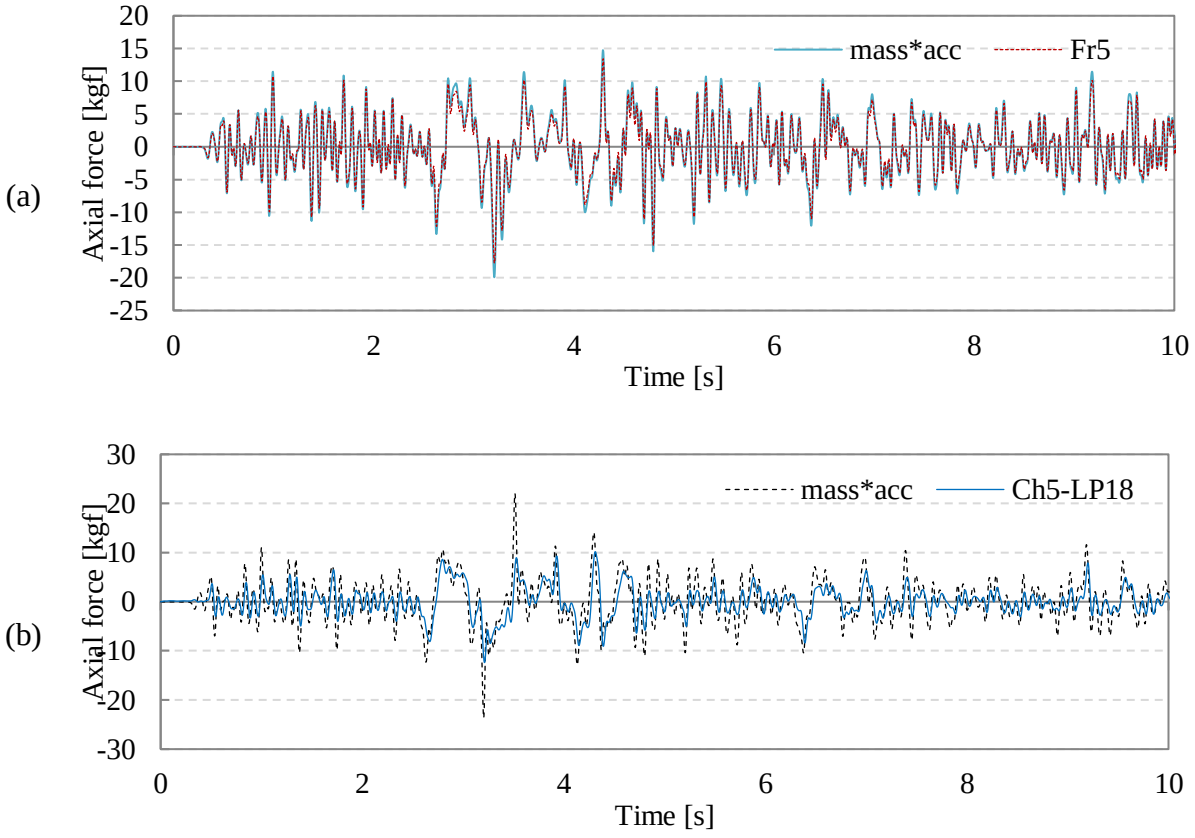

Figure 7-27 – Axial force in grid element vs. the corresponding tributary area mass times grid acceleration in (a) numerical model (Fr5), and (b) filtered experiment (Ch5-LP18)

7.4.6 *Comparisons of results in a sinusoidal motion test with filtering*

Similarly, the graphs shown in Figure 7-28 through to Figure 7-31 compare the results from numerical analysis with corresponding experimental results for a sinusoidal motion with an input frequency of 3 Hz and displacement amplitude of 20 mm. The conclusions drawn from this sinusoidal test example are similar to those discussed in Section 7.4.5 for the example ground motion test.

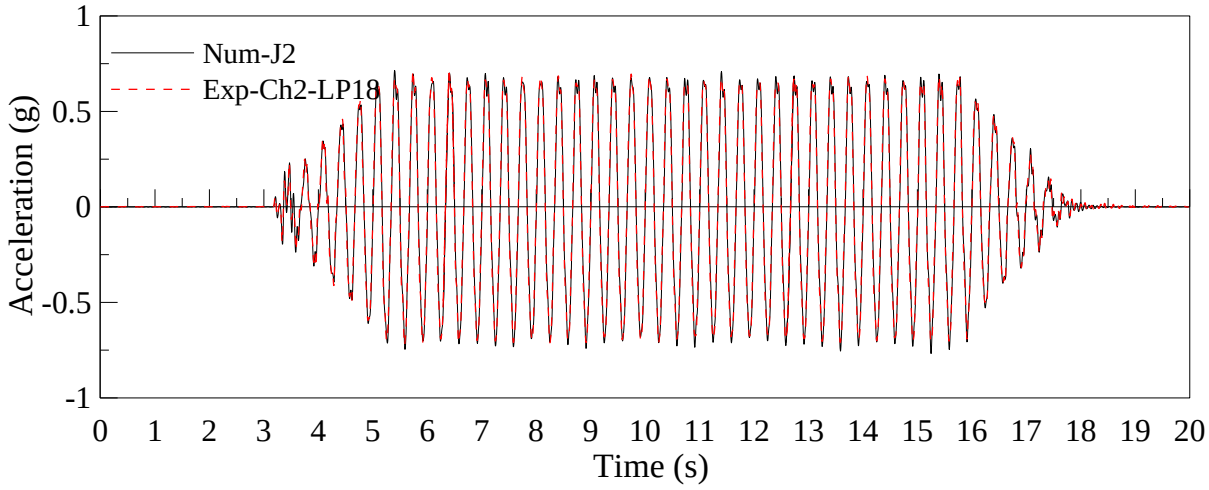

Figure 7-28 – Comparisons between frame acceleration response in the experiments (Ch2) and numerical model (J2) with low-pass 18 Hz filtering – Sinusoidal test

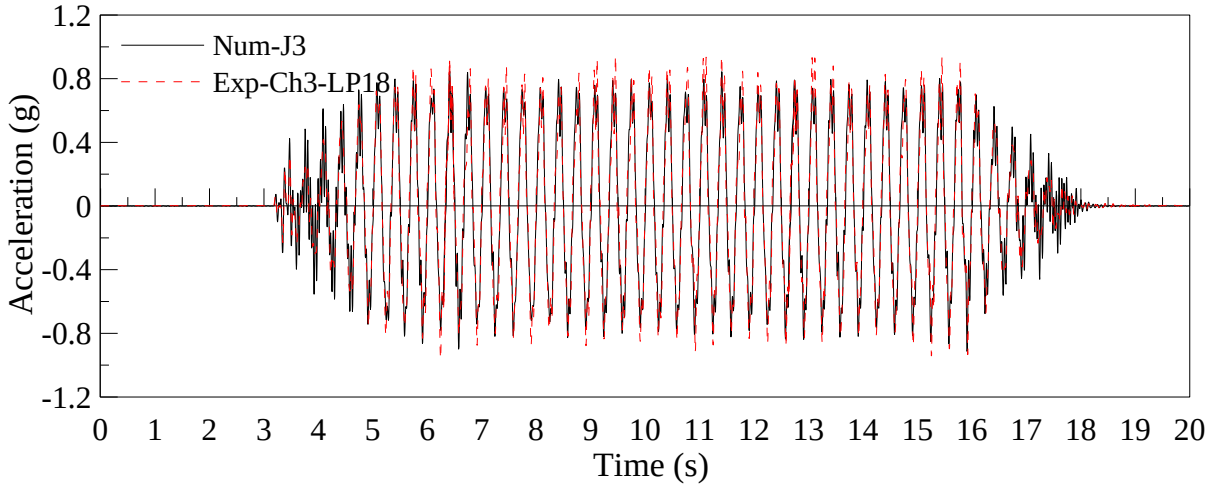

Figure 7-29 – Horizontal acceleration in ceiling grid centre in experiment (Ch3) and model (J3) with low-pass 18 Hz filtering – Sinusoidal test

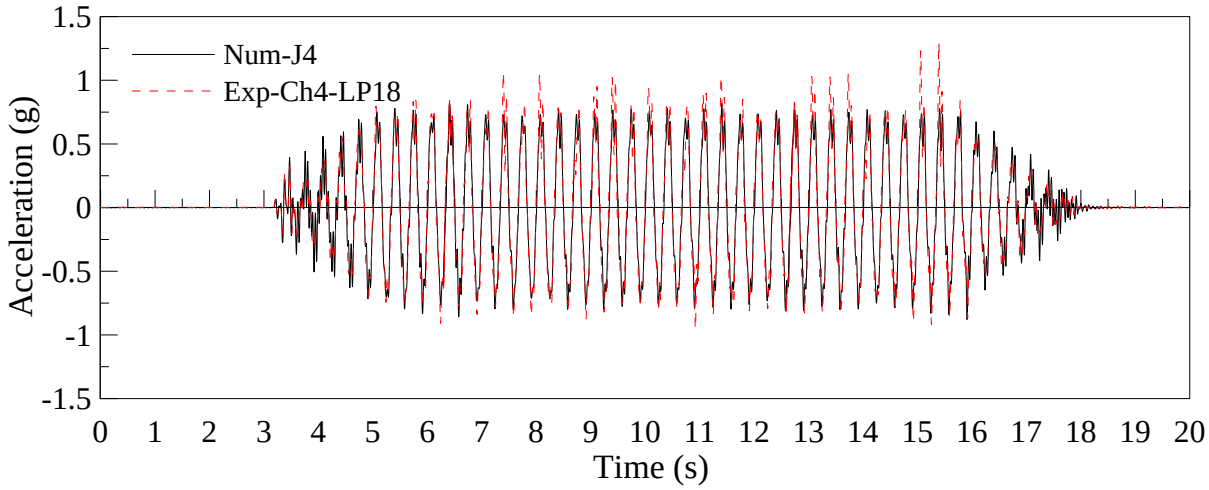

Figure 7-30 – Horizontal acceleration in ceiling grid end in experiment (Ch4) and model (J4) with low-pass 18 Hz filtering – Sinusoidal test

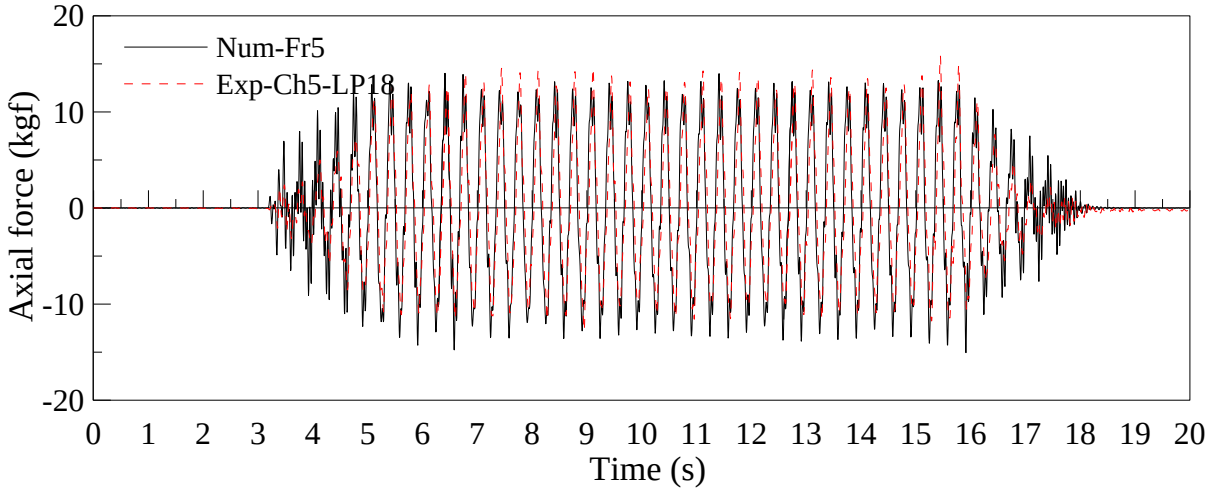

Figure 7-31 – Axial force in ceiling grid in experiment (Ch5) and numerical model (Fr5) with low-pass 18 Hz filtering – Sinusoidal test

7.4.7 *Comparisons of results for all tests*

7.4.7.1 Horizontal acceleration on shake table and frame top

Figure 7-32 and Figure 7-33 show that a relatively good similarity existed between the PFAs (acceleration recorded at the top of the frame on Ch2 and j2) although in some cases the numerical model resulted in larger values. This was specially observed in GM tests. As it was seen in previous section's graphs, the frame model response showed a clear amplification at resonance frequencies (12-13 Hz) which could result in larger accelerations in the frame.

In all of the following figures, the red straight lines indicate the state of experimental and numerical analyses results being equal (i. e. experiment=numerical).

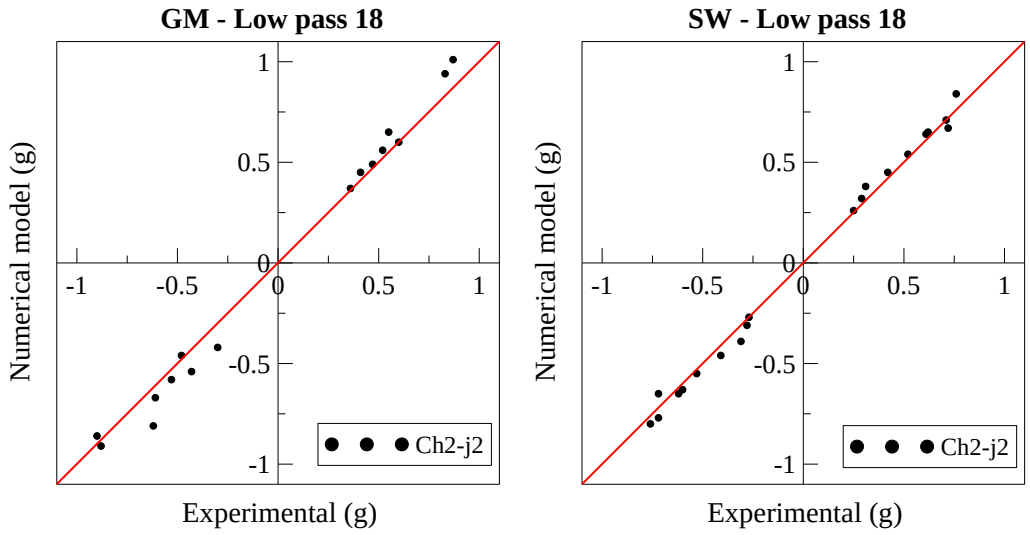

(a) (b)

Figure 7-32 – Peak floor acceleration (Ch2-j2) in (a) ground motion tests, and (b) sinusoidal tests with low-pass filtering of 18 Hz

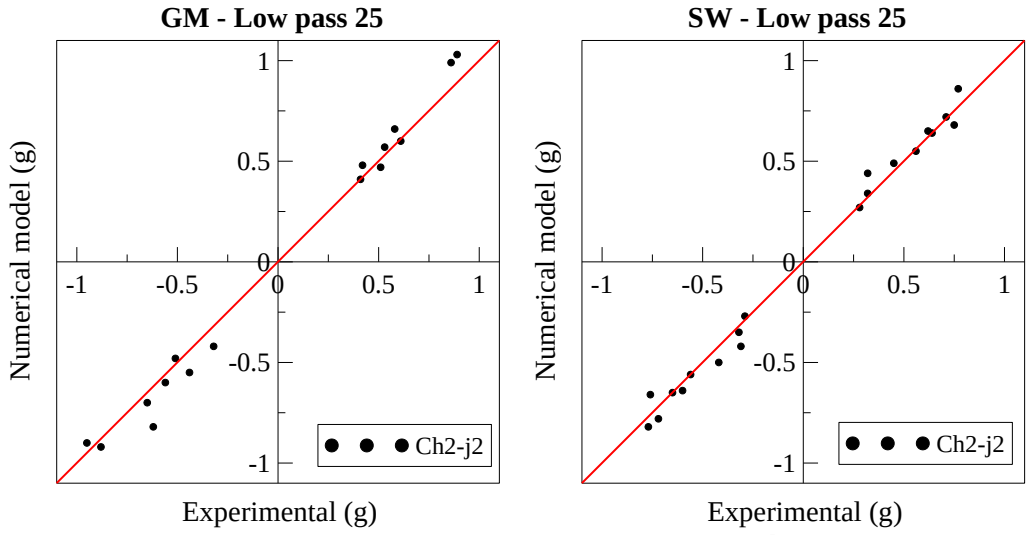

(a) (b)

Figure 7-33 – Peak floor acceleration (Ch2-j2) in (a) ground motion tests, and (b) sinusoidal tests with low-pass filtering of 25 Hz

7.4.7.2 Horizontal acceleration on ceiling grids

Graphs presented in Figure 7-34 and Figure 7-35 compare the accelerations recorded on the ceiling grids in the experiments vs. the numerical model (Refer to Figure 7-10 for the location of the instruments). The peak acceleration data was collected both at the end of longitudinal grids and centre of the ceiling. The results showed a good agreement between numerical predictions and experimental results, especially at lower accelerations. At higher accelerations, the model underestimated the response. A portion of these large accelerations

were found to be caused by the pounding between grids and ceiling tiles as the tiles slid and vibrated within the grid modules. This impact was not included in the model and the low-pass filtering was applied to partially eliminate this effect from the ceiling response. Moreover, with the lower filtering onset (18 Hz) numerical results were closer to the experimental results. It must be noted that these plots summarise the peak response in tests which was the point of significant difference. As shown in Section 7.4.5.3, the two response histories showed a good similarity in lower amplitudes but were more noticeably different at peaks.

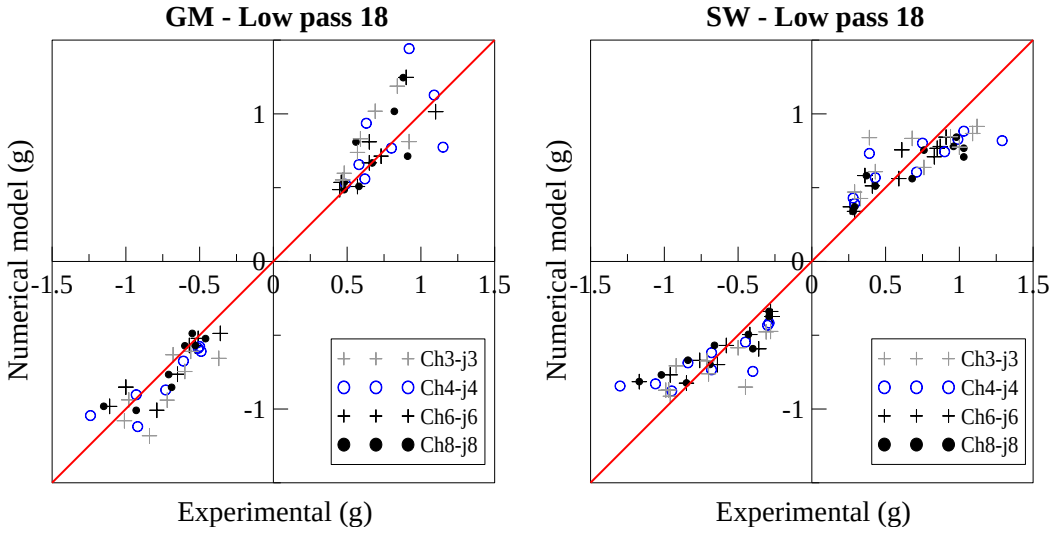

Figure 7-34 – Peak grid acceleration in experiments (Ch3 to Ch8) vs. peak grid acceleration in numerical model (j3 to j8) in (a) ground motion tests, and (b) sinusoidal tests with low-pass filtering of 18 Hz

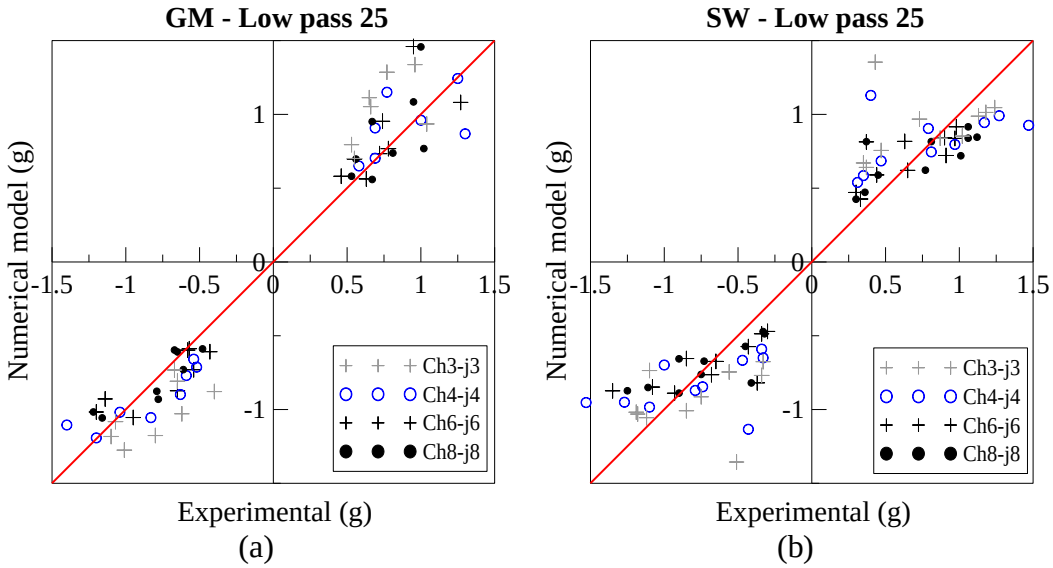

Figure 7-35 – Peak grid acceleration in experiments (Ch3 to Ch8) vs. peak grid acceleration in numerical model (j3 to j8) in (a) ground motion tests, and (b) sinusoidal tests with low-pass filtering of 25 Hz

One of the coefficients included in the design of a ceiling is component spectral shape coefficient that takes into account amplification of input horizontal acceleration within the component (herein, ceiling). This coefficient is considered as 2 for suspended ceilings in NZ seismic design Standard (natural period less than 0.75s) (NZS1170.5, 2004).

The results obtained from the experiments and numerical analyses were used to evaluate the amplification of the PFA (i.e. acceleration at the top of the test frame) as it was transferred through the ceiling grids. The ratio between the accelerations recorded on the ceiling grids and PFA are compared for the experimental results in Figure 7-36 and for the numerical analyses results in Figure 7-37. According to Figure 7-36, despite the low-pass filtering, this ratio in some experiments exceeded the Standard mandated value of 2. However, majority of the ratios remain between 1 and 2. Using the same acceleration time histories in the modelled frame and ceiling, the ratios follow a relatively similar trend in Figure 7-37. The filtering level showed an influence on reducing this acceleration amplification in the numerical results.

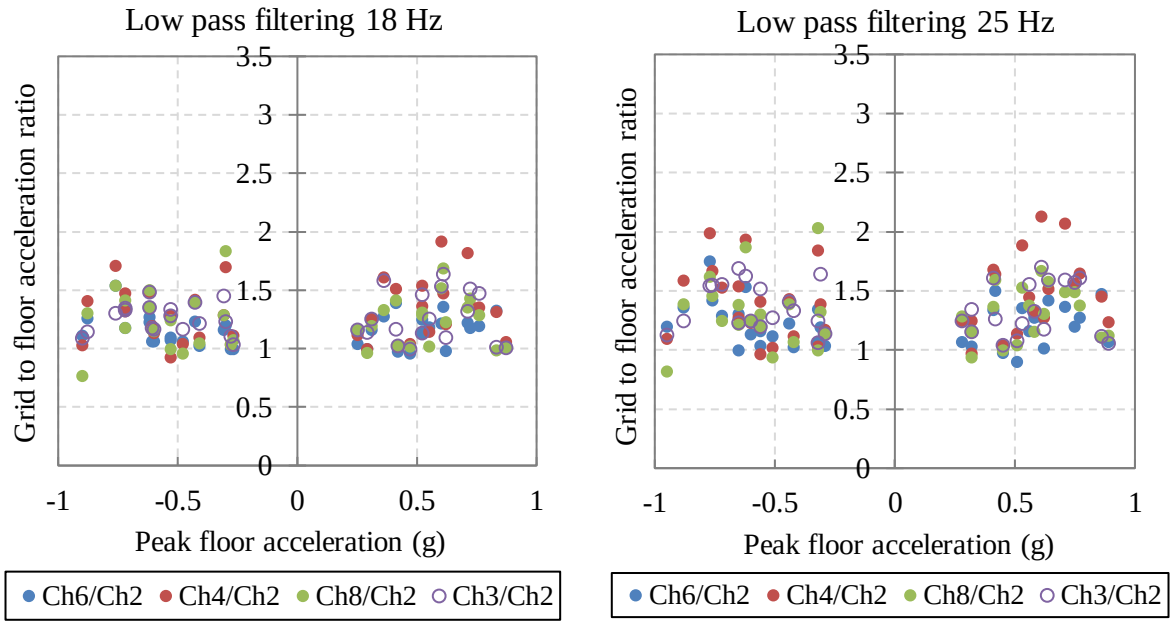

Figure 7-36 – Amplification of ceiling grids acceleration in experiments with sinusoidal and ground motions: Grid acceleration to acceleration at the top of the frame (PFA) with low pass filtering of 18 and 25 Hz

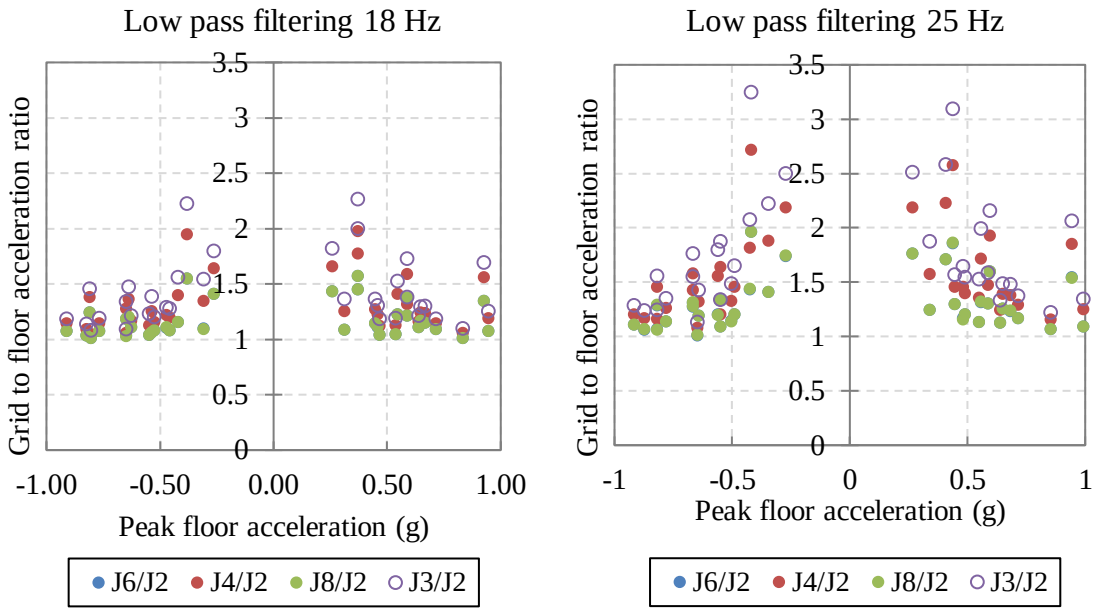

Figure 7-37 – Amplification of ceiling grids acceleration in analyses with sinusoidal and ground motions: Grid acceleration to acceleration at the top of the frame (PFA) with low pass filtering of 18 and 25 Hz

7.4.7.3 Axial force on ceiling grids

The axial force induced in the ceiling grids were measured through load cells (Refer to Figure 7-10 for the location of the instruments). These measurements were compared with the axial forces in similar locations of the ceiling model in Figure 7-38 and Figure 7-39. The comparisons show that the model overestimated the axial forces. This was especially noticed in tests with ground motion inputs.

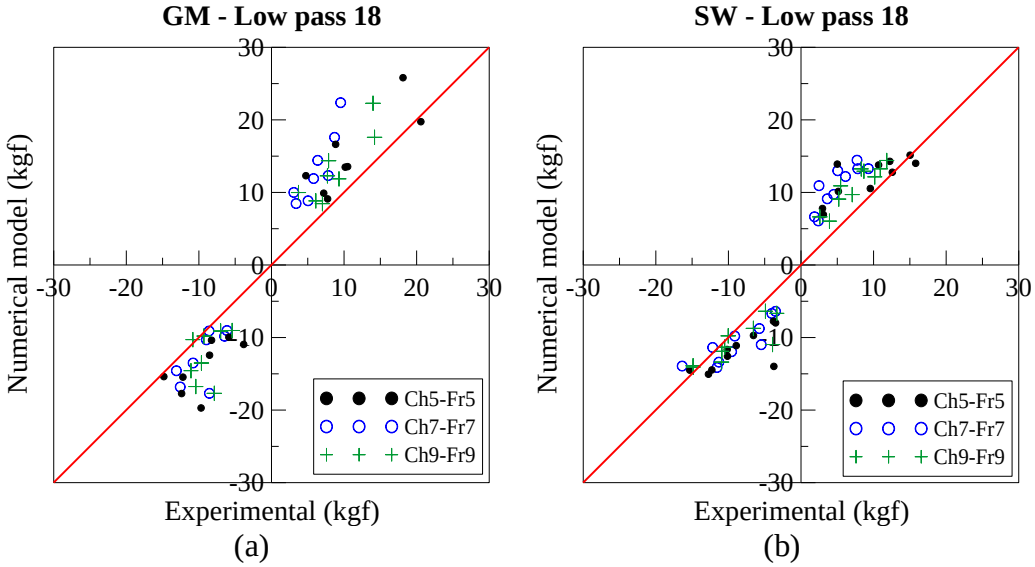

Figure 7-38 – Peak grid acceleration in experiments (Ch5 to Ch9) vs. peak grid acceleration in numerical model (Fr5 to Fr9) in (a) ground motion tests, and (b) sinusoidal tests with low-pass filtering of 18 Hz

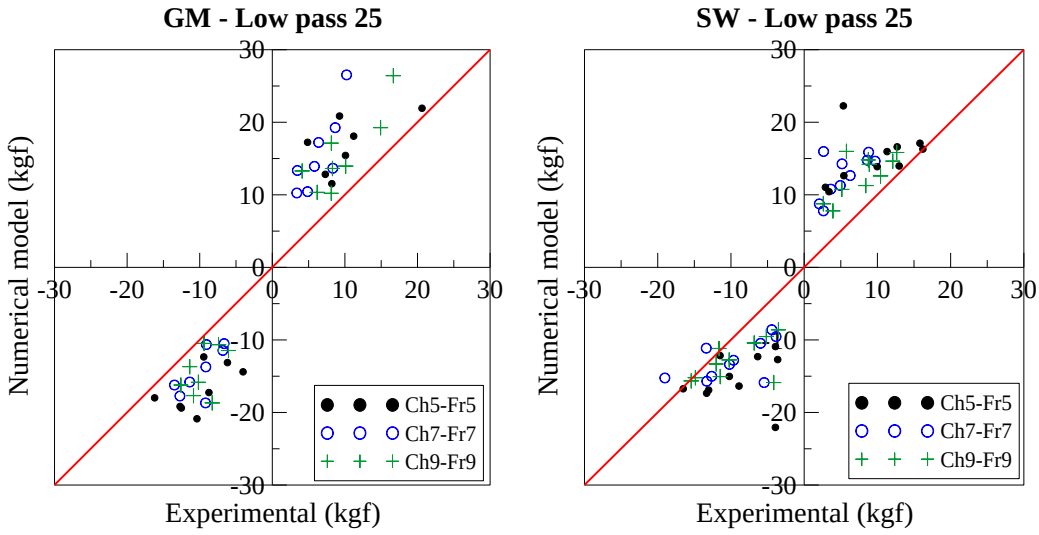

Figure 7-39 – Peak grid acceleration in experiments (Ch5 to Ch9) vs. peak grid acceleration in numerical model (Fr5 to Fr9) in (a) ground motion tests, and (b) sinusoidal tests with low-pass filtering of 25 Hz

In making comparisons and verifications however, the probable inefficiencies/inconsistencies in the experimental results must be taken into account. For example, in the experiments with sinusoidal input motions, it was noticed that the load cells consistently recorded smaller values in one direction. This means despite the symmetry of the input motion, the positive and negative output axial forces were not similar and, in some cases, twice larger. The comparison between load cell recordings on three longitudinal grids in sinusoidal tests in Figure 7-40 shows the absence of symmetry, especially in load cell on Ch7 and Ch9. This occurred despite the relatively symmetrical accelerations recorded on the same grids (Figure 7-41). The 3 load cells recordings for each sinusoidal test in the negative side seem more consistent. Therefore, it seems more reasonable to exclude the positive recordings on Ch7 from the overall results.

The comparisons reported in this section show that considering the limits and simplifying assumptions, this model can provide a relatively good estimate for the experimental results. This excludes the high frequency impact due to grid and tile pounding which was assumed to occur at very short periods of time and have negligible damaging effect. The model is simple and can be easily replicated and used for preliminary design purposes. The overestimation of the model response can be considered a conservative safety factor.

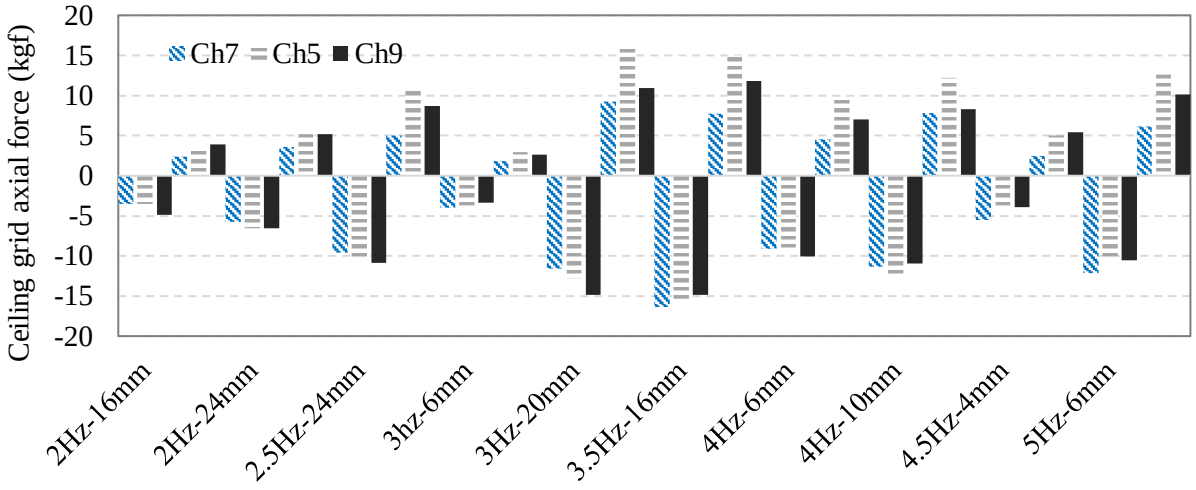

Figure 7-40 – Axial loads in load cells in sinusoidal experiments (low-pass 18 Hz)

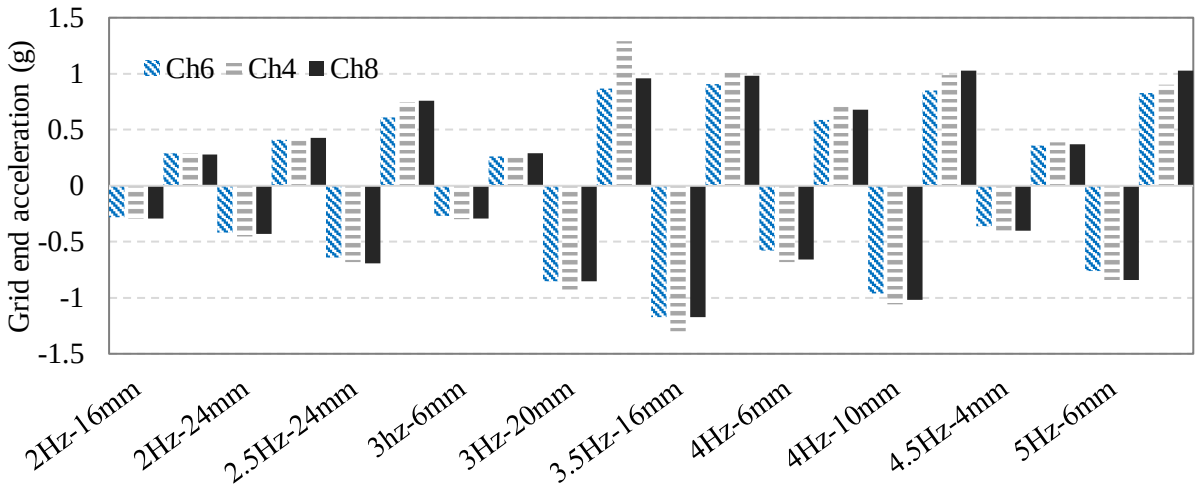

Figure 7-41 – Acceleration on grid ends in sinusoidal experiments (low-pass 18 Hz)

7.4.8 *Effect of filtering level*

Comparing the results shown for ground motion and sinusoidal tests without and with filtering shows an obvious difference in peak values as well as high frequency response (Compare plots in Section 7.4.3 and Section 7.4.4 with Section 7.4.5 and Section 7.4.6, respectively). With the filtering applied, the scatter in results was reduced significantly. However, the two levels of filtering do not appear to have a significantly different effect on the overall results. Figure 7-42 shows all results collected in all experiments and corresponding numerical analyses for grid accelerations, with two levels of filtering. Figure 7-43 shows a similar comparison for axial forces in ceiling grids.

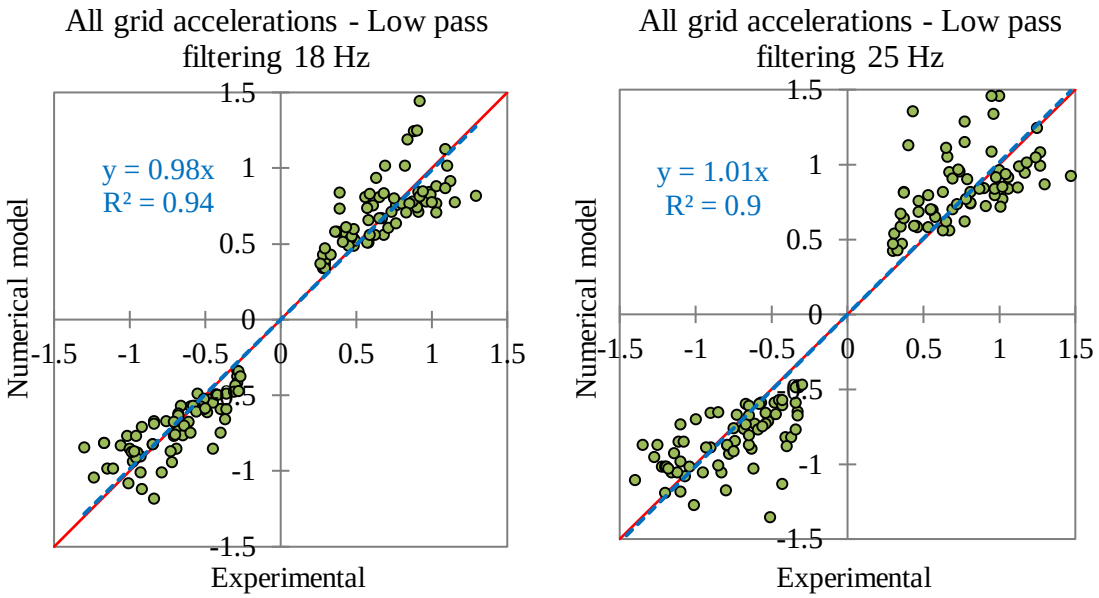

Figure 7-42 – Comparison of all acceleration data in ceiling longitudinal grids in experiments and numerical analyses with two levels of filtering

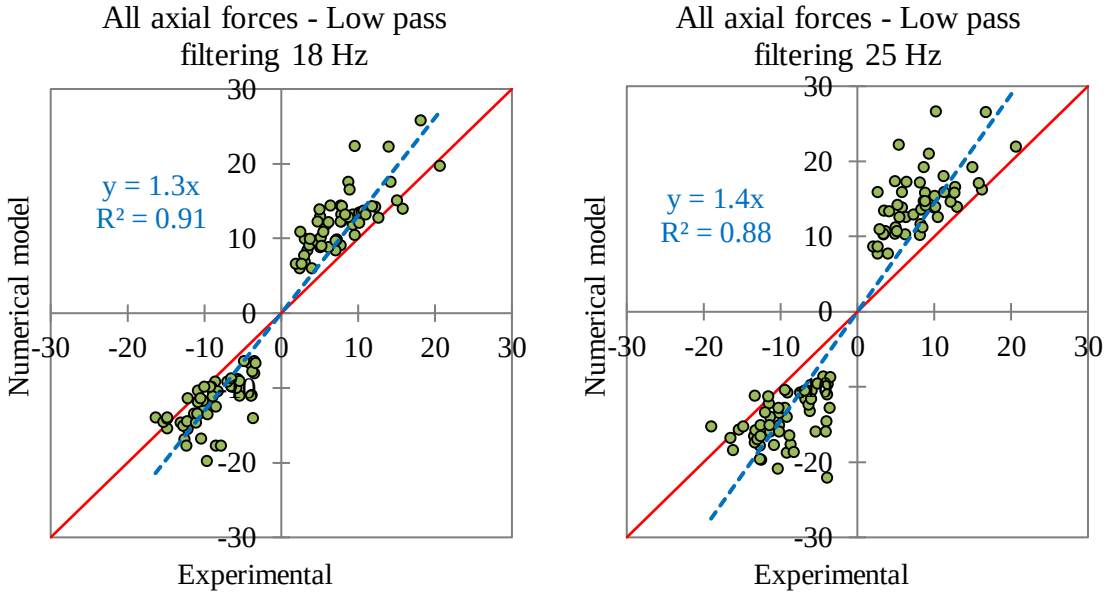

Figure 7-43 – Comparison of all axial force data in ceiling longitudinal grids in experiments and numerical analyses with two levels of filtering

The low-pass filtering of 18 Hz appeared to be more effective in the removal of scatters. However, this effect did not result in the appearance of significantly different trends in results, except for the ratio between peak floor and peak ceiling accelerations. The conclusion drawn from the comparison between the two levels of filtering was that, the frequency range removed was far enough from the natural frequency of the system and both levels can be assumed acceptable and unbiased.

7.4.9 *Numerical model of ceiling specimen incorporating the tile-grid impact*

7.4.9.1 Modelling objectives and assumptions

In this Phase, the objective was to create a numerical model which includes the contact between tiles and grids in order to consider the impact among these components. The model developed for this purpose is named as the "grid and tile model" herein. The purpose of the modelling is not to replicate the experimental results but rather show the occurrence of pounding and creation of consequential large accelerations. Therefore, it was found unnecessary for this model to be of the same dimensions as the perimeter-fixed ceiling used in the experiments. Only a quarter of the ceiling specimen tested in experiments was modelled here (4 tiles and their grids). This also shortened the analysis time by reducing the number of elements and the complexity of the model.

There were a number of additional simplifications assumed in the process of creating this model. One assumption arises from the engagement between hanger wires and ceiling tiles. The ceiling vertical hanger wires are fixed to the ceiling grids through loops that pass through holes at approximately mid-height of the web of tees. This means that in some areas the looped wire restricted the movement of the tiles. This restricting element was not included in the model. Moreover, the friction between tile and grid surfaces was not directly included in the model. To partially incorporate these effects, the initial stiffness of the gap elements was increased. This provided a small resistance and prevented the tiles from sliding as a free body at the onset of motion. The input acceleration was unidirectional and in one horizontal direction (X). This means that the effect of vertical excitation was excluded in this model.

7.4.9.2 Details of grid and tile model

For this model, material properties and cross sections were chosen similar to the model described in Section 7.3.1. The model consisted of four 600 mm by 1200 mm tiles framed by cross tees and main tees (Figure 7-45). The tiles are modelled using shell elements. Hanger wires were excluded from this model and their vertical restriction in tension was replaced by applying vertical restraints on all cross tee-main tee joints. The mass of each tile is uniformly distributed as area dead load. The contact between the tiles and grids was modelled using multilinear elastic link elements (springs) allowing for 2.5 mm gap on each side of the tiles (Figure 7-44). This gap width was chosen based on the measurements of the ceiling tiles used in the experiments. On average, ceiling tiles were found to be 5 mm smaller than the grid modules in each direction (i.e. width and length). The elastic springs were compression-only

elements and had negligible stiffness in tension. These springs were defined on four corners of the tile assembly and at each corner two springs were defined in x and y directions. At each stroke of motion, two springs acted in compression and two were ineffective or in tension. At the closure of gaps in compression, the second and relatively much greater stiffness of the multilinear spring element simulated the pounding effect between the tile assembly and grids. Figure 7-46 shows a schematic plan view of the grid and tile model in exaggerated dimensions with the joints and frames labelled for later reference in the following sections.

Disp (m)	F (N)
-1	-9810
-0.02501	-9810
-0.025	-9.81
0	0
1	9.81E-05

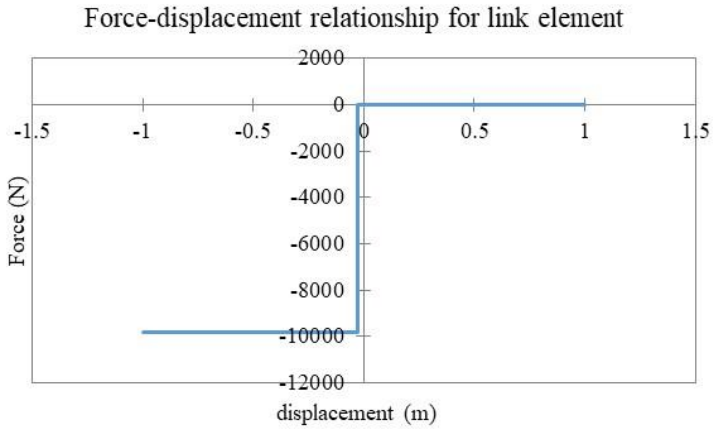

Figure 7-44 – Multilinear elastic link element used at free ends of the ceiling grids

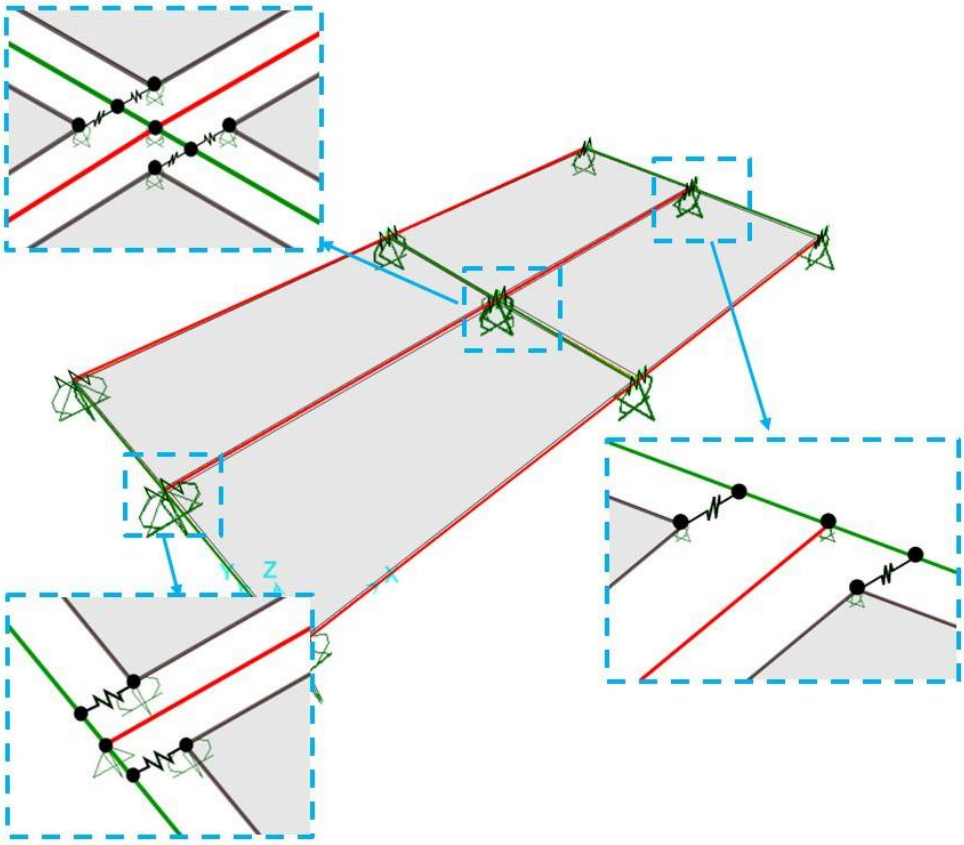

Figure 7-45 – The grid and tile model

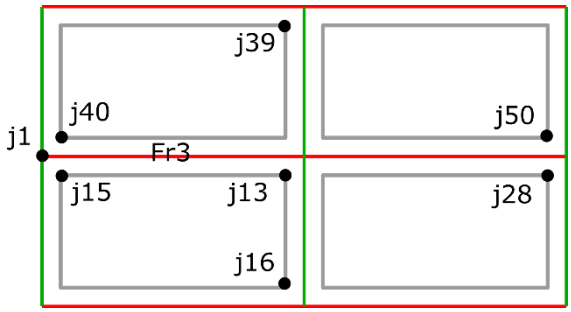

Figure 7-46 – Schematic view of the grid and time model with elements labelled

7.4.9.3 Loading

The input motions used in this model were the acceleration time histories recorded at the top of the test frame (i.e. PFA) in the experiments. The recordings from this accelerometer (marked as Ch 2 in Section 7.2.3) were used without any filtering. This motion was applied in a unidirectional (X direction) similar to the condition provided by the shake table. No vertical excitation was included in the analyses. Figure 7-47 and Figure 7-48 show the input acceleration time histories used in the grid and tile model. Figure 7-49 shows the displacement time history corresponding to this motion obtained from the potentiometer at the frame top in the experiment.

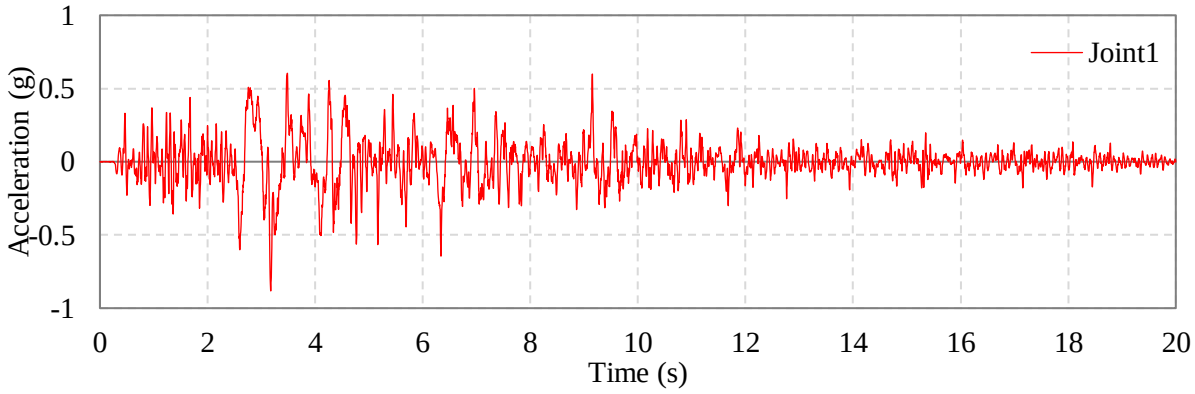

Figure 7-47 – Horizontal acceleration input motion in test with ground motion input (Northridge 1063-1)

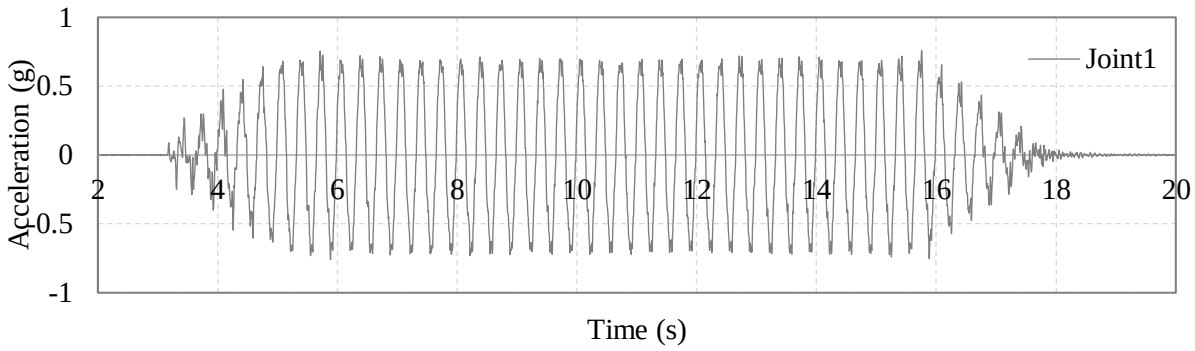

Figure 7-48 – Horizontal acceleration input motion in test with sinusoidal motion input (3Hz-20mm)

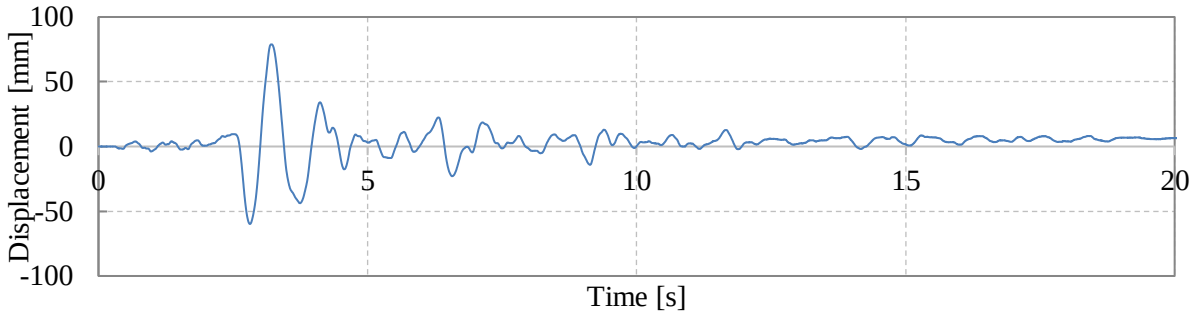

Figure 7-49 – Horizontal displacement at the top of the frame (peak floor displacement) from ground motion input (Northridge 1063-1)

7.4.9.4 Results and discussions

The displacement time history recorded at the corner of one of the ceiling tiles in the model is shown in Figure 7-50. As it can be seen, the displacement has a cap of 2.5 mm and that is the instance of gap closure and pounding between tiles and grids. Large accelerations and axial forces are expected at these instances.

The results obtained from the grid and tile model in Figure 7-51 show clear instances of amplified response due to the closure of 2.5 mm gap and impact between tile and grid elements. A similar response was observed in the axial force in ceiling grids in the model as shown in Figure 7-52.

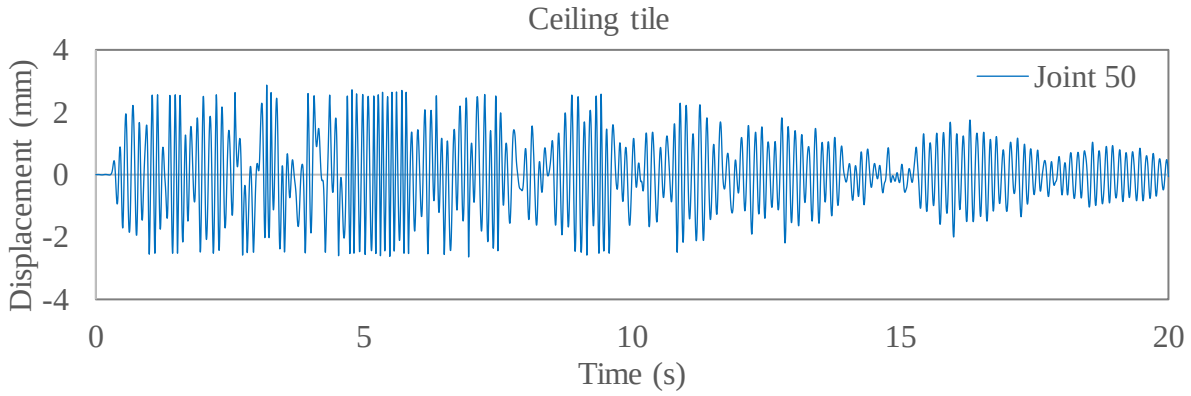

Figure 7-50 – Horizontal displacement of the tile in analysis with ground motion input (Northridge 1063-1)

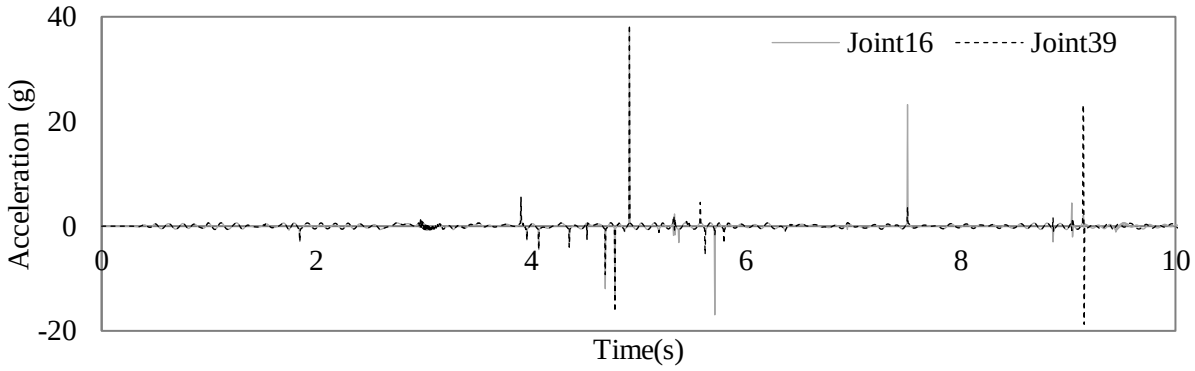

Figure 7-51 – Horizontal acceleration recorded on tile corner in analysis with ground motion input (Northridge 1063-1)

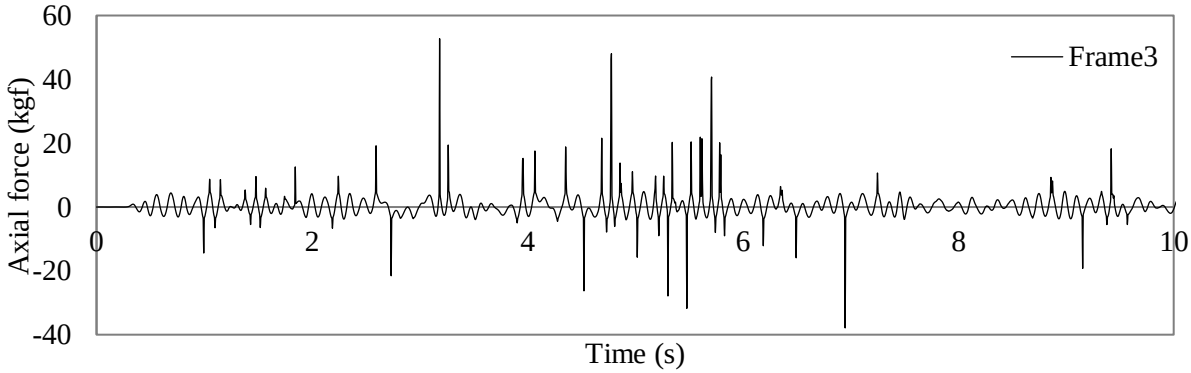

Figure 7-52 – Axial force recorded on ceiling grid in analysis with ground motion input (Northridge 1063-1)

Ignoring these spikes as in Figure 7-53, shows that the accelerations on the tiles in the numerical analysis were relatively similar to the acceleration recorded on grid ends in the experiment. Discrepancies however, exist due to the different conditions in the experiment compared to the numerical model and the simplified assumptions made in the modelling such as ignoring friction and engagement of hangers.

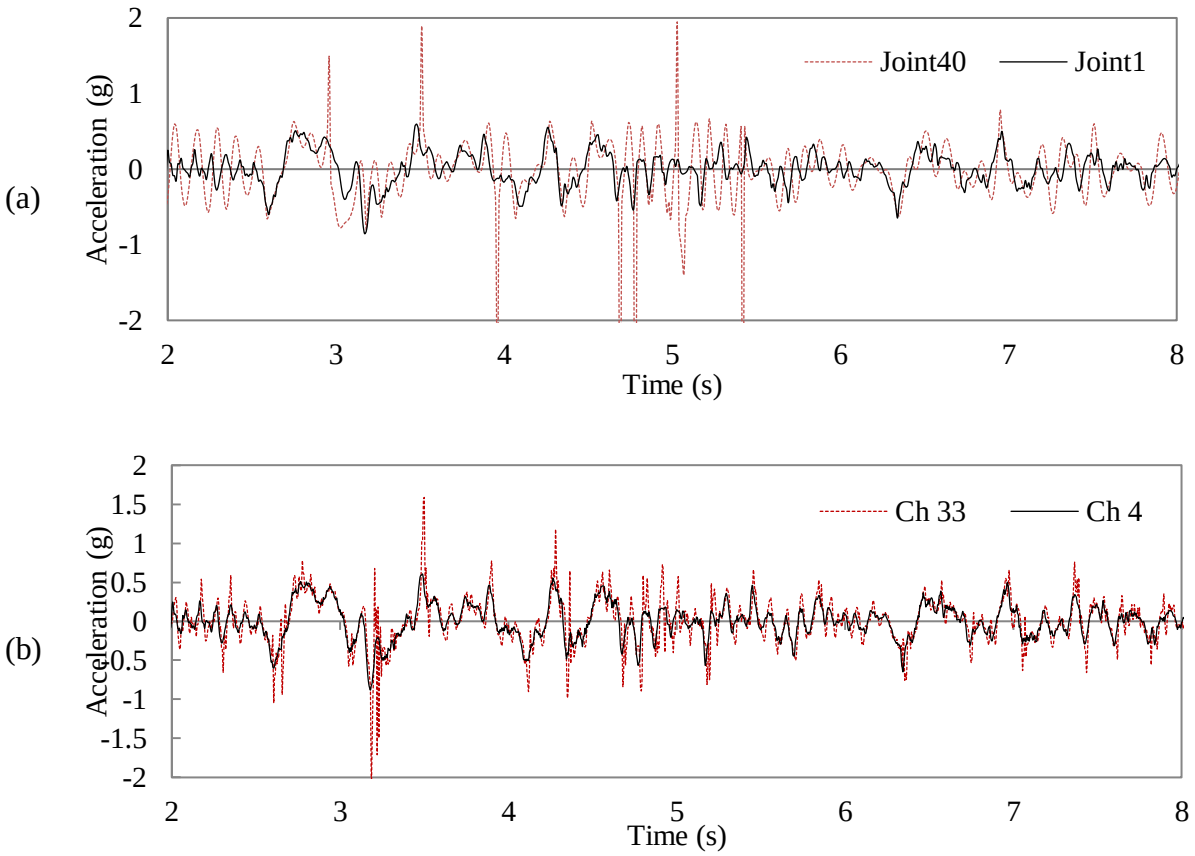

Figure 7-53 – Horizontal acceleration recorded on (a) tile corners in analysis vs. (b) experimental results with ground motion input (Northridge 1063-1)

Figure 7-54 through to Figure 7-57 show similar results obtained from the tile and grid model with a sinusoidal input motion (3Hz-20mm).

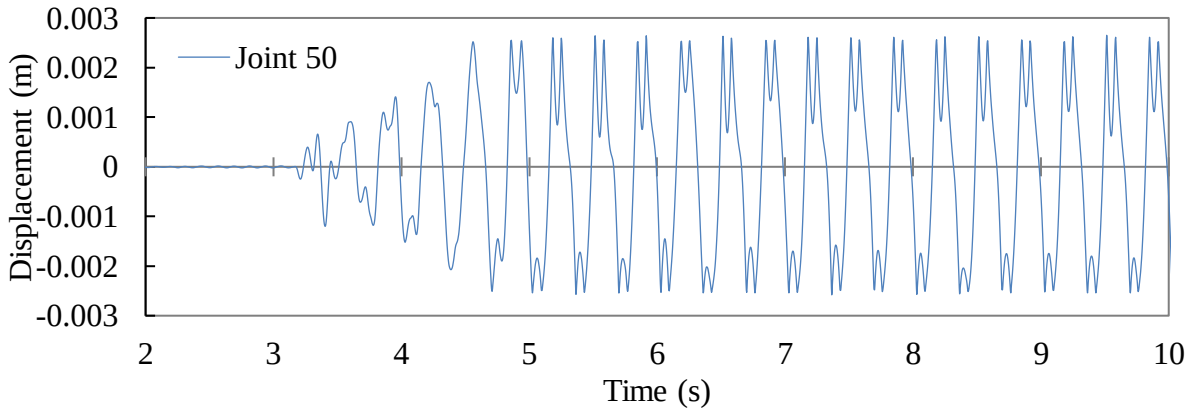

Figure 7-54 – Horizontal displacement of the tile in analysis with sinusoidal motion input (3Hz-20mm)

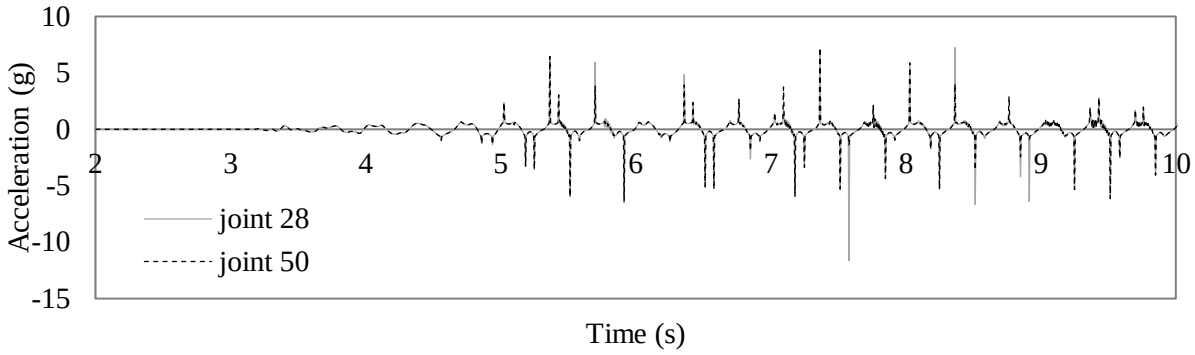

Figure 7-55 – Horizontal acceleration recorded on tile corner in analysis with sinusoidal motion input (3Hz-20mm)

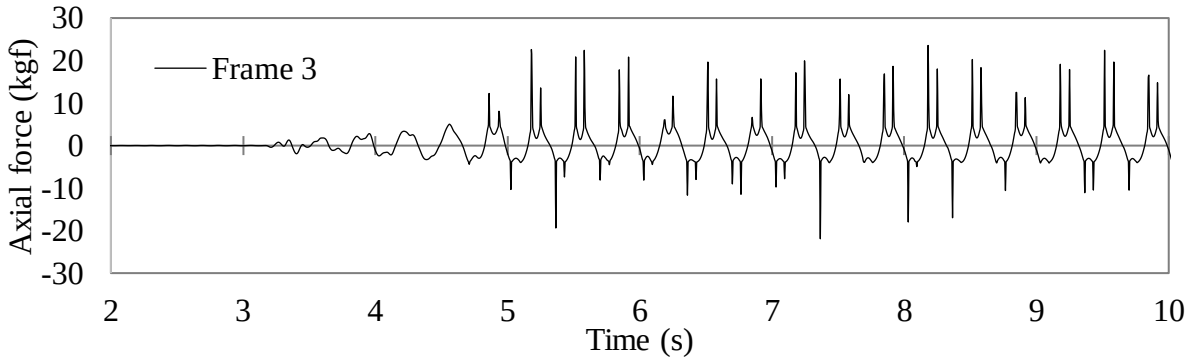

Figure 7-56 – Axial force recorded on ceiling grid with sinusoidal motion input (3Hz-20mm)

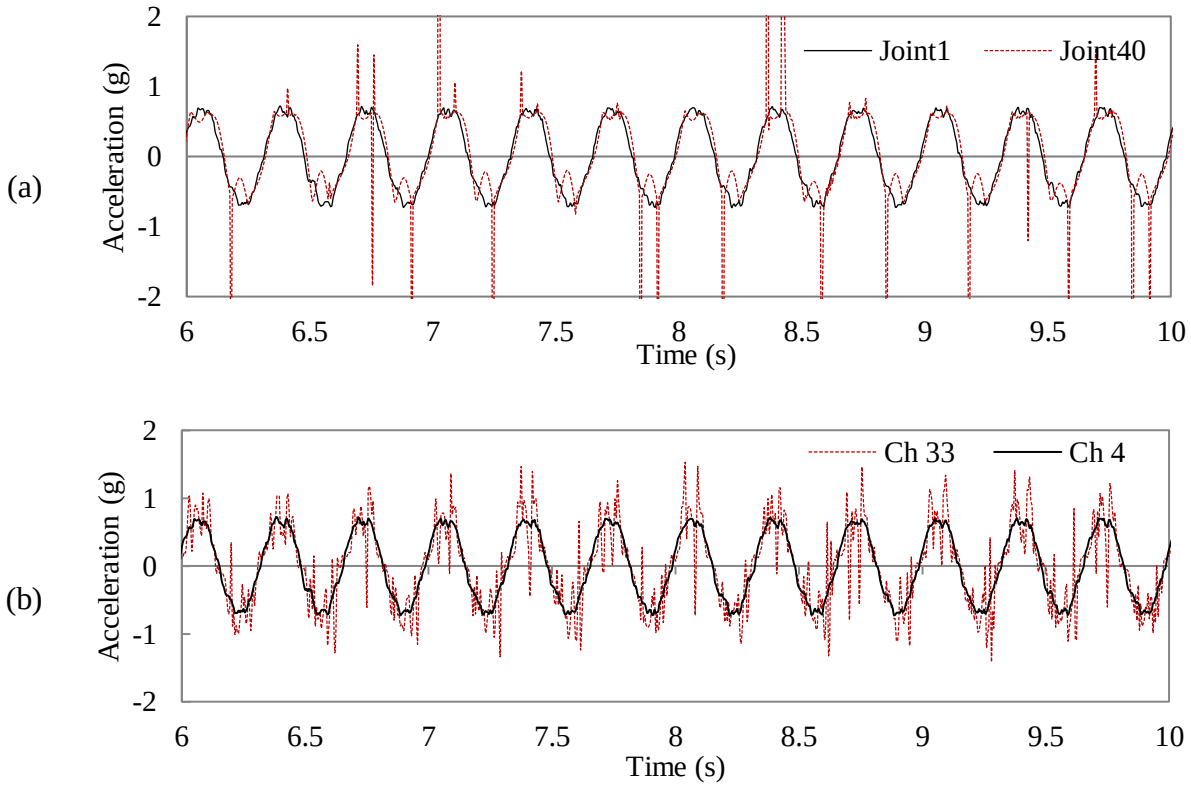

Figure 7-57 – (a) Horizontal acceleration recorded on tile corner in analysis vs. (b) horizontal acceleration recorded on longitudinal grid ends in experiment with sinusoidal motion input (3Hz-20mm)

7.5 Summary and Conclusions

Numerical models of shake table tests on a perimeter-fixed ceiling were developed in the finite element software SAP2000. The first model aimed at reproducing/replicating the experimental results and the second model showed the effect of pounding between ceiling elements. In the first Phase of this chapter, the model of the test frame was built using line elements for beams, columns and ceiling grids. No ceiling tiles were included in this model and the masses were applied as frame loads. The absence of tiles excluded the effect of tile vibration and the pounding between these two components. In the second phase of the modelling, a smaller grid and tile assembly (only 4 of the 16 tiles with their grids) was modelled using shell elements to represent the tiles and line elements for ceiling grid members. The contact between tiles and grids was modelled using multilinear elastic link elements. This model was used to check the occurrence of pounding between tiles and grids.

1. In the 1st phase, the general trend of results obtained from the simple frame and ceiling model showed a reasonable compatibility with the experimental results. The only discrepancies were concentrated in the high frequency peaks. This model was very practical to develop and to analyze.
2. The two levels of filtering (i.e. 18 Hz and 25 Hz) appeared to be effective in removing the scatter in the results and some of the spikes. The ceiling acceleration amplification ratios were more conservative compared to those obtained through experiments.
3. The model of the ceiling grid and tiles showed that the spikes in the acceleration and axial force response histories occurred at the closure of gaps between tiles and grids.
4. In the simple model of frame and ceiling including filtering, the accelerations obtained in the ceiling grids were generally lower than the experimental results. The ratios between ceiling grid accelerations and peak floor accelerations were mainly lower than the experimental results. However, this model overestimated the peak axial forces in the ceiling grids.

7.6 References

Langill, T. J. (2009). Mechanical properties of hot-dip galvanized steel. In Structures Congress 2009: Don't Mess with Structural Engineers: Expanding Our Role (pp. 1-6).

Effect of galvanizing on high performance steels and their weldments. Summary of the IZA ZC-21 project

Seismosoft [2013] "SeismoSignal v5.1 – A computer program for signal processing of

strong-motion data," available from http://www.seismosoft.com.

CSI, S. V. (2010). 8, 2002. Integrated Finite Element Analysis and Design of Structures Basic Analysis Reference Manual. Computers and Structures, Inc., Berkeley, California, USA.

Zaghi, A. E., Soroushian, S., Echevarria Heiser, A., Maragakis, M., & Bagtzoglou, A. (2016). Development and Validation of a Numerical Model for Suspended-Ceiling Systems with Acoustic Tiles. Journal of Architectural Engineering, 22(3), 04016008.

Ryu, K. P., & Reinhorn, A. M. (2014, July). Simplified analytical modeling of a suspended ceiling system. In Proceedings of the 10 th National Conference in Earthquake Engineering (pp. 21-25).

Paganotti G (2010). *"Behaviour of Suspended Ceiling System during Seismic Events: Development of Fragility Curves"*. Masters Thesis, Politecnico Di Milano, Italy.

CHAPTER 8

IMPLICATIONS OF RESEARCH FINDINGS

8 IMPLICATIONS OF RESEARCH FINDINGS

8.1 Introduction

Following the review of existing Standards and manufacturer guidelines in the first chapter of this thesis, a list of areas for potential improvement were identified. The experimental and analytical sections of this study sought answers to these raised issues and ambiguities. This chapter aims at discussing the implications of these findings on the existing state of the seismic design and installation of suspended ceilings. Where applicable, conclusions and recommendations are provided based on the experiments carried out during this research project.

8.2 Findings and implications

8.2.1 *The design working life of the suspended ceiling system*

As mentioned in Chapter 1, NZ Standard for the design and installation of suspended ceilings (AS/NZS 2785:2000, Clause 3.1.2) requires ceilings not providing structural stability to be designed for a working life of 15 years without maintenance.

For a building with a 50-year design life, it is not clear as to what level of earthquake the ceiling should be designed, e.g. is it the 15-year earthquake, or the earthquake related to the design life of the building? This becomes an issue specially in design for ULS as for this limit state, the level of earthquake varies with the design working life assumed.

According to Clause 8.6 of NZS 1170.5:2004, the minimum shaking level for the design of ceilings is SLS with a ductility factor of 1. This implies that for such a ceiling, any greater shaking level (i.e. >0.25 ULS shaking) could result in collapse. The main reason for this low level of design is the rare occurrence of injury or loss of life due to the collapse of ceilings in previous earthquakes. The current financial incentives to reduce the initial build cost act as a strong disincentive to designing higher performing ceilings. Consequently, often a more resilient design that would reduce the likelihood of seismic damage over the life of the structure comes second place when competing against the immediate advantages of lower cost and higher financial benefit.

Although the standard requires ceilings that provide structural stability to the building to be designed for the design life not less than that of the building, the common suspended ceilings do not provide such stability to a building (e.g. as a diaphragm). Nevertheless, ceilings play an important role in maintaining uninterrupted occupancy. Therefore, for determining the

annual probability of exceedance of a seismic design event, it seems reasonable to assume the design life of the suspended ceiling to be equal to that of the supporting structure. This important decision also depends on the extent of the possible damage and its acceptability in different areas of the building, for example on egress routs or areas of congregation.

8.2.2 *Suspended ceiling system's ductility factor for the ULS design*

NZ Standard 1170.5:2004 requires a ductility factor of 1 to be considered for the SLS design of ceilings. The maximum allowable deflections of the grid members under service loads at mid-span are defined by the AS/NZS 2785:2000 Standard for SLS. When design for ULS is required, higher ductility factors are provided with part response factors below 1, resulting in reduced seismic demands (NZS 1170.5:2004, Table 8.2). Based on Table C8.2, in the commentary of NZS 1170.5:2004 for the ductility factors for common parts in buildings, suspended (lay-in tile proprietary) ceilings are recommended to be designed assuming a ductility of $\mu=2$. This means that for ULS design the seismic demand for a ceiling with this ductility can be reduced by a factor of 0.55. The standard provides no further criteria for this choice.

According to the USG design guide (USG, 2012), use of higher ductility factors for ULS design is allowed based on a structural engineer's recommendation/approval: "A ductility of 1.0 must be assumed, except on the advice of a Chartered professional structural engineer for a specific ceiling." (p. 25). However, the choice of an appropriate ductility factor for a ceiling system directly depends on the proprietary system manufactured. In order to make an informed decision, the structural engineer requires sufficient information at his/her disposal to assign an appropriate ductility factor (higher than 1) to a proprietary product. This information needs to be provided by the manufacturer.

In the early stages of this research, suspended ceilings were treated as elastic non-ductile systems where the failure of the first component was assumed to trigger system failure. This assumption was confirmed in the static tests carried out on various components of suspended ceilings in this research project, where little ductility was observed in the force-displacement responses. Figure 8-1 shows an example of the brittle failure in a typical grid joint captured in monotonic tension and compression tests in Chapter 4 of this thesis. It has been observed in previous earthquakes and experimental studies (Badillo-Almaraz et al., 2007, Ryu et al., 2012) that suspended ceilings can experience brittle and cascading failure. As the ceiling grids and tiles all contribute to the integrity and stiffness of the suspension system and

normally no additional mechanical fasteners are used on grid intersections, loss of a tile or grid joint is considered as the onset of an abrupt system failure and therefore any small residual capacity is ignored.

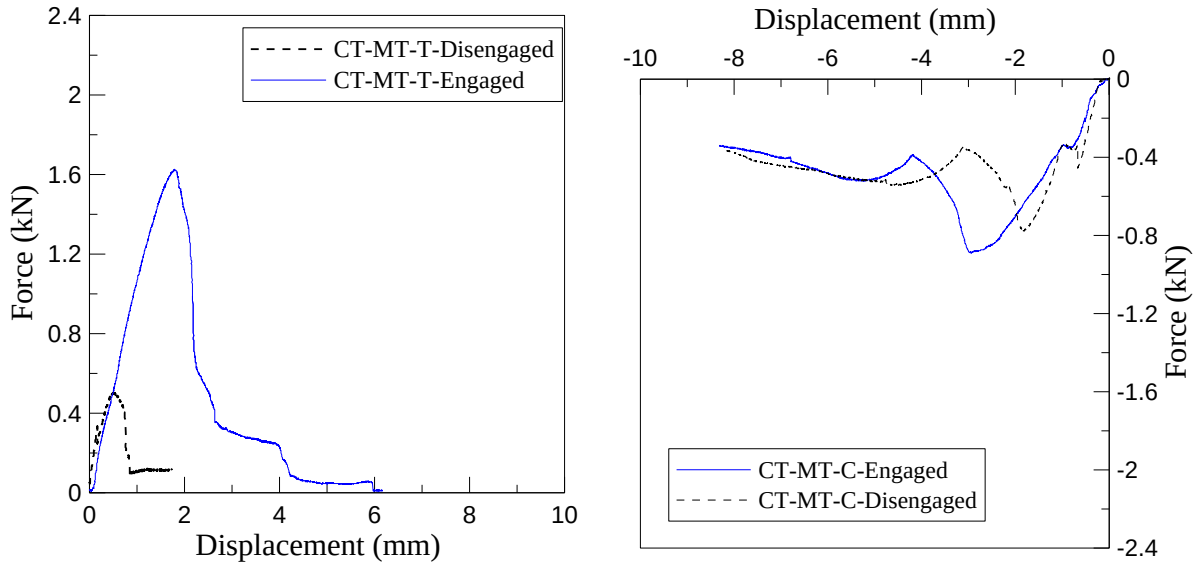

(a) (b)

Figure 8-1 – Force-displacement relationship for a typical suspended ceiling grid joint in (a) tension and (b) compression (Refer to Chapter 4)

Investigating the possibility of increasing the deformability and load bearing capacity of the existing ceiling systems was one of the objectives of the experiments conducted as part of this research project. In these experiments, the load bearing and deformation capacities of the joints between suspended ceiling grid members (cross tee - main tee) were tested under tension and compression loads (Refer to Chapter 4). A proprietary seismic clip (originally produced by USG (2012) as seismic separation joint) was added to the cross tee - main tee joints as a modification. The results obtained from these experiments showed that the addition of the seismic clips increased the load bearing capacity of the joints. Moreover, with the addition of seismic clips, the connection's failure mode was no longer brittle. The connections with seismic clips experienced a number of failure and yielding phases while still carrying forces as large as those of the as-built connection (i.e. without seismic clip) (Figure 8-2).

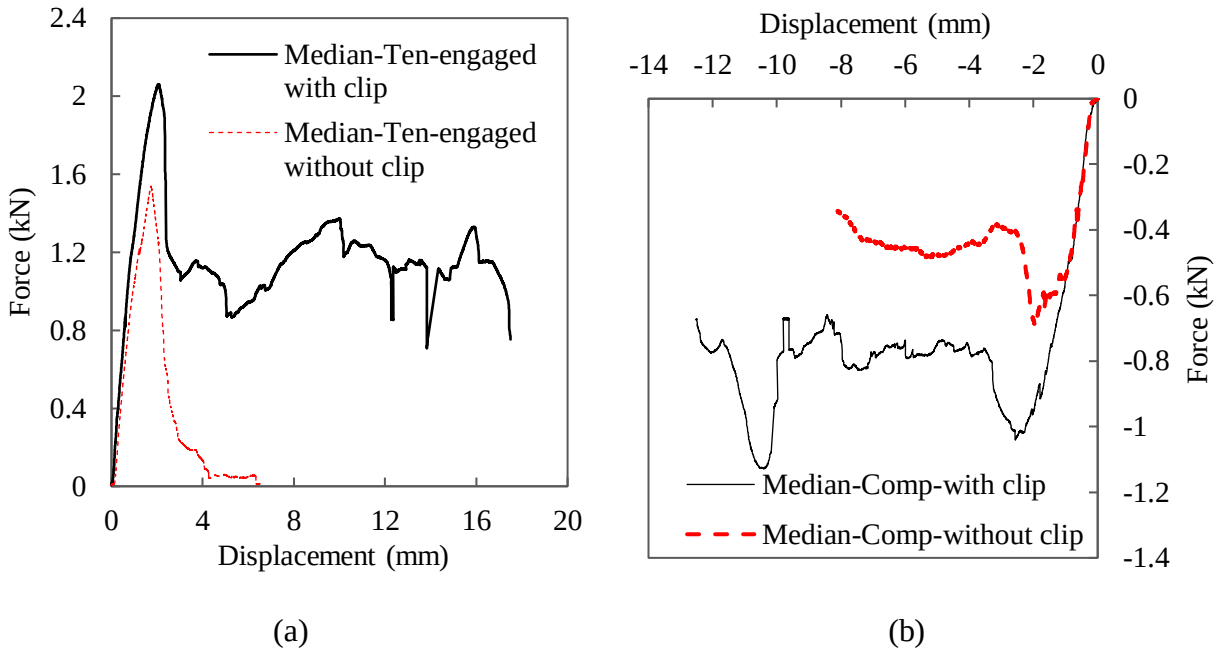

Figure 8-2 – Comparison between the cross tee – main tee joint median capacity with and without seismic clip under (a) tension, and (b) compression load

Having mentioned this, until the applicability of this improvement method on different ceiling systems (rather than single joints) is tested under dynamic loading, a ductility factor higher than 1 is not recommended for common suspended ceilings. The ductility of a component needs to be considered in a broader context including other elements to make sure the system allows for the development of the post yield phase with sufficient gaps and no brittle failure occurs in other components before the ductile element reaches yield point. Also, the effect of such deformations on other components supported by the grid system (e.g. tiles, luminaries, services, etc.) needs to be considered in a system level experiment.

Based on our limited findings it seems to be reasonable to apply a conservative ductility factor of 1 to current ceilings for ultimate limit state design. To advise the applicability of ductility factors greater than 1, it seems necessary for the manufacturers of ceiling systems to demonstrate with sufficient supporting evidence (e.g. force-displacement relationship), any similar enhancements and ductile behaviour in their products both in terms of components and overall system.

8.2.3 *Understanding the mechanics of the force transfer within the components of suspended ceilings and development of a hierarchy of strength*

The load bearing capacity of a suspended ceiling depends on the capacity of its components,

i.e. fixtures and grid/suspension system. It is quite difficult to obtain the strength of the proprietary suspension systems (i.e. cross tees, main tees and their connections) due to the confidentiality of manufacturer information. Another possible source is tests conducted on similar elements. As discussed in Chapter 2 of this thesis, Paganotti et al. (2011) quantified the failure forces for main tees, cross tees and their intersection joints using two major ceiling manufacturers in NZ in a series of monotonic tension and compression experiments. However, the strength reduction factor appropriate for these experimental results is not clear in the available documents. As mentioned in Chapter 1, the NZ Standard for cold-formed steel members (AS/NZS 4600:2005) requires a capacity reduction factor of 0.9 for members subject to tension and 0.6-0.7 for riveted connections. Comparing the experimental failure forces obtained by Paganotti et al. (2011) and the capacity values used in the manufacturer's guidelines does not indicate a clear and consistent capacity reduction factor can be applied generally. This needs to be more clearly determined in the compliant ceiling design standards.

8.2.4 *Ceiling grid acceleration – axial force relationship*

As discussed in Chapter 2 of this thesis, a linear and direct relationship was demonstrated between the axial forces induced in the ceiling grids and the accelerations in the grids. The axial force could be calculated, with some proximity, based on the simplified tributary area associated with each grid line as shown in Figure 8-3 and the peak acceleration on the grid which can be calculated based on the parameters defined in Section 8 of NZS 1170.5:2004, discussed in Chapter 1 of this thesis. The seismic mass considered over this tributary area consists of the mass of the tiles and grids, and the mass of any services and luminaries supported by the ceiling grid, with a minimum service load of 30 N/m^2.

The seismic forces in the direction of main tees and cross tees can be calculated using Equation 8-1 and Equation 8-2, respectively:

$$F_{MT} = a_{\max,MT} \times m \times L_{MT} \times 1.2 \qquad \text{Equation 8-1}$$

$$F_{CT} = a_{\max,CT} \times m \times L_{CT} \times 0.6 \qquad \text{Equation 8-2}$$

where $a_{max,MT}$ and $a_{max,CT}$ are peak accelerations in the main tee and cross tee considered, m is the unit area seismic mass and L_{MT} and L_{CT} are the total lengths of main tees and cross tees in each direction. Since the spacing of cross tees (i.e. 0.6 m) is half of the spacing between main tees (i.e. 1.2 m), their tributary areas are different.

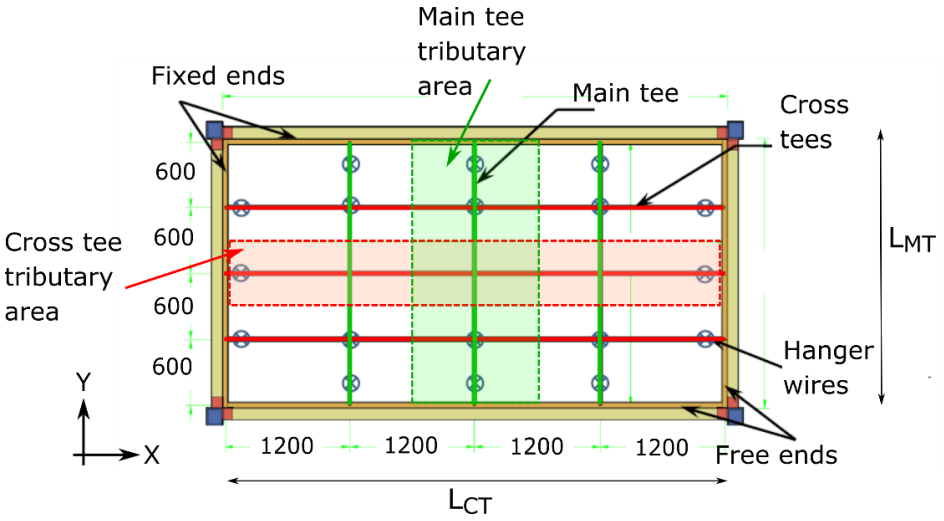

Figure 8-3 – Schematic view of tributary areas for cross tees and main tees in a suspended ceiling (dimensions in mm)

Comparing the forces calculated based on the equations above with the experimental fragility curves obtained for the weakest component of the ceiling in the cross tee or main tee directions can determine the probability of failure at the considered seismic demand level. This simple and effective method was proposed for the initial design of a suspended ceiling with known component capacities in Chapter 2 of this thesis. In Section 8.4 this method has been utilised for estimating the capacity of the example ceiling discussed.

8.2.5 *Part spectral shape coefficient for suspended ceilings*

In Chapter 3 of this thesis, the horizontal and vertical accelerations induced in the ceiling suspension system (i.e. grids) were compared with the input or floor accelerations in a series of shake table tests on perimeter-fixed ceilings. The comparison showed that the amplification of input acceleration varied in different locations of the system but appeared to also depend on the frequency and amplitude of excitation. The level of amplification in floor horizontal acceleration as it is transferred to the ceiling grids was observed to be greater than the factor of 2 recommended by the NZ design Standard NZS 1170.5 (2004). This implied that grid members could be subject to much larger accelerations, in the worst cases up to 4.5 times the peak floor acceleration. Moreover, in these experiments, large vertical accelerations were recorded on ceiling grid members which resulted in vibrations and uplift in ceiling tiles.

Upon the application of low-pass filtering to the recorded acceleration outputs, these amplification factors were observed to consistently decrease and mostly remain below the

code recommended factor of 2. The filtering eliminated the high frequency contents in the acceleration and axial force time histories which were assumed to result from the impact between ceiling tiles and grids and vertical excitations due to the flexibility of the specimens. Based on these observations, tile hold-down clips were recommended for limiting the impact between ceiling grids and tiles and preventing the possible tile dislodgment. As most of these high frequency peaks in grid accelerations occurred in very short periods of time and only occurred once or a few times during the length of shaking, it seems reasonable to use the code mandated factor of 2. A larger factor (e.g. 3) is recommended to provide a margin of safety.

8.2.6 *Alternative ceiling systems or solutions*

As part of this research and through an extensive series of shake table tests, the possibility of using a modified free-floating ceiling -called fully-floating- in a high seismic area was investigated (Refer to Chapter 5 of this thesis). The modifications included:

i. trimming element fixed to all tee ends instead of spacer bars,
ii. large gaps (100 mm) between the trimming element and perimeters on all sides, and
iii. elastic isolation material filling the gap between the trimming element and walls/beams

As the fully-floating ceiling partly followed the simple pendulum theory, large displacements and accelerations were observed at resonant input frequencies. However, the isolation material appeared effective in damping the ceiling displacement and avoiding the large acceleration peaks due to pounding and impact. Throughout the tests on this fully-floating ceiling, damage was only observed in the form of panel dislodgement which was assumed to be caused by large ceiling accelerations due to impact combined with the vertical movement of the untied/loose tiles induced by significant vertical accelerations. No grid failure was observed in these experiments.

The results obtained through these experiments implied that upon the provision of sufficient clearances around rigid penetrating objects, this system could be effective in reducing the demands transferred to the ceiling system. The stiffness of the isolation material used could also vary based on the limitations on the allowable displacements.

In another part of this research, a series of shake table tests were carried out on the combination of a back-braced ceiling and low-damage partition walls (Refer to Chapter 6 of this thesis). The braces were installed in the form of splay wires and vertical struts. All grid ends were sliding on the supporting perimeter angles as per the recommendations of the

ceiling manufacturer. During these tests, large relative displacements were recorded on the braced ceiling which in some cases resulted in the closure of the 20-mm gap provided on perimeters and pounding of grid ends against perimeter supports. This pounding imposed large accelerations on the ceiling grid. Moreover, grid spreading was observed in the tests which resulted in tile dislodgement at larger displacements.

Based on the results obtained from these experiments, it was concluded that the inherent slackness in splay wire bracing could result in perimeter gap closure and unforeseen impact on the ceiling grid system. Where large relative displacements/drifts are also expected in the structure, the perimeter gaps may need to be increased or filled with isolation material to dampen the probable impact. More rigid bracing could alternatively be used to limit the ceiling's lateral flexibility.

To avoid grid spreading, a trimming element was recommended in the form of trimming angles riveted to all grid ends, transforming the ceiling to an integrated rigid body separate from the perimeter structure.

The low-damage drywalls tested remained undamaged. However, it was expected that in the presence of paint and cosmetic finish on corners, some cracks will appear in the surface. The system was only tested under unidirectional loading. In order for the two adjacent walls to move out of plane without causing damage under bidirectional loading, sufficient gaps need to be provided on the intersection of the wall boards.

8.3 Research limitations and shortcomings

The experimental nature of research involves uncertainties and unforeseen obstacles. Any study also includes boundaries to the quantity and quality of the work that is plausible within one project's time and budget and by one limited team of researchers. The following paragraphs list the limitations of this study and the shortcomings identified. In the following chapter a list of potential future areas of research has also been provided which is based on the recognised limitations of this study.

The dimensions, location and capacity of the shaking table available was one of the early limitations identified in this study. This restriction affected the dimension of the test specimens and to some extent the applied demand. The shaking table was only capable of applying unidirectional excitation. In real conditions, suspended ceilings are subject to bidirectional horizontal loading as well as vertical excitations. This limitation must be recognised in the interpretation of the findings of this research.

Time was another important limiting factor which meant some variations of the experiments had to be eliminated due to the schedule set in the lab and limited resource. It would have been beneficial and practical to delve more deeply in the properties of the isolation foam material used in the fully-floating ceiling experiment and experiment different installation techniques. It would have been also beneficial to test the seismic clips proposed in Chapter 4 on a full-scale ceiling specimen on the shaking table. This would have enabled us to evaluate the effectiveness of the proposed strengthening under dynamic loading and in conjunction with other components of the ceiling.

The numerical analysis software chosen for the simulation phase of this study came with some limitations. The first model of the ceiling specimen and testing frame did not include the ceiling tiles for simplification of the analysis. Ceiling tiles and their impact against the ceiling grids have been found to cause some high frequency peaks in the acceleration response of the specimen. Ignoring this element in the model resulted in the elimination of this effect. The model also did not include vertical excitation in agreement with the experimental test setup.

8.4 Seismic design example of a suspended ceiling based on NZ Standard

The suspended ceiling example presented in Chapter 1 of this thesis (Section 1.7.1) is presented in this section with design plots added for the estimation of grid lengths. The seismic forces calculated in Chapter 1, Table 1-12 are used here as the demand values. The design plots shown in Figure 8-5 were introduced in Chapter 2 of this thesis, and were derived based on the ceiling components capacities and fragility curves and using the method mentioned in Section 8.2.4. The design is presented in the following steps:

8.4.1 *Calculation of seismic demand:*

The horizontal seismic design coefficient was calculated in detail in Section 1.7.1 based on the requirements of NZS 1170.5:2004, Section 8.

8.4.2 *Envelope fragility curves*

Figure 8-4 shows an example for the envelop fragility curves produced for cross tees and their connections from two manufacturers discussed in Chapter 2. These example curves were produced for 12 m long cross tees and their connections for a ceiling with total seismic mass of 9.5 kg/m^2. Paganotti's (2010) experimental fragility curves for cross tees, their connections and 3.2 mm aluminium rivet fixtures were used as the basis for these curves. Similar fragility curves were produced for cross tees with other lengths as well as main tees

and their connections. Note that in creating these envelope curves, the capacities of the members, connections and end fixtures have been considered and the curves represent the weakest component of the ceiling in each direction (i.e. cross tee and main tee direction).

Table 8-1 – Seismic forces based on NZS 1170.5:2004

Seismic weight for SLS design (including 5.5 kg/m^2 tiles, 1 kg/m^2 grid system and 3 kg/m^2 service load)	$W_p = (5.5+1+3)\times 9.81 = 93.2\ N/m^2$
Horizontal SLS design earthquake actions	$F_{ph} = C_p(T_p)\cdot C_{ph}\cdot R_p \cdot W_p = 0.6\times 93.2 = 56 N/m^2$
Horizontal ULS design earthquake actions	$F_{ph} = C_p(T_p)\cdot C_{ph}\cdot R_p \cdot W_p = 2.4\times 93.2 = 223.7 N/m^2$

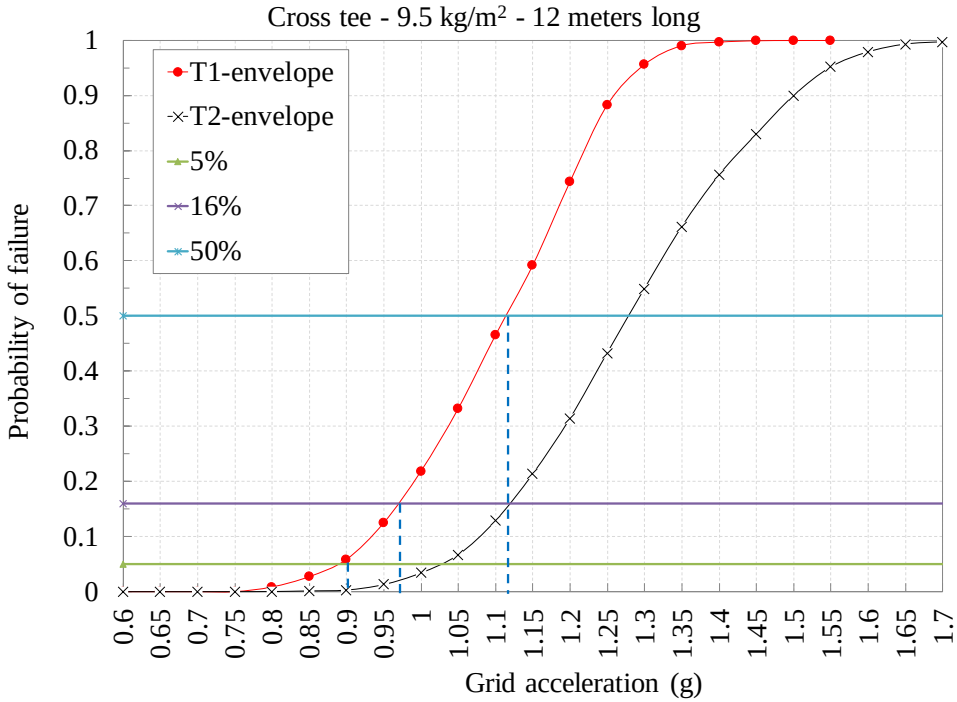

Figure 8-4 – Envelope fragility curves for ceiling components of two manufacturers (Type 1, T1 & Type 2, T2)

8.4.3 *Design plots*

The ceiling grid accelerations associated with 5%, 16% and 50% failure probability were derived from these plots as shown in Figure 8-4. For example, in the case of 12 m long cross tee shown, the grid acceleration associated with 16% failure probability is approximately 0.97

g for manufacturer type 1 and 1.12 g for manufacturer type 2. These failure probabilities along with the length of the cross tee or main tee considered were used for creating design plots shown in Figure 8-5 for the ceiling discussed in this example (seismic mass of 9.5 kg/m^2).

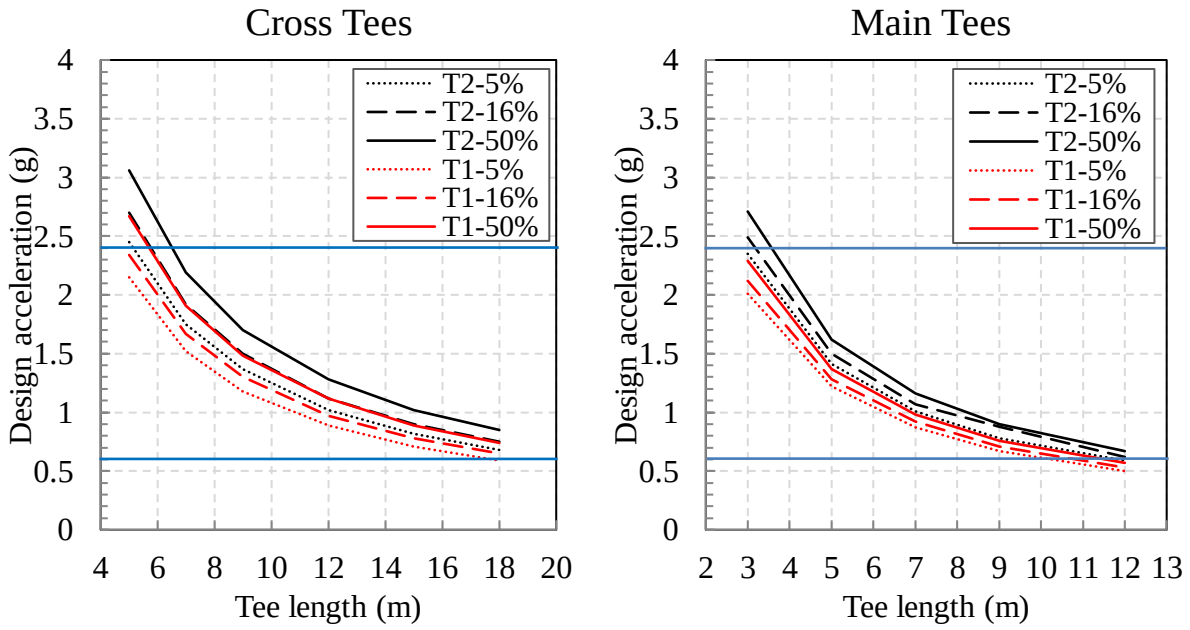

Figure 8-5 –Design plots for the example ceiling

8.4.4 *Estimation of allowable lengths*

Based on the calculations shown in

Table 1-12, the example ceiling should be designed for two design accelerations:

i. SLS level design for ceiling category P.7, which covers ordinary application areas, offices etc. = 0.6 g
ii. ULS level design for ceiling category P.4, which covers all areas leading to exit and egress routs and doors = 2.4 g

These two design accelerations are marked with horizontal blue lines on the cross tee and main tee design plots shown in Figure 8-5. The information provided through these plots indicate that, for a perimeter-fixed ceiling with conditions mentions earlier, the SLS level demand of 0.6 g allows less than 18 m cross tee length from manufacturer T1, with 5% probability of failure. The same level of seismic demand allows for approximately 10 m main tee length with the same failure probability. Slight variations in allowable length can be seen in Figure 8-5, with change in ceiling manufacturer and failure probability. These dimensions

(i.e. 10 m × 18 m) results in an area beyond the allowable limit for perimeter-fixed ceilings (i.e. 93 m^2). This area is either separated into smaller sections using seismic separation joints or back-bracing is used alternatively (ASTM E580, 2011).

For the ceilings designed to resist an ULS demand, the permitted cross tees length appears to be approximately 4 m for a low failure probability. For the main tees, plots associated with the second manufacturer allow for approximately 3 m of length in a perimeter-fixed lateral resisting system.

Based on the information presented here, it appears that for ultimate limit state level design, use of perimeter-fixed ceilings is not recommended for areas larger than those mentioned above, and back bracing may be a more suitable option.

8.4.5 *Comparison of Standard mandated seismic force with manufacturer's guidelines*

In Chapter 1 of this thesis and in the review of seismic design methods available, in an example the difference between the results from NZ standard with those based on manufacturer's guidelines was mentioned. This discrepancy was assumed to arise from the different return period factors taken for Christchurch; both guidelines applied a serviceability level return period factor of R_s = 0.33 for Christchurch (Canterbury area), instead of the factor 0.25 used in the Standard. This was due to the raised concern for Christchurch after the Canterbury 2010 & 2011 earthquake sequence. The seismic coefficients based on three sources are shown in Table 8-2. The ratio between the seismic action coefficient calculated based on NZS 1170.5:2004 to those of the guidelines was 0.6/0.8 = 0.75 which is equal to 0.25/0.33. To check this assumption, seismic action coefficient was calculated for two other areas in NZ based on these three sources as shown in Table 8-3 and Table 8-4.

Example of a ceiling on the forth story of an office building in Christchurch:

Table 8-2 – Comparison of seismic forces for an example in Christchurch

Armstrong	USG	NZS 1170.5:2004
Zone 1 (Z = 0.396)	Zone 2a (Z = 0.3)	Z = 0.3 R_s = 0.25 $C_h(0)$ = 1.33 (Soil C)
Height factor (H>9 m), H = 2	Zone & Height factor (H = 9.1-12) = 4.6	Height factor = 3 $C_i(T_p)$ = 2
Seismic force = 0.396×2W = 0.79W	Seismic force = 0.1729*×4.6W = 0.8W	Seismic force = 0.3×1.33×0.25×3×2W = 0.6W

* *Factor advised by USG (2012) for standardising the seismic force in guideline.*

Example of a ceiling on the second story of an office building in Auckland:

Table 8-3 – Comparison of seismic forces for an example in Auckland

Armstrong	USG	NZS 1170.5:2004
Zone 1 (Z = 0.13)	Zone 1a (Z = 0.13)	Z = 0.13 R_s = 0.25 $C_h(0)$ = 1.33 (Soil C)
Height factor (3-6 m), H = 1.33	Zone & Height factor = 1	Height factor = 1.98 $C_i(T_p)$ = 2
Seismic force = 0.13×1.33W = 0.17W	Seismic force = 0.1729×1W = 0.17W	Seismic force = 0.13×1.33×0.25×1.98×2W = 0.17W

Example of a ceiling on the second story of an office building in Wellington:

Table 8-4 – Comparison of seismic forces for an example in Wellington

Armstrong	USG	NZS 1170.5:2004
Zone 5 (Z = 0.5)	Zone 3 (Z = 0.46)	Z = 0.4 R_s = 0.25 $C_h(0)$ = 1.33 (Soil C)
Height factor (3-6 m), H = 1.33	Zone & Height factor = 3.6	Height factor = 1.98 $C_i(T_p)$ = 2
Seismic force = 0.5×1.33W = 0.66W	Seismic force = 0.1729×3.6W = 0.62W	Seismic force = 0.4×1.33×0.25×1.98×2W = 0.53W

In the three examples shown above, some discrepancy is still noticed between the NZ standard and the manufacturers as well as between the manufacturers themselves. The exact source of these inconsistencies could not be identified due to the limited information provided in the guidelines. It was also difficult to exactly compare the similarity -or difference- of criteria used by the guidelines for determining the zone factors with the soil class and seismicity risk factors provided in the NZ standard. Use of maps for determining the zone factor for different locations throughout the country -as provided by the guidelines- also results in a level of inaccuracy and approximation. It is probable that upon the choice of a different soil type in the calculations based on the NZ standard, more discrepancies would be identified with the guidelines approach. The seismic demand calculated according to the NZ standard was lower than those of the manufacturer guidelines in all three examples shown. In light of this example and the inherent consistency, it is recommended that NZ standards provide a coherent design method including both demand and capacity aspects and appropriate factors.

8.5 Conclusions

As a concluding note to this research project, the findings in experimental and analytical sections were used in this chapter to address the issues faced during this study. These findings and their implications were reinterpreted to find possible links with the practical application and design of ceiling systems in NZ. Issues such as ceiling ductility factor in ULS design, spectral shape factor, and improvement methods were discussed in this chapter. Finally, a design example was provided for a typical perimeter-fixed ceiling incorporating both demand and capacity aspects.

8.6 References

Armstrong (2013). *"Seismic Design Guide New Zealand Version, Suspended Ceiling Systems"*. Armstrong, Auckland, New Zealand.

Australian/New Zealand Standard. (1999). *Methods for Fire Test on Building Materials, Components and Structures - Simultaneous Determination of Ignitability, Flame Propagation, Heat Release and Smoke Release (AS/NZS 1530.3:1999)*. Wellington, NZ: Standards New Zealand.

Australian/New Zealand Standard. (2000). *Acoustics - Measurements of sound insulation in buildings and of buildings elements - Laboratory measurement of room-to-room airborne sound insulation of a suspended ceiling with a plenum above it (AS/NZS 2499:2000).* Wellington, NZ: Standards New Zealand.

Australian/New Zealand Standard. (2000). *Suspended ceilings - Design and Installation (AS/NZS 2785:2000).* Wellington, NZ: Standards New Zealand.

Badillo-Almaraz, H., Whittaker, A. S., & Reinhorn, A. M. (2007). Seismic fragility of suspended ceiling systems. *Earthquake Spectra, 23*(1), 21-40.

British Standards Institution. (1987). *Fire Tests on Building Materials and Structures - Method for determination of the fire resistance of elements of construction (general principles) (NZS/BS 476.20:1987).*

New Zealand Standard. (2004). *Structural Design Actions Part 5: Earthquake Actions-New Zealand (NZS 1170.5:2004)*. Wellington, NZ: Standards New Zealand.

Paganotti, G. (2010). *Behaviour of Suspended Ceiling System during Seismic Events: Development of Fragility Curves*. (Masters Thesis, Politecnico Di Milano, Italy).

Paganotti, G., MacRae, G. A., & Dhakal, R. P. (2011, April). Development of typical NZ ceiling system seismic fragilities. In *Ninth Pacific Conference on Earthquake Engineering (PCEE)* (pp. 14-16).

Ryu, K. P., Reinhorn, A. M., & Filiatrault, A. (2012). Full scale dynamic testing of large area suspended ceiling system. In *Proceedings 15th World Conference on Earthquake Engineering, September 23-28, 2012, Lisbon Portugal-Paper* (Vol. 5474).

USG Australia. (2012). *Generic Seismic Design for USG DONN Exposed Grid Suspended Ceilings*, Auckland, NZ.

CHAPTER 9

CONCLUSIONS & RECOMMENDATIONS

9 CONCLUSIONS AND RECOMMENDATIONS

This study was conducted with the main objective of investigating the seismic performance of suspended ceiling systems as one of the common non-structural elements (NSEs) in NZ. The main objectives of the research presented were set out in the first chapter of this thesis as:

i. Evaluating the mechanics of the force transfer within the components of suspended ceilings commonly used in NZ and establishing a strength hierarchy for the critical components,
ii. Development of a simple method for deducing the global capacity of the suspended ceiling system from components capacities. Providing fragility functions in terms of ceiling acceleration for the suspended ceiling using the component capacity data,
iii. Verification of the simple method of estimating seismic actions in connections and members based on PFA via shake table tests,
iv. Development of a simple numerical model for the perimeter-fixed ceiling in SAP2000 software and performing nonlinear time history analyses. Verification of the numerical model using the obtained experimental results,
v. Experimental investigations on the feasibility of a low-damage fully-floating (pendulum) ceiling for seismic applications and use of perimeter isolation material through full scale shake table tests,
vi. Experimental evaluation of the out-of-plane performance of an existing low-damage drywall partition system and its compatibility with existing suspended ceilings in a series of shake table tests,
vii. Recommendations for improving the existing design practice incorporating the findings from this research.

The objectives were investigated throughout different chapters of this thesis. The main findings and conclusions drawn from these investigations are presented in this chapter, along with the statement of limitations and potential areas for future research.

9.1 Main Findings

9.1.1 *Component-based seismic fragility of suspended ceilings*

A thorough review of current standards and guidelines for the design and installation of suspended ceilings was carried out in this thesis along with a summary of common ceiling damage types in recent earthquakes. Using the experiments carried out by Paganotti et al.

(2011) on typical NZ suspended ceilings, component fragility curves were reviewed and reinterpreted to develop system level fragility functions. Among the suspended ceiling system components tested in Paganotti's study, single rivet end-fixtures and cross tee – main tee connections were the most critical elements of the ceilings, and governed the system capacity. With the fragility curves corresponding to these components, the overall fragility of the ceiling system was derived based on the assumption of linear accumulation of seismic force in ceiling components. These fragility studies led to the following conclusions:

- The simple analytical method employing component fragility functions proposed for the analysis of perimeter-fixed suspended ceilings was found effective.
- The comparison between the analytical fragility curves proposed for the perimeter-fixed ceilings in this study with experimental fragility curves derived by other researchers (Badillo-Almaraz, 2007; Ryu, 2013) showed that the proposed method is relatively conservative in estimating the fragility of the system but can be used as an initial estimation of the probability of failure at a given acceleration intensity.
- The linear relationship between the peak grid acceleration, the length of the grid members and the overall seismic mass in conjunction with the system fragility curves was demonstrated as an initial design method for perimeter-fixed ceilings.
- Design examples were provided utilizing the proposed method for ceilings at different elevations of a structure showing different probabilities of failure for ceilings with different areas and weights.

9.1.2 *Experimental investigations on the seismic performance of perimeter-fixed ceilings*

Preparation, execution and preliminary results of a series of shake table tests on two perimeter-fixed suspended ceiling specimens were presented in this section of the research. The ceilings were perimeter-fixed type using the common fix-and-float installation method constructed in accordance with the typical NZ practice and designed for areas of high seismic risk. Using the recorded responses of the ceilings under a range of applied motions on a shake table, the relationship between the applied acceleration and the force induced in the ceiling grid members and connections was quantified, followed by discussions on the effect of grid members' layout and end-fixings on the overall performance of the suspended ceilings.

Based on the results and observations in this section:

- The linear correlation between grid axial forces and grid accelerations appeared to be reasonable and conservative (hence acceptable for design purposes).
- Lower axial forces were obtained in experiments compared to the expected analytical values -based on the linear correlation. This was considered to result from the initial assumptions made about the tributary areas for the mass and the constant acceleration along the entire grids.
- The boundary conditions and connections on the transverse grids were observed to affect the distribution of tributary area mass and consequent axial forces in longitudinal grids. For instance, use of clips on the free end of grids increased the stiffness and contribution of boundary connections to the load carried.
- The grid accelerations were observed to vary along the grid lengths in the direction of excitation.
- The amplification of the input acceleration in different locations of the system appeared to depend on the frequency and amplitude of excitation as well as the inherent flexibility of the specimen.
- The level of amplification in floor acceleration as it is transferred to the ceiling grids was observed to be greater than the factor recommended by the NZ Earthquake Loading Standard NZS 1170.5:2004 and in some cases this amplification was more significant than previously thought.
- Upon the application of low-pass filtering to the recorded acceleration outputs, it was observed that these amplification factors were consistently reduced and remained below the code recommended factor. The filtering eliminated the high frequency contents in the acceleration and axial force time histories which were assumed to have resulted from the impact between ceiling tiles and grids and vertical excitations due to the flexibility of the specimens.
- These high frequency large amplifications which occurred at short periods of time were considered a small concern for the overall design, especially when considered with the overestimation of axial forces predicted.
- The series of experiments concluded with one-off damage observed in one of the cross tee - main tee connections that could potentially lead to tile dislodgement. The axial force recorded on the grid at the instance of this damage was similar to the capacity obtained through previous experiments (Chapter 2 of this thesis) for that type of connection.

9.1.3 *Effect of seismic clips on the performance of ceiling grid joints*

According to the experiments carried out by Paganotti et al. (2011), and as discussed in Chapter 2 of this thesis, the weakest components of a perimeter-fixed suspended ceiling were the cross tee – main tee (CT-MT) connections and rivet fixtures around the perimeters of the ceiling grids. Considering the overall capacity of the ceiling system, any strengthening solution must take into account the effect of all contributing elements. In a perimeter-fixed ceiling, although the rivet fixtures can be strengthened by increasing the rivet size, the CT-MT connections remain the weakest element in the seismic load path of suspended ceiling systems. To investigate the possibility of improving this weakness, monotonic tension compression experiments were carried out on specimens of CT – MT connections with the following configurations; i) the connection used in as-built practice, and ii) the connection with an added cross-shaped seismic clip. During the tests, different failure modes were observed in the connection area and force-displacement relationships were derived for both configurations. Based on these experiments:

- Using seismic clips improved CT-MT connection performance in two ways: i) increasing the maximum and residual load bearing capacity, and ii) adding ductility.
- Comparisons in tension and compression tests showed that using seismic clips in all cases increased the failure force in the connection.
- When seismic clips were added, initial failure always occurred in the CT clip, followed by larger deformations and buckling in the seismic clips.
- With the addition of seismic clips, the connection's failure mode was no longer brittle. The connection with seismic clips experienced a number of failure and yielding phases while still carrying forces as large as that of the as-built CT-MT joint.
- This ductility together with substantial residual load carrying capacity in the grid system could delay the spread of damage and allow for the safe evacuation of occupants while still showing signs of damage.
- To transfer this component level gain to the performance of the whole suspended ceiling system, use of these 4-way seismic clips must be accompanied by strengthening other critical components of the ceiling such as the splices on MTs and increasing the size or number of end fixing rivets.

9.1.4 *Experimental evaluation of fully-floating ceilings as a low-damage solution*

Some of the common incidents of damage in ceilings were identified in previous seismic

events to be caused by relative displacements between rigid objects surrounding suspended ceilings and inertial forces induced by the acceleration transferred through the structure to the grid members. Inspired by this observation, the main objective of this phase of the study was set to investigate the possibility and practicality of a ceiling system which was isolated from the surrounding structure or had flexible connections with it. A novel pendulum-type fully-floating ceiling system with and without an isolation layer around the perimeter was tested on a shake table using sinusoidal and earthquake induced ground motions.

Based on the results of these experiments:

- The recorded response of the tested fully-floating ceiling was consistent with the simple pendulum theory; including (i) independence of the natural frequency of the system and its peak displacement to its mass, and (ii) resonance induced large displacements at input frequencies close to the natural frequency of the ceiling.
- Changing the number and arrangement of the vertical hanger wires did not affect the natural frequency of the fully-floating ceiling or the ceiling peak displacement. However, a more spread-out layout of hangers covering perimeters rather than center of the ceiling reduced the displacement perpendicular to the direction of excitation resulting in a linear motion pattern.
- The addition of perimeter isolation elastic material was found effective in inducing extra damping and protecting the ceiling from pounding impact; resulting in much reduced ceiling displacements and accelerations. Overall, a 100-mm thick isolation foam was found enough to safeguard the floating ceiling from any untoward effects causing any noticeable damage.
- The only form of damage observed throughout ground motion and sinusoidal tests was panel dislodgement at the successive pounding incident.
- The panel failure was assumed to be caused by large ceiling accelerations due to impact combined with the vertical movement of the untied/loose tiles due to significant vertical acceleration induced. No grid failure occurred in these experiments.
- Based on these observations it was concluded that with sufficient gaps provided between the ceiling and rigid objects i.e. walls, services, columns etc. the use of isolated fully-floating ceiling could be practical.

9.1.5 *Compatibility between low-damage drywall partitions and common suspended ceilings*

Two series of full-scale unidirectional shake table tests were conducted on combined suspended ceiling – low damage drywall systems. The first suspended ceiling was back-braced to the structure above with horizontal gaps placed between the free ends of ceiling grids and vertical wall supports. The second ceiling - referred to as perimeter-fixed - was restrained laterally by connecting to the drywalls on two adjacent sides while being free to move on the opposite sides. The low-damage drywall system proposed in a previous study by Tasligedik (2014), was designed to tilt during out-of-plane story deformations, and slide at the top and bottom during in-plane deformations, thereby avoiding damage. The shake table tests were planned to investigate the in-plane and out-of-plane performance of the low-damage drywall partitions, as well as the displacement compatibility between these walls and the two types of suspended ceilings.

- In the braced ceiling experiment, where no connection is made between ceiling grid ends and surrounding walls, inter-story drifts up to 1.35% were achieved with no damage in the grid system or partitions.
- During these experiments, it was found that the braced-back ceiling did not touch the low-damage drywall during small earthquake excitations. However, for larger excitations impact occurred between the grid ends and supporting wall structure, causing large ceiling accelerations but no further damage.
- These large displacements were concluded to be due to the slackness of sway wire braces and the inherent flexibility of this bracing solution. Thorough evaluation of the required gap between grid ends or use of damping/isolation gap filling material was recommended.
- Grid spreading at the ceiling boundary caused some tile dislodgement at high drift values on the corners of the back-braced ceiling.
- The use of ceiling grid end framing elements was proposed to address the grid spreading and tile dislodgement issues. These perimeter angles were proposed to be riveted only to grid ends while maintaining a sufficient clearance from the walls.
- The perimeter-fixed ceiling showed no damage in the ceiling system or the drywalls up to the drift levels achieved during these unidirectional tests.

- The tested perimeter-fixed ceiling appeared to have enough flexibility to accommodate the relative displacement between two perpendicular walls up to the inter-story drifts achieved.
- It was concluded that the low-damage drywall partition was compatible with both the perimeter-fixed ceiling and the back-braced ceiling tested, provided that grid spreading is prevented, and that a clash avoidance space be placed between adjacent wallboards for horizontal shaking at different angles.

9.1.6 *Numerical modelling of perimeter-fixed ceilings*

Numerical models of the perimeter-fixed ceilings tested in this research were developed in the finite element analysis program SAP2000. The primary objective of this simulation was to develop a simple model to replicate the experimental results with an acceptable level of accuracy. Such a model could be used for system level investigation of the seismic performance of suspended ceilings of different configurations for a given floor acceleration time history.

Two types of models were developed in the numerical modelling section:

i. Model of the steel test frame and ceiling specimen excluding the interaction between ceiling grids and tiles
ii. Model of a grid and tile assembly to simulate the effect of pounding between tiles and grids

The following conclusions were drawn based on these simulations:

- The general trend of results obtained from the frame and ceiling model showed a reasonable compatibility with the experimental results and the model was very practical to develop and to analyze.
- The discrepancies were concentrated in the high frequency peaks. These high frequency peaks were assumed to be caused partly by electronic noise from the testing machine and partly by the impact between grids and tiles.
- Low pass filtering was applied to experimental output time histories and experimental shake table accelerations used as input for numerical analyses, to eliminate the effect of high frequency content. The two levels of filtering (i.e. 18 Hz and 25 Hz) appeared to be effective in removing the scatter in the results and some of the spikes.
- The accelerations obtained in the ceiling grids in this model were generally lower than the experimental results on the same joints.

- The model overestimated the peak axial forces in the ceiling grids when compared with experimental results. This was concluded to also result from the initial assumptions made about the tributary areas and constant accelerations along the grids.
- The model of the ceiling grid and tiles showed a reasonable agreement between the experimental and numerical acceleration time histories excluding the peaks.
- The model showed the effect of impact at the closure of gaps defined between tiles and grids elements, through high frequency spikes in the acceleration and axial force response histories. However, due to the simplifying assumptions made regarding the stiffness of the gap elements and the actual frictions between grids, tiles and hanger wires, the numerical peaks could not be verified with the experimental results.

9.2 Recommendations for Future Research

The following sections list the potential areas for future research which could not be covered in this study due to limits of time, resources and scope.

9.2.1 *Effect of seismic clips*

In this research, monotonic tests showed the effectiveness of seismic clips on the load-bearing capacity and ductility of a cross tee – main tee joints. However, it was also pointed out that this joint improvement must be accompanied by strengthening the splices on main tees and increasing the size or the number of end fixing rivets. The possibility of strengthening main tees splices using 2-way seismic separation clips needs to be further investigated through experiments.

As one of the failure modes recorded in tension tests was tearing in the CT web, it is recommended that similar investigations be conducted on the effects of seismic clips on heavy-duty grids.

Finally, the effect of these clips on the overall performance of the suspended ceilings needs to be investigated in a full-scale ceiling specimen under bidirectional dynamic loads. This specially concerns the interpretation of joint ductility into system ductility, and its impact on other components of the ceiling such as tiles and services.

9.2.2 *The fully-floating ceiling*

Based on the experiments carried out, the fully-floating ceiling isolated with perimeter foam showed a satisfactory performance in excitations with floor accelerations matching (in some cases, exceeding) an ULS level event. Although the outcomes from this investigation are

promising and point towards viability of the fully floating ceilings as a low damage solution, more investigation is needed to confirm its ability to interact positively with surrounding structural and non-structural elements. Some of the areas that could be further investigated include

- Applying isolation material as tension – compression springs (as opposed to compression only in these experiments) by gluing the isolation material to the specimen as well as supports. This could potentially further reduce the acceleration amplification by eliminating the impact between the specimen and isolation material.
- Effect of various isolation materials with different stiffness and damping properties and their effect on the seismic response of the ceiling.
- Full-scale experiments on a suspended ceiling combined with services, luminaries, etc.

9.2.3 *Numerical modelling of perimeter-fixed ceiling*

The numerical analyses carried out in this research was verified with the experimental results available. The response simulated was relevant to that of a similar ceiling exposed to any floor acceleration used as input. However, in order for these analyses to be applicable to other ceiling configurations and types, the model needs to be verified with a more extensive set of earthquake data. The numerical modelling can be further investigated with ground and floor acceleration time histories in an instrumented building in a seismic event. This will be more productive if such information could be available for a building where post-earthquake ceiling damage data was recorded.

9.3 References

Badillo-Almaraz, H., Whittaker, A. S., & Reinhorn, A. M. (2007). Seismic fragility of suspended ceiling systems. *Earthquake Spectra*, *23*(1), 21-40.

Paganotti, G., MacRae, G. A., & Dhakal, R. P. (2011, April). Development of typical NZ ceiling system seismic fragilities. In *Ninth Pacific Conference on Earthquake Engineering (PCEE)* (pp. 14-16).

Ryu, K. P., Reinhorn, A. M., & Filiatrault, A. (2013). Capacity evaluation of suspended ceiling systems. *Technical Report MCEER-13-XXXX*.

Tasligedik, A. S. (2014). *Damage mitigation strategies for non-structural infill walls* (Doctral thesis, Civil and Natural Resources Engineering Department. University of Canterbury,

Christchurch/New Zealand), pp. 304.

APPENDIX A

RANDOM MOTIONS

10 ORIGINAL AND FILTERED GROUND MOTIONS USED IN EXPERIMENTS ON PERIMETER FIXED CEILING SPECIMENS

The time histories below are presented in either their unfiltered format (herein original) or after filtering for the purpose of the experiments (herein filtered).

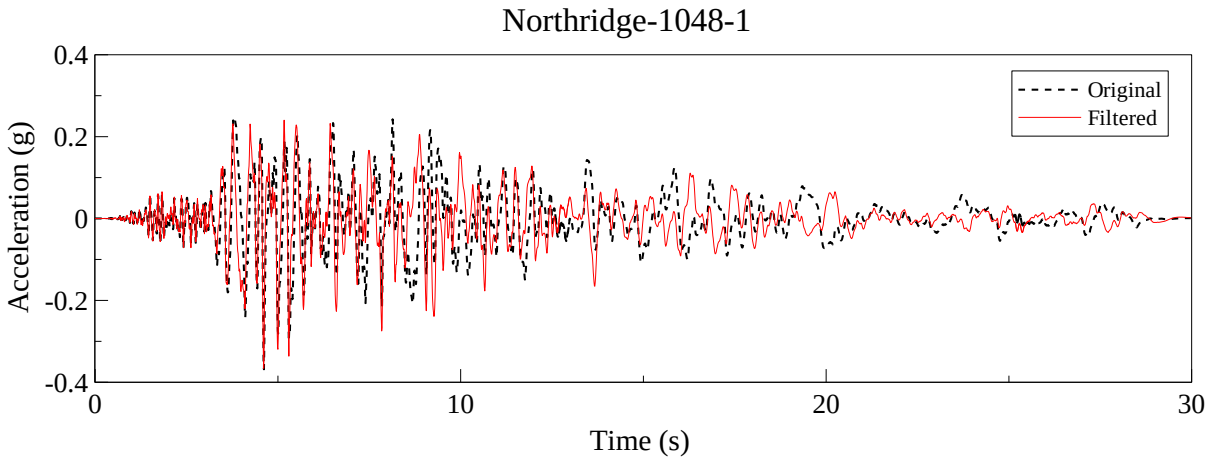

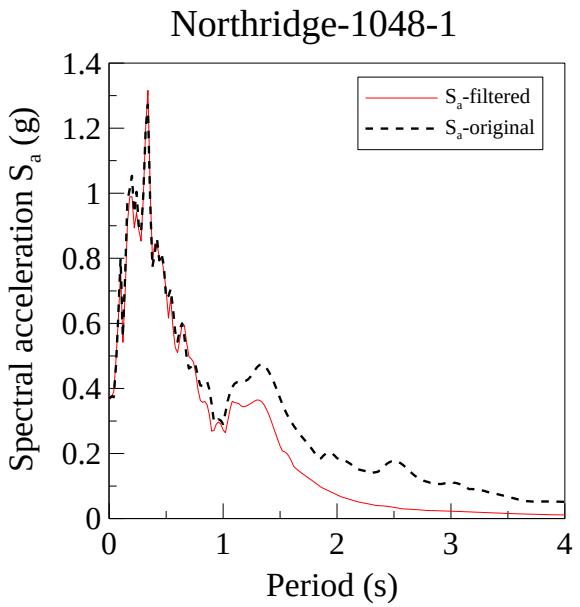

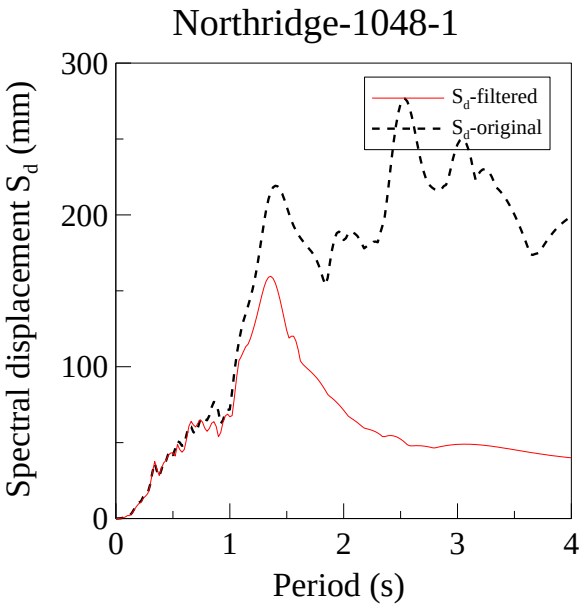

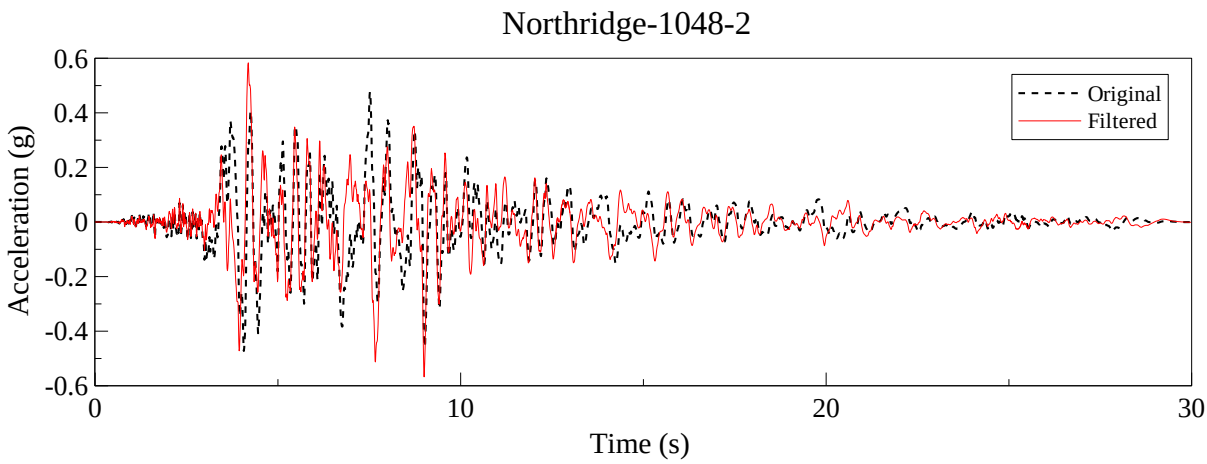
Northridge-1048-2
Acceleration (g)
Time (s)
Original
Filtered
0.6
0.4
0.2
0
-0.2
-0.4
-0.6
0
10
20
30

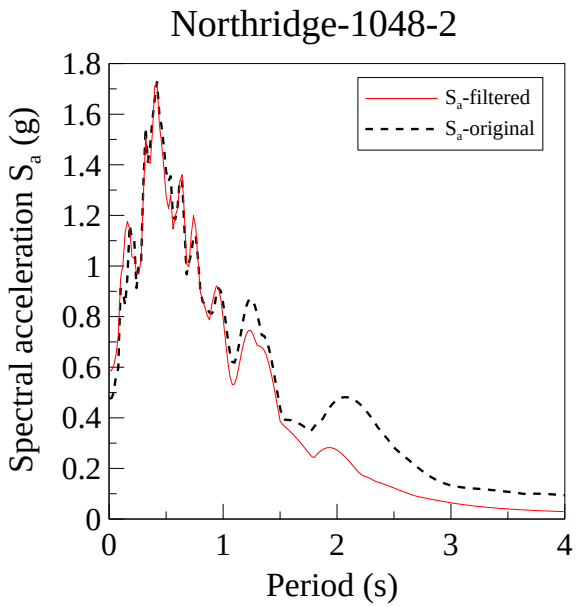
Northridge-1048-2
Spectral acceleration S_a (g)
Period (s)
S_a-filtered
S_a-original
1.8
1.6
1.4
1.2
1
0.8
0.6
0.4
0.2
0
0
1
2
3
4

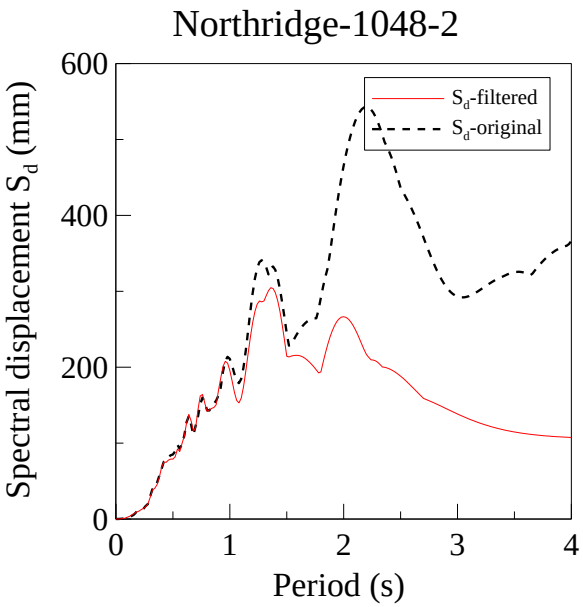
Northridge-1048-2
Spectral displacement S_d (mm)
Period (s)
S_d-filtered
S_d-original
600
400
200
0
0
1
2
3
4

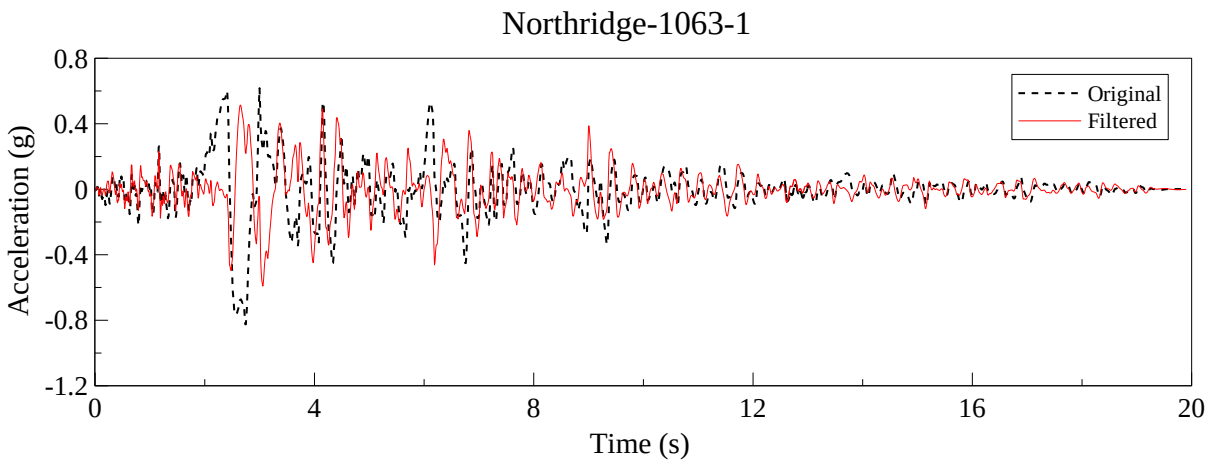
Northridge-1063-1
Original
Filtered
Acceleration (g)
Time (s)
0.8
0.4
0
-0.4
-0.8
-1.2
0
4
8
12
16
20

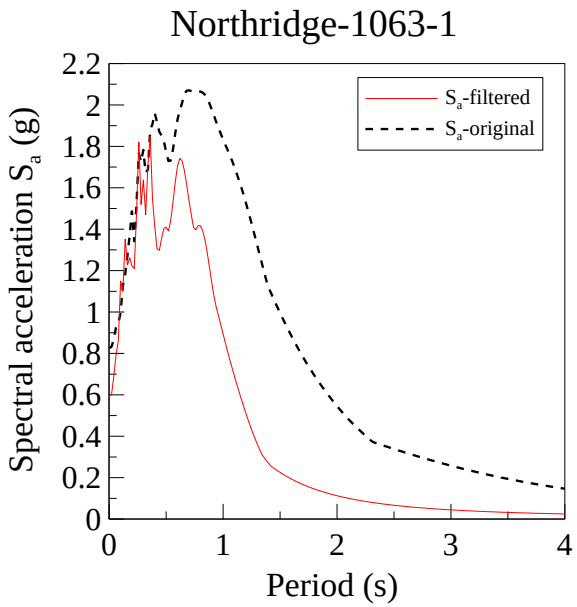
Northridge-1063-1
S$_a$-filtered
S$_a$-original
Spectral acceleration S$_a$ (g)
Period (s)
2.2
2
1.8
1.6
1.4
1.2
1
0.8
0.6
0.4
0.2
0
0
1
2
3
4

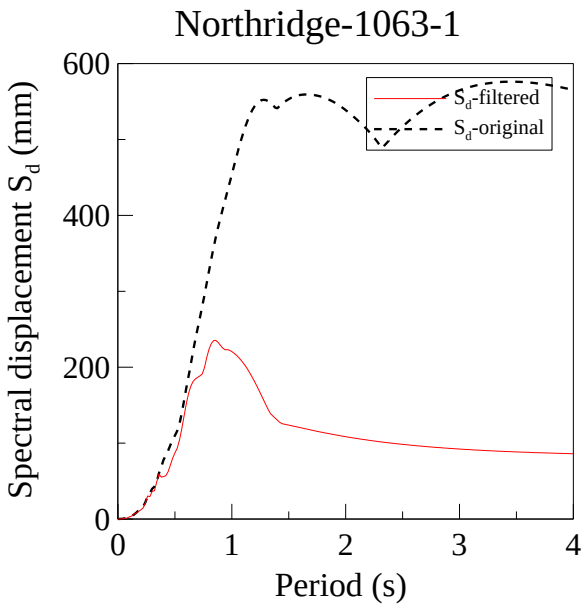
Northridge-1063-1
S$_d$-filtered
S$_d$-original
Spectral displacement S$_d$ (mm)
Period (s)
600
400
200
0
0
1
2
3
4

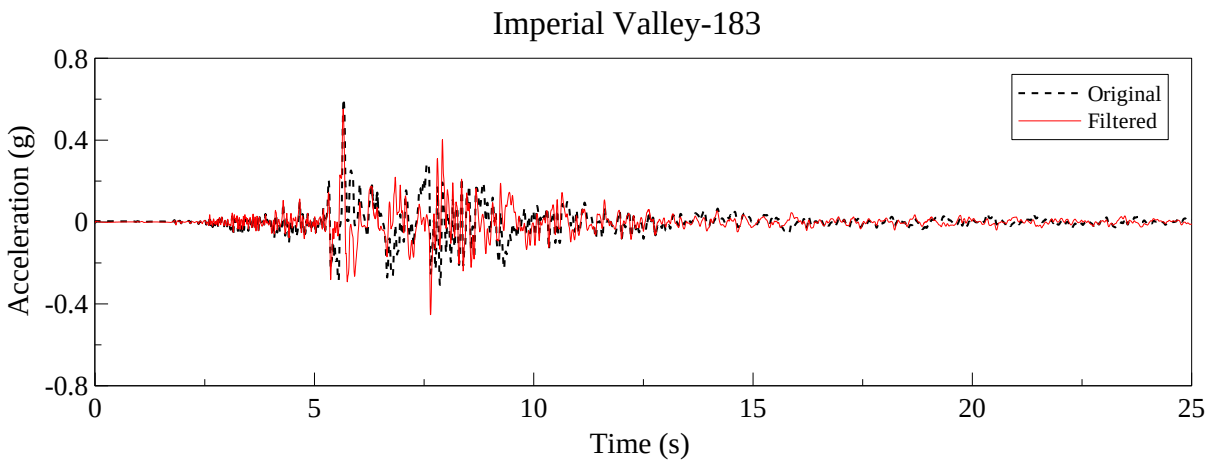
Imperial Valley-183
Original
Filtered
Acceleration (g)
Time (s)
0.8
0.4
0
-0.4
-0.8
0
5
10
15
20
25

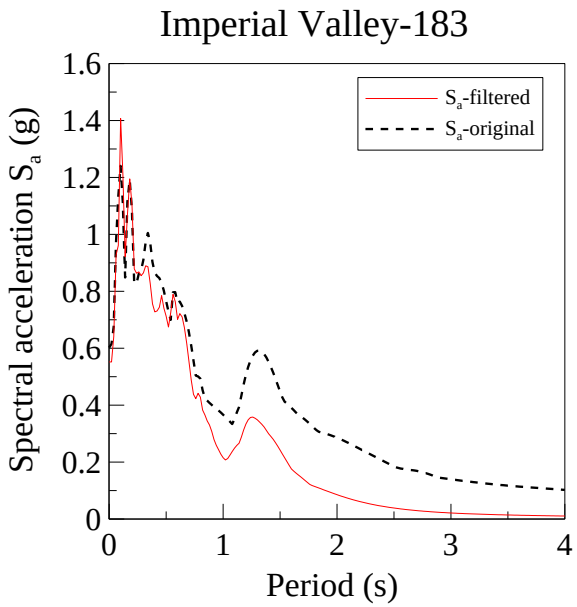
Imperial Valley-183
S$_a$-filtered
S$_a$-original
Spectral acceleration S$_a$ (g)
Period (s)
1.6
1.4
1.2
1
0.8
0.6
0.4
0.2
0
0
1
2
3
4

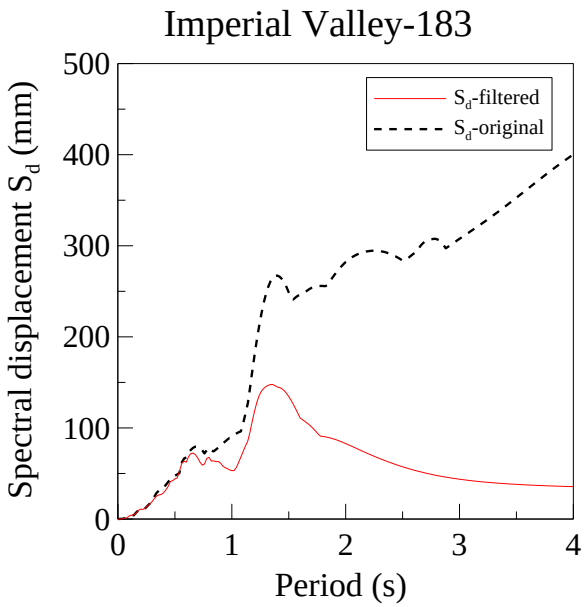
Imperial Valley-183
S$_d$-filtered
S$_d$-original
Spectral displacement S$_d$ (mm)
Period (s)
500
400
300
200
100
0
0
1
2
3
4

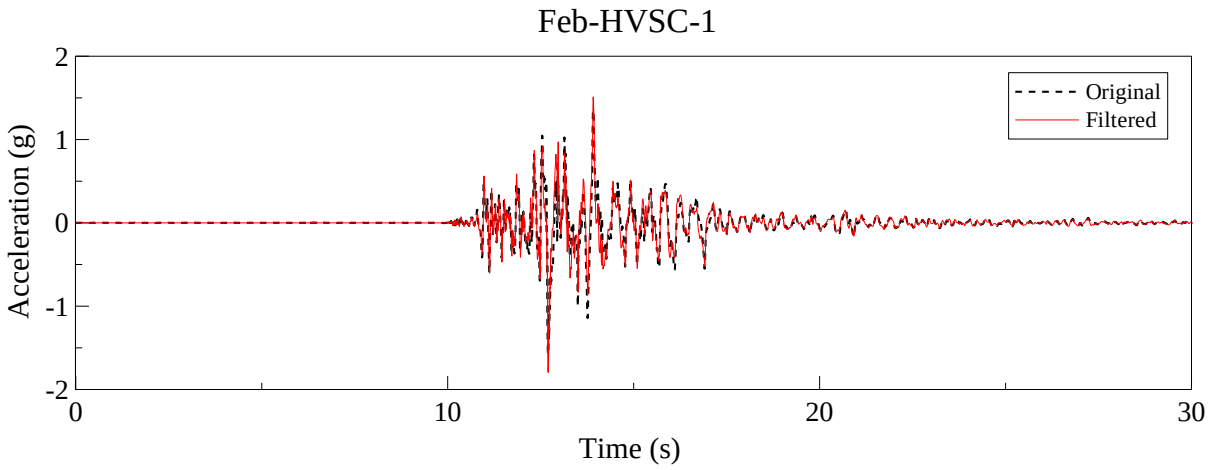
Feb-HVSC-1
Original
Filtered
Acceleration (g)
Time (s)

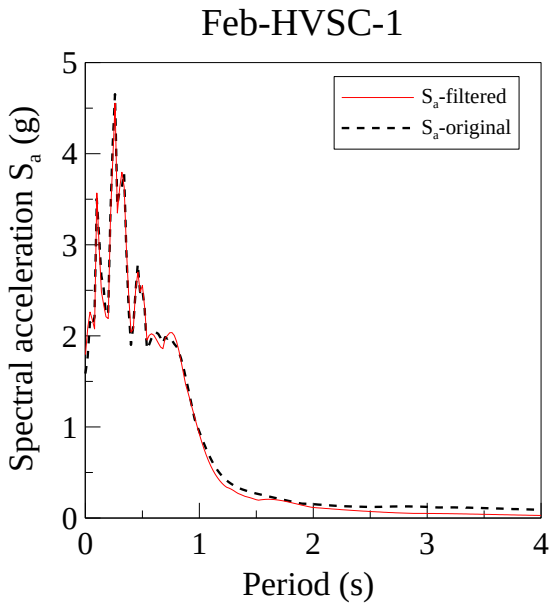
Feb-HVSC-1
S_a-filtered
S_a-original
Spectral acceleration S_a (g)
Period (s)

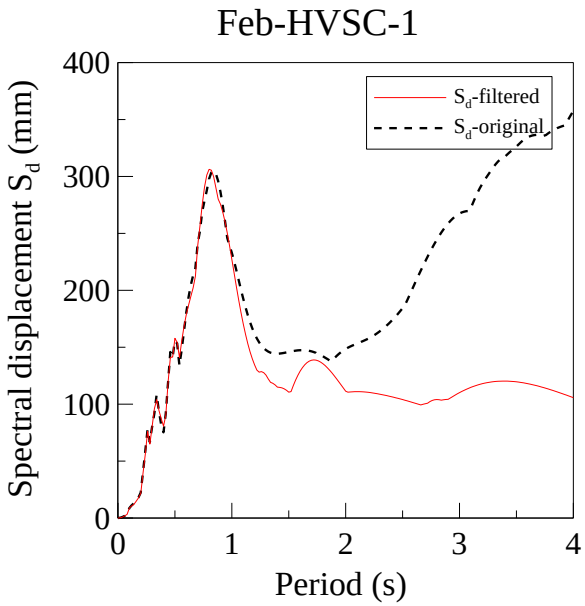
Feb-HVSC-1
S_d-filtered
S_d-original
Spectral displacement S_d (mm)
Period (s)

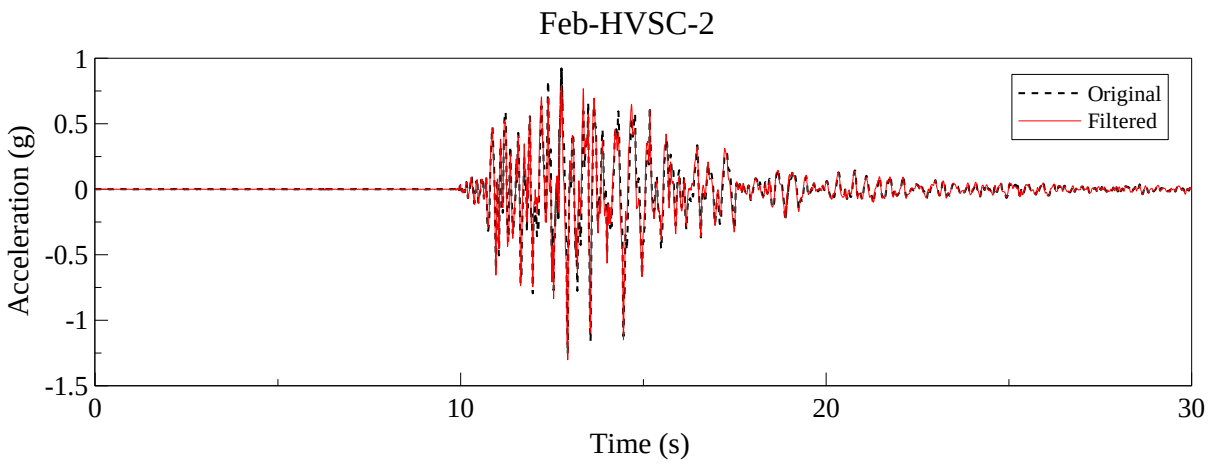
Feb-HVSC-2
Original
Filtered
Acceleration (g)
Time (s)
1
0.5
0
-0.5
-1
-1.5
0
10
20
30

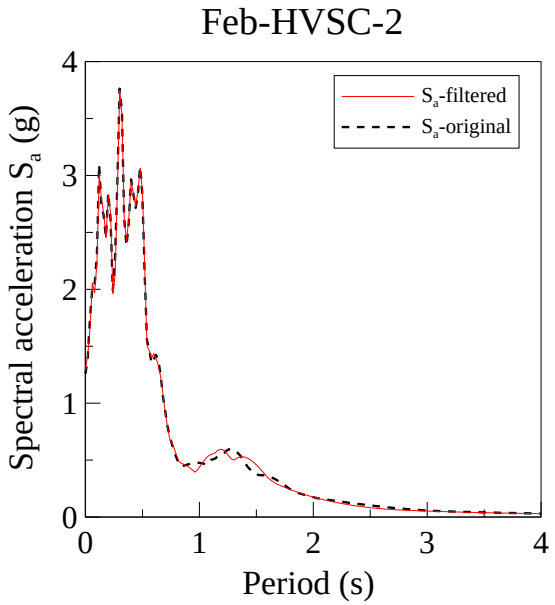
Feb-HVSC-2
S_a-filtered
S_a-original
Spectral acceleration S_a (g)
Period (s)
4
3
2
1
0
0
1
2
3
4

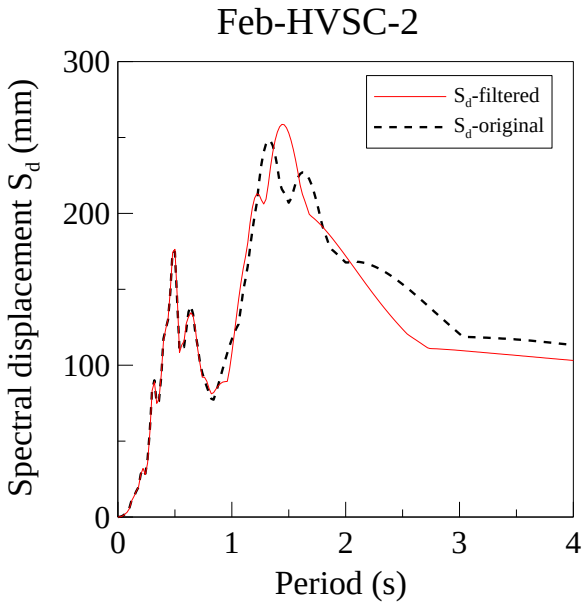
Feb-HVSC-2
S_d-filtered
S_d-original
Spectral displacement S_d (mm)
Period (s)
300
200
100
0
0
1
2
3
4

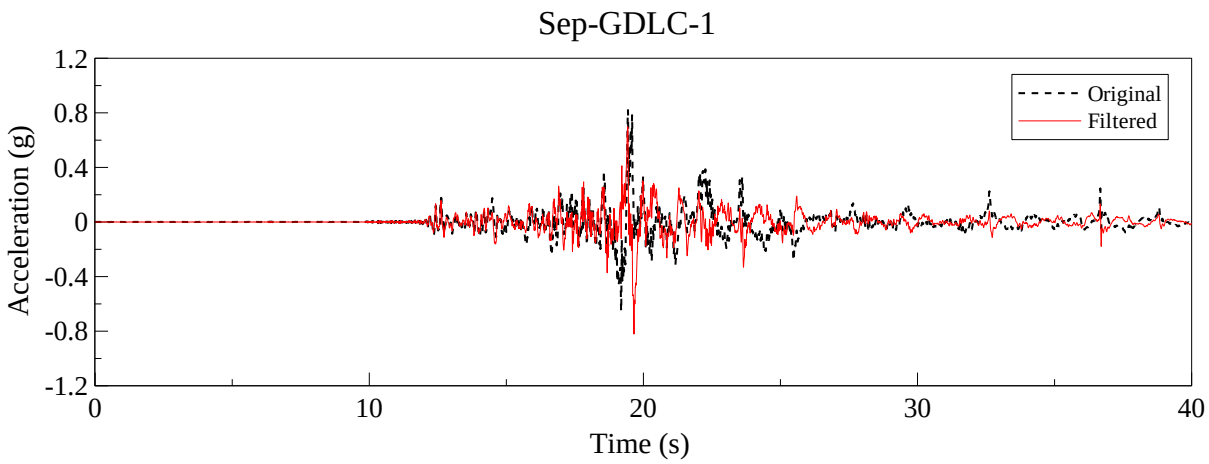
Sep-GDLC-1
Original
Filtered
Acceleration (g)
Time (s)
1.2
0.8
0.4
0
-0.4
-0.8
-1.2
0
10
20
30
40

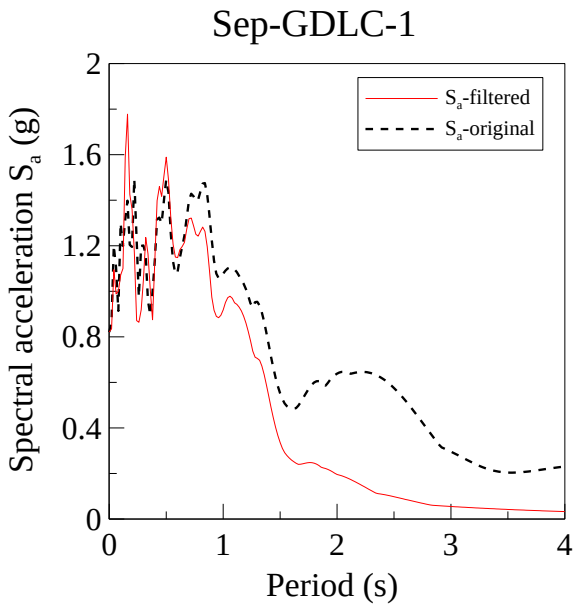
Sep-GDLC-1
S_a-filtered
S_a-original
Spectral acceleration S_a (g)
Period (s)
2
1.6
1.2
0.8
0.4
0
0
1
2
3
4

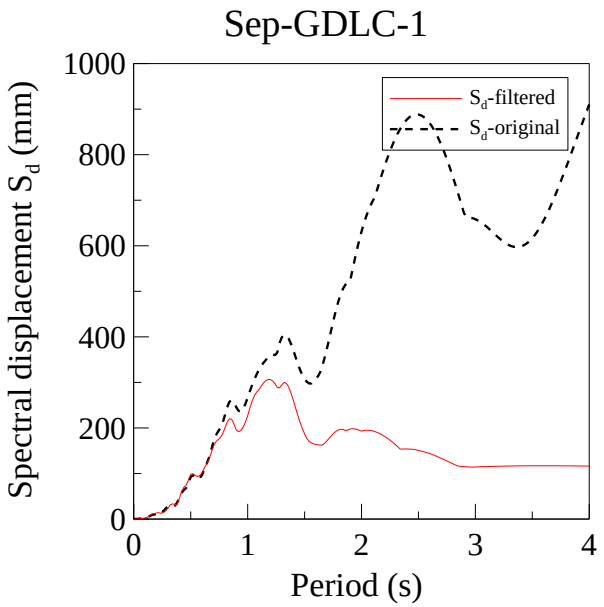
Sep-GDLC-1
S_d-filtered
S_d-original
Spectral displacement S_d (mm)
Period (s)
1000
800
600
400
200
0
0
1
2
3
4

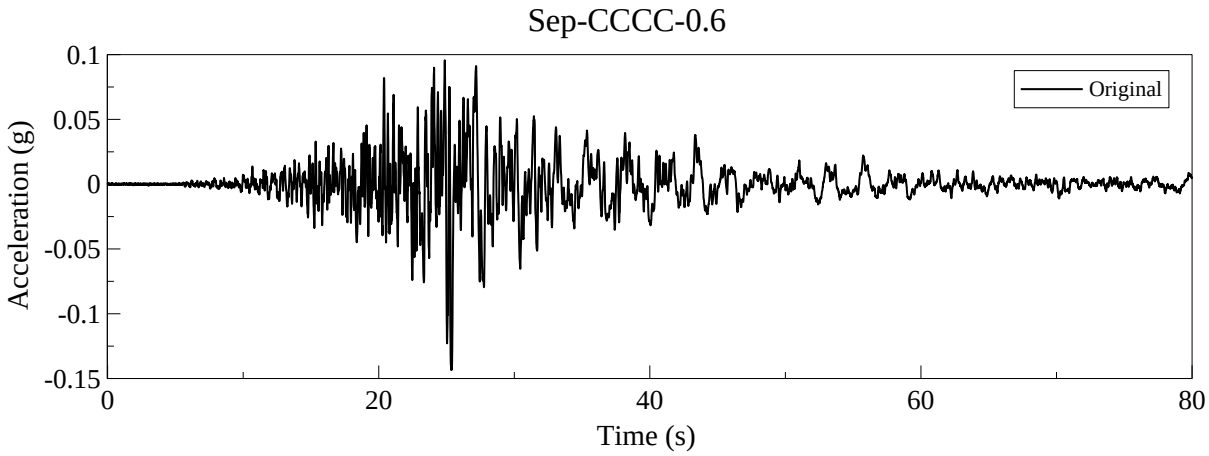
Sep-CCCC-0.6
Original
Acceleration (g)
0.1
0.05
0
-0.05
-0.1
-0.15
0
20
40
60
80
Time (s)

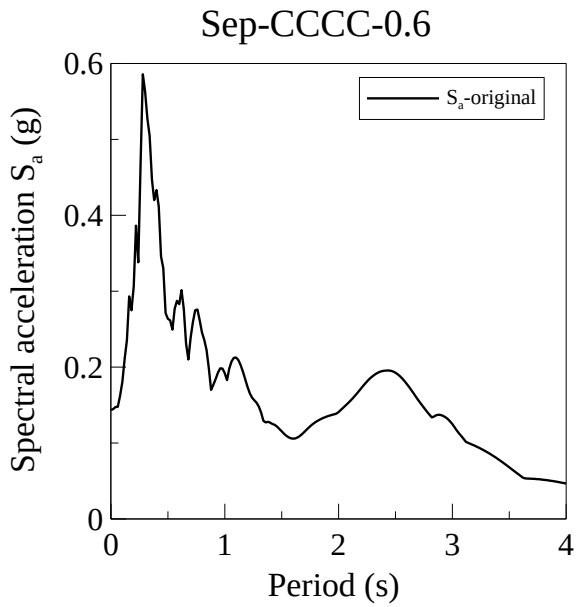
Sep-CCCC-0.6
S$_a$-original
Spectral acceleration S$_a$ (g)
0.6
0.4
0.2
0
0
1
2
3
4
Period (s)

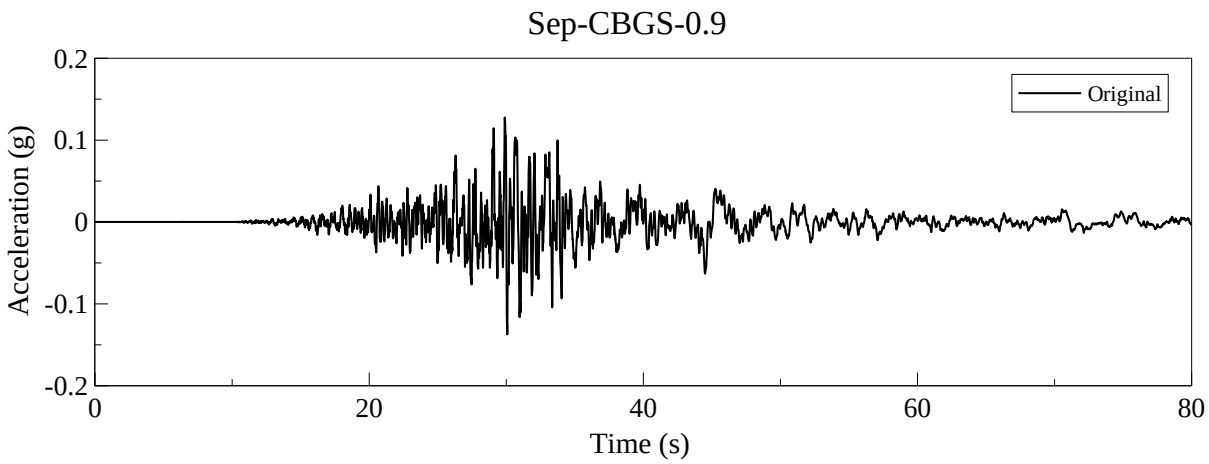
Sep-CBGS-0.9
Original
Acceleration (g)
Time (s)
0.2
0.1
0
-0.1
-0.2
0
20
40
60
80

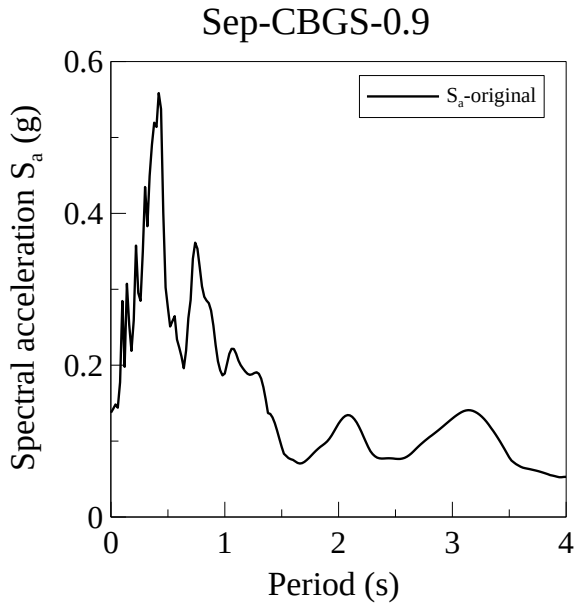
Sep-CBGS-0.9
Sa-original
Spectral acceleration Sa (g)
Period (s)
0.6
0.4
0.2
0
0
1
2
3
4

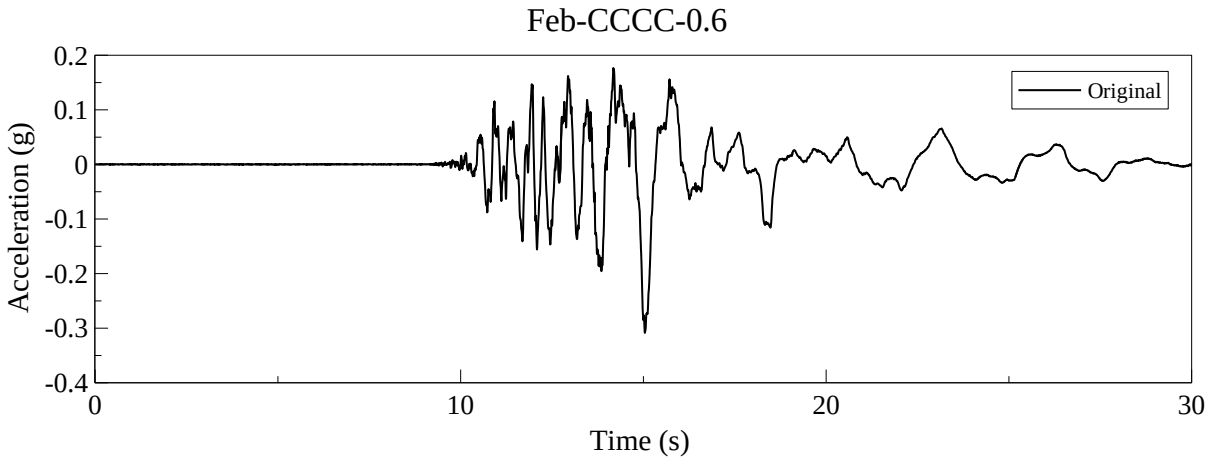
Feb-CCCC-0.6
Original
Acceleration (g)
Time (s)
0.2
0.1
0
-0.1
-0.2
-0.3
-0.4
0
10
20
30

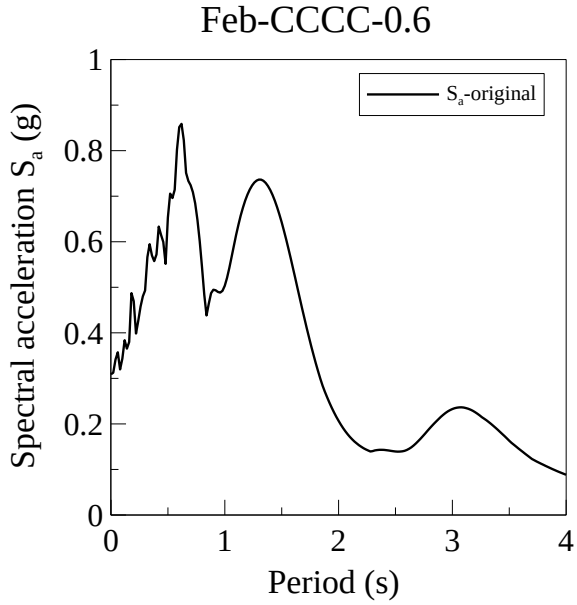
Feb-CCCC-0.6
S_a-original
Spectral acceleration S_a (g)
Period (s)
1
0.8
0.6
0.4
0.2
0
0
1
2
3
4

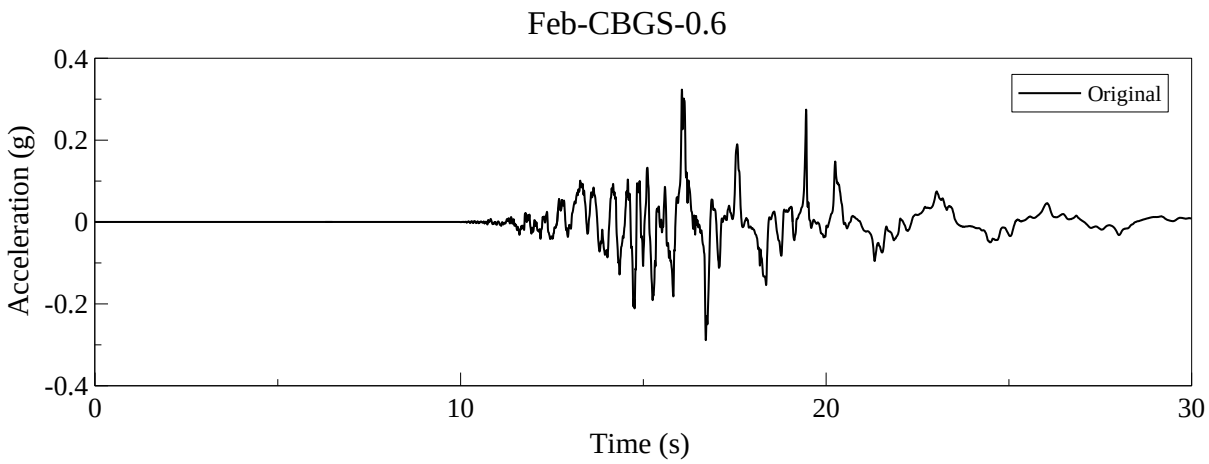
Feb-CBGS-0.6
Original
Acceleration (g)
Time (s)
0.4
0.2
0
-0.2
-0.4
0
10
20
30

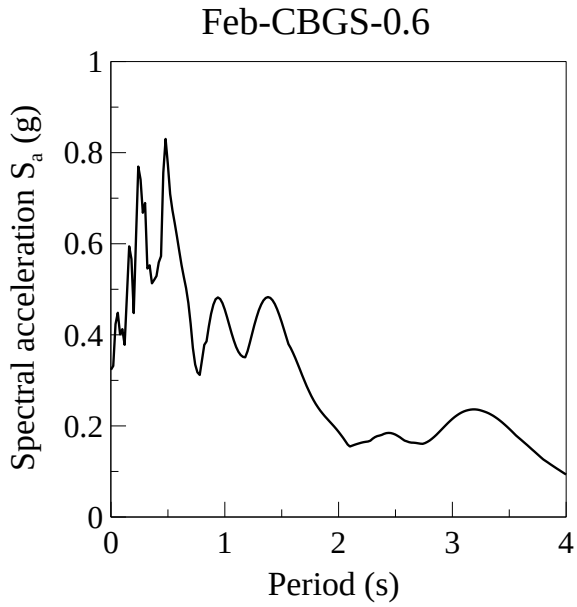
Feb-CBGS-0.6
Spectral acceleration S_a (g)
Period (s)
1
0.8
0.6
0.4
0.2
0
0
1
2
3
4

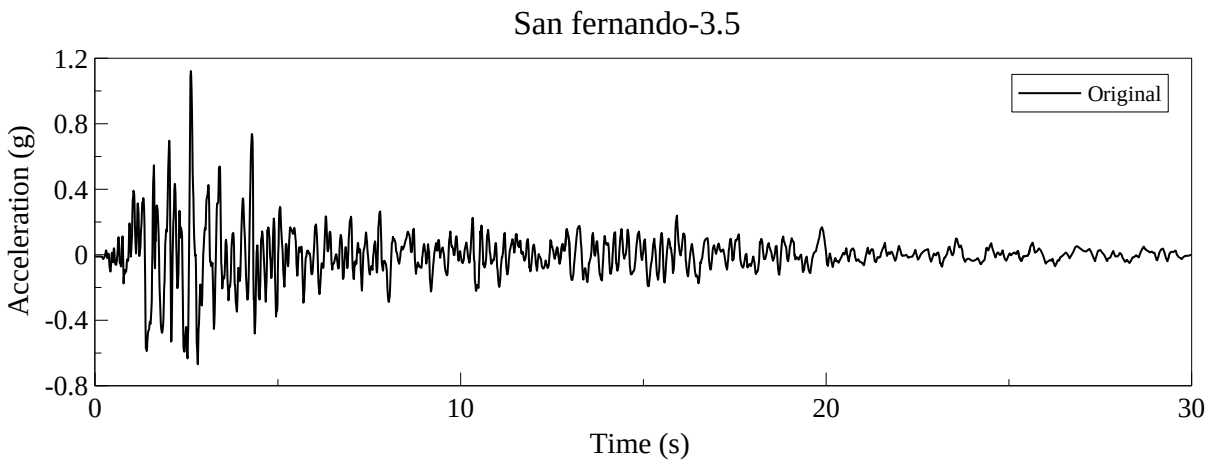
San fernando-3.5
Original
Acceleration (g)
Time (s)
1.2
0.8
0.4
0
-0.4
-0.8
0
10
20
30

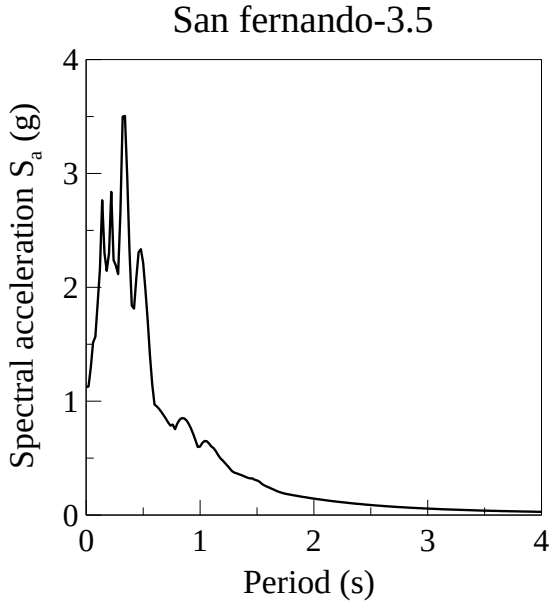
San fernando-3.5
Spectral acceleration S_a (g)
Period (s)
4
3
2
1
0
0
1
2
3
4

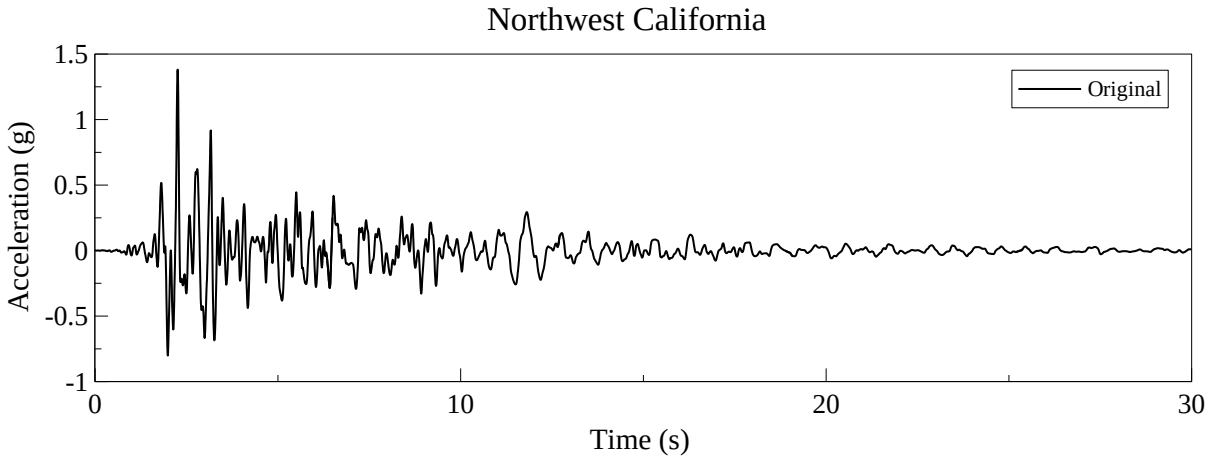
Northwest California
Original
Acceleration (g)
1.5
1
0.5
0
-0.5
-1
0
10
20
30
Time (s)

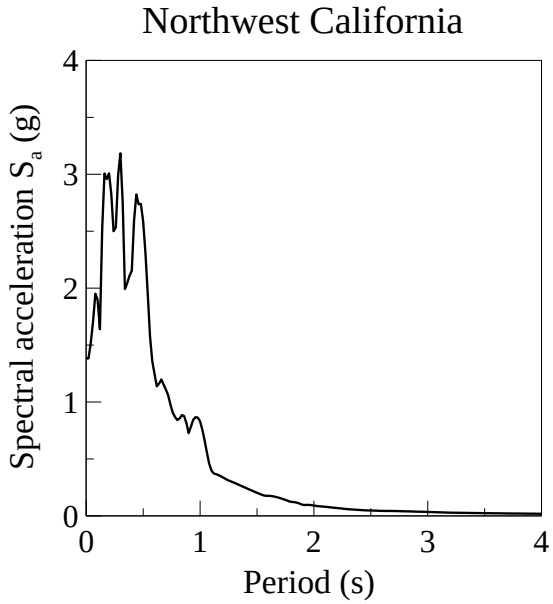
Northwest California
Spectral acceleration S_a (g)
4
3
2
1
0
0
1
2
3
4
Period (s)

APPENDIX B

INSTRUMENTATION

11 LIST AND LOCATION OF INSTRUMENTS ON SPECIMENS AND TEST FRAME

11.1 Test frame

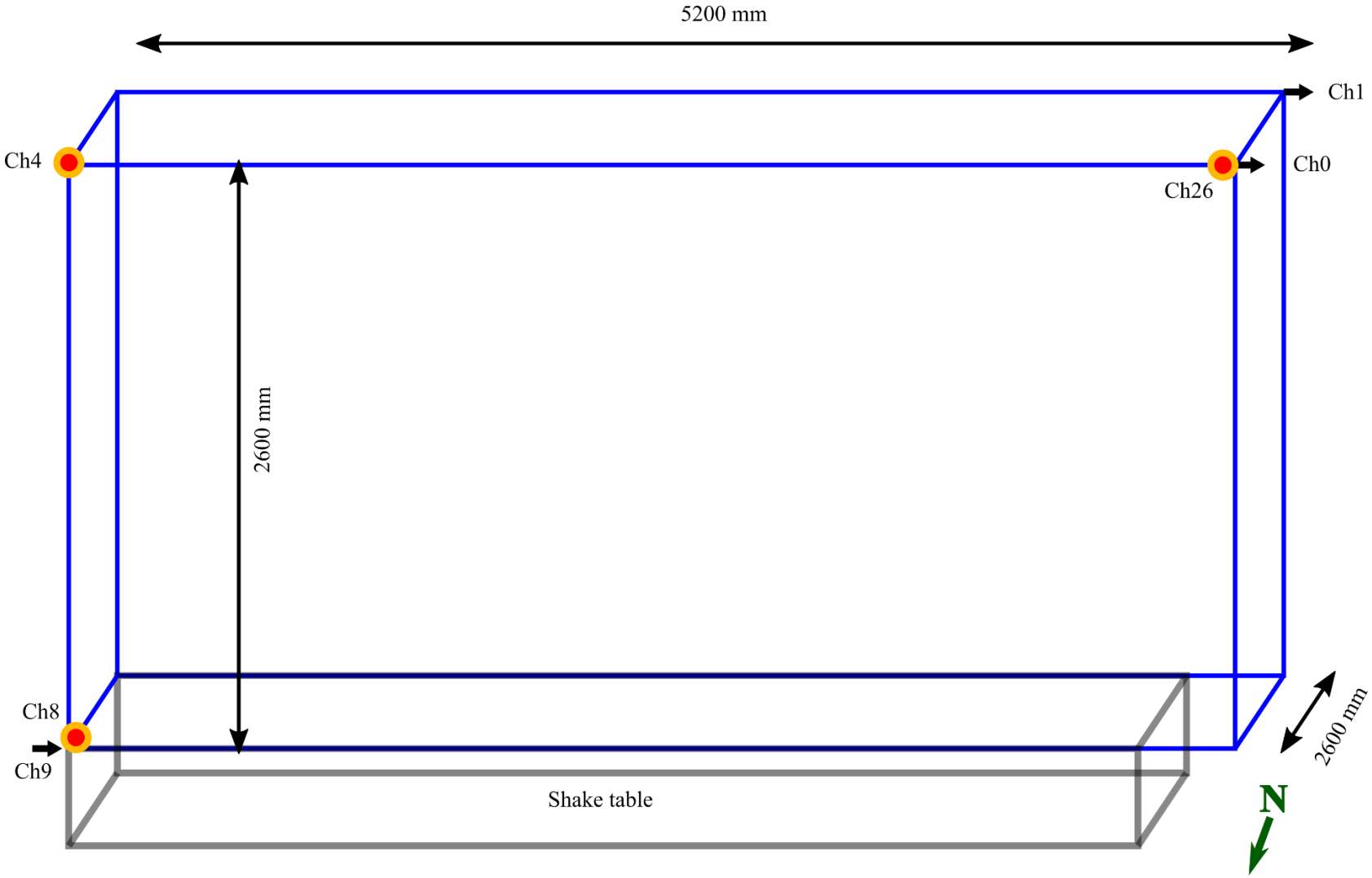

Table 5 – Instruments on test frame

Instrument ID	Instrument type	Direction
Ch0	Potentiometer	E-W
Ch1	Potentiometer	E-W
Ch4	Accelerometer	E-W
Ch8	Accelerometer	E-W
Ch9	Potentiometer	E-W
Ch26	Accelerometer	Vertical

11.2 Perimeter-fixed ceiling Pr-F-A

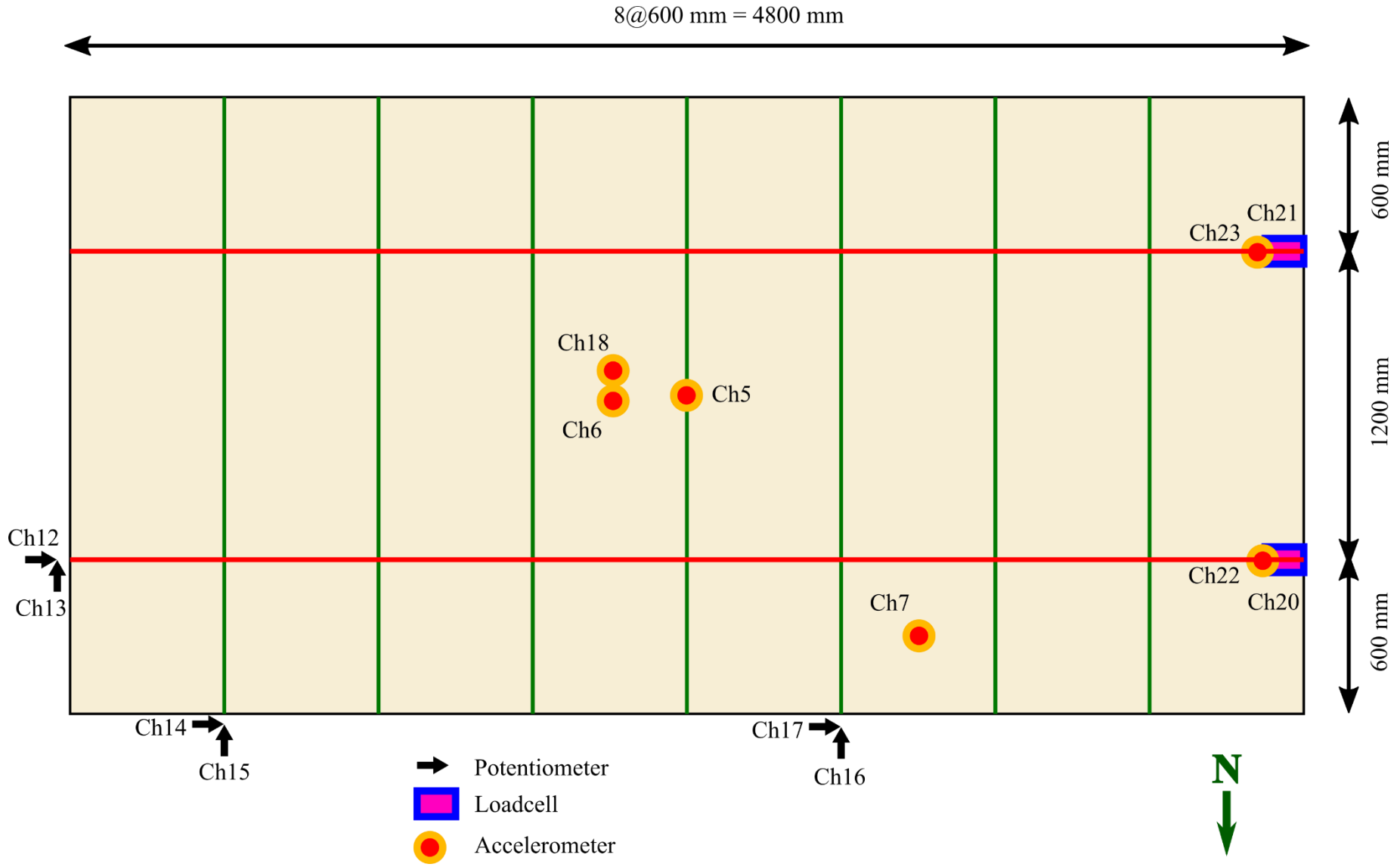

Table 6 – Instruments on Pr-F-A specimen

Instrument ID	Instrument type	Direction
Ch5	Accelerometer	E-W
Ch6	Accelerometer	E-W
Ch7	Accelerometer	E-W
Ch12	Potentiometer	E-W
Ch13	Potentiometer	N-S
Ch14	Potentiometer	E-W
Ch15	Potentiometer	N-S
Ch16	Potentiometer	N-S
Ch17	Potentiometer	E-W
Ch18	Accelerometer	Vertical
Ch20	Load cell	E-W
Ch21	Load cell	E-W
Ch22	Accelerometer	E-W
Ch23	Accelerometer	E-W

11.3 Perimeter-fixed ceiling Pr-F-B

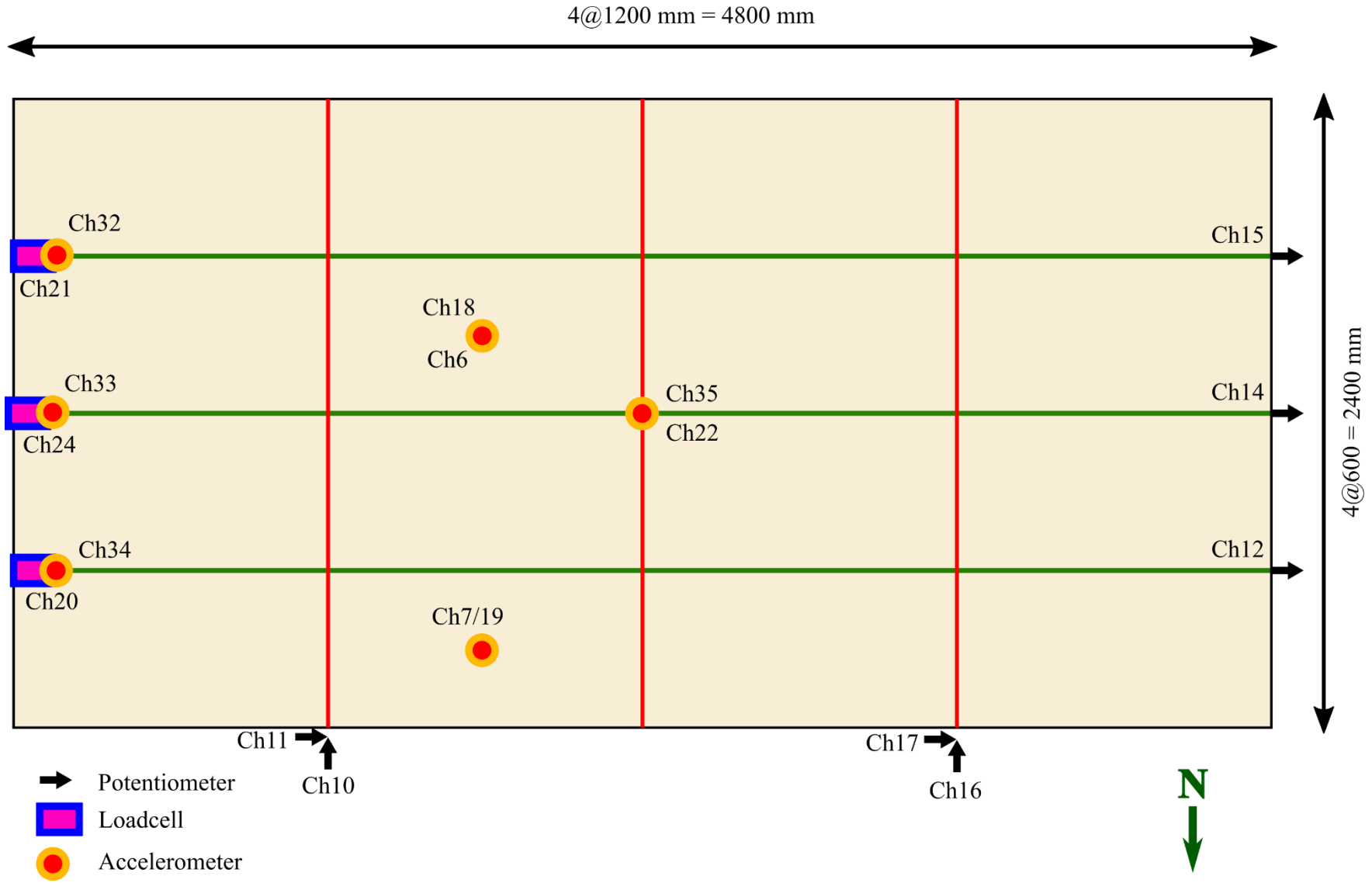

Table 7 – Instruments on Pr-F-B specimen

Instrument ID	Instrument type	Direction
Ch6	Accelerometer	E-W
Ch7	Accelerometer	E-W
Ch10	Potentiometer	N-S
Ch11	Potentiometer	E-W
Ch12	Potentiometer	E-W
Ch14	Potentiometer	E-W
Ch15	Potentiometer	E-W
Ch16	Potentiometer	N-S
Ch17	Potentiometer	E-W
Ch18	Accelerometer	Vertical
Ch19	Accelerometer	E-W
Ch20	Load cell	E-W
Ch21	Load cell	E-W
Ch22	Accelerometer	E-W
Ch24	Load cell	E-W
Ch32	Accelerometer	E-W
Ch33	Accelerometer	E-W
Ch34	Accelerometer	E-W
Ch35	Accelerometer	Vertical

11.4 Fully-floating ceiling

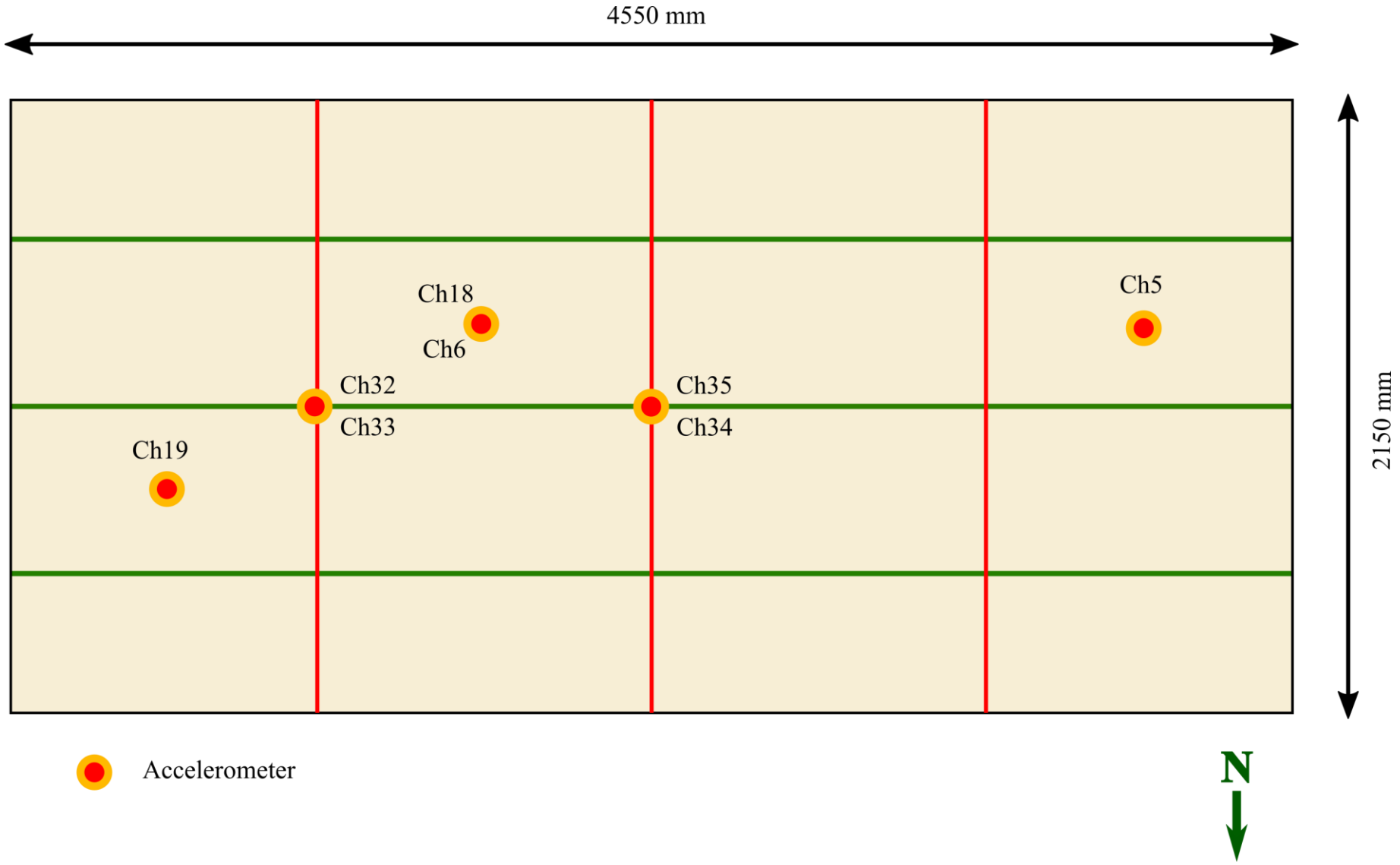

Table 8 – Instruments on fully-floating ceiling specimen

Instrument ID	Instrument type	Direction
Ch5	Accelerometer	E-W
Ch6	Accelerometer	E-W
Ch18	Accelerometer	Vertical
Ch19	Accelerometer	Vertical
Ch32	Accelerometer	N-S
Ch33	Accelerometer	E-W
Ch34	Accelerometer	Vertical
Ch35	Accelerometer	E-W

11.5 Low-damage drywall

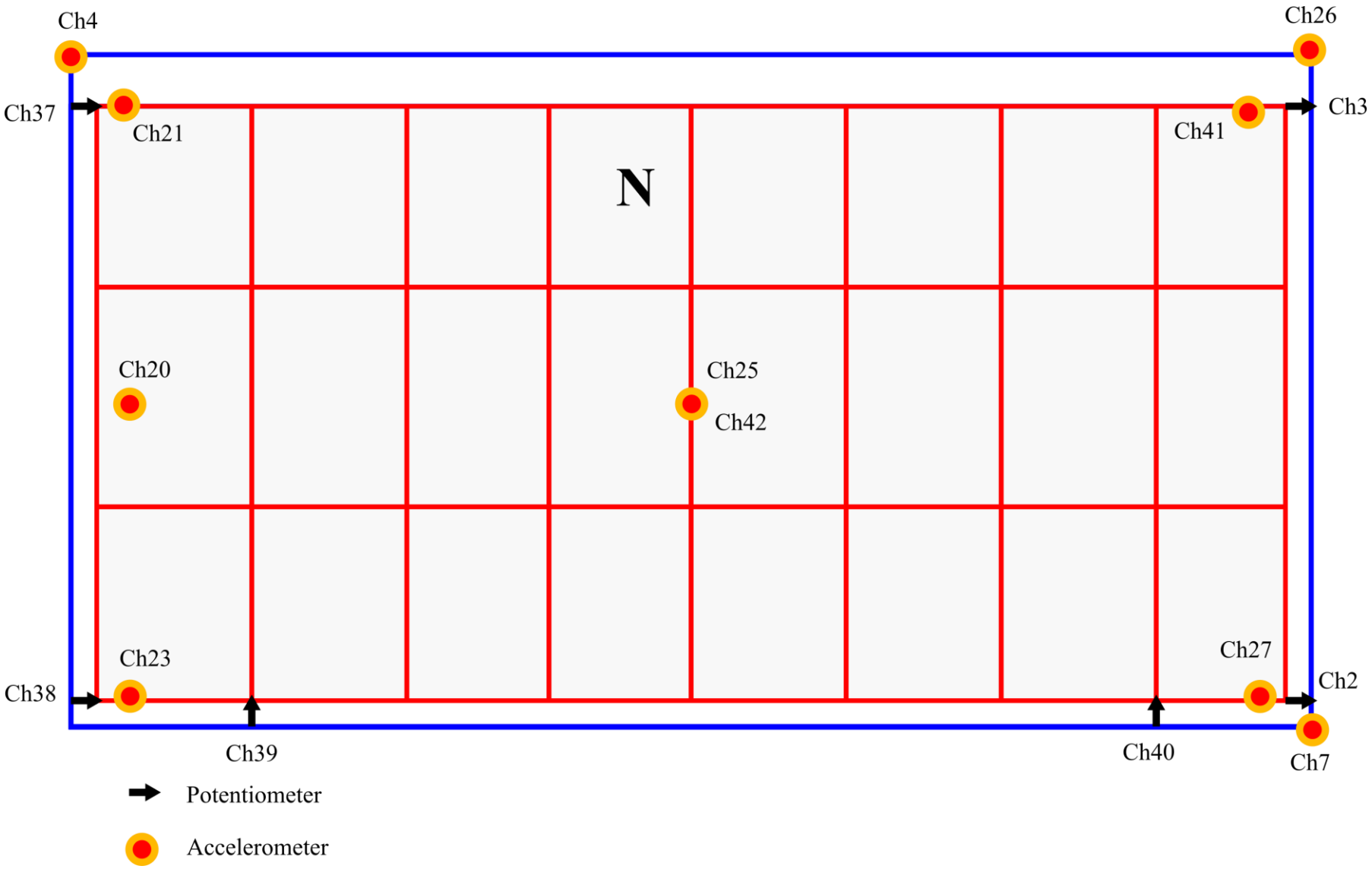

11.6 Braced ceiling

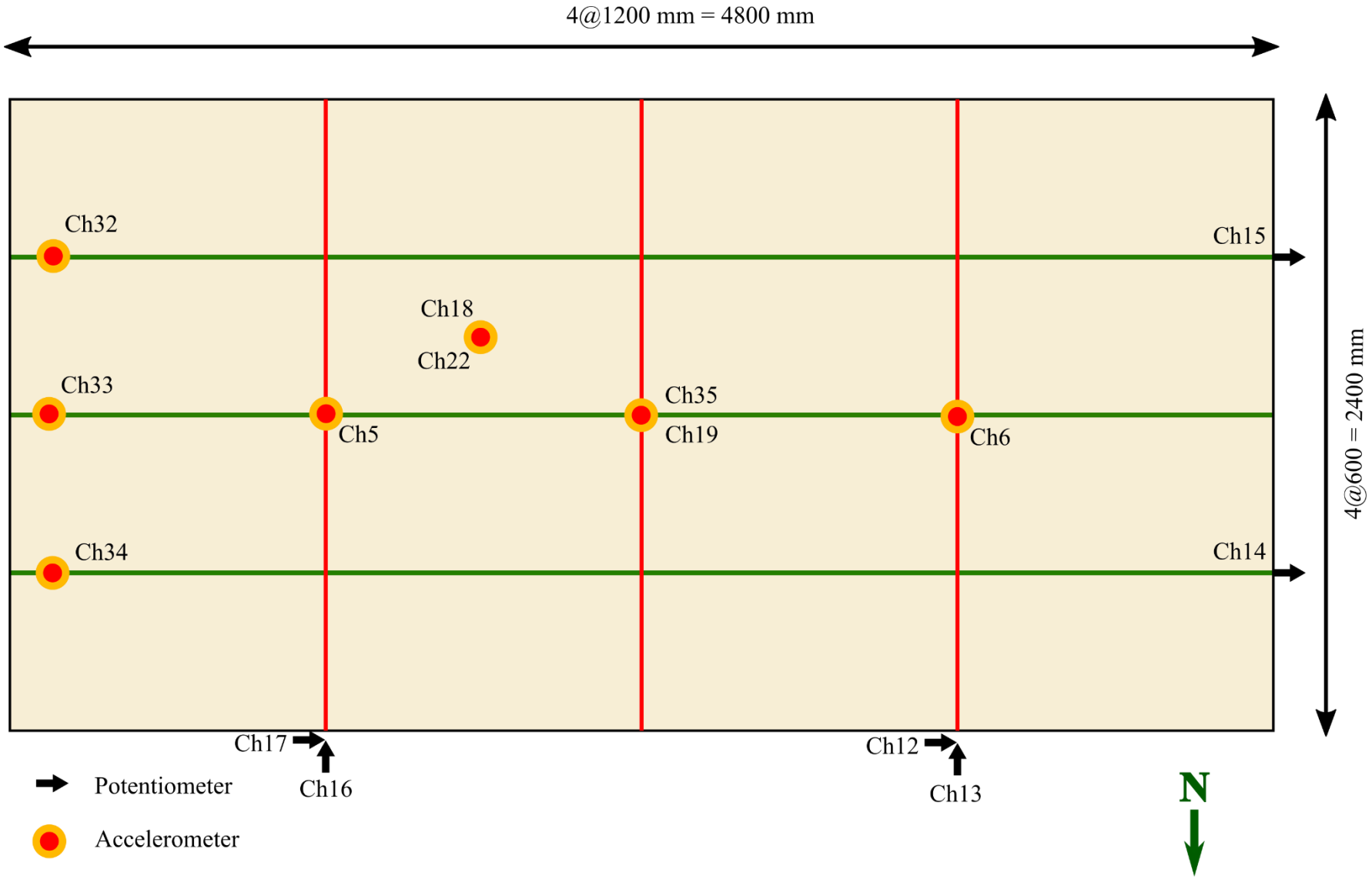

11.7 Unbraced ceiling

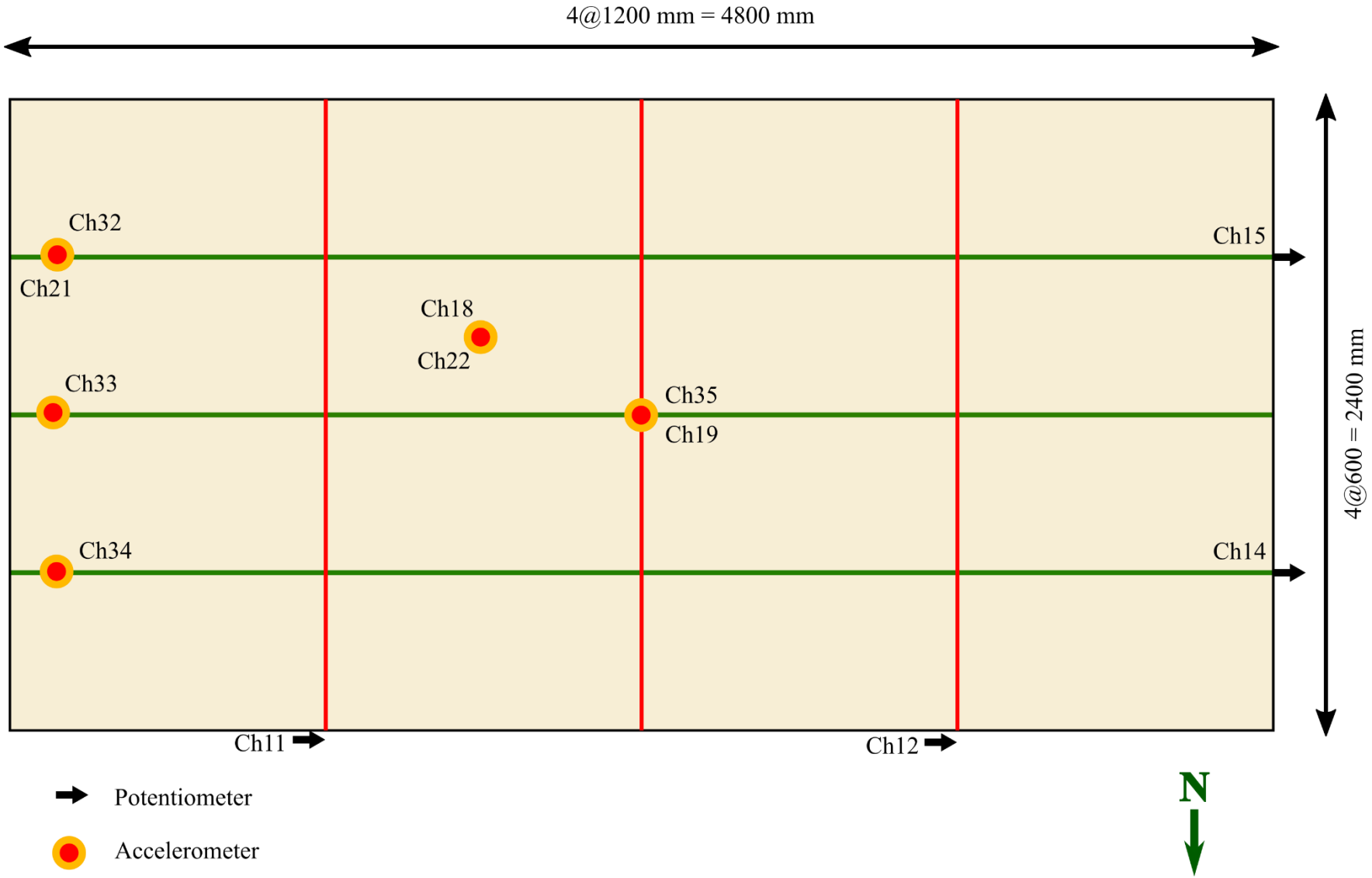

Table 9 – Instruments on drywall and two ceiling specimens

Instrument ID	Instrument type	Direction	Instrument ID	Instrument type	Direction
Ch2	Potentiometer	E-W	Ch20	Accelerometer	E-W
Ch3	Potentiometer	E-W	Ch21	Accelerometer	E-W
Ch4	Accelerometer	E-W	Ch22	Accelerometer	E-W
Ch5	Accelerometer	E-W	Ch23	Accelerometer	E-W
Ch6	Accelerometer	E-W	Ch25	Accelerometer	E-W
Ch7	Accelerometer	Vertical	Ch26	Accelerometer	Vertical
Ch8	Accelerometer	E-W	Ch27	Accelerometer	E-W
Ch9	Potentiometer	E-W	Ch32	Accelerometer	E-W
Ch11	Potentiometer	E-W	Ch33	Accelerometer	E-W
Ch12	Potentiometer	E-W	Ch34	Accelerometer	E-W
Ch13	Potentiometer	N-S	Ch35	Accelerometer	E-W
Ch14	Potentiometer	E-W	Ch37	Potentiometer	E-W
Ch15	Potentiometer	E-W	Ch38	Potentiometer	E-W
Ch16	Potentiometer	N-S	Ch39	Potentiometer	Vertical
Ch17	Potentiometer	E-W	Ch40	Potentiometer	Vertical
Ch18	Accelerometer	Vertical	Ch41	Accelerometer	E-W
Ch19	Accelerometer	Vertical	Ch42	Accelerometer	Vertical

APPENDIX C

PHOTOS FROM EXPERIMENTS

12 PHOTOS

12.1 Test frame

Figure 6 – Frame lower beams and extension beams on shake table

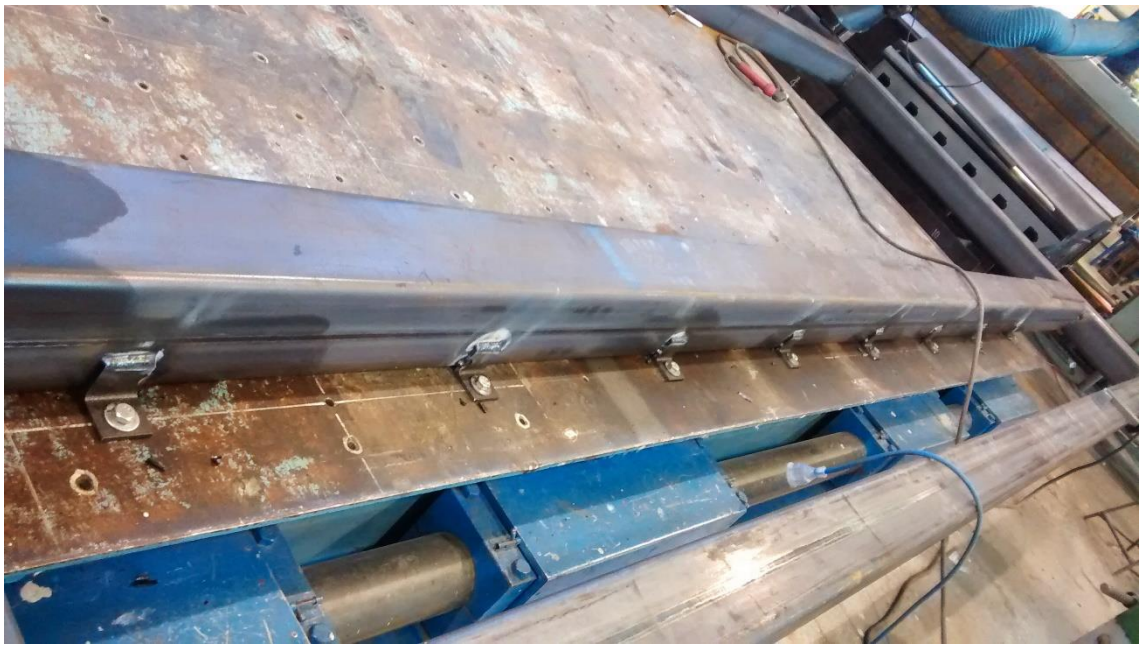

Figure 7 – Fixtures of frame lower beams to shake table

Figure 8 – Frame overhang on west end

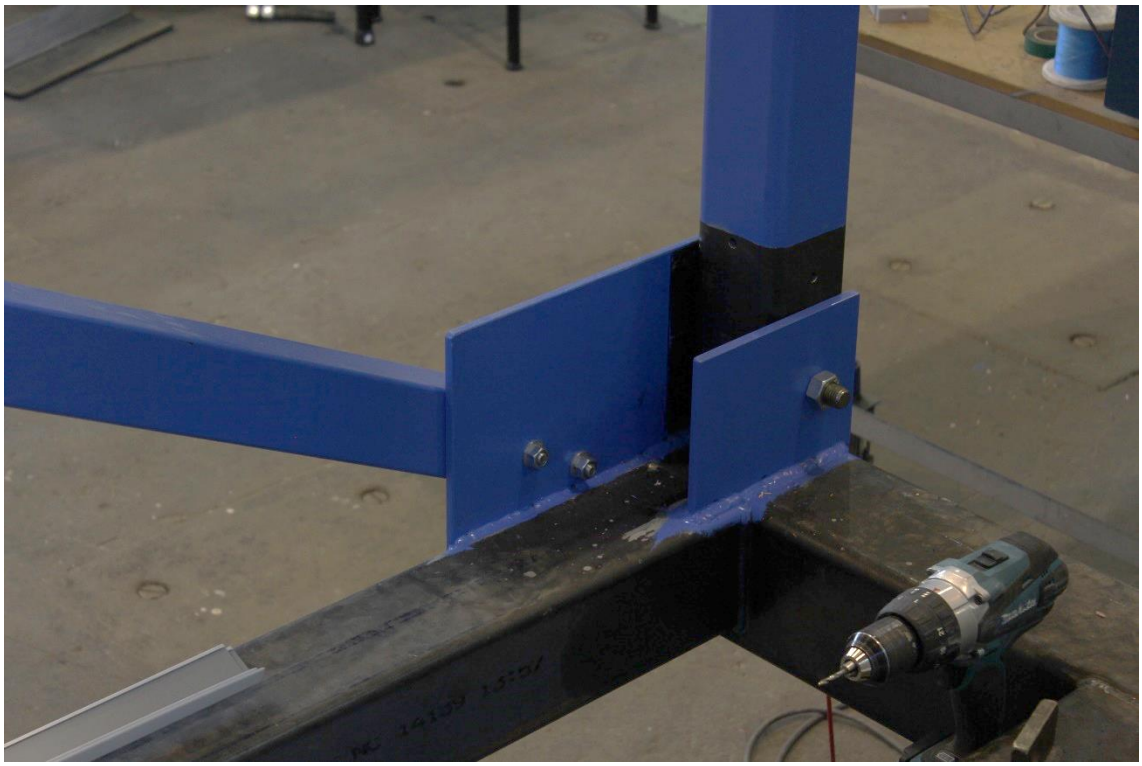

Figure 9 – Bottom connection of beams, column and brace

Figure 10 – Top connection of beams, column and brace

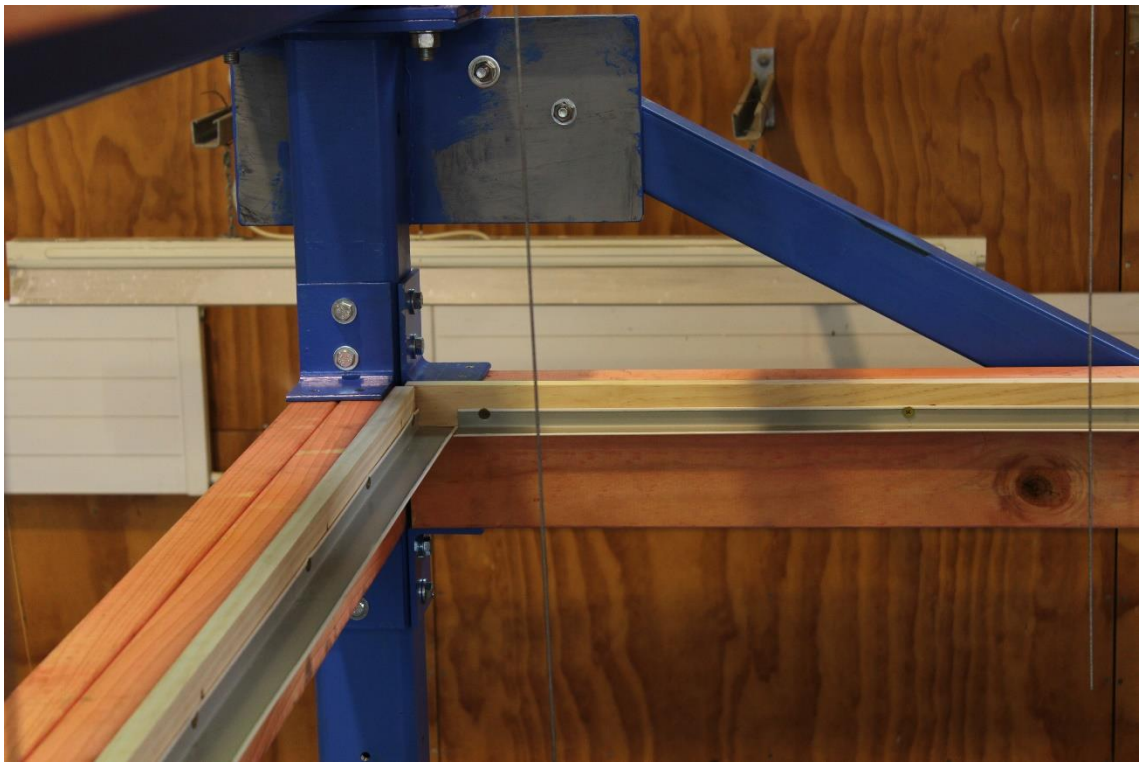

Figure 11 – Connection of ceiling perimeter beams to frame

12.2 Experiments on perimeter-fixed ceilings

Figure 12 – Detail of end clip, end hanger and potentiometer

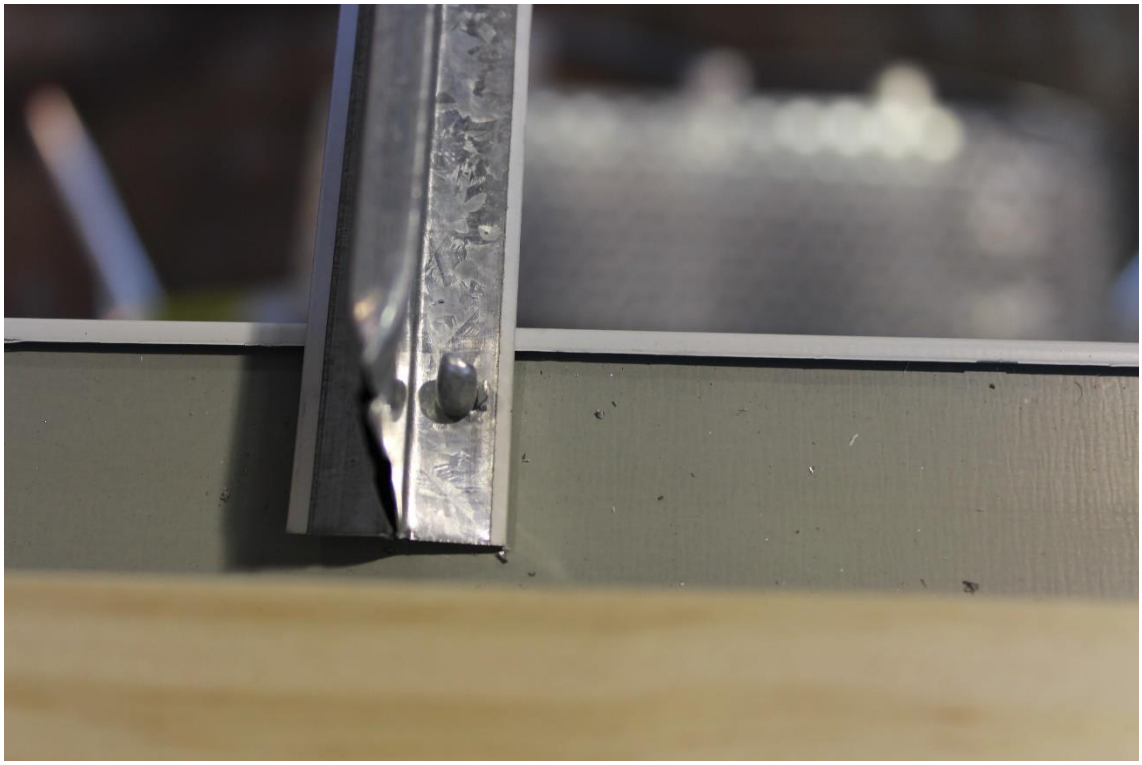

Figure 13 – Detail of riveted fixture on ceiling grid

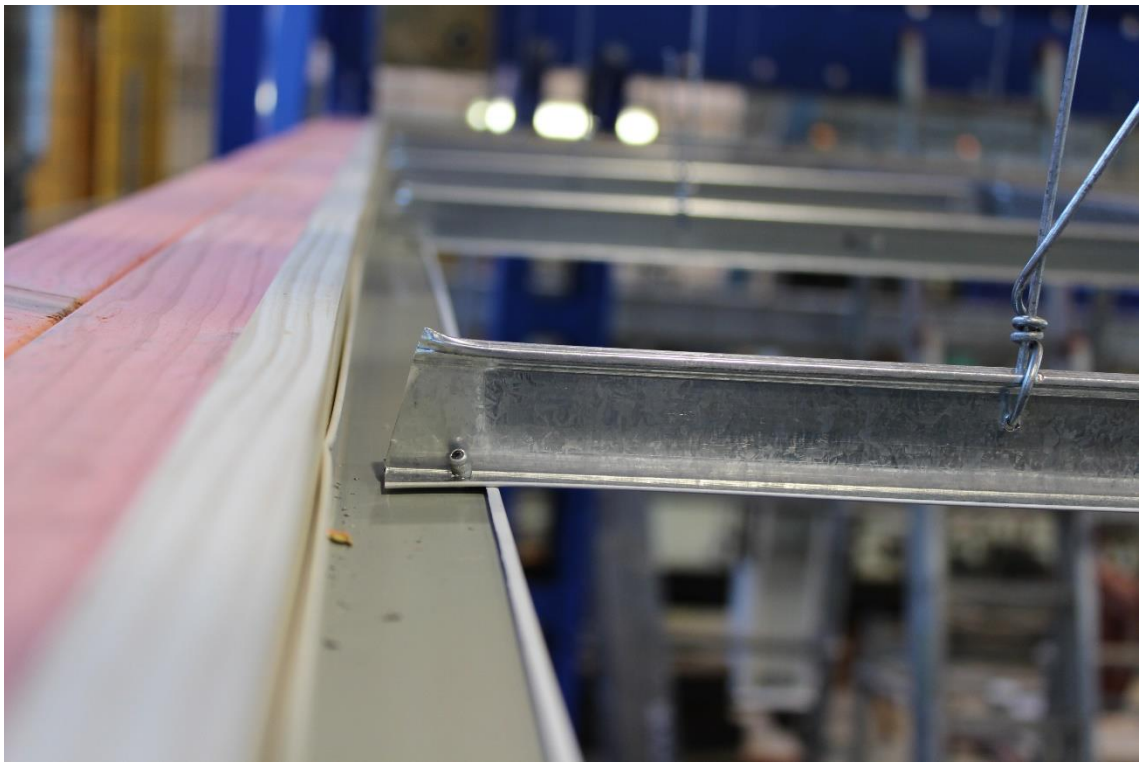

Figure 14 – Detail of end fixture rivet and hangers on ceiling grid

Figure 15 – Detail of hanger fixture to roof beams

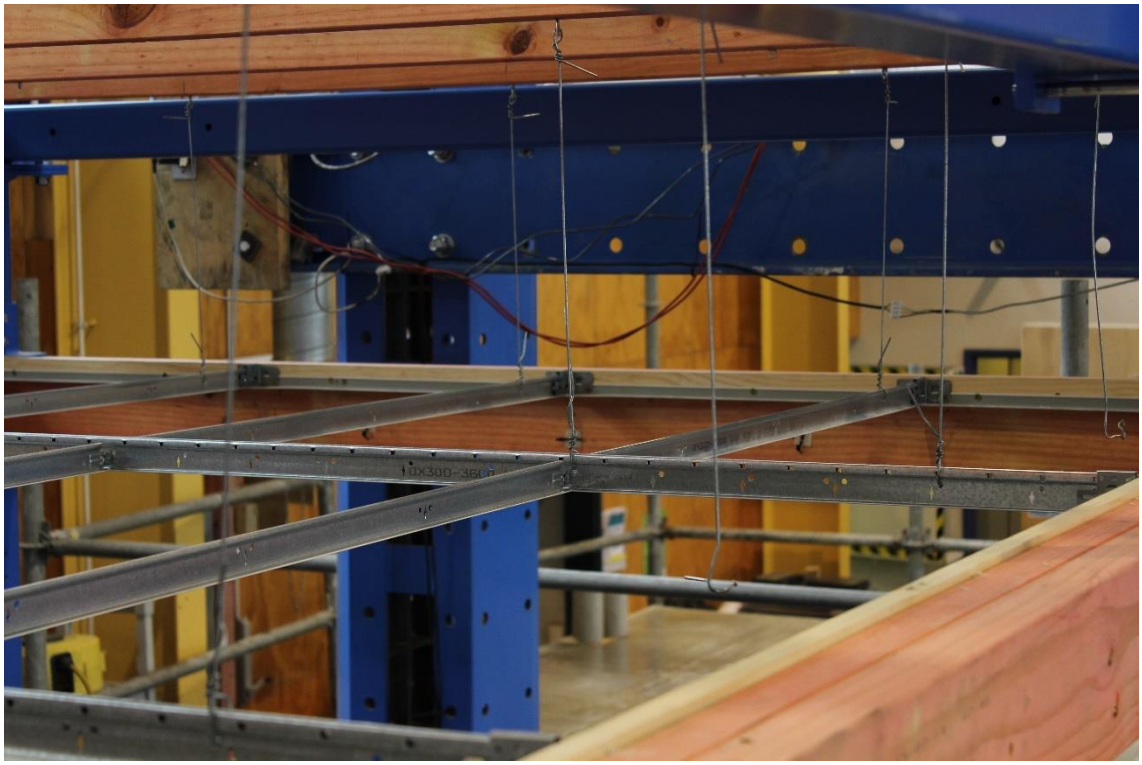

Figure 16 – Detail of end clip, hangers on CT-MT joints and grid ends

Figure 17 – Instruments on perimeter-fixed ceiling specimen

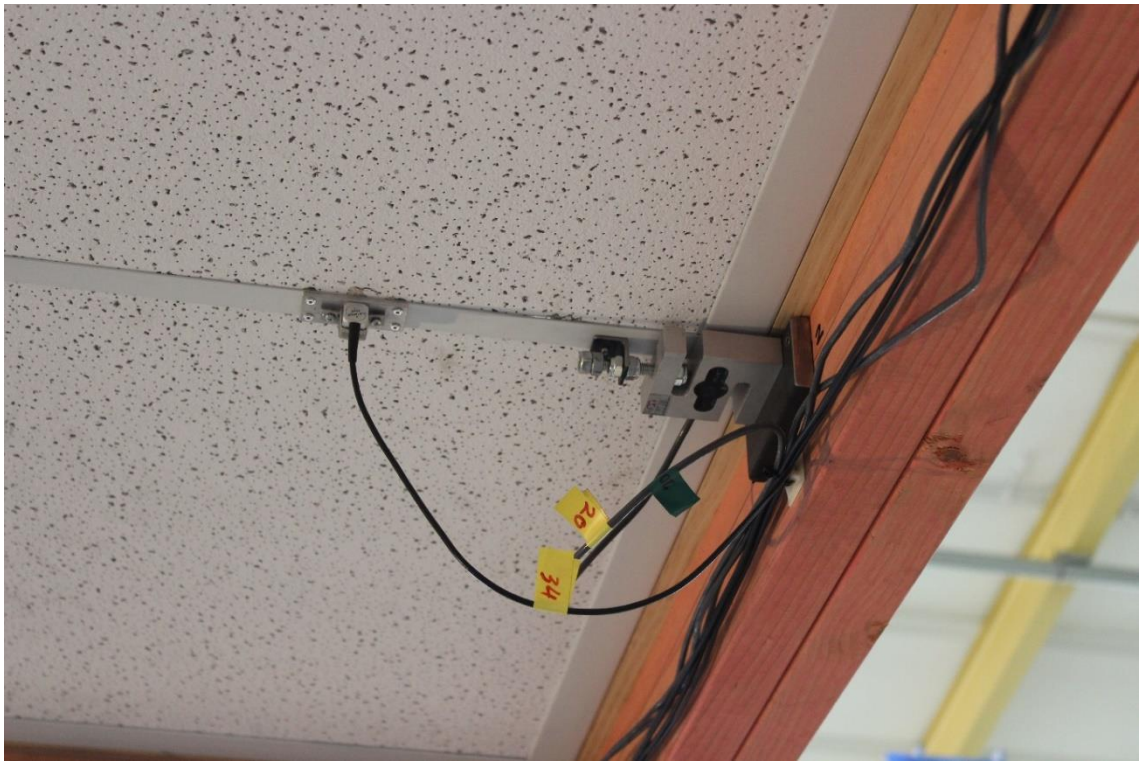

Figure 18 – Detail of load cell and accelerometer installed on grid end

Figure 19 – Detail of potentiometer and accelerometer installed on grid end

Figure 20 – Detail of potentiometer and accelerometer installed on grid ends

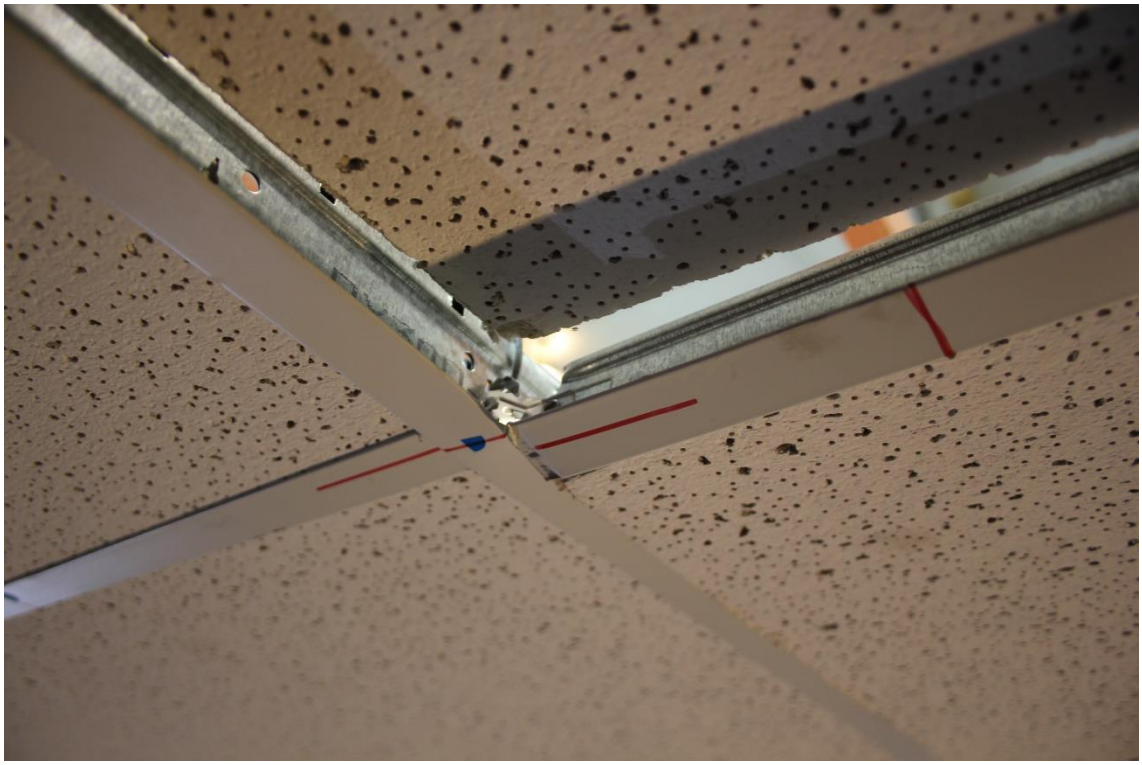

Figure 21 – Damage to CT-MT clip in Pr-F-B specimen

Figure 22 – Damage to CT-MT clip in Pr-F-B specimen

12.3 Experiments of fully-floating ceiling system

Figure 23 – View of fully-floating ceiling on test frame

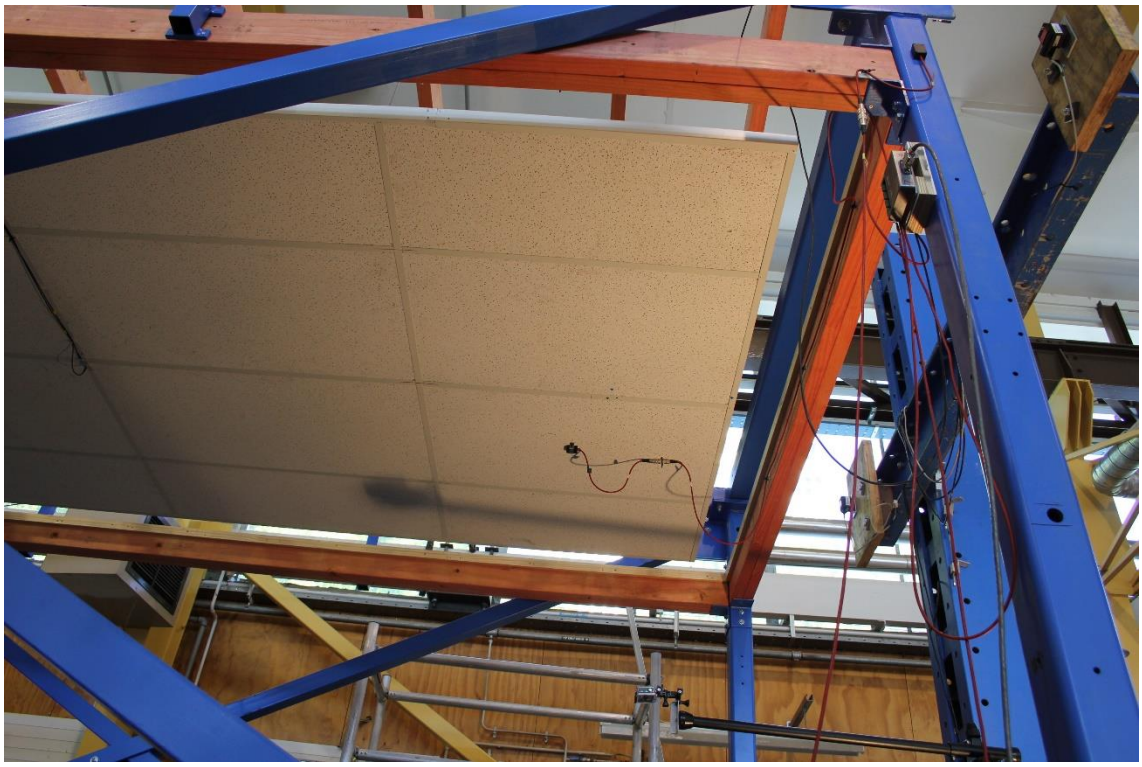

Figure 24 - Fully-floating ceiling with perimeter gaps, west end

Figure 25 - Fully-floating ceiling with perimeter gaps, east end

Figure 26 – Perimeter gap in fully-floating ceiling

Figure 27 – Fully-floating ceiling with sand bags for tests with added mass

Figure 28 - Fully-floating ceiling with hanger layout A

Figure 29 – Fully-floating ceiling with steel angle covering the perimeter gap before the placement of isolation foam

Figure 30 - Fully-floating ceiling with steel angle covering the perimeter gap before the placement of isolation foam, Hanger layout B

Figure 31 - Fully-floating ceiling with perimeter gaps filled with isolation foam

Figure 32 – Damage incident in the fully-floating ceiling: panel dislodgement

12.4 Experiments on low-damage drywall & ceiling

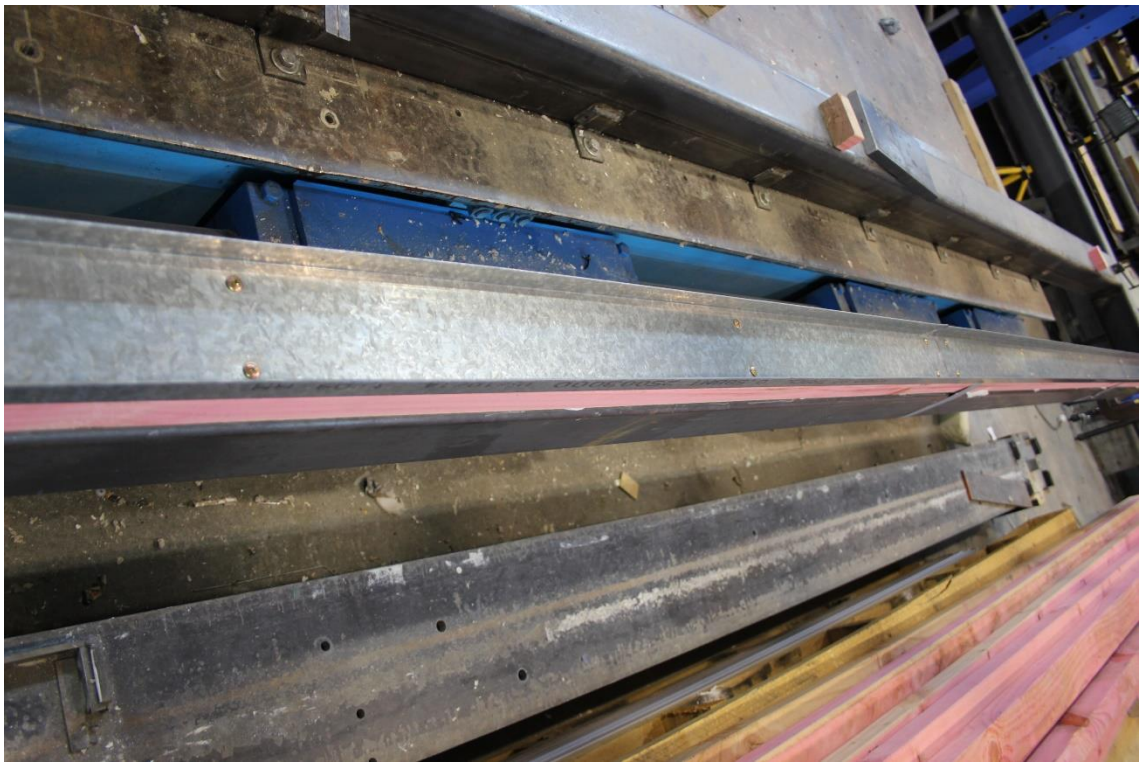

Figure 33 – Lower channel fixed to the frame beam for the installation of low-damage drywall

Figure 34 – Installation process of low-damage drywall: placement of timber studs

Figure 35 – Installation process of low-damage drywall: use of nail guns for fixing wall studs to frame columns

Figure 36 – Installation process of low-damage drywall: placement of inner frames

Figure 37 – Installation process of the low-damage drywall: pivot points

Figure 38 – Installation process of low-damage drywall: gaps on the upper end of wall studs

Figure 39 – Installation process of low-damage drywall: gaps on the lower end of last wall studs to allow rotation

Figure 40 – Installation process of low-damage drywall: installation of drywall boards

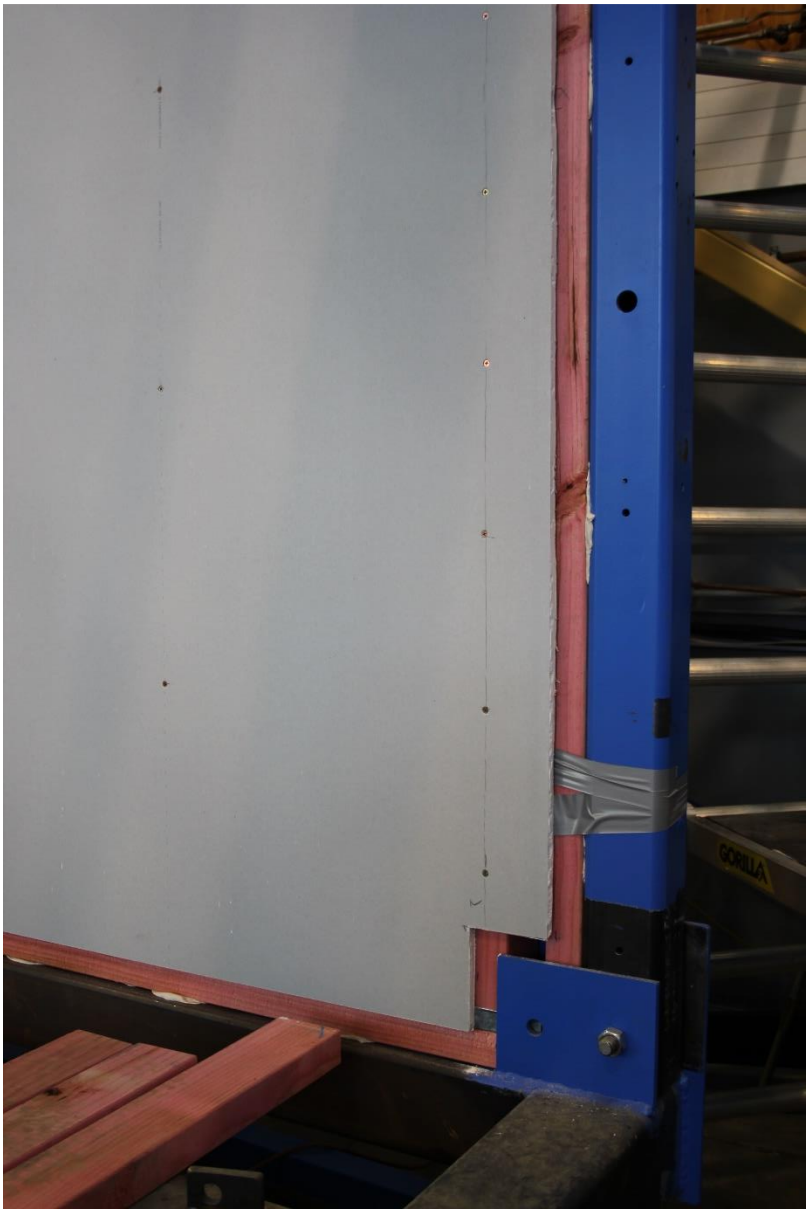

Figure 41 – Installation process of low-damage drywall: wall board corner detail

Figure 42 – Installation process of low-damage drywall: addition of the ceiling

Figure 43 – Installation process of low-damage drywall: ceiling bracing

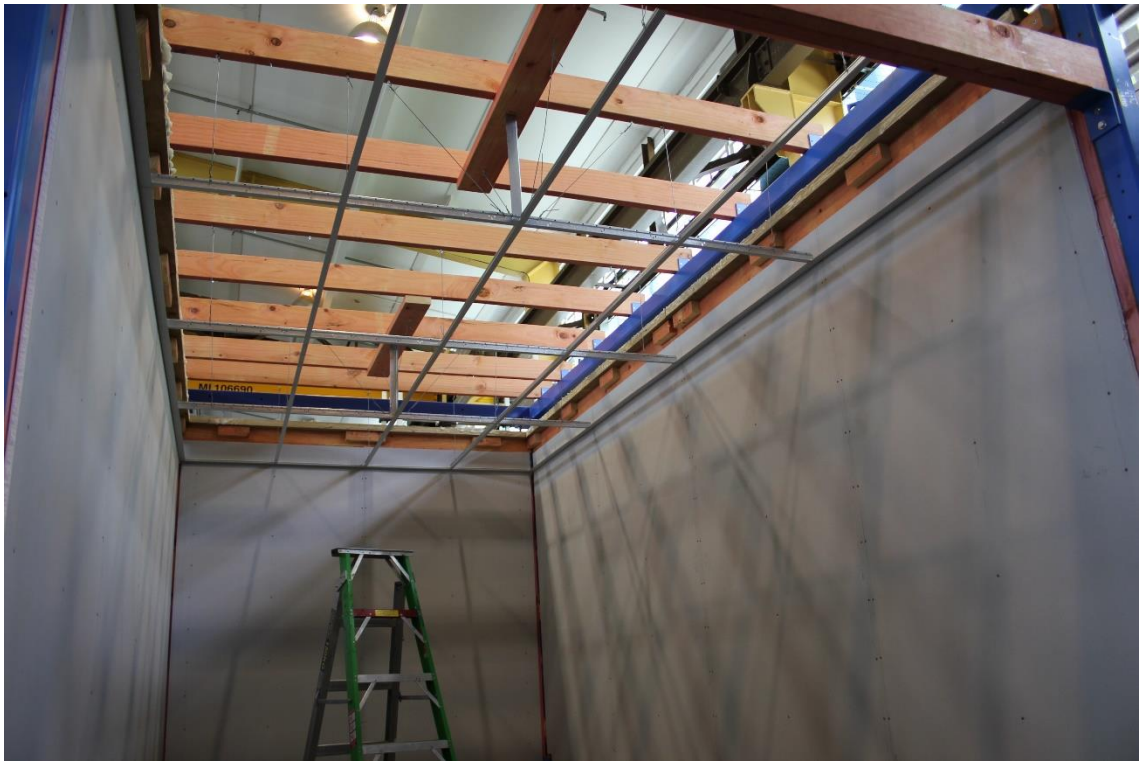

Figure 44 – Installation process of low-damage drywall: interior view before tile placement

Figure 45 – Low-damage drywall: exterior view, north face

Figure 46 – Low-damage drywall: exterior view, east wnd

Figure 47 – Panel dislodgement in braced ceiling, NW corner

Figure 48 – Panel dislodgement in braced ceiling, NW corner

Figure 49 – Panel dislodgement in braced ceiling, NE corner

12.5 Experiments on CT-MT joints with seismic clip

Figure 50 – Test specimen without seismic clip

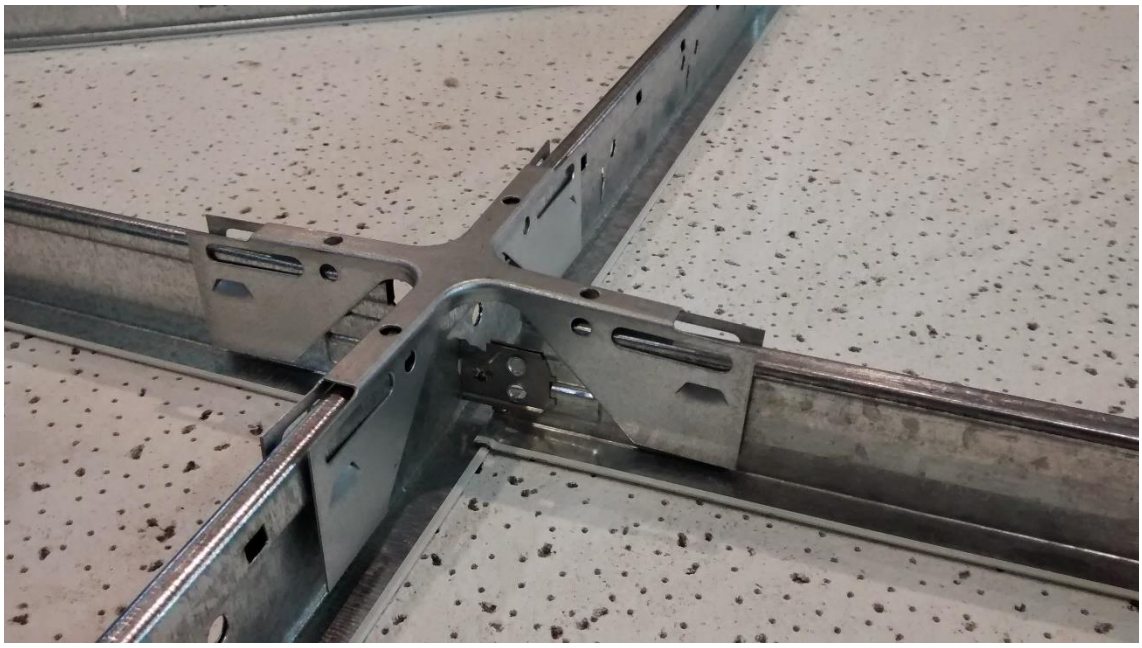

Figure 51 – Test specimen with seismic clip

Figure 52 – Test setup in compression

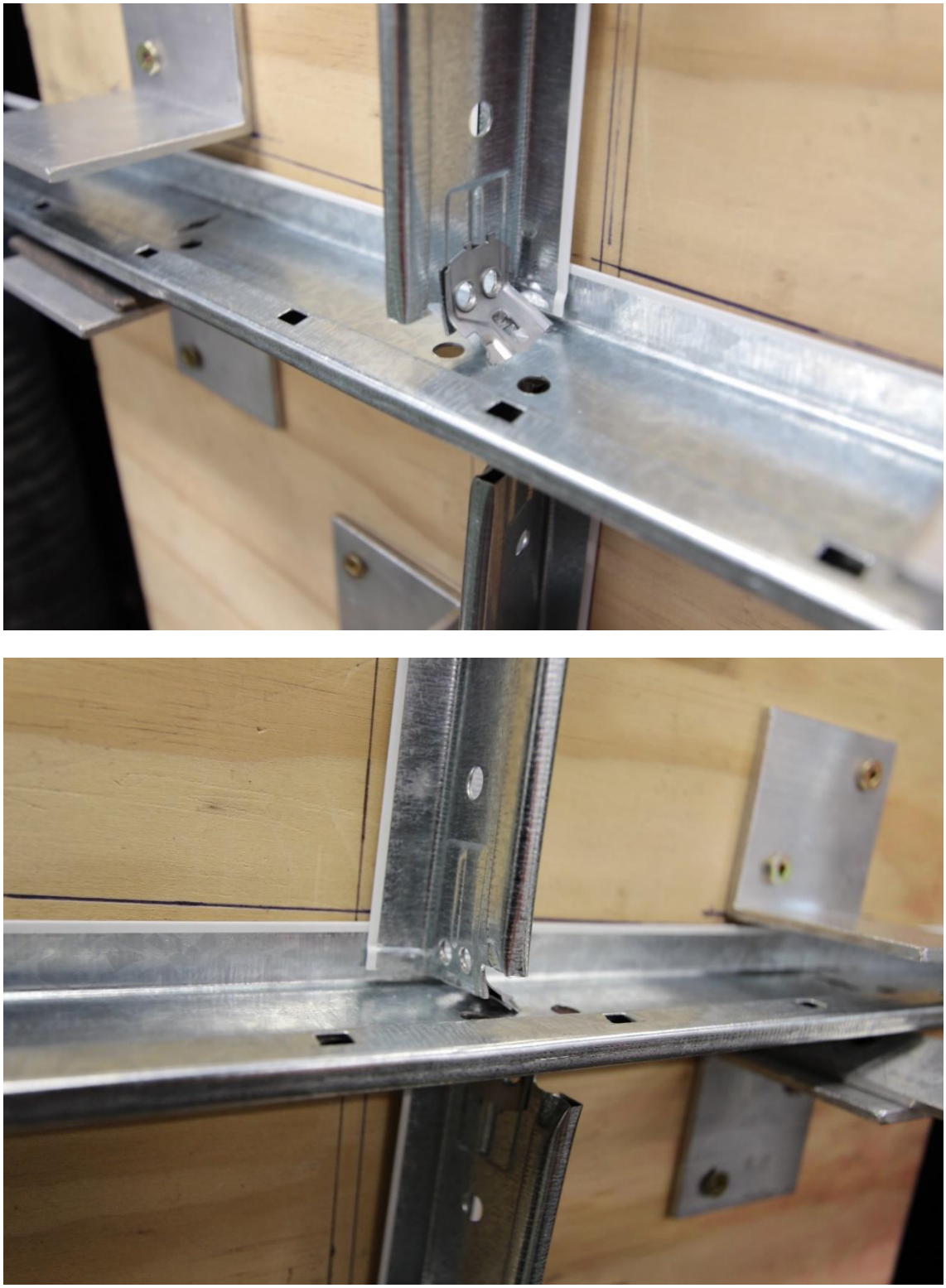

Figure 53 – Failure of connection in compression: buckling of CT clip

Figure 54 – Failure of connection in compression: buckling of CT clip

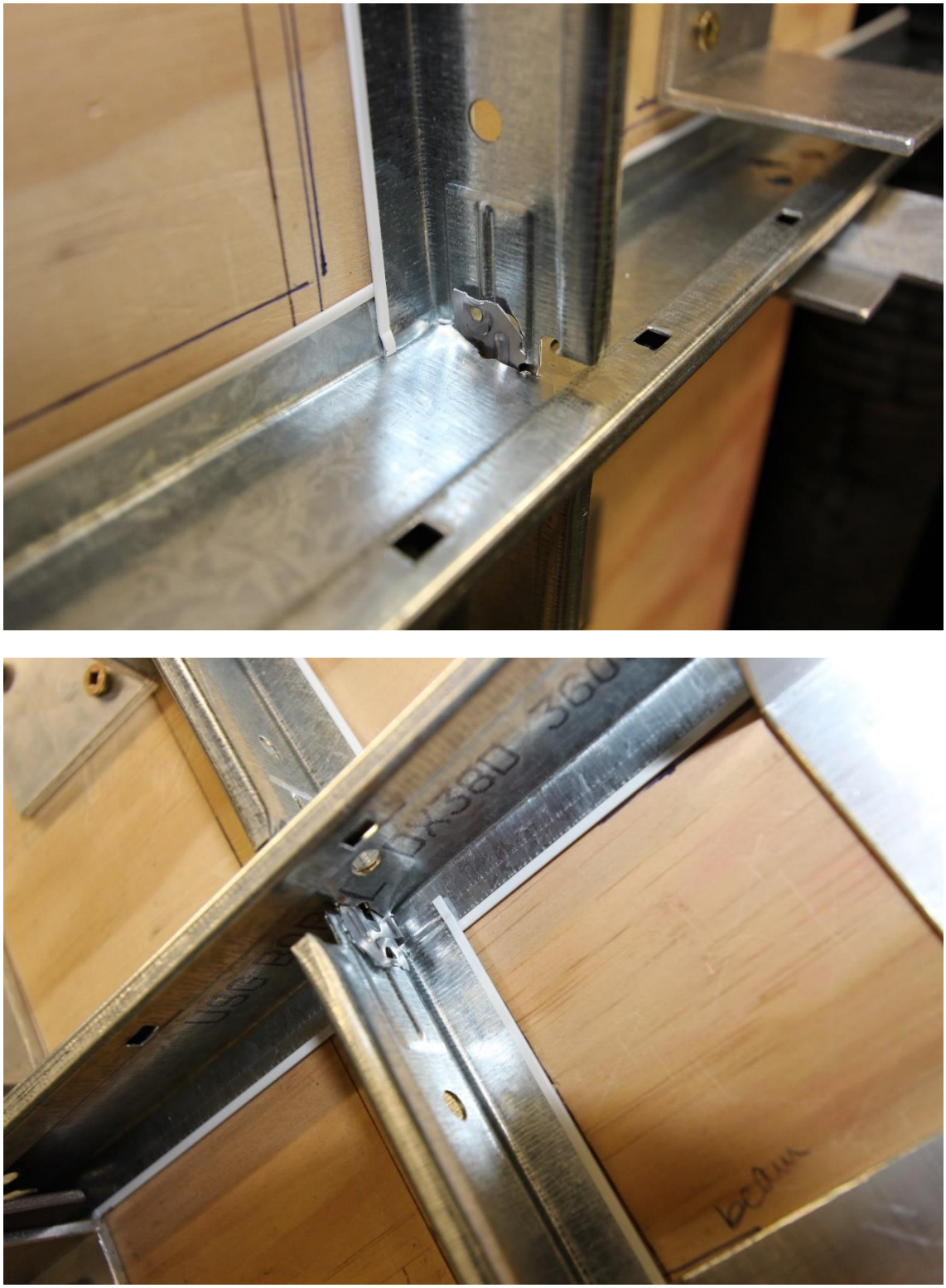

Figure 55 – Failure of connection in compression: tearing of MT web

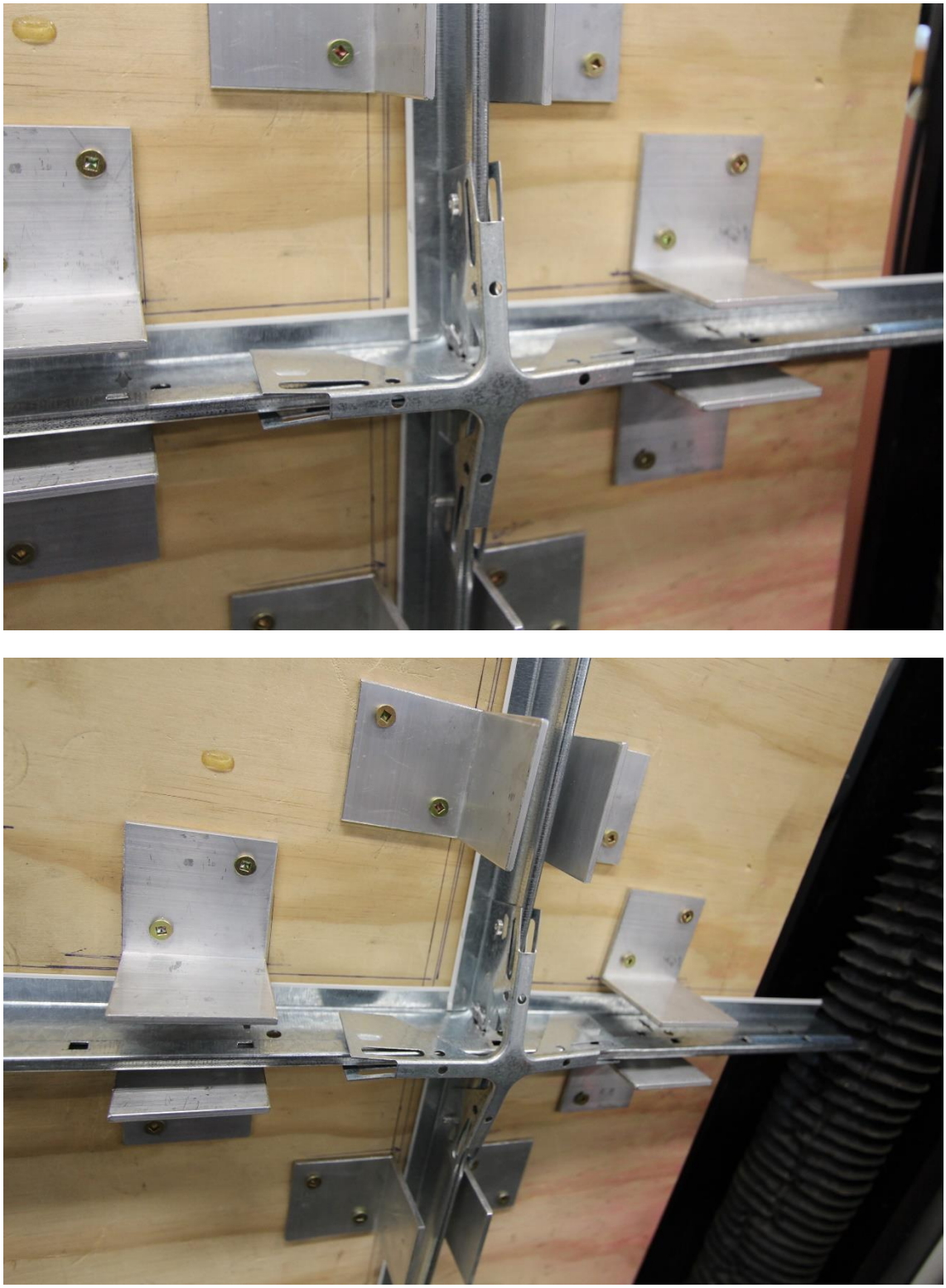

Figure 56 – Test of connection with seismic clip under compression

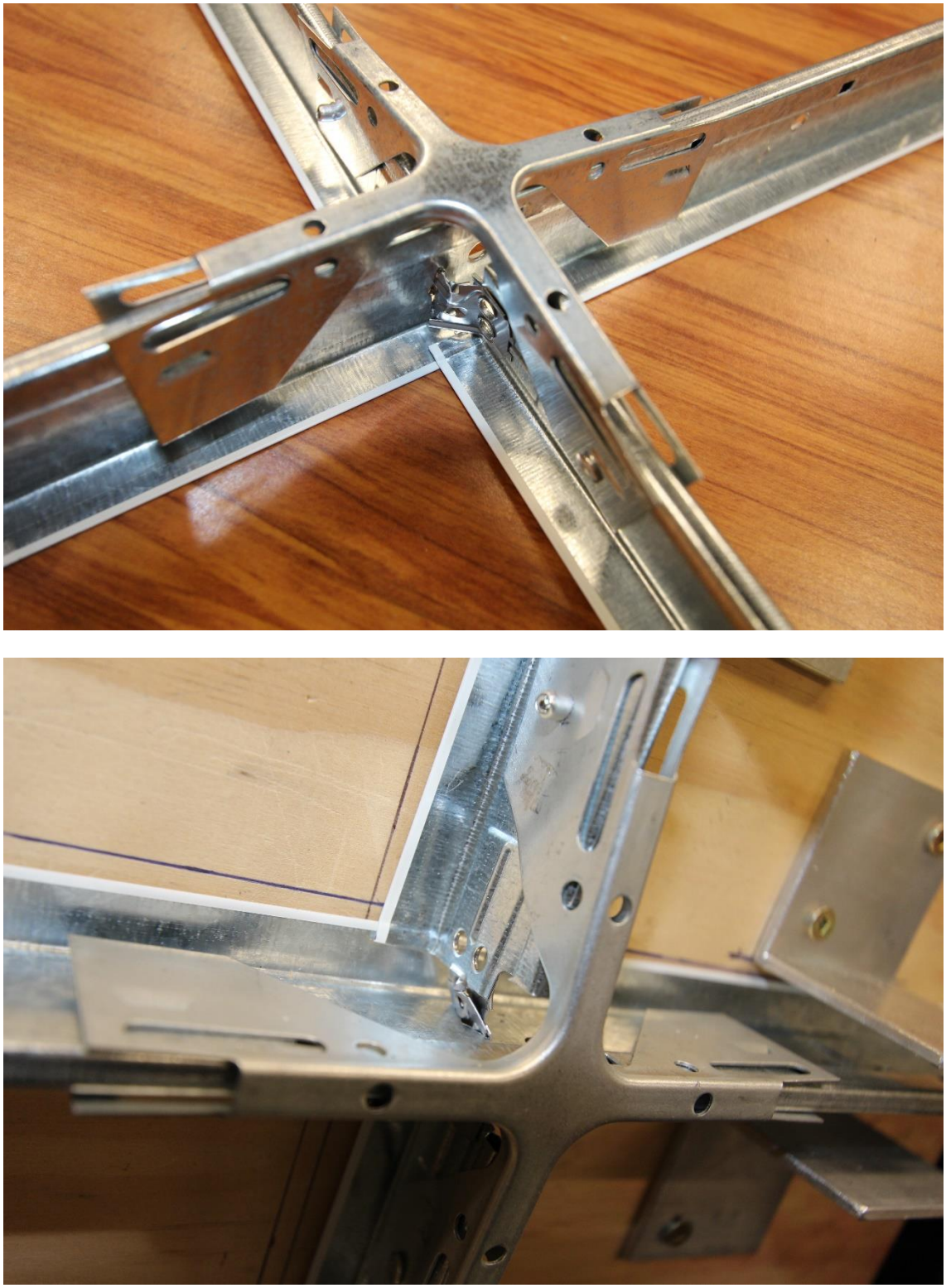

Figure 57 – Failure of connection in compression: buckling of CT clip

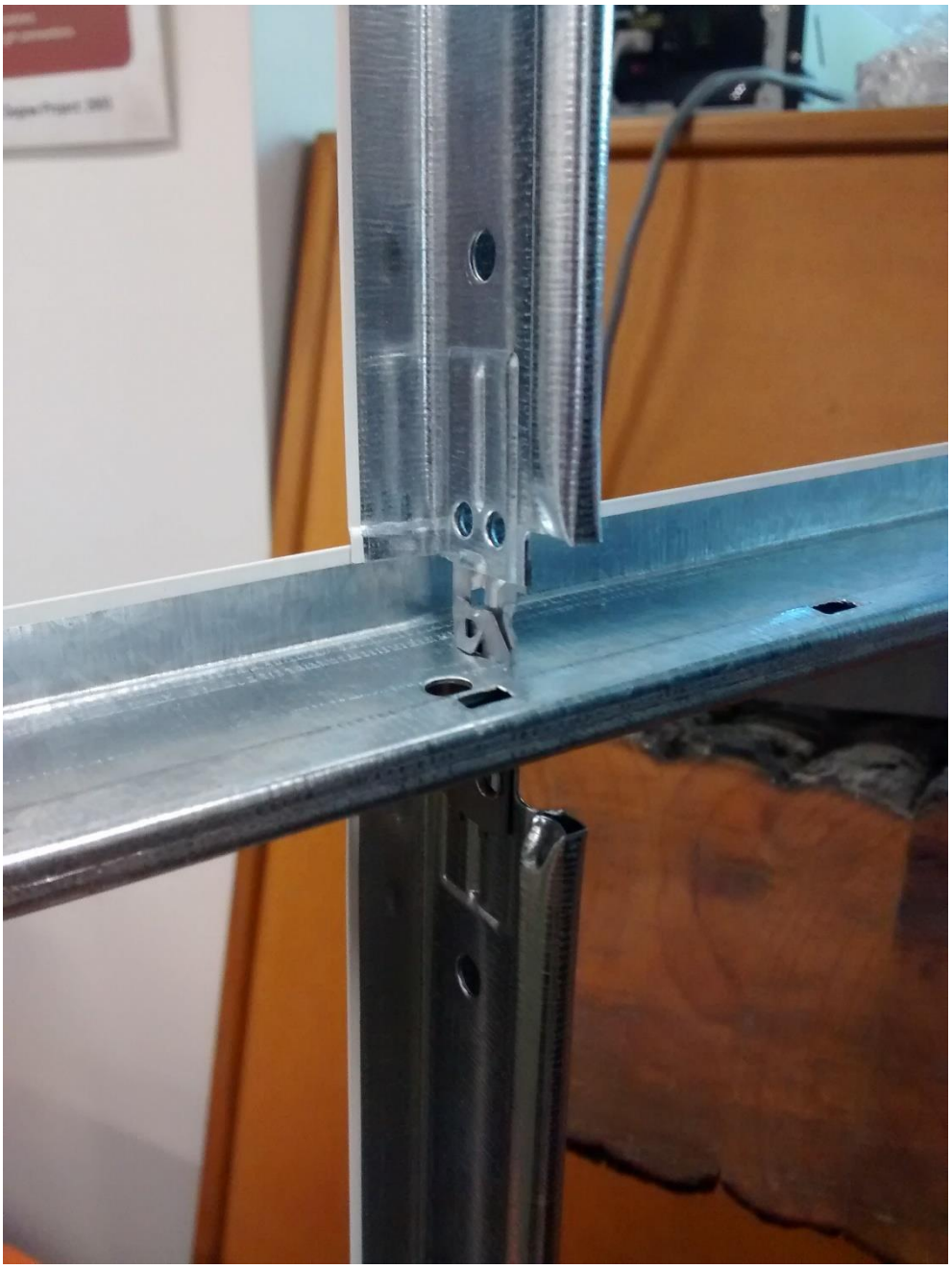

Figure 58 – Failure of connection in tension

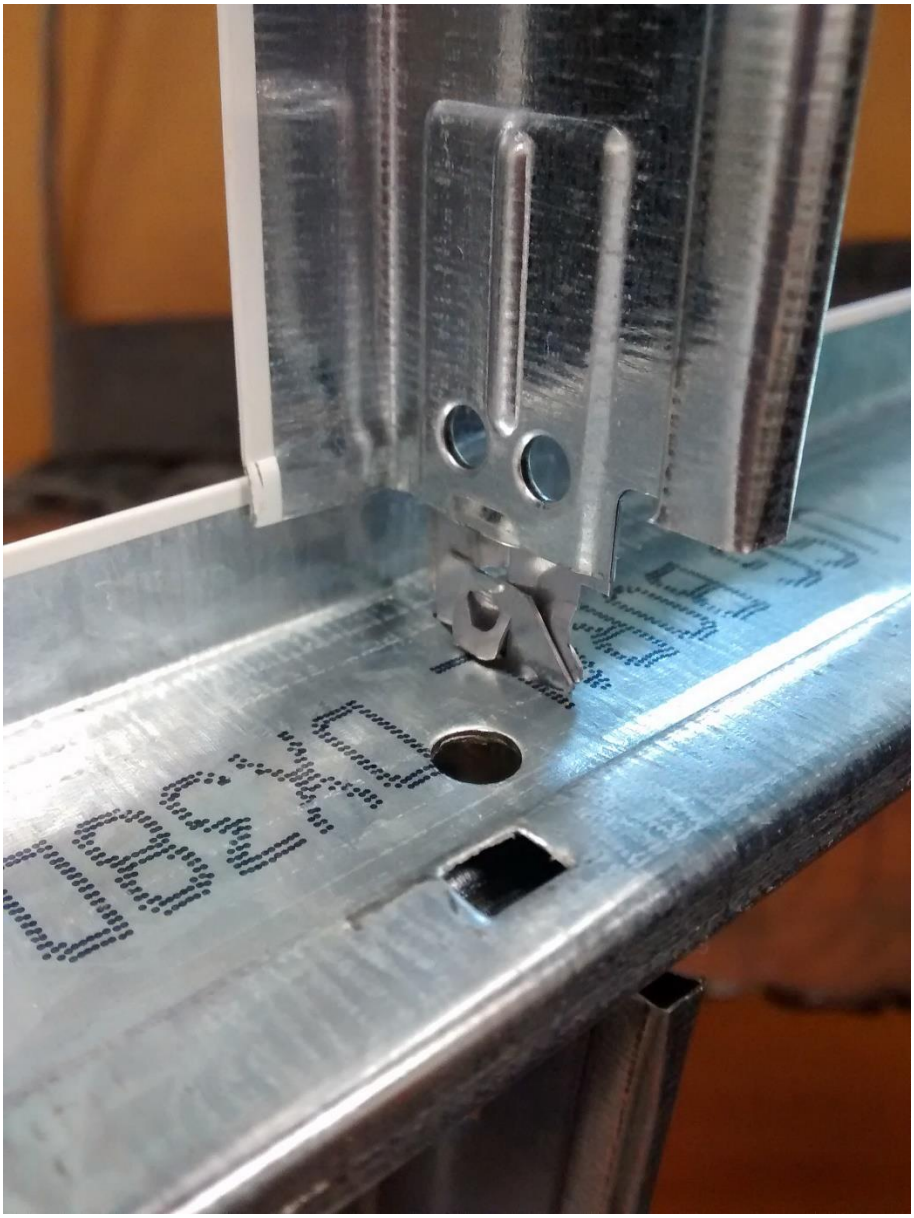

Figure 59 – Engagement of CT clip in tension

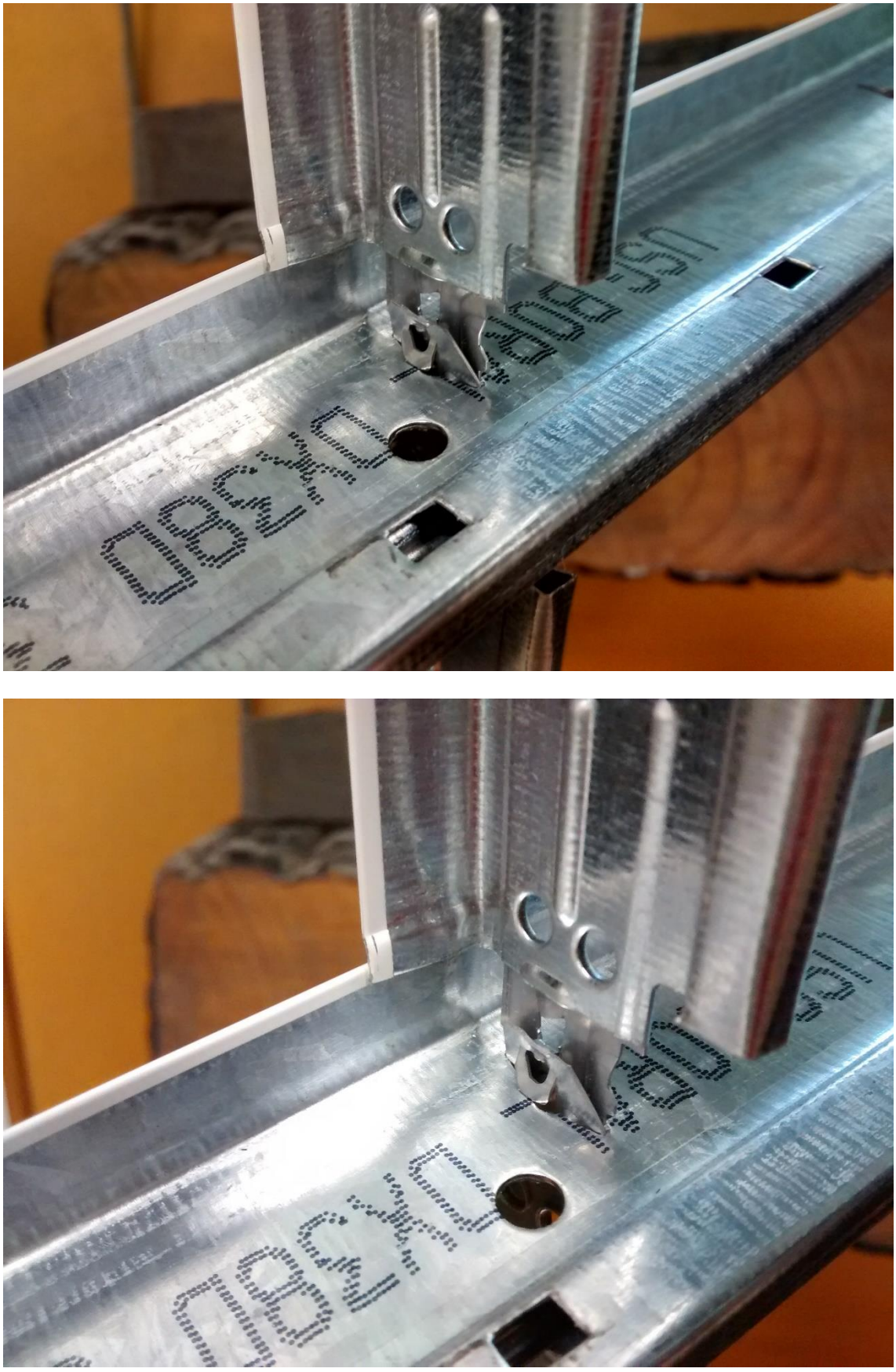

Figure 60 – Engagement and failure of CT clip in tension

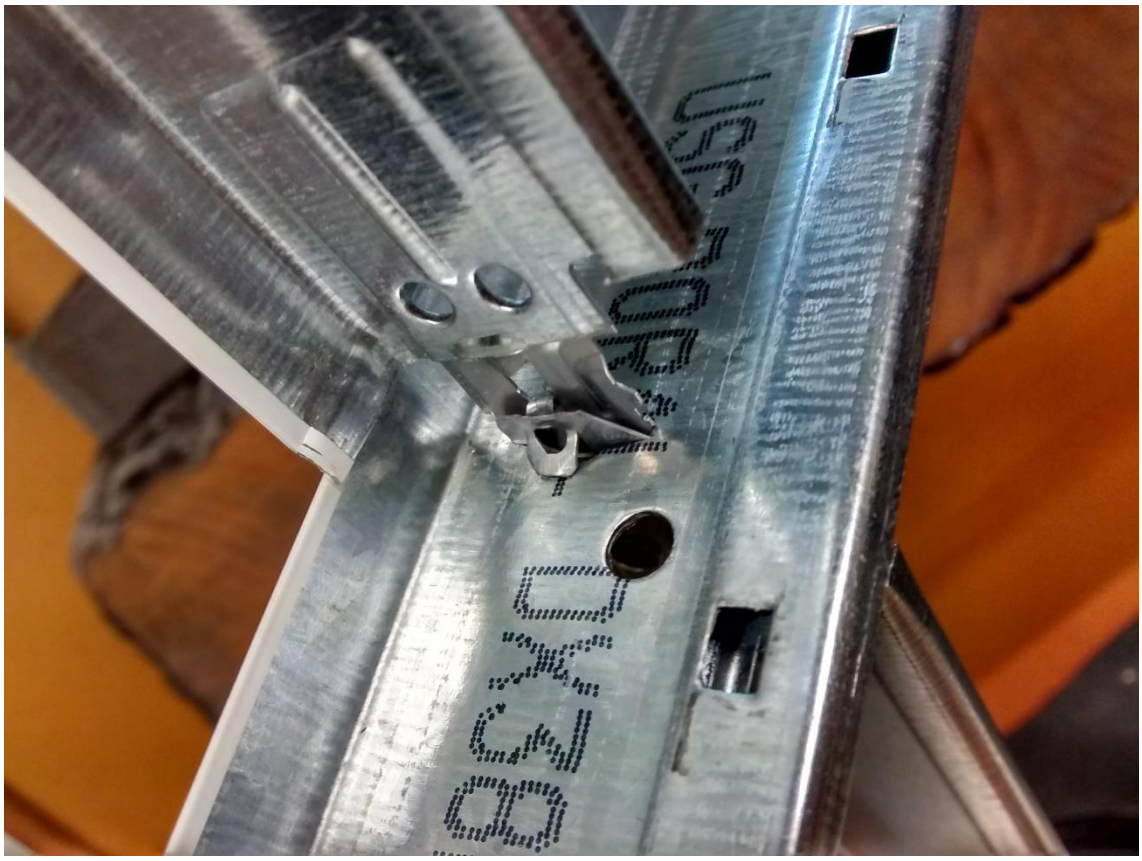

Figure 61 – Engagement and failure of CT clip in tension

Figure 62 – Example of disengaged CT clip in tension

Figure 63 – Deformation of seismic clip in tension

Figure 64 – Connection failure in tension: rivet failure

Figure 65 – Connection failure in tension: tearing of MT web

Figure 66 – Connection failure in tension: tearing of MT web